Methods in Molecular Biology 3075

Springer Protocols

Duško Lainšček · Melita Vidaković
Yonglun Luo · Karim Benabdellah
Editors

CRISPR Delivery

cost
EUROPEAN COOPERATION IN SCIENCE & TECHNOLOGY

Funded by the European Union

OPEN ACCESS

Humana Press

METHODS IN MOLECULAR BIOLOGY

Series Editor
John M. Walker
School of Life and Medical Sciences
University of Hertfordshire
Hatfield, Hertfordshire, UK

For further volumes:
http://www.springer.com/series/7651

For over 35 years, biological scientists have come to rely on the research protocols and methodologies in the critically acclaimed Methods in Molecular Biology series. The series was the first to introduce the step-by-step protocols approach that has become the standard in all biomedical protocol publishing. Each protocol is provided in readily-reproducible step-by step fashion, opening with an introductory overview, a list of the materials and reagents needed to complete the experiment, and followed by a detailed procedure that is supported with a helpful notes section offering tips and tricks of the trade as well as troubleshooting advice. These hallmark features were introduced by series editor Dr. John Walker and constitute the key ingredient in each and every volume of the Methods in Molecular Biology series. Tested and trusted, comprehensive and reliable, all protocols from the series are indexed in PubMed.

Manuscript Instructions https://drive.google.com/file/d/1K4Az5vpAFVzYadJ3jKx2-QSo7Dqa_SNA/view?usp=sharing

CRISPR Delivery

Edited by

Duško Lainšček

Department of Synthetic Biology and Immunology, Centre for Technologies of Gene and Cell Therapy, National Institute of Chemistry, Ljubljana, Slovenia

Melita Vidaković

Department of Molecular Biology, Institute for Biological Research - National Institute of the Republic of Serbia, University of Belgrade, Belgrade, Serbia

Yonglun Luo

Department of Biomedicine, Aarhus University, Aarhus C, Denmark

Karim Benabdellah

Department of Genomic Medicine, Andalusian Regional Government Centre for Genomics and Oncological Research (GENYO), Pfizer-University of Granada, Granada, Spain

Humana Press

Editors
Duško Lainšček
Department of Synthetic Biology and Immunology
Centre for Technologies of Gene and Cell Therapy
National Institute of Chemistry
Ljubljana, Slovenia

Yonglun Luo
Department of Biomedicine
Aarhus University
Aarhus C, Denmark

Melita Vidaković
Department of Molecular Biology
Institute for Biological Research - National
Institute of the Republic of Serbia
University of Belgrade
Belgrade, Serbia

Karim Benabdellah
Department of Genomic Medicine
Andalusian Regional Government Centre for
Genomics and Oncological Research (GENYO)
Pfizer-University of Granada
Granada, Spain



ISSN 1064-3745 ISSN 1940-6029 (electronic)
Methods in Molecular Biology
ISBN 978-1-0716-5546-7 ISBN 978-1-0716-5547-4 (eBook)
https://doi.org/10.1007/978-1-0716-5547-4

© The Editor(s) (if applicable) and The Author(s) 2027 This book is an open access publication.

Open Access This book is licensed under the terms of the Creative Commons Attribution-NonCommercial-NoDerivatives 4.0 International License (http://creativecommons.org/licenses/by-nc-nd/4.0/), which permits any noncommercial use, sharing, distribution and reproduction in any medium or format, as long as you give appropriate credit to the original author(s) and the source, provide a link to the Creative Commons license and indicate if you modified the licensed material. You do not have permission under this license to share adapted material derived from this book or parts of it.
The images or other third party material in this book are included in the book's Creative Commons license, unless indicated otherwise in a credit line to the material. If material is not included in the book's Creative Commons license and your intended use is not permitted by statutory regulation or exceeds the permitted use, you will need to obtain permission directly from the copyright holder.
This work is subject to copyright. All commercial rights are reserved by the author(s), whether the whole or part of the material is concerned, specifically the rights of translation, reprinting, reuse of illustrations, recitation, broadcasting, reproduction on microfilms or in any other physical way, and transmission or information storage and retrieval, electronic adaptation, computer software, or by similar or dissimilar methodology now known or hereafter developed. Regarding these commercial rights a non-exclusive license has been granted to the publisher. Unless otherwise expressly agreed by the Publisher in writing, the Publisher does not authorize use or reproduction of all or any part of this work in any manner for the purpose of training, fine-tuning, evaluating, or developing artificial intelligence models, technologies, or systems. In accordance with Article 4(3) of the EU Directive 2019/790 on copyright and related rights in the Digital Single Market, the Publisher expressly reserves all rights with respect to this work under the text and data mining exception of the directive.
The use of general descriptive names, registered names, trademarks, service marks, etc. in this publication does not imply, even in the absence of a specific statement, that such names are exempt from the relevant protective laws and regulations and therefore free for general use.
The publisher, the authors and the editors are safe to assume that the advice and information in this book are believed to be true and accurate at the date of publication. Neither the publisher nor the authors or the editors give a warranty, expressed or implied, with respect to the material contained herein or for any errors or omissions that may have been made. The publisher remains neutral with regard to jurisdictional claims in published maps and institutional affiliations.

This Humana imprint is published by the registered company Springer Science+Business Media, LLC, part of Springer Nature.
The registered company address is: 1 New York Plaza, New York, NY 10004, U.S.A.

If disposing of this product, please recycle the paper.

This publication is based upon work from COST Action Genome Editing for the Treatment of Human Disease Network (GenE-HumDi; COST Action CA21113), supported by COST (European Cooperation in Science and Technology). COST (European Cooperation in Science and Technology) is a funding agency for research and innovation networks. Our Actions help connect research initiatives across Europe and enable scientists to grow their ideas by sharing them with their peers. This boosts their research, career and innovation (www.cost.eu)





Preface

Genome editing technologies have revolutionized our ability to precisely manipulate genetic information, opening unprecedented opportunities for both fundamental research and therapeutic applications. Over the past decade, a variety of powerful tools, including CRISPR/Cas systems, base editors, and prime editors, have significantly expanded the genome engineering toolbox, enabling efficient and precise modification of genetic and epigenetic information across diverse species, including humans. Among these, the RNA-guided CRISPR/Cas system has emerged as a particularly versatile and transformative platform since its adaptation for programmable gene editing in 2012. This rapid technological progress has already led to important clinical milestones, including the recent approval of the first CRISPR-based therapies for the treatment of sickle cell disease and transfusion-dependent beta-thalassemia.

Despite these groundbreaking advances, a major challenge remains: the safe and efficient delivery of genome editing components into target cells and tissues. Delivery is now widely recognized as one of the principal bottlenecks in the field, as it directly affects editing efficiency, specificity, toxicity, and ultimately clinical efficacy. Without reliable delivery strategies, even the most advanced genome editing tools cannot fully realize their potential in medicine, agriculture, or basic research.

Over the past 4 years, the GenE-HumDi COST Action has fostered an active and collaborative international research network dedicated to advancing genome editing toward clinical application. Supported by the European Cooperation in Science and Technology (COST), this initiative brings together academia and industry scientists, translational researchers, clinicians, regulatory experts, and industrial partners with the shared goal of improving and translating gene editing protocols for the treatment of human diseases. Through continuous discussion, knowledge exchange, and coordinated efforts across working groups (WGs), delivery has emerged as one of the most dynamic areas within the GenE-HumDi consortium.

The collective expertise generated during this period, spanning diverse platforms, cell types, and translational challenges, has laid the foundation for this book, which represents a key scientific outcome of the GenE-HumDi COST Action. Contributed by leading scientists in the field, this volume provides an up-to-date overview of the evolving landscape of genome editing delivery strategies, with a particular focus on CRISPR-based systems. It offers a comprehensive collection of current delivery approaches, ranging from viral vectors and lipid nanoparticles to physical methods such as electroporation, and presents detailed protocols for the development and implementation of specific CRISPR–Cas delivery modalities.

In line with the *Methods in Molecular Biology* philosophy, this volume is designed to provide practical, detailed, and reproducible protocols that can be readily implemented across laboratories. Each chapter combines a concise overview of the underlying principles with step-by-step methodologies, critical parameters, and expert notes aimed at facilitating reproducibility and experimental success. As the field of genome editing continues to advance, the development of tailored delivery solutions has become increasingly important across different applications. Depending on the specific objectives and biological context, such as cell type, target tissue, or therapeutic strategy, the selection of an appropriate delivery method is essential for achieving successful editing outcomes. For example, in vivo approaches must overcome complex

biological barriers and ensure precise cell targeting, whereas ex vivo strategies prioritize cell viability, expansion, and therapeutic functionality. To address these diverse challenges, ongoing innovations in nanotechnology, biomaterials, and synthetic biology are opening new avenues for the development of safer, more efficient, and highly precise delivery platforms.

The book is structured to reflect the multidimensional nature of genome editing and its delivery. Most importantly, its primary objective is to provide the research community with a comprehensive inventory of methods for CRISPR delivery. Building on an extensive overview of the diverse delivery strategies currently available, this volume presents 21 chapters dedicated to delivery technologies, organized into three main categories: (1) viral delivery, (2) non-viral delivery, and (3) physical delivery approaches, preceded by a brief state-of-the-art overview of the field. Together, these contributions aim to serve as a practical resource for researchers, clinicians, students, and industry professionals committed to improving CRISPR delivery and accelerating its translation into real-world applications.

The initial chapters provide a comprehensive and up-to-date overview of the field, including the fundamental principles of CRISPR-based genome editing and the molecular and cellular machineries involved in DNA modification processes. Particular attention is given to the mechanisms of DNA repair underlying conventional genome editing approaches based on CRISPR-induced double-strand breaks (DSBs). In addition, emerging DSB-independent technologies, such as base editing and prime editing, are discussed as more precise and efficient alternatives for targeted genome modification. These approaches, while highly promising, introduce additional challenges due to the increased size and complexity of their associated protein components, such as deaminases and reverse transcriptases, thereby reinforcing the need for improved delivery strategies.

The subsequent chapters focus on the major delivery platforms, encompassing viral systems, such as lentiviral, γ-retroviral, and adeno-associated virus (AAV) vectors, as well as non-viral approaches, including lipid nanoparticles, electroporation-based delivery, extracellular vesicles, and other synthetic carriers. Together, these sections offer both conceptual frameworks and experimentally validated protocols for a wide range of delivery formats, including DNA, mRNA, and ribonucleoprotein (RNP) complexes. Subsequent chapters further address delivery in specific cellular contexts of high relevance for both research and clinical translation. Detailed protocols are presented for genome editing in hematopoietic stem cells (HSCs), T cells, and other immune populations, as well as in additional clinically relevant cell types and tissues. Particular attention is given to key parameters that influence editing outcomes, including cell handling, delivery conditions, and post-editing analysis.

This work was supported by the European Cooperation in Science and Technology through the Genome Editing for the Treatment of Human Disease Network (GenE-HumDi; COST Action CA21113). We gratefully acknowledge all contributing authors and the broader GenE-HumDi community for their valuable contributions and continued support.

Ljubljana, Slovenia — *Duško Lainšček*
Belgrade, Serbia — *Melita Vidaković*
Aarhus C, Denmark — *Yonglun Luo*
Granada, Spain — *Karim Benabdellah*

Contents

Preface . . . . . *v*
Contributors . . . . . *ix*

Part I Overview

1 CRISPR/Cas Systems: Biological Basis and Genome Editing Applications 3
Ece Cakiroglu and Serif Senturk

2 DNA Repair Mechanisms 19
Pelin Dilsiz and Fatma Zehra Hapil

3 Prime Editing: An Overview 41
Emilio M. García-Tenorio, Mar Alvarez, Eva Richard and Lourdes R. Desviat

4 Base Editing: Mechanisms and Therapeutic Applications 59
Fabio Catalano

5 An Overview of Programmable Epigenetic Editing Based on CRISPR Tools for Gene Expression Regulation 75
Marija Djordjević, Svetlana Dinić, Ana Sarić, Aleksandra Uskoković and Melita Vidaković

6 Overview of Delivery Methods for Gene Editing 93
Bilge Debelec Butuner

Part II Viral Delivery Methods

7 Production of Lentiviral Vectors Encoding the CRISPR–Cas13d System for RNA Targeting 127
Roberta Stilhano and Leonardo Martin

8 Production and Storage of High-Capacity Adenoviral Vectors for the Delivery of Advanced CRISPR Systems 143
Xiaoling Wang, Jin Liu, Josephine M. Janssen and Manuel A. F. V. Gonçalves

9 Adeno-Associated Viral Vector (AAV)-Mediated In Vivo CRISPR-Cas9 Delivery 175
Andrea Llanos-Ardaiz, Nerea Zabaleta, Laura Torella and Gloria Gonzalez-Aseguinolaza

Part III Non-Viral Delivery Methods

10 Lipid Nanoparticle-Mediated Delivery of CRISPR–Cas9 Components for Genome Editing 201
Amalie Lykke Olsen, Camilla Blunk Brandt, Rasmus Karred Larsen and Yonglun Luo

11 CRISPR/Cas9 Delivery Using Extracellular Vesicles 219
Peter Pečan and Mateja Manček-Keber

12 Preparation of Polymeric Nanoparticles for Gene Delivery 237
Emre Şefik Çağlar and Emine Saldamlı

13 Quantitative Analysis of CRISPR Encoding Plasmid DNA–Nanocarrier Interactions by Gel Electrophoresis and Densitometry 257
Cecilia Vasti, Laura E. Valenti and Carla E. Giacomelli

14 Cell-Penetrating Peptide Delivery for CRISPR Applications 275
Abhik Paul, Hye Young Lee and Jan Tuma

15 Oligo-Modified Poly (β-Amino Ester)-Mediated mRNA Delivery: A Protocol for Gene Editing Applications 299
Laia Martí-Melero, Sara Pérez Martín, Salvador Borrós Gómez and Marta Guerra-Rebollo

16 Virus-Like Particles as a Nonviral CRISPR/Cas Editing Delivery Tool 311
Antonio Carusillo, Asma Naseem and Alessia Cavazza

Part IV Physical Delivery Methods

17 Production and Purification of Cas9 Protein for Ribonucleoprotein Complex Formation 327
Mojca Skrbinek and Jure Bohinc

18 Electroporation for High-Efficiency Delivery of CRISPR to Hematopoietic Cells 341
Nikoletta Y. Papaioannou, Panayiota L. Papasavva, Petros Patsali and Carsten W. Lederer

19 An Electroporation-Based Protocol for Ex Vivo Base Editing: From Design to Quantitative Assessment 367
Irene Peña-Gutierrez, Davide Mazzeo, Alex Bassons-Bascuñana, Sibtain Haider, Laura Garcia-Garcia, Beatriz Olalla-Sastre, Paula Río, Sergio López-Manzaneda and Manuel Mataix

20 Nucleofection-Based CRISPR/Cas Delivery in Human T Cells for Immunotherapy Applications 389
María Ortiz-Bueno, Alejandro Millán-López, Kornel Labun and Karim Benabdellah

21 Delivery of Targeting Constructs into Zygotes Using Electroporation 411
Michaela Vaskovicova, Vojtech Dolejs, Pavla Dostalova, Csilla Sustr Michalikova, Jan Prochazka and Radislav Sedlacek

Contributors

Mar Alvarez • *Centro de Biología Molecular Severo Ochoa UAM-CSIC, Universidad Autónoma de Madrid, Madrid, Spain*

Alex Bassons-Bascuñana • *Centro de Investigación Biomédica en Red de Enfermedades Raras (CIBERER), Madrid, Spain; Regenerative Medicine and Tissue Engineering, Instituto de Investigación Sanitaria Fundación Jiménez Díaz (IIS-FJD), Madrid, Spain; Department of Bioengineering, University Carlos III Madrid (UC3M), Madrid, Spain*

Karim Benabdellah • *Department of Genomic Medicine, Pfizer-University of Granada-Andalusian Regional Government Centre for Genomics and Oncological Research (GENYO), Granada, Spain*

Jure Bohinc • *Department of Synthetic Biology and Immunology, National Institute of Chemistry, Ljubljana, Slovenia; Interdisciplinary Doctoral Study of Biomedicine, Faculty of Medicine, University of Ljubljana, Ljubljana, Slovenia*

Camilla Blunk Brandt • *Department of Biomedicine, Aarhus University, Aarhus C, Denmark; Steno Diabetes Center Aarhus, Aarhus University Hospital, Aarhus N, Denmark*

Emre Şefik Çağlar • *Department of Pharmaceutical Biotechnology, Faculty of Pharmacy, University of Health Sciences, İstanbul, Türkiye*

Ece Cakiroglu • *Izmir International Biomedicine and Genome Institute, Dokuz Eylul University, Izmir, Türkiye*

Antonio Carusillo • *Center for Genomic Medicine and Rare Diseases, Department of Medical and Surgical Sciences for Children and Adults, University of Modena and Reggio Emilia, Modena, Italy*

Fabio Catalano • *Department of Clinical Genetics, Erasmus MC University Medical Center, Rotterdam, The Netherlands; Department of Pediatrics, Erasmus MC University Medical Center, Rotterdam, The Netherlands; Center for Lysosomal and Metabolic Diseases, Erasmus MC University Medical Center, Rotterdam, The Netherlands*

Alessia Cavazza • *Center for Genomic Medicine and Rare Diseases, Department of Medical and Surgical Sciences for Children and Adults, University of Modena and Reggio Emilia, Modena, Italy; Infection, Immunity & Inflammation Research, and Teaching Department, UCL Great Ormond Street Institute of Child Health, University College London, London, UK*

Bilge Debelec Butuner • *Faculty of Pharmacy, Department of Pharmaceutical Biotechnology, Ege University, Izmir, Türkiye*

Lourdes R. Desviat • *Centro de Biología Molecular Severo Ochoa UAM-CSIC, Universidad Autónoma de Madrid, Madrid, Spain; Instituto Universitario de Biología Molecular (IUBM), Madrid, Spain; Instituto de Investigación Sanitaria Hospital La Paz (IdiPaz), Madrid, Spain; Centro de Investigación Biomédica en Red de Enfermedades Raras (CIBERER), Instituto de Salud Carlos III (ISCIII), Madrid, Spain*

Pelin Dilsiz • *Department of Molecular Biology and Genetics, Faculty of Science and Letters, Istanbul Technical University, Istanbul, Turkey; Research Institute for Health Sciences and Technologies (SABITA), Istanbul Medipol University, Istanbul, Turkey*

Svetlana Dinić • *Department of Molecular Biology, Institute for Biological Research, National Institute of the Republic of Serbia, University of Belgrade, Belgrade, Serbia*
Marija Djordjević • *Department of Molecular Biology, Institute for Biological Research, National Institute of the Republic of Serbia, University of Belgrade, Belgrade, Serbia*
Vojtech Dolejs • *Czech Centre for Phenogenomics, Laboratory of Transgenic Models of Diseases, Institute of Molecular Genetics of the Czech Academy of Sciences, Vestec, Prague, Czech Republic*
Pavla Dostalova • *Czech Centre for Phenogenomics, Laboratory of Transgenic Models of Diseases, Institute of Molecular Genetics of the Czech Academy of Sciences, Vestec, Prague, Czech Republic*
Laura Garcia-Garcia • *Biomedical Innovation Unit, Centro de Investigaciones Energéticas, Medioambientales y Tecnológicas (CIEMAT), Madrid, Spain; Advanced Therapies Unit, Instituto de Investigación Sanitaria Fundación Jiménez Díaz (IIS-FJD, UAM), Madrid, Spain; Centro de Investigación Biomédica en Red de Enfermedades Raras (CIBERER), Madrid, Spain*
Emilio M. García-Tenorio • *Centro de Biología Molecular Severo Ochoa UAM-CSIC, Universidad Autónoma de Madrid, Madrid, Spain; Instituto Universitario de Biología Molecular (IUBM), Madrid, Spain*
Carla E. Giacomelli • *Universidad Nacional de Córdoba, Facultad de Ciencias Químicas, Departamento de Fisicoquímica, Ciudad Universitaria, Córdoba, Argentina; Consejo Nacional de Investigaciones Científicas y Técnicas (CONICET), Instituto de Investigaciones en Fisicoquímica de Córdoba (INFIQC), Ciudad Universitaria, Córdoba, Argentina*
Salvador Borrós Gómez • *GEMAT/VIR2CELL Group, Institut Químic de Sarrià (IQS), Barcelona, Spain*
Manuel A. F. V. Gonçalves • *Department of Cell and Chemical Biology, Leiden University Medical Center, Leiden, The Netherlands*
Gloria Gonzalez-Aseguinolaza • *DNA & RNA Medicine Division, CIMA, University of Navarra, Pamplona, Navarra, Spain; IdiSNA, Navarra Institute for Health Research, Pamplona, Navarra, Spain*
Marta Guerra-Rebollo • *GEMAT/VIR2CELL Group, Institut Químic de Sarrià (IQS), Barcelona, Spain*
Sibtain Haider • *Institute for Transfusion Medicine and Gene Therapy, Medical Center-University of Freiburg, Freiburg, Germany; Center for Chronic Immunodeficiency (CCI), Medical Center-University of Freiburg, Freiburg, Germany*
Fatma Zehra Hapil • *Department of Medical Biology, Faculty of Medicine, Akdeniz University, Antalya, Turkey*
Josephine M. Janssen • *Department of Cell and Chemical Biology, Leiden University Medical Center, Leiden, The Netherlands*
Kornel Labun • *Institute of Genetics and Biotechnology, Faculty of Biology, University of Warsaw, Warsaw, Poland; Laboratory of RNA Biology, International Institute of Molecular and Cell Biology, Warsaw, Poland*
Rasmus Karred Larsen • *Department of Biomedicine, Aarhus University, Aarhus C, Denmark; Steno Diabetes Center Aarhus, Aarhus University Hospital, Aarhus N, Denmark*
Carsten W. Lederer • *Blood Disorder Genetics & Thalassemia Department, The Cyprus Institute of Neurology & Genetics, Nicosia, Cyprus*

Hye Young Lee • *The Department of Cellular and Integrative Physiology, The University of Texas Health Science Center at San Antonio, San Antonio, TX, USA*
Jin Liu • *Department of Cell and Chemical Biology, Leiden University Medical Center, Leiden, The Netherlands*
Andrea Llanos-Ardaiz • *DNA & RNA Medicine Division, CIMA, University of Navarra, Pamplona, Navarra, Spain*
Sergio López-Manzaneda • *Biomedical Innovation Unit, Centro de Investigaciones Energéticas, Medioambientales y Tecnológicas (CIEMAT), Madrid, Spain; Advanced Therapies Unit, Instituto de Investigación Sanitaria Fundación Jiménez Díaz (IIS-FJD, UAM), Madrid, Spain; Centro de Investigación Biomédica en Red de Enfermedades Raras (CIBERER), Madrid, Spain; Regenerative Medicine and Tissue Engineering, Instituto de Investigación Sanitaria Fundación Jiménez Díaz (IIS-FJD), Madrid, Spain*
Yonglun Luo • *Department of Biomedicine, Aarhus University, Aarhus C, Denmark; Steno Diabetes Center Aarhus, Aarhus University Hospital, Aarhus N, Denmark*
Mateja Manček-Keber • *Department of Synthetic Biology and Immunology, National Institute of Chemistry, Ljubljana, Slovenia*
Laia Martí-Melero • *GEMAT/VIR2CELL Group, Institut Químic de Sarrià (IQS), Barcelona, Spain*
Leonardo Martin • *Department of Pharmaceutical Sciences, Laboratory of Physiopharmacology, University of Antwerp, Antwerp, Belgium; Infla-Med Centre of Excellence, University of Antwerp, Antwerp, Belgium*
Sara Pérez Martín • *GEMAT/VIR2CELL Group, Institut Químic de Sarrià (IQS), Barcelona, Spain*
Manuel Mataix • *Biomedical Innovation Unit, Centro de Investigaciones Energéticas, Medioambientales y Tecnológicas (CIEMAT), Madrid, Spain; Advanced Therapies Unit, Instituto de Investigación Sanitaria Fundación Jiménez Díaz (IIS-FJD, UAM), Madrid, Spain; Centro de Investigación Biomédica en Red de Enfermedades Raras (CIBERER), Madrid, Spain*
Davide Mazzeo • *Biomedical Innovation Unit, Centro de Investigaciones Energéticas, Medioambientales y Tecnológicas (CIEMAT), Madrid, Spain; Advanced Therapies Unit, Instituto de Investigación Sanitaria Fundación Jiménez Díaz (IIS-FJD, UAM), Madrid, Spain; Centro de Investigación Biomédica en Red de Enfermedades Raras (CIBERER), Madrid, Spain*
Csilla Sustr Michalikova • *Czech Centre for Phenogenomics, Laboratory of Transgenic Models of Diseases, Institute of Molecular Genetics of the Czech Academy of Sciences, Vestec, Prague, Czech Republic*
Alejandro Millán-López • *Department of Genomic Medicine, Pfizer-University of Granada-Andalusian Regional Government Centre for Genomics and Oncological Research (GENYO), Granada, Spain; Cell Therapy Group, Maimonides Institute of Biomedical Research in Córdoba (IMIBIC), Córdoba, Spain*
Asma Naseem • *Infection, Immunity & Inflammation Research, and Teaching Department, UCL Great Ormond Street Institute of Child Health, University College London, London, UK*
Beatriz Olalla-Sastre • *Biomedical Innovation Unit, Centro de Investigaciones Energéticas, Medioambientales y Tecnológicas (CIEMAT), Madrid, Spain; Advanced Therapies Unit, Instituto de Investigación Sanitaria Fundación Jiménez Díaz (IIS-FJD, UAM), Madrid, Spain; Centro de Investigación Biomédica en Red de Enfermedades Raras (CIBERER), Madrid, Spain*

Amalie Lykke Olsen • *Department of Biomedicine, Aarhus University, Aarhus C, Denmark*
María Ortiz-Bueno • *Department of Genomic Medicine, Pfizer-University of Granada-Andalusian Regional Government Centre for Genomics and Oncological Research (GENYO), Granada, Spain*
Nikoletta Y. Papaioannou • *Blood Disorder Genetics & Thalassemia Department, The Cyprus Institute of Neurology & Genetics, Nicosia, Cyprus*
Panayiota L. Papasavva • *Blood Disorder Genetics & Thalassemia Department, The Cyprus Institute of Neurology & Genetics, Nicosia, Cyprus*
Petros Patsali • *Blood Disorder Genetics & Thalassemia Department, The Cyprus Institute of Neurology & Genetics, Nicosia, Cyprus*
Abhik Paul • *The Department of Cellular and Integrative Physiology, The University of Texas Health Science Center at San Antonio, San Antonio, TX, USA*
Peter Pečan • *Department of Synthetic Biology and Immunology, National Institute of Chemistry, Ljubljana, Slovenia; Graduate School of Biomedicine, University of Ljubljana, Ljubljana, Slovenia*
Irene Peña-Gutierrez • *Biomedical Innovation Unit, Centro de Investigaciones Energéticas, Medioambientales y Tecnológicas (CIEMAT), Madrid, Spain; Advanced Therapies Unit, Instituto de Investigación Sanitaria Fundación Jiménez Díaz (IIS-FJD, UAM), Madrid, Spain; Centro de Investigación Biomédica en Red de Enfermedades Raras (CIBERER), Madrid, Spain*
Jan Prochazka • *Czech Centre for Phenogenomics, Laboratory of Transgenic Models of Diseases, Institute of Molecular Genetics of the Czech Academy of Sciences, Vestec, Prague, Czech Republic*
Eva Richard • *Centro de Biología Molecular Severo Ochoa UAM-CSIC, Universidad Autónoma de Madrid, Madrid, Spain; Instituto Universitario de Biología Molecular (IUBM), Madrid, Spain; Instituto de Investigación Sanitaria Hospital La Paz (IdiPaz), Madrid, Spain; Centro de Investigación Biomédica en Red de Enfermedades Raras (CIBERER), Instituto de Salud Carlos III (ISCIII), Madrid, Spain*
Paula Río • *Biomedical Innovation Unit, Centro de Investigaciones Energéticas, Medioambientales y Tecnológicas (CIEMAT), Madrid, Spain; Advanced Therapies Unit, Instituto de Investigación Sanitaria Fundación Jiménez Díaz (IIS-FJD, UAM), Madrid, Spain; Centro de Investigación Biomédica en Red de Enfermedades Raras (CIBERER), Madrid, Spain*
Emine Saldamli • *Department of Pharmaceutical Technology, Faculty of Pharmacy, İstanbul University,* İ*stanbul, Türkiye*
Ana Sarić • *Department of Molecular Biology, Institute for Biological Research, National Institute of the Republic of Serbia, University of Belgrade, Belgrade, Serbia*
Radislav Sedlacek • *Czech Centre for Phenogenomics, Laboratory of Transgenic Models of Diseases, Institute of Molecular Genetics of the Czech Academy of Sciences, Vestec, Prague, Czech Republic*
Serif Senturk • *Izmir International Biomedicine and Genome Institute, Dokuz Eylul University, Izmir, Türkiye; Izmir Biomedicine and Genome Center, Izmir, Türkiye*
Mojca Skrbinek • *Department of Synthetic Biology and Immunology, National Institute of Chemistry, Ljubljana, Slovenia; Interdisciplinary Doctoral Study of Biomedicine, Faculty of Medicine, University of Ljubljana, Ljubljana, Slovenia*

Roberta Stilhano • *Department of Physiological Sciences, Santa Casa de São Paulo School of Medical Sciences, São Paulo, SP, Brazil*
Laura Torella • *DNA & RNA Medicine Division, CIMA, University of Navarra, Pamplona, Navarra, Spain*
Jan Tuma • *Department of Pathophysiology, Faculty of Medicine in Pilsen, Charles University, Pilsen, Czechia*
Aleksandra Uskoković • *Department of Molecular Biology, Institute for Biological Research, National Institute of the Republic of Serbia, University of Belgrade, Belgrade, Serbia*
Laura E. Valenti • *Universidad Nacional de Córdoba, Facultad de Ciencias Químicas, Departamento de Fisicoquímica, Ciudad Universitaria, Córdoba, Argentina; Consejo Nacional de Investigaciones Científicas y Técnicas (CONICET), Instituto de Investigaciones en Fisicoquímica de Córdoba (INFIQC), Ciudad Universitaria, Córdoba, Argentina*
Michaela Vaskovicova • *Czech Centre for Phenogenomics, Laboratory of Transgenic Models of Diseases, Institute of Molecular Genetics of the Czech Academy of Sciences, Vestec, Prague, Czech Republic*
Cecilia Vasti • *Universidad Nacional de Córdoba, Facultad de Ciencias Químicas, Departamento de Fisicoquímica, Ciudad Universitaria, Córdoba, Argentina; Consejo Nacional de Investigaciones Científicas y Técnicas (CONICET), Instituto de Investigaciones en Fisicoquímica de Córdoba (INFIQC), Ciudad Universitaria, Córdoba, Argentina*
Melita Vidaković • *Department of Molecular Biology, Institute for Biological Research, National Institute of the Republic of Serbia, University of Belgrade, Belgrade, Serbia*
Xiaoling Wang • *Department of Cell and Chemical Biology, Leiden University Medical Center, Leiden, The Netherlands*
Nerea Zabaleta • *DNA & RNA Medicine Division, CIMA, University of Navarra, Pamplona, Navarra, Spain*

Part I

Overview



Chapter 1

CRISPR/Cas Systems: Biological Basis and Genome Editing Applications

Ece Cakiroglu and Serif Senturk

Abstract

Clustered regularly interspaced short palindromic repeats (CRISPR) and associated (Cas) systems have revolutionized the field of genome engineering by providing versatile, efficient, and programmable tools for precise genetic manipulation. Originally identified as an adaptive immune mechanism in prokaryotes, CRISPR/Cas systems have been extensively repurposed for a wide range of applications across molecular biology, biotechnology, and medicine. This chapter provides a comprehensive overview of the molecular mechanisms underlying CRISPR/Cas immunity. Furthermore, the classification of CRISPR/Cas systems into distinct types and subtypes is discussed, highlighting their structural and functional diversity. Advances in genome editing technologies, including CRISPR-mediated knockout, base editing, and prime editing, are explored with an emphasis on their mechanisms and applications. The chapter also examines emerging CRISPR-based platforms for transcriptional regulation, epigenome editing, and RNA targeting, which enable precise and reversible modulation of gene expression without altering genomic DNA. In addition, the transformative impact of CRISPR technologies on functional genomics is addressed, particularly through high-throughput screening approaches that facilitate the identification of gene function and genetic vulnerabilities. CRISPR-based diagnostic tools and therapeutic strategies are also reviewed, underscoring their potential in disease detection and treatment. Despite significant progress, challenges such as off-target effects, delivery limitations, and safety concerns remain critical considerations. Overall, this chapter highlights the expanding capabilities of CRISPR/Cas systems and their growing importance in both fundamental research and clinical applications.

Keywords CRISPR/Cas, gRNA, Cas classification, Mechanisms

1 Emergence of CRISPR/Cas Systems

The conceptual and technological significance of the CRISPR system as we understand it today has emerged from the accumulation of fragmented observations and delayed insights spanning several decades. Prior to the introduction of the term "Clustered Regularly Interspaced Short Palindromic Repeats (CRISPR)" by Jansen et al. [1], the existence of these sequences had already been documented, although their biological relevance remained unclear.

Duško Lainšček et al. (eds.), *CRISPR Delivery*, Methods in Molecular Biology, vol. 3075,
https://doi.org/10.1007/978-1-0716-5547-4_1,
© The Author(s) 2027

The story begins in 1987, when Ishino et al. reported the presence of unusual, regularly spaced repetitive DNA sequences located downstream of the iap gene in the genome of *Escherichia coli* [2]. However, these repeats could not be placed into a functional context, nor were they recognized as components of a broader biological system. Throughout the 1990s, similar repeat structures were independently identified in a range of bacterial and archaeal species [3–5]. Notably, the work of Mojica et al. demonstrated that these elements were conserved across phylogenetically distant organisms, suggesting that they were unlikely to be random genomic features [6]. During this period, the characteristic architecture of the system—comprising direct repeats interspaced by unique sequences later termed "spacers"—was described, although its function remained unresolved.

In 2002, Jansen and colleagues not only coined the term CRISPR but also identified a set of genes located adjacent to these repeat arrays, later termed CRISPR-associated (cas) genes [1]. This finding marked an important shift, as CRISPR loci began to be considered as components of a putative functional system rather than isolated genomic anomalies.

The first compelling insights into the function of CRISPR emerged in 2005. Independent studies, including that of Mojica et al., revealed that spacer sequences share homology with bacteriophage and plasmid DNA [7]. These observations led to the hypothesis that CRISPR constitutes an adaptive immune system in prokaryotes. Experimental validation of this model was provided in 2007 by Barrangou et al., who demonstrated in *Streptococcus thermophilus* that acquisition of new spacers from infecting phages confers sequence-specific resistance [8]. This study established CRISPR as an adaptive and heritable defense mechanism.

Building on these foundational discoveries, the CRISPR system was rapidly repurposed as a genome engineering tool. In 2012, Emmanuelle Charpentier and Jennifer Doudna demonstrated that the CRISPR/Cas9 system can be programmed with a single guide RNA to direct site-specific DNA cleavage, thereby laying the groundwork for modern genome editing technologies [9]. Shortly thereafter, in 2013, studies led by Feng Zhang and George Church established the functionality of CRISPR/Cas9 in eukaryotic cells [10, 11].

Together, these findings established CRISPR/Cas as an RNA-guided defense system providing adaptive and heritable immunity against foreign nucleic acids and enabled its widespread adoption in biomedical research.

CRISPR/Cas systems are now broadly classified into distinct classes and types based on effector composition and mechanism of action, and they operate through coordinated stages of spacer acquisition, CRISPR RNA biogenesis, and target interference.

2 Molecular Mechanism of CRISPR/Cas Immunity

CRISPR/Cas systems function through a coordinated, multistep process that enables sequence-specific recognition and elimination of foreign nucleic acids. This process is generally divided into three stages: adaptation, expression, and interference (Fig. 1).

The adaptation stage involves the acquisition of short DNA fragments from invading genetic elements, such as bacteriophages or plasmids, and their integration into the CRISPR array as new spacer sequences. This process is primarily mediated by the conserved Cas1–Cas2 protein complex, which recognizes foreign DNA and catalyzes spacer integration at the leader-proximal end of the CRISPR locus

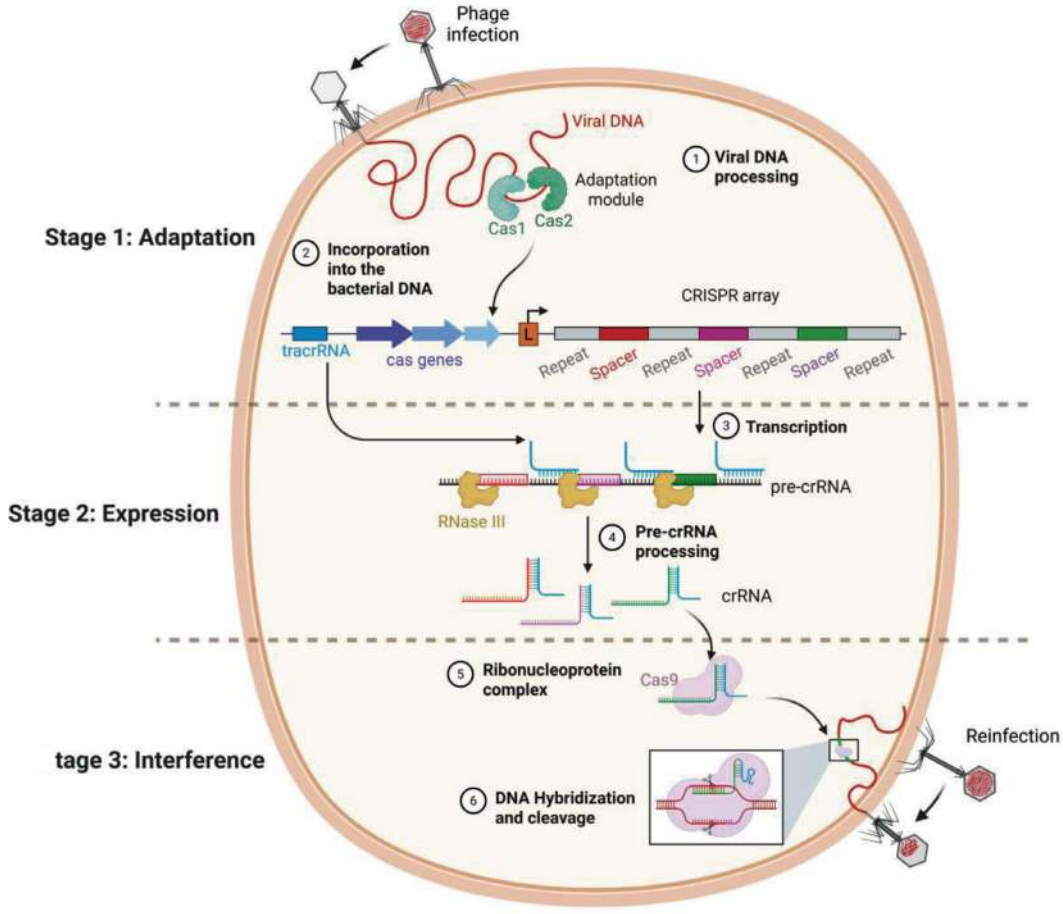


Fig. 1 Molecular mechanism of CRISPR/Cas immunity. CRISPR/Cas systems mediate adaptive immunity through three stages: adaptation, expression, and interference. During adaptation, fragments of invading DNA are incorporated into the CRISPR array as spacers. The array is then transcribed and processed into guide crRNAs that associate with Cas proteins. In the interference stage, these complexes recognize and cleave complementary foreign nucleic acids, providing sequence-specific protection against reinfection

[12]. As a result, the CRISPR array serves as a molecular record of past infections.

During the expression stage, the CRISPR array is transcribed into a long precursor RNA (pre-crRNA), which is subsequently processed into shorter CRISPR RNAs (crRNAs), each containing a single spacer sequence flanked by repeat-derived elements. In Class 2 systems, such as Type II, this process requires the trans-activating CRISPR RNA (tracrRNA) and host RNase activity for proper maturation. The resulting crRNA, together with associated Cas proteins, forms an effector complex capable of guiding target recognition [13].

The interference stage is characterized by the detection and cleavage of invading nucleic acids. The crRNA within the effector complex directs sequence-specific binding to complementary target sequences, typically requiring the presence of a protospacer adjacent motif (PAM) in DNA-targeting systems. Upon target recognition, the Cas effector protein induces cleavage of the foreign nucleic acid, thereby neutralizing the threat [14]. In some systems, target binding also triggers collateral cleavage activity, further enhancing the defensive response [15, 16].

Together, these three stages establish CRISPR/Cas systems as adaptive and heritable immune mechanisms that provide sequence-specific protection against recurrent genetic invasion.

3 Classification of CRISPR/Cas Systems

CRISPR/Cas systems are broadly divided into two major classes based on the composition of their effector modules: Class 1 and Class 2 [17–19] (Fig. 2). This classification reflects fundamental differences in the architecture and mechanism of target recognition and cleavage.

Class 1 systems, which include Types I, III, and IV, are characterized by multi-subunit effector complexes composed of several Cas proteins. These systems are more prevalent in nature and are widely distributed across bacterial and archaeal genomes and rely on coordinated interactions between multiple protein components to mediate target recognition and degradation [17, 19]. Among them, Type I systems are the most prevalent in nature and utilize a Cascade (CRISPR-associated complex for antiviral defense) complex for target binding, followed by recruitment of the nuclease–helicase Cas3 for target degradation. Type III systems, in contrast, exhibit dual targeting capabilities and can act on both DNA and RNA. In addition to direct nucleic acid cleavage, they often couple target recognition to cyclic oligoadenylate (cOA) signaling pathways mediated by Cas10, leading to activation of auxiliary nucleases and amplification of the immune response [20–22]. Type IV systems are less well characterized and are frequently associated with plasmids rather than

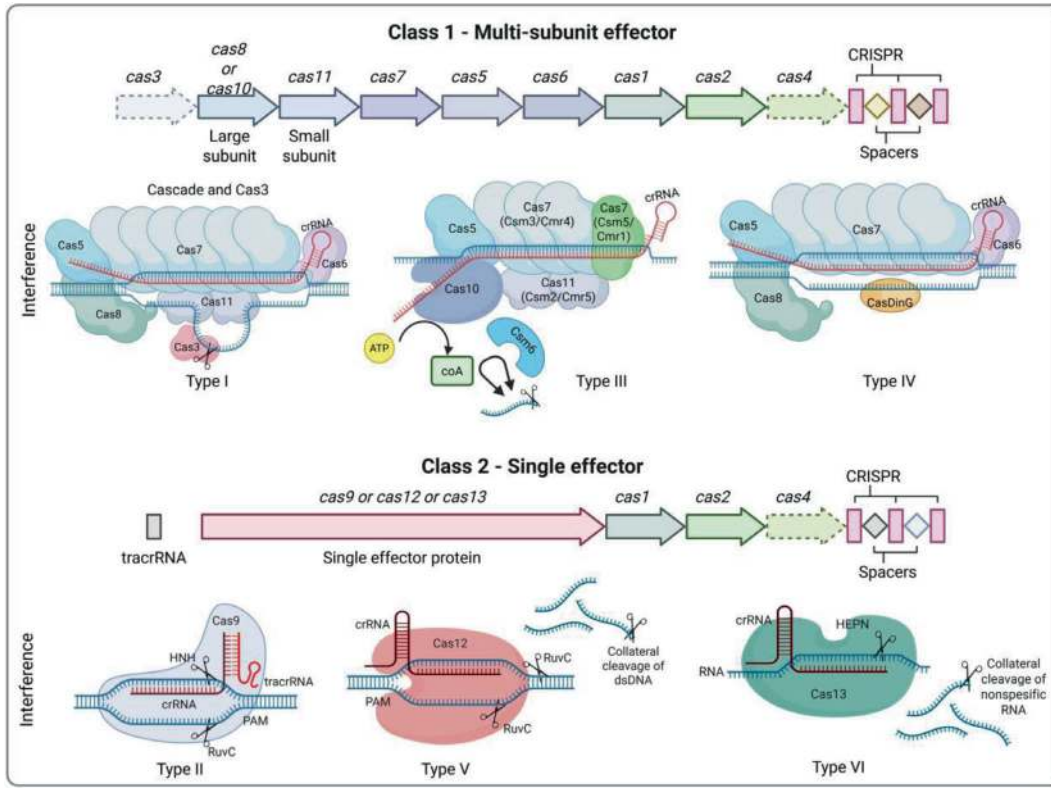


Fig. 2 Classification of CRISPR/Cas systems. CRISPR/Cas systems are divided into two main classes based on their effector architecture. Class 1 (Types I, III, IV) uses multi-subunit protein complexes for target recognition and cleavage. Class 2 (Types II, V, VI) utilizes a single, multidomain effector protein (e.g., Cas9, Cas12, or Cas13). Both classes employ RNA-guided mechanisms to target DNA or RNA, as shown in the genomic organization and interference schematics

chromosomal loci. Unlike other CRISPR systems, they often lack adaptation modules such as Cas1 and Cas2, and their functional role is thought to involve plasmid maintenance or inter-plasmid competition rather than classical antiviral defense [17, 23].

Class 2 systems, which include Types II, V, and VI, are defined by the presence of a single, multidomain effector protein responsible for target recognition and cleavage [17, 19]. This structural simplicity distinguishes them from Class 1 systems and underlies their widespread adoption as genome engineering tools. Type II systems employ the well-characterized Cas9 endonuclease, which introduces site-specific double-strand breaks in DNA in a guide RNA-dependent manner [9]. Type V systems utilize Cas12 family nucleases, which also target DNA but generate staggered double-strand breaks and exhibit collateral single-stranded DNA cleavage activity upon activation [16, 24]. Type VI systems, represented by Cas13, are unique in their ability to target RNA molecules and display collateral RNA

cleavage, enabling both antiviral defense and RNA-targeting applications [15, 25].

Overall, the classification of CRISPR/Cas systems highlights the evolutionary diversification of prokaryotic immune strategies, ranging from structurally complex, multicomponent machineries in Class 1 systems to streamlined, single-effector platforms in Class 2 systems. Despite these differences, all CRISPR/Cas systems share a common functional logic based on RNA-guided recognition of foreign nucleic acids.

3.1 The Type II CRISPR/Cas9 System

Among CRISPR/Cas systems, the Type II system has emerged as the most extensively studied and widely utilized platform. This system is characterized by its reliance on a single effector protein, Cas9, which mediates RNA-guided DNA cleavage.

In the native system, Cas9 is guided by a dual RNA complex composed of crRNA and tracrRNA. These RNA molecules form a structure that directs Cas9 to complementary DNA sequences. In engineered systems, this dual RNA configuration is simplified into a single guide RNA (sgRNA), which retains the necessary structural and functional features for target recognition and Cas9 activation [9].

Target recognition by Cas9 requires the presence of a PAM sequence adjacent to the target site. PAM recognition initiates conformational changes in Cas9, enabling local DNA unwinding and formation of an RNA–DNA hybrid between the guide RNA and the target strand. Cas9 contains two nuclease domains, HNH and RuvC, which cleave the complementary and noncomplementary DNA strands, respectively, resulting in a double-strand break [9].

The generation of double-strand breaks is central to the utility of Cas9 in genome editing. Cellular DNA repair pathways, including nonhomologous end joining (NHEJ) and homology-directed repair (HDR), can be exploited to introduce targeted genetic modifications [10, 11]. The simplicity and programmability of the CRISPR/Cas9 system have enabled its rapid adoption across diverse fields, including functional genomics, disease modeling, and therapeutic development.

3.2 The Type V CRISPR/Cas12 System

Type V CRISPR/Cas systems are characterized by the use of Cas12 family nucleases, which represent a distinct class of single-effector proteins with structural and functional features that differentiate them from Cas9 [25]. Similar to Cas9, Cas12 proteins mediate RNA-guided targeting of double-stranded DNA; however, their mechanism of cleavage and post-cleavage behavior exhibit notable differences.

Cas12 is guided by a single CRISPR RNA (crRNA) and does not require a tracrRNA, reflecting a simplified RNA architecture compared to Type II systems [24]. Target recognition is initiated through base pairing between the crRNA and the complementary DNA sequence, accompanied by recognition of a PAM sequence, typically located upstream of the target site. Upon target binding,

Cas12 undergoes conformational activation that enables cleavage of both DNA strands.

Unlike Cas9, which generates blunt-ended double-strand breaks, Cas12 introduces staggered cuts that result in 5′ or 3′ overhangs, depending on the subtype [24]. In addition to its site-specific nuclease activity, Cas12 exhibits a unique property known as collateral cleavage, in which activation by a target DNA molecule triggers nonspecific cleavage of single-stranded DNA [16]. This property has been extensively exploited in nucleic acid detection platforms, enabling highly sensitive and specific diagnostic applications.

The structural simplicity and distinct cleavage characteristics of Cas12 have expanded the CRISPR toolbox, offering alternative strategies for genome editing and molecular diagnostics.

3.3 The Type VI CRISPR/Cas13 System

Type VI CRISPR/Cas systems are uniquely adapted for RNA targeting and are defined by the Cas13 family of effector proteins [15, 26]. Unlike DNA-targeting systems such as Cas9 and Cas12, Cas13 mediates RNA-guided cleavage of single-stranded RNA, thereby providing a mechanism for post-transcriptional regulation of gene expression.

Cas13 is guided by a crRNA that directs the effector to complementary RNA targets. Target recognition induces conformational changes that activate the ribonuclease activity of Cas13, leading to cleavage of the target RNA [26]. A defining feature of Cas13 is its collateral cleavage activity, whereby activation results in nonspecific degradation of nearby RNA molecules [15, 26]. While this property may contribute to antiviral defense in prokaryotes, it has also been harnessed for highly sensitive RNA detection technologies [27].

The RNA-targeting capability of Cas13 distinguishes it from other CRISPR systems and enables applications that do not involve permanent genomic alterations. This makes Cas13 particularly attractive for transient gene regulation, transcriptome engineering, and antiviral strategies.

4 Applications of CRISPR/Cas Systems

The transformation of CRISPR/Cas systems from prokaryotic immune mechanisms into programmable molecular tools has enabled a wide spectrum of applications across basic research (Fig. 3), biotechnology, and medicine (Fig. 4). Continuous engineering of CRISPR-associated proteins and guide RNA architectures has further expanded the functional capabilities of these systems beyond double-stranded DNA cleavage, allowing precise and versatile manipulation of genetic information.

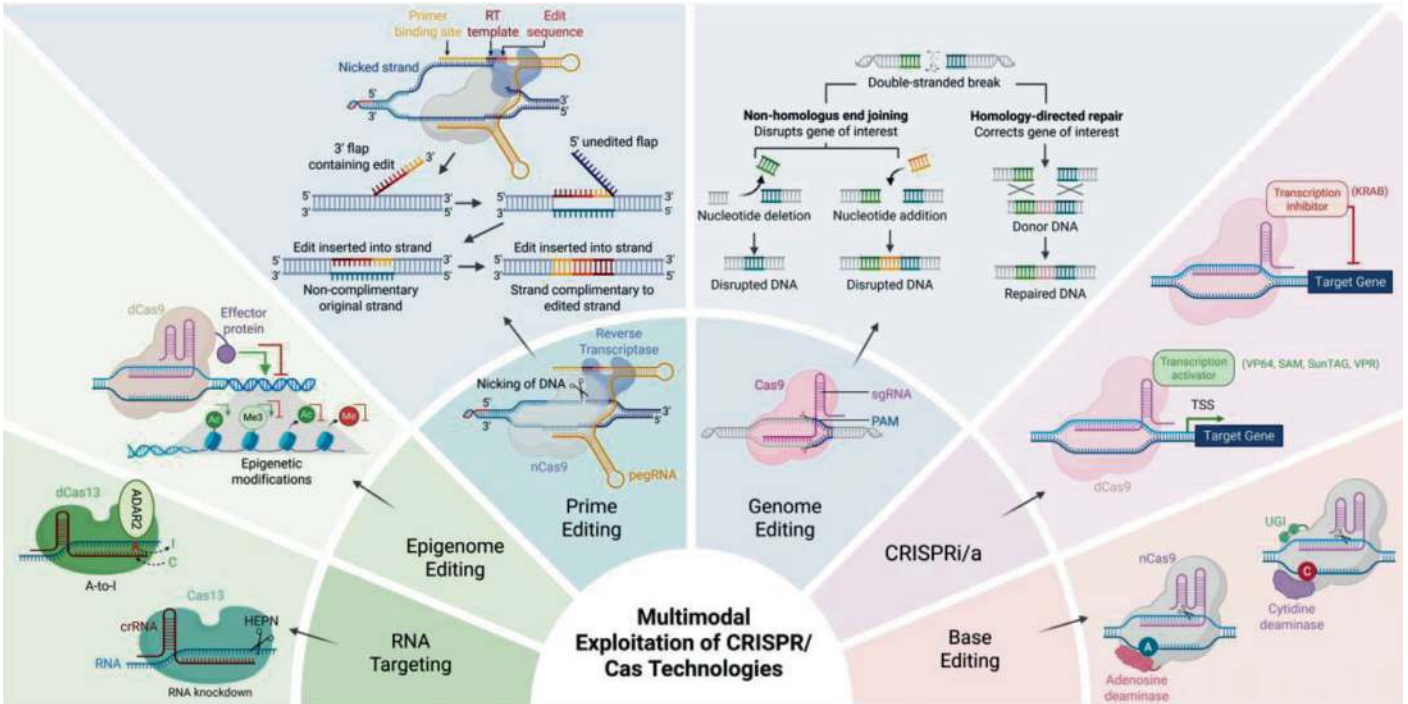


Fig. 3 Multimodal exploitation of CRISPR/Cas technologies. CRISPR/Cas systems have been engineered into a versatile molecular toolbox for diverse genetic and epigenetic manipulations. Genome editing utilizes Cas9-induced double-strand breaks for gene disruption (NHEJ) or precise correction (HDR). Base editing and prime editing enable programmable nucleotide conversions and flexible sequence insertions/deletions without double-strand breaks. CRISPRi/a and epigenome editing employ catalytically inactive Cas (dCas) fusions to modulate gene expression through transcriptional regulation or chromatin modification. Finally, RNA targeting (e.g., Cas13) allows for programmable RNA knockdown and transcript-level editing, expanding the scope of CRISPR applications to the transcriptome

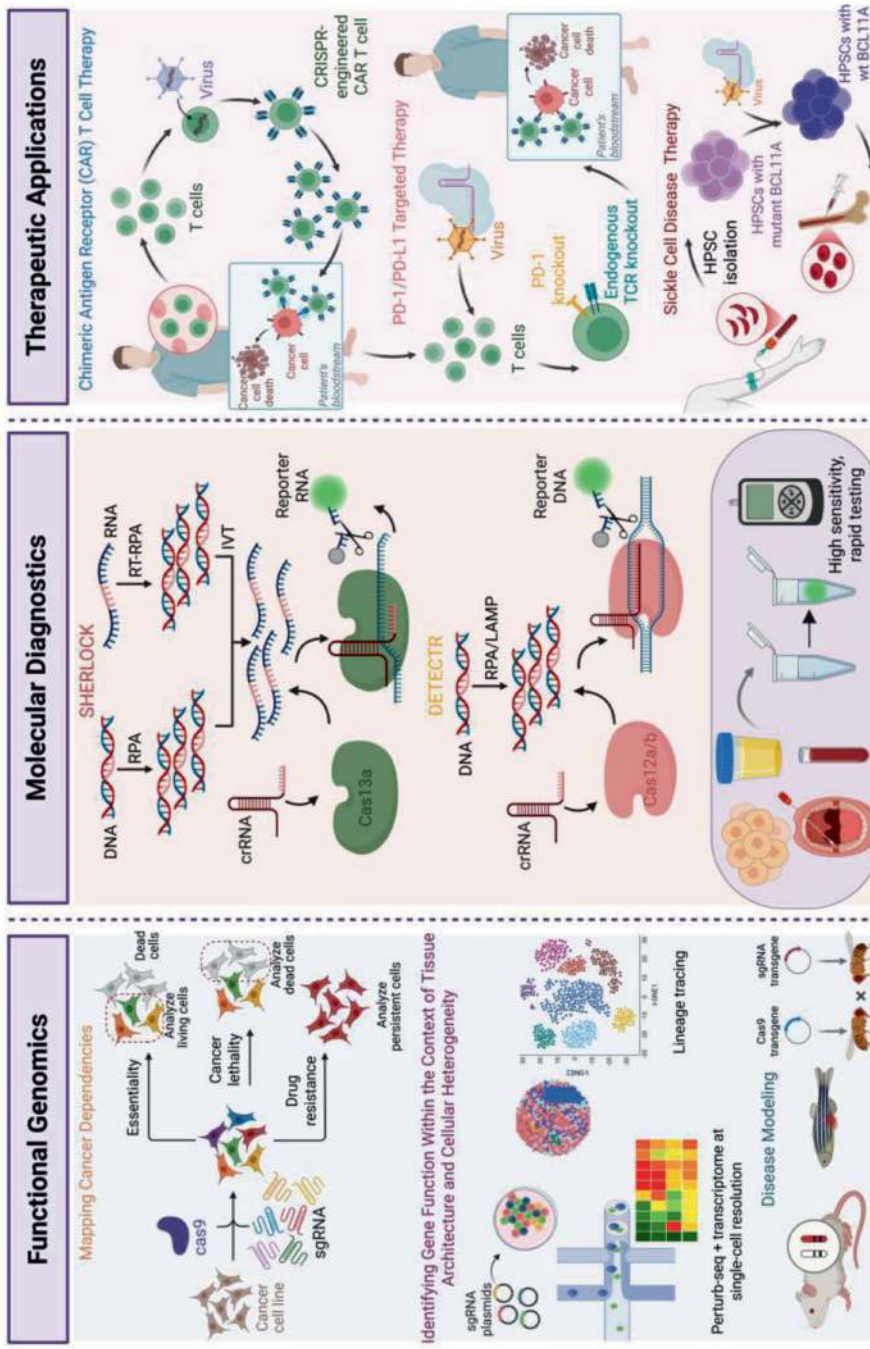


Fig. 4 Biomedical applications of CRISPR/Cas technologies. The figure illustrates the clinical and research integration of CRISPR systems across three primary domains. Functional genomics utilizes high-throughput screens and Perturb-seq to map cancer dependencies, drug resistance, and gene functions within complex tissue architectures. Molecular Diagnostics leverages the collateral cleavage activity of Cas13 (SHERLOCK) and Cas12 (DETECTR) for rapid, high-sensitivity detection of DNA and RNA. Therapeutic Applications highlight the development of CRISPR-engineered CAR T cells, PD-1 knockout immunotherapies, and the treatment of hematological disorders like sickle cell disease through HPSC modification

4.1 Genome Editing via Double-Strand Breaks

The foundational application of CRISPR/Cas systems involves the induction of site-specific double-strand breaks (DSBs) in DNA. These breaks are repaired by endogenous cellular pathways, primarily nonhomologous end joining (NHEJ) and homology-directed repair (HDR). NHEJ-mediated repair often introduces insertions or deletions (indels), resulting in gene disruption and enabling efficient gene knockout strategies. In contrast, HDR allows precise sequence modifications through the use of exogenous donor templates [10, 11]. The simplicity of guide RNA design enables rapid targeting of multiple loci, facilitating multiplex genome editing [11]. This has accelerated studies in functional genomics, enabling systematic interrogation of gene function and regulatory networks.

4.2 Base Editing Technologies

Base editing represents a major advancement in CRISPR-based genome engineering by enabling precise nucleotide conversions without introducing double-strand breaks. These systems typically consist of a catalytically impaired Cas protein (dCas9 or nickase Cas9) fused to a nucleobase deaminase enzyme.

Cytosine base editors (CBEs) mediate C-G to T-A transitions through cytosine deamination [28], while adenine base editors (ABEs) enable A-T to G-C conversions via adenine deamination [29]. These systems operate within a defined "editing window" determined by guide RNA positioning and enzyme configuration. Importantly, base editing minimizes reliance on HDR and reduces the frequency of large insertions, deletions, and chromosomal rearrangements associated with DSB-based editing.

Base editing has proven particularly valuable for modeling and correcting point mutations, which constitute a significant proportion of disease-associated genetic variants [30]. However, challenges such as off-target deamination and bystander editing remain important considerations [31, 32].

4.3 Prime Editing

Prime editing further expands the precision of CRISPR-based genome engineering by enabling targeted insertions, deletions, and all possible base-to-base conversions without requiring double-strand breaks or donor DNA templates. This system utilizes a fusion protein consisting of a Cas9 nickase and a reverse transcriptase, guided by a prime editing guide RNA (pegRNA) [33]. The pegRNA encodes both the target recognition sequence and the desired edit, which is copied into the genomic DNA through a reverse transcription process [33, 34]. This approach provides a versatile and highly precise editing platform capable of introducing a wide range of genetic modifications. Although prime editing offers significant advantages in terms of precision and versatility, its efficiency can vary depending on the target context and requires careful optimization.

4.4 CRISPR Interference and Activation (CRISPRi/a)

Catalytically inactive Cas proteins (dCas variants) have been repurposed for transcriptional regulation without altering DNA sequence [35, 36]. CRISPR interference (CRISPRi) utilizes dCas proteins to block transcription by sterically hindering RNA polymerase or transcription factor binding [35–38]. Conversely, CRISPR activation (CRISPRa) employs dCas fused to transcriptional activators to enhance gene expression [36, 38].

These systems enable precise and reversible modulation of gene expression, allowing functional interrogation of regulatory elements and gene networks [39]. Multiplexed CRISPRi/a approaches facilitate the study of combinatorial gene regulation and cellular state transitions [39, 40].

4.5 Epigenome Editing

CRISPR-based epigenome editing extends the functionality of dCas systems by targeting chromatin-modifying enzymes to specific genomic loci [41, 42]. Fusion of dCas proteins to histone acetyltransferases, DNA methyltransferases, or demethylases enables locus-specific modification of epigenetic marks, resulting in altered gene expression profiles [41, 43, 44].

This approach provides a powerful tool for studying the causal role of epigenetic modifications in gene regulation and disease, offering insights that cannot be obtained through conventional genetic perturbation methods.

4.6 RNA Targeting and Transcriptome Engineering

RNA-targeting CRISPR systems, particularly those based on Cas13, enable direct manipulation of RNA molecules without altering genomic DNA. These systems can be used for transcript knockdown, RNA editing, and modulation of alternative splicing [45, 46].

RNA editing platforms, such as those based on Cas13 fused to adenosine deaminases, allow programmable A-to-I editing at the transcript level [46]. This enables transient and reversible modification of gene expression, providing an additional layer of control over cellular function.

4.7 Functional Genomics and CRISPR Screens

CRISPR-based screening technologies have revolutionized functional genomics by enabling systematic, high-throughput interrogation of gene function [47, 48]. Pooled CRISPR knockout, activation, and interference screens allow identification of genes involved in diverse biological processes, including proliferation, differentiation, drug resistance, and immune evasion [38, 49] (Fig. 4).

Compared to RNA interference-based approaches, CRISPR screens offer improved specificity and the ability to generate complete loss-of-function phenotypes [50]. These methods have been widely applied in cancer research to identify genetic vulnerabilities and therapeutic targets [51].

In addition to loss-of-function approaches, CRISPR activation (CRISPRa) and interference (CRISPRi) platforms enable systematic

gain- and partial-loss-of-function screening, allowing more nuanced interrogation of gene regulatory networks [38]. The integration of CRISPR screening with single-cell transcriptomics has further expanded the resolution of functional genomics by enabling simultaneous perturbation and transcriptional profiling at the single-cell level [52]. Moreover, advances in combinatorial and multiplexed CRISPR screening approaches permit the investigation of genetic interactions and synthetic lethality, which are particularly relevant for identifying novel therapeutic strategies in cancer [53].

Recent developments have also incorporated spatial transcriptomics and lineage tracing into CRISPR screening frameworks, enabling the study of gene function within the context of tissue architecture and cellular heterogeneity [54, 55]. Furthermore, the integration of CRISPR screening data with large-scale cancer dependency datasets, such as DepMap, has facilitated the identification of context-specific essential genes and predictive biomarkers for targeted therapies [51]. Collectively, these advances position CRISPR screening as a central platform for systems-level functional genomics and precision oncology.

4.8 Molecular Diagnostics

The collateral cleavage activities of Cas12 and Cas13 have been harnessed for the development of sensitive nucleic acid detection platforms [16, 27]. Technologies such as SHERLOCK and DETECTR utilize CRISPR-based detection of specific DNA or RNA sequences, coupled with signal amplification through nonspecific cleavage of reporter molecules [16, 27, 56].

These systems enable rapid, sensitive, and portable diagnostic assays with applications in infectious disease detection, genetic testing, and environmental monitoring.

Recent developments have further improved the sensitivity and field applicability of CRISPR-based diagnostics, enabling attomolar detection limits and integration with isothermal amplification techniques such as recombinase polymerase amplification (RPA) and loop-mediated isothermal amplification (LAMP) [16, 27, 57]. In addition, the combination of CRISPR detection systems with microfluidic platforms and lateral flow assays has facilitated the development of point-of-care diagnostics suitable for resource-limited settings [56, 58].

Emerging CRISPR-based diagnostic platforms are increasingly capable of multiplexed detection, allowing simultaneous identification of multiple pathogens or genetic variants within a single assay [59]. Beyond pathogen detection, these technologies are being adapted for the detection of circulating tumor DNA (ctDNA) and other biomarkers, enabling applications in early cancer diagnosis and real-time disease monitoring [60, 61]. The integration of CRISPR diagnostics with portable and digital readout systems further enhances their potential for decentralized and rapid testing environments.

5 Therapeutic Applications

CRISPR/Cas systems are increasingly being explored for therapeutic applications, including gene therapy, regenerative medicine, and immunotherapy [62–64]. Genome editing strategies aim to correct pathogenic mutations, disrupt disease-associated genes, or introduce protective genetic changes [65]. In addition, CRISPR-engineered immune cells, such as CAR-T cells, are being developed for cancer treatment [66, 67].

Despite their promise, clinical applications face challenges related to delivery efficiency, off-target effects, immune responses, and long-term safety [68, 69]. Ongoing research focuses on improving specificity, developing novel delivery systems, and refining editing technologies to enhance therapeutic potential.

Recent clinical studies have demonstrated the feasibility of CRISPR-based therapies in humans, particularly for hematological disorders such as sickle cell disease and β-thalassemia, highlighting the translational potential of genome editing technologies [62, 65]. Advances in delivery systems, including lipid nanoparticles, viral vectors such as adeno-associated viruses (AAV), and emerging non-viral platforms, have improved in vivo editing efficiency, although tissue specificity and immunogenicity remain important challenges [68, 70].

In addition to ex vivo editing strategies, in vivo genome editing approaches are being actively developed, enabling direct targeting of tissues such as liver, muscle, and retina [71–73]. The incorporation of CRISPR technologies into combinatorial therapeutic strategies, including immunomodulation and synthetic biology-based circuits, is expected to further enhance their clinical potential [74].

Acknowledgments

The publication is based upon work by COST Action CA21113: Genome Editing for the Treatment of Human Diseases (https://www.genehumdi.eu), supported by European Cooperation in Science and Technology (COST). This work was supported by the Health Institutes of Türkiye (TÜSEB; Project number: 15429) and Dokuz Eylul University, Department of Scientific Research Projects (ADEP Project number: TSA-2024-3353). Figures were created with BioRender.com.

Competing interests The authors declare no competing interests.

References

1. Jansen R, Embden JDA, van, Gaastra W, Schouls LM (2002) Identification of genes that are associated with DNA repeats in prokaryotes. Mol Microbiol 43:1565–1575
2. Ishino Y, Shinagawa H, Makino K et al (1987) Nucleotide sequence of the iap gene, responsible for alkaline phosphatase isozyme conversion in *Escherichia coli*, and identification of the gene product. J Bacteriol 169:5429–5433
3. Martin B, Humbert O, Camara M et al (1992) A highly conserved repeated DNA element located in the chromosome of *Streptococcus pneumoniae*. Nucleic Acids Res 20:3479–3483
4. Bachellier S, Clément JM, Hofnung M, Gilson E (1997) Bacterial interspersed mosaic elements (BIMEs) are a major source of sequence polymorphism in *Escherichia coli* intergenic regions including specific associations with a new insertion sequence. Genetics 145:551–562
5. van Belkum A, Scherer S, van Alphen L, Verbrugh H (1998) Short-sequence DNA repeats in prokaryotic genomes. Microbiol Mol Biol Rev 62:275–293
6. Mojica FJ, Díez-Villaseñor C, Soria E, Juez G (2000) Biological significance of a family of regularly spaced repeats in the genomes of Archaea, Bacteria and mitochondria. Mol Microbiol 36:244–246
7. Mojica FJM, Díez-Villaseñor C, García-Martínez J, Soria E (2005) Intervening sequences of regularly spaced prokaryotic repeats derive from foreign genetic elements. J Mol Evol 60:174–182
8. Barrangou R, Fremaux C, Deveau H et al (2007) CRISPR provides acquired resistance against viruses in prokaryotes. Science 315:1709–1712
9. Jinek M, Chylinski K, Fonfara I et al (2012) A programmable dual-RNA-guided DNA endonuclease in adaptive bacterial immunity. Science 337:816–821
10. Mali P, Yang L, Esvelt KM et al (2013) RNA-guided human genome engineering via Cas9. Science 339:823–826
11. Cong L, Ran FA, Cox D et al (2013) Multiplex genome engineering using CRISPR/Cas systems. Science 339:819–823
12. Fineran PC, Charpentier E (2012) Memory of viral infections by CRISPR-Cas adaptive immune systems: acquisition of new information. Virology 434:202–209
13. Charpentier E, Richter H, van der Oost J, White MF (2015) Biogenesis pathways of RNA guides in archaeal and bacterial CRISPR-Cas adaptive immunity. FEMS Microbiol Rev 39:428–441
14. Reeks J, Naismith JH, White MF (2013) CRISPR interference: a structural perspective. Biochem J 453:155–166
15. East-Seletsky A, O'Connell MR, Knight SC et al (2016) Two distinct RNase activities of CRISPR-C2c2 enable guide-RNA processing and RNA detection. Nature 538:270–273
16. Chen JS, Ma E, Harrington LB et al (2018) CRISPR-Cas12a target binding unleashes indiscriminate single-stranded DNase activity. Science 360:436–439
17. Makarova KS, Wolf YI, Alkhnbashi OS et al (2015) An updated evolutionary classification of CRISPR–Cas systems. Nat Rev Microbiol 13:722–736
18. Shmakov S, Abudayyeh OO, Makarova KS et al (2015) Discovery and functional characterization of diverse Class 2 CRISPR-Cas systems. Mol Cell 60:385–397
19. Koonin EV, Makarova KS, Zhang F (2017) Diversity, classification and evolution of CRISPR-Cas systems. Curr Opin Microbiol 37:67–78
20. Niewoehner O, Garcia-Doval C, Rostøl JT et al (2017) Type III CRISPR-Cas systems produce cyclic oligoadenylate second messengers. Nature 548:543–548
21. Kazlauskiene M, Kostiuk G, Venclovas Č et al (2017) A cyclic oligonucleotide signaling pathway in type III CRISPR-Cas systems. Science 357:605–609
22. Huang F, Zhu B (2020) The cyclic oligoadenylate signaling pathway of type III CRISPR-Cas systems. Front Microbiol 11:602789
23. Pinilla-Redondo R, Mayo-Muñoz D, Russel J et al (2020) Type IV CRISPR-Cas systems are highly diverse and involved in competition between plasmids. Nucleic Acids Res 48:2000–2012
24. Zetsche B, Gootenberg JS, Abudayyeh OO et al (2015) Cpf1 is a single RNA-guided endonuclease of a class 2 CRISPR-Cas system. Cell 163:759–771
25. Makarova KS, Wolf YI, Iranzo J et al (2020) Evolutionary classification of CRISPR-Cas systems: a burst of class 2 and derived variants. Nat Rev Microbiol 18:67–83
26. Abudayyeh OO, Gootenberg JS, Konermann S et al (2016) C2c2 is a single-component programmable RNA-guided RNA-targeting CRISPR effector. Science 353:aaf5573
27. Gootenberg JS, Abudayyeh OO, Lee JW et al (2017) Nucleic acid detection with CRISPR-Cas13a/C2c2. Science 356:438–442
28. Komor AC, Kim YB, Packer MS et al (2016) Programmable editing of a target base in

genomic DNA without double-stranded DNA cleavage. Nature 533:420–424
29. Gaudelli NM, Komor AC, Rees HA et al (2017) Programmable base editing of A•T to G•C in genomic DNA without DNA cleavage. Nature 551:464–471
30. Qi T, Wu F, Xie Y et al (2020) Base editing mediated generation of point mutations into human pluripotent stem cells for modeling disease. Front Cell Dev Biol 8:590581
31. Zuo E, Sun Y, Wei W et al (2019) Cytosine base editor generates substantial off-target single-nucleotide variants in mouse embryos. Science 364:289–292
32. Jeong YK, Song B, Bae S (2020) Current status and challenges of DNA base editing tools. Mol Ther 28:1938–1952
33. Anzalone AV, Randolph PB, Davis JR et al (2019) Search-and-replace genome editing without double-strand breaks or donor DNA. Nature 576:149–157
34. Shuto Y, Nakagawa R, Zhu S et al (2024) Structural basis for pegRNA-guided reverse transcription by a prime editor. Nature 631:224–231
35. Qi LS, Larson MH, Gilbert LA et al (2013) Repurposing CRISPR as an RNA-guided platform for sequence-specific control of gene expression. Cell 152:1173–1183
36. Gilbert LA, Larson MH, Morsut L et al (2013) CRISPR-mediated modular RNA-guided regulation of transcription in eukaryotes. Cell 154:442–451
37. Larson MH, Gilbert LA, Wang X et al (2013) CRISPR interference (CRISPRi) for sequence-specific control of gene expression. Nat Protoc 8:2180–2196
38. Gilbert LA, Horlbeck MA, Adamson B et al (2014) Genome-scale CRISPR-mediated control of gene repression and activation. Cell 159:647–661
39. Pickar-Oliver A, Gersbach CA (2019) The next generation of CRISPR-Cas technologies and applications. Nat Rev Mol Cell Biol 20:490–507
40. McCarty NS, Graham AE, Studená L, Ledesma-Amaro R (2020) Multiplexed CRISPR technologies for gene editing and transcriptional regulation. Nat Commun 11: 1281
41. Hilton IB, D'Ippolito AM, Vockley CM et al (2015) Epigenome editing by a CRISPR-Cas9-based acetyltransferase activates genes from promoters and enhancers. Nat Biotechnol 33:510–517
42. Thakore PI, Black JB, Hilton IB, Gersbach CA (2016) Editing the epigenome: technologies for programmable transcription and epigenetic modulation. Nat Methods 13:127–137
43. Vojta A, Dobrinić P, Tadić V et al (2016) Repurposing the CRISPR-Cas9 system for targeted DNA methylation. Nucleic Acids Res 44:5615–5628
44. Liu XS, Wu H, Ji X et al (2016) Editing DNA methylation in the mammalian genome. Cell 167(233-247):e17
45. Abudayyeh OO, Gootenberg JS, Essletzbichler P et al (2017) RNA targeting with CRISPR-Cas13. Nature 550:280–284
46. Cox DBT, Gootenberg JS, Abudayyeh OO et al (2017) RNA editing with CRISPR-Cas13. Science 358:1019–1027
47. Wang T, Wei JJ, Sabatini DM, Lander ES (2014) Genetic screens in human cells using the CRISPR-Cas9 system. Science 343:80–84
48. Shalem O, Sanjana NE, Hartenian E et al (2014) Genome-scale CRISPR-Cas9 knockout screening in human cells. Science 343:84–87
49. Joung J, Konermann S, Gootenberg JS et al (2017) Genome-scale CRISPR-Cas9 knockout and transcriptional activation screening. Nat Protoc 12:828–863
50. Smith I, Greenside PG, Natoli T et al (2017) Evaluation of RNAi and CRISPR technologies by large-scale gene expression profiling in the Connectivity Map. PLoS Biol 15:e2003213
51. Tsherniak A, Vazquez F, Montgomery PG et al (2017) Defining a cancer dependency map. Cell 170:564–576.e16
52. Dixit A, Parnas O, Li B et al (2016) Perturb-Seq: dissecting molecular circuits with scalable single-cell RNA profiling of pooled genetic screens. Cell 167:1853–1866. e17
53. Shen JP, Zhao D, Sasik R et al (2017) Combinatorial CRISPR-Cas9 screens for de novo mapping of genetic interactions. Nat Methods 14:573–576
54. Baccin C, Al-Sabah J, Velten L et al (2020) Combined single-cell and spatial transcriptomics reveal the molecular, cellular and spatial bone marrow niche organization. Nat Cell Biol 22:38–48
55. Dhainaut M, Rose SA, Akturk G et al (2022) Spatial CRISPR genomics identifies regulators of the tumor microenvironment. Cell 185:1223–1239.e20
56. Gootenberg JS, Abudayyeh OO, Kellner MJ et al (2018) Multiplexed and portable nucleic acid detection platform with Cas13, Cas12a, and Csm6. Science 360:439–444
57. Li L, Li S, Wu N et al (2019) HOLMESv2: A CRISPR-Cas12b-assisted platform for nucleic acid detection and DNA methylation quantitation. ACS Synth Biol 8:2228–2237
58. Atceken N, Kahya A, Yigci D, Tasoglu S (2026) CRISPR-on-chip for point-of-care diagnostics. ACS Nano 20:2561–2577

59. Ackerman CM, Myhrvold C, Thakku SG et al (2020) Massively multiplexed nucleic acid detection with Cas13. Nature 582:277–282
60. Chen M, Wu D, Tu S et al (2021) CRISPR/Cas9 cleavage triggered ESDR for circulating tumor DNA detection based on a 3D graphene/AuPtPd nanoflower biosensor. Biosens Bioelectron 173:112821
61. Chen K, Shen Z, Wang G et al (2022) Research progress of CRISPR-based biosensors and bioassays for molecular diagnosis. Front Bioeng Biotechnol 10:986233
62. DeWitt MA, Magis W, Bray NL et al (2016) Selection-free genome editing of the sickle mutation in human adult hematopoietic stem/progenitor cells. Sci Transl Med 8:360ra134
63. Valenti MT, Serena M, Carbonare LD, Zipeto D (2019) CRISPR/Cas system: an emerging technology in stem cell research. World J Stem Cells 11:937–956
64. Stadtmauer EA, Fraietta JA, Davis MM et al (2020) CRISPR-engineered T cells in patients with refractory cancer. Science 367:eaba7365
65. Frangoul H, Altshuler D, Cappellini MD et al (2021) CRISPR-Cas9 gene editing for sickle cell disease and β-thalassemia. N Engl J Med 384:252–260
66. Eyquem J, Mansilla-Soto J, Giavridis T et al (2017) Targeting a CAR to the TRAC locus with CRISPR/Cas9 enhances tumour rejection. Nature 543:113–117
67. Ren J, Liu X, Fang C et al (2017) Multiplex genome editing to generate universal CAR T cells resistant to PD1 inhibition. Clin Cancer Res 23:2255–2266
68. Lino CA, Harper JC, Carney JP, Timlin JA (2018) Delivering CRISPR: a review of the challenges and approaches. Drug Deliv 25:1234–1257
69. Bairqdar A, Karitskaya PE, Stepanov GA (2024) Expanding horizons of CRISPR/Cas technology: clinical advancements, therapeutic applications, and challenges in gene therapy. Int J Mol Sci 25:13321
70. Duan L, Ouyang K, Xu X et al (2021) Nanoparticle Delivery of CRISPR/Cas9 for genome editing. Front Genet 12:673286
71. Gillmore JD, Gane E, Taubel J et al (2021) CRISPR-Cas9 in vivo gene editing for transthyretin amyloidosis. N Engl J Med 385:493–502
72. Nelson CE, Wu Y, Gemberling MP et al (2019) Long-term evaluation of AAV-CRISPR genome editing for Duchenne muscular dystrophy. Nat Med 25:427–432
73. Maeder ML, Stefanidakis M, Wilson CJ et al (2019) Development of a gene-editing approach to restore vision loss in Leber congenital amaurosis type 10. Nat Med 25:229–233
74. Dong A, Soleimani Samarkhazan H, Tavakoli F (2026) Beyond CRISPR: next-gen precision engineering of CAR-NK cells for enhanced persistence, trafficking, and tumor eradication. Cancer Cell Int 26: 120

Open Access This chapter is licensed under the terms of the Creative Commons Attribution-NonCommercial-NoDerivatives 4.0 International License (http://creativecommons.org/licenses/by-nc-nd/4.0/), which permits any noncommercial use, sharing, distribution and reproduction in any medium or format, as long as you give appropriate credit to the original author(s) and the source, provide a link to the Creative Commons license and indicate if you modified the licensed material. You do not have permission under this license to share adapted material derived from this chapter or parts of it.

The images or other third party material in this chapter are included in the chapter's Creative Commons license, unless indicated otherwise in a credit line to the material. If material is not included in the chapter's Creative Commons license and your intended use is not permitted by statutory regulation or exceeds the permitted use, you will need to obtain permission directly from the copyright holder.





Chapter 2

DNA Repair Mechanisms

Pelin Dilsiz and Fatma Zehra Hapil

Abstract

DNA undergoes a wide range of chemical reactions every day, and such DNA lesions might have deleterious consequences as they not only affect cellular components and biological processes but can also accumulate permanently in the genome. Since DNA alterations eventually lead to multiple detrimental consequences, including genomic instability and cancer predisposition, these lesions must be efficiently detected and repaired by tightly regulated mechanisms to maintain genome integrity. Various DNA repair mechanisms contribute to the correction of the alterations that occur every day to prevent genomic instability, providing key insights into genome editing. Genome editing is a significant exogenous mutagen, in which conventional editing strategies cause double-strand breaks, and nickases induce single-strand breaks, albeit base editing depends on the modulation of base excision repair, and prime editing results in mismatches. A comprehensive understanding of DNA repair mechanisms is strategically important for genome editing applications. In this chapter, we discuss the pivotal DNA repair mechanisms to provide a better insight into the role of DNA repair mechanisms in genome editing.

Keywords Base excision, Direct repair of DNA alkylation, DNA repair, Homology directed repair, Microhomology-mediated repair, Mismatch repair, Nonhomologous end joining, Nucleotide excision, Single strand annealing

1 Introduction

DNA, the code of life, is preserved within the nuclei of eukaryotic cells and is constantly exposed to different endogenous or exogenous mutagens despite being deliberately protected.

Each human cell is estimated to experience over 70,000 DNA lesions every day. Single-strand DNA (ssDNA) breaks account for 75% of lesions and might result from base hydrolysis or oxidative damage during metabolism. DNA double-strand breaks (DSBs), which are more hazardous but far less common, might also result from ssDNA breaks [1]. Approximately 26,000 bases are lost per day, predominantly purines, due to spontaneous hydrolysis of the glycosidic bond [2]. Therefore, the maintenance of genome integrity

Duško Lainšček et al. (eds.), *CRISPR Delivery*, Methods in Molecular Biology, vol. 3075,
https://doi.org/10.1007/978-1-0716-5547-4_2,
© The Author(s) 2027

should be tightly regulated to eliminate such a high rate of modifications or lesions.

From a molecular perspective, genome editing can be considered an exogenous mutagen. Conventional genome editing generates double-strand breaks, in which the repair process is essential for generating knockouts or knock-ins, whereas nickases induce single-strand breaks. Base editing relies on modulation of base excision repair. Prime editing, on the other hand, results in mismatches, the repair of which limits editing efficiency. Thus, a comprehensive knowledge of DNA repair mechanisms is fundamental to understanding and applying genome editing.

A typical human cell coordinates multiple pathways to repair different lesions. Small base modifications are generally repaired by base excision repair, while larger lesions that alter the three-dimensional structure of the DNA double helix are repaired by nucleotide excision repair. DNA mismatches are corrected by a specific repair pathway called DNA mismatch repair. In cases of double-strand DNA breaks, cells rely on three different pathways: nonhomologous end joining, homology directed repair, and microhomology-mediated end joining.

2 Direct Repair of DNA Alkylation

DNA alkylation refers to the attachment of an alkyl moiety to a noncanonical position of DNA. DNA alkylation is usually caused by endogenous or exogenous factors, including S-adenosylmethionine, lipid peroxidation products, diet- and tobacco-derived nitrosamines, pollution, and many cancer drugs (e.g., temozolomide and nitrosoureas) [3]. DNA alkylation, if not repaired, induces genotoxicity or cytotoxicity. For example, O(6)-methylguanine pairs with thymine unless being repaired by direct repair, which might either cause a mutation or be further recognized by the mismatch repair system. Recognition by the mismatch repair system is followed by several cycles of repair attempts since removal of thymine causes resynthesis of a new T-. This process can ultimately lead to the formation of double-strand breaks, resulting in genomic instability and cytotoxicity [3].

Direct reversal is a specialized, error-free mode of DNA repair that allows the removal of certain alkyl groups without interrupting the backbone or resynthesizing the DNA. O^6-methylguanine-DNA methyltransferase (MGMT) and Alkylation B (AlkB) Homolog (ALKBH) are the pioneering enzymes involved in direct repair of O-alkylations and N-alkylations, respectively [4]. High MGMT and ALKBH activities reduce mutagenesis and cancer risk but also confer resistance to alkylating chemotherapies [5].

MGMT is a methyltransferase expressed in almost all organisms [6]. It scans the genome and recognizes the base flipping caused by DNA alkylation [7]. In human MGMT, Cys145 is positioned in the conserved PCHRV motif and is deprotonated via a His146–Glu172–water network to a thiolate (S^-) nucleophile [8]. The thiolate of Cys145 attacks the alkylated oxygen (O6 of guanine or O4 of thymine), breaking the C–O bond and forming S-alkyl-Cys145 while restoring normal guanine (or thymine) [7,8]. Once the alkyl group is removed, the base flips back to the double helix, dissociating MGMT, which is irreversibly inactivated due to the transfer of the alkyl group to the cysteine residue. Following alkylation, MGMT is rapidly degraded; thus, this direct repair mechanism is often referred to as "suicide repair," as the enzyme sacrifices itself to protect genome integrity. ALKBH proteins are Fe(II)/α-ketoglutarate-dependent dioxygenases that directly reverse alkylation on DNA and RNA by oxidative demethylation, regenerating the normal base and releasing formaldehyde or an aldehyde. ALKBH1 is essentially responsible for repairing tRNA or mitochondrial genome alkylations [9,10], whereas ALKBH2 and ALKBH3 are considered the major ALKBH proteins in nuclear genome repair. The most well-known targets for direct repair by ALKBH2 and ALKBH3 are 1-methyladenine, 3-methylcytosine, 3-methylthymine, and 1-methylguanine, with the last two being the predominant targets [5].

Similar to MGMT, the alkylated base is recognized by ALKBH because it flips out from the double-stranded DNA. The catalytic pocket of ALKBH contains α-ketoglutarate (α-KG, also known as 2-oxoglutarate) and nonheme Fe(II). Following binding to substrate (the alkylated base), two oxygen molecules bind to the Fe(II) to create Fe(IV)=O (ferryl) in addition to leading to oxidative decarboxylation of α-KG to succinate + CO_2. Then, Fe(IV)=O attacks a H atom at the alkyl group via σ- or π-channels to generate substrate radical + Fe(III)–OH [11]. This hydroxyl group bound to Fe rebounds to the carbon radical to yield the N-hydroxymethyl intermediate, which is unstable. The unstable hydroxy-methyl intermediate spontaneously decomposes in water to formaldehyde and remains the base unmodified, completing the direct reversal without DNA synthesis [11].

3 Base Excision Repair

Base excision repair (BER) is the primary pathway to repair small and non-helix-distorting base modifications that result from oxidation, alkylation, deamination, and spontaneous base loss [12]. BER is divided into two pathways: short-patch BER, in which one nucleotide is being replaced, and long-patch BER, in which 2–13 nucleotides are replaced. Both sub-pathways start with the recognition of DNA

damage by a DNA glycosylase. DNA glycosylases, which comprise a family of more than 11 enzymes, scan the genome, recognize specific types of damaged or modified bases due to being flipped out, and hydrolyze the N-glycosidic bond between the damaged base and the deoxyribose sugar to create an abasic (AP) site [13]. In short patch BER, the phosphodiester backbone 5′ to the AP site is cleaved either by intrinsic lyase activity of glycosylase when the glycosylase that recognized the lesion is multifunctional or AP endonuclease 1 (APE1) when the glycosylase is monofunctional and therefore lacks intrinsic lyase activity. Cleavage of the phosphodiester backbone yields a 3′-hydroxyl and 5′-deoxyribose phosphate (5′-dRP) termini. If the site is not oxidized or reduced, and the cell is neither in ATP shortage nor in S phase, then DNA Polymerase β removes 5′-dRP (the sugar moiety at the 5′ end), operating its lyase activity and fills the gap by its polymerase activity [14–16]. Following the addition of this single nucleotide, XRCC1 recruits DNA ligase III to seal the nick since it acts as a scaffolding protein between DNA Pol β and DNA ligase III [13] (Fig. 1).

The long-patch BER is preferred in cases where the AP site is oxidized, reduced, or somehow modified to make it inaccessible by DNA Pol β, there is shortage of cellular ATP, or the cell goes through the S phase of the cell cycle [17]. In this case, Flap Endonuclease-1(FEN1) and proliferating cell nuclear antigen (PCNA) become readily available. At least four different mechanisms of long patch BER have been proposed so far. These mechanisms share a critical stage, in which PCNA seems to mediate the process by binding to the damaged DNA and recruiting required proteins such as FEN1 and DNA Ligase I to the vicinity of the lesion. In the simplest mechanism, FEN1 discards an extra 5′ base following the removal of the lesion by DNA glycosylase and creation of AP site by APE1, which in turn provides an accessible site for DNA Pol β [18] to allow the resynthesis of the missing bases. In strand displacement DNA synthesis, DNA-damage sensor 9-1-1 triggers DNA Pol β to synthesize a longer patch [19] by creating a 5′-flap, which is further removed by FEN1 as well. In both mechanisms, the missing phosphodiester bond is formed by DNA ligase-1 via sealing the nick [12, 17]. Alternatively, in case 5′ end remains inaccessible for DNA Pol β, then PCNA and RFC bound to DNA recruits and activates DNA Pol δ/ε. Strand-displacement synthesis by DNA Pol δ/ε causes a flap in a process dependent on single-strand DNA-binding protein RPA, which is preceded by the removal of the flap by FEN1 [20]. During this process, the first nucleotide is either added by DNA Pol β, followed by elongation via DNA Pol δ/ε [21], or the entire sequence is synthesized by DNA Pol δ/ε [22]. Abovementioned pathways require DNA nick sensor PARP1, which predominantly functions via ADP-ribosylating (PARylating) certain proteins, including itself [23]. The nick generated by APE1 is recognized by PARP1, which in turn loosens the chromatin structure by PARylating histones and nonhistone proteins [24]. PARP1

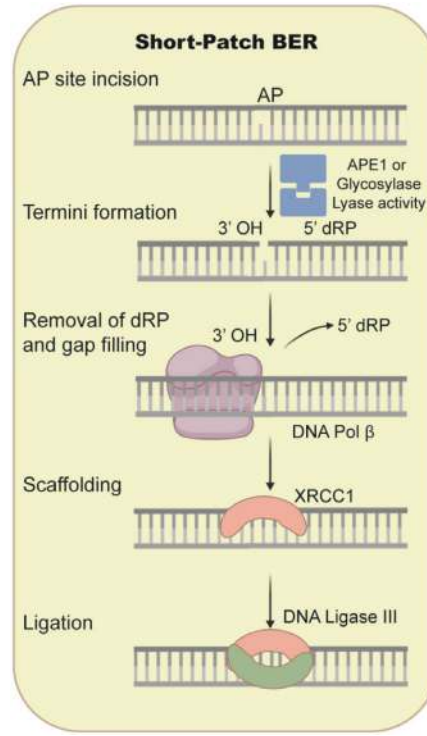


Fig. 1 Schematic illustration of the short patch base-excision repair mechanism. The small non-helix-distorting lesions are repaired by short patch BER when the lesion is accessible by Polymerase Beta, there is no ATP shortage, or the cell is not in the S phase. When there is a non-helix-distorting base modification in the DNA, the DNA glycosylases detect and remove the modified base, creating an AP site. Next, the phosphodiester backbone is removed either by intrinsic lyase activity of some DNA glycosylases or the activity of AP endonuclease 1, which generates a 3′-OH and 5′-deoxyribose phosphate ends. DNA Pol β removes the sugar moiety at the 5′-deoxyribose phosphate end and fills the one-nucleotide gap. XRCC1, a scaffolding protein, recruits DNA ligase III to seal the remaining nick

also PARylates FEN1, which is essential for being recruited to the repair complex [25]. However, PARP1 limits FEN1- and DNA Pol β-mediated strand displacement when it is accumulated on DNA by restricting the access of essential proteins to the site of the lesion. In short patch repair, XRCC-mediated recruitment of DNA Pol β and Ligase III prevents further trapping of PARP1 and thus enables completion of the repair [26] (Fig. 2).

In long patch BER, PARP1 accumulation on DNA inhibits the activity of FEN1 and DNA Pol β, which overall restricts the repair process [27]. The auto-PARylation of PARP1 releases it from the DNA, which allows FEN1 and DNA Pol β action [28]. In case PARP1 auto-PARylation is impaired, particularly during S phase, then an alternative pathway takes place, in which PARP1-activated RECQ1 helicase unwinds the DNA and creates an eight-nucleotide

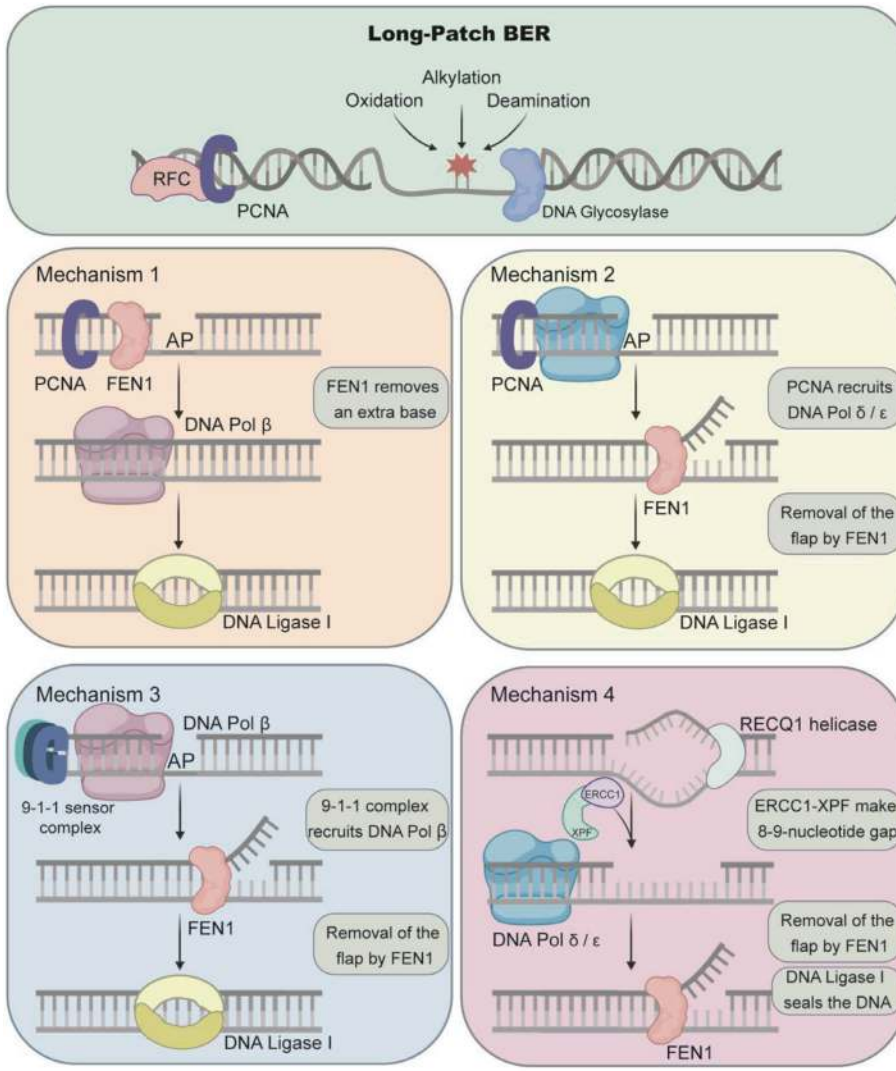


Fig. 2 Representation of long patch base-excision repair mechanism. Long patch BER occurs when (i) the site is either oxidized or reduced to block DNA Pol β binding, (ii) the cell undergoes ATP shortage, or (iii) the cell is in the S phase of the cell cycle. There are at least four alternative routes of long patch BER

flap that is further directed to the 5′ end by ERCC1–XPF to create a nine-nucleotide gap. This gap is processed by DNA Pol δ/ε, the 3′ flap is removed by FEN1, and finally 20 nucleotides are synthesized [29], which is further sealed by DNA ligase I (Fig. 2).

4 Nucleotide Excision Repair

Nucleotide excision repair (NER) is a universal cut-and-patch pathway that removes helix-distorting DNA lesions such as UV-induced cyclobutane pyrimidine dimers, 6–4 photoproducts, and bulky

chemical adducts occurring due to environmental mutagens and chemotherapeutic agents [30].

In prokaryotic organisms, cyclobutane pyrimidine dimers and 6–4 photoproducts might be repaired by photolyase-mediated direct repair as well. Photolyase, a monomeric protein with two chromophore cofactors, is expressed in many prokaryotic species but is absent in human cells. When the organism is exposed to violet/blue light, the light photon is absorbed by folate, which is found on the surface of the enzyme and acts as a photo-antenna [31]. Folate, upon absorbing the photons, generates an excitation energy and transfers it to the flavin cofactor to generate FADH. The excited electron from FADH is transferred to the cyclobutane pyrimidine dimer to separate it into two pyrimidines and turn the enzyme into its resting form. Since photolyase is not expressed in mammals, repair of cyclobutane pyrimidine dimers and 6–4 photoproducts merely relies on NER.

NER is a functional repair pathway in all eukaryotes. It operates through two sub-pathways, the global genome NER (GG-NER) and transcription-coupled NER (TC-NER), that differ in their damage recognition mechanisms yet share common downstream stages. GG-NER surveys the entire genome for helix-distorting lesions, while TC-NER repairs lesions that restrict the activity of RNA Polymerase II during transcription.

GG-NER starts with detecting the damage by the XPC–RAD23B–CETN2 complex. This complex, rather than chemical, nature of the damage senses structural distortion and destabilization of the DNA double helix. XPC, the first protein of the NER mechanism constantly and nonspecifically binds to and dissociates from DNA even in the absence of DNA damage, making it a protein shuttling between the nucleus and cytoplasm [32]. XPC–RAD23B–Centrin-2 heterotrimeric complex scans the genome for helix distortions. In the presence of a NER lesion in the genome, RAD23B dissociates [33], and most possibly, allows the damage-specific binding domain of XPC to bind specifically to the lesion [34]. Centrin-2 is known to foster damage-specific binding of XPC, and bridge XPC and XPA, which is another protein essential for the damage verification during NER [35].

XPC is sufficient to recognize 6–4 photoproducts, albeit such a recognition module is not sufficient to detect cyclobutane pyrimidine dimers. Thus, UV-DNA damage binding (UV-DDB, also known as XPE) is additionally recruited. UV-DDB detects cyclobutane pyrimidine dimers via its DDB2 domain, flips out the damaged bases, and recruits XPC to the site of the lesion [35]. Interestingly, XPC–RAD23B and UV-DDB seem to reciprocally enhance each other's recruitment to cyclobutane pyrimidine dimers [36]. A ubiquitin ligase associated with UV-DDB, namely CUL4, subsequently polyubiquitinates UV-DDB and XPC [37], which facilitates XPC binding to the lesion.

Stable binding of XPC provides an initiation signal to the other factors involved in the NER [38]. The first recruited is the TFIIH complex, which is a horseshoe-shaped heterodecameric complex

composed of three subunits with cyclin-dependent kinase (CDK)-activating kinase (CAK) activity and a seven-subunit core complex. Within the core complex, five subunits—p62, p44, p34, p52, and p8—constitute the structural backbone and regulate the activity of the other two subunits, XPB translocase and XPD helicase [30]. Owing to their helicase and translocase activities, XPB and XPD generate ~25–30 nucleotide DNA repair bubble, where XPB binds to the double-stranded, and XPD binds to the single-stranded DNA [39]. The repair function of TFIIH, which is a transcription factor, is primarily attributed to its modulation by XPA. XPA bridges XPB and XPD by binding to the DNA with the help of XPC and Centrin-2 and holds them at the 5′ of the repair bubble [39]. Given that XPC detects not only NER lesions, but also DNA mismatches [40], further verification of the damage is required, which is predominantly performed by XPB and XPD [39]. In addition to bridging XPB and XPD, XPA interacts with the single-stranded DNA-binding complex RPA [41], which is essential for the stabilization of XBG binding and stimulation of ERCC1–XPF [42].

In a nutshell, DNA damage is initially detected by XPC, either alone or in cooperation with UV-DDB. Centrin-2 facilitates the recruitment of XPA by making a complex with XPC. XPC, on the other hand, recruits the TFIIH complex via direct physical interaction with the XPB subunit. CAK complex dissociates from TFIIH and releases the XPD subunit to bind to the DNA [30]. XPA connects XPB with the translocase activity and XPD with the helicase activity, which altogether unwind the DNA around the lesion, restricted within a repair bubble. RPA, together with XPA, binds and stabilizes the exposed single-stranded DNA (Fig. 3).

After detecting and validating the damage, NER proceeds with incision. XPF/ERCC1 complex is the endonuclease involved in 5′ incision, which is recruited to the NER complex via the interaction between ERCC1 and XPA [43]. Besides binding to ssDNA, ERCC1 interacts with XPF via its helix–hairpin–helix (HhH) motif, which has the catalytic endonuclease activity [44]. Following 5′ cut by ERCC1/XPF, RPA bound to ssDNA positions RFC [45], which displaces XPF from the NER complex. Concomitantly, the 3′ cut is performed by XPG endonuclease [46], altogether yielding around 24–32 nucleotides being removed from the DNA. In addition to the removal of the lesion-containing fragment, the catalytic activities of XPF and XPG also cause DNA demethylation and chromatin looping to initiate the transcription of NER proteins [47]. PCNA is recruited to the site upon interacting with XPG and via the clamp-loading activity of RFC [45]. As in long-patch BER, PCNA and RFC recruit DNA Pol δ/ε, which fills the gap by DNA synthesis, and the remaining nick is sealed by DNA Ligase I [45]. Moreover, DNA Pol κ might alternatively be recruited to the complex via ubiquitinated PCNA and XRCC1 when PCNA is ubiquitinated due to UV-exposure, and translesion synthesis should take place [48].

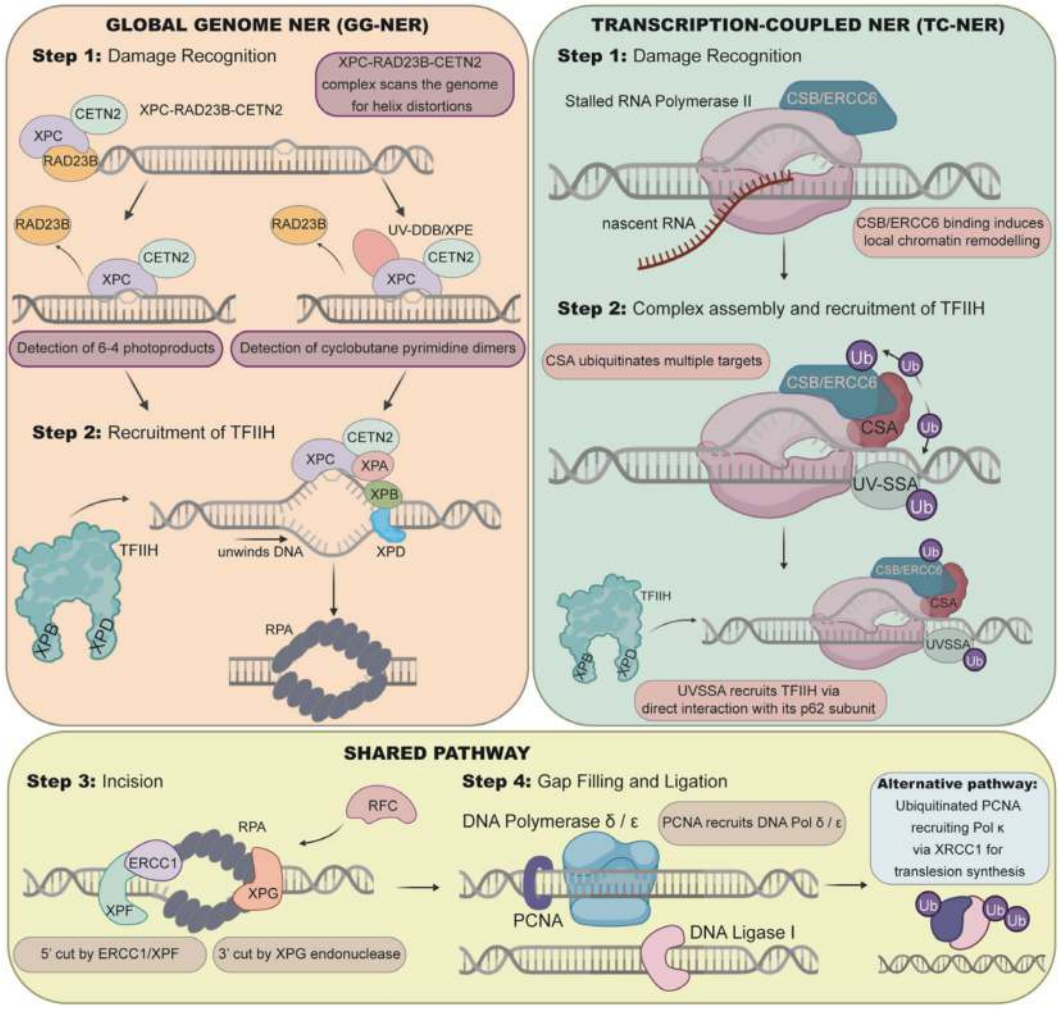


Fig. 3 The mechanisms of global-genome and transcription-coupled nucleotide-excision repair. The two distinct lesion recognition subpathways converge into a shared DNA repair mechanism. GG-NER surveys the entire genome for helix-distorting DNA damage, such as UV-induced cyclobutane pyrimidine dimers (CPDs) or 6–4 photoproducts. XPC–RAD23B is the primary damage sensor, facilitated by UV-DDB, which is required for sensing CPDs or hidden lesions. TC-NER is initiated when an elongating RNA Polymerase II (RNA Pol II) stalls at a bulky lesion

Transcription-coupled NER (TC-NER) takes place when RNA Polymerase II is stalled due to helix-distorting lesions during transcription elongation. It further triggers the recruitment of CSB (ERCC6), which stably associates with the arrested polymerase, albeit it dynamically associates and dissociates during regular transcription [49]. CSB is an SWI/SNF-related ATPase that promotes local chromatin remodeling, thereby enabling access to the damaged DNA [50]. CSA (ERCC8) is then recruited as part of a $CRL4^{CSA}$

ubiquitin E3 ligase complex and contributes to the ubiquitination of NER components, ensuring an orderly progression of the repair process. CSA also ubiquitinates CSB and RPB1 [51] and contributes to the assembly of UVSSA, ELOF1, STK19, and associated factors [52]. UVSSA recruits TFIIH to the repair site via direct interaction with the p62 subunit of TFIIH core complex [52,53] (Fig. 3). After the specific recognition of the lesion during TC-NER, where RNA Polymerase II is the main "damage sensor," the repair proceeds by following the shared pathway with GG-NER (Fig. 3).

5 Mismatch Repair

DNA mismatch repair (MMR) corrects base mismatches and small insertion/deletion loops generated during replication and recombination. It improves replication fidelity up to 50–1000 times [54]. By doing so, MMR preserves genome integrity and shapes how cells respond to unintended or intended damage, such as cancer therapies or advanced genome editing techniques such as prime editing.

Although the mechanism is mainly conserved, MMR in prokaryotes is simpler compared to eukaryotes. In bacteria, MutS, an ATP-hydrolyzing protein, detects mismatches and small insertion–deletion associated mispairs. It further recruits another ATPase, MutL, and they activate MutH, which nicks the newly synthesized, hemimethylated strand [54]. Detecting the mismatch by MutS is driven by MutS-mediated scanning of the genome for distortions in the sugar-phosphate backbone, deformability, and flexibility of DNA [55], particularly at replisome regions [56].

In eukaryotes, mismatches are recognized by one of the MutS homologs; MutSα (MSH2–MSH6 heterodimer), which preferentially recognizes base mismatches and 1 nucleotide insertion loops, or MutSβ (MSH2–MSH3 heterodimer), which detects 1 nucleotide deletions or 2–6 nucleotide insertion–deletion loops, especially found in noncoding regions [57]. Since human DNA is not DAM-methylated as in prokaryotes, discrimination between the newly synthesized and the nascent strand relies on the presence of replication-associated nicks and the existence of PCNA on the newly synthesized strand [58]. Thus, ligating the replication-associated nicks by DNA ligase shortens the action window for MMR [59]. MutSα/β is positioned near the replisome through interacting with PCNA [60], and tracks with DNA polymerases during the S phase [61]. MutSα/β recruits MutLα (MLH1–PMS2 heterodimer), or rarely MutLγ (MLH1–MLH3 heterodimer), to the mismatch [62]. Upon recruitment of MutL, the pre-existing PCNA binds and activates the latent endonuclease PMS2 subunit of MutL (or Pms1 in yeast) to incise the daughter strand [60], if a nick is not already present. The ATP-binding domain of the MLH1 subunit of MutL seems to play a redundant

role in the recognition and preservation of the present nicks in DNA to enable strand discrimination [63]. This double-nick defines the error-containing segment to be excised. Once the mismatch is recognized and DNA is nicked, ATP bound to MutS is displaced from the site, which allows recruited Exonuclease-1 (EXO1) to remove the nicked segment via $5' \rightarrow 3'$ excision [64]. When EXO1 is not present, multiple nucleases including FEN1 [65], DNA2 [66], or FANCD2-associated nuclease 1 (FAN1) [67] may play an active role in excising the damaged strand. In the DNA2-mediated compensatory mechanism, helicase activity of DNA2 is not crucial, although the nuclease activity is essential to enhance Pol δ-dependent strand displacement [66]. After EXO1 or backup nucleases excise the error-containing segment, the resulting single-stranded gap is coated by RPA and then synthesized by replicative polymerases (Pol δ or Pol ε) using the intact strand as template in a PCNA-dependent reaction, which is then followed by the sealing activity of DNA ligase I [68] (Fig. 4).

6 Double Strand DNA Break Repair Mechanisms

DNA double-strand breaks (DSBs) represent one of the most deleterious forms of DNA damage due to the high risk of initiating unwanted recombination events, and provoke a rapid, alarm-like cellular response to preserve the genome integrity. DNA double-strand breaks can arise from (i) endogenous sources such as replication stress, reactive oxygen species (ROS), meiotic recombination, and V(D)J recombination, (ii) exogenous sources such as ionizing radiation, chemotherapeutic agents, environmental toxins, or (iii) interventions such as conventional CRISPR/Cas9-mediated genome editing. Indeed, the success of conventional CRISPR/Cas9 relies on the induction of DSBs, and knock-in strategies often involve the modulation of DSB repair pathways.

The cellular response to DSBs involves a sophisticated network of DNA repair pathways, primarily nonhomologous end joining (NHEJ), alternative end joining (alt-EJ), homology-directed repair (HDR), and single-strand annealing (SSA), along with complex signaling cascades collectively termed the DNA damage response (DDR). These pathways are tightly regulated and coordinated with the cell cycle checkpoints to ensure accurate repair before cell division. The choice between repair pathways depends on multiple factors, including cell cycle phase, chromatin context, the nature of the DNA ends, and the availability of homologous templates. Defects in DSB repair mechanisms are associated with genomic instability, cancer predisposition, immunodeficiency, neurodegeneration, and premature aging syndromes.

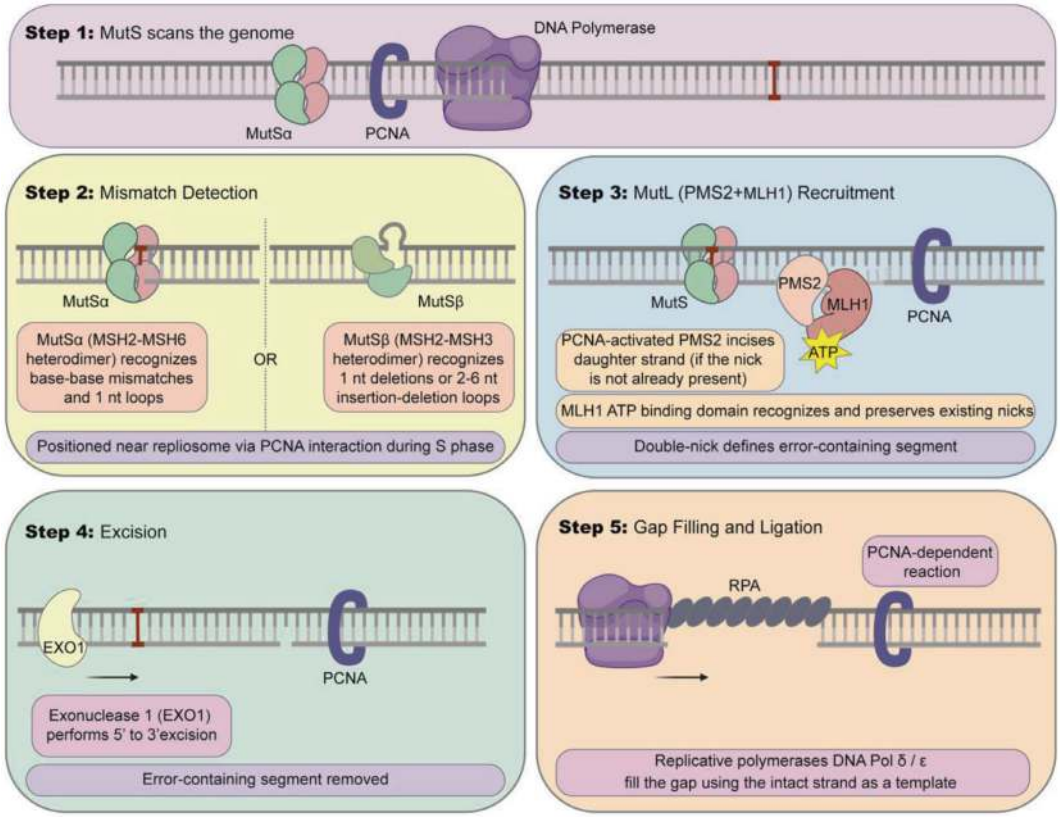


Fig. 4 Schematic illustration of the mismatch repair mechanism. Mismatch recognition complexes (MutSα for base mismatches or 1 nucleotide insertions or deletions (indels), and MutSβ for longer indel loops) scan the genome by following the replicasome with the help of the PCNA sliding clamp. Once a mismatch is found, the newly synthesized strand is detected by the presence of nicks remaining from the replication. MutL preserves the pre-existing nicks and generates new nicks, when necessary, followed by EXO1-mediated excision. The resulting single-stranded gap, which is secured by RPA, is resynthesized by DNA Polymerase δ and sealed by DNA Ligase I to restore genomic fidelity

6.1 Nonhomologous End Joining

Nonhomologous end joining (NHEJ) is the predominant DSB repair pathway in mammalian cells that is active throughout the cell cycle, yet exclusively critical in G1 or early S phases [69]. It functions when a sister chromatid template is unavailable for homology-directed repair. NHEJ directly ligates the broken ends of the DNA in the absence of extensive homology, which makes it an essentially faster, but potentially more error-prone, repair mechanism compared to HDR. This "error-prone" nature of NHEJ provides 1–2 nucleotides of insertions and deletions (indels) that cause frame-shift mutations and thus knock out the genome-edited cells [70].

In NHEJ, the "damage sensor" role is attributed to Ku70/Ku80 heterodimer, a preformed ring/basket-shaped heterodimer abundant in the nucleus that has a strong affinity to duplex DNA

ends [71]. Owing to its basket shape, Ku70/80 encircles the DNA ends with Ku70 being located at a closer position to the DNA [71]. The binding of Ku70/80 protects the DNA ends from undesired exonuclease activities and recruits other proteins involved in NHEJ, such as DNA–PKcs, X-ray repair cross-complementing protein 4 (XRCC4), XRCC4-like factor (XLF), paralog of XRCC4 and XLF (PAXX), and DNA ligase IV.

DNA–PKcs, the master kinase involved in the NHEJ, is recruited to the break by interacting with the C-terminal region of Ku80. Once DNA–PKc is bound, it pushes Ku70/80 approximately 15 nucleotides upstream to occupy the terminal nucleotides via its HhH motif [71]. This causes a conformational rearrangement in DNA–PKcs, including exposing the DNA end-binding helix, allowing stable association with DNA ends and activating its catalytic function [71]. DNA–PKcs is a member of the phosphatidylinositol 3-kinase-related kinase (PIKK) family [72] and phosphorylates numerous substrates involved in DNA repair and cell cycle checkpoint activation. The DNA–PK complex tethers the two broken ends of the DNA and further orchestrates subsequent processing and ligation steps.

DNA end processing in NHEJ is carried out by several nucleases and polymerases that prepare incompatible ends for ligation. Artemis (SNM1C/DCLRE1C), activated by DNA–PKcs, has endonuclease activity that coordinates hairpin structures and overhangs [73]. XLF and XRCC4–LIG4 make a bridge between the ends [74]. DNA Pol μ and λ fill in the gaps, while terminal deoxynucleotidyl transferase (TdT) adds random nucleotides, particularly during V(D)J recombination in developing lymphocytes. The final ligation step is performed by the DNA ligase IV–XRCC4 complex, which is often stabilized by XLF (XRCC4-like factor, also known as Cernunnos) (Fig. 5).

6.2 Homology Directed Repair

Homology-directed repair (HDR) is the first choice of the cell to repair the double-strand break, thanks to its accuracy. Nevertheless, HDR is only performed in S or G2 phase of the cell cycle where sister chromatids are available as homologous templates. This cell cycle phase-restriction appears to be modulated by cyclin-dependent kinase (CDK)-mediated phosphorylation of certain elements involved in HDR.

HDR starts with the recognition of double-strand break by MRE11–RAD50–NBS1/MRX (MRN) complex in combination with CtIP. MRN approaches the break site with the help of (i) PARP1 [75] that yields PAR regions that the MRN complex can bind, and (ii) MRN-interacting protein (MRNIP), which generates MRN-condense droplets to enrich the double-strand break site with MRN complexes [76]. Once the MRN complex is recruited to the DNA by RAD50, it scans through nucleosomes until a double-strand break is detected by MRE11 [77]. If the break is already recognized and occupied with Ku proteins, the MRN complex removes the Ku

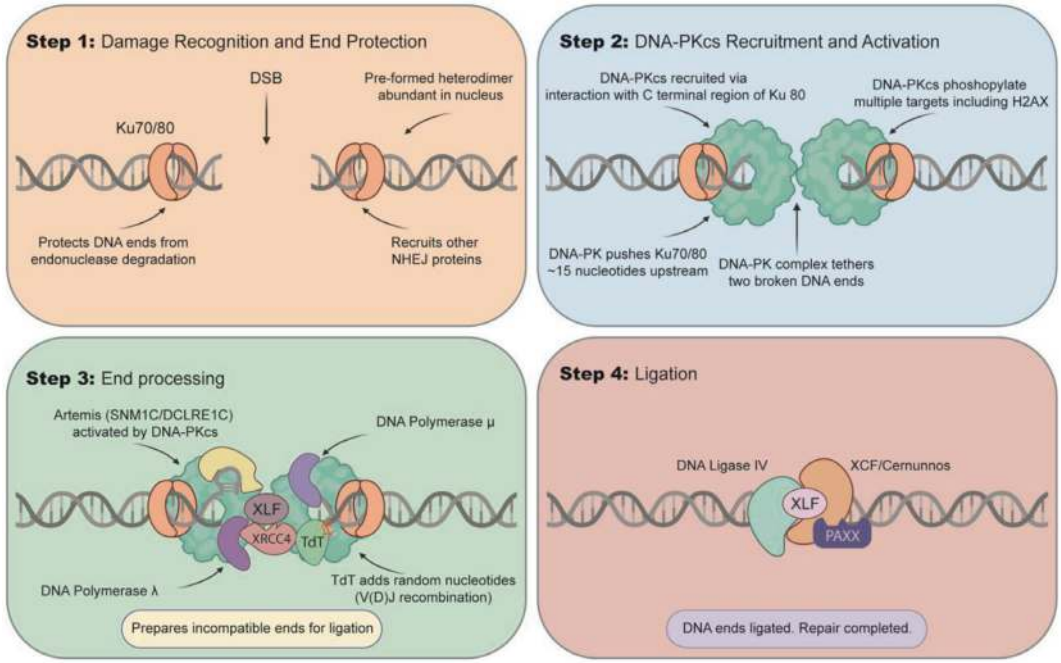


Fig. 5 Nonhomologous end joining mediated double-strand DNA break repair. NHEJ starts with the recognition of a double-strand break by Ku proteins. Ku70/80 heterodimer recruits DNA–PKcs, which phosphorylates several targets, including H2AX and some NHEJ components. After essential end-processing by enzymes such as Artemis and specialized polymerases, the double helix is sealed by the DNA Ligase IV–XRCC4–XLF complex. This mechanism frequently introduces small insertions or deletions (indels) at the repair junction

proteins from the break site, most probably due to HDR being the primary choice of the cell to repair the double-strand break since it is more accurate [77]. In the absence of a DNA double-strand break, ATP-bound Rad50 and NBS1 cover MRE11 to inhibit its enzymatic activity and block ATM recruitment [78]. Once a DNA end is detected, hydrolysis of ATP by Rad50 induces a conformational change in the complex to make the ATM binding motif accessible and release the MRE11 active site for enzymatic activity [79]. ATM recruitment to the FxF/Y motif in the C-terminal domain of NBS1 [80] activates ATM by inducing its dimerization and autophosphorylation. Activated ATM phosphorylates H2AX, MDC1, CtIP, BRCA1, MRN components, and many others to build DDR foci and allow resection [81]. H2AX phosphorylation extends to megabases of DNA, which amplifies the repair signal, increases protein accessibility, and creates a bias towards double-strand break repair instead of single-strand annealing [82]. In the telomere ends, telomere-binding proteins such as TRF2 occupy Rad50, which makes the C-terminal of NBS1 inaccessible for ATM binding [78].

Following activation of ATM and MRE11, CtIP and MRE11 initiate 3' to 5′ end resection to create short single-stranded DNA

ends. CtIP, which is activated in S or G2 phase by CDK-mediated phosphorylation, further stimulates MRE11 endonuclease activity to create entry points for long-range nucleases. Long-range resection is executed by two partially redundant routes: EXO1 performs processive $5' \rightarrow 3'$ exonucleolytic resection, while the DNA2 nuclease acts with a helicase such as Bloom syndrome helicase (BLM) to cleave the displaced 5′-strands during helicase-driven resection [83]. The produced single-stranded DNA is rapidly coated by RPA. In addition to protecting single-stranded DNA, RPA recruits and activates a protein kinase called ATR, which has similar phosphorylation targets to ATM and DNA–PKcs. 53BP1 binds to DNA via interacting with the ubiquitin chains on histones, and together with RPA, it forms a barrier to limit the end resection [84].

H2AX phosphorylation triggers a cascade that involves RNF8 E3 Ubiquitin Ligase, which ubiquitinates H1 on K63 [85]. These ubiquitins serve as a recognition signal for RNF168 [86], which further amplifies histone ubiquitination and helps recruit damage repair proteins [86]. BRCA1-associated RING domain protein 1 (BARD1) binds to ubiquitinated histones and recruits BRCA1 to the nucleosomes in the vicinity of the break site [87]. BARD1 also recognizes H4K20me0, which marks the newly replicated chromatin and directs BRCA1 to the regions where a sister chromatid becomes accessible [88]. BRCA1 promotes end resection by dephosphorylating and repositioning 53BP1 [84], and additionally binds to and recruits EXO1, which provides a platform for long-range end resection [89]. Resected single-strand DNA ends provide a docking site for PALB2, which recruits BRCA2, the protein required for the displacement of RPA by RAD51 [90]. RAD51 is an ATPase brought by BRCA2 to the synapse that searches for a homologous double-stranded DNA (donor DNA) when bound to ATP, and catalyzes strand invasion [91] to form the D loop. Once the D loop is formed, the 3′ OH end of the invading strand is extended by the DNA polymerases using the homologous double-stranded DNA as a template. This "D-loop extension" is an essential early post-invasion step in all HDR sub-pathways. From this point on, alternative sub-pathways might take place. In synthesis-dependent strand annealing (SDSA), helicases such as BLM disrupt the extended D loop, the newly extended invading strand dissociates and anneals to the other resected end of the break (the second end), which is complementary to the newly synthesized sequence. Any remaining gaps are filled and ligated, yielding a noncrossover product [92,93]. If the extended D-loop is not dismantled, the second end of the break can be "captured," which in turn results in a double Holliday Junction intermediate after the synthesis and ligation. Specialized nucleases or helicase-topoisomerase complexes then resolve or dissolve the dHJ, producing either cross-over or noncrossover products [92,93]. The break-induced replication is the third sub-pathway, which occurs when only one end of the break finds homology and results in the

formation of a replication fork-like structure. DNA synthesis in such a replication fork-like structure might cause loss of heterozygosity and translocations, and therefore, the mutagenic characteristic of this pathway is critically high. Although DNA Pol δ is considered the primary DNA polymerase involved in HDR, Pol η and Pol κ are reported to extend D-loops in vitro. Double depletion of Pol η and Pol κ reduces HDR frequency by approximately twofold, indicating redundant roles in D-loop extension [94] (Fig. 6).

6.3 Alternative End Joining/ Microhomology-Mediated End Joining

Alternative end joining (aEJ), also known as the microhomology-mediated end joining (MMEJ) or theta-mediated end joining (TMEJ), is an error-prone double-strand break repair mechanism that is utilized when the two main double-strand repair mechanisms (NHEJ and HDR) compromised. In HDR-deficient cells, MMEJ contributes to the accumulation of mutations, thus inducing tumorigenesis [95]. MMEJ, as the name implies, uses short stretches of homology to join DNA ends, typically leaving deletions and sometimes insertions.

The main steps of MMEJ are summarized as recognition, resection, annealing, flap removal, gap filling, and ligation. Recognition of the double-strand break in MMEJ is independent of Ku proteins but involves the MRN complex, which is the recognition module of HDR. Although both HDR and MMEJ employ CDK-activated players and can occur during the S and G2 phases of the cell cycle [96], DSB repair in the M phase predominantly relies on MMEJ. One of the reasons is that MMEJ, unlike HDR, does not require a sister chromatid. Another reason is that some of the proteins involved in MMEJ are phosphorylated by M-phase kinases, which favors and enhances their activities.

MMEJ starts end resection that is promoted by CDK-activated CtIP and MRE11, following PARP1-facilitated binding of the MRN complex to the double-strand breaks [97]. This limited resection yields 3′ single-strand DNA overhangs of 5–25 nucleotides length on each side of the break [98]. At this point, if RPA is loaded onto the single-stranded DNA, a bias toward HDR blocks MMEJ [99]. Once the overhangs are generated, Polθ, the main executor of the MMEJ, comes into play. Polθ binds to 3′ overhangs by its helicase domain, removes RPA, searches for homology, and builds the bridge when a microhomology is found. It then initiates its polymerization activity using the 3′ free end as a primer, and the microhomology-bearing end as a template [100]. If the polymerization is aborted for any reason, then Polδ excises a single nucleotide to generate a free 3′ OH end [101], and Polθ looks for another microhomology to complete the synthesis [102]. Given its non-processive action [103], synthesis by Polθ produces partially filled gaps and short 5′ or 3′ flaps rather than a complete duplex in one shot. These flaps are then removed by FEN1 [104] and APE2 [105], and other polymerases fill the gaps, and the final sealing of the nick is performed by Ligase III–XRCC1, or by Ligase I in the absence of Ligase III [106].

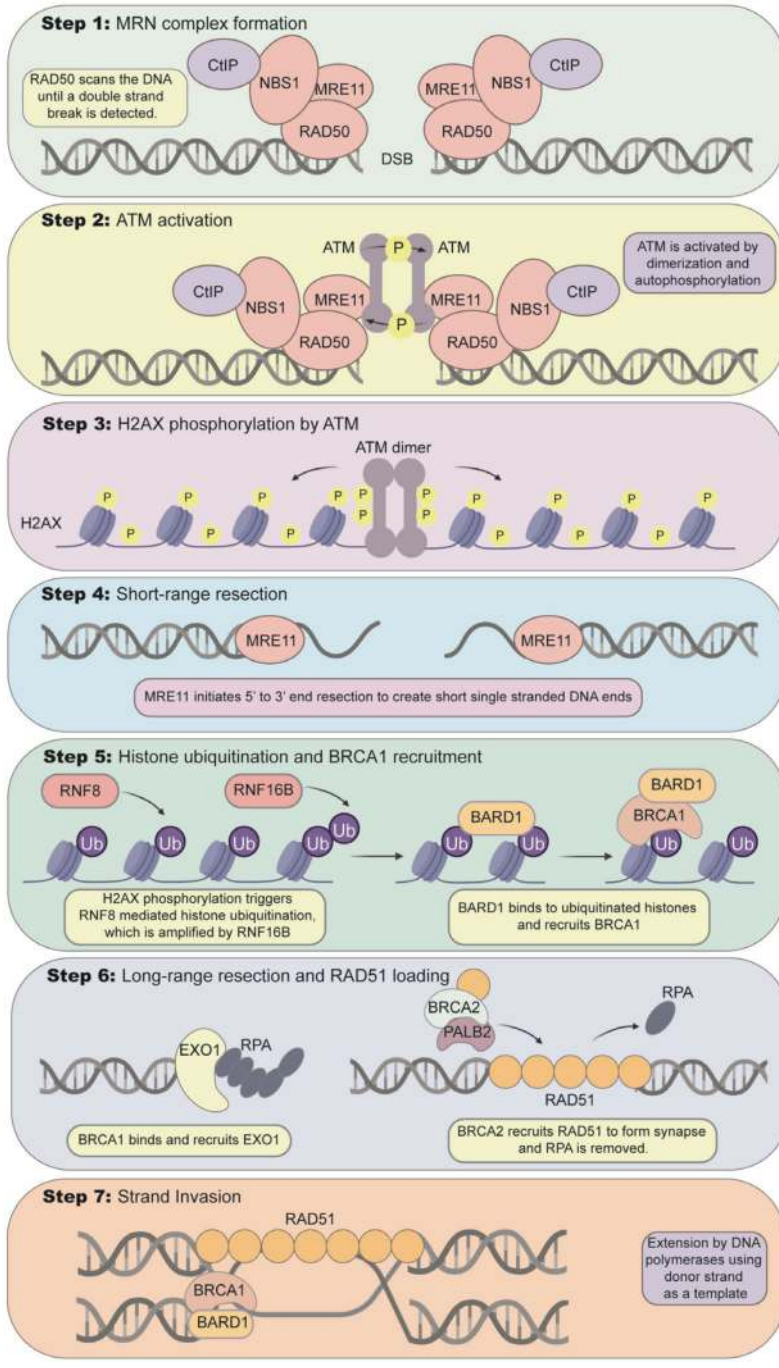


Fig. 6 The mechanism of homology-directed repair. MRN complex (MRE11, RAD50, and NBS1) scans the genome via RAD50 and stalls when a double-strand break (DSB) is detected. If Ku proteins are bound to this DSB, binding of MRN proteins removes the Ku proteins. Binding to DSB causes a conformational change in the MRN complex, exposing the active site of MRE11 and enabling recruitment of ATM, which phosphorylates several targets involved in HDR, including itself and H2AX. HDR, with a coordinated action of MRE11, EXO1, RPA, BRCA1, BRCA2, and RAD51 proteins, repairs the DSB by using the homologous chromosome as a template, and therefore is specific to S and G2 phases of the cell cycle

6.4 Single Strand Annealing

Single-strand annealing (SSA) is a double-strand break repair pathway that is preferred, especially if the break is in the long repeat sequences. SSA repairs the double-strand breaks by long-range resection, RAD52-family-mediated annealing of direct repeats, flap cleavage, ligation, and invariably deletes the sequence between repeats. It is a conserved, mutagenic, homology-directed backup pathway that helps rescue broken chromosomes but also drives deletions, rearrangements, and cancer-associated genome instability. Additionally, it is known to influence CRISPR editing outcomes extensively.

In SSA, double-strand break recognition and end resection are performed by a coordinated action of the MRN complex, CtIP, EXO1, and helicases [107]. This end resection yields long 3′ single-strand DNA wrapped by RPA to inhibit the formation of secondary structures and generate a repair intermediate. RAD52 brings these RPA-covered single-strand DNAs together to form a synapse-like structure by annealing homologous sequences. Flaps generated by nonhomologous sequences are removed by the XPF–ERCC1 complex directed by the mismatch repair factor MSH2–MSH3 [108]. After the flap removal, DNA polymerases fill the gaps, and the resultant nick is sealed by DNA ligases, which cause deletion of some repeat sequences. However, the exact mechanism of SSA still remains to be elucidated.

Acknowledgments

The publication is based upon work by COST Action CA21113: Genome Editing for the Treatment of Human Diseases (https://www.genehumdi.eu), supported by European Cooperation in Science and Technology (COST).

Competing Interests The authors declare no competing interests.

References

1. Tubbs A, Nussenzweig A (2017) Endogenous DNA damage as a source of genomic instability in cancer. Cell 168:644–656
2. Saul RL, Ames BN (1986) Background levels of DNA damage in the population BT—mechanisms of DNA damage and repair: implications for carcinogenesis and risk assessment. In: Simic MG, Grossman L, Upton AC, Bergtold DS (eds), Springer, Boston, MA, USA, pp 529–535
3. Drabløs F, Feyzi E, Aas PA, Vaagbø CB, Kavli B, Bratlie MS et al. (2004) Alkylation damage in DNA and RNA—repair mechanisms and medical significance. DNA Repair (Amst) 3:1389–1407
4. Fahrer J, Christmann M (2023) DNA alkylation damage by nitrosamines and relevant DNA repair pathways. Int J Mol Sci 24(5), 4684.
5. Gutierrez R, O'Connor TR (2021) DNA direct reversal repair and alkylating agent drug resistance. Cancer Drug Resist (Alhambra, Calif) 4:414–423
6. Fang Q (2024) The versatile attributes of MGMT: its repair mechanism, crosstalk with other DNA repair pathways, and its role in cancer. Cancers (Basel) 16.
7. T G S, Siddiqui SA, Dubey KD (2022) Unraveling key interactions and the mechanism of demethylation during hAGT-mediated DNA repair via simulations. Front Mol Biosci 9:975046
8. Jena NR, Shukla PK, Jena HS, Mishra PC, Suhai S (2009) O6-methylguanine repair by

O6-alkylguanine-DNA alkyltransferase. J Phys Chem B 113:16285–16290
9. Kawarada L, Suzuki T, Ohira T, Hirata S, Miyauchi K, Suzuki T (2017) ALKBH1 is an RNA dioxygenase responsible for cytoplasmic and mitochondrial tRNA modifications. Nucleic Acids Res 45:7401–7415
10. Luo Z, Li Y, He C, Wu D, Dai W, Hu L, et al. (2026) ALKB-1-dependent tRNA methylation is required for efficient paternal mitochondrial elimination. Nat Commun 17, 2144.
11. Waheed SO, Ramanan R, Chaturvedi SS, Lehnert N, Schofield CJ, Christov CZ et al. (2020) Role of structural dynamics in selectivity and mechanism of non-heme Fe(II) and 2-oxoglutarate-dependent oxygenases involved in DNA repair. ACS Cent Sci 6:795–814
12. Krokan HE, Bjørås M (2013) Base excision repair. Cold Spring Harb Perspect Biol 5:a012583
13. Rathnaiah G, Sweasy JB (2025) Protein-protein interactions in base excision repair. Biomolecules 15(6):890.
14. Matsumoto Y, Kim K (1995) Excision of deoxyribose phosphate residues by DNA polymerase beta during DNA repair. Science 269:699–702
15. Sobol RW, Horton JK, Kühn R, Gu H, Singhal RK, Prasad R et al. (1996) Requirement of mammalian DNA polymerase-beta in base-excision repair. Nature 379:183–186
16. Caldecott KW (2020) Mammalian DNA base excision repair: dancing in the moonlight. DNA Repair (Amst) 93:102921
17. Gohil D, Sarker AH, Roy R (2023) Base excision repair: mechanisms and impact in biology, disease, and medicine. Int J Mol Sci 24(18), 14186.
18. Prasad R, Dianov GL, Bohr VA, Wilson SH (2000) FEN1 stimulation of DNA polymerase beta mediates an excision step in mammalian long patch base excision repair. J Biol Chem 275:4460–4466
19. Toueille M, El-Andaloussi N, Frouin I, Freire R, Funk D, Shevelev I et al. (2004) The human Rad9/Rad1/Hus1 damage sensor clamp interacts with DNA polymerase beta and increases its DNA substrate utilisation efficiency: implications for DNA repair. Nucleic Acids Res 32:3316–3324
20. DeMott MS, Zigman S, Bambara RA (1998) Replication protein A stimulates long patch DNA base excision repair. J Biol Chem 273:27492–27498
21. Podlutsky AJ, Dianova II, Podust VN, Bohr VA, Dianov GL (2001) Human DNA polymerase beta initiates DNA synthesis during long-patch repair of reduced AP sites in DNA. EMBO J 20:1477–1482
22. Pascucci B, Stucki M, Jónsson ZO, Dogliotti E, Hübscher U (1999) Long patch base excision repair with purified human proteins. DNA ligase I as patch size mediator for DNA polymerases delta and epsilon. J Biol Chem 274:33696–33702
23. Wei H, Yu X (2016) Functions of PARylation in DNA damage repair pathways. Genomics Proteomics Bioinform 14:131–139
24. Ciccarone F, Zampieri M, Caiafa P (2017) PARP1 orchestrates epigenetic events setting up chromatin domains. Semin Cell Dev Biol 63:123–134
25. Sun Y, Jenkins LM, El Touny LH, Zhu L, Yang X, Jo U et al. (2025) Flap endonuclease 1 repairs DNA-protein cross-links via ADP-ribosylation-dependent mechanisms. Sci Adv 11:eads2919
26. Demin AA, Hirota K, Tsuda M, Adamowicz M, Hailstone R, Brazina J et al. (2021) XRCC1 prevents toxic PARP1 trapping during DNA base excision repair. Mol Cell 81:3018–3030. e5
27. Sukhanova M, Khodyreva S, Lavrik O (2010) Poly(ADP-ribose) polymerase 1 regulates activity of DNA polymerase beta in long patch base excision repair. Mutat Res 685:80–89
28. Conceição CJF, Moe E, Ribeiro PA, Raposo M (2025) PARP1: a comprehensive review of its mechanisms, therapeutic implications and emerging cancer treatments. Biochim Biophys Acta Rev Cancer 1880:189282
29. Woodrick J, Gupta S, Camacho S, Parvathaneni S, Choudhury S, Cheema A et al. (2017) A new sub-pathway of long-patch base excision repair involving 5' gap formation. EMBO J 36:1605–1622
30. Theil AF, Häckes D, Lans H (2023) TFIIH central activity in nucleotide excision repair to prevent disease. DNA Repair (Amst) 132:103568
31. Sancar A, Lindsey-Boltz LA, Unsal-Kaçmaz K, Linn S (2004) Molecular mechanisms of mammalian DNA repair and the DNA damage checkpoints. Annu Rev Biochem 73:39–85
32. Hoogstraten D, Bergink S, Ng JMY, Verbiest VHM, Luijsterburg MS, Geverts B et al. (2008) Versatile DNA damage detection by the global genome nucleotide excision repair protein XPC. J Cell Sci 121:2850–2859
33. Bergink S, Toussaint W, Luijsterburg MS, Dinant C, Alekseev S, Hoeijmakers JHJ et al. (2012) Recognition of DNA damage by XPC coincides with disruption of the XPC-RAD23 complex. J Cell Biol 196:681–688
34. Mu H, Geacintov NE, Broyde S, Yeo J-E, Schärer OD (2018) Molecular basis for damage recognition and verification by XPC-RAD23B and TFIIH in nucleotide excision repair. DNA Repair (Amst) 71:33–42

35. Nishi R, Sakai W, Tone D, Hanaoka F, Sugasawa K (2013) Structure-function analysis of the EF-hand protein centrin-2 for its intracellular localization and nucleotide excision repair. Nucleic Acids Res 41:6917–6929
36. An S, Kusakabe M, Kim H-S, Kozono H, Cheon NY, Kim J, et al. (2025) XPC-RAD23B enhances UV-DDB binding to DNA to facilitate lesion search in nucleotide excision repair. Nucleic Acids Res 53(11), gkaf463.
37. Sugasawa K, Okuda Y, Saijo M, Nishi R, Matsuda N, Chu G et al. (2005) UV-induced ubiquitylation of XPC protein mediated by UV-DDB-ubiquitin ligase complex. Cell 121:387–400
38. Volker M, Moné MJ, Karmakar P, van Hoffen A, Schul W, Vermeulen W et al. (2001) Sequential assembly of the nucleotide excision repair factors in vivo. Mol Cell 8:213–224
39. Kokic G, Chernev A, Tegunov D, Dienemann C, Urlaub H, Cramer P (2019) Structural basis of TFIIH activation for nucleotide excision repair. Nat Commun 10: 2885
40. Sugasawa K, Okamoto T, Shimizu Y, Masutani C, Iwai S, Hanaoka F (2001) A multistep damage recognition mechanism for global genomic nucleotide excision repair. Genes Dev 15:507–521
41. Kim M, Kim H-S, D'Souza A, Gallagher K, Jeong E, Topolska-Wós A et al. (2022) Two interaction surfaces between XPA and RPA organize the preincision complex in nucleotide excision repair. Proc Natl Acad Sci USA 119:e2207408119
42. de Laat WL, Appeldoorn E, Sugasawa K, Weterings E, Jaspers NG, Hoeijmakers JH (1998) DNA-binding polarity of human replication protein A positions nucleases in nucleotide excision repair. Genes Dev 12:2598–2609
43. Orelli B, McClendon TB, Tsodikov OV, Ellenberger T, Niedernhofer LJ, Schärer OD (2010) The XPA-binding domain of ERCC1 is required for nucleotide excision repair but not other DNA repair pathways. J Biol Chem 285:3705–3712
44. Tripsianes K, Folkers G, Ab E, Das D, Odijk H, Jaspers NGJ et al. (2005) The structure of the human ERCC1/XPF interaction domains reveals a complementary role for the two proteins in nucleotide excision repair. Structure 13:1849–1858
45. Mocquet V, Lainé JP, Riedl T, Yajin Z, Lee MY, Egly JM (2008) Sequential recruitment of the repair factors during NER: the role of XPG in initiating the resynthesis step. EMBO J 27:155–167
46. O'Donovan A, Davies AA, Moggs JG, West SC, Wood RD (1994) XPG endonuclease makes the 3' incision in human DNA nucleotide excision repair. Nature 371:432–435
47. Le May N, Fradin D, Iltis I, Bougnères P, Egly J-M (2012) XPG and XPF endonucleases trigger chromatin looping and DNA demethylation for accurate expression of activated genes. Mol Cell 47:622–632
48. Ogi T, Limsirichaikul S, Overmeer RM, Volker M, Takenaka K, Cloney R et al. (2010) Three DNA polymerases, recruited by different mechanisms, carry out NER repair synthesis in human cells. Mol Cell 37:714–727
49. van den Boom V, Citterio E, Hoogstraten D, Zotter A, Egly J-M, van Cappellen WA et al. (2004) DNA damage stabilizes interaction of CSB with the transcription elongation machinery. J Cell Biol 166:27–36
50. Xu J, Wang W, Xu L, Chen J-Y, Chong J, Oh J et al. (2020) Cockayne syndrome B protein acts as an ATP-dependent processivity factor that helps RNA polymerase II overcome nucleosome barriers. Proc Natl Acad Sci USA 117:25486–25493
51. Nakazawa Y, Hara Y, Oka Y, Komine O, van den Heuvel D, Guo C et al. (2020) Ubiquitination of DNA damage-stalled RNAPII promotes transcription-coupled repair. Cell 180:1228–1244.e24
52. Mevissen TET, Kümmecke M, Schmid EW, Farnung L, Walter JC (2024) STK19 positions TFIIH for cell-free transcription-coupled DNA repair. Cell 187:7091–7106.e24
53. van der Weegen Y, Golan-Berman H, Mevissen TET, Apelt K, González-Prieto R, Goedhart J et al. (2020) The cooperative action of CSB, CSA, and UVSSA target TFIIH to DNA damage-stalled RNA polymerase II. Nat Commun 11: 2104
54. Hsieh P, Yamane K (2008) DNA mismatch repair: molecular mechanism, cancer, and ageing. Mech Ageing Dev 129:391–407
55. Jayaraj A, Thayer KM, Beveridge DL, Hingorani MM (2023) Molecular dynamics of mismatch detection-How MutS uses indirect readout to find errors in DNA. Biophys J 122:3031–3043
56. Liao Y, Schroeder JW, Gao B, Simmons LA, Biteen JS (2015) Single-molecule motions and interactions in live cells reveal target search dynamics in mismatch repair. Proc Natl Acad Sci USA 112:E6898–E6906
57. Kadyrova LY, Mieczkowski PA, Kadyrov FA (2023) Genome-wide contributions of the MutSα- and MutSβ-dependent DNA mismatch repair pathways to the maintenance of genetic stability in Saccharomyces cerevisiae. J Biol Chem 299:104705
58. Putnam CD (2021) Strand discrimination in DNA mismatch repair. DNA Repair (Amst) 105:103161
59. Reyes GX, Kolodziejczak A, Devakumar LJPS, Kubota T, Kolodner RD, Putnam CD et al. (2021) Ligation of newly replicated DNA controls the timing of DNA mismatch repair. Curr Biol 31:1268–1276.e6
60. Goellner EM, Smith CE, Campbell CS, Hombauer H, Desai A, Putnam CD et al.

(2014) PCNA and Msh2-Msh6 activate an Mlh1-Pms1 endonuclease pathway required for Exo1-independent mismatch repair. Mol Cell 55:291–304
61. Haye JE, Gammie AE (2015) The eukaryotic mismatch recognition complexes track with the replisome during DNA synthesis. PLoS Genet 11:e1005719
62. Kolodner RD, Marsischky GT (1999) Eukaryotic DNA mismatch repair. Curr Opin Genet Dev 9:89–96
63. Collingwood BW, Bhalkar AN, Manhart CM (2025) Mlh1-Pms1 couples ATP-driven DNA compaction with nick-dependent endonuclease activation. Nucleic Acids Res 53(22), gkaf1252.
64. Ortega J, Lee GS, Gu L, Yang W, Li G-M (2021) Mispair-bound human MutS-MutL complex triggers DNA incisions and activates mismatch repair. Cell Res 31:542–553
65. Desai A, Gerson S (2014) Exo1 independent DNA mismatch repair involves multiple compensatory nucleases. DNA Repair (Amst) 21:55–64
66. Kadyrova LY, Dahal BK, Gujar V, Daley JM, Sung P, Kadyrov FA (2022) The nuclease activity of DNA2 promotes exonuclease 1-independent mismatch repair. J Biol Chem 298:101831
67. Kratz K, Artola-Borán M, Kobayashi-Era S, Koh G, Oliveira G, Kobayashi S et al. (2021) FANCD2-associated nuclease 1 partially compensates for the lack of exonuclease 1 in mismatch repair. Mol Cell Biol 41:e0030321
68. Marti TM, Kunz C, Fleck O (2002) DNA mismatch repair and mutation avoidance pathways. J Cell Physiol 191:28–41
69. Takata M, Sasaki MS, Sonoda E, Morrison C, Hashimoto M, Utsumi H et al. (1998) Homologous recombination and non-homologous end-joining pathways of DNA double-strand break repair have overlapping roles in the maintenance of chromosomal integrity in vertebrate cells. EMBO J 17:5497–5508
70. Song B, Yang S, Hwang G-H, Yu J, Bae S (2021) Analysis of NHEJ-based DNA repair after CRISPR-mediated DNA cleavage. Int J Mol Sci 22(12), 6397.
71. Vogt A, He Y (2023) Structure and mechanism in non-homologous end joining. DNA Repair (Amst) 130:103547
72. Lees-Miller JP, Cobban A, Katsonis P, Bacolla A, Tsutakawa SE, Hammel M et al. (2021) Uncovering DNA-PKcs ancient phylogeny, unique sequence motifs and insights for human disease. Prog Biophys Mol Biol 163:87–108
73. Watanabe G, Lieber MR (2022) Dynamics of the Artemis and DNA-PKcs complex in the repair of double-strand breaks. J Mol Biol 434:167858
74. Graham TGW, Walter JC, Loparo JJ (2016) Two-stage synapsis of DNA ends during non-homologous end joining. Mol Cell 61:850–858
75. Kieffer SR, Lowndes NF (2022) Immediate-early, early, and late responses to DNA double stranded breaks. Front Genet 13:793884
76. Wang Y-L, Zhao W-W, Bai S-M, Feng L-L, Bie S-Y, Gong L et al. (2022) MRNIP condensates promote DNA double-strand break sensing and end resection. Nat Commun 13: 2638
77. Myler LR, Gallardo IF, Soniat MM, Deshpande RA, Gonzalez XB, Kim Y et al. (2017) Single-molecule imaging reveals how Mre11-Rad50-Nbs1 initiates DNA break repair. Mol Cell 67:891–898.e4
78. Fan Y, Kuybu F, Cui H, Lammens K, Chen J-X, Kugler M et al. (2025) Structural basis for DNA break sensing by human MRE11-RAD50-NBS1 and its regulation by telomeric factor TRF2. Nat Commun 16: 8320
79. Liu Y, Sung S, Kim Y, Li F, Gwon G, Jo A et al. (2016) ATP-dependent DNA binding, unwinding, and resection by the Mre11/Rad50 complex. EMBO J 35:743–758
80. Warren C, Pavletich NP (2022) Structure of the human ATM kinase and mechanism of Nbs1 binding. Elife 11, e74218.
81. Shibata A, Jeggo PA (2021) ATM's role in the repair of DNA double-strand breaks. Genes (Basel) 12(9), 1370.
82. Xie A, Puget N, Shim I, Odate S, Jarzyna I, Bassing CH et al. (2004) Control of sister chromatid recombination by histone H2AX. Mol Cell 16:1017–1025
83. Carusillo A, Mussolino C (2020) DNA damage: from threat to treatment. Cells 9(7), 1665.
84. Isono M, Niimi A, Oike T, Hagiwara Y, Sato H, Sekine R et al. (2017) BRCA1 directs the repair pathway to homologous recombination by promoting 53BP1 dephosphorylation. Cell Rep 18:520–532
85. Thorslund T, Ripplinger A, Hoffmann S, Wild T, Uckelmann M, Villumsen B et al. (2015) Histone H1 couples initiation and amplification of ubiquitin signalling after DNA damage. Nature 527:389–393
86. Doil C, Mailand N, Bekker-Jensen S, Menard P, Larsen DH, Pepperkok R et al. (2009) RNF168 binds and amplifies ubiquitin conjugates on damaged chromosomes to allow accumulation of repair proteins. Cell 136:435–446
87. Becker JR, Clifford G, Bonnet C, Groth A, Wilson MD, Chapman JR (2021) BARD1 reads H2A lysine 15 ubiquitination to direct homologous recombination. Nature 596:433–437
88. Nakamura K, Saredi G, Becker JR, Foster BM, Nguyen NV, Beyer TE et al. (2019) H4K20me0 recognition by BRCA1-BARD1 directs homologous recombination to sister chromatids. Nat Cell Biol 21:311–318
89. Salunkhe S, Daley JM, Kaur H, Tomimatsu N, Xue C, Raina VB et al. (2024) Promotion of DNA

end resection by BRCA1-BARD1 in homologous recombination. Nature 634:482–491
90. Wang Y, Coulombe Y, Yueh W-T, Conway GD, Milano L, Glass DJ et al. (2025) PALB2 and 53BP1 govern post-resection homologous recombination DNA repair. Mol Cell 85:2824–2838.e8
91. Appleby R, Bollschweiler D, Chirgadze DY, Joudeh L, Pellegrini L (2023) A metal ion-dependent mechanism of RAD51 nucleoprotein filament disassembly. IScience 26:106689
92. Li J, Sun H, Huang Y, Wang Y, Liu Y, Chen X (2019) Pathways and assays for DNA double-strand break repair by homologous recombination. Acta Biochim Biophys Sin (Shanghai) 51:879–889
93. Hu J, Crickard JB (2024) All who wander are not lost: the search for homology during homologous recombination. Biochem Soc Trans 52:367–377
94. Sebesta M, Burkovics P, Juhasz S, Zhang S, Szabo JE, Lee MYWT et al. (2013) Role of PCNA and TLS polymerases in D-loop extension during homologous recombination in humans. DNA Repair (Amst) 12:691–698
95. Seol J-H, Shim EY, Lee SE (2018) Microhomology-mediated end joining: good, bad and ugly. Mutat Res 809:81–87
96. Truong LN, Li Y, Shi LZ, Hwang PY-H, He J, Wang H et al. (2013) Microhomology-mediated end joining and homologous recombination share the initial end resection step to repair DNA double-strand breaks in mammalian cells. Proc Natl Acad Sci USA 110:7720–7725
97. Patterson-Fortin J, D'Andrea AD (2020) Exploiting the microhomology-mediated end-joining pathway in cancer therapy. Cancer Res 80:4593–4600
98. McVey M, Lee SE (2008) MMEJ repair of double-strand breaks (director's cut): deleted sequences and alternative endings. Trends Genet 24:529–538
99. Deng SK, Gibb B, de Almeida MJ, Greene EC, Symington LS (2014) RPA antagonizes microhomology-mediated repair of DNA double-strand breaks. Nat Struct Mol Biol 21:405–412
100. Li C, Zhu H, Jin S, Maksoud LM, Jain N, Sun J et al. (2023) Structural basis of DNA polymerase θ mediated DNA end joining. Nucleic Acids Res 51:463–474
101. Li Y, Returan M, Guerin AT, Averill AM, Oladapo D, Doublié S et al. (2025) Coordinated transfer of DNA between Pol θ and Pol δ resets microhomology choice during double-strand break repair. Proc Natl Acad Sci USA 122:e2513018122
102. Carvajal-Garcia J, Cho J-E, Carvajal-Garcia P, Feng W, Wood RD, Sekelsky J et al. (2020) Mechanistic basis for microhomology identification and genome scarring by polymerase theta. Proc Natl Acad Sci USA 117:8476–8485
103. Fijen C, Drogalis Beckham L, Terino D, Li Y, Ramsden DA, Wood RD et al. (2024) Sequential requirements for distinct Polθ domains during theta-mediated end joining. Mol Cell 84:1460–1474
104. Chatterjee S, Starrett GJ (2024) Microhomology-mediated repair machinery and its relationship with HPV-mediated oncogenesis. J Med Virol 96:e29674
105. Fleury H, MacEachern MK, Stiefel CM, Anand R, Sempeck C, Nebenfuehr B et al. (2023) The APE2 nuclease is essential for DNA double-strand break repair by microhomology-mediated end joining. Mol Cell 83:1429–1445.e8
106. Sfeir A, Symington LS (2015) Microhomology-mediated end joining: a back-up survival mechanism or dedicated pathway?. Trends Biochem Sci 40:701–714
107. Chang HHY, Pannunzio NR, Adachi N, Lieber MR (2017) Non-homologous DNA end joining and alternative pathways to double-strand break repair. Nat Rev Mol Cell Biol 18:495–506
108. Bhargava R, Onyango DO, Stark JM (2016) Regulation of single-strand annealing and its role in genome maintenance. Trends Genet 32:566–575

Open Access This chapter is licensed under the terms of the Creative Commons Attribution-NonCommercial-NoDerivatives 4.0 International License (http://creativecommons.org/licenses/by-nc-nd/4.0/), which permits any noncommercial use, sharing, distribution and reproduction in any medium or format, as long as you give appropriate credit to the original author(s) and the source, provide a link to the Creative Commons license and indicate if you modified the licensed material. You do not have permission under this license to share adapted material derived from this chapter or parts of it.

The images or other third party material in this chapter are included in the chapter's Creative Commons license, unless indicated otherwise in a credit line to the material. If material is not included in the chapter's Creative Commons license and your intended use is not permitted by statutory regulation or exceeds the permitted use, you will need to obtain permission directly from the copyright holder.





Chapter 3

Prime Editing: An Overview

Emilio M. García-Tenorio, Mar Alvarez, Eva Richard and Lourdes R. Desviat

Abstract

CRISPR tools are revolutionizing the landscape of genetic therapies, with the potential to cure a range of previously untreatable diseases. Among all the available genome editing technologies, prime editing is an especially versatile tool that enables precise genetic modifications, including point mutations, insertions, and deletions, without inducing double-strand breaks or requiring a donor DNA template. Through structural modifications and the development of novel systems with additional functionalities, prime editing has expanded its applicability with improved precision, efficacy, and safety. It is already being tested in clinical trials for chronic granulomatous disease, and many preclinical studies are underway. However, significant challenges remain for its broad applicability as a potential curative therapy for human genetic diseases, mainly related to ensuring efficient and safe delivery to target tissues.

Keywords Prime editing, pegRNA, CRISPR/Cas, Genome editing, Personalised medicine

1 Introduction

Gene-editing technologies based on CRISPR/Cas approaches have emerged as powerful tools, enabling precise genetic modifications at specific genomic loci, with potential therapeutic applications. These technologies have already entered the clinical phase, with one therapy (Casgevy) approved for the treatment of sickle cell disease and beta-thalassemia [1]. However, despite their success, approaches based on active Cas endonucleases have limitations, as they rely on inducing double-strand breaks (DSBs), which can be genotoxic, have unpredictable repair outcomes, and lead to off-target cleavage events. These drawbacks have prompted the development of second-generation gene editing modalities, which are more precise and safer, including base editors (BEs) and prime editors (PEs), that do not induce DSBs [2]. These repurposed CRISPR/Cas editors combine the binding activity of catalytically impaired Cas endonucleases with catalytic domains of DNA deaminases or reverse transcriptases (RT), respectively. Although BEs are powerful tools for

Duško Lainšček et al. (eds.), *CRISPR Delivery*, Methods in Molecular Biology, vol. 3075,
https://doi.org/10.1007/978-1-0716-5547-4_3,
© The Author(s) 2027

precise nucleotide conversions without the need for DNA cleavage, they remain restricted to specific base transitions. Moreover, the dependence of BEs on protospacer adjacent motif (PAM) requirements and a limited editing window (typically four to five nucleotides) restricts their targeting scope. Additionally, BEs often exhibit bystander editing, leading to unintended edits in adjacent nucleotides [3]. To overcome these limitations, David Liu's laboratory developed a more versatile and precise method for genome modification named prime editing (PE) [4].

PEs do not rely on DSBs or donor DNA templates and can introduce all types of DNA point mutations, small insertions, and deletions at target sites in the genome. PEs consist of an engineered RT fused with a modified Cas9 nickase (nCas9) and utilize a modified guide RNA called prime editing guide RNA (pegRNA) that possesses an additional 3′ extension containing a reverse transcription template (RTT), which encodes the desired sequence for editing, and a primer-binding site (PBS), complementary to the genomic target [5]. This innovative approach significantly reduces off-target and bystander editing and has enormous potential in the therapeutic landscape of human genetic diseases, as it can theoretically reverse >90% of all known pathogenic mutations and disease-associated genetic variants [6].

Efficient PE has been demonstrated in many cell types and in in vivo models of disease [6]. In vivo delivery is simplified by the fact that no exogenous DNA template is required. Additionally, off-target edits are minimized in PE as hybridization events with the spacer and the PBS encoded by the pegRNA are required for productive editing. Nevertheless, the editing efficiency of the first generation of PEs was relatively limited, underscoring the need for improvement. This was achieved in successive versions of the PE systems, mainly through: (i) incorporating an additional guide RNA that nicks the nonedited DNA strand to promote the use of the newly synthesized edited strand as template for repairing the nicked complementary strand [4], (ii) modifying the RT and Cas proteins enhancing thermostability, processivity and affinity [5], (iii) engineering the pegRNA to protect it from degradation [7], (iv) modulating DNA mismatch repair mechanisms [8], and (v) fusing the N-terminal domain of the La protein to the PE, to stabilize the pegRNA [9].

Still, there are significant challenges for clinical translation of PE. One major hurdle is the need for extensive and expensive optimization steps required before identifying a lead candidate PE drug. For in vivo studies, efficient and safe delivery of editing components to target tissues remains a limiting step, as with other genetic therapies. The size of most current PE systems is relatively large, which in effect hinders delivery. Consistent with this, PE systems have been engineered in split-intein configurations to deliver in dual AAV systems for in vivo applications [10–12]. More compact versions of the RT with a smaller size have been developed, making them more suitable

for delivery vectors with size limitations such as AAV [13]. Although PE as a therapeutic tool is still in its infancy, it has already entered the clinical trials phase for autosomal recessive p47^{phox}-deficient chronic granulomatous disease (CGD) (ClinicalTrials.gov number: NCT06559176). CGD is predominantly caused by a two-nucleotide deletion in exon 2 (delGT) of the *NCF1* gene, and a PE has been developed to correct this [14].

Overall, the preclinical and clinical data that will emerge in the following years will lay the foundation of PE applications as personalized medicine approaches to address human genetic diseases.

2 Mechanism of Action

The fundamental mechanism of all PEs consists of several main steps: (i) recognition of the spacer sequence adjacent to a PAM by the nCas enzyme and nicking of the DNA (ii) hybridization of the PBS sequence to the nicked strand, (iii) elongation of the reverse transcription (RT) template, and finally, (iv) incorporation of the generated sequence with the edit into the genome (Fig. 1) [4].

The process starts when the PE–pegRNA complex binds to the genomic target complementary to the spacer sequence, in the presence of a PAM. This allows for Cas enzyme, usually a H840A nickase, which only cleaves one strand of the DNA, to introduce a nick in the

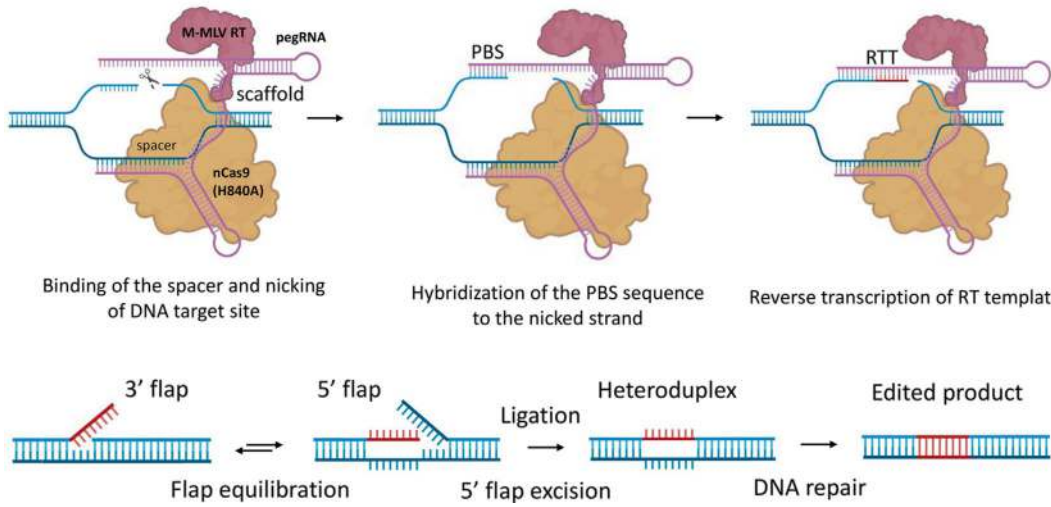


Fig. 1 Mechanism of action of PE. The prime editor complex binds to the target site via the pegRNA spacer sequence, allowing DNA nicking (top left). The single-strand overhang generated after the cut is annealed to the PBS (top center), creating a primer for reverse transcription of the RTT, which introduces the edition, shown in red (top right). Finally, the edited sequence is incorporated into the genome by a process of flap equilibration (bottom left), followed by 5′ flap excision and ligation (bottom center), and resolution of the heteroduplex by DNA repair mechanisms (bottom right)

strand containing the PAM sequence, usually located 3 bp upstream of this motif. At this point, the generated 3′ flap single-stranded DNA hybridizes to the PBS located at the 3′ end of the pegRNA, creating a primer for reverse transcription. This is then extended by the RT domain of the PE, using the RTT sequence in the pegRNA, therefore introducing the desired edit. As a result, the edited 3' flap enters a dynamic equilibrium, competing to hybridize with the original DNA sequence, thereby displacing the endogenous 5′ flap, which is excised by endonucleases. The remaining nick is then repaired by ligation, leaving a heteroduplex intermediate with one DNA strand carrying the edit, mismatched to the original sequence. Finally, the heteroduplex is resolved by cellular mismatch repair mechanisms (MMR), leading to either permanent incorporation or removal of the edit.

Some PE modalities, such as PE3, employ a second gRNA, also known as nicking guide RNA (ngRNA), to nick the nontarget strand. The purpose of this strategy is to bias the MMR system to use the edited strand as a template for correction, therefore increasing the efficiency of incorporation of the desired edit.

3 Versions of PEs

Following publication of the initial PE, known as PE1 [4], the toolbox of PE modalities has considerably expanded. To date, more than seven generations have been developed, all of them aiming to enhance particular aspects of PE outcomes, with the list continuing to expand. However, the naming system is perhaps unclear, since components of the different versions can usually be employed in combination, and there is a lack of standard nomenclature in these cases. In addition, many alternative architectures and gene constructs are being studied, with new modifications which, however, have not been formally cataloged as new generations. Moreover, some of the more sophisticated PE strategies can be grouped under new categories, such as PE-nucleases (PEn), bidirectional PE, and recombinase-based PE systems.

3.1 Generations of PEs

PE1, the first proof-of-concept for PE, employed a simple MMLV-RT coupled to nCas9 H840A nickase and a standard pegRNA. Nonetheless, its modest efficiency improved with the development of the PE2 editor, which introduced five mutations in the RT that improved its activity and stability, leading to a fivefold increase in editing efficiency. The same authors [4] further proposed a third approach (PE3), where an ngRNA is used to nick the non-edited strand upstream or downstream of the edit in order to bias the DNA repair system towards productive editing. A similar variant of this approach is PE3b, which uses an ngRNA that is complementary to

the edit, therefore only introducing the nick after the prime edit has been installed, effectively reducing indel formation.

PE4 and PE5 systems [8] also aim to increase editing efficiency and reduce the abundance of editing byproducts by transiently co-expressing a dominant negative variant of MLH1 protein, which inhibits the MMR system. In the case of the PE5 system, an ngRNA is employed as in PE3. This approach improved editing efficiency.

Phage-assisted protein evolution by PACE/PANCE, combined with rational engineering, has also allowed the creation of the PE6 suite of editors [13], featuring more compact RT variants (PE6a-c), and Cas9 with enhanced activities (PE6e-g).

Finally, the PE7 system has been developed by fusing the PE to the N-terminal domain of endogenous protein La, which binds to the 3′ polyuridinated end of the pegRNA, protecting it from degradation by exonucleases [9]. This strategy has effectively increased pegRNA stability and achieved a notable boost in editing efficiency, even for some of the more challenging cell types and gene targets.

In addition to the seven generations of editors, new modalities are still emerging to improve PE outcomes. Precise PE (pPE) uses an nCas9 with mutations that relax nick positioning, achieving a drastic reduction of indels with similar editing efficiencies. This performance was further improved by introducing additional mutations, leading to the development of extra-precise prime editing (xPE) and very-precise prime editing (vPE), which also includes La protein as in PE7, further increasing the edit: indel ratio [15]. Another strategy is PE with a prolonged editing window (proPE), where the pegRNA is replaced with a combination of an engRNA, responsible for nicking the DNA at the target site, and a non-cleaving tpgRNA, which binds to a nearby site through a truncated spacer and delivers the RTT-PBS extension sequence. As a result, editing outcomes are enhanced for target-distal and low-efficiency edits [16].

3.2 PE Architectures

In combination with all the strategies mentioned above, many genetic innovations have been attempted in order to optimize PE construct expression, protein activity, or stability. Some of these have aimed to increase protein nuclear localization, as in PE* by encoding additional NLS signal peptides [17]. This is also the case of PEmax, one of the most widely used versions up to date, whose features include a codon-optimized RT and additional Cas9 mutations for improved expression and activity [8]. Another editor known as improved PE (iPE), also explored removal of cryptic splice sites of the RT sequence, and fusion of the RT in both the N- and C-termini, in addition to the previous strategies. The same study also developed Exo-PE, a prime editor based on iPE, which introduces an aptamer into the pegRNA to recruit a co-expressed 5′ exonuclease. This complex favors the removal of the 5′ flap, therefore promoting edit integration [18].

Some other architectures employ fusion of the PE with auxiliary protein or domains to increase editor expression and activity, such as CMP-PE1-V [19], hyPE2 [20], or the IN-PE systems [21]. Another important point of architecture optimization is reducing the size of the editor, for instance, by using a truncated RT without the RNAseH domain [11]. Another main approach for size reduction has been the development of split PE, where the Cas enzyme and the RT are expressed from separate constructs, usually coupled to intein domains that allow reconstitution of the intact editor by protein trans-splicing. This facilitates in vivo delivery of PE systems in dual AAV vectors, circumventing their capacity limitation [12].

Additionally, different PAM-preference Cas variants have also been engineered to broaden the scope of possible target sites for PE [22].

3.3 PE-Nucleases

Recently, the use of PEs harnessing wild-type Cas9 nucleases has been proposed as a prominent alternative to increase the editing efficiency by leveraging diverse DSB repair pathways other than mismatch repair, which may reject the edit. PE-nucleases (PEn) have been described to boost desired editing outcomes in HeLa and K562 cells [23]. Nonetheless, they tend to incorporate tandem duplications of the template due to imprecise correction by NHEJ, an issue that has been compensated for by the use of DNA-PK inhibitors [24]. However, the ability of NHEJ to integrate a sequence at the DSB by an end-to-end joining mechanism has also been exploited to develop PRINS editing (PRImed INSertions strategy). Here, the PEn uses a springRNA where the template has no homology sequence, promoting small insertions by NHEJ with up to 50% efficiency [24].

3.4 Bidirectional PE

Compared to conventional PE, bidirectional PE systems are based on dual pegRNAs, which target and edit complementary strands, with the purpose of increasing the efficiency and the range of possible modifications (insertions, deletions, sequence replacement). In the case of twin PE, both pegRNAs encode for both strands of the same heterologous sequence, leading to the synthesis of complementary DNA flaps that overlap and anneal to each other [25]. The same principle applies to other related strategies: in PRIME-Del, both pegRNAs incorporate a sequence at the end of the DNA flap that is homologous to the sequence downstream of the opposite spacer, which improves deletion efficiency [26]. On the other hand, in GRAND editing, the DNA flaps generated on both sides are only partially complementary and overlap on a short sequence. This provides a primer for gap filling in both directions, using the ssDNA segments as a template. As a result, the size of potential insertions is increased up to 250 bp [27].

Additionally, Bi-WT–PE systems feature a wild-type Cas9 nuclease instead of a nickase, which allows for versatile and large-scale

genomic editing [28]. This is the case of PEDAR, analogous to twin PE but inducing DSBs, which leads to long sequence deletions, up to 10 kb between both target sites [29].

3.5 Recombinase-Based PE Systems

Even with bidirectional PE methods, the introduction of large sequences, such as complete exons or gene coding sequences, remains challenging. This has encouraged the development of systems that combine PE with site-specific recombinases to address this purpose.

One of the first approaches, known as prime-editing-assisted site-specific integrase gene editing (PASSIGE), features a two-step mechanism, where twin PE is first used to introduce an *attB* site into the desired genomic location, which will be used by site-specific recombinase Bxb1 to insert a donor sequence, provided by a plasmid that also includes the *attP* site. This has allowed for integration of plasmids over 5 kb, and it has also been applied for targeted genomic inversions with over 50% editing efficiency [25].

On the other hand, the PASTE strategy (programmable addition via site-specific targeting elements), uses a single pegRNA (atgRNA) to install the *attB* site, assisted by a ngRNA, enabling recombination by Bxb, which is fused to the PE. With a single delivery, PASTE has achieved integration of up to 36 kb DNA cargo and has been successfully tested for in vivo gene integration in the liver by adenoviral vectors [30].

4 pegRNA Design Strategies and Improvements

Selection of the pegRNA sequence is a crucial step of PE optimization. It involves a series of careful considerations when designing the spacer, RTT, and PBS sequences, as well as structural modifications.

First, regarding the spacer sequence, the use of a 5′ terminal guanine (G) is beneficial for pegRNA expression, as it promotes transcription initiation by RNA polymerase III [5]. In order to avoid secondary structure formation by annealing of the spacer with the PBS, another approach is to design several mismatches within the spacer (mpegRNA), therefore reducing the complementarity. This leads to an increase in efficiency in parallel with a reduction of indels, as a result of preventing prolonged retrotranscription activity [31]. Second, PBS optimal length ranges between 10 and 15 nts, although it is variable for each locus, with an average GC content in the 40%–60% interval [4]. With respect to the RTT, it is recommended to keep it at a short length, with the edit no further than 30 nucleotides of the DNA nick, as using longer RTTs tends to impair the editing outcome [4]. A minimal right homology arm (RHA) length of five to ten nucleotides is also convenient [32]. In addition, one of the most common strategies to improve pegRNA design is the addition of same-sense bystander mutations to the RTT

(spegRNA), which improve editing efficiency as they bypass repair of the edit by the MMR system [8].

In order to assist with pegRNA design, different software tools have been developed, such as PRIDICT [33], based on a predictive model trained by deep learning, which scores all the possible pegRNAs for a given site and edition. However, predictive algorithms currently lack translatability, as the in silico results often do not correlate with the experimental outcomes for different cell types.

Aside from sequence design, many strategies have been attempted to improve pegRNA by altering its secondary structure, mainly that of the 3′ end. This is the case of engineered pegRNAs (epegRNAs), where a structured RNA motif (evopreQ1, tevopreQ1, mpknot, tmpknot) is added to the 3′ terminus in order to protect it from degradation by exonucleases [7]. Another strategy is the incorporation of aptamers, which can be coupled to the pegRNA to favor interaction with other helper protein domains [34].

5 Therapeutic Applications

5.1 Preclinical Studies

Preclinical PE studies span diverse organ systems and translational routes, from blood and immune disorders to retinal, skin, neuromuscular, and liver-directed metabolic diseases, and they also cover a broad range of experimental contexts, including immortalized cell lines, patient-derived primary cells, organoids or tissue explants, and in vivo animal models. Importantly, editing efficiency is not directly comparable across diseases because readouts differ (DNA-level correction vs protein restoration vs functional rescue) and, in some situations, particularly liver disease, corrected cells can expand over time, so apparent efficacy may be partly shaped by selection and repopulation. The selected examples shown below are grouped by study type (in vitro, in vivo, and ex vivo). The details of studies addressing different diseases using PE approaches are summarized in Table 1.

5.1.1 In Vitro Studies

Duchenne muscular dystrophy. In Δex51 models, PE enabled partial restoration of dystrophin-related readouts and improved disease-relevant phenotypes [46]. PE has also been applied to other variants, with moderate on-target editing reported depending on the sequence context and design [47].

Spinal muscular atrophy. A PE-based strategy has been developed to delete an intronic splicing silencer, promoting inclusion of exon 7 in SMN2 and restoring SMN expression. The effect was demonstrated in iPSCs and in iPSC-derived motor neurons [48].

Alzheimer's disease. PE has been used in human cells to install both a protective APP variant and a pathogenic variant, with marked sequence-dependent differences in editing efficiency [49].

Table 1
Preclinical PE studies

Indication (gene, mutation)	Preclinical model and outcomes				PE system and delivery method	References
	In vitro (cell lines)		Ex vivo (primary/ patient cells)	In vivo (local/ systemic)		
Leber congenital amaurosis (LCA) (*Rpe65*, p.R44X)				✓ **M**	PE2 (AAV, subretinal injection)	[35]
Retinitis pigmentosa (RP) (*RHO*, p.P23H, p.V345L, p.P347L; *Pde6b*, p.Y347X)			✓ **M**	✓ **H**	PE (dual-AAV subretinal injection; *RHO* and *Pde6b*)	[36]
Phenylketonuria (PKU) (*PAH*, c.1222 C>T; *Pah* p.F263S)	✓ **H**			✓ **H**	PE2 (plasmid; AAV; dual-AAV8; AdV)	[10, 11]
Tyrosinemia type 1 (TT1) (*Fah*)			✓ **L**	✓ **H**	PE3 (hydrodynamic injection; ex vivo + transplant)	[35, 37]
Alpha-1 antitrypsin deficiency (AATD) (*SERPINA1*, p.E342K)	✓**M(HEK)**	✓**L(hPSCs)**		✓ **M**	PE2, PE2* (plasmid)/PE2 (dual-AAV8)	[17]
Sickle cell disease (SCD) (*HBB*, p.E6V)	✓ **H**		✓ **H**		PE3 (RNP electroporation)/ PE3, PE3b (plasmid)	[38]
X-linked Severe combined immunodeficiency (SCID) (*IL2RG*, c.458 T>C)	✓ **H**		✓ **H**		PE2 (mRNA/pegRNA electroporation)	[39]
Cystic fibrosis (CF) (*CFTR*, p.F508del and 3 bp deletion)	✓ **H**		✓ **H**		PE6 (RNA electroporation)	[40]

Table 1 (continued)

Indication (gene, mutation)	Preclinical model and outcomes				PE system and delivery method	References
	In vitro (cell lines)		Ex vivo (primary/ patient cells)	In vivo (local/ systemic)		
Recessive dystrophic epidermolysis bullosa (RDEB) (*COL7A1*, c.3631 C> T/c.2005C>T)			✓ **M**		PE2 (plasmid)	[41]
β-thalassemia (*HBB*, IVS-II-654)	✓ **H**				PE3 (plasmid; mRNA; pegRNA; zygote microinjection)	[42]
Tay-Sachs disease (*HEXA*, 1278+ TATC insertion)	✓ **H**				PE3 (rabbit embryo microinjection)/PE3b (plasmid)	[43]
Cataract disorder (*Crygc*, G-del in exon 3)	✓ **H**				PE3 (plasmid)/PE3 (mouse embryo microinjection)	[44]
Oculocutaneous albinism (*Tyr*, p.P302L)	✓ **H**				PE2 (RNP)	[45]
Duchenne muscular dystrophy DMD) (*DMD*, ΔEx51)	✓ **H**		✓ **H**		PE2 (plasmid)	[46,47]
Spinal muscular atrophy (SMA) (*SMN2*, exon 7 inclusion)	✓**M (HEK)**	✓**H (iPSCs)**			PE2 (plasmid)	[48]
Alzheimer´s disease (AD) (*APP*, p.A673T and p.V717I)	✓ **H**				PE2/PE3 (plasmid)	[49]

✓ Evidence reported in this setting **H** High ≥20% editing or strong functional rescue **M** Medium: 5%–20% editing **L** Low <5% editing

5.1.2 Ex Vivo and In Vivo Studies

Ex vivo editing is currently one of the most practical translational routes for PE, as it allows controlled delivery, standardized processing, and extensive characterization of the edited product before administration. This approach has been applied for sickle cell disease [38], X-linked Severe Combined Immunodeficiency [39], cystic fibrosis [40], and recessive dystrophic epidermolysis bullosa [41].

In vivo, outcomes depend on whether an effective delivery route can be matched to the relevant target tissue. Local administration offers greater experimental control and is most advanced in anatomically accessible, compartmentalized tissues such as the eye, where subretinal or intravitreal administration enables high local exposure and sensitive functional readouts. Preclinical studies have been reported in inherited retinal diseases, correcting pathogenic variants in Leber congenital amaurosis [35] and retinitis pigmentosa [36].

Systemic in vivo delivery remains constrained by tissue targeting and safety considerations, with most advanced studies having the liver as the primary target. Liver-directed PE is especially appealing for recessive metabolic diseases because even partial hepatocyte correction can translate into measurable biochemical benefit. Consistent with this, several preclinical studies have evaluated PE in monogenic disorders targeting the liver, such as phenylketonuria [10], tyrosinemia type 1 [35], or alpha-1 antitrypsin deficiency [17].

5.2 Clinical Trials

Clinical translation of PE is still in its early stages. To date, the most mature clinical evidence comes from ex vivo autologous hematopoietic stem and progenitor cell (HSPC) editing, where manufacturing control and extensive product testing are feasible. In parallel, liver-directed in vivo programs are advancing through lead optimization and IND/CTA-enabling development (Investigational New Drug application [IND]/Clinical Trial Application [CTA]), toward first-in-human evaluation, driven by the need for scalable, tissue-selective delivery. The programs below illustrate these two leading translational tracks.

Chronic Granulomatous Disease (CGD): PM359 (Prime-0101; NCT06559176) is the first PE-based therapy to report first-in-human clinical data. It targets autosomal-recessive $p47^{phox}$ deficiency-associated CGD (p47-CGD), caused by *NCF1* mutations affecting the NADPH oxidase complex and leading to severe, recurrent infections and inflammatory complications. The most common pathogenic variant is the two-nucleotide deletion (delGT) in exon 2, reported to be present in ~80% of individuals with p47-CGD, a subtype estimated to represent ~25% of CGD cases. PM359 is an autologous CD34+ HSPC therapy: patient cells are edited ex vivo with PE to correct delGT, followed by reinfusion after busulfan myeloablative conditioning. The initial results support a favorable early genomic safety profile [14].

Wilson disease (WD) is an autosomal recessive disorder caused by ATP7B mutations, leading to toxic copper accumulation (primarily in the liver and also in the brain), and potentially resulting in liver failure or progressive neurological disease without transplantation. Prime Medicine has described a liver-directed prime editing program using GalNAc-LNPs to deliver PE components for precise correction of common *ATP7B* mutations, indicating that correction in a meaningful fraction of hepatocytes could be potentially disease-modifying or curative. At present, this program remains preclinical; company guidance targets IND/CTA submission in the first half of 2026 to enable a Phase 1 study, with initial clinical data expected in 2027.

6 Challenges

CRISPR/Cas technologies are anticipated to become essential tools for the treatment and management of a wide range of diseases. However, broader in vivo application still requires further work to improve editing efficiency, specificity, and safety, as well as to optimize delivery strategies and refine the spatial and structural configuration of CRISPR-Cas systems.

6.1 Efficiency, Specificity, and Safety

Despite notable progress in PE, achieving consistently high levels of efficiency and specificity across diverse cell types, tissues, and organisms remains a major challenge. In vivo PE efficiencies often remain substantially lower than those achieved in vitro or with other genome-editing platforms. Although optimized systems have demonstrated remarkably high efficiencies, overall, PE performance is often inconsistent and frequently falls below desired levels.

PE efficiency is highly influenced by the genomic target, the nature of the intended genetic modification, and the cellular context, highlighting the need for continued optimization to ensure robust and reproducible outcomes. Notably, PE outcomes are strongly influenced by cellular DNA repair context. Transient inhibition of MMR (PE4/PE5 systems) can markedly increase PE efficiencies and improve edit-to-indel ratios in MMR-proficient cells [8]. However, this dependence on repair pathway modulation highlights a translational challenge: gains in efficiency may be context-dependent and may require careful evaluation of genome-wide fidelity and long-term safety when manipulating repair processes.

With respect to specificity and safety, key barriers include minimizing off-target activity, unintended mutations, and broader genotoxicity. PE is generally more precise than conventional CRISPR-Cas9 nuclease editing and is often described as resistant to bystander editing and as having reduced off-target activity. Nevertheless, measurable off-target events have been reported in some settings. These events may alter gene expression, disrupt gene function, or contribute

to genomic rearrangements, underlining the importance of comprehensive safety profiling, especially for clinical translation [50].

Mechanistic studies also show that PE can generate characteristic byproducts in some contexts, including pegRNA scaffold-derived insertions consistent with reverse transcriptase readthrough or template switching, and larger on-target deletions or tandem duplication-like insertions arising from mis-joining of edited DNA intermediates, underscoring the need for systematic long-read and genome-wide safety assessment and continued editor/pegRNA engineering [8,15].

Another important safety consideration is immunogenicity. Pre-existing adaptive immune responses against bacterially derived Cas9 proteins have been documented in humans. In particular, commonly used Cas9 orthologs, such as Streptococcus pyogenes Cas9 (SpCas9) and Staphylococcus aureus Cas9 (SaCas9), may elicit immune responses [51]. These findings highlight the need to evaluate the immunological implications of PE components and to develop strategies that minimize inflammation and immune activation in therapeutic applications [12].

A major obstacle for PE is the development of efficient, tissue-appropriate, and scalable delivery systems. Considerable efforts are therefore focused on optimizing both viral platforms, particularly AAVs, and nonviral approaches such as lipid nanoparticles (LNPs) and virus-like particle-based systems.

6.2 Delivery Strategies

A major obstacle for PE is the development of efficient, tissue-appropriate, and scalable delivery systems. Considerable efforts are therefore focused on optimizing both viral platforms, particularly AAVs, and nonviral approaches such as lipid nanoparticles (LNPs) and virus-like particle-based systems.

The large size of the PE machinery poses substantial challenges for intracellular delivery. Widely used AAV vectors have a limited packaging capacity (~4.7 kb), making it difficult to package a complete PE system within a single vector. This constraint has driven the development of dual-AAV strategies, in which the editor is split across two vectors and reconstituted in target cells, although this can reduce overall efficiency and introduce variability in reassembly [52]. In parallel, efforts to identify and engineer smaller RNA-guided endonucleases, including TnpB and IscB, aim to enable more compact editing systems that may ultimately simplify delivery [52–54].

Beyond size limitations, AAV-based delivery raises additional translational concerns. Prolonged expression of the editor can increase the likelihood of cytolytic immune responses, expand the window for off-target effects, and carry potential risks associated with vector persistence or integration. It can also limit redosing if corrective editing is incomplete. In contrast, LNP-based delivery avoids persistent expression but still faces challenges, including

efficient synthesis and encapsulation of long PE mRNAs, constraints in nuclear delivery, dose-dependent toxicity, and potential innate immune activation [10].

Alternative delivery modalities capable of accommodating large cargoes have also been explored. Notably, helper-dependent adenoviral (HDAd) vectors offer a large packaging capacity (~37 kb) and have been reported to efficiently deliver PE5max into human cells [40,55].

Overall, improved delivery strategies remain essential for the clinical translation of PE, and while nonviral systems are highly promising, further optimization is still required to enhance tissue specificity, delivery efficiency, and cargo stability.

7 Conclusions

Preclinical studies show that prime editing can correct molecular defects and improve functional outcomes across a range of monogenic disease models. However, clinical translation will largely depend on whether an effective delivery route can be matched to the relevant target tissue. Local administration and ex vivo workflows offer greater experimental control and the opportunity for extensive product characterization, whereas systemic in vivo delivery can achieve meaningful efficacy but remains constrained by tissue targeting and safety considerations. Together, these findings underline the need for continued advances in delivery platforms and editor engineering. As PE continues to evolve, its clinical applications will require further innovation in improved editor, advanced delivery technologies, and streamlined regulatory frameworks to unlock its full potential.

Acknowledgments

The publication is based upon work by COST Action CA21113: Genome Editing for the Treatment of Human Diseases (https://www.genehumdi.eu), supported by European Cooperation in Science and Technology (COST). E.M.G.-T. holds a fellowship from the FPU program (grant FPU22/03244). The group is funded by the Spanish Ministry of Science and Innovation and the European Regional Development Fund (grant PID2022-137238OB-I00 to L.R.D. and E.R.) and Fundación Ramón Areces (XXII Concurso Nacional para la adjudicación de Ayudas a la Investigación en Ciencias de la Vida y de la Materia, grant to L.R.D.). Centro de Biología Molecular Severo Ochoa receives an institutional grant from Fundación Ramón Areces and is a Severo Ochoa Center of Excellence (MICIU/AEI, Award CEX2021-001154-S). Figure created with Biorender.

Competing Interests The authors declare no competing interests.

References

1. Singh A, Irfan H, Fatima E et al. (2024) Revolutionary breakthrough: FDA approves CASGEVY, the first CRISPR/Cas9 gene therapy for sickle cell disease. Ann Med Surg (Lond) 86:4555–4559
2. Anzalone AV, Koblan LW, Liu DR (2020) Genome editing with CRISPR-Cas nucleases, base editors, transposases and prime editors. Nat Biotechnol 38:824–844
3. Rees HA, Liu DR (2018) Base editing: precision chemistry on the genome and transcriptome of living cells. Nat Rev Genet 19:770–788
4. Anzalone AV, Randolph PB, Davis JR et al. (2019) Search-and-replace genome editing without double-strand breaks or donor DNA. Nature 576:149–157
5. Doman JL, Sousa AA, Randolph PB et al. (2022) Designing and executing prime editing experiments in mammalian cells. Nat Protoc 17:2431–2468
6. Brooks IR, Graham C, Kazemizadeh A, Jacków-Malinowska J (2025) Prime editing in mammals: From promise to practicalities. Mol Ther Nucleic Acids 36:102719
7. Nelson JW, Randolph PB, Shen SP et al. (2022) Engineered pegRNAs improve prime editing efficiency. Nat Biotechnol 40:402–410
8. Chen PJ, Hussmann JA, Yan J et al. (2021) Enhanced prime editing systems by manipulating cellular determinants of editing outcomes. Cell 184:5635–5652.e29
9. Yan J, Oyler-Castrillo P, Ravisankar P et al. (2024) Improving prime editing with an endogenous small RNA-binding protein. Nature 628:639–647
10. Brooks DL, Whittaker MN, Qu P et al (2023) Efficient in vivo prime editing corrects the most frequent phenylketonuria variant, associated with high unmet medical need. Am J Hum Genet S0002-9297(23)00358–0
11. Böck D, Rothgangl T, Villiger L et al. (2022) In vivo prime editing of a metabolic liver disease in mice. Sci Transl Med 14:eabl9238
12. Davis JR, Banskota S, Levy JM et al. (2024) Efficient prime editing in mouse brain, liver and heart with dual AAVs. Nat Biotechnol 42:253–264
13. Doman JL, Pandey S, Neugebauer ME et al. (2023) Phage-assisted evolution and protein engineering yield compact, efficient prime editors. Cell 186:3983–4002.e26
14. Gori JL, Haddad E, Frangoul H, et al. (2025) Prime editing for p47phox-deficient chronic granulomatous disease. N Engl J Med 394(12):1195–1203.
15. Chauhan VP, Sharp PA, Langer R (2025) Engineered prime editors with minimal genomic errors. Nature 646:1254–1260
16. Krausz SL, Simon DA, Bartos Z et al. (2025) ProPE expands the prime editing window and enhances gene editing efficiency where prime editing is inefficient. Nat Catal 8:1100–1116
17. Liu P, Liang S-Q, Zheng C et al. (2021) Improved prime editors enable pathogenic allele correction and cancer modelling in adult mice. Nat Commun 12: 2121
18. Truong D-JJ, Geilenkeuser J, Wendel SV et al. (2024) Exonuclease-enhanced prime editors. Nat Methods 21:455–464
19. Park S-J, Jeong TY, Shin SK et al. (2021) Targeted mutagenesis in mouse cells and embryos using an enhanced prime editor. Genome Biol 22: 170
20. Song M, Lim JM, Min S et al. (2021) Generation of a more efficient prime editor 2 by addition of the Rad51 DNA-binding domain. Nat Commun 12: 5617
21. Velimirovic M, Zanetti LC, Shen MW et al. (2022) Peptide fusion improves prime editing efficiency. Nat Commun 13: 3512
22. Kweon J, Yoon J-K, Jang A-H et al. (2021) Engineered prime editors with PAM flexibility. Mol Ther 29:2001–2007
23. Adikusuma F, Lushington C, Arudkumar J et al. (2021) Optimized nickase- and nuclease-based prime editing in human and mouse cells. Nucleic Acids Res 49:10785–10795
24. Peterka M, Akrap N, Li S et al. (2022) Harnessing DSB repair to promote efficient homology-dependent and -independent prime editing. Nat Commun 13: 1240
25. Anzalone AV, Gao XD, Podracky CJ et al. (2022) Programmable deletion, replacement, integration and inversion of large DNA sequences with twin prime editing. Nat Biotechnol 40:731–740
26. Choi J, Chen W, Suiter CC et al. (2022) Precise genomic deletions using paired prime editing. Nat Biotechnol 40:218–226
27. Wang J, He Z, Wang G et al. (2022) Efficient targeted insertion of large DNA fragments without DNA donors. Nat Methods 19:331–340
28. Tao R, Wang Y, Hu Y et al. (2022) WT-PE: prime editing with nuclease wild-type Cas9 enables versatile large-scale genome editing. Signal Transduct Target Ther 7:108
29. Jiang T, Zhang X-O, Weng Z, Xue W (2022) Deletion and replacement of long genomic sequences using prime editing. Nat Biotechnol 40:227–234
30. Yarnall MTN, Ioannidi EI, Schmitt-Ulms C et al. (2023) Drag-and-drop genome insertion of large sequences without double-strand DNA cleavage using CRISPR-directed integrases. Nat Biotechnol 41:500–512

31. Fei J, Zhao D, Pang C et al. (2025) Mismatch prime editing gRNA increased efficiency and reduced indels. Nat Commun 16: 139
32. Yu G, Kim HK, Park J et al. (2023) Prediction of efficiencies for diverse prime editing systems in multiple cell types. Cell 186:2256–2272.e23
33. Mathis N, Allam A, Kissling L et al. (2023) Predicting prime editing efficiency and product purity by deep learning. Nat Biotechnol 41:1151–1159
34. Chen R, Cao Y, Liu Y et al. (2023) Enhancement of a prime editing system via optimal recruitment of the pioneer transcription factor P65. Nat Commun 14: 257
35. Jang H, Jo DH, Cho CS et al. (2022) Application of prime editing to the correction of mutations and phenotypes in adult mice with liver and eye diseases. Nat Biomed Eng 6:181–194
36. Fu Y, He X, Ma L et al. (2025) In vivo prime editing rescues photoreceptor degeneration in nonsense mutant retinitis pigmentosa. Nat Commun 16: 2394
37. Kim Y, Hong S-A, Yu J et al. (2021) Adenine base editing and prime editing of chemically derived hepatic progenitors rescue genetic liver disease. Cell Stem Cell 28:1614–1624. e5
38. Everette KA, Newby GA, Levine RM et al. (2023) Ex vivo prime editing of patient haematopoietic stem cells rescues sickle-cell disease phenotypes after engraftment in mice. Nat Biomed Eng 7:616–628
39. Hou Y, Ureña-Bailén G, Mohammadian Gol T et al. (2022) Challenges in gene therapy for somatic reverted mosaicism in X-linked combined immunodeficiency by CRISPR/Cas9 and prime editing. Genes (Basel) 13:2348
40. Sousa AA, Hemez C, Lei L et al. (2025) Systematic optimization of prime editing for the efficient functional correction of CFTR F508del in human airway epithelial cells. Nat Biomed Eng 9:7–21
41. Hong S-A, Kim S-E, Lee A-Y et al. (2022) Therapeutic base editing and prime editing of COL7A1 mutations in recessive dystrophic epidermolysis bullosa. Mol Ther 30:2664–2679
42. Zhang H, Sun R, Fei J et al. (2022) Correction of Beta-Thalassemia IVS-II-654 Mutation in a Mouse Model Using Prime Editing. Int J Mol Sci 23:5948
43. Qian Y, Zhao D, Sui T et al. (2021) Efficient and precise generation of Tay-Sachs disease model in rabbit by prime editing system. Cell Discov 7:50
44. Lin J, Liu X, Lu Z et al. (2021) Modeling a cataract disorder in mice with prime editing. Mol Ther Nucleic Acids 25:494–501
45. Petri K, Zhang W, Ma J et al. (2022) CRISPR prime editing with ribonucleoprotein complexes in zebrafish and primary human cells. Nat Biotechnol 40:189–193
46. Chemello F, Chai AC, Li H et al. (2021) Precise correction of Duchenne muscular dystrophy exon deletion mutations by base and prime editing. Sci Adv 7:eabg4910
47. Happi Mbakam C, Rousseau J, Tremblay G et al. (2022) Prime editing permits the introduction of specific mutations in the gene responsible for Duchenne muscular dystrophy. Int J Mol Sci 23:6160
48. Zhou M, Tang S, Duan N et al. (2022) Targeted-deletion of a tiny sequence via prime editing to restore SMN expression. Int J Mol Sci 23:7941
49. Tremblay G, Rousseau J, Mbakam CH, Tremblay JP (2022) Insertion of the icelandic mutation (A673T) by prime editing: a potential preventive treatment for familial and sporadic Alzheimer's disease. CRISPR J 5:109–122
50. Liang S-Q, Liu P, Ponnienselvan K et al. (2023) Genome-wide profiling of prime editor off-target sites in vitro and in vivo using PE-tag. Nat Methods 20:898–907
51. Hyeon H, Hwang S, Luo Y et al. (2025) CRISPR-Cas technologies: emerging tools from research to clinical application. J Microbiol 63:e2504012
52. Lee J, Kweon J, Kim Y (2025) Emerging trends in prime editing for precision genome editing. Exp Mol Med 57:1381–1391
53. Karvelis T, Druteika G, Bigelyte G et al. (2021) Transposon-associated TnpB is a programmable RNA-guided DNA endonuclease. Nature 599:692–696
54. Altae-Tran H, Kannan S, Demircioglu FE et al. (2021) The widespread IS200/IS605 transposon family encodes diverse programmable RNA-guided endonucleases. Science 374:57–65
55. Li C, Georgakopoulou A, Newby GA et al. (2023) In vivo HSC prime editing rescues sickle cell disease in a mouse model. Blood 141:2085–2099

Open Access This chapter is licensed under the terms of the Creative Commons Attribution-NonCommercial-NoDerivatives 4.0 International License (http://creativecommons.org/licenses/by-nc-nd/4.0/), which permits any noncommercial use, sharing, distribution and reproduction in any medium or format, as long as you give appropriate credit to the original author(s) and the source, provide a link to the Creative Commons license and indicate if you modified the licensed material. You do not have permission under this license to share adapted material derived from this chapter or parts of it.

The images or other third party material in this chapter are included in the chapter's Creative Commons license, unless indicated otherwise in a credit line to the material. If material is not included in the chapter's Creative Commons license and your intended use is not permitted by statutory regulation or exceeds the permitted use, you will need to obtain permission directly from the copyright holder.





Chapter 4

Base Editing: Mechanisms and Therapeutic Applications

Fabio Catalano

Abstract

Base editing enables the direct, programmable conversion of one nucleotide into another at a defined genomic site without introducing a double-strand break. First reported in 2016, a decade later, it has expanded into a broad family of molecular tools that has now entered clinical trials. This chapter reviews the development of base editing from its origins, including the early transition of cytosine and adenine base editors, to the more recent emergence of transversion editors. For each class, this section describes the mechanism, the optimization of on-target efficiency, product purity, and specificity, as well as the key strengths and limitations. The following discussion focuses on delivery, which remains one of the central bottlenecks for clinical translation, with particular attention to lipid nanoparticles, engineered virus-like particles, and other emerging strategies. Finally, a review of the current clinical landscape is presented. This already includes the first ex vivo multiplex base-edited cell therapy in T-cell leukemia, ex vivo hematopoietic stem cell transplantation targeting hemoglobin disorders, the first systemic in vivo base editing in humans, and, importantly, the first personalized N-of-1 in vivo base-editing therapy, which was developed within a remarkably short time. These developments show that base editing has moved from a proof-of-concept to a clinically-ready platform with incredible speed, and that the central questions for the field, perhaps, concern the pace at which the surrounding technology, for example delivery, can keep up with base editors themselves.

Keywords Base editing, Cytosine base editing, Adenine base editing, Mitochondrial DNA editing, Lipid nanoparticles, Virus-like particles, Gene therapy

1 Introduction

The idea that human genetic diseases might one day be treated by directly correcting the underlying DNA mutation was first formally articulated by Friedmann and Roblin in 1972 [1]. At the time, scientists had only recently begun to learn how to modify mammalian cells using naturally occurring viruses, and progress toward any clinical use was premature at best. Knowledge of vector biodistribution, toxicity, and long-term safety was scarce [2, 3]. And yet, driven by a mixture of enthusiasm and a regulatory landscape that had not yet caught up with the science, the field moved quickly into the clinic, perhaps more quickly than it should have [2]. In 1990, the first approved

Duško Lainšček et al. (eds.), *CRISPR Delivery*, Methods in Molecular Biology, vol. 3075,
https://doi.org/10.1007/978-1-0716-5547-4_4,
© The Author(s) 2027

gene therapy trial was carried out in a 4-year-old girl named Ashanthi De Silva, who had adenosine deaminase deficiency, a form of severe combined immunodeficiency [4, 5]. She is widely remembered as the first patient to receive an approved gene therapy and as an early proof that the approach could, in principle, work [5]. As Wolff and Lederberg wrote in 1994, scientists felt on the verge of a revolution [2]. What followed, however, revealed that more work was needed before gene therapy could meet the standards of safety and scientific rigor required for human use. Subsequent trials often showed limited efficacy, significant toxicity, or both [6, 7]. The death of Jesse Gelsinger in 1999 after adenoviral gene transfer marked a turning point, making clear that the field needed to return to the drawing board [6, 8]. Today, more than 30 years after that first gene therapy trial, we are also living a new gene therapy revolution, this time driven by new molecular tools that enable DNA changes with unprecedented precision. One of the most promising of these tools is base editing. Base editing, a new variant of the CRISPR/Cas system, enables the direct, programmable conversion of one nucleotide into another at a defined genomic site without introducing a double-strand break [9]. It is arguably one of the most precise genome-editing approaches currently available, and one of the most promising for therapeutic use [10]. The past few years have already produced a remarkable set of clinical firsts: the first patient treated with an ex vivo base-edited cell therapy (2022) [11], the first patient treated with base editing in vivo (2022) [12], and the first infant treated with a personalized in vivo base-editing approach (2025) [13]. This chapter discusses the path that led to base editing, describes its mechanisms and main variants, and reviews the current clinical landscape and the challenges that remain.

2 Cytosine Base Editors

The first base editor systems were the cytosine base editor BE1, BE2, and BE3, introduced by Komor et al. [9]. These systems were built by fusing catalytically inactive Cas9 (dCas9), or Cas9 nickase, to APOBEC1 (apolipoprotein B mRNA editing enzyme catalytic polypeptide 1), a cytidine deaminase. APOBEC1 naturally mediates C-to-U editing in the apoB mRNA, converting a CAA codon into a UAA stop codon and thereby generating the shorter apoB48 isoform [14, 15]. Komor and colleagues reasoned that this chemistry could be applied to the single-stranded DNA that is normally exposed when Cas9 binds its target sequence [9]. The first cytosine base editor they presented, **BE1**, showed conversion of **C-to-T** and proved that this simple and elegant idea could, in principle, work. However, this first architecture had some major limitations. Uracil in DNA is efficiently recognized by the uracil DNA glycosylase (UNG) enzyme,

which hydrolyzes the N-glycosidic bond between the base and the deoxyribose, thereby creating an abasic site [9, 10]. This can reduce editing efficiency and contributes to undesired by-products, including reversion toward the original C:G base pair. In short, competition between BE1 edit and UNG-mediated repair limits the overall editing efficiency. To address this, the same authors developed **BE2**. In this version, a uracil glycosylase inhibitor (UGI) is fused to BE1 to locally inhibit UNG activity and increase editing efficiency [9]. The next version, **BE3**, substantially increased efficiency by replacing the dCas9 with a Cas9 nickase (Fig. 1). This introduces a single-strand nick in the non-edited strand that directs cellular mismatch repair to recognize the nicked strand as "damaged," and to use the opposite, uracil-containing strand as a template for repair, resulting in a more efficient incorporation of the desired edit [9, 10]. The creative work of Komor and colleagues established a completely new paradigm in genome editing, with obvious implications for gene therapy. Follow-up work focused on refining and expanding the concept that a molecular effector able to chemically modify a specific base could be used to change the genetic information. In the context of CBEs, from BE3 onwards, development split into three parallel tracks.

The first track was improving efficiency and reducing by-products. To improve editing efficiency, the first efforts focused on further stabilizing the uracil intermediate. In 2017, Komor and colleagues introduced **BE4** and **SaBE4**, by adding a second UGI domain in tandem, and refining the linker architecture to better protect the uracil intermediate (Fig. 1). These versions had an improved editing efficiency and lower rate of by-products compared to BE3 [16]. Next, in 2018, Koblan and colleagues observed that editing efficiency could be enhanced by increasing the expression of the editor. This was achieved through codon optimization and improved nuclear localization signals. The resulting version, **BE4max**, showed a substantial increase in efficacy [17]. The same authors also replaced the deaminase with an *ancestrally reconstructed* APOBEC1 homolog, generating **AncBE4max**, which further improved editing performance at many loci in mammalian cells (Fig. 1) [17].

The second track tackled the fact that BE3 acts across a window of several nucleotides. This problem manifests when multiple cytosines are present in the editing window, and can result in the installation of bystander substitutions together with the intended edit. In 2017, Kim and colleagues hypothesized that the broad editing window of BE3 was caused by the high activity of APOBEC1, and tested whether variants with reduced activity could result in more precise editing [18]. They introduced mutations into APOBEC1 at residues predicted to affect either its catalytic activity or substrate binding, obtaining variants that retained useful deamination activity, while showing a substantial reduction in bystander activity. An example is the **YE1–BE3** variant [18].

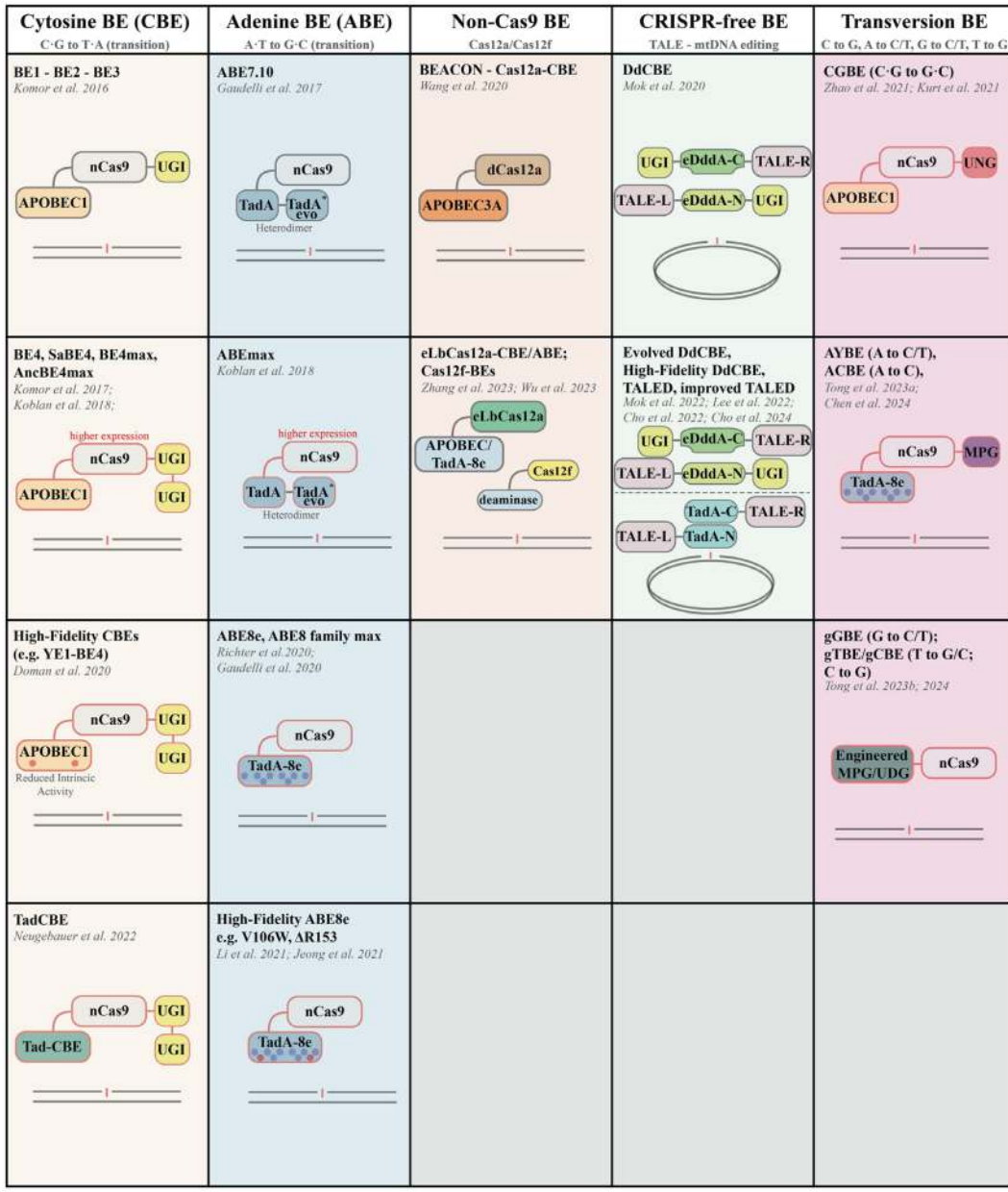


Fig. 1 Overview of the main base editor classes and representative stages of development. Columns group editors by class: cytosine base editors (CBEs), adenine base editors (ABEs), non-Cas9 base editors, CRISPR-free base editors, and transversion base editors. Within each column, entries are arranged as representative successive developments within that editor class. Schematics show the principal architectural components of each editor, including the DNA-targeting module (nCas9, dCas12a/eLbCas12a, Cas12f, or paired TALEs), the catalytic module (for example, APOBEC1, APOBEC3A, TadA/TadA-8e, Tad-CBE, split DddA halves, or engineered glycosylase-related components). Linear DNA schematics denote nuclear DNA; the circular DNA schematic in the CRISPR-free BE column denotes mitochondrial DNA (mtDNA)

The third track of development was safety. Some cytosine base editors, particularly those based on APOBEC1, could induce unwanted deamination events outside the intended target site, both on DNA and RNA targets [19]. In 2020, Doman, Raguram, Newby, and Liu showed that this type of unwanted editing was largely driven by the intrinsic ability of the deaminase to act on exposed single-stranded DNA outside the intended Cas9 target [20]. Based on this, they compared editor variants with reduced intrinsic deaminase activity for their capacity to minimize unguided off-target deamination. They found several variants, for example, the **YE1–BE4**, that displayed background-level Cas9-independent DNA and RNA deamination in human cells while retaining useful on-target activity (Fig. 1) [20].

The developments described so far were all based on improving the original architecture described by Komor and colleagues in 2016. But by this stage, the field had shifted to a basic architecture driven by work on adenine base editors that had already begun in the meantime. Adenine base editors were built using an engineered TadA, an enzyme that naturally catalyzes adenosine deamination in tRNA in *E. coli*, and that was evolved to act on single-stranded DNA in mammalian cells [21]. TadA-derived adenosine base editors were smaller and generally showed lower unguided off-target activity compared to APOBEC1-derived cytosine base editors [10, 21]. Therefore, scientists wonder whether TadA could be engineered to mediate cytosine deamination instead of adenine, retaining its small size and precision. Neugebauer and colleagues tested this exact hypothesis using phage-assisted continuous evolution to reengineer the highly active adenine deaminase TadA-8e so that it could efficiently deaminate cytidine [22]. The resulting TadA-derived cytosine base editors (**TadCBEs**) matched or exceeded BE4max in on-target activity across nine endogenous sites in HEK293T cells, while Cas-independent off-target DNA editing was markedly reduced and RNA off-target editing was undetectable [22]. Whether TadCBEs will displace APOBEC1-based editors in clinical contexts remains unclear, but they currently offer a particularly attractive combination of size, activity, and specificity.

3 Adenine Base Editors

The cytosine base editors described so far can only install C-to-T transitions. Following the same logic established by Komor and colleagues in 2016, Gaudelli and colleagues introduced adenine base editors (ABEs) in 2017 to address **A-to-G** transitions (Fig. 1) [21]. Because no naturally occurring enzyme was known to deaminate adenine in DNA, Gaudelli and colleagues evolved TadA, an enzyme from *E. coli* that normally deaminates adenine in tRNA, to act on the single-stranded DNA exposed during the Cas9 binding to

DNA [21, 23]. The resulting editors culminated in **ABE7.10**, which was built by fusing Cas9 nickase to a heterodimeric deamination unit composed of wild-type TadA fused to an evolved TadA* [21]. This heterodimer design reflected the native TadA homodimer, and conferred better DNA editing activity than constructs built from evolved subunits alone (Fig. 1). Its mechanism of action involves conversion of adenine to inosine, which is interpreted as guanine by DNA polymerases and repair machinery, leading to an A-to-G transition. Crucially, inosine in DNA is removed much less efficiently than uracil, which meant that the first generation of ABEs already showed high product purity and very low indel formation [10, 21].

After the introduction of ABE7.10, subsequent development followed a logic partially similar to that of CBE development. In 2018, Koblan and colleagues showed that expression was also a major bottleneck for adenine base editing and developed **ABEmax** through codon optimization, improved nuclear localization signals, and optimization of the deaminase component, substantially increasing editing efficiency in mammalian cells (Fig. 1) [17].

A second increase in activity was reported in 2020 from two independent groups simultaneously. Richter and colleagues used phage-assisted evolution to generate TadA-8e, a hyperactive adenine base editor carrying eight additional mutations, which was incorporated into **ABE8e** as a monomer, and showed a 590-fold higher apparent deamination rate compared to ABE7.10 (Fig. 1) [24]. In parallel, Gaudelli and colleagues used a library of evolved TadA variants to generate the broader ABE8 family, consisting of 20 evolved TadA variants, tested in both heterodimeric (ABE8.1-20-d) and monodimeric (ABE8.1-20-m) configurations [25]. Together, these developments yielded a new generation of ABEs with substantially higher activity across the editing window, including at positions that had previously been edited less efficiently.

Two further problems were addressed in 2021. First, it became clear that ABEs were not entirely chemically specific, as, in some contexts, low-level cytosine deamination had been reported at the target site [26]. Jeong and colleagues showed that a D108Q substitution in TadA7.10 reduced this unwanted cytosine editing activity by about tenfold while preserving useful adenine editing [26]. Additionally, like CBEs, the field had realized that ABEs could induce guide-independent RNA deamination at the transcriptome level [27]. Li and colleagues addressed this through structure-guided engineering and developed ABE variants with minimized RNA off-targeting activity [28]. Their work identified residues involved in RNA recognition, including R153, and showed that deletion of R153 or disruption of TadA–RNA interactions could substantially reduce unwanted RNA editing while maintaining useful DNA on-target activity (Fig. 1) [28]. Similarly, although early ABE variants showed low levels of guide-independent genomic DNA deamination, later work indicated that

some highly evolved ABEs, particularly ABE8e editors, can display guide-independent DNA off-target activity [24, 25, 29]. To tackle this, higher-fidelity derivatives were developed, such as the V106W variant, which displays reduced DNA and RNA off-target activity (Fig. 1) [24, 25, 29].

Overall, the current state of the art consists of high-fidelity ABE8-derived editors, with modifications that reduce both DNA and RNA off-target activity while retaining the high on-target efficiency that distinguishes ABE8e from earlier variants.

4 Cytosine Base Editing Versus Adenine Base Editing

Comparing cytosine and adenine base editors is not straightforward, in part because these editors have continued to evolve over the years and direct comparison studies are limited. Nevertheless, some differences have remained generally consistent. In mouse embryos, Lee and colleagues compared ABE7.10 with a panel of CBE variants from BE2 to BE4. ABE7.10 was notably precise, as it almost exclusively generated the expected A-to-G transition. The CBEs, by contrast, produced a higher burden of bystander edits, proximal off-target changes, and other unanticipated products, even in their more advanced forms. Among these, SaBE3 and BE4 performed the best [30]. A follow-up study from the same group, using identical guide RNAs for both editor types, extended this to whole-genome sequencing. Consistent with the earlier study, they found that BE4, but not ABE7.10, generated elevated de novo single-nucleotide variants genome-wide [31]. These first side-by-side comparisons showed that CBEs carry a higher off-target DNA burden than ABEs at comparable on-target activity. This result has been reproduced in various contexts since. For example, Fiumara and colleagues compared CBEs and ABEs in primary T cells and $CD34^+$ hematopoietic stem and progenitor cells [32]. They found that ABE8.20-m generally outperformed BE4max in both efficiency and precision. At the B2M gene and nearly all additional loci tested, ABE8.20-m was more efficient and more precise at the target site. Importantly, both editors produced some genotoxic by-products, but these were more evident for BE4max compared to ABE8.20-m [32]. A complementary comparison by Tálas and colleagues further showed that increased-fidelity Cas9 variants that display a reduced mismatch tolerance could reduce off-targeting more effectively when incorporated into ABE and ABE8e scaffolds than into CBE scaffolds, suggesting that ABEs are generally easier to make highly selective [33]. Overall, these comparisons indicate that CBEs currently rely on a more challenging and less controllable chemistry than ABEs, and suggest that ABEs should be favored over CBEs whenever a choice exists.

5 Transversion Base Editors

Both CBE and ABE eventually resolve into the desired edit through a transition, that is, a change between chemically similar bases (pyrimidine to pyrimidine, or purine to purine) [9, 21, 29]. Together, these chemistries cover a large fraction of known pathogenic point mutations, but not all of them. To account for this, base editing-mediated transversions (pyrimidine to purine, or vice versa) have been described.

Zhao et al. [34] and, independently, Kurt and colleagues [35] showed that the uracil intermediate produced during cytosine base editing could be redirected toward a **C-to-G** transversion using C-to-G base editors (**CGBE**; Fig. 1). The architecture of these editors consisted of a cytidine deaminase fused to a Cas9 nickase and an UNG enzyme [34, 35]—the exact same enzyme that had to be inhibited during CBE editing to retain the uracil intermediate. The rationale was that, during CGBEs, uracil excision is promoted by the UNG enzyme, creating an abasic site. The subsequent processing of this site through endogenous lesion-tolerance and repair pathways biases its resolution towards the desired C:G-to-G:C outcome. The exact downstream repair route is still not fully resolved, but these studies established the basic principle that glycosylase-mediated generation of an abasic site can ultimately resolve in transversion events [34, 35]. Later work introduced a series of CGBEs with distinct editing profiles that improved efficiency and product purity when matched to the target sequence [36]. The same work also showed that the outcome of CGBE editing depends strongly on the repair context, with the same editor performing differently depending on the target sequence and on how the cell handles the abasic intermediate [36].

A similar logic of using glycosylase-mediated transversion was then extended to adenine editing. Tong and colleagues developed **AYBE** by fusing ABE8e to N-methylpurine DNA glycosylase (MPG), so that the inosine intermediate produced by adenine deamination is excised rather than read as guanine, as happens with standard ABEs (Fig. 1) [37]. This reroutes repair toward **A-to-C** and **A-to-T** transversions. Chen and colleagues later reported a related system using an evolved mAAG glycosylase, giving rise to the **ACBE** class of editors for **A-to-C** editing (Fig. 1) [38]. More recently, the same group that developed AYBE showed that MPG could be engineered to act directly on unmodified guanine in DNA, but without any deaminase component [39]. The resulting glycosylase-based guanine base editor (**gGBE**), consisting of an engineered MPG fused to Cas9 nickase, enabled G-to-C and G-to-T transversion editing. In parallel, engineered uracil–DNA glycosylase variants, again without a deaminase, were shown to support programmable **T-to-G** and **T-to-C**, as well as **C-to-G** editing in mammalian cells (**gTBE/gCBE**; Fig. 1) [40].

Taken together, these developments expand the possible base-conversion outcomes, but they are still at an early stage

compared with transition editors. Unlike CBEs and ABEs, which usually converge on a single predictable product, glycosylase-dependent transversion editors tend to generate mixtures of intended edits, by-products, and indels because the abasic intermediate can be processed by several competing repair pathways, which can differ depending on the target cell [34, 35, 37–39]. For this reason, these systems are still less reliable than classical transition editors.

6 Non-Cas9 Base Editing

The extension of programmable base editing beyond the Cas9 scaffold started mainly with the goal of expanding the editable sequence space, which can be limited by PAM availability. The first major non-Cas9 base editors in mammalian cells were built on catalytically impaired Cas12a, which recognizes T-rich PAMs. One example of Cas12a-derived cytosine base editors was reported in 2020 with the BEACON architecture, which fused dCas12a to an engineered APOBEC3A deaminase, and achieved C-to-T editing with low DNA damage response and minimal RNA off-target activity (Fig. 1) [41]. This was followed in 2022 by improved Cas12a-derived CBEs and ABEs that combined highly active deaminases with engineered LbCas12a variants, enabling both cytosine and adenine editing at expanded T-rich PAM sites (Fig. 1) [42]. These developments were also relevant for multiplex base editing, as Cas12a can process guide arrays and is therefore more naturally suited to multiplex editing than Cas9-derived systems [42]. In parallel, hypercompact Cas12f-derived base editors also emerged, motivated in part by the cargo limitations of common delivery systems such as adeno-associated virus (AAV) vectors (Fig. 1) [43, 44]. Taken together, non-Cas9 base editors expand target accessibility, facilitate multiplex editing, and may offer advantages in settings such as AAV-based delivery, where Cas9-derived editors are limited.

7 CRISPR-Free Base Editing

Not all base editing problems are accessible to CRISPR/Cas technology. Mitochondrial DNA editing is the clearest example, as guide RNAs cannot be efficiently imported into mitochondria, which rules out CRISPR-based approaches [45]. For years, this left mtDNA essentially unreachable by precise base editing, until CRISPR-free base editors were developed [45].

The first such development was the double-stranded DNA deaminase A (DddA)-derived cytosine base editor, or **DdCBE**, introduced in 2020 (Fig. 1) [45]. DddA differs from the deaminases described so far in that it acts on double-stranded DNA rather than single-stranded

DNA [45, 46]. In DdCBE, split halves of DddA are fused to two programmable transcription activator-like effector (TALE) DNA-binding proteins, along with a UGI, enabling **C-to-T** editing [45]. This architecture has been subsequently refined. Evolved DddA variants reported in 2022 improved activity and, importantly, relaxed the strong sequence-context preferences of the original DdCBE [47]. Additionally, high-fidelity DdCBEs described in 2023 substantially reduced the unguided DNA deamination, without sacrificing on-target efficiency (Fig. 1) [48].

In parallel, non-Cas9 *adenine editing*, **TALED**, was introduced in 2022 and enabled the first targeted **A-to-G** editing in human mitochondrial DNA [49]. Early versions, however, induced extensive transcriptome-wide RNA off-target editing, a problem that was even more pronounced than that seen with TadA-based ABEs 9 (Fig. 1) [50]. Engineered variants reported in 2024 reduced these RNA off-target events by more than 99% and also addressed the cytotoxicity seen with original TALED constructs [50]. Direct comparisons with CRISPR-derived base editors are still limited, partly because CRISPR-free systems were largely developed for mitochondrial targets. What is clear is that TALE-based architectures broaden the possible therapeutic targets, so far most notably in mitochondrial DNA.

8 Delivery of (Base) Editors

While base editors themselves have advanced rapidly, getting a functional base editor into the right cell type remains a challenge for many clinical targets.

Delivery is especially limiting for base editing because these are relatively large fusion proteins that are difficult to package and deliver efficiently in vivo [51]. In particular, the size of many base editor systems exceeds the cargo capacity of AAV, one of the most common delivery platforms, often forcing the use of split-intein or dual-AAV strategies that can reduce efficiency and complicate manufacturing [51]. At the same time, persistent expression from DNA-based viral delivery is not ideal for base editors, because prolonged editor exposure may increase the risk of bystander and off-target deamination [10, 52]. For this reason, transient delivery approaches such as lipid nanoparticles (LNPs) carrying base editor mRNA and guide RNA, or virus-like particles delivering ribonucleoproteins, are especially attractive for base editing and have already shown effective delivery in vivo [52].

Besides these well-established technologies and limitations, it is useful to consider where the field is going next. While split-intein dual-AAV and LNP–mRNA strategies have brought the technology in vivo to the clinic, both have limitations that become obvious for extrahepatic tissues. The great majority of Mendelian diseases that could in principle be corrected by base editing also affect tissues other than the liver, such as muscle, lung, brain, retina, and heart. In this

context, the most tangible progress has come from reengineering LNPs themselves. One example is the Selective ORgan Targeting, or SORT, strategy [53]. This showed that adding a specific lipid component to standard LNP formulations could systematically redirect delivery toward the lung, spleen, or other target organs following intravenous administration [53]. This concept has now been demonstrated directly for base editing: dual SORT LNPs have been used to deliver base editors simultaneously to liver and lung, achieving approximately 40% correction in liver cells and 10% in lung AT2 cells in a disease mouse model [54]. The clinical translation of SORT LNP technology is already underway with trials RCT1100 and RCT2100, both consisting of inhaled mRNA therapies formulated using the SORT LNP platform. For RCT1100, a study for primary ciliary dyskinesia, the first patient was dosed in January 2024, while for RCT2100, a study for cystic fibrosis, the first patients were dosed in September 2024. A complementary, but still preclinical approach, peptide-encoded organ-selective targeting (POST), uses specific amino acid sequences on the LNP surface to redirect systemic delivery to extrahepatic organs [55].

Complementary to these LNP innovations, a different class of delivery vehicle has also emerged. Engineered virus-like particles (eVLPs) are protein-based nanoparticles that can package and deliver base editor ribonucleoproteins transiently, without introducing any DNA into the cell [56]. The Liu lab, which developed many of the base editors described in this chapter, has also been systematically evolving eVLPs, and fifth-generation eVLPs now show a twofold to fourfold increase in mammalian cell delivery potency compared to their immediate predecessors, achieved through directed evolution of the capsid rather than rational design [56]. The transient nature of eVLP delivery is especially appealing for base editing: because the edit itself is permanent, there is no need for sustained editor expression, and transience directly reduces the window for off-target activity and immune recognition [56]. Related to this are extracellular vesicles (EVs), cell-derived lipid-bilayer nanoparticles that are inherently biocompatible, can be engineered to carry gene editing cargo, and, crucially, have been shown to cross biological barriers, including the blood–brain barrier [57].

Overall, the delivery problem for base editing, or editing in general, is now being tackled with the same systematic creativity that has characterized the evolution of the editors themselves. Therefore, the next major advances in base editing will likely also come from solving how to deliver these tools precisely to the cells that need them.

9 Clinical Landscape

Base editing has rapidly moved to the clinic since its first appearance a decade ago. To date, it has marked a series of clinical landmarks that helped shape the clinical trajectory of the entire gene editing field.

9.1 Ex Vivo *Editing for Cell Therapy*

The first published clinical application of base editing was ex vivo cytosine base editing in relapsed or refractory T-cell acute lymphoblastic leukemia. In 2023, Chiesa and colleagues reported the first clinical use of multiplex base-edited allogeneic anti-CD7 CAR T cells, termed BE-CAR7, in three children with relapsed T-cell acute lymphoblastic leukemia [11]. These cells were made from healthy-donor T cells and base-edited at three separate loci: CD7 was disrupted to prevent fratricide, the endogenous T-cell receptor was disrupted to reduce graft-versus-host disease, and CD52 was disrupted to make the cells compatible with lymphodepleting therapy [11]. This made the study both the first report of base editing in humans and the first use of multiplex base editing to generate an allogeneic cell therapy product [11]. For some of these patients, who had exhausted other options, the approach could induce rapid remissions. The first patient achieved molecular remission within 28 days, and another showed morphologic and molecular remission with no evidence of CNS disease at the same time point [11]. This study showed for the first time that base editing could be used effectively to address a therapeutic problem in humans.

Another application of ex vivo base editing comes from autologous hematopoietic stem cell programs targeting hemoglobin disorders. Gupta and colleagues recently reported base editing of the HBG1/HBG2 promoters, specifically the BCL11A binding motif, to reactivate fetal hemoglobin in sickle cell disease [58]. In this trial, the primary endpoint, freedom from severe vaso-occlusive crises for 12 consecutive months, was met in the evaluable cohort. Shortly afterward, Lai and colleagues reported a phase 1 trial of five patients with transfusion-dependent β-thalassemia treated with base editing on autologous $CD34^+$ cells [59]. All five patients became independent from red blood cell transfusions. Together, these studies strongly support the therapeutic potential of base editing for ex vivo cell therapies.

9.2 *Systemic* In Vivo *Delivery*

The first proof of concept for in vivo use of base editing in humans comes from interim report data from VERVE-101, an adenine base editor delivered systemically as a lipid nanoparticle to inactivate PCSK9 in adults with heterozygous familial hypercholesterolemia and advanced atherosclerotic cardiovascular disease [12]. In early dose cohorts, treated patients showed substantial PCSK9 and LDL-cholesterol reductions. Patients also experienced infusion-related reactions and transient elevations in liver transaminases [12]. Overall, VERVE-101 has so far shown that systemic in vivo base editing is feasible in humans and could produce therapeutic benefits.

9.3 *Personalized* In Vivo *Therapy*

Another clinical first came in 2025, when Musunuru and colleagues described the treatment of an infant with severe carbamoyl-phosphate synthetase 1 deficiency using a bespoke lipid nanoparticle formulation carrying a patient-specific adenine base editor [13]. This was the first published N-of-1 in vivo base-editing therapy, and represented a landmark achievement for the whole gene editing field.

Importantly, the patient-specific base editing strategy was designed, manufactured, safety-tested, and delivered within months of the diagnosis being made [13]. After two infusions at approximately seven and eight months of age, dietary protein tolerance improved, and nitrogen-scavenger medication could be halved without serious adverse events. Despite the promise of these early outcomes, the follow-up was too short to draw general safety, efficacy, and durability conclusions, as reported by the authors of the study. Even so, this early report showed that for a patient with no other real option, personalized in vivo base editing is feasible to develop and deliver rapidly [13]. Future studies will expand this intermediate landmark to answer questions such as whether this personalized model is scalable in cost and manufacturing, and whether the regulatory framework will develop as fast as the science to facilitate these approaches.

10 Conclusions

Across cancer, metabolic diseases, hemoglobinopathies, and cardiovascular diseases, neurological disorders, base editing has now shown clinical feasibility, whether ex vivo or in vivo, in children or adults, in a variety of trials and applications, and with development times that can support personalized precision gene therapies. That is a remarkable body of evidence, accumulated in just about a decade. In short, the question for the next phase of base editing developments is not whether this technology is therapeutically feasible. Rather, the key questions are whether this technology can be safely expanded to all types of point mutations and whether it can be delivered efficiently and precisely to the relevant cells and tissues. In other words, assuming that transversion base editing will develop as fast as transition base editing, and assuming that long-term safety will stay consistent with early reports, progress will depend on whether the surrounding technologies, particularly those required for efficient and precise delivery, can develop at the same pace as base editing.

Acknowledgments

The publication is based upon work by COST Action CA21113: Genome Editing for the Treatment of Human Diseases (https://www.genehumdi.eu), supported by European Cooperation in Science and Technology (COST). F.C. is supported by Metakids (grant No. 2024-110), the United for Metabolic Disorders Catalyst Grant (grant No. 2024-CG-003), and the Society for Inborn Errors of Metabolism in the Dutch-speaking area (Vereniging tot bevordering van onderzoek naar Erfelijke Stofwisselingsziekten in het Nederlandse taalgebied).

Competing Interests The author declares no competing interests.

References

1. Friedmann T, Roblin R (1972) Gene therapy for human genetic disease?. Science 175(4025):949–955
2. Wolff JA, Lederberg J (1994) An early history of gene transfer and therapy. Hum Gene Ther 5(4):469–480
3. Friedmann T (1992) A brief history of gene therapy. Nat Genet 2(2):93–98
4. Onodera M, Nelson DM, Sakiyama Y et al. (1999) Gene therapy for severe combined immunodeficiency caused by adenosine deaminase deficiency: improved retroviral vectors for clinical trials. Acta Haematol 101(2):89–96
5. Blaese RM, Culver KW, Miller AD et al. (1995) T lymphocyte-directed gene therapy for ADA-SCID: initial trial results after 4 years. Science 270(5235):475–480
6. Thomas CE, Ehrhardt A, Kay MA (2003) Progress and problems with the use of viral vectors for gene therapy. Nat Rev Genet 4(5):346–358
7. Branca MA (2005) Gene therapy: cursed or inching towards credibility?. Nat Biotechnol 23(5):519–521
8. Lehrman S (1999) Virus treatment questioned after gene therapy death. Nature 401(6753):517–518
9. Komor AC, Kim YB, Packer MS et al. (2016) Programmable editing of a target base in genomic DNA without double-stranded DNA cleavage. Nature 533:7603
10. Rees HA, Liu DR (2018) Base editing: precision chemistry on the genome and transcriptome of living cells. Nat Rev Genet 19(12):770–788
11. Chiesa R, Georgiadis C, Syed F et al. (2023) Base-edited CAR7 T cells for relapsed T-cell acute lymphoblastic leukemia. N Engl J Med 389(10):899–910
12. Tual-Chalot S, Stellos K (2024) First-in-human gene editing for lipid lowering: the initial results. Cardiovasc Res 120(4):e5
13. Musunuru K, Grandinette SA, Wang X et al. (2025) Patient-specific in vivo gene editing to treat a rare genetic disease. N Engl J Med 392(22):2235–2243
14. Lau PP, Zhu HJ, Baldini A et al. (1994) Dimeric structure of a human apolipoprotein B mRNA editing protein and cloning and chromosomal localization of its gene. Proc Natl Acad Sci USA 91(18):8522–8526
15. Chan L, Chang BHJ, Nakamuta M et al (1997) Apobec-1 and apolipoprotein B mRNA editing. Biochim Biophys Acta 1345(1):11–26
16. Komor AC, Zhao KT, Packer MS, et al (2017) Improved base excision repair inhibition and bacteriophage Mu Gam protein yields C:G-to-T:A base editors with higher efficiency and product purity. Sci Adv 3(8), eaao4774.
17. Koblan LW, Doman JL, Wilson C et al. (2018) Improving cytidine and adenine base editors by expression optimization and ancestral reconstruction. Nat Biotechnol 36(9):843–848
18. Kim YB, Komor AC, Levy JM et al. (2017) Increasing the genome-targeting scope and precision of base editing with engineered Cas9-cytidine deaminase fusions. Nat Biotechnol 35(4):371–376
19. Yu Y, Leete TC, Born DA et al. (2020) Cytosine base editors with minimized unguided DNA and RNA off-target events and high on-target activity. Nat Commun 11(1):2052
20. Doman JL, Raguram A, Newby GA et al. (2020) Evaluation and minimization of Cas9-independent off-target DNA editing by cytosine base editors. Nat Biotechnol 38(5):620–628
21. Gaudelli NM, Komor AC, Rees HA et al. (2017) Programmable base editing of T to G C in genomic DNA without DNA cleavage. Nature 551(7681):464–471
22. Neugebauer ME, Hsu A, Arbab M et al. (2022) Evolution of an adenine base editor into a small, efficient cytosine base editor with low off-target activity. Nat Biotechnol 41(5):673–685
23. Wolf J, Gerber AP, Keller W (2002) tadA, an essential tRNA-specific adenosine deaminase from Escherichia coli. EMBO J 21(14):3841–3851
24. Richter MF, Zhao KT, Eton E et al. (2020) Phage-assisted evolution of an adenine base editor with improved Cas domain compatibility and activity. Nat Biotechnol 38(7):883–891
25. Gaudelli NM, Lam DK, Rees HA et al. (2020) Directed evolution of adenine base editors with increased activity and therapeutic application. Nat Biotechnol 38(7):892–900
26. Jeong YK, Lee SH, Hwang GH et al. (2021) Adenine base editor engineering reduces editing of bystander cytosines. Nat Biotechnol 39(11):1426–1433
27. Grünewald J, Zhou R, Garcia SP et al. (2019) Transcriptome-wide off-target RNA editing induced by CRISPR-guided DNA base editors. Nature 569(7756):433–437
28. Li J, Yu W, Huang S et al. (2021) Structure-guided engineering of adenine base editor with minimized RNA off-targeting activity. Nat Commun 12(1):2287
29. Rees HA, Wilson C, Doman JL, et al. (2019) Analysis and minimization of cellular RNA editing by DNA adenine base editors. Sci Adv 5(5), eaax5717.
30. Lee HK, Willi M, Miller SM, et al. (2018) Targeting fidelity of adenine and cytosine base editors in mouse embryos. Nat Commun 9(1):4804.
31. Lee HK, Smith HE, Liu C et al. (2020) Cytosine base editor 4 but not adenine base

editor generates off-target mutations in mouse embryos. Commun Biol 3(1):19
32. Fiumara M, Ferrari S, Omer-Javed A et al. (2023) Genotoxic effects of base and prime editing in human hematopoietic stem cells. Nat Biotechnol 42(6):877–891
33. Tálas A, Simon DA, Kulcsár PI, et al. (2021) BEAR reveals that increased fidelity variants can successfully reduce the mismatch tolerance of adenine but not cytosine base editors. Nat Commun 12(1):6353.
34. Zhao D, Li J, Li S et al. (2020) Glycosylase base editors enable C-to-A and C-to-G base changes. Nat Biotechnol 39(1):35–40
35. Kurt IC, Zhou R, Iyer S et al. (2021) CRISPR C-to-G base editors for inducing targeted DNA transversions in human cells. Nat Biotechnol 39(1):41–46
36. Koblan LW, Arbab M, Shen MW et al. (2021) Efficient C G-to-G C base editors developed using CRISPRi screens, target-library analysis, and machine learning. Nat Biotechnol 39(11):1414–1425
37. Tong H, Wang X, Liu Y et al. (2023) Programmable A-to-Y base editing by fusing an adenine base editor with an N-methylpurine DNA glycosylase. Nat Biotechnol 41(8):1080–1084
38. Chen L, Hong M, Luan C et al. (2024) Adenine transversion editors enable precise, efficient A• T-to-C•G base editing in mammalian cells and embryos. Nat Biotechnol 42(4):638–650
39. Tong H, Liu N, Wei Y, et al. (2023) Programmable deaminase-free base editors for G-to-Y conversion by engineered glycosylase. Natl Sci Rev 10(8), nwad143.
40. Tong H, Wang H, Wang X et al. (2024) Development of deaminase-free T-to-S base editor and C-to-G base editor by engineered human uracil DNA glycosylase. Nat Commun 15(1):4897
41. Wang X, Ding C, Yu W, et al. (2020) Cas12a base editors induce efficient and specific editing with low DNA damage response. Cell Rep 31(9), 107723.
42. Chen F, Lian M, Ma B, et al. (2022) Multiplexed base editing through Cas12a variant-mediated cytosine and adenine base editors. Commun Biol 5(1):1163.
43. Zhang S, Song L, Yuan B et al. (2023) TadA reprogramming to generate potent miniature base editors with high precision. Nat Commun 14(1):413
44. Wu T, Liu C, Zou S et al. (2023) An engineered hypercompact CRISPR-Cas12f system with boosted gene-editing activity. Nat Chem Biol 19(11):1384–1393
45. Mok BY, de Moraes MH, Zeng J et al. (2020) A bacterial cytidine deaminase toxin enables CRISPR-free mitochondrial base editing. Nature 583(7817):631
46. Yin L, Shi K, Aihara H (2023) Structural basis of sequence-specific cytosine deamination by double-stranded DNA deaminase toxin DddA. Nat Struct Mol Biol 30(8):1153–1159
47. Mok BY, Kotrys AV, Raguram A et al. (2022) CRISPR-free base editors with enhanced activity and expanded targeting scope in mitochondrial and nuclear DNA. Nat Biotechnol 40(9):1378–1387
48. Lee S, Lee H, Baek G et al. (2022) Precision mitochondrial DNA editing with high-fidelity DddA-derived base editors. Nat Biotechnol 41(3):378–386
49. Cho SI, Lee S, Mok YG et al. (2022) Targeted A-to-G base editing in human mitochondrial DNA with programmable deaminases. Cell 185(10):1764–1776
50. Cho SI, Lim K, Hong S et al. (2024) Engineering TALE-linked deaminases to facilitate precision adenine base editing in mitochondrial DNA. Cell 187(1):95–109
51. Davis JR, Wang X, Witte IP et al. (2022) Efficient in vivo base editing via single adeno-associated viruses with size-optimized genomes encoding compact adenine base editors. Nat Biomed Eng 6(11):1272–1283
52. Kulkarni JA, Witzigmann D, Thomson SB et al. (2021) The current landscape of nucleic acid therapeutics. Nature Nanotechnology 16(6):630–643
53. Cheng Q, Wei T, Farbiak L et al. (2020) Selective organ targeting (SORT) nanoparticles for tissue-specific mRNA delivery and CRISPR-Cas gene editing. Nat Nanotechnol 15(4):313–320
54. Kim M, Song ES, Chen JC, et al. (2025) Dual SORT LNPs for multi-organ base editing. Nat Biotechnol 44(4):578–586.
55. Chang T, Zheng Y, Jiang M et al. (2026) Peptide codes for organ-selective mRNA delivery. Nat Mater 25(1):146–159
56. Raguram A, An M, Chen PZ et al. (2025) Directed evolution of engineered virus-like particles with improved production and transduction efficiencies. Nat Biotechnol 43(10): 1635–1647
57. Ramos-Zaldívar HM, Polakovicova I, Salas-Huenuleo E et al. (2022) Extracellular vesicles through the blood–brain barrier: a review. Fluids Barriers CNS 19(1):60
58. Gupta AO, Sharma A, Frangoul H, et al. (2026) Base editing of HBG1 and HBG2 promoters for sickle cell disease. N Engl J Med 394(18):1824–1835.
59. Lai Y, Liu R, Wang L et al. (2026) Clinical application of base editing for treating β-thalassaemia. Nature 8:1–10

Open Access This chapter is licensed under the terms of the Creative Commons Attribution-NonCommercial-NoDerivatives 4.0 International License (http://creativecommons.org/licenses/by-nc-nd/4.0/), which permits any noncommercial use, sharing, distribution and reproduction in any medium or format, as long as you give appropriate credit to the original author(s) and the source, provide a link to the Creative Commons license and indicate if you modified the licensed material. You do not have permission under this license to share adapted material derived from this chapter or parts of it.

The images or other third party material in this chapter are included in the chapter's Creative Commons license, unless indicated otherwise in a credit line to the material. If material is not included in the chapter's Creative Commons license and your intended use is not permitted by statutory regulation or exceeds the permitted use, you will need to obtain permission directly from the copyright holder.





Chapter 5

An Overview of Programmable Epigenetic Editing Based on CRISPR Tools for Gene Expression Regulation

Marija Djordjevič, Svetlana Dinič, Ana Sarič, Aleksandra Uskokovič and Melita Vidakovič

Abstract

Epigenetic regulation provides a dynamic and reversible layer of gene control that functions independently of changes in DNA sequence, primarily mediated by DNA methylation, histone modifications, and higher-order chromatin organization. Aberrant epigenetic states contribute to a wide range of human diseases. However, conventional epigenetic therapies based on small-molecule inhibitors lack locus specificity and often cause global chromatin disturbances. The emergence of programmable epigenetic editing technologies has transformed the field by enabling targeted rewriting of chromatin states at defined genomic loci. Catalytically inactive CRISPR/Cas9 platforms fused to transcriptional activators, repressors, or chromatin-modifying enzymes now allow precise addition or removal of epigenetic marks without altering the underlying DNA sequence. This chapter provides an overview of the conceptual and technical foundations of CRISPR-based epigenetic editing, including tools for gene activation and repression, DNA methylation, histone modifications, and multiplexed systems that permit coordinated regulation of multiple genomic loci or epigenetic marks. Delivery methods for in vitro and in vivo applications are discussed, with an emphasis on viral and nonviral platforms that enable tissue-specific, durable gene regulation. Finally, recent preclinical and clinical studies highlight the potential of programmable epigenetic editing as a next-generation therapy for precise and reversible gene control.

Keywords Epigenetic modifications, Epigenetic editing, CRISPR/dCas9 tools, Gene regulation, Next-generation gene therapies

1 Introduction

Epigenetics encompasses heritable and reversible modifications in gene expression that occur independently of changes in DNA sequence. These regulatory processes govern chromatin structure and transcriptional activity, thereby shaping cellular identity, developmental trajectories, and physiological adaptation. The principal epigenetic mechanisms include DNA methylation, post-translational histone modifications, noncoding RNA molecules, and ATP-dependent chromatin remodeling, which together establish dynamic

Duško Lainšček et al. (eds.), *CRISPR Delivery*, Methods in Molecular Biology, vol. 3075,
https://doi.org/10.1007/978-1-0716-5547-4_5,
© The Author(s) 2027

transcriptional programs in response to developmental and environmental cues (Fig. 1) [1].

DNA methylation occurs predominantly at cytosine residues within CpG dinucleotides and is catalyzed by DNA methyltransferases (DNMT1, DNMT3A/3B, and DNMT3L). Promoter-associated methylation is generally linked to transcriptional repression through recruitment of methyl-CpG binding proteins and chromatin compaction [2]. Histone modifications, including acetylation, methylation, phosphorylation, ubiquitination, PARylation, SUMOylation, and citrullination, further regulate chromatin accessibility [3]. Noncoding RNAs (ncRNAs) regulate gene expression epigenetically, without altering DNA sequences by directing modifications of chromatin, DNA, and histones. Long noncoding RNAs (lncRNAs) act as scaffolds or guides for chromatin-modifying enzymes, while small RNAs such as miRNAs and piRNAs regulate DNA methyltransferases. These mechanisms are crucial for gene activation or silencing, imprinting and disease development, particularly in cancer

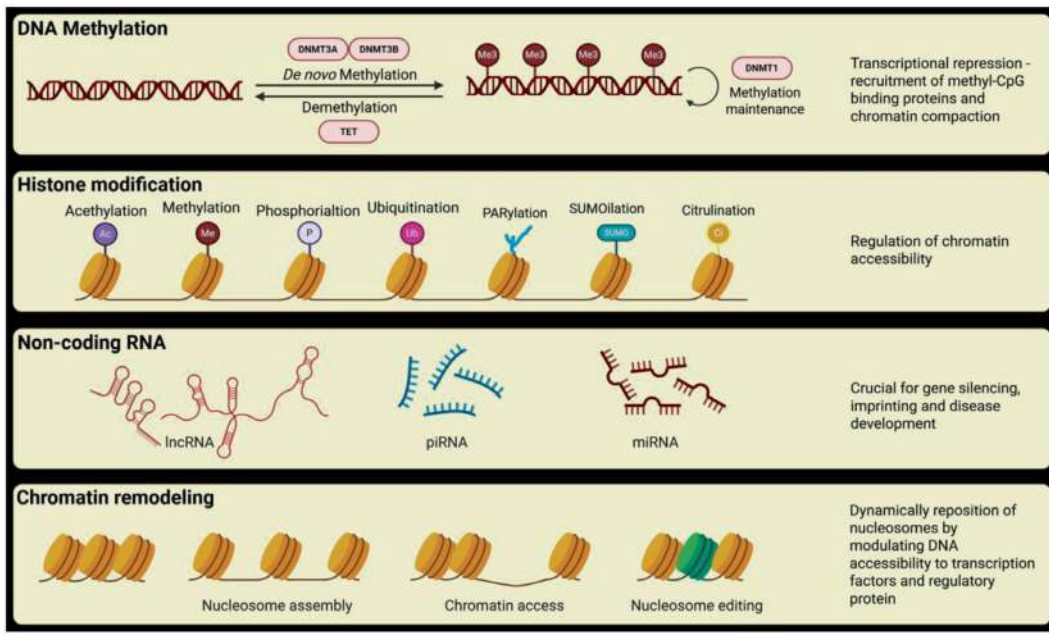


Fig. 1 Major epigenetic mechanisms regulating gene expression. This schematic summarizes key layers of epigenetic regulation. DNA methylation involves the addition of methyl groups (Me3) to cytosine residues by DNMT3A/3B (de novo methylation) and maintenance by DNMT1, while TET enzymes mediate demethylation. These modifications generally lead to transcriptional repression through chromatin compaction and recruitment of methyl-CpG binding proteins. Histone modifications, including acetylation, methylation, phosphorylation, ubiquitination, PARylation, SUMOylation, and citrullination, occur on histone tails and regulate chromatin accessibility and gene activity. Noncoding RNAs (lncRNAs, piRNAs, and miRNAs) contribute to gene silencing, genomic imprinting, and disease processes through both transcriptional and post-transcriptional regulatory mechanisms. Chromatin remodeling complexes dynamically reposition or modify nucleosomes via assembly, sliding, or editing, thereby modulating DNA accessibility to transcription factors and regulatory proteins

and immune responses [4]. Chromatin remodeling complexes such as SWI/SNF, ISWI, and INO80 dynamically reposition nucleosomes, thereby modulating DNA accessibility to transcription factors and regulatory proteins (Fig. 1) [5].

Under physiological conditions, epigenetic regulation plays an essential role in embryonic development, lineage commitment, cellular plasticity, and maintenance of tissue-specific transcriptional programs. Dysregulation of epigenetic homeostasis contributes to a broad range of pathological conditions, including cancer, neurodevelopmental disorders, metabolic disease, and immune dysfunction [6–8]. Importantly, accumulating evidence suggests that epigenetic alterations frequently act as drivers rather than passive markers of disease, underscoring the therapeutic relevance of targeted epigenetic modulation [9].

2 Emergence of Programmable Epigenetic Editing

Clinical manipulation of epigenetic processes has traditionally relied on small-molecule inhibitors targeting chromatin-modifying enzymes, most notably DNMT inhibitors (DNMTi) and histone deacetylase inhibitors (HDACi). Agents such as azacitidine, decitabine, vorinostat, and panobinostat have demonstrated clinical benefit in selected hematological malignancies and certain solid tumors [10]. However, their therapeutic efficacy is constrained by fundamental limitations inherent to their global mode of action. Azacitidine and decitabine are nucleoside analogs that become incorporated into DNA and trap DNMT enzymes, leading to passive genome-wide DNA hypomethylation and reactivation of silenced genes. These drugs are approved for the treatment of myelodysplastic syndromes and acute myeloid leukemia [11]. Similarly, HDACi such as vorinostat and romidepsin increase histone acetylation levels and promote transcriptional activation of multiple genes, and they are clinically approved for cutaneous T-cell lymphoma and related hematologic malignancies [12]. Despite their therapeutic value, these agents exhibit pleiotropic effects across thousands of genomic loci, contributing to dose-limiting toxicities, variable patient responses and difficulties in predicting transcriptional outcomes.

Although small-molecule epigenetic drugs have shown that epigenetic states are pharmacologically tractable, their lack of locus specificity and reversible yet widespread chromatin perturbation remain major limitations. Therefore, precise functional dissection of gene regulatory networks (via targeted enhancers, silencers, or promoters) and selective correction of disease-associated epigenetic lesions remain unattainable with conventional approaches. These constraints have stimulated the development of targeted epigenome editing strategies capable of precise, locus-specific chromatin modification.

The conceptual framework governing epigenetic intervention has transitioned from global pharmacological perturbation (systemically acting) toward programmable, locus-specific epigenome engineering approaches (targeted acting).

2.1 Conceptual Shift Toward Locus-Specific CRISPR-Based Epigenome Engineering

The start of CRISPR-derived technologies has enabled a fundamental shift from global pharmacological modulation to programmable epigenome engineering. Catalytically inactive Cas9 (dCas9) retains high-fidelity DNA-binding capability guided by short single-guide RNA (sgRNA) sequences while lacking nuclease activity [13]. This property allows precise targeting of specific genomic loci without inducing DNA cleavage. By fusing dCas9 to epigenetic editors that deposit or remove epigenetic marks, programmable complexes can be generated to locally modify chromatin structure. Once recruited to promoters, enhancers or other regulatory regions through sequence-specific sgRNAs, these fusion proteins establish defined chromatin environments, enabling targeted rewriting of epigenetic states and modulation of gene expression [14]. Epigenetic editors are chromatin-modifying enzymes that function as epigenetic writers, erasers, or readers. Writers catalyze the deposition of epigenetic marks, such as DNMTs that methylate cytosine residues in CpG dinucleotides (DNMT3A/3B) or histone acetyltransferases (HATs) like p300/CBP that add acetyl groups to lysine residues on histone tails, generally promoting transcriptional activation through chromatin relaxation. In contrast, erasers remove these modifications and often contribute to gene repression or chromatin compaction. Prominent examples include ten–eleven translocation (TET) dioxygenases, which catalyze oxidative DNA demethylation and histone deacetylases (HDACs) or lysine demethylases (KDMs), which reverse acetylation and methylation marks on histones [15]. Epigenetic readers, such as proteins containing bromodomains or chromodomains, recognize specific chromatin modifications and recruit additional transcriptional or remodeling complexes, thereby translating epigenetic marks into functional gene expression programs [16]. Bromodomain-containing protein 4 (BRD4) recognizes and binds acetylated histones [17], while chromodomain protein families, such as the HP1 family and the Polycomb group, are involved in heterochromatin formation and gene silencing, typically recognizing H3K9me3 and H3K27me3, respectively [18].

This strategy enables direct manipulation of endogenous regulatory elements without altering nucleotide sequence, preserving genomic integrity while providing dynamic control over transcriptional output. Unlike permanent genetic modifications, epigenetic editing offers reversibility, temporal precision, and adaptability, making it particularly well-suited for interrogating gene regulatory mechanisms and for developing therapeutic interventions that require tunable control.

2.2 CRISPR-Based Epigenetic Editing Platforms

CRISPR-based epigenetic editing platforms have emerged as powerful tools for interrogating and manipulating gene regulation at defined genomic loci. Their development was initially driven by the need to experimentally validate the causal role of specific epigenetic marks in gene regulation, enabling researchers to move beyond correlative epigenomic observations toward direct functional testing. By coupling dCas proteins with chromatin-modifying enzymes, these systems were introduced into experimental models to demonstrate that targeted deposition or removal of epigenetic marks can modulate transcriptional programs, thereby establishing a mechanistic framework for studying epigenetic control and exploring therapeutic gene regulation (Fig. 2).

Transcriptional activation (CRISPRa) is commonly achieved through fusion to the catalytic core of the p300 histone acetyltransferase, which deposits an acetylation mark on the histone H3 at lysine 27 (H3K27ac) at promoters and enhancers, resulting in robust transcriptional induction. Similarly, recruitment of the TET1 catalytic domain enables site-specific DNA demethylation and gene reactivation. CRISPR gene activation can also occur through fusing dCas9 with VP64, a strong transcriptional activation domain. Guided by dCas9, VP64 recruits transcriptional machinery to specific sequences, causing targeted gene regulation. Transcriptional activation using these systems can be achieved by directing effector domains to specific genomic regions, thereby influencing either transcriptional initiation or elongation, depending on the targeted sequence. An enhanced activator configuration, VPR, was developed by fusing dCas9 with a tripartite activation module composed of VP64 (four copies of VP16 viral protein activation domain, linked together), P65 (a subunit of the transcription factor NF-κB), and Rta (replication and transcription activator from the Epstein–Barr virus), which collectively function as strong transcriptional activators. These domains cooperatively recruit components of the transcriptional machinery to promote gene expression. In practice, the VPR system generally produces stronger activation than the original dCas9–VP64 construct. A key advantage of VPR is its relatively simple design: it operates via a single fusion protein rather than requiring additional engineered components, such as modified guide RNAs or peptide arrays. This streamlines delivery, making it a common choice for CRISPR activation (Fig. 2) [19].

Conversely, transcriptional repression (CRISPRi) in CRISPR-based epigenetic editing systems is typically achieved by fusing dCas9 to repressive chromatin-modifying domains, such as the Krüppel-associated box (KRAB; a transcriptional repression domain from a family of zinc finger proteins known as KRAB-ZFPs), or to DNA methyltransferase complexes, including DNMT3A and its cofactor DNMT3L. The KRAB domain mediates transcriptional silencing primarily by recruiting KAP1/TRIM28 and associated heterochromatin-forming complexes, leading to histone modifications such

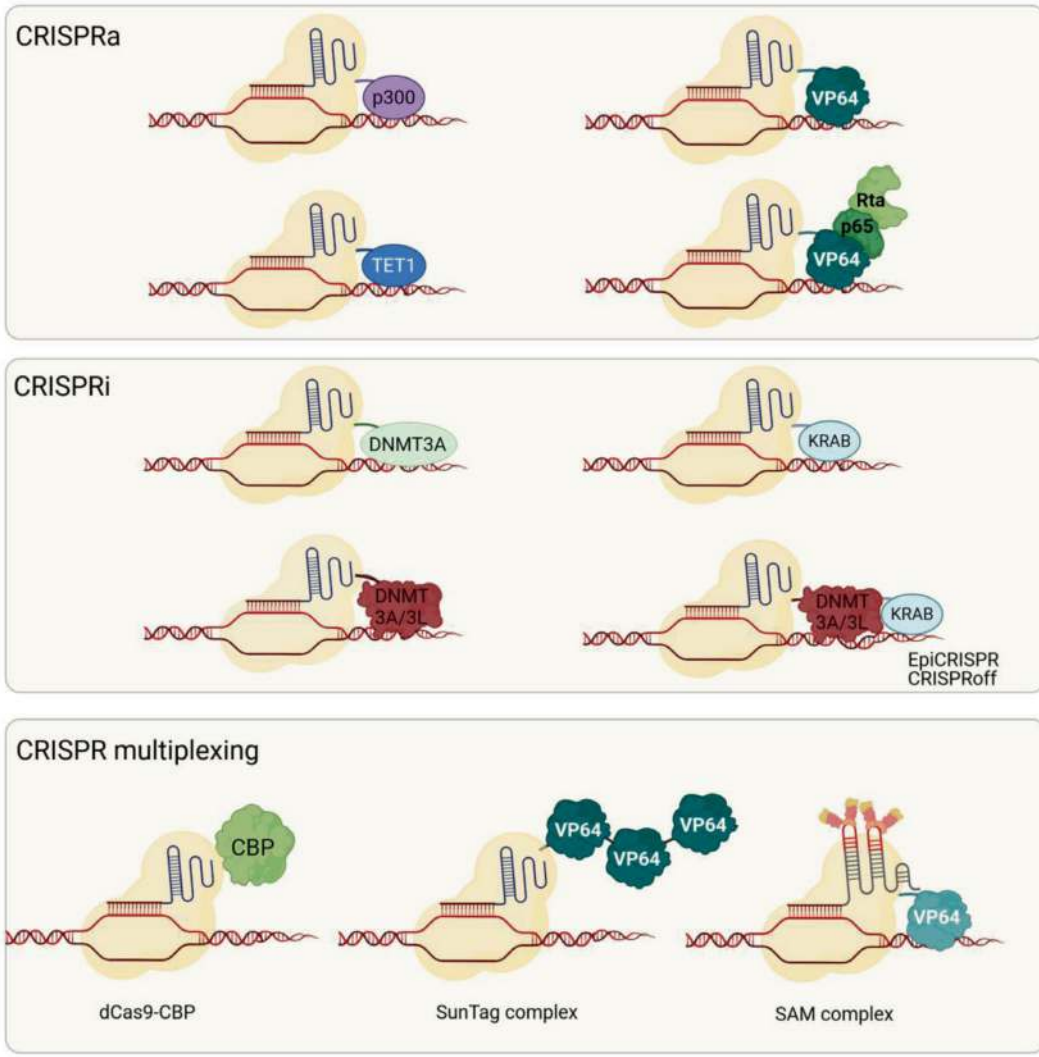


Fig. 2 CRISPR-based transcriptional and epigenetic regulation strategies. Schematic overview of CRISPR-mediated gene regulation using catalytically inactive Cas9 (dCas9) fused to diverse effector domains. Top panel (CRISPRa): Transcriptional activation approaches in which dCas9 is fused to activators such as p300, TET1, or VP64, or to multi-component activator complexes (e.g., VP64–p65–Rta; VPR activator). These systems enhance gene expression through histone acetylation, DNA demethylation, or recruitment of transcriptional machinery. Middle panel (CRISPRi): Transcriptional repression strategies employing dCas9 fused to repressive or epigenetic silencing domains, including DNMT3A, DNMT3A/3L, and KRAB. These effectors promote gene silencing via DNA methylation and/or chromatin compaction. Combined systems (e.g., DNMT3A/3L with KRAB; EpiCRISPR/CRISPRoff) enable more stable and heritable repression. Bottom panel (CRISPR multiplexing): Strategies to enhance or diversify gene regulation include dCas9 fused to CBP, SunTag systems for multivalent recruitment of VP64 activators, and SAM complexes that recruit multiple transcriptional activators via modified gRNAs. These approaches enable amplification of regulatory effects at a single locus and, when combined with multiple gRNAs, allow simultaneous targeting of multiple loci

as H3K9 trimethylation [20], whereas DNMT3A/3L catalyzes de novo DNA methylation at CpG sites. Together, these mechanisms enable targeted establishment of stable transcriptional repression and epigenetic memory at promoters or regulatory elements, allowing durable gene silencing without altering the underlying DNA sequence [21,22]. Recently developed platforms such as EpiCRISPR and CRISPRoff combine KRAB-mediated repression with targeted DNA methylation to establish heritable epigenetic memory, enabling gene silencing across multiple cell generations (Fig. 2) [23,24].

Additional innovations incorporate chromatin remodeling enzymes, histone acetyltransferase and demethylases, expanding the functional repertoire of epigenome editing beyond classical histone and DNA modifications [25]. dCas9 is fused to CBP (dCas9-CBP), a histone acetyltransferase domain capable of rearranging chromatin structure in some loci across *Drosophila* cell lines [26]. More sophisticated architectures, including SunTag and synergistic activation mediator (SAM) systems, amplify effector recruitment, significantly enhancing regulatory potency [27]. The SAM system is a second-generation CRISPR activation platform in which dCas9–VP64 is combined with modified single-guide RNAs containing MS2 aptamer loops that recruit additional transcriptional activators such as p65 and HSF1, thereby enabling robust, multiplexable activation of endogenous genes [28]. The SunTag-based epigenetic editing platforms constitute a highly versatile strategy for amplifying and multiplexing chromatin-modifying activities at defined genomic loci. This system employs a repetitive GCN4 peptide array (series of repeated short sequences from yeast transcription factor GCN4) fused to dCas9, enabling recruitment of multiple effector proteins via high-affinity antibody–peptide interactions, thereby markedly enhancing local enzymatic activity and amplifying gene regulation at a target DNA site [29,30]. By facilitating simultaneous delivery of multiple epigenetic writers and erasers, SunTag architectures enable combinatorial regulation of DNA methylation and histone modifications, supporting precise dissection of causal relationships between chromatin states and transcriptional outputs. Compared with single-effector CRISPR platforms, SAM and SunTag provide superior transcriptional potency through multivalent recruitment, and they occupy an intermediate position between simple transcriptional modulators (dCas9–VP64 or dCas9–KRAB) and direct chromatin-modifying fusions (dCas9–DNMT3A or dCas9–p300), offering scalable and modular control of gene expression while retaining programmability and multiplex capacity. Another system, SunTag-p65-HSF1 (SPH), combines components of SAM and SunTag activators, fusing the SunTag epitope tag with the P65-HSF activation domains used in SAM. This method has been shown to activate genes at two- to threefold higher than SAM, SunTag and VPR (Fig. 2) [31].

2.3 Delivery Strategies for CRISPR/dCas9-Based Epigenetic Editing

Efficient delivery of CRISPR/dCas9-based epigenetic editors is a central determinant of experimental robustness in vitro and therapeutic feasibility in vivo, as the large size of dCas9 fusion proteins and the requirement for coordinated gRNA expression impose technical constraints on vector design and cellular uptake. CRISPR-based epigenome editors have been delivered using a variety of strategies: plasmid DNA transfection, viral vector–mediated delivery (adeno-associated virus (AAV) and lentivirus), mRNA delivery using lipid nanoparticles (LNPs), and direct delivery of ribonucleoprotein complexes via electroporation or nanoparticle systems. In addition, physical delivery approaches such as nucleofection and in vivo electroporation have been employed in experimental models to facilitate the introduction of epigenome-editing components into target cells or tissues.

In vitro, most foundational studies relied on plasmid-based transient transfection in human cell lines to establish proof-of-principle epigenetic remodeling. Targeted DNA methylation using dCas9/DNMT3A was first demonstrated following lipid-mediated plasmid transfection in HEK293 and other mammalian cells, resulting in locus-specific CpG methylation and transcriptional repression [21]. Similarly, dCas9–TET1-mediated targeted DNA demethylation and gene reactivation were validated in cultured cells using lipofectamin-based plasmid transfection prior to in vivo adaptation [32]. Histone modification editing has likewise been established predominantly through transient plasmid delivery: dCas9–p300 acetyltransferase was introduced by lipid-based transfection to induce promoter- and enhancer-specific H3K27ac and transcriptional activation [32], whereas dCas9–LSD1-mediated enhancer repression was achieved through plasmid-based expression in human cells [25]. Early CRISPR interference and activation systems (dCas9–KRAB and dCas9–VP64) were delivered via plasmid transfection and lentiviral vectors to enable either transient or stable expression, depending on experimental requirements [2]. Signal amplification architectures such as the SunTag system were similarly validated in vitro using plasmid co-transfection of dCas9–GCN4 arrays and scFv-effector fusions [29] and later refined for multiplex chromatin editing through optimized plasmid delivery strategies in human stem and somatic cells [30]. For applications requiring durable repression or transcriptional memory, lentiviral delivery has frequently been employed to achieve stable integration and prolonged effector expression, whereas electroporation or nucleofection is preferred in primary cells and pluripotent stem cells to improve efficiency while limiting prolonged overexpression.

However, each approach presents specific limitations, including vector cargo size constraints, the risk of prolonged expression, and challenges with delivery efficiency and tissue specificity. Therefore, alternative delivery strategies, such as transient delivery of ribonucleoprotein complexes, are increasingly being investigated to improve

the safety, controllability, and effectiveness of CRISPR-based epigenome editing systems. To address this limitation, a delivery strategy termed robust enveloped delivery of epigenome-editor ribonucleoproteins (RENDER) has been recently developed. This approach enables transient delivery of programmable epigenetic regulators into human cells as ribonucleoprotein complexes. Using RENDER, several CRISPR-based systems, including epigenetic repressors such as CRISPRi, DNMT3A-3L-dCas9, and CRISPRoff, as well as the activator TET1-dCas9, can be introduced into cells by electroporation to modulate gene expression [34].

Efficient delivery of CRISPR/dCas9-based epigenetic effectors remains a principal determinant of in vivo efficacy and clinical translation, and multiple viral and nonviral platforms have been engineered for this purpose. For in vivo applications, delivery strategies must additionally address tissue tropism, immunogenicity, vector persistence, and packaging constraints. Recombinant AAVs are currently the most extensively validated system for in vivo epigenome editing, owing to their favorable safety profile, defined serotype tropism, and capacity for long-term transgene expression in post-mitotic tissues. Systemic administration of hepatotropic AAV encoding dCas9–DNMT3A targeted to the *Pcsk9* promoter induced stable DNA methylation and long-term LDL cholesterol reduction in murine liver [35]. In the central nervous system, stereotaxic injection of AAV9 delivering dCas9-based transcriptional activators to the hippocampus resulted in persistent upregulation of endogenous *Kcna1* and significant seizure reduction in rodent epilepsy models [36], establishing proof-of-concept for therapeutic CRISPRa in neuronal tissue. To address vector size constraints, compact "all-in-one" AAV systems incorporating smaller dCas orthologs fused to KRAB- or MeCP2-based repressors have been developed and successfully applied to neural tissues, where they achieved robust chromatin remodeling and gene repression in vivo [37]. Beyond viral approaches, LNP formulations have been adapted for transient hepatic delivery of mRNA encoding dCas9 epigenetic regulators, enabling efficient yet nonintegrative expression and potent locus-specific chromatin modification with reduced risk of long-term vector persistence [38]. Methodologically, these in vivo studies typically combine vector engineering (serotype selection or nanoparticle formulation), tissue-targeted administration (systemic intravenous injection or stereotaxic delivery), and locus-specific gRNA design to achieve programmable recruitment of epigenetic writers or repressors.

Across both in vitro and in vivo systems, rigorous validation of on-target epigenetic remodeling typically combines chromatin immunoprecipitation, bisulfite sequencing, and transcriptomic profiling to confirm locus specificity and functional gene regulation. Despite substantial progress, challenges remain, including immune recognition of Cas proteins, variable chromatin accessibility, large effector size, and the need for precise temporal control of epigenetic mark

deposition and erasure, underscoring the importance of continued optimization of delivery platforms for translational epigenome engineering. Importantly, the clinical feasibility of AAV- and LNP-based delivery platforms has already been established in human genome editing trials, thereby reinforcing the translational potential of analogous delivery strategies for programmable epigenetic regulation [39].

2.4 Improving Specificity in CRISPR/dCas-Mediated Epigenetic Editing

Despite rapid advances in programmable epigenetic editing, off-target activity remains a key challenge that may limit therapeutic applications of CRISPR/dCas-based systems. Although dCas proteins do not introduce double-strand DNA breaks, unintended binding of the gRNA–dCas complex to partially homologous genomic sites can still recruit chromatin-modifying enzymes and alter local epigenetic states at nontarget loci. Such effects may lead to unintended changes in gene expression, particularly when potent effector domains such as DNMT3A, TET1, p300, or KRAB are used.

Several complementary approaches have been explored to reduce nonspecific genomic interactions and improve locus-selective activity [40]. These strategies include the engineering and directed evolution of DNA-binding components, particularly optimization of gRNA sequences and modifications that increase target discrimination. Adjustments in gRNA architecture, such as truncated or chemically modified sgRNAs, can further refine targeting accuracy [41]. In parallel, the development of synthetic high-fidelity dCas variants and alternative Cas orthologues, including Cas9 and Cas12a proteins derived from different bacterial species, provides enzymes with altered protospacer adjacent motif (PAM) requirements and improved specificity profiles [42]. Among alternative CRISPR nucleases, several compact type II-C Cas9 orthologues have attracted attention because of their intrinsically high targeting fidelity. Notably, NmeCas9 from *Neisseria meningitidis* and CjeCas9 from *Campylobacter jejuni* display substantially reduced off-target activity compared with the widely used SpCas9 [43,44]. The improved accuracy of these enzymes has been linked to structural and mechanistic features that impose stricter target recognition requirements. In particular, they employ longer gRNA targeting sequences and recognize more restrictive PAM sequences, which together enhance discrimination between correct and mismatched genomic targets.

Additional approaches involve the implementation of multi-component CRISPR cascade systems, derived from Class 1 CRISPR complexes, as well as advanced effector-domain recruitment strategies that enable more controlled assembly of regulatory complexes at target loci. Pickar-Oliver and colleagues have recently engineered multi-protein Class 1 CRISPR complexes known as Cascade, originally derived from *Escherichia coli* (EcoCascade) and *Listeria monocytogenes* (LmoCascade) [45]. Similar to other Cas-based tools, Cascade components can be fused to effector domains such as p300 or KRAB, enabling targeted gene activation or repression, respectively. Finally,

technologies enabling spatiotemporal regulation of DNA-binding modules and associated effector domains, for example, through inducible or light-controlled systems, offer further opportunities to minimize unintended activity while maintaining efficient epigenetic modulation [46]. Besides the properties of the gRNAs, the method used to attach effector domains to dCas9 can significantly affect targeting specificity. For instance, when dCas9 is directly fused to the DNMT3A, the system may display higher levels of unintended off-target activity. In contrast, recruitment-based approaches, such as the SunTag system, configuration SpdCas9–SunTag–DNMT3A, tend to improve targeting control by bringing several enzyme molecules to the same genomic locus at once. With this strategy, even a single gRNA can be sufficient to produce strong and efficient epigenetic modification [47].

Together, these developments illustrate ongoing efforts to enhance the precision and safety of programmable epigenetic editing technologies, which will be critical for their reliable use in functional genomics and future therapeutic applications.

3 Epigenetic Editing: from In Vitro Systems to Clinical Translation

3.1 In Vitro Epigenetic Editing for Disease Modeling and Correction

In recent years, several in vitro epigenetic editing studies have provided compelling demonstrations of targeted chromatin modulation as a therapeutic strategy for disease-associated transcriptional dysregulation. Hilton et al. first established that dCas9 fused to the catalytic domain of p300 enables potent, locus-specific histone acetylation, leading to robust activation of developmentally silenced genes and disease-relevant regulatory elements in human cells [33]. Building on this foundation, Liu et al. demonstrated targeted DNA demethylation using dCas9–TET1 to reactivate hypermethylated tumor suppressor genes in cancer cell lines, restoring physiological transcriptional programs and suppressing malignant phenotypes [48]. Recently developed platforms such as CRISPRoff and EpiCRISPR combine KRAB-mediated repression with targeted DNA methylation to establish heritable epigenetic memory, enabling stable gene silencing across multiple cell generations. The CRISPRoff system has been developed by Nuñez et al. to establish durable epigenetic silencing of pathogenic gene expression programs implicated in neurodevelopmental and oncogenic disorders [23]. By employing the EpiCRISPR platform fused to the DNMT3A/3L methyltransferase complex and the KRAB repression domain, the authors achieved targeted hypermethylation of the *Arx* promoter, leading to transcriptional repression of *Arx* in pancreatic α-cells, which was sufficient to initiate partial reprogramming of α-cells toward an insulin-producing phenotype [24].

Disease-focused in vitro applications have included reactivation of fetal γ-globin expression in erythroid progenitors as a therapeutic strategy for sickle cell disease and β-thalassemia, achieved through epigenetic repression of the BCL11A enhancer [49]. In the field of neurodegenerative disease, targeted DNA methylation editing was applied to the amyloid precursor protein (APP) locus using a dCas9–DNMT3A fusion in cultured primary neurons derived from APP knock-in mice. Directed methylation of the APP promoter reduced APP transcription, lowered amyloid-β production and significantly improved neuronal survival, demonstrating that locus-specific methylation editing can correct pathogenic gene expression signatures associated with Alzheimer's disease [50]. In cancer epigenetics, CRISPR-based demethylation screens using dCas9–TET1 have been implemented in colorectal cancer cell lines to identify functionally relevant epigenetically silenced genes. By systematically removing DNA methylation at selected promoters, investigators uncovered regulatory loci that influence tumor cell proliferation and transcriptional networks, illustrating how programmable demethylation can reveal causal epigenetic drivers of oncogenesis [51]. Another line of investigation has focused on synthetic chromatin writing to model transcriptional regulation associated with therapy resistance in melanoma. A programmable histone kinase system (dCas9-dMSK1) was used to deposit H3S28 phosphorylation at endogenous promoters in human cancer cells, resulting in activation of specific gene networks and altered cellular responses to BRAF inhibitor treatment. These experiments demonstrated that targeted histone phosphorylation can directly modulate transcriptional programs relevant to cancer cell fitness and drug resistance [52]. Epigenome editing has also been applied in cellular endocrine disease modeling and regenerative medicine. Using a dCas9–p300 histone acetyltransferase fusion targeted to transcription factor loci such as *NR5A1*, *GATA4*, and *DMRT1*, investigators successfully converted human fibroblasts into Leydig-like cells in vitro. The induced cells displayed elevated H3K27ac at regulatory elements, expressed steroidogenic genes and produced testosterone, illustrating how targeted chromatin acetylation can drive lineage reprogramming relevant to treatment strategies for male hypogonadism [53]. Finally, programmable chromatin engineering approaches have been used to dissect immune cell function and inflammatory disease pathways. Targeting the Foxp3 locus with dCas9-p300 or dCas9-TET1 editors in cultured T cells demonstrated that locus-specific acetylation or demethylation could stabilize regulatory T-cell identity and sustain transcription of immune-regulatory genes under inflammatory conditions. These findings highlight the potential of epigenetic editing for manipulating immune cell phenotypes and modeling autoimmune disease mechanisms [54].

Recent refinements have further optimized effector recruitment, minimized off-target activity, and enabled multiplex targeting across regulatory landscapes, expanding the applicability of SunTag and SAM platforms in functional genomics, disease modeling, and therapeutic epigenome engineering [55]. These multiplexed CRISPR activation platforms have been widely applied in in vitro epigenetic editing experiments to achieve robust transcriptional activation through multivalent recruitment of transcriptional and chromatin-modifying factors. The SunTag system, consisting of a dCas9 fusion containing tandem GCN4 peptide repeats that recruit multiple copies of antibody-linked activators such as VP64 and TET1, provides strong signal amplification and has been used to induce epigenetic remodeling and transcriptional activation of endogenous loci in cultured mammalian cells [32]. Similarly, the SAM system, which combines dCas9–VP64 with MS2-aptamer-modified sgRNAs recruiting p65 and HSF1 activators, has been extensively used for genome-scale activation screens in human cell lines, enabling systematic identification of genes controlling cancer proliferation, drug resistance, and immune signaling pathways [56]. These platforms have proven particularly valuable for dissecting regulatory networks in cancer and developmental biology, as well as for multiplexed activation of lineage-specific transcription factors during cellular reprogramming.

Together, these recent in vitro experiments illustrate the versatility of programmable epigenome editing for modeling disease mechanisms and correcting aberrant transcriptional states across neurological disorders, cancer, endocrine dysfunction, and immune regulation. By directly writing or erasing specific chromatin marks at endogenous loci, CRISPR-based epigenetic editors provide a mechanistically precise framework for investigating the causal role of epigenetic alterations in human disease.

3.2 In Vivo Epigenetic Editing for Therapeutic Gene Regulation

In vivo epigenetic editing experiments have further validated the translational potential of targeted chromatin remodeling, with multiple landmark studies demonstrating durable phenotypic correction in animal disease models, notably in neurological and metabolic disorders. In epilepsy models, AAV-mediated delivery of dCas9-based transcriptional activators targeting the endogenous *Kcna1* locus produced sustained seizure suppression and functional recovery, establishing CRISPRa as a viable neuromodulatory strategy [36]. In Alzheimer's disease models, locus-specific repression of amyloid-beta precursor protein gene using dCas9–DNMT3A or compact dCas9–KRAB–MeCP2 constructs reduced amyloid burden, restored synaptic function, and improved cognition [37]. In metabolic disease, Thakore et al. achieved efficient silencing of the Pcsk9 gene in murine liver using AAV-mediated delivery of dCas9–KRAB, resulting in long-term reduction of circulating cholesterol levels and

protection against hyperlipidemia [57]. Liao et al. introduced an in vivo CRISPR-based transcriptional gene activation platform that enables locus-specific chromatin remodeling through directed assembly of transcriptional regulators, facilitating controlled upregulation of endogenous genes. They employed AAV delivery of dCas9–p300 to epigenetically activate utrophin expression, which significantly improved muscle integrity and contractile function, thereby compensating for dystrophin deficiency. Therapeutic application of this strategy has resulted in measurable disease amelioration in models of acute kidney injury, type 1 diabetes, and Duchenne muscular dystrophy [58]. Similarly, targeted epigenetic activation of fetal hemoglobin in vivo has shown therapeutic efficacy in murine models of hemoglobinopathies, offering a nonmutagenic alternative to conventional genome editing [49]. Recent advances in nonviral delivery have further expanded translational prospects. Namely, LNP-mediated delivery of the CRISPR–Cas9 gene-editing therapeutic NTLA-2001 via intravenous infusion is designed to disrupt the *TTR* gene in hepatocytes and thereby reduce hepatic production of both wild-type and mutant transthyretin following a single treatment. It has enabled efficient, transient chromatin remodeling in hepatocytes, achieving therapeutic modulation of metabolic gene networks with minimal immunogenicity [59].

Collectively, these studies demonstrate that programmable epigenetic editing can achieve persistent phenotypic correction in vivo, offering a versatile and potentially safer alternative to permanent genome modification for treating a broad spectrum of human diseases.

3.3 Recently Developed Clinical Trials

Several clinical programs have begun translating programmable epigenetic modulation into human studies, moving beyond traditional small-molecule epigenetic drugs toward locus-specific gene-regulation strategies. Notably, nChroma Bio has initiated a Phase 1/2 open-label clinical trial (NCT07200193) of CRMA-1001, an epigenetic silencer designed to durably suppress hepatitis B virus (HBV) gene expression by targeted epigenetic silencing (methylation) of viral covalently closed circular DNA (cccDNA) and integrated HBV sequences. This represents one of the first in-human assessments of a programmable epigenetic modulator (nChroma Bio-press release). Concurrently, Tune Therapeutics has leveraged its TEMPO epigenome editing platform to develop candidate therapies such as TUNE-401 for chronic HBV, which are designed to reprogram regulatory chromatin states at disease-relevant loci and are advancing toward clinical validation (Tune Therapeutics pipeline overview, 2025). In the neuromuscular disease space, Epicrispr Biotechnologies has advanced its lead candidate EPI-321 into an early Phase I/II study for facioscapulohumeral muscular dystrophy (FSHD), employing AAV-delivered epigenetic editing constructs to repress pathogenic

gene expression through targeted chromatin modification rather than genomic DNA cutting (Epicrispr Biotechnologies clinical listing). A further illustration of epigenome-targeting therapies entering clinical evaluation is OTX-2002, a candidate developed by Omega Therapeutics. This therapeutic uses a bicistronic mRNA construct designed to direct epigenetic regulation of the MYC locus, leading to durable repression of MYC-driven transcriptional activity. The therapy is currently being assessed in an early-phase clinical study for hepatocellular carcinoma (NCT05497453), highlighting the growing clinical interest in programmable epigenetic modulation as a treatment strategy. These emerging clinical efforts build on a broader ecosystem of companies, including Chroma Medicine (acquired by nChroma), Omega Therapeutics, and others, that are pursuing locus-specific epigenetic control across a range of indications, underscoring both the translational momentum and the diversity of therapeutic contexts in which programmable epigenetic modulation is being tested.

The clinical translation of programmable epigenetic editors represents a rapidly advancing frontier in precision medicine. By enabling locus-specific and potentially reversible regulation of gene expression, these technologies offer promising therapeutic opportunities for diseases in which aberrant gene regulation plays a central role, including cancer, cardiovascular disorders, neurodegenerative, and metabolic diseases. As several candidates progress from preclinical development toward early clinical testing, continued improvements in delivery efficiency, specificity, and durability will be essential to fully realize their therapeutic potential. At the same time, progress in this field is closely accompanied by an expanding intellectual property landscape. Biotechnology companies are actively building patent portfolios around both emerging and prospective epigenome-editing approaches, protecting key targets and technological platforms while positioning themselves for future partnerships, investment and commercialization [60].

3.4 Advantages of Programmable Epigenetic Editing

Programmable epigenetic editing offers several decisive advantages over conventional therapeutic approaches. Foremost is locus specificity, which enables selective modulation of disease-relevant regulatory elements while minimizing global chromatin disruption. This precision substantially reduces off-target transcriptional effects and cytotoxicity [61]. The reversibility of epigenetic modifications provides dynamic temporal control, facilitating both transient perturbations for mechanistic studies and stable reprogramming for therapeutic purposes. Multiplexed targeting permits coordinated regulation of entire gene networks, an essential feature for controlling complex cellular phenotypes such as differentiation, lineage conversion, and stress responses [28]. Importantly, epigenome editing preserves endogenous genomic context, maintaining native promoter–enhancer

interactions and higher-order chromatin architecture. This physiological mode of regulation enhances functional fidelity compared with ectopic transgene expression and reduces unintended transcriptional rewiring [61].

4 Outlook

The convergence of programmable DNA-binding platforms with enzymatic epigenetic effectors has transformed gene regulation into a precise, modular, and scalable discipline. Ongoing refinements in editor architecture, delivery strategies, and effector engineering are rapidly advancing clinical translational potential. As understanding of chromatin dynamics deepens, programmable epigenome editing is set to become a cornerstone technology for functional genomics, regenerative medicine, and precision therapeutics. Advances in technology development, together with strategic protection of innovation, are expected to shape the path toward broader clinical adoption of epigenetic editing therapies.

Acknowledgments

The publication is based upon work by COST Action CA21113: Genome Editing for the Treatment of Human Diseases (https://www.genehumdi.eu), supported by European Cooperation in Science and Technology (COST). This work was supported by the Ministry of Science, Technological Development, and Innovation of the Republic of Serbia, contract number 451-03-33/2026-03/200007. The results presented in this manuscript are in line with Sustainable Development Goal 3 (Good Health and Well-being) of the United Nations 2030 Agenda.

Conflict of Interest The authors have no conflicts of interest to declare that are relevant to the content of this chapter.

References

1. Allis CD, Jenuwein T (2016) The molecular hallmarks of epigenetic control. Nat Rev Genet 17:487–500
2. Greenberg MVC, Bourc'his D (2019) The diverse roles of DNA methylation in mammalian development and disease. Nat Rev Mol Cell Biol 20:590–607
3. Bannister AJ, Kouzarides T (2011) Regulation of chromatin by histone modifications. Cell Res 21:381–395
4. Mattick JS et al. (2023) Long non-coding RNAs: definitions, functions, challenges and recommendations. Nat Rev Mol Cell Biol 24:430–447
5. Clapier CR, Iwasa J, Cairns BR, Peterson CL (2017) Mechanisms of action and regulation of ATP-dependent chromatin-remodelling complexes. Nat Rev Mol Cell Biol 18:407–422
6. Olawade DB et al. (2025) Reversing epigenetic dysregulation in neurodegenerative diseases:

mechanistic and therapeutic considerations. Int J Mol Sci 26:4929
7. Feinberg AP, Levchenko A (2023) Epigenetics as a mediator of plasticity in cancer. Science 379:eaaw3835
8. Wu YL et al. (2023) Epigenetic regulation in metabolic diseases: mechanisms and advances in clinical study. Sig Transduct Target Ther 8:98
9. Kelly TK, De Carvalho DD, Jones PA (2010) Epigenetic modifications as therapeutic targets. Nat Biotechnol 28:1069–1078
10. Dai W et al. (2024) Epigenetics-targeted drugs: current paradigms and future challenges. Sig Transduct Target Ther 9:332
11. Jones P, Issa JP, Baylin S (2016) Targeting the cancer epigenome for therapy. Nat Rev Genet 17:630–641
12. West AC, Johnstone RW (2014) New and emerging HDAC inhibitors for cancer treatment. J Clin Invest 124:30–39
13. Qi L, Larson M, Gilbert L et al. (2013) Repurposing CRISPR as an RNA-guided platform for sequence-specific control of gene expression. Cell 152:1173–1183
14. de Groote ML, Verschure PJ, Rots MG (2012) Epigenetic editing: targeted rewriting of epigenetic marks to modulate expression of selected target genes. Nucleic Acids Res 40:10596–10613
15. Hyun K, Jeon J, Park K, Kim J (2017) Writing, erasing and reading histone lysine methylations. Exp Mol Med 49(4):e324
16. Musselman C, Lalonde ME, Côté J et al. (2012) Perceiving the epigenetic landscape through histone readers. Nat Struct Mol Biol 19:1218–1227
17. Sartor GC et al. (2019) Enhancement of BDNF expression and memory by HDAC inhibition requires BET bromodomain reader proteins. J. Neurosci. 39:612–626
18. DasGupta A, Lee TL, Li C, Saltzman AL (2020) Emerging roles for chromo domain proteins in genome organization and cell fate in *C. elegans.* Front Cell Dev Biol 8:590195
19. Adli M (2018) The CRISPR tool kit for genome editing and beyond. Nat Commun 9: 1911
20. Olga Rosspopoff DT (2023) Take a walk on the KRAB side. Trends in Genetics 39:844–857
21. Vojta A et al. (2016) Repurposing the CRISPR-Cas9 system for targeted DNA methylation. Nucleic Acids Res 44:5615–5628
22. Stepper P et al. (2017) Efficient targeted DNA methylation with chimeric dCas9-Dnmt3a-Dnmt3L methyltransferase. Nucleic Acids Res 45:1703
23. Nuñez JK et al. (2021) Genome-wide programmable transcriptional memory by CRISPR-based epigenome editing. Cell 184:2503–2519
24. Đorđević M et al. (2023) EpiCRISPR targeted methylation of Arx gene initiates transient switch of mouse pancreatic alpha to insulin-producing cells. Front. Endocrinol. 14:1134478
25. Kearns NA et al. (2015) Functional annotation of native enhancers with a Cas9-histone demethylase fusion. Nat Methods 12:401–403
26. Sajwan S, Mannervik M (2019) Gene activation by dCas9-CBP and the SAM system differ in target preference. Sci Rep 9: 18104
27. Chavez A et al. (2016) Comparison of Cas9 activators in multiple species. Nat Methods 13:563–567
28. Konermann S et al. (2015) Genome-scale transcriptional activation by an engineered CRISPR–Cas9 complex. Nature 517:583–588
29. Tanenbaum ME et al. (2014) A protein-tagging system for signal amplification in gene expression and fluorescence imaging. Cell 159:635–646
30. Policarpi C et al. (2024) Systematic epigenome editing captures the context-dependent instructive function of chromatin modifications. Nat Genet 56:1168–1180
31. Zhou H et al. (2018) In vivo simultaneous transcriptional activation of multiple genes in the brain using CRISPR–dCas9-activator transgenic mice. Nat Neurosci 21:440–446
32. Morita S et al. (2016) Targeted DNA demethylation *in vivo* using dCas9–peptide repeat and scFv–TET1 catalytic domain fusions. Nat Biotechnol 34:1060–1065
33. Hilton IB et al. (2015) Epigenome editing by a CRISPR-Cas9-based acetyltransferase activates genes from promoters and enhancers. Nat Biotechnol 33:510–517
34. Xu D et al. (2025) Programmable epigenome editing by transient delivery of CRISPR epigenome editor ribonucleoproteins. Nat Commun 16: 7948
35. Pan R et al. (2025) Editing DNA methylation in vivo. Nat Commun 17:527
36. Colasante G et al. (2020) In vivo CRISPRa decreases seizures and rescues cognitive deficits in a rodent model of epilepsy. Brain 143:891–905
37. Kantor B et al. (2024) The therapeutic implications of *all-in-one* AAV-delivered epigenome-editing platform in neurodegenerative disorders. Nat Commun 15: 7259
38. Tremblay F et al (2025) A potent epigenetic editor targeting human PCSK9 for durable reduction of low-density lipoprotein cholesterol levels. Nat Med 31:1329–1338
39. Roth GV, Gengaro IR, Qi LS (2024) Precision epigenetic editing: technological advances, enduring challenges, and therapeutic applications. Cell Chem Biol S2451-9456(24):00309-X

40. Sgro A, Blancafort P (2020) Epigenome engineering: new technologies for precision medicine. Nucleic Acids Res 48:12453–12482
41. Ryan DE et al. (2018) Improving CRISPR-Cas specificity with chemical modifications in single-guide RNAs. Nucleic Acids Res 46:792–803
42. Zhao L et al. (2023) PAM-flexible genome editing with an engineered chimeric Cas9. Nat Commun 14: 6175
43. Amrani N et al. (2018) NmeCas9 is an intrinsically high-fidelity genome-editing platform. Genome Biol 19: 214
44. Kim E et al. (2017) In vivo genome editing with a small Cas9 orthologue derived from Campylobacter jejuni. Nat. Commun. 8: 14500
45. Pickar-Oliver A et al. (2019) Targeted transcriptional modulation with type I CRISPR–Cas systems in human cells. Nat Biotechnol 37:1493
46. Polstein LR, Gersbach CA (2015) A light-inducible CRISPR-Cas9 system for control of endogenous gene activation. Nat Chem Biol 11:198–200
47. Huang YH et al. (2017) DNA epigenome editing using CRISPR-Cas SunTag-directed DNMT3A. Genome Biol 18: 176
48. Liu XS et al. (2016) Editing DNA methylation in the mammalian genome. Cell 167:233–247. e17
49. Amistadi S et al. (2025) Dissecting the epigenetic regulation of the fetal hemoglobin genes to unravel a novel therapeutic approach for β -hemoglobinopathies. Nucleic Acids Res 53:637
50. Park H et al. (2022) CRISPR/dCas9-Dnmt3a-mediated targeted DNA methylation of APP rescues brain pathology in a mouse model of Alzheimer's disease. Transl Neurodegener 11:41
51. Tejedor JR et al. (2023) CRISPR/dCAS9-mediated DNA demethylation screen identifies functional epigenetic determinants of colorectal cancer. Clin Epigenetics 15: 133
52. Li J et al. (2021) Programmable human histone phosphorylation and gene activation using a CRISPR/Cas9-based chromatin kinase. Nat Commun 12: 896
53. Huang H et al. (2023) Epigenome editing based on CRISPR/dCas9p300 facilitates transdifferentiation of human fibroblasts into Leydig-like cells. Exp Cell Res 425:113551
54. Okada M et al. (2017) Stabilization of Foxp3 expression by CRISPR-dCas9-based epigenome editing in mouse primary T cells. Epigenet Chromat 10:24
55. Morita S, Horii T, Hatada I (2024) Optimized protocol for the regulation of DNA methylation and gene expression using modified dCas9-SunTag platforms. Methods Mol Biol 2842:155–165
56. Joung J et al. (2017) Genome-scale CRISPR-Cas9 knockout and transcriptional activation screening. Nat Protoc 12:828–863
57. Thakore PI et al. (2018) RNA-guided transcriptional silencing in vivo with *S. aureus* CRISPR-Cas9 repressors. Nat Commun 9: 1674
58. Liao HK et al. (2017) In vivo target gene activation via CRISPR/Cas9-mediated trans-epigenetic modulation. Cell. 171:1495–1507
59. Gillmore JD et al. (2021) CRISPR-Cas9 in vivo gene editing for transthyretin amyloidosis. N Engl J Med 385:493–502
60. Yuan L et al. (2026) Epigenome editing based treatment: progresses and challenges. Mol Ther 34:46–67
61. Thakore PI et al. (2016) Highly specific epigenome editing by CRISPR-Cas9 repressors for silencing of distal regulatory elements. Nat Methods 12:1143–1149

Open Access This chapter is licensed under the terms of the Creative Commons Attribution-NonCommercial-NoDerivatives 4.0 International License (http://creativecommons.org/licenses/by-nc-nd/4.0/), which permits any noncommercial use, sharing, distribution and reproduction in any medium or format, as long as you give appropriate credit to the original author(s) and the source, provide a link to the Creative Commons license and indicate if you modified the licensed material. You do not have permission under this license to share adapted material derived from this chapter or parts of it.

The images or other third party material in this chapter are included in the chapter's Creative Commons license, unless indicated otherwise in a credit line to the material. If material is not included in the chapter's Creative Commons license and your intended use is not permitted by statutory regulation or exceeds the permitted use, you will need to obtain permission directly from the copyright holder.





Chapter 6

Overview of Delivery Methods for Gene Editing

Bilge Debelec Butuner

Abstract

The clinical success of CRISPR-based interventions depends primarily on the efficient delivery of editing components into target cells. While base and prime editing have refined genomic precision, achieving therapeutic efficacy requires specialized vehicles that can navigate systemic circulation, escape endosomes, and ensure cell-specific entry. Delivery platforms are traditionally categorized into viral and nonviral systems. Viral vectors, namely adeno-associated vectors (AAV), lentiviral vectors, and adenoviral vectors, employ evolved mechanisms to achieve high transduction efficiency and predictable biodistribution, yet remain constrained by immunogenicity and the risk of insertional mutagenesis. In contrast, nonviral approaches, including synthetic nanoparticles and physical methods, offer superior scalability and transient expression profiles, reducing long-term genomic risks. Next-generation platforms such as virus-like particles (VLPs), engineered extracellular vesicles (EVs), and functionalized nanoparticles have emerged to bridge this gap. These hybrid systems synergize the entry efficiency of viral proteins with the low-immunogenicity profiles of synthetic carriers. Ultimately, the optimal delivery method is determined by the CRISPR cargo format and target cell characteristics, balancing safety, immunogenicity, and scalability. This chapter emphasizes that the strategic selection of a delivery vehicle must be harmonized with the specific cargo and the unique biological requirements of the target tissue to ensure therapeutic success.

Keywords CRISPR delivery, Genome editing, Viral vectors, Nonviral delivery, Physical delivery

1 Introduction to Genome Editing Tool Delivery Systems

The therapeutic potential of CRISPR systems is closely linked to the efficiency of their delivery to target cells in vitro and in vivo. While advanced methods such as base editing and prime editing have made critical advances in gene-editing technologies, the delivery of CRISPR components remains the primary hurdle to clinical translation [1].

Successful therapeutic application is hindered by several fundamental constraints: the high molecular weight of the Cas9 protein (~160 kDa), as well as the high anionic charge and hydrophilicity of the sgRNA-bound RNP complex, which causes poor membrane permeability, present significant barriers to passive membrane translocation. These physicochemical properties necessitate specialized delivery vehicles to facilitate cellular entry [2]. Additionally, the

Duško Lainšček et al. (eds.), *CRISPR Delivery*, Methods in Molecular Biology, vol. 3075,
https://doi.org/10.1007/978-1-0716-5547-4_6,
© The Author(s) 2027

editing machinery is susceptible to nuclease-mediated degradation in physiological fluids, and, once internalized, the cargo must evade lysosomal degradation via efficient endosomal escape. Furthermore, in vivo delivery of CRISPR components, whether as RNP, mRNA, or plasmid DNA, necessitates overcoming a series of physiological barriers, including systemic circulation, the space of Disse, and the hepatocyte membrane. Consequently, an effective delivery vehicle must provide robust protection of the CRISPR payload in the extracellular environment while facilitating cellular internalization and controlled intracellular release of cargo for genomic modification [3, 4].

The optimal delivery method is determined by the CRISPR cargo format and target cell characteristics, balancing the inherent advantages and limitations of each platform with respect to safety, immunogenicity, and scalability. The strategic selection of a delivery vehicle must be harmonized with the specific cargo and the biological requirements of the target tissue [5]. Although in vitro and in vivo delivery approaches share the same obstacles, such as cellular specificity, membrane crossing, and endosomal escape, in vivo delivery systems must navigate anatomical barriers, including blood circulation, tissue-specific niches, and the immune system, to reach the target site, alike from in vitro [4].

Delivery approaches are broadly classified as viral and nonviral systems (Fig. 1). Viral vectors such as adeno-associated virus (AAV), lentiviral, and adenoviral vectors represent the most mature class of delivery platforms, exploiting natural mechanisms for cellular entry and intracellular trafficking. Their primary advantages include high transduction efficiency and predictable biodistribution, while safety concerns limit their clinical translation [5]. Nonviral strategies include nanoparticles with various chemical compositions, extracellular vesicles, and direct physical methods. These systems prioritize transient expression and manufacturing scalability, addressing the limitations of viral vectors such as immunogenicity and insertional mutagenesis [1, 5]. Although each of these strategies possesses distinct advantages, their inherent limitations continue to pose hurdles to widespread clinical implementation. Next-generation approaches, including virus-like particles, engineered extracellular vesicles, and functionalized nanoparticles, have emerged to synergize the high transduction efficiency of viral vectors with the superior safety profiles of nonviral systems. These platforms are mostly utilized for the delivery of mRNA and RNP formats, demonstrating improvements in targeted delivery, biocompatibility, and safety.

This chapter presents a comprehensive overview of genome-editing delivery systems for distinct cargo formats, focusing on major applications and highlighting their advantages and limitations for clinical translation. An overview of the delivery methods, including their compatible CRISPR cargo formats, major applications, and advantages/limitations, is summarized in Table 1.

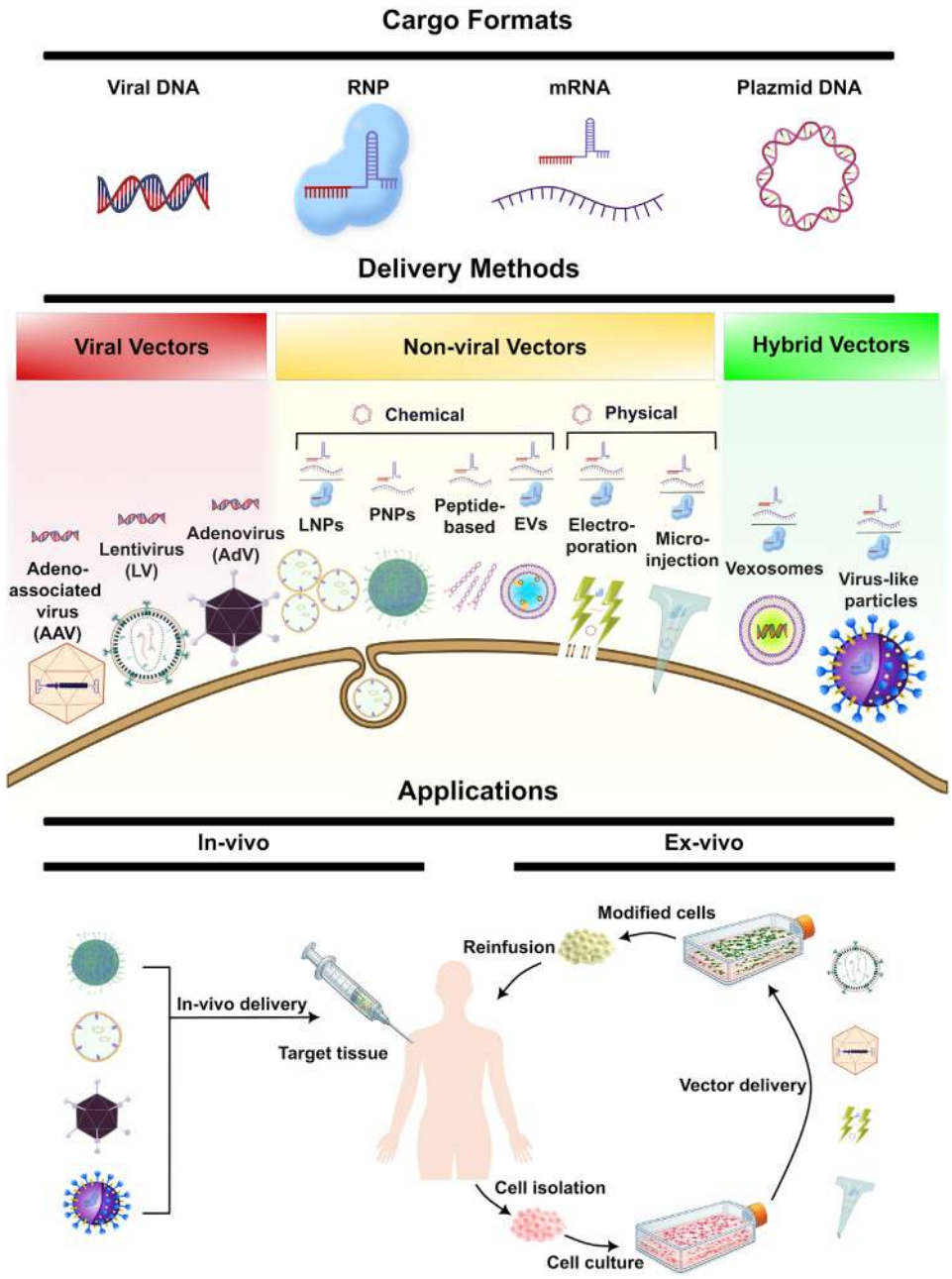


Fig. 1 Overview of delivery platforms for nucleic acid and genome-editing cargoes and their therapeutic applications. Schematic representation of the major cargo formats used in gene and cell therapy, including viral DNA, ribonucleoprotein (RNP) complexes, mRNA, and plasmid DNA. These cargos can be delivered using viral vectors, including adeno-associated virus (AAV), lentivirus (LV), and adenovirus (AdV), as well as nonviral vectors, which are subdivided into chemical approaches such as lipid nanoparticles (LNPs), polymeric nanoparticles (PNPs), peptide-based carriers, and extracellular vesicles (EVs), and physical approaches including electroporation and microinjection. In addition, hybrid delivery systems, such as engineered vesicles and virus-like particles (VLPs), are also depicted. The lower panel illustrates the principal therapeutic applications of these delivery platforms in in vivo settings, where cargos are administered directly to the patient for targeted tissue delivery, and in ex vivo approaches, in which cells are isolated, genetically modified outside the body, expanded, and subsequently reinfused into the patient

Table 1
Viral and nonviral delivery methods for CRISPR-Cas genome editing tools

Delivery type	Delivery method	Major applications	Cargo format	Advantages	Limitations
Viral	Adeno-associated virus	In vivo	DNA	High efficiency in dividing/nondividing cells Low immunogenicity Efficient in vivo delivery	Limited packaging capacity Prolonged expression
	Lentivirus	In vitro Ex vivo	DNA	High efficiency in dividing/nondividing cells Larger packaging capacity Long-term transgene expression in daughter cells	Random integration Insertional mutagenesis
	Adenovirus	In vivo	DNA	High efficiency in dividing/nondividing cells Larger packaging capacity No genome integration	High immunogenicity Inflammatory responses
Nonviral chemical	Lipid nanoparticles	In vitro In vivo	DNA mRNA RNP	High biocompatibility Transient expression Easy production	Lack of target specificity Endosomal escape constraints
	Polymeric nanoparticles	In vitro In vivo	DNA mRNA RNP	Customizable targeting Tunable chemistry High biocompatibility Easy production	Low delivery efficiency Safety concerns Complex formulation issues for target specificity
	Peptide-based nanoparticles	In vitro Ex vivo In vivo	mRNA RNP	High efficiency Relatively higher safety	Variable efficiency depending on cell type Sensitivity to protease degradation
	Extracellular vesicles	In vitro Ex vivo In vivo	mRNA RNP	High biocompatibility Natural targeting properties No immunogenicity	Challenging isolation, characterization, and cargo loading
	Electroporation	In vitro Ex vivo	DNA mRNA RNP	High efficiency Suitable for various cell types	Physical cell damage Cell death Unsuitable for in vivo

Nonviral physical	Microinjection	In vitro Ex vivo	DNA mRNA RNP	High reproducibility Direct delivery Suitable for dosage control	Physical cell damage Low throughput Unsuitable for in vivo
	Hydrodynamic injection	In vivo	DNA RNP	High efficiency for the liver	Unsuitable for other organs
	iTOP	Ex vivo	RNP	High cell viability High efficiency Suitable for various cell types, including primary T cells	Unsuitable for in vivo
Hybrid	Virus-like particles	In vitro Ex vivo In vivo	mRNA RNP	High efficiency No genome integration	Limited packaging capacity Manufacturing complexity

2 Viral Delivery Systems

Viral vectors provide superior efficiency in delivering genetic material ex vivo and in vivo by exploiting innate mechanisms of membrane translocation and intracellular trafficking. Their surface proteins enable effective bypass of cellular barriers, allowing delivery of various molecular cargoes. While originally evolved for viral replication, these engineered systems currently serve as foundational platforms for therapeutic gene editing [6]. A viral vector is composed of three primary elements: the protein capsid or envelope, which both encapsulates the genetic payload and determines the tissue tropism as well as antigenic profile; the transgene payload, whose expression is responsible for the intended cellular effect; and the regulatory cassette, comprising promoters and enhancers that govern episomal or integrative expression. The design and optimization of these components vary across platforms, each presenting distinct trade-offs in expression kinetics and stability. By engineering these modules, viral vectors can be tailored to deliver gene-editing machinery into therapeutically relevant tissues. Their innate capacity for cell-specific targeting and efficient intracellular trafficking remains a primary driver for their widespread implementation in clinical gene therapy [7]. Although viral vectors include vaccinia, measles, herpes simplex, alphavirus, vesicular stomatitis, influenza, and baculoviruses, three platforms, namely adeno-associated virus, lentiviral, and adenoviral vectors, are predominantly employed for the delivery of gene editing systems, gaining significant attention in ongoing clinical trials [4, 8].

With over three decades of development, viral vectors remain the most efficient platforms for delivering plasmid-based nucleic acids both in vitro and in vivo, with several systems having achieved clinical approval. Despite their high transduction rates and broad tropism, significant limitations persist, including the risk of insertional mutagenesis, which may lead to oncogenesis, limited packaging capacity, and restricted efficacy in nondividing cells. Furthermore, complex manufacturing requirements and potential immunogenicity can hinder their repeated administration in therapeutic contexts. To address these challenges, engineered viral variants have been developed with improved safety profiles and enhanced targeting capabilities [9]. Despite the improvements achieved with these artificially modified viral vectors, distinct vector-specific challenges continue to impede their broader implementation. For adeno-associated virus platforms, the primary bottleneck remains the transition from small-scale production to large-scale, GMP-compliant manufacturing, which slows the clinical development pipeline. In contrast, the clinical utility of adenoviral vectors is frequently compromised by potent immune responses, necessitating strategies to mitigate severe inflammatory side effects. For lentiviral systems, research remains focused on refining integration profiles to minimize the risk of

insertional mutagenesis and enhance long-term safety. Addressing these vector-specific limitations is essential for expanding the therapeutic scope of gene-editing technologies to a wider array of clinical indications [8].

Overall, these advancements have facilitated the successful implementation of viral-based delivery across in vitro, ex vivo, and in vivo platforms, supporting preclinical and clinical genome editing trials.

2.1 Adeno-Associated Virus Vectors

Adeno-associated viruses (AAVs) are small, nonenveloped viruses from the Parvoviridae characterized by a ~4.9 kb single-stranded DNA genome. In modified AAV systems, the rep and cap genes, which are essential for replication and packaging, are provided in trans, rendering the resulting vectors replication-deficient [10]. AAVs have emerged as the premier platform for in vivo gene therapy. As a nonintegrating platform, it offers a high safety profile due to the low frequency of genomic integration. Furthermore, their minimal immunogenicity and limited tropism for antigen-presenting cells facilitate sustained therapeutic expression in post-mitotic tissues. Its ability to maintain episomal transgene expression for long periods is advantageous for nondividing tissues such as the retina and central nervous system, although its limited packaging capacity remains a key disadvantage [11].

AAVs are extensively utilized to deliver ZFNs and CRISPR-Cas9. By inducing targeted double-strand breaks (DSBs), these systems promote homology-directed repair (HDR) for precise donor integration. Clinical and preclinical studies have successfully deployed AAVs to target diverse organs, including the central nervous system and the liver [6].

A critical limitation of AAV is its ~4.7 kb packaging capacity, which is frequently exceeded by next-generation editors. To circumvent this, dual-vector strategies employing split-intein systems have been developed to reconstitute base editors (CBEs and ABEs) and prime editors (PE) in vivo. Significant mutation reversions in models of Niemann-Pick disease and hereditary deafness have been achieved using dual-AAV systems [12, 13]. Recent engineering efforts have produced compact, single-vector ABEs, such as Nme2-ABE8e and size-optimized ABE8e variants, which achieve up to 66% editing efficiency in the liver, thereby streamlining production and reducing required dosages [14]. The ~6.3 kb coding sequence of PEs, which exceeds the packaging limit of AAVs, necessitates sophisticated optimization. Strategies including nuclear localization signal (NLS) refinement, codon optimization, and the development of miniature PEs have improved editing titers [15]. While dual-rAAV8 systems have demonstrated up to 46% efficiency in the murine liver and 42% in the cortex, efficiency in sensitive tissues like the retina remains a challenge, highlighting the need for further refinement [16, 17].

Clinical translation of AAV-mediated CRISPR systems remains in the early stages, with EDIT-101, under development for the treatment of Leber congenital amaurosis type 10 (LCA10). EDIT-101 targets a pathogenic intronic mutation in CEP290, utilizing AAV5 to deliver *Staphylococcus aureus* Cas9 and dual guide RNAs via subretinal injection [18].

These studies demonstrate the central role of AAVs in advancing in vivo genome editing. The strategic selection of capsid serotypes is essential for achieving precise tissue tropism: AAV5 is optimized for subretinal delivery, whereas AAV8 is preferable for hepatic applications. Furthermore, AAV9 and its engineered variants provide the systemic distribution necessary to cross the blood-brain barrier and achieve widespread transduction within the central nervous system [19].

The established safety profile and clinical longevity of AAV episomes underscore their potential for treating genetic disorders. Future research must prioritize the optimization of manufacturing scales to ensure affordability, the engineering of capsids to bypass pre-existing neutralizing antibodies, and the continued miniaturization of editing machinery to maximize therapeutic efficacy within the constraints of the AAV capsid. Overall, high in vivo transduction efficiency, broad tissue tropism, and the capacity for persistent episomal expression in nondividing cells establish AAVs as a primary platform for therapeutic gene editing. Furthermore, their low frequency of genomic integration minimizes the risk of insertional mutagenesis, enhancing their safety profile for clinical applications.

2.2 Lentiviral Vectors

Lentiviral vectors (LVs) are widely utilized for in vitro and ex vivo gene editing due to their capacity for stable genomic integration. Derived from retroviruses, these single-stranded RNA vehicles are capable of transducing both dividing and nondividing cells. Their relatively large packaging capacity (~8 kb) facilitates the delivery of all gene editing components within a single vector backbone. While the random integration of LVs into the host genome ensures stable transgene expression, it concurrently introduces the risk of insertional mutagenesis. To mitigate these risks, integration-deficient lentiviral vectors (IDLVs) have been developed. IDLVs incorporate a point mutation within the integrase protein to prevent genomic incorporation, thereby enhancing their safety profile [20]. Although IDLVs typically exhibit lower transgene expression levels, these can be optimized by including the IS2 element, which enhances transgene expression while maintaining target cell specificity [21]. Further safety refinements include implementing self-inactivating, transient CRISPR systems. These strategies employ a dual-gRNA approach: one guide targets the gene of interest, while a second "self-targeting" gRNA disrupts the Cas9 sequence itself. This mechanism ensures transient nuclease activity, significantly reducing off-target effects associated with prolonged Cas9 expression [20].

Unlike episomal systems, LVs facilitate the inheritance of CRISPR components by daughter cells, ensuring a persistent therapeutic effect in highly proliferative populations such as T-lymphocytes and hematopoietic stem cells (HPSCs) [22]. A nonintegrating lentiviral system encoding guide RNA and donor DNA for delivery of Cas9 protein to HSPCs was also developed, enabling transient endonuclease activity and the inclusion of all editing tools within a single ("all-in-one") vector, and demonstrating efficient one-time correction of the sickle cell disease mutation [23]. LVs are the most actively investigated vehicles for generating chimeric antigen receptor (CAR)-T cells, serving as the backbone for both established laboratory-based manufacturing and emerging direct-injection therapies. The current clinical standard for CAR-T therapy follows an ex vivo autologous manufacturing model. To overcome the bottlenecks of ex vivo manipulation, such as high costs and complex logistics, researchers are developing strategies for direct in vivo CAR-T generation, where LVs are administered systemically to program T cells within the patient's body. Because in vivo delivery lacks a controlled environment, LVs must be engineered with extreme precision to avoid off-target sequestration in organs such as the liver. Pseudotyping and decoration of LVs by antibody-derived moieties may serve to ensure the target cell specificity [24]. Several LV-based in vivo programs have moved into Phase I clinical trials, including UB-VV111 (targeting CD19) [25], INT2104 (targeting CD7), and ESO-T01 (targeting BCMA). Early evidence suggests these vectors can successfully generate functional CAR-T cells in vivo that achieve tumor control without the need for traditional lymphodepleting chemotherapy [24].

LVs hold immense potential to transition gene editing from expensive, logistically intensive ex vivo models to scalable, off-the-shelf in vivo therapies that could dramatically broaden patient access. Their key advantages lie in a robust packaging capacity for complex therapeutic designs, the ability to induce stable genomic integration for long-term expression, and a modular envelope that facilitates precise targeting of specific cell lineages through pseudotyping. However, these systems face critical disadvantages, including the theoretical risk of insertional mutagenesis and the challenge of navigating systemic biological barriers such as complement-mediated inactivation and rapid sequestration by macrophages in the liver and spleen. Despite these limitations, the evolution of high-safety third-generation systems and engineered immune-stealth features continues to solidify LVs as a versatile and foundational modality for advanced cellular reprogramming [26, 27].

2.3 Adenoviral Vectors

Adenoviral (AdV) vectors are nonenveloped, double-stranded DNA viruses, capable of transducing both quiescent and proliferating cells. A primary advantage of the AdV platform is its substantial packaging capacity (>35 kb), which easily accommodates large expression cassettes of the editing machinery. Unlike lentiviral systems,

AdVs remain episomal, thereby mitigating the risks of insertional mutagenesis and reducing the potential for long-term off-target editing. While early-generation AdVs were associated with acute and chronic inflammatory responses, modular engineering has significantly enhanced their safety profile for clinical gene delivery [20]. To mitigate the cytotoxicity and in vivo immunogenicity associated with leaky viral gene expression in early-region-deleted AdVs, helper-dependent vectors (HDAds) have been investigated for genome editing [28]. By deleting all viral coding sequences, HDAds minimize chronic toxicity and expand the cloning capacity to approximately 37 kb while maintaining high transduction efficiency [29]. Furthermore, this expanded capacity facilitates the delivery of sophisticated editing machinery, such as BEs [30] and PEs [31]. Despite these refinements, pre-existing immunity remains a formidable barrier; widespread natural exposure to AdVs often results in high titers of neutralizing antibodies, which can trigger acute immune reactions and compromise transgene persistence. HDAds effectively transduce integrated complexes comprising Cas nickases fused to deaminase or reverse transcriptase domains, respectively, alongside their cognate gRNAs. This single-vector approach circumvents the requirement for multi-vector systems, potentially enhancing editing efficiency across diverse cell types [32]. AdV-mediated CRISPR delivery has demonstrated efficacy across several ex vivo and in vivo disease models and successfully corrected mutations in Duchenne muscular dystrophy (DMD) [33] and cystic fibrosis [34]. Beyond monogenic disorders, the platform shows promise in oncology. Disrupting the epidermal growth factor receptor (EGFR) via AdV-CRISPR has been shown to inhibit tumor progression in human lung cancer xenografts [35]. Other significant applications include targeting PCSK9 in murine livers to reduce LDL cholesterol [36] and disrupting CCR5 in CD4+ T cells to confer resistance to HIV infection [37].

As a summary, AdVs remain episomal and possess a much larger payload capacity. They are highly efficient at transducing a broad range of cell types but are limited by high innate immunogenicity and the prevalence of pre-existing immunity in human populations, which can lead to rapid clearance and inflammatory complications [38, 39].

In conclusion, viral platforms are specifically engineered for DNA-based CRISPR systems that require constitutive intracellular transcription and long-term expression; however, they are not preferable for CRISPR formats such as RNPs, where transient nuclease activity is required to mitigate off-target effects [40].

3 Nonviral Delivery Systems

Nonviral systems have two major groups, namely, chemical nanocarriers and physical methods. Chemical carriers include lipid nanoparticles (LNPs), inorganic nanoparticles, polymeric nanoparticles, peptide-based nanoparticles, and extracellular vesicles (EVs)

[2, 20, 41]. The clinical application of CRISPR-Cas9 systems within nonviral delivery utilizes various biomolecular formats, including pDNA, mRNA, and RNP complexes. While early investigations focused primarily on pDNA-based transfection, the current paradigm for systemic, nonviral in vivo delivery has shifted toward RNA-based platforms, which have demonstrated significant efficacy in preliminary clinical trials. In contrast, RNP delivery has gained considerable traction for ex vivo applications due to its rapid kinetics and reduced off-target profile; however, its transition to systemic in vivo therapeutic use in patients remains a significant challenge. Generally, delivery vectors are engineered to accommodate a specific Cas9 format, although recent advancements in polymer and nanoparticle research have yielded hybrid platforms capable of co-delivering two or more of these distinct molecular configurations [42]. While physical methods are highly effective for generating in vitro knockout cell lines and animal models, their utility for systemic in vivo therapy remains limited. Conversely, although synthetic nonviral systems offer superior safety and modularity, they often exhibit lower delivery efficiency compared to viral vectors.

3.1 Chemical Nanocarriers

Researchers have investigated various delivery strategies based on lipidic, polymeric, inorganic, peptide-based, bioderived, and hybrid nanoparticles, focusing on the delivery of mRNA and RNP formats, to realize the therapeutic potential of the CRISPR/Cas9 systems for clinical applications. Nanocarriers utilize endocytic pathways for cellular entry, requiring successful endosomal escape to release mRNA and RNP into the cytosol. There, mRNA is translated into the Cas9 protein, which translocates to the nucleus to initiate genome editing [2, 42].

3.2 Lipid Nanoparticles

LNPs are an increasingly attractive nonviral platform by their use in COVID-19 mRNA vaccines and systemic CRISPR therapies targeting the liver. Extensive research has documented the delivery of CRISPR systems via LNPs, utilizing various cargo formats and ultimately overcoming biological barriers for in vivo delivery [2, 43]. These platforms have demonstrated the capacity to encapsulate an expansive repertoire of CRISPR-derived gene editors for diverse therapeutic applications [44].

LNPs are complex chemical assemblies typically comprising ionizable lipids, phospholipids, cholesterol, and polyethylene glycol (PEG) lipids. The components and the specific formulation conditions of LNPs directly dictate the physicochemical properties of the particles, such as morphology, hydrodynamic diameter, surface potential, and internal packing density. These characteristics are primary determinants of colloidal stability and systemic biodistribution. The LNP functions by sequestering CRISPR cargoes through electrostatic interactions, providing a protective shield against nuclease degradation and minimizing immune recognition during systemic circulation [45]. Furthermore, recent innovations in LNP chemistry,

specifically the engineering of biodegradable ionizable lipids, have significantly enhanced particle stability and extended circulation half-life. These advancements concurrently mitigate cellular toxicity and diminish systemic immunogenicity, thereby facilitating increased cargo delivery efficiency to target tissues [6].

Specifically, LNPs function by encapsulating negatively charged mRNA or RNPs within a pH-responsive lipid shell, facilitating endosomal escape upon entry into the cell. While exceptionally effective for hepatic delivery, targeting nonhepatic tissues remains an active area of research [45]. In clinical and preclinical models, robust efficacy for in vivo editing, particularly within the liver, has been demonstrated. Hepatic tropism is primarily driven by the adsorption of apolipoprotein E (ApoE) onto the LNP surface, which facilitates uptake via low-density lipoprotein receptors (LDLR) [46]. This endogenous targeting mechanism has enabled the efficient disruption of therapeutic targets such as PCSK9 and ANGPTL3, resulting in significant reductions in circulating lipid levels [47, 48]. To expand the therapeutic reach of CRISPR beyond hepatic tissues, significant research has focused on selective organ targeting (SORT) LNPs. By incorporating a supplemental lipid component to modulate surface charge and protein corona composition, SORT LNPs can be redirected to extrahepatic sites [49, 50]. For instance, cationic lipid-enriched formulations preferentially accumulate in the lungs, whereas anionic lipid-enriched variants favor splenic delivery [51]. Conversely, studies have shown that transient macrophage depletion can further refine biodistribution by reducing immune-mediated clearance [52].

Local administration strategies offer an alternative route to bypass systemic barriers. Intramuscular and intratumoral injections have facilitated successful genome editing in skeletal muscle for dystrophin restoration and in glioblastoma models, respectively [45, 53]. Furthermore, inhalation-based nebulization [43] and intracameral injections [54] have shown promise for pulmonary and ocular genome editing. The physicochemical tuning of LNPs, including adjustments to particle size, lipid molar ratios, and apparent pKa, remains a primary determinant of organ specificity, with higher pKa formulations generally favoring pulmonary targeting.

Surface functionalization represents another sophisticated approach for achieving cell-type specificity. The conjugation of PEG lipids with antibodies, aptamers, or peptides allows for highly targeted delivery, such as aptamer-mediated tumor targeting or specialized ionizable lipids designed for bone tissue and immune cell engagement [55]. Recent applications of these technologies include the successful treatment of primary hyperoxaluria type 1 via HAO1 disruption and the restoration of Rpe65 expression in models of hereditary retinal dystrophy [56]. Additionally, spleen-tropic LNPs engineered for

T-cell targeting hold significant potential for advancing HIV resistance and cancer immunotherapy [57].

In conclusion, LNPs offer high biocompatibility, lower immunogenicity compared with viral vectors, and compatibility with established, scalable manufacturing processes, providing a versatile and clinically relevant nonviral strategy for in vivo therapeutic applications.

3.3 Polymeric Nanoparticles

Polymeric nanoparticles represent a critical class of delivery vehicles for genome-editing machineries, based on their advantageous safety profiles and biocompatibility. Polymers for gene delivery are characterized by repeating structural units containing amine functional groups within their backbone. Depending on the specific pKa of these groups, the amines maintain a positive charge across neutral-to-acidic pH ranges, facilitating electrostatic interactions with nucleic acids and their subsequent compaction into polyplexes [3, 58].

These macromolecules exhibit significant architectural diversity, ranging from strictly linear to highly branched configurations. Beyond structural topology, the polymer's molecular weight is a primary determinant of both nucleic acid condensation efficiency and overall transfection potency. Polyethylenimine (PEI), one of the most efficient polymers, has been extensively investigated for gene delivery. Both linear and branched variants of PEI are frequently used in the formulation of delivery vehicles, as their high charge density enables robust cargo protection and effective cellular internalization [3]. Polymers, such as poly(lactic-co-glycolic acid) (PLGA) and layered double hydroxides (LDHs), demonstrate favorable biocompatibility and biodegradability, supporting their in vivo application for clinical translation [1, 59]. Furthermore, poly(β-amino ester) (PBAE) nanoparticles have been used to encapsulate Cas9 plasmid DNA targeting the HPV16-E7 oncogene via intratumoral administration, resulting in efficient delivery of the pCas9 cargo and significant inhibition of neoplastic progression in HPV16-associated cervical malignancy models [60]. In another approach, both cholesterol- and ethanolamine-containing poly(glycidyl methacrylate) (PGEA) nanoparticles were engineered for the in vivo delivery of a dual-expression plasmid encoding Cas9 and gRNAs to disrupt the Fbn1 gene, a determinant of Marfan syndrome [61].

Synthetic nanomaterials offer substantial design flexibility, as the composition of nanocarriers, considering their physicochemical properties, including hydrodynamic diameter, morphology, surface potential, and molecular composition, enables circumventing biological barriers and refining tissue-specific targeting. In addition, polymeric carriers allow for precise tuning of surface chemistry. These materials can be functionalized with specific ligands to facilitate receptor-mediated endocytosis, allowing for cell-type-specific targeting [59, 62].

These platforms accommodate distinct CRISPR cargoes across plasmid DNA, mRNA, and RNP formats, while simultaneously facilitating the co-delivery of synergistic therapeutic agents. The chemical synthesis of these vectors supports both scalable and cost-effective manufacturing protocols. Despite these operational advantages, polymeric nanoparticles, as nonviral systems, typically exhibit lower transduction and transfection efficiencies than their viral counterparts and require extensive physicochemical optimization to reach therapeutic thresholds [58, 63].

3.4 Peptide-Based Nanoparticles

Positively charged peptides derived from HIV-1 have been shown to significantly enhance DNA cellular uptake. Subsequent research established that short sequences of basic amino acids are sufficient to facilitate nucleic acid binding through electrostatic interactions. These findings led to the formal classification of these sequences as cell-penetrating peptides (CPPs) due to their capacity to mediate intracellular access. CPPs are short sequences, typically comprising 5–30 amino acids, characterized by an enrichment of cationic or amphipathic residues. CPPs have been increasingly investigated as nonviral delivery vehicles for CRISPR–Cas9 genome-editing systems, particularly on RNP and mRNA, thereby enabling transient genomic modification. These peptides facilitate the intracellular delivery of macromolecules by mediating either direct membrane translocation or various endocytic uptake pathways [64,65]. However, the precise pathways through which CPPs enter cells remain a subject of ongoing investigation. While early models proposed direct translocation across the plasma membrane, more recent evidence points to active endocytosis as the primary route of uptake. Notably, comparative studies have indicated that many CPPs fail to facilitate significant endosomal escape. This suggests that the primary function of these peptides may be limited to promoting cell-surface association in low-serum environments, rather than directly driving cargo translocation into the cytosol [3].

The use of CPPs, such as TAT, relies on endocytic uptake, which requires efficient endosomal escape to release cargo into the cytosol. To address this, endosomolytic sequences like the influenza-derived HA2 peptide are often employed to produce chimeric CPPs, enabling pH-dependent conformational transitions within acidic endosomes to facilitate membrane destabilization [66]. Self-delivering Cas9 plasmids incorporating CPP-like elements can achieve efficient genomic modification in primary human cells with lower cytotoxicity than traditional electroporation [67]. Furthermore, the modularity of CPPs has been exploited for tissue-specific applications, such as engineered neuron-targeting nanocomplexes that combine PepFect14 with a rabies virus glycoprotein fragment, thereby demonstrating selective editing in neuronal populations [65]. Beyond isolated peptide delivery, CPPs are increasingly integrated into hybrid platforms, such as

CPP-functionalized lipid nanoparticles designed to enhance blood–brain barrier penetration via transferrin receptor targeting [68].

In addition, proteins composed of longer amino acid chains have also been investigated as nucleic acid-binding proteins for gene delivery applications. Initial research focused on the utilization of endogenous proteins such as histones, which were evolutionarily specialized in the condensation of the genome [69]. Subsequently, the high-mobility group box protein family was also evaluated for their DNA-binding capacities. While these proteins demonstrate high efficiency in compacting genetic material, they lack intrinsic mechanisms for endosomal escape. Consequently, their functional delivery is often dependent on the co-administration of lysosomotropic agents, such as chloroquine, which facilitates cytosolic entry by inducing endosomal escape and subsequent membrane rupture [3].

Despite current limitations, ongoing research on CPP–polymer and CPP–lipid hybrid platforms, as well as the capacity of vector design based on a vast repertoire of human proteins with highly specialized functions, suggests peptide-based gene delivery systems have significant potential for clinical translation.

3.5 Extracellular Vesicles

Extracellular vesicles (EVs) are lipid bilayer biological nanoparticles secreted by cells for intercellular communication. EVs have emerged as a promising delivery approach for therapeutics, including CRISPR-based gene-editing tools [70]. The intrinsic cargo capacity and lipid bilayer encapsulation of EVs render them highly effective delivery vehicles for therapeutic macromolecules. As they are derived from host cells, they exhibit superior biocompatibility and can evade the reticuloendothelial system. EVs can facilitate the transport of CRISPR components in various formats, including RNPs, mRNA/sgRNA complexes, or plasmid DNA, while simultaneously shielding these payloads from enzymatic degradation and enhancing systemic stability [71]. Cargo loading is typically achieved through either endogenous or exogenous strategies. Endogenous methods involve engineering donor cells to express or recruit CRISPR components into EVs during biogenesis. In contrast, exogenous strategies involve loading the cargo after vesicle isolation using membrane-permeabilization techniques such as electroporation, surfactant treatment, or microfluidic loading. Endogenous approaches generally offer superior consistency and reproducibility; furthermore, the EV lipid bilayer can extend the functional half-life and bioavailability of CRISPR cargoes in vivo. However, standardized high-throughput loading remains technically challenging [72, 73].

Reflecting these mechanistic advantages, engineered EVs are increasingly utilized for in vivo CRISPR delivery [74]. The functional delivery of dCas9-VPR/sgRNA complexes via engineered extracellular vesicles enables the targeted upregulation of endogenous hepatocyte growth factor, demonstrating a potent therapeutic strategy

for counteracting liver damage in murine models [75]. RNP-loaded EVs have demonstrated significant functional benefits in preclinical models. Engineered EVs, loaded with RNPs by a high-throughput microfluidic electroporation system, exhibited facilitated auditory recovery in a mouse model, demonstrating the efficacy of this platform for treating dominant progressive hearing loss [76].

In cancer treatment, targeted disruption of PARP-1, which induced apoptosis and enhanced sensitivity to chemotherapy via EV-mediated RNP delivery, was demonstrated in ovarian tumor models [77]. Further, Duchenne muscular dystrophy (DMD), a monogenic disease, has been targeted by EV-mediated delivery of CRISPR-Cas9 components, exhibiting increased dystrophin expression in treated animal models [78]. Similarly, EVs engineered with RNP achieved 90% editing efficiency in primary skeletal muscle cells derived from DMD patient-induced pluripotent stem cells (iPSCs) [79].

Recent methodological advancements incorporate the fusogenic protein VSV-G, which promotes endosomal escape and the translocation of cargo into the recipient cell cytosol, enhancing intracellular delivery. These platforms utilize an engineered mini-intein protein with self-cleavage activity to tether molecular cargoes to an EV-sorting domain, subsequently facilitating their release into the cytosol of recipient cells [80]. Further, the safeEXO platform, which delivers RNPs, mRNA, and other nucleic acids with dose-dependent editing and minimal immunogenicity in vivo, has been used to develop safeEXO-CAS-ITGA6 vesicles that edit EMX1 in lung epithelial cells in mice [81]. An alternative methodology for engineered EVs has utilized chemically inducible heterodimerization in conjunction with fusogenic components to produce FKBP/FRB/VSV-G-EVs, facilitating the encapsulation and delivery of CRISPR components. This approach has been successfully employed for ex vivo inactivation of Pcsk9 in primary hepatocytes, resulting in significant downstream functional modulation of LDL receptor activity [82]. Other approaches in engineered EVs that incorporate active cargo-loading modules, T-cell-targeting domains, and fusogenic glycoproteins have been employed to deliver RNP complexes into primary human CD4+ T cells, revealing the potential of EV-based delivery in T-cell immunotherapies [83].

Overall, in addition to efficient delivery, EVs exhibit superior biocompatibility and offer distinct opportunities for targeted tissue delivery. EVs are internalized through diverse endocytic pathways and can bypass restrictive biological barriers, including the blood–brain barrier via transcytosis [84]. Furthermore, their tropism can be refined through surface engineering with ligands, antibodies, or peptides to facilitate cell-selective uptake. Despite the promising advancements, the clinical transition of these platforms remains constrained by significant variability in EV yield and the heterogeneity of vesicle populations. To achieve reproducible, scalable,

and safe EV-mediated genome editing, therapeutic applications strictly necessitate the establishment of standardized manufacturing protocols, precise regulation of cargo loading and release kinetics, and comprehensive characterization of in vivo biodistribution and persistence [85].

4 Physical Delivery Methods

Physical transfection methods enable direct access and high potency, bypassing the requirement for viral or chemical vectors. They circumvent the limited cargo size or format inherent to viral platforms and the endocytic rate limitations associated with chemical carriers. The physical delivery methods are electroporation, hydrodynamic delivery, micro-injection, iTOP (induced transduction by osmocytosis and propanebetaine), GONAD (Genome editing via Oviductal Nucleic Acids Delivery), TRIAMF (Transmembrane Internalization Assisted by Membrane Filtration), and mechanical cell deformation [1]. These techniques leverage electrical, thermal, or mechanical forces to transiently disrupt the plasma membrane, facilitating the passive diffusion or active translocation of molecular cargoes into the cytosol. A prominent example is electroporation, which utilizes high-intensity electric fields to induce reversible membrane permeabilization. Beyond simple perforation, the applied field generates electrophoretic forces that drive the migration of anionic cargoes, such as plasmid DNA or RNPs, directly into the intracellular environment [86].

Despite the high efficiency of physical transfection, its clinical in vivo utility is often restricted by the invasive nature of the required procedures. In the context of gene editing, in vivo electroporation has successfully delivered genetic material to murine epidermal and retinal tissues [87, 88]. Furthermore, silicon nanoneedles have been employed to deliver plasmid DNA encoding vascular endothelial growth factor (VEGF) into murine muscle, promoting therapeutic neovascularization [89]. Nevertheless, the inherent invasiveness of these methods necessitates the continued use of delivery vectors for most systemic therapeutic applications.

Physical delivery methods are particularly advantageous for hard-to-transfect primary cells, including neurons, stem cells, and hematopoietic lineages. In vitro editing of these populations remains a critical approach for elucidating human gene function. Beyond research, physical transfection, specifically electroporation, is superior for ex vivo clinical applications, such as adoptive cell immunotherapy. While traditional viral-based ex vivo engineering is limited by high manufacturing costs and prolonged expansion timelines, physical methods enable high-throughput, cost-effective genomic modification [86]. Recent clinical reports underscore this potential. Xu et al. demonstrated the long-term persistence (>19 months) of

CRISPR-edited hematopoietic stem cells delivered via electroporation, with no associated adverse complications [90]. Similarly, a Phase 1 trial by Stadtmauer et al. utilized electroporation to deliver Cas9 RNPs for multiplex editing of T cells in patients with refractory cancer [91].

Although there are challenges for in vivo applications and limitations in certain tissues, such as the brain, lung, and spinal cord [20], their relatively high efficiency for ex vivo applications is promising for future investigations into technical improvements.

4.1 Electroporation

Electroporation is used for clinical ex vivo editing and is a conventional technique for creating animal models and studying disease pathogenicity. By applying controlled electrical pulses, transient pores are created in the cell membrane, allowing the entry of plasmid DNA, mRNA, and RNP complexes [1]. The primary drawbacks of electroporation are its relatively low gene-editing efficiency and high levels of associated cell death. The electrical pulses required to open the cell membrane can be harsh, often reducing the overall survival rate of the treated cells. Despite these challenges, electroporation is a standard tool in both basic research and clinical therapy [92].

Several biophysical and biological variables, including electric field strength, pulse duration and frequency, cell diameter, and cargo concentration, determine the efficacy of electroporation. Extending the pulse duration generally produces larger membrane pores that remain open for longer intervals, thereby facilitating molecular entry. However, optimizing these parameters requires a careful balance. Even transient membrane disruption can cause significant perturbations in cellular homeostasis, leading to DNA damage, mitochondrial stress, and, in severe cases, cell death. Despite these challenges, electroporation remains a relatively straightforward method for delivering exogenous molecules and offers distinct advantages over viral vectors. Viral platforms are exceptionally expensive, particularly when scaling for clinical-grade production. In contrast, electroporation is a more cost-effective alternative, though it still requires specialized equipment that meets good manufacturing practice (GMP) standards, and technologies that remain relatively limited in the current market [92].

Technical advancements have expanded the utility of electroporation in both fundamental research and clinical medicine. Ex vivo modification of primary cells by electroporation for adoptive cell therapy is one of the most significant applications at the clinical level [93]. This technique also allows the combined delivery of different cargos, which is critical in genome engineering when a DNA repair template is required [94, 95]. In addition, correction of hematopoietic stem cells (HSCs) for sickle cell disease [96] and corneal epithelial cells for corneal dystrophies [97].

Recent progress in micro- and nanofluidic technologies has enabled single-cell electroporation to achieve a high-throughput process

and improve cell viability [98, 99]. Specifically, nanostraw-mediated electroporation platforms allow for precise dosage control and the efficient delivery of molecular cargoes into diverse cell populations, including primary cells [100, 101]. However, optimization of electroporation parameters remains critical, particularly for sensitive populations such as stem cells, to balance transient membrane disruption, which can further lead to DNA damage and mitochondrial stress. If these physiological stressors are not minimized, they can trigger apoptotic pathways and lead to cell death. While ongoing optimization aims to improve transfection efficiency and minimize cellular disruption, the future of this platform depends on the development of automated, GMP-compliant systems. Such advancements are essential to increase the accessibility of these therapies and streamline their clinical translation.

4.2 Hydrodynamic Delivery

Hydrodynamics-based transfection involves rapid, high-pressure infusion of a large volume of fluid containing gene-editing components into a rodent's tail vein. Typically, the injection volume corresponds to 8%–10% of the subject's total body weight, equivalent to approximately 20–25 mL for an adult rat. The resulting physical pressure transiently disrupts the vascular endothelium and cell membranes, facilitating the entry of CRISPR cargoes into parenchymal cells. Research has demonstrated varying degrees of success with this method, including a genetic correction rate of approximately 1 in 250 murine hepatocytes and a 2.6% modification rate when targeting the PTEN gene in the liver [6, 20, 92]. Current studies demonstrate that hydrodynamic delivery is a robust tool for investigating off-target effects and long-term effects of genome editing, such as carcinogenesis in mouse models [102, 103]. Despite these experimental results, hydrodynamic delivery remains unsuitable for clinical translation. The procedure causes a sudden and severe increase in venous blood pressure, leading to transient cardiac dysfunction, acute hepatic expansion, and significant risk of mortality in treated subjects [92].

4.3 Microinjection

Mechanical transfection, also called mechano-transfection, utilizes physical forces, such as direct contact with solid structures or fluid, to induce shear stress that transiently permeabilizes the plasma membrane. These mechanical disruptions create transient pores that facilitate the passive diffusion of molecular cargoes into the cytosol. Microinjection is an example of mechanical transfection and bypasses the requirement for diffusion by directly depositing the delivery buffer and its associated materials into the intracellular compartment. This direct translocation ensures precise cargo localization while minimizing the volumetric constraints often associated with other transfection modalities [86]. Microinjection offers the highest degree of precision, allowing the direct deposition of all three

CRISPR cargo formats into the cytoplasm or nucleus of a single cell, such as zygotes. This remains the foundational method for generating genetically modified organism (GMO) models in research [6]. This procedure utilizes a specialized microneedle and is conducted under high-magnification microscopy. The primary advantages of microinjection include the absence of cargo size constraints, nearly 100% delivery efficiency with no collateral damage to surrounding tissues, and the guaranteed deposition of material directly into the target cell. CRISPR components can be introduced into either the cytoplasm or the pronucleus of fertilized eggs, a strategy widely employed to develop in vivo models in species such as *Zebrafish, Caenorhabditis elegans*, and mice. Furthermore, the high accuracy of this method allows researchers to rigorously compare the genome-editing efficacy of different plasmid-based CRISPR systems targeting the same locus [86]. Microinjection is currently a powerful tool for generating disease models by gene editing [104–106]. Despite these technical strengths, microinjection is inherently limited to low-throughput applications because it requires manual intervention for each cell during the injection cycle.

4.4 Mechanical Cell Deformation

Mechanical cell deformation, facilitated by microfluidic architectures that use electrical pulses, hydrodynamic pressure, or optical energy, induces transient membrane permeability, enabling intracellular uptake of macromolecules. The diverse array of microfluidic-based mechanoporation strategies is discussed extensively in the literature [20,107,108]. This approach provides a highly efficient delivery platform for hard-to-transfect cell populations. Studies utilized this method to introduce DNA plasmids encoding CRISPR-Cas components into breast cancer and lymphoma cell lines with significant efficiency [109]. Furthermore, RNPs were delivered into SKBR-3 breast cancer cells [110], indicating that mechanoporation is a valuable tool for delivering distinct cargo formats. As a technical advancement, a microfluidics-based cell mechanoporation platform has been designed to deliver both mRNA and CRISPR systems into primary human T cells, enabling efficient, stable, and clinically scalable gene delivery. The platform uses controlled mechanical deformation within microfluidic droplets to transiently permeabilize cell membranes, thereby minimizing cytotoxicity while preserving editing efficiency [111].

Compared to conventional electroporation, mechanical membrane deformation is often considered superior for the intracellular translocation of macromolecules. This approach, which utilizes physical compressive or shear forces rather than high-voltage electrical stimuli, minimizes the potential for electric field-induced cellular stress and better preserves the functional integrity of sensitive target populations [1].

4.5 iTOP (Induced Transduction by Osmocytosis and Propane Betaine)

iTOP represents a specialized chemical methodology for the intracellular delivery of proteins and other functional biomolecules. This approach utilizes a hyperosmolar transduction buffer containing propane betaine and sodium chloride to stimulate macropinocytosis, thereby facilitating the endocytic uptake of exogenous cargo. Through the iTOP platform, both separate Cas9/sgRNA components and RNPs can be efficiently transduced into target cells. As a relatively recent development, its application to in vivo CRISPR delivery has not yet been demonstrated, and the method's comprehensive safety and longitudinal efficacy profiles remain under investigation [1].

Preliminary studies indicate that iTOP enables high-efficiency RNP delivery across a range of primary cell types. For example, Astolfo et al. reported that two sequential applications of the iTOP protocol achieved a 26% transfection efficiency in human embryonic stem cells (hESCs) [112]. The platform was evaluated across multiple human cell lines, including primary T cells, human induced pluripotent stem cells (hiPSCs), Jurkat, ARPE-19, and HEK293 cells for the delivery of CRISPR components. Gene-editing efficiencies and post-treatment cellular viabilities were compared with standard delivery modalities, specifically electroporation and lipofection, achieving editing efficiencies ranging from 40% to 95% and post-transduction viability consistently between 70% and 95%, depending on the specific cell architecture [113].

These findings suggest that iTOP is a highly effective, low-toxicity alternative for genome engineering in sensitive primary and pluripotent cell populations, and that it likely requires further optimization to achieve the efficiencies observed with traditional physical or viral modalities.

4.6 GONAD (Genome Editing via Oviductal Nucleic Acids Delivery)

The GONAD technique has represented a significant shift from traditional transgenic methodologies when initially described by Takahashi et al. in 2015. The procedure involves a dorsolateral incision to expose the ovaries and oviducts, followed by the intraluminal injection of genome-editing components via a glass capillary pipette. Immediately following injection, the oviduct is subjected to electroporation using tweezer-type electrodes before the reproductive organs are returned to their anatomical positions. A primary advantage of GONAD is the circumvention of labor-intensive stages inherent to conventional transgenesis, including embryo isolation, ex vivo microinjection, and subsequent surgical embryo transfer. However, a significant limitation is the high incidence of pregnancy loss, as one out of five mice. Because the success of the procedure depends on the delicate manipulation of oviductal tissue and the precise delivery of nucleic acids, results are highly dependent on operator proficiency [114]. To address these limitations, the improved-GONAD (i-GONAD) platform was developed. These technical enhancements have expanded

the system's utility for generating knockout, knock-in, and large-deletion models [115, 116]. Unlike traditional microinjection, i-GONAD does not require specialized embryo handling skills or complex micromanipulation equipment. Consequently, this platform addresses several bottlenecks in transgenic technology by reducing the total number of animals required for model generation and lowering the technical barrier for implementation in the laboratory.

4.7 TRIAMF (Transmembrane Internalization Assisted by Membrane Filtration)

The therapeutic potential of RNP-edited hematopoietic stem and progenitor cells (HSPCs) for monogenic disorders has driven the development of cost-effective, nonviral delivery platforms. The TRIAMF method, designed by Yen et al. in 2018, utilizes mechanical deformation to facilitate molecular uptake. When a cell is forced through a constriction smaller than its diameter, the lipid bilayer undergoes mechanical stretching, creating transient pores that allow for the passive diffusion of biochemical cargoes. This mechanism is particularly effective in HSPCs, which are highly susceptible to such membrane pore formation. The TRIAMF system has been systematically optimized for the delivery of RNPs into HSPCs to achieve robust genomic modification [117]. Compared with large-scale electroporation using identical RNP concentrations, TRIAMF demonstrates higher gene-editing efficiency but lower post-treatment cell viability. A distinct advantage of this platform is its compatibility with standard HSPC culture media, eliminating the requirement for specialized, high-conductivity electroporation buffers. Technically, TRIAMF is more cost-effective and simpler to implement than electroporation, as it does not require complex microfluidic fabrication. Scaling the process for clinical applications involves increasing either the total processing volume or the membrane surface area of the filtration interface [1, 118].

5 Hybrid Systems

Viral platforms provide efficient gene editing and sustained expression for DNA cargos, whereas nonviral approaches enable transient but safer delivery of mRNA or RNP formats of CRISPR. Next-generation platforms are currently shifting toward hybrid systems, such as virus-like particles (VLPs), which combine the high-efficiency entry mechanisms of viral capsids with the transient, nonintegrating nature of RNP delivery [119].

5.1 Virus-Like Particles

VLPs are noninfectious assemblies, typically derived from Moloney Murine Leukemia Virus (MMLV) or Human Immunodeficiency Virus (HIV) proteins and are engineered to encapsulate mRNAs, proteins, or RNPs. They have emerged as versatile platforms for delivering genome-editing machinery by leveraging the inherent

advantages of viral systems. Specifically, high efficiency in intracellular delivery, robust endosomal escape, and the ability to maintain modularity for incorporating diverse envelope glycoproteins for cell-specific targeting represent virus-like properties. However, VLPs facilitate the transient presence of genome-editing agents, significantly mitigating the risks associated with off-target activity and insertional mutagenesis, unlike viruses. This integration of viral transduction efficiency with the safety profile of nonviral kinetics renders VLPs a compelling modality for therapeutic applications [120, 121]. VLPs are employed for various gene-editing cargoes, specifically mRNA, CRISPR-RNP, and PE-RNP, resulting in ex vivo and in vivo therapeutic editing [122–124]. Furthermore, they achieve substantial editing efficiencies across multiple cell types, enabling targeting of specific subpopulations via envelope pseudotyping [125, 126]. Given the aforementioned advantages over traditional viral vector delivery, VLPs hold significant potential for personalized medicine tailored to individual genetic mutations [6].

On the other hand, VLPs face significant technical hurdles, including limited cargo capacity, structural stability, and the complexities of large-scale manufacturing. To overcome volume constraints, the development of bespoke VLPs utilizing modified capsid monomers has been proposed to increase particle diameter and surface area without compromising structural integrity [127]. Furthermore, enhancing VLP stability through specialized formulations, such as surface PEGylation, may reduce protein aggregation and facilitate immune evasion, thereby extending the functional longevity of the vector. The systematic optimization of manufacturing workflows remains critical to generating high-quality base- and prime-editing agents at the scale required for rigorous preclinical evaluation and subsequent clinical translation [128]. Engineered VLPs employed for the delivery of base and prime editing tools, achieving comparable editing efficiencies in the liver and eye [124].

Despite the advancements in engineering therapeutic VLPs as gene editing platforms, the comprehensive characterization of increasingly complex virus-derived architectures is a primary obstacle to their clinical translation. Robust orthogonal methodologies for evaluating critical quality attributes (CQAs) are essential for these platforms before therapeutic implementation [129].

5.2 Vexosomes

Beyond the integration of EVs, specifically exosomes, as gene delivery vehicles, exosome-enveloped viral vectors, called vexosomes, represent a sophisticated advancement in the field. This strategy deploys the intrinsic biological advantages of EVs, including broad cellular tropism, minimal immunogenicity, and the capacity for scalable production. By encapsulating viral vectors within these endogenous vesicles, the therapeutic potential of gene delivery platforms is significantly enhanced [130]. The production of vexosomes involves

introducing plasmids encoding the viral genome into packaging cells. During viral replication and protein synthesis, viral components accumulate within the cytoplasm. These viral components are subsequently sequestered by cellular receptors located in the phagosomes, endosomes, and plasma membrane, enabling EVs to encapsulate viral elements during their secretion into the extracellular environment [4]. Oncolytic AAV components encapsulated by capsid-free EVs were successfully delivered to malignant cells [131]. Further, precision targeting can be achieved by engineering AAV/EV surfaces with specific ligands or peptides. The efficacy of targeted AAV/EVs in both in vitro and in vivo models has been demonstrated in the literature, exhibiting that these vectors can traverse the blood–brain barrier to facilitate genetic modification in neural tissue [132]. Furthermore, specific AAV serotypes within the EV envelope have been used to target distinct cell populations [133, 134], demonstrating the platform's modularity across diverse tissue types. Additionally, immune-evasive capability has been demonstrated by systemically administering AAV9/EVs into mice with pre-existing anti-AAV9 immunity, achieving successful transduction where traditional vectors failed. This study revealed that by encapsulating AAVs, EVs enable the vector to evade pre-existing neutralizing antibodies directed against the viral capsid [135]. Overall, although the ability of vexosomes to combine the high transduction efficiency of viral vectors with the low immunogenicity of EVs suggests a promising pathway for optimizing genome editing, the clinical transition of vexosome-mediated CRISPR delivery remains largely unexplored and requires further investigation to ensure efficiency, long-term safety, and precision.

6 Conclusions

The design of the delivery strategy, depending on both the cargo format and the target cell, is a major determinant of gene editing quality. DNA-based delivery strategies primarily utilize viral systems, resulting in sustained expression and increased editing efficiency; however, this also increases the probability of cleavage at off-target genomic sites. Conversely, delivering mRNA or RNPs by nonviral or physical methods results in a transient burst of nuclease activity. These transient delivery systems are widely considered the safest approach for therapeutic applications, as the editing machinery is degraded shortly after the desired modification is achieved [2, 136].

The capacity of viral platforms to be engineered for specific tissue tropism and sustained transgene expression supports their broad integration into clinical practice. However, despite their high transduction efficiency, viral systems present significant clinical challenges, including immunogenicity and the risk of insertional mutagenesis. Next-generation hybrid platforms are particularly advantageous for

delivering CRISPR RNPs or mRNA, as they facilitate tissue-specific targeting, enhance biocompatibility, and mitigate the risks of persistent transgene expression or insertional mutagenesis. Consequently, they represent a robust framework for transient and safe in vivo genome editing.

Overall, a comprehensive understanding of the interplay among the delivery vehicle, the cargo format, and the biological barriers of the target tissue is essential for the therapeutic delivery of CRISPR systems. As delivery engineering and tissue-specific targeting continue to evolve, the transition from bench to bedside will likely be dominated by platforms that offer precise control over the spatial and temporal activity of the CRISPR system.

Acknowledgments

The publication is based upon work by COST Action CA21113: Genome Editing for the Treatment of Human Diseases (https://www.genehumdi.eu), supported by European Cooperation in Science and Technology (COST). The AI-assisted tool Gemini was used to check grammar and spelling. No generative AI was used to create or draft content.

Conflict of Interest The author declares no conflicts of interest.

References

1. Liu C, Zhang L, Liu H, Cheng K (2017) Delivery Strategies of the CRISPR-Cas9 Gene-Editing System for Therapeutic Applications. J Control Release 266:17–26. https://doi.org/10.1016/j.jconrel.2017.09.012
2. Yip BH (2020) Recent advances in CRISPR/Cas9 delivery strategies. Biomolecules 10:839
3. Honrath S, Burger M, Leroux J-C (2025) Hurdles to healing: overcoming cellular barriers for viral and nonviral gene therapy. Int J Pharmaceut 674:125470
4. Tang S, Chen X, Tong X, Zhu L (2025) Overcoming the delivery challenges in CRISPR/Cas9 gene editing for effective cancer treatment: a review of delivery systems. Int J Med Sci 22:3625–3649
5. Seijas A, Cora D, Novo M et al (2025) CRISPR/Cas9 delivery systems to enhance gene editing efficiency. Int J Mol Sci 26:4420
6. Cavazza A, Molina-Estévez FJ, Reyes ÁP et al (2025) Advanced delivery systems for gene editing: a comprehensive review from the GenE-HumDi COST Action Working Group. Mol Ther Nucl Acids 36:102457
7. Bulcha JT, Wang Y, Ma H et al. (2021) Viral vector platforms within the gene therapy landscape. Sig Transduct Target Ther 6:53
8. Li X, Le Y, Zhang Z et al. (2023) Viral vector-based gene therapy. Int J Mol Sci 24:7736
9. Xu X, Wan T, Xin H et al. (2019) Delivery of CRISPR/Cas9 for therapeutic genome editing. J Gene Med 21:e3107
10. Drouin LM, Agbandje-McKenna M (2013) Adeno-associated virus structural biology as a tool in vector development. Future Virol 8:1183–1199
11. Trends and challenges of AAV-delivered gene editing therapeutics for CNS disorders: implications for neurodegenerative disease. Mol Ther Nucl Acids. https://www.cell.com/molecular-therapy-family/nucleic-acids/fulltext/S2162-2531(25)00189-1?_returnURL=https%3A%2F%2Flinkinghub.elsevier.com%2Fretrieve%2Fpii%2FS2162253125001891%3Fshowall%3Dtrue. Accessed 21 Mar 2026
12. In vivo base editing restores sensory transduction and transiently improves auditory function in a mouse model of recessive deafness. Sci Transl Med. https://www.science.

org/doi/10.1126/scitranslmed.aay9101. Accessed 23 Mar 2026
13. Cytosine and adenine base editing of the brain, liver, retina, heart and skeletal muscle of mice via adeno-associated viruses—PubMed. https://pubmed.ncbi.nlm.nih.gov/31937940/. Accessed 23 Mar 2026
14. Davis JR, Wang X, Witte IP et al. (2022) Efficient in vivo base editing via single adeno-associated viruses with size-optimized genomes encoding compact adenine base editors. Nat Biomed Eng 6:1272–1283. https://doi.org/10.1038/s41551-022-00911-4
15. Gao Z, Ravendran S, Mikkelsen NS et al. (2022) A truncated reverse transcriptase enhances prime editing by split AAV vectors. Mol Ther 30:2942–2951. https://doi.org/10.1016/j.ymthe.2022.07.001
16. Davis JR, Banskota S, Levy JM et al. (2024) Efficient prime editing in mouse brain, liver and heart with dual AAVs. Nat Biotechnol 42:253–264. https://doi.org/10.1038/s41587-023-01758-z
17. Lan T, Chen H, Tang C et al. (2023) Mini-PE, a prime editor with compact Cas9 and truncated reverse transcriptase. Mol Ther Nucleic Acids 33:890–897. https://doi.org/10.1016/j.omtn.2023.08.018
18. Gene editing for CEP290-associated retinal degeneration. New Engl J Med. https://www.nejm.org/doi/10.1056/NEJMoa2309915. Accessed 23 Mar 2026
19. Wang J-H, Gessler DJ, Zhan W et al. (2024) Adeno-associated virus as a delivery vector for gene therapy of human diseases. Sig Transduct Target Ther 9:78. https://doi.org/10.1038/s41392-024-01780-w
20. Demirci S, Essawi K, Germino-Watnick P et al. (2022) Advances in CRISPR delivery methods: perspectives and challenges. CRISPR J 5:660–676. https://doi.org/10.1089/crispr.2022.0051
21. Sánchez-Hernández S, Gutierrez-Guerrero A, Martín-Guerra R et al. (2018) The IS2 element improves transcription efficiency of integration-deficient lentiviral vector episomes. Mol Ther Nucleic Acids 13:16–28. https://doi.org/10.1016/j.omtn.2018.08.007
22. Jargalsaikhan B-E, Muto M, Ema M (2025) The era of gene therapy: the advancement of lentiviral vectors and their pseudotyping. Viruses 17. https://doi.org/10.3390/v17081036
23. Uchida N, Drysdale CM, Nassehi T et al. (2021) Cas9 protein delivery non-integrating lentiviral vectors for gene correction in sickle cell disease. Mol Ther Methods Clin Dev 21:121–132. https://doi.org/10.1016/j.omtm.2021.02.022
24. Baek Y, Seo YR, Kim S et al. (2026) From ex vivo to in vivo: advances in lentiviral vector engineering for CAR-T therapy. Immune Netw 26:e13. https://doi.org/10.4110/in.2026.26.e13
25. Garcia J (2024) A phase 1, multicenter, open-label study of UB-VV111 in combination with rapamycin in relapsed/refractory CD19+ B-cell malignancies. Blood 144(Supplement 1), 1750.1-1750.1.
26. Pierini S, Qureshi R, Pustylnikov S et al. (2026) In vivo CAR-T therapies-a new era of programmable immunity. Int J Mol Sci 27:1737. https://doi.org/10.3390/ijms27041737
27. Barbieri E, Heldt CL (2026) Challenges and opportunities in lentivirus viral vector manufacturing for in vivo applications. Biomedicines 14:369
28. Tasca F, Wang Q, Gonçalves MAFV (2020) Adenoviral vectors meet gene editing: a rising partnership for the genomic engineering of human stem cells and their progeny. Cells 9:953. https://doi.org/10.3390/cells9040953
29. Ricobaraza A, Gonzalez-Aparicio M, Mora-Jimenez L et al. (2020) High-capacity adenoviral vectors: expanding the scope of gene therapy. Int J Mol Sci 21:3643. https://doi.org/10.3390/ijms21103643
30. Li C, Georgakopoulou A, Mishra A et al. (2021) In vivo HSPC gene therapy with base editors allows for efficient reactivation of fetal γ-globin in β-YAC mice. Blood Adv 5:1122–1135. https://doi.org/10.1182/bloodadvances.2020003702
31. Wang Q, Liu J, Janssen JM et al. (2021) Broadening the reach and investigating the potential of prime editors through fully viral gene-deleted adenoviral vector delivery. Nucleic Acids Res 49:11986–12001. https://doi.org/10.1093/nar/gkab938
32. Chen PJ, Liu DR (2023) Prime editing for precise and highly versatile genome manipulation. Nat Rev Genet 24:161–177. https://doi.org/10.1038/s41576-022-00541-1
33. Wang Q, Capelletti S, Liu J et al. (2024) Selection-free precise gene repair using high-capacity adenovector delivery of advanced prime editing systems rescues dystrophin synthesis in DMD muscle cells. Nucleic Acids Res 52:2740–2757. https://doi.org/10.1093/nar/gkae057
34. Chen PJ, Liu DR (2023) Prime editing for precise and highly versatile genome manipulation. Nat Rev Genet 24:161–177. https://doi.org/10.1038/s41576-022-00541-1
35. Cheng H, Zhang F, Ding Y (2021) CRISPR/Cas9 delivery system engineering for genome editing in therapeutic applications.

Pharmaceutics 13:1649. https://doi.org/10.3390/pharmaceutics13101649
36. Ding Q, Strong A, Patel KM et al. (2014) Permanent alteration of PCSK9 with in vivo CRISPR-Cas9 genome editing. Circ Res 115:488–492. https://doi.org/10.1161/CIRCRESAHA.115.304351
37. Li C, Guan X, Du T et al. (2015) Inhibition of HIV-1 infection of primary CD4+ T-cells by gene editing of CCR5 using adenovirus-delivered CRISPR/Cas9. J Gen Virol 96:2381–2393. https://doi.org/10.1099/vir.0.000139
38. Hackett NR, Crystal RG (2025) Four decades of adenovirus gene transfer vectors: history and current use. Mol Ther 33:2192–2204. https://doi.org/10.1016/j.ymthe.2025.03.062
39. Boucher P, Cui X, Curiel DT (2020) Adenoviral vectors for in vivo delivery of CRISPR-Cas gene editors. J Control Release 327:788–800. https://doi.org/10.1016/j.jconrel.2020.09.003
40. Foley RA, Sims RA, Duggan EC et al (2022) Delivering the CRISPR/Cas9 system for engineering gene therapies: recent cargo and delivery approaches for clinical translation. Front Bioeng Biotechnol 10. https://doi.org/10.3389/fbioe.2022.973326
41. Tsuchida CA, Wasko KM, Hamilton JR, Doudna JA (2024) Targeted nonviral delivery of genome editors in vivo. Proc Natl Acad Sci USA 121:e2307796121. https://doi.org/10.1073/pnas.2307796121
42. Lin Y, Wagner E, Lächelt U (2022) Non-viral delivery of the CRISPR/Cas system: DNA versus RNA versus RNP. Biomater Sci 10:1166–1192. https://doi.org/10.1039/D1BM01658J
43. Wu F, Li N, Xiao Y et al. (2026) Lipid nanoparticles for delivery of CRISPR gene editing components. Small Methods 10:2401632. https://doi.org/10.1002/smtd.202401632
44. Huang K, Zapata D, Tang Y et al. (2022) In vivo delivery of CRISPR-Cas9 genome editing components for therapeutic applications. Biomaterials 291:121876. https://doi.org/10.1016/j.biomaterials.2022.121876
45. Mohammadian Farsani A, Mokhtari N, Nooraei S et al. (2024) Lipid nanoparticles: the game-changer in CRISPR-Cas9 genome editing. Heliyon 10:e24606. https://doi.org/10.1016/j.heliyon.2024.e24606
46. Wu F, Li N, Xiao Y et al. (2026) Lipid nanoparticles for delivery of CRISPR gene editing components. Small Methods 10:e2401632. https://doi.org/10.1002/smtd.202401632
47. Lee RG, Mazzola AM, Braun MC et al. (2023) Efficacy and safety of an investigational single-course CRISPR base-editing therapy targeting PCSK9 in nonhuman primate and mouse models. Circulation 147:242–253. https://doi.org/10.1161/CIRCULATIONAHA.122.062132
48. Phase 1 trial of CRISPR-Cas9 gene editing targeting ANGPTL3. New Engl J Med. https://www.nejm.org/doi/full/10.1056/NEJMoa2511778. Accessed 27 Mar 2026
49. Selective organ targeting (SORT) nanoparticles for tissue-specific mRNA delivery and CRISPR–Cas gene editing. Nat Nanotechnol. https://www.nature.com/articles/s41565-020-0669-6. Accessed 27 Mar 2026
50. Wang X, Liu S, Sun Y et al. (2023) Preparation of selective organ-targeting (SORT) lipid nanoparticles (LNPs) using multiple technical methods for tissue-specific mRNA delivery. Nat Protoc 18:265–291. https://doi.org/10.1038/s41596-022-00755-x
51. Haley RM, Padilla MS, El-Mayta RD et al. (2025) Lipid nanoparticles for in vivo lung delivery of CRISPR-Cas9 ribonucleoproteins allow gene editing of clinical targets. ACS Nano 19:13790–13804. https://doi.org/10.1021/acsnano.4c16617
52. Transient macrophage depletion circumvents scavenging and redirects biodistribution of mRNA-lipid nanoparticles. ACS Nano. https://pubs.acs.org/doi/10.1021/acsnano.5c02001. Accessed 27 Mar 2026
53. Taha EA, Lee J, Hotta A (2022) Delivery of CRISPR-Cas tools for *in vivo* genome editing therapy: Trends and challenges. J Control Release 342:345–361. https://doi.org/10.1016/j.jconrel.2022.01.013
54. Vasudevan A, Jozić A, Curtis AG et al. (2025) Lipid nanoparticle-mediated intracameral mRNA delivery facilitates gene expression and editing in the anterior chamber of the eye. J Control Release 379:1022–1028. https://doi.org/10.1016/j.jconrel.2025.01.068
55. Mrksich K, Padilla MS, Mitchell MJ (2024) Breaking the final barrier: evolution of cationic and ionizable lipid structure in lipid nanoparticles to escape the endosome. Adv Drug Deliv Rev 214:115446. https://doi.org/10.1016/j.addr.2024.115446
56. Jiang Y, Chen S, Hsiao S et al. (2025) Efficient and safe in vivo treatment of primary hyperoxaluria type 1 via LNP-CRISPR-Cas9-mediated glycolate oxidase disruption. Mol Ther 33:104–118. https://doi.org/10.1016/j.ymthe.2024.10.003
57. A multistep platform identifies spleen-tropic lipid nanoparticles for in vivo T cell–targeted delivery of gene-editing proteins. Sci Adv. https://www.science.org/doi/10.1126/sciadv.ady5579. Accessed 27 Mar 2026

58. Lee H, Rho W-Y, Kim Y-H et al (2025) CRISPR-Cas9 gene therapy: non-viral delivery and stimuli-responsive nanoformulations. Molecules 30. https://doi.org/10.3390/molecules30030542
59. Mendes BB, Conniot J, Avital A et al. (2022) Nanodelivery of nucleic acids. Nat Rev Methods Primers 2:24. https://doi.org/10.1038/s43586-022-00104-y
60. Zhu D, Shen H, Tan S et al. (2018) Nanoparticles based on poly (β-amino ester) and HPV16-targeting CRISPR/shRNA as potential drugs for HPV16-related cervical malignancy. Mol Ther 26:2443–2455. https://doi.org/10.1016/j.ymthe.2018.07.019
61. Zhang X, Xu C, Gao S et al. (2019) CRISPR/Cas9 delivery mediated with hydroxyl-rich nanosystems for gene editing in aorta. Adv Sci 6:1900386. https://doi.org/10.1002/advs.201900386
62. Luo J, Cui Y, Xu L et al. (2025) Layered double hydroxides for regenerative nanomedicine and tissue engineering: recent advances and future perspectives. J Nanobiotechnol 23:370. https://doi.org/10.1186/s12951-025-03448-1
63. Liu X, Gao M, Bao J (2025) Precisely targeted nanoparticles for CRISPR-Cas9 delivery in clinical applications. Nanomaterials 15. https://doi.org/10.3390/nano15070540
64. Patel SG, Sayers EJ, He L et al. (2019) Cell-penetrating peptide sequence and modification dependent uptake and subcellular distribution of green florescent protein in different cell lines. Sci Rep 9: 6298. https://doi.org/10.1038/s41598-019-42456-8
65. de Morais CCP, de L, Correia EM, Bonamino MH, de Vasconcelos ZFM (2024) Cell-penetrating peptides and CRISPR-Cas9: a combined strategy for human genetic disease therapy. Hum Gene Ther 35:781–797. https://doi.org/10.1089/hum.2024.020
66. Peptide-mediated delivery of CRISPR enzymes for the efficient editing of primary human lymphocytes—PubMed. https://pubmed.ncbi.nlm.nih.gov/37147433/. Accessed 27 Mar 2026
67. Cationic lipid-mediated delivery of proteins enables efficient protein-based genome editing in vitro and in vivo—PubMed. https://pubmed.ncbi.nlm.nih.gov/25357182/. Accessed 27 Mar 2026
68. In vitro and in vivo characterization of CPP and transferrin modified liposomes encapsulating pDNA—PubMed. https://pubmed.ncbi.nlm.nih.gov/32485318/. Accessed 27 Mar 2026
69. Revival of bioengineered proteins as carriers for nucleic acids— ScienceDirect. https://www.sciencedirect.com/org/science/article/pii/S1043180224000594. Accessed 27 Mar 2026
70. Rädler J, Gupta D, Zickler A, Andaloussi SE (2023) Exploiting the biogenesis of extracellular vesicles for bioengineering and therapeutic cargo loading. Mol Ther 31:1231–1250. https://doi.org/10.1016/j.ymthe.2023.02.013
71. Sharma V, Mukhopadhyay CD (2024) Exosome as drug delivery system: current advancements. Extracellular Vesicle 3:100032. https://doi.org/10.1016/j.vesic.2023.100032
72. René CA, Parks RJ (2024) Bioengineering extracellular vesicle cargo for optimal therapeutic efficiency. Mol Ther Method Clin Dev 32:101259. https://doi.org/10.1016/j.omtm.2024.101259
73. Han Y, Jones TW, Dutta S et al. (2021) Overview and update on methods for cargo loading into extracellular vesicles. Processes 9:356. https://doi.org/10.3390/pr9020356
74. Lu Y, Godbout K, Lamothe G, Tremblay JP (2023) CRISPR-Cas9 delivery strategies with engineered extracellular vesicles. Mol Ther Nucleic Acids 34:102040. https://doi.org/10.1016/j.omtn.2023.102040
75. Lainšček D, Kadunc L, Keber MM et al. (2018) Delivery of an artificial transcription regulator dCas9-VPR by extracellular vesicles for therapeutic gene activation. ACS Synth Biol 7:2715–2725. https://doi.org/10.1021/acssynbio.8b00192
76. Pan X, Li Y, Huang P et al. (2024) Extracellular vesicles for developing targeted hearing loss therapy. J Control Release 366:460–478. https://doi.org/10.1016/j.jconrel.2023.12.050
77. Kim SM, Yang Y, Oh SJ et al. (2017) Cancer-derived exosomes as a delivery platform of CRISPR/Cas9 confer cancer cell tropism-dependent targeting. J Control Release 266:8–16. https://doi.org/10.1016/j.jconrel.2017.09.013
78. Majeau N, Fortin-Archambault A, Gérard C et al. (2022) Serum extracellular vesicles for delivery of CRISPR-CAS9 ribonucleoproteins to modify the dystrophin gene. Mol Ther 30:2429–2442. https://doi.org/10.1016/j.ymthe.2022.05.023
79. Gee P, Lung MSY, Okuzaki Y et al. (2020) Extracellular nanovesicles for packaging of CRISPR-Cas9 protein and sgRNA to induce therapeutic exon skipping. Nat Commun 11: 1334. https://doi.org/10.1038/s41467-020-14957-y

80. Liang X, Gupta D, Xie J et al. (2025) Engineering of extracellular vesicles for efficient intracellular delivery of multimodal therapeutics including genome editors. Nat Commun 16: 4028. https://doi.org/10.1038/s41467-025-59377-y
81. Dubey S, Chen Z, Jiang YJ et al. (2024) Small extracellular vesicles (sEVs)-based gene delivery platform for cell-specific CRISPR/Cas9 genome editing. Theranostics 14:2777–2793. https://doi.org/10.7150/thno.92133
82. Ilahibaks NF, Kluiver TA, de Jong OG et al. (2024) Extracellular vesicle-mediated delivery of CRISPR/Cas9 ribonucleoprotein complex targeting proprotein convertase subtilisin-kexin type 9 (Pcsk9) in primary mouse hepatocytes. J Extracell Vesicles 13:12389. https://doi.org/10.1002/jev2.12389
83. Stranford DM, Simons LM, Berman KE et al. (2024) Bioengineering multifunctional extracellular vesicles for targeted delivery of biologics to T cells. Nat Biomed Eng 8:397–414. https://doi.org/10.1038/s41551-023-01142-x
84. Mehdizadeh S, Mamaghani M, Hassanikia S et al. (2025) Exosome-powered neuropharmaceutics: unlocking the blood-brain barrier for next-gen therapies. J Nanobiotechnology 23: 329. https://doi.org/10.1186/s12951-025-03352-8
85. van Haasteren J, Li J, Scheideler OJ et al. (2020) The delivery challenge: fulfilling the promise of therapeutic genome editing. Nat Biotechnol 38:845–855. https://doi.org/10.1038/s41587-020-0565-5
86. Fajrial AK, He QQ, Wirusanti NI et al. (2020) A review of emerging physical transfection methods for CRISPR/Cas9-mediated gene editing. Theranostics 10:5532–5549. https://doi.org/10.7150/thno.43465
87. Wu W, Lu Z, Li F et al. (2017) Efficient in vivo gene editing using ribonucleoproteins in skin stem cells of recessive dystrophic epidermolysis bullosa mouse model. Proc Natl Acad Sci USA 114:1660–1665. https://doi.org/10.1073/pnas.1614775114
88. Latella MC, Di Salvo MT, Cocchiarella F et al. (2016) In vivo editing of the human mutant rhodopsin gene by electroporation of plasmid-based CRISPR/Cas9 in the mouse retina. Mol Ther Nucleic Acids 5:e389. https://doi.org/10.1038/mtna.2016.92
89. Chiappini C, De Rosa E, Martinez JO et al. (2015) Biodegradable silicon nanoneedles delivering nucleic acids intracellularly induce localized in vivo neovascularization. Nat Mater 14:532–539. https://doi.org/10.1038/nmat4249
90. Xu L, Wang J, Liu Y et al. (2019) CRISPR-edited stem cells in a patient with HIV and acute lymphocytic leukemia. N Engl J Med 381:1240–1247. https://doi.org/10.1056/NEJMoa1817426
91. Stadtmauer EA, Fraietta JA, Davis MM et al (2020) CRISPR-engineered T cells in patients with refractory cancer. Science 367:eaba7365. https://doi.org/10.1126/science.aba7365
92. Taghdiri M, Mussolino C (2024) Viral and non-viral systems to deliver gene therapeutics to clinical targets. Int J Mol Sci 25. https://doi.org/10.3390/ijms25137333
93. Ren J, Liu X, Fang C et al. (2017) Multiplex genome editing to generate universal CAR T cells resistant to PD1 inhibition. Clin Cancer Res 23:2255–2266. https://doi.org/10.1158/1078-0432.CCR-16-1300
94. Lotfi M, Morshedi Rad D, Mashhadi SS et al. (2023) Recent advances in CRISPR/Cas9 delivery approaches for therapeutic gene editing of stem cells. Stem Cell Rev Rep 19:2576–2596. https://doi.org/10.1007/s12015-023-10585-3
95. Houghton BC, Panchal N, Haas SA et al. (2022) Genome editing with TALEN, CRISPR-Cas9 and CRISPR-Cas12a in combination with AAV6 homology donor restores T cell function for XLP. Front Genome Ed 4:828489. https://doi.org/10.3389/fgeed.2022.828489
96. Frangoul H, Altshuler D, Cappellini MD et al. (2021) CRISPR-Cas9 gene editing for sickle cell disease and β-Thalassemia. N Engl J Med 384:252–260. https://doi.org/10.1056/NEJMoa2031054
97. Chen J, Davison CW, Ellis J et al. (2026) CRISPR base editing correction of TGFBI mutations in autosomal dominant corneal dystrophies. Invest Ophthalmol Vis Sci 67:60. https://doi.org/10.1167/iovs.67.2.60
98. Mi Y, Xu J, Liu Q et al. (2021) Single-cell electroporation with high-frequency nanosecond pulse bursts: simulation considering the irreversible electroporation effect and experimental validation. Bioelectrochemistry 140:107822. https://doi.org/10.1016/j.bioelechem.2021.107822
99. Mondal N, Yadav KS, Dalal DC (2023) Enhanced drug uptake on application of electroporation in a single-cell model. J Membr Biol 256:243–255. https://doi.org/10.1007/s00232-023-00283-z
100. Pop MA, Almquist BD (2021) Controlled delivery of microRNAs into primary cells using nanostraw technology. Adv Nanobiomed Res 1:2000061. https://doi.org/10.1002/anbr.202000061

101. Lard M, Ho BD, Beech JP et al. (2022) Use of dielectrophoresis for directing T cells to microwells before nanostraw transfection: modelling and experiments. RSC Adv 12:30295–30303. https://doi.org/10.1039/d2ra05119b
102. Chen T, Barzi M, Furey N et al. (2025) CRISPR/Cas9 gene therapy increases the risk of tumorigenesis in the mouse model of hereditary tyrosinemia type I. JHEP Rep 7:101327. https://doi.org/10.1016/j.jhepr.2025.101327
103. Monteagudo V, Flores LCB, Lopes M et al. (2025) Newborn intravenous injection of liposomal CRISPR/Cas9 complex has no incidence of off-targets or tumors in mice. Pharmaceutics 17:656. https://doi.org/10.3390/pharmaceutics17050656
104. Xie D, Wang J, Huang L et al. (2025) A novel X-linked retinitis pigmentosa beagle dog model for ophthalmic research established rapidly by editing the RPGR gene in zygotes. Exp Eye Res 261:110697. https://doi.org/10.1016/j.exer.2025.110697
105. Zhang F, Peng Y, Fan D et al. (2025) Engineering a CRISPR-associated IscB system for developing miniature genome-editing tools in human cells and mouse embryos. Nat Commun 16: 10693. https://doi.org/10.1038/s41467-025-65724-w
106. Chen W, Zhang X, Fan R et al. (2026) Generating golden Syrian hamsters with conditional alleles via zygote microinjection of CRISPR/Cas9. Animal Model Exp Med 9:308–318. https://doi.org/10.1002/ame2.70107
107. Chakrabarty P, Gupta P, Illath K et al. (2022) Microfluidic mechanoporation for cellular delivery and analysis. Mater Today Bio 13:100193. https://doi.org/10.1016/j.mtbio.2021.100193
108. Zhang G, Mu R, Ma Y, Li B (2025) Intracellular delivery enabled by squeezing mechanoporation. Small Methods e2500338. https://doi.org/10.1002/smtd.202500338
109. Han X, Liu Z, Jo MC et al. (2015) CRISPR-Cas9 delivery to hard-to-transfect cells via membrane deformation. Sci Adv 1:e1500454. https://doi.org/10.1126/sciadv.1500454
110. Han X, Liu Z, Ma Y et al. (2017) Cas9 ribonucleoprotein delivery via microfluidic cell-deformation chip for human T-cell genome editing and immunotherapy. Adv Biosyst 1:e1600007. https://doi.org/10.1002/adbi.201600007
111. Kim Y-J, Bang S, Chung AJ (2026) Safe and efficient CRISPR genome editing of primary human T cells using a droplet-based cell mechanoporation platform. Small n/a:e12553. https://doi.org/10.1002/smll.202512553
112. D'Astolfo DS, Pagliero RJ, Pras A et al. (2015) Efficient intracellular delivery of native proteins. Cell 161:674–690. https://doi.org/10.1016/j.cell.2015.03.028
113. Kholosy WM, Visscher M, Ogink K et al. (2021) Simple, fast and efficient iTOP-mediated delivery of CRISPR/Cas9 RNP in difficult-to-transduce human cells including primary T cells. J Biotechnol 338:71–80. https://doi.org/10.1016/j.jbiotec.2021.07.006
114. Takahashi G, Gurumurthy CB, Wada K et al. (2015) GONAD: genome-editing via oviductal nucleic acids delivery system: a novel microinjection independent genome engineering method in mice. Sci Rep 5: 11406. https://doi.org/10.1038/srep11406
115. Bold-Erdene A, Miura K, Yamasaki N et al. (2025) Effect of gamma-ray exposure on the genome-editing efficiency of improved genome-editing via oviductal nucleic acids delivery (i-GONAD). Exp Anim 74:457–462. https://doi.org/10.1538/expanim.25-0036
116. Leonova EI, Chirinskaite AV, Akhmarov II et al (2025) Improved genome editing via oviductal nucleic acids delivery-based in vivo electroporation technique for knockout mice generation. J Vis Exp. https://doi.org/10.3791/68704
117. Yen J, Fiorino M, Liu Y et al. (2018) TRIAMF: a new method for delivery of Cas9 ribonucleoprotein complex to human hematopoietic stem cells. Sci Rep 8: 16304. https://doi.org/10.1038/s41598-018-34601-6
118. Wilbie D, Walther J, Mastrobattista E (2019) Delivery aspects of CRISPR/Cas for in vivo genome editing. Acc Chem Res 52:1555–1564. https://doi.org/10.1021/acs.accounts.9b00106
119. Lyu P, Lu B (2022) New advances in using virus-like particles and related technologies for eukaryotic genome editing delivery. Int J Mol Sci 23. https://doi.org/10.3390/ijms23158750
120. Ikwuagwu B, Tullman-Ercek D (2022) Virus-like particles for drug delivery: a review of methods and applications. Curr Opin Biotechnol 78:102785. https://doi.org/10.1016/j.copbio.2022.102785
121. Lyu P, Wang L, Lu B (2020) Virus-like particle mediated CRISPR/Cas9 delivery for efficient and safe genome Editing. Life 10:366. https://doi.org/10.3390/life10120366
122. Segel M, Lash B, Song J et al. (2021) Mammalian retrovirus-like protein PEG10 packages its own mRNA and can be pseudotyped for mRNA delivery. Science 373:882–889. https://doi.org/10.1126/science.abg6155
123. An M, Raguram A, Du SW et al. (2024) Engineered virus-like particles for transient delivery of prime editor ribonucleoprotein complexes in vivo. Nat Biotechnol

42:1526–1537. https://doi.org/10.1038/s41587-023-02078-y
124. Banskota S, Raguram A, Suh S et al. (2022) Engineered virus-like particles for efficient in vivo delivery of therapeutic proteins. Cell 185:250–265. https://doi.org/10.1016/j.cell.2021.12.021 e16
125. Hamilton JR, Tsuchida CA, Nguyen DN et al. (2021) Targeted delivery of CRISPR-Cas9 and transgenes enables complex immune cell engineering. Cell Reports 35:109207. https://doi.org/10.1016/j.celrep.2021.109207
126. Choi JG, Dang Y, Abraham S et al. (2016) Lentivirus pre-packed with Cas9 protein for safer gene editing. Gene Ther 23:627–633. https://doi.org/10.1038/gt.2016.27
127. Biela AP, Naskalska A, Fatehi F et al. (2022) Programmable polymorphism of a virus-like particle. Commun Mater 3:7. https://doi.org/10.1038/s43246-022-00229-3
128. Janns JH, Mikkelsen JG (2024) Gene editing by ferrying of CRISPR/Cas ribonucleoprotein complexes in enveloped virus-derived particles. Hum Gene Ther 35:604–616. https://doi.org/10.1089/hum.2024.105
129. Dipalo LL, Mikkelsen JG, Gijsbers R, Carlon MS (2025) Trojan Horse-like vehicles for CRISPR-Cas delivery: engineering extracellular vesicles and virus-like particles for precision gene editing in cystic fibrosis. Hum Gene Ther 36:1021–1052. https://doi.org/10.1089/hum.2024.258
130. Farzanehpour M, Miri A, Alvanegh AG, Gouvarchinghaleh HE (2023) Viral vectors, exosomes, and vexosomes: potential armamentarium for delivering CRISPR/Cas to cancer cells. Biochem Pharmacol 212:115555. https://doi.org/10.1016/j.bcp.2023.115555
131. Saari H, Turunen T, Lõhmus A et al. (2020) Extracellular vesicles provide a capsid-free vector for oncolytic adenoviral DNA delivery. J Extracell Vesicles 9:1747206. https://doi.org/10.1080/20013078.2020.1747206
132. Wood MJA, O'Loughlin AJ, Samira L (2011) Exosomes and the blood-brain barrier: implications for neurological diseases. Ther Deliv 2:1095–1099.https://doi.org/10.4155/tde.11.83
133. Orefice NS, Souchet B, Braudeau J et al. (2019) Real-time monitoring of exosome enveloped-AAV spreading by endomicroscopy approach: a new tool for gene delivery in the brain. Mol Ther Methods Clin Dev 14:237–251. https://doi.org/10.1016/j.omtm.2019.06.005
134. Hudry E, Andres-Mateos E, Lerner EP et al. (2018) Efficient gene transfer to the central nervous system by single-stranded Anc80L65. Mol Ther Methods Clin Dev 10:197–209. https://doi.org/10.1016/j.omtm.2018.07.006
135. Meliani A, Boisgerault F, Fitzpatrick Z et al. (2017) Enhanced liver gene transfer and evasion of preexisting humoral immunity with exosome-enveloped AAV vectors. Blood Adv 1:2019–2031. https://doi.org/10.1182/bloodadvances.2017010181
136. Shchukina EI, Mazunin IO, Eremin II, Moskalev AA (2025) Gene therapy techniques and delivery methods. Sovrem Tekhnologii Med 17:56–67. https://doi.org/10.17691/stm2025.17.6.06

Open Access This chapter is licensed under the terms of the Creative Commons Attribution-NonCommercial-NoDerivatives 4.0 International License (http://creativecommons.org/licenses/by-nc-nd/4.0/), which permits any noncommercial use, sharing, distribution and reproduction in any medium or format, as long as you give appropriate credit to the original author(s) and the source, provide a link to the Creative Commons license and indicate if you modified the licensed material. You do not have permission under this license to share adapted material derived from this chapter or parts of it.

The images or other third party material in this chapter are included in the chapter's Creative Commons license, unless indicated otherwise in a credit line to the material. If material is not included in the chapter's Creative Commons license and your intended use is not permitted by statutory regulation or exceeds the permitted use, you will need to obtain permission directly from the copyright holder.



Part II

Viral Delivery Methods



Chapter 7

Production of Lentiviral Vectors Encoding the CRISPR–Cas13d System for RNA Targeting

Roberta Stilhano and Leonardo Martin

Abstract

The CRISPR–Cas13d system has been shown to be a potent tool for target RNA knockdown, offering advantages over DNA-editing systems by providing a non-genotoxic method to modulate gene expression. Efficient delivery of Cas13d and its guide RNAs into target cells is essential to achieve a strong knockdown effect, particularly in cell lines that are difficult to transfect and primary cells. Lentiviral vectors (LVs) are ideal for delivering large gene-editing tools due to their large packaging capacity and ability to transduce both dividing and nondividing cells. Here, we describe a detailed protocol for the production of high-titer, third-generation LVs with a dual-expression cassette for Cas13d and a customizable guide RNA. The method describes the cloning of target-specific guide RNAs, the transfection of HEK293T cells with packaging and transfer plasmids, the harvest and concentration of viral supernatants, and the determination of viral titer. The generated lentiviral particles can be used for stable transduction and efficient RNA knockdown in a broad range of mammalian cell types.

Keywords Lentivirus, CRISPR–Cas13d, RNA knockdown, Viral production, Guide RNA cloning

1 Introduction

The discovery and modifications of CRISPR–Cas systems have transformed the field of molecular biology [1–3]. Although DNA-targeting Cas9 has been widely used for genome editing, the Cas13 family of enzymes is designed to target and cleave single-stranded RNA [4]. Among these, Cas13d, derived from the bacterium "*Ruminococcus flavefaciens*" (RfxCas13d), is particularly effective for RNA knockdown due to its compact size and high catalytic activity in mammalian cells [5,6]. This tool enables the reversible and transient suppression of gene expression, which is highly useful for exploring essential genes, noncoding RNAs, and developing therapeutic tools [7].

A key challenge in applying CRISPR–Cas13d is the efficient delivery of its two core components: the Cas13d and a CRISPR RNA (crRNA, also known as guide RNA or gRNA). Although plasmid transfection can be used for certain cell types, it is not very

Duško Lainšček et al. (eds.), *CRISPR Delivery*, Methods in Molecular Biology, vol. 3075,
https://doi.org/10.1007/978-1-0716-5547-4_7,
© The Author(s) 2027

efficient for primary cells, neurons, or immune cells. Lentiviral vectors provide a robust solution, enabling stable genomic integration and long-term, constitutive expression of both components from a single vector [8,9]. Third-generation lentiviral packaging platforms, which separate the viral genes into several plasmids to improve biosafety and prevent the generation of replication-competent virus, are commonly used for gene delivery applications [10] (Fig. 1).

Here, we detail a comprehensive protocol for producing, concentrating, and titering third-generation lentivirus encoding a mammalian codon-optimized RfxCas13d and a user-defined gRNA. The transfer plasmid backbone is designed with two independent polymerase II and polymerase III promoters to drive Cas13d and gRNA expression, respectively. Following production in HEK-293T/17

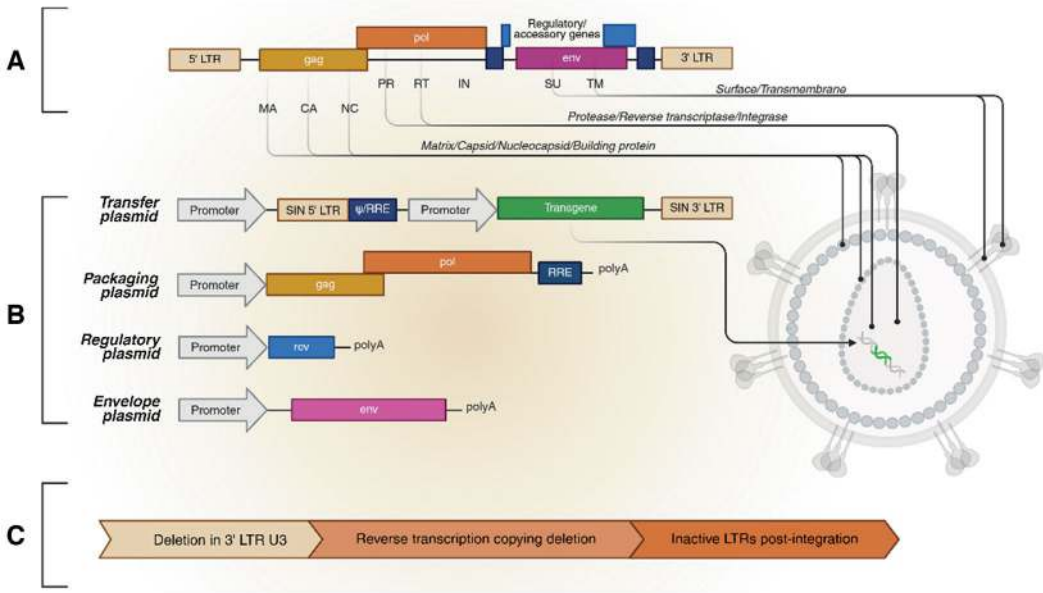


Fig. 1 Organization of third-generation lentiviral vector systems used for gene delivery. (**A**) Schematic representation of the wild-type HIV-1 genome. The viral RNA genome is flanked by 5′ and 3′ long terminal repeats (LTRs) and contains the canonical structural genes gag, pol, and env, together with regulatory and accessory elements. The gag gene encodes structural proteins forming the viral core, whereas pol encodes the viral enzymes protease, reverse transcriptase, and integrase required for reverse transcription and genomic integration. The env gene encodes the surface and transmembrane glycoproteins responsible for host cell entry. (**B**) Architecture of a third-generation lentiviral vector production system. Viral functions are separated into four plasmids to enhance biosafety and prevent the formation of replication-competent lentivirus. These include: (i) the transfer plasmid, containing self-inactivating (SIN) LTRs, the packaging signal (Ψ), Rev response element (RRE), and the transgene cassette; (ii) the packaging plasmid encoding gag and pol; (iii) a regulatory plasmid encoding Rev; and (iv) an envelope plasmid, typically expressing the vesicular stomatitis virus glycoprotein (VSV-G) to broaden viral tropism. (**C**) Principle of self-inactivation in SIN vectors. A deletion in the U3 region of the 3′ LTR is copied to the 5′ LTR during reverse transcription, resulting in transcriptionally inactive LTRs after integration. This modification improves biosafety by preventing promoter activity within the integrated vector genome

cells, the virus is concentrated by ultracentrifugation, and its functional titer is determined via antibiotic resistance selection. This robust protocol routinely yields viral titers of (10^7–10^8) TU/mL, sufficient for efficient transduction of most mammalian cell types.

2 Materials

2.1 Reagents

2.1.1 Cell Culture and Plating

1. Human embryonic kidney (HEK293T/17) cells (low passage, <15) (*see* **Note 1**)
2. Complete DMEM: Dulbecco's Modified Eagle Medium high glucose supplemented with 10% fetal bovine serum and 1% penicillin–streptomycin (e.g., Thermo Fisher Scientific)
3. Trypsin–EDTA solution: 0.25% trypsin–EDTA with phenol red (e.g., Thermo Fisher Scientific)
4. Phosphate-buffered saline (PBS), pH 7.2
5. Sterile conical tubes: 15 mL
6. Sterile conical tubes: 50 mL
7. Tissue culture flasks: 75 cm^2, vented cap
8. Cell culture dishes: 10 cm diameter

2.1.2 Plasmid, Primers, and Cloning

1. Plasmid pLentiRNACRISPR_005-hU6-DR_BsmBI-EFS-RfxCas13d-NLS-2A-Puro-WPRE (e.g., Addgene)
2. psPAX2 packaging plasmid (e.g., Addgene)
3. pMD2.G envelope plasmid (e.g., Addgene)
4. Oligonucleotide primers: forward and reverse
5. Q5® Site-Directed Mutagenesis Kit (e.g., New England Biolabs)
6. *Esp*3I (*BsmB*I) restriction enzyme (Thermo Fisher Scientific, Waltham, MA, USA)
7. LB broth, Miller formulation: Luria–Bertani medium prepared according to manufacturer's instructions
8. LB agar: Luria–Bertani medium supplemented with agar
9. Ampicillin sodium salt
10. 1 mg/mL Puromycin in sterile water
11. Plasmid purification kit (e.g., QIAGEN Plasmid Plus Maxi Kit, Qiagen, Hilden, Germany)
12. NEB 5-alpha competent *Escherichia coli* cells (New England Biolabs)
13. Agarose: ultrapure grade

14. TAE buffer (50×): Tris–acetate–EDTA buffer
15. 1 kb Plus DNA ladder
16. DNA gel loading dye (6×)
17. Elution buffer (EB): 10 mM Tris-Cl, pH 8.5
18. SOC medium (Thermo Fisher Scientific)
19. 70%–75% Ethanol solution

2.1.3 Transfection

1. Ultrapure water (DNAse/RNAse free)
2. 2 M $CaCl_2$ solution: $CaCl_2$ dissolved in ultrapure water to a final concentration of 2 M
3. 500 mM HEPES buffer, pH 7.1: HEPES dissolved in ultrapure water and adjusted to pH 7.1 (*see* **Note 2**)
4. 2 M NaCl solution: NaCl dissolved in ultrapure water to a final concentration of 2 M
5. 150 mM Na_2HPO_4 solution, pH 7.0: Na_2HPO_4 dissolved in ultrapure water and adjusted to pH 7.0 (*see* **Note 2**)
6. HEPES-buffered saline (HBS): 10 mL 500 mM HEPES, 12.5 mL 2 M NaCl, and 1 mL 150 mM Na_2HPO_4, adjusted to a final volume of 100 mL with ultrapure water (*see* **Note 2**)

2.1.4 LVs Purification and Concentration

1. 0.45 μm PVDF syringe filter (e.g., Merck Millipore)
2. Polypropylene centrifuge tubes (e.g., Nalgene, Thermo Fisher Scientific)
3. 10% w/v Sucrose solution: sucrose dissolved in ultrapure water

2.2 Equipment

1. High-speed refrigerated centrifuge (e.g., Sorvall LYNX 6000, Thermo Fisher Scientific, Waltham, MA, USA)
2. Fixed-angle rotor compatible with high-speed centrifugation (e.g., Fiberlite™ F21-8 × 50 y, Thermo Fisher Scientific, Waltham, MA, USA)
3. Dry block heater
4. Spectrophotometer (e.g., NanoDrop 2000c, Thermo Fisher Scientific, Waltham, MA, USA)
5. Chemiluminescence imaging system (e.g., iBright™ CL1500, Thermo Fisher Scientific, Waltham, MA, USA)
6. Microcentrifuge
7. CO_2 cell culture incubator
8. Automated cell counter
9. Water bath and dry bath incubator
10. Inverted light microscope

3 Methods

3.1 Guide Design

This step describes the design of guide RNAs (gRNAs) targeting the gene of interest using online tools.

1. Obtain the sequence of the target gene from the Ensembl website (www.ensembl.org/index.html)
2. Select the appropriate species.
3. Type the name of the gene of interest and click "go."
4. From the search results, identify the canonical transcript; in the "Flag" column, it will be labeled "Ensembl canonical."
5. Click the corresponding RefSeq accession number, which begins with NM_.
6. Copy the transcript ID, which begins with "ENST."
7. Go to the Cas13 guide design website (https://cas13design.nygenome.org/) (*see* **Note 3**).
8. Select "Human" for Human genes or "Model organisms" to find genes from other species.
9. Scroll down to the "transcript ID" field and paste the transcript ID copied in the previous step.
10. Choose the six top-scoring gRNAs for each RNA annotation (3′ UTR, 5′ UTR, and CDS) based on minimal off-target effects and maximal efficiency.

3.2 Cloning Using Q5 Mutagenesis Methodology

This step describes the cloning of designed gRNAs into the Cas13d vector using site-directed mutagenesis.

1. Access the website https://nebasechanger.neb.com.
2. Paste the pLentiRNACRISPR_005-hU6-DR_BsmBI-EFS-RfxCas13d-NLS-2A-Puro-WPRE vector sequence in fasta format.
3. In the "select input mode and set mutations" field, choose indel/substitution.
4. In the "search for target sequence" field, paste the restriction site sequence.
5. Click find.
6. In the "Replacement sequence" field, paste the gRNA sequence designed in the previous step.
7. Click "build primers."
8. Copy the primer sequences and submit them for synthesis.
9. Prepare the reaction in a PCR tube as shown in Table 1.

10. Mix the reagents and transfer to a thermocycler.
11. The PCR thermal cycling conditions were shown in Table 2 (*see* **Note 4**).
12. In a PCR tube, assemble the following reagents as shown in Table 3:
13. Incubate at room temperature for 5 min.

3.3 Transformation

This step describes the transformation of recombinant plasmids into competent *Escherichia coli* cells.

1. Thaw one tube of NEB 5-alpha Competent *E. coli* cells on ice.
2. Add 5 μL of the KLD reaction mixture to the competent cells.
3. Gently mix by inverting the tube 4–5 times. Do not vortex.
4. Incubate the mixture on ice for 30 min.
5. Heat-shock the cells at 42°C for 30 s.

Table 1

PCR reaction mixture (25 μL total volume). PCR reactions were prepared using Q5 hot start high-fidelity 2× master mix. Primers were used at 0.5 μM each, and template DNA at 1–25 ng per reaction. Nuclease-free water was added to a final volume of 25 μL

	25 μL RXN	Final concentration
Q5 hot start high-fidelity 2× master mix	12.5 μL	1×
10 μM Forward primer	1.25 μL	0.5 μM
10 μM Reverse primer	1.25 μL	0.5 μM
Template DNA (1–25 ng/μL)	1 μL	1–25 ng
Nuclease-free water	9 μL	

Table 2

PCR thermal cycling conditions. Thermal cycling was performed with an initial denaturation at 98°C for 30 s, followed by 25 cycles (98°C for 10 s, 50–72°C for 10–30 s, 72°C for 20–30 s/kb), a final extension at 72°C for 2 min, and a hold at 4–10°C

Step	Temp	Time
Initial denaturation	98°C	30 s
	98°C	10 s
25 Cycles	50–72°C	10–30 s
	72°C	20–30 s/kb
Final extension	72°C	2 min
Hold	4–10°C	

Table 3
KLD reaction mixture for mutagenesis. KLD reactions were assembled with PCR product, 2× KLD reaction buffer (1× final), and 10× KLD enzyme mix (1× final), with nuclease-free water added to a total volume of 10 μL

	Volume (μL)	Final concentration
PCR product	1	
2× KLD reaction buffer	5	1×
10× KLD enzyme mix	1	1×
Nuclease-free water	3	

6. Immediately place the tube on ice for 5 min.
7. Add 950 μL of room-temperature SOC medium to the cells.
8. Incubate at 37°C for 1 h with shaking at 250 rpm (orbital shaker, ~19 mm orbit).
9. Mix the cells by inverting the tube.
10. Plate 50–100 μL of the transformation mixture onto LB agar plates containing ampicillin (100 μg/mL).
11. Choose some colonies and add them to a tube containing 5 mL of LB broth with ampicillin (100 μg/mL).
12. Incubate the plates overnight at 37°C.
13. Select several individual colonies and inoculate each into a tube containing 5 mL of LB broth supplemented with ampicillin (100 μg/mL).
14. Incubate the cultures at 37°C for 16 h with shaking at 180 rpm (orbital shaker, ~19 mm orbit).

3.4 Plasmid Miniprep

This step describes the purification of plasmid DNA from bacterial cultures using a commercial miniprep kit. Plasmid DNA was purified using a commercial miniprep kit (e.g., QIAprep Spin Miniprep Kit, Qiagen) according to the manufacturer's instructions with minor modifications as described below.

1. Transfer 1.5 mL of each bacterial culture to a microcentrifuge tube and centrifuge at 6800×*g* for 3 min at room temperature (*see* **Note 5**).
2. Discard the supernatant and resuspend the bacterial pellet in 250 μL Buffer P1 (*see* **Note 6**).
3. Add 250 μL Buffer P2 and mix thoroughly by inverting the tube 4–6 times, until the solution becomes clear. Do not allow the lysis step to proceed for more than 5 min.
4. Add 350 μL Buffer P3 and mix immediately by inverting the tube 4–6 times.

5. Centrifuge at 13,000 rpm (~17,900×*g*) for 10 min in a benchtop microcentrifuge.
6. Carefully transfer 800 µL of the supernatant to a QIAprep 2.0 spin column and centrifuge for 30–60 s. Discard the flow-through.
7. Wash the column with 0.5 mL Buffer PB. Centrifuge for 30–60 s and discard the flow-through (*see* **Note 7**).
8. Wash the column with 0.75 mL Buffer PE. Centrifuge for 30–60 s and discard the flow-through.
9. Centrifuge the empty column for 1 min to remove residual wash buffer.
10. Place the spin column into a clean 1.5 mL microcentrifuge tube.
11. Elute the plasmid DNA by adding 30 µL Elution buffer (EB) or nuclease-free water to the center of the membrane. Let the column stand for 1 min, then centrifuge for 1 min (*see* **Note 8**).
12. Measure DNA concentration and purity using 1 µL of the eluted plasmid on a NanoDrop spectrophotometer.
13. Submit the purified plasmids for Sanger sequencing to identify colonies containing the correct insert.
14. Select the positive clone for midiprep-scale plasmid preparation. This positive clone will be named pLenti-U6-gRNA-Cas13d-Puro.
15. After midiprep, quantify the plasmid DNA again using a NanoDrop spectrophotometer.

3.5 Calcium Phosphate Transfection

This step describes the production of lentiviral particles in HEK293T cells using calcium phosphate transfection.

Caution: All procedures involving lentiviral vector production must be performed in a biosafety level 2 (BSL-2) cabinet and according to institutional biosafety guidelines.

3.5.1 Day 1: Seeding Producer Cells

1. Seed 2.0–2.5 × 10^6 HEK-293T/17 cells per 10 cm dish.
2. Prepare a total of 10 dishes.
3. Incubate overnight at 37°C in a humidified incubator with 5% CO_2.

3.5.2 Day 2: Calcium Phosphate Transfection

1. Replace the culture medium with 10 mL of fresh complete DMEM prewarmed to 37°C.
2. Adjust the concentration of pLenti-U6-gRNA-Cas13d-Puro, psPAX2, and pMD2.G to 1 µg/µL in nuclease-free water.
3. For the transfection of ten 10-cm dishes, prepare the following DNA/CaCl2 mixture in a sterile 15-mL conical tube as shown in Table 4.

Table 4
DNA/$CaCl_2$ mixture for lentiviral transfection. Plasmid DNA (pLenti-U6-gRNA-Cas13d-Puro, psPAX2, and pMD2.G) was combined with 2 M $CaCl_2$ and nuclease-free water to the indicated final volumes for transfection of one or ten 10-cm dishes

Reagent	1 plate (μL)	10 plates (μL)
pLenti-U6-gRNA-Cas13d-Puro (1 μg/μL)	20	200
psPAX2 (1 μg/μL)	15	150
pMD2.G (1 μg/μL)	6	60
$CaCl_2$ (2 M)	62	620
Nuclease-free water	397	3970
Total volume	**500**	**5000**

4. Add the components in the following order: water, plasmids, and then $CaCl_2$.
5. Mix thoroughly by gentle pipetting.
6. In a second sterile 15 mL conical tube, add 5 mL of HBS.
7. Add the 5 mL DNA/$CaCl_2$ mixture dropwise to the 5 mL HBS while continuously mixing the HBS tube gently, or vortexing at low speed, to allow precipitate formation.
8. Incubate the mixture at room temperature for 15–30 min to allow calcium phosphate-DNA precipitate formation. Do not exceed 30 min.
9. Add the transfection mixture dropwise to the cells, using 1 mL per dish.
10. Gently swirl each plate until the medium regains a uniform red color.
11. Incubate the cells at 37°C and 5% CO_2.
12. After 4–5 h, carefully remove the medium and slowly add 6 mL of fresh DMEMs to each dish (*see* **Note 9**).
13. Incubate the cells for an additional 48 h.

3.5.3 Day 4: Lentiviral Harvest and Concentration

1. Collect the culture supernatant from each plate into 50-mL centrifuge tubes.
2. Close the tubes and spray them with 75% ethanol before removing them from the biosafety cabinet.
3. Centrifuge at 500×*g* for 5 min at 4°C to pellet detached cells and debris.
4. Filter the pooled supernatant through a 0.45 μm filter unit (*see* **Note 10**).

5. Add 4 mL of 10% sucrose to a polypropylene copolymer ultracentrifuge tube and slowly layer 26 mL of filtered supernatant on top.
6. Centrifuge at 40,000×*g* for 2 h at 4°C using a high-speed refrigerated centrifuge (e.g., Sorvall LYNX 6000, Thermo Fisher Scientific, Waltham, MA, USA) equipped with a suitable fixed-angle rotor (e.g., Fiberlite™ F21-8 × 50 y).
7. Carefully discard the supernatant.
8. Resuspend the viral pellet, which may not be visible, in 1× PBS by pipetting 10–15 times around the pellet and then 15 times up and down.
9. Clarify the final concentrate by a brief centrifugation (~5 s at maximum speed) in a benchtop centrifuge.
10. Aliquot the supernatant and store at −80°C.

3.6 Lentiviral Titration by Puromycin Selection

This step describes the determination of functional lentiviral titer using puromycin selection.

3.6.1 Day 1: Seeding Target Cells

1. Seed HEK-293T/17 cells in a 24-well plate at a density of $3–5 \times 10^4$ cells/well.
2. Prepare at least three wells for each viral dilution and three wells as non-transduced controls.
3. Incubate overnight at 37°C and 5% CO_2.
4. Ensure that the cells are evenly distributed and well separated in each well.

3.6.2 Day 2: Transduction

1. Count the cells in one representative well before transduction. The cell number should be approximately $3–5 \times 10^5$ cells/well at the time of infection.
2. Remove the culture medium.

For Nonconcentrated Lentiviral Supernatant:

1. Transduce cells with 250, 125, 62.5, 31.5, and 16.625 µL of crude viral supernatant.
2. Adjust the final transduction volume to 250 µL with fresh DMEM.
3. Keep two or three wells as noninfected controls.
4. Perform each condition in triplicate.

For Concentrated Lentiviral Vector:

1. Prepare serial dilutions of the concentrated vector (Fig. 2).
2. Transduce cells using a fixed volume from each dilution in 250 µL of fresh DMEM (*see* **Note 11**).

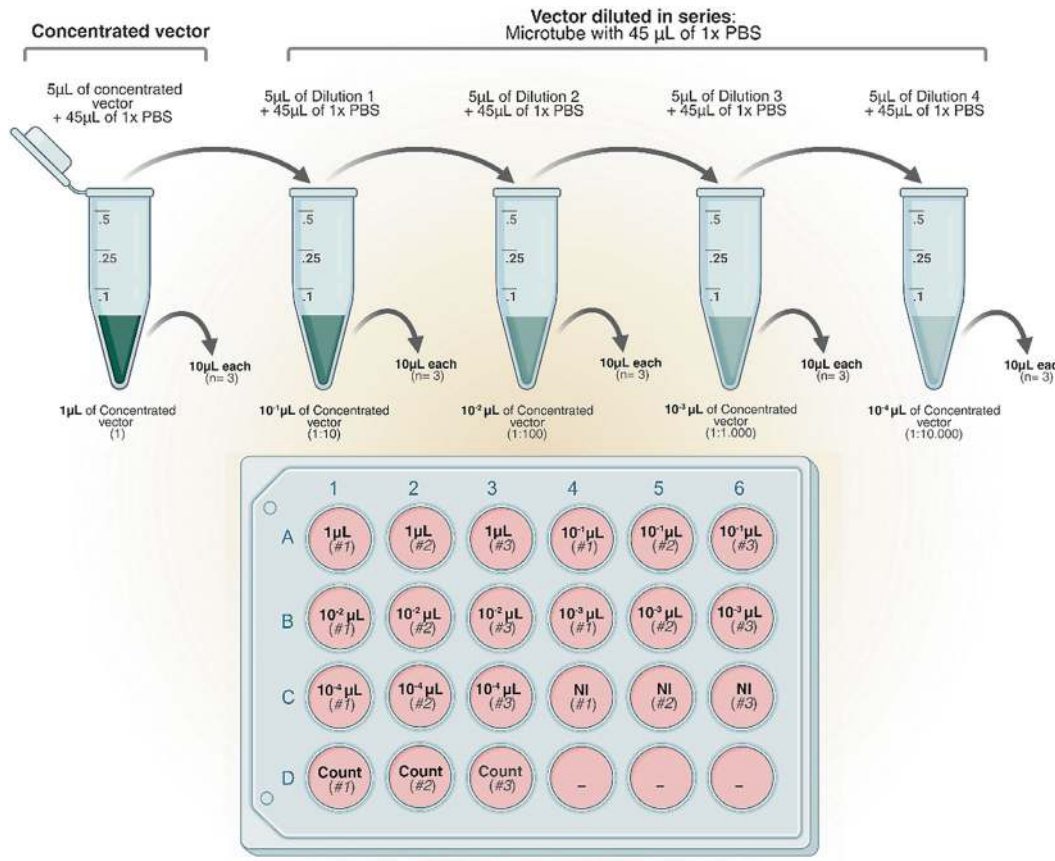


Fig. 2 Serial dilution of concentrated lentiviral vector for transduction assays and vector titration. The concentrated lentiviral vector was subjected to a tenfold serial dilution in 1× PBS. The first dilution was prepared by mixing 5 µL of concentrated vector with 45 µL of 1× PBS, followed by sequential dilutions using 5 µL from the previous dilution mixed with 45 µL of 1× PBS, generating dilutions from 10^{-1} to 10^{-4} relative to the original stock. For transduction, 10 µL from each dilution was added to cells in 250 µL of fresh DMEM per well. Each dilution was tested in triplicate in a 24-well plate to ensure reliable estimation of transduction efficiency. Noninfected wells (NI) were included as negative controls, and wells within the optimal dilution range were used for vector titer calculation

3.6.3 Day 3

1. Remove media and add 500 µL of fresh DMEMs to each well.

3.6.4 Day 4: Puromycin Selection

1. Replace the culture medium.
2. Add puromycin to each well to a final concentration of 1–2 µg/mL.
3. Example: add 0.5 µL of puromycin stock (1 mg/mL) to 500 µL medium to obtain a final concentration of 1 µg/mL.
4. Replace the medium every other day with fresh medium containing puromycin.
5. Continue selection until all non-transduced control cells are dead.

Determination of Functional Titer:

1. Select wells in which the transduction rate is not too high, ideally within the 10%–30% range, to minimize errors caused by multiple transduction events.
2. Count the surviving cells after puromycin selection.
3. Calculate the functional titer using the following formula (see Table 5):

$$\mathrm{TU/mL} = (N \times F \times D)/V \quad (1)$$

Worked Example:

1. You plated 1×10^5 cells and added 10 µL of a 1:100 diluted virus.
2. After puromycin selection, 2×10^4 cells survived.

- $N = 1 \times 10^5$
- $F = 2 \times 10^4 / 1 \times 10^5 = 0.2$
- $D = 100$
- $V = 0.01$ mL

$$\mathrm{TU/mL} = (1 \times 10^5 \times 0.2 \times 100)/0.01 = 2 \times 10^8 \ \mathrm{TU/mL}$$

To provide an integrated overview of the experimental pipeline, the complete workflow for lentiviral vector production and functional titration is summarized schematically in Fig. 3. This diagram outlines the sequential steps from in silico guide RNA design and cloning into the transfer vector to lentiviral production in HEK293T cells, followed by viral harvest, concentration, and determination of functional titer. The figure also incorporates approximate time indications for each phase, facilitating experimental planning and highlighting the overall timeline required to generate high-titer lentiviral preparations for CRISPR–Cas13d delivery.

Table 5

Parameters for lentiviral titer calculation. Functional titer (TU/mL) was calculated as ($N \times F \times D$) / V, where N is the number of cells at transduction, F is the fraction of puromycin-resistant cells, D is the dilution factor, and V is the volume of virus added (mL)

Parameter	Definition
N	Number of cells present at the time of transduction
F	Fraction of cells that survived puromycin selection
D	Viral dilution factor
V	Volume of virus added (in mL)

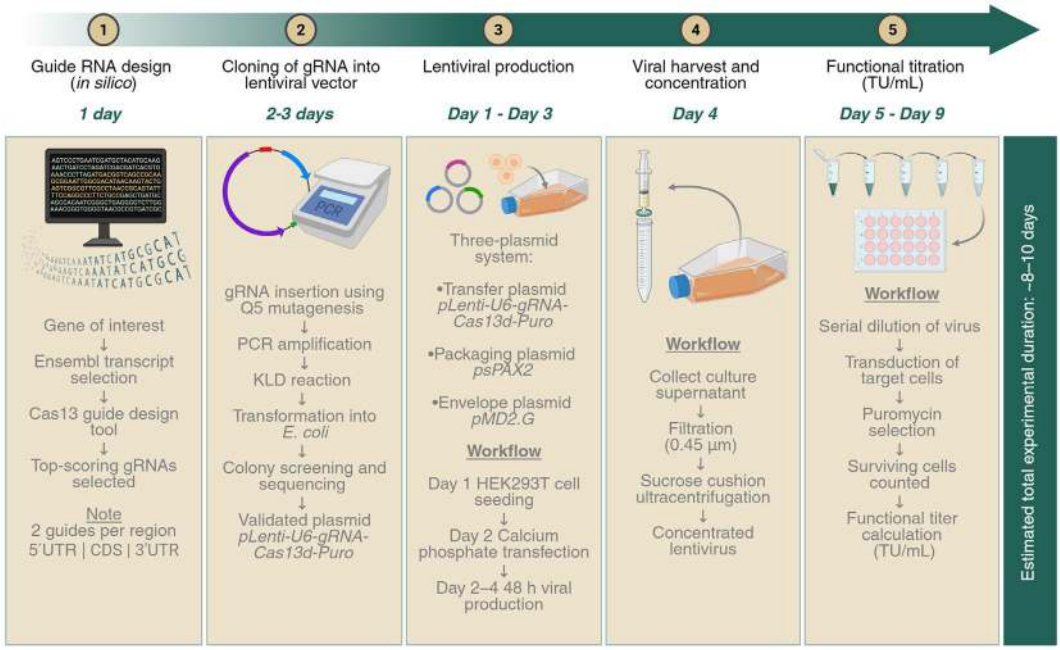


Fig. 3 Workflow and experimental timeline for lentiviral vector production and titration for CRISPR–Cas13d delivery. Schematic overview of the pipeline from guide RNA design and cloning to lentiviral production, concentration, and functional titration. Approximate time points for each step are indicated, with a total duration of ~8–10 days

4 Notes

1. For optimal lentiviral production, HEK293T cells are preferably used at low passage numbers, ideally no higher than passage 15, since prolonged passaging may be associated with reduced viral titers, potentially as a result of changes in cell growth, viability, and transfection efficiency [11].
2. The pH of the solutions must exactly match the values specified in the protocol. In particular, the final pH of the HBS must be 7.05; otherwise, transfection efficiency may be compromised.
3. To design guide RNAs for other CRISPR–Cas systems, different software tools should be used. For Cas9 guide design, we recommend CHOPCHOP (https://chopchop.cbu.uib.no/)
4. The PCR product can be stored at −20°C.
5. Before pelleting the bacteria, transfer 15 µL of the culture to a 0.5 mL tube containing glycerol. This glycerol stock can be stored at −80°C for up to 1 year.

6. Buffer P1 should be prepared by adding LyseBlue reagent (1:1000) and RNase A solution. After preparation, Buffer P1 must be stored at 2–8°C.
7. This step is only required when using endA+ strains or other bacterial strains with high nuclease activity or elevated carbohydrate content. Since DH5α is an endA− strain, this step is not necessary.
8. Although the original Qiagen protocol recommends elution with 50 µL of EB buffer, we prefer to use 30 µL in order to obtain a more concentrated DNA sample.
9. At this step, the calcium phosphate–DNA precipitate may be visible under the microscope.
10. Cleared supernatants may be stored at 4°C for 5–7 days. They can be used directly, stored as aliquots at −80°C, or concentrated if necessary. Repeated freeze–thaw cycles markedly reduce viral titer.
11. For concentrated vector preparations, it is preferable to prepare serial dilutions and add a constant volume from each dilution, rather than pipetting extremely small volumes directly.

Acknowledgments

The publication is based upon work by COST Action CA21113: Genome Editing for the Treatment of Human Diseases (https://www.genehumdi.eu), supported by European Cooperation in Science and Technology (COST). R.S.S. was supported by the Fundação de Amparo à Pesquisa do Estado de São Paulo (FAPESP) (grant number 2019/10922-9 and 2021/00168-5) and Conselho Nacional de Desenvolvimento Científico e Tecnológico (CNPq, Project Number: 406018/2022-7). L.M. is supported by Special University Research Fund (BOF N. 54207), Seal of Excellence grants, University of Antwerp, Flemish Government (BE), and received funding from FWO under the umbrella of the Partnership Fostering a European Research Area for Health (ERA.NET, ERA4Health CARDINNOV) (GA N. 101095426 of the EU Horizon Europe Research and Innovation Program). The figure was created with BioRender.

Competing Interests The authors declare no competing interests.

References

1. Jinek M, Chylinski K, Fonfara I et al. (2012) A programmable dual-RNA-guided DNA endonuclease in adaptive bacterial immunity. Science 337(6096):816–21
2. Mali P, Yang L, Esvelt KM et al. (2013) RNA-guided human genome engineering via Cas9. Science 339(6121):819–23.
3. Cong L, Ran FA, Cox D et al. (2013) Multiplex genome engineering using CRISPR/Cas systems. Science 339(6121):819–23
4. Abudayyeh OO, Gootenberg JS, Konermann S et al. (2016) C2c2 is a single-component programmable RNA-guided RNA-targeting CRISPR effector. Science 353(6299):aaf5573
5. Konermann S, Lotfy P, Brideau NJ et al. (2018) Transcriptome Engineering with RNA-Targeting Type VI-D CRISPR Effectors. Cell 173(3):665–676
6. Yan WX, Chong S, Zhang H et al. (2018) Cas13d is a compact RNA-targeting Type VI CRISPR effector positively modulated by a WYL-domain-containing accessory protein. Mol Cell 70(2):327–339
7. Abudayyeh OO, Gootenberg JS, Essletzbichler P et al. (2017) RNA targeting with CRISPR-Cas13. Nature 550:280–284
8. Zufferey R, Nagy D, Mandel RJ et al (1997) Multiply attenuated lentiviral vector achieves efficient gene delivery in vivo. Nat Biotechnol (9):871-875
9. Dull T, Zufferey R, Kelly M et al. (1998) A third-generation lentivirus vector with a conditional packaging system. J Virol 72:8463–8471
10. Kutner RH, Zhang XY, Reiser J (2009) Production, concentration and titration of pseudotyped HIV-1-based lentiviral vectors. Nat Protoc 4:495–505
11. Brown LY, Dong W, Kantor B (2020) An improved protocol for the production of lentiviral vectors. STAR Protoc 1:100152

Open Access This chapter is licensed under the terms of the Creative Commons Attribution-NonCommercial-NoDerivatives 4.0 International License (http://creativecommons.org/licenses/by-nc-nd/4.0/), which permits any noncommercial use, sharing, distribution and reproduction in any medium or format, as long as you give appropriate credit to the original author(s) and the source, provide a link to the Creative Commons license and indicate if you modified the licensed material. You do not have permission under this license to share adapted material derived from this chapter or parts of it.

The images or other third party material in this chapter are included in the chapter's Creative Commons license, unless indicated otherwise in a credit line to the material. If material is not included in the chapter's Creative Commons license and your intended use is not permitted by statutory regulation or exceeds the permitted use, you will need to obtain permission directly from the copyright holder.





Chapter 8

Production and Storage of High-Capacity Adenoviral Vectors for the Delivery of Advanced CRISPR Systems

Xiaoling Wang, Jin Liu, Josephine M. Janssen and Manuel A.F.V. Gonçalves

Abstract

Genome editing based on engineered CRISPR systems is advancing rapidly, with the field increasingly moving toward approaches that avoid the induction of mutagenic double-stranded DNA breaks (e.g., RNA-programmable base editing, prime editing, and donor DNA transposition). These nuclease-free strategies often rely on large or multi-component molecular assemblies that can include gene-sized donor DNA substrates. There is, nonetheless, a paucity of vehicles capable of delivering such large and complex genome-editing components effectively and, ideally, in defined stoichiometric ratios. High-capacity adenoviral vector particles (AdVPs) offer an attractive set of features to address these challenges, including robust cell transduction levels regardless of mitotic status, exceptional payload capacity (up to ~36 kb), strict chromosomal nonintegrating character, and the complete absence of viral coding sequences. Hence, AdVPs can serve as biological nanoparticles suitable for the evaluation and application of next-generation CRISPR technologies in physiologically relevant cellular contexts, regardless of the size and number of the attendant tools. Here, after summarizing the key characteristics of earlier- and latest-generation adenoviral vector platforms, we describe protocols for producing AdVPs, including vectors that deliver multiplexing, prime-editing, and orthogonal nuclease constructs. Finally, we highlight important considerations for designing AdVP production reagents and validate a storage buffer that preserves AdVP functionality after repeated freeze-thaw cycles.

Keywords Genome editing, Gene editors, Prime editing, Donor DNA, Adenoviral vectors, High-capacity, Third generation, Helper-dependent, Virus-like particles

1 Introduction

Adenoviral vectors are based on vertebrate viruses in the *Adenoviridae* family, with over 100 distinct types identified in humans alone [1]. Human adenoviruses are classified into seven species, designated A through G, with the most-studied prototypic adenovirus, type 5 from species C, typically causing cold-like symptoms [1,2]. Structurally, these virus particles (virions) consist of a protein-capped linear double-stranded DNA genome of approximately 36,000 base-pairs (bp)

Duško Lainšček et al. (eds.), *CRISPR Delivery*, Methods in Molecular Biology, vol. 3075,
https://doi.org/10.1007/978-1-0716-5547-4_8,
© The Author(s) 2027

packaged inside a nonenveloped icosahedral protein capsid (~100 nm) mostly formed by hexons, penton bases, and fiber proteins [3]. The fiber proteins protrude from the capsid surface to engage, via their apical knob domains, specific cell-surface receptors to enter host cells through clathrin-mediated endocytosis [4]. As endosomes mature, acidification triggers conformational rearrangements in capsid proteins, exposing membrane-penetrating motifs that mediate endosomal escape. The partially disassembled capsid then traffics along microtubules to the nuclear envelope, where it docks and delivers the viral DNA through a nuclear pore [4]. Consequently, adenoviruses do not require nuclear envelope breakdown, allowing efficient infection of both dividing and nondividing or post-mitotic cells. Once in the nucleus, viral and cellular factors support viral gene expression, genome replication, virion assembly, and host-cell lysis [1,4]. Hence, building on the fine-tuned cell-entry mechanisms evolved by their parental viruses, replication-defective adenoviral vectors serve as efficient delivery vehicles for exogenous DNA transfer into target cells regardless of their replication status [1,5]. The transgenic DNA can be tailored to introduce viral- or tumor-specific vaccine antigens, therapeutic proteins, or gene-editing tools into cell nuclei, including multicomponent or large CRISPR-derived enzymes and donor DNA substrates for gene-sized chromosomal knock-ins [1,6,7].

Adenoviral vector platforms are divided into three main categories (Fig. 1). First-generation adenoviral vectors lack the early region 1 (*E1*), which encodes transcription factors that activate the viral gene expression program and modulate host-cell protein synthesis. Hence, removing *E1* disrupts viral DNA replication and creates space for exogenous DNA insertion [6–8]. To further expand DNA payload capacity and suppress residual viral gene expression, second-generation vectors combine *E1* deletion with additional deletions (typically in the *E2A* or *E4* viral DNA regions) (Fig. 1). First- and second-generation adenoviral vectors are produced in complementing packaging cell lines that supply in trans the missing gene functions [9]. Of note, the *E3* region is optional in both first- and second-generation adenoviral vectors because it is dispensable for replication and encapsidation in producer cells cultured in vitro [9]. Despite their genomic deletions, first- and second-generation adenoviral vectors are not fully inert. Indeed, low-level ("leaky") expression of remaining viral coding sequences can still occur in transduced cells in a vector-dose-dependent manner [1,10]. This residual viral gene expression contributes to vector cytotoxicity in vitro and to vector immunogenicity in vivo, which renders these vectors mostly applicable for vaccination purposes. A radical solution to the de novo "leaky" viral gene expression phenomenon is the development of high-capacity adenoviral vector particles (AdVPs), also called helper-dependent or third-generation AdVPs (Fig. 1) [6,11–13]. These virus-like particles lack all viral coding sequences, retaining only short noncoding *cis*-acting elements, namely inverted

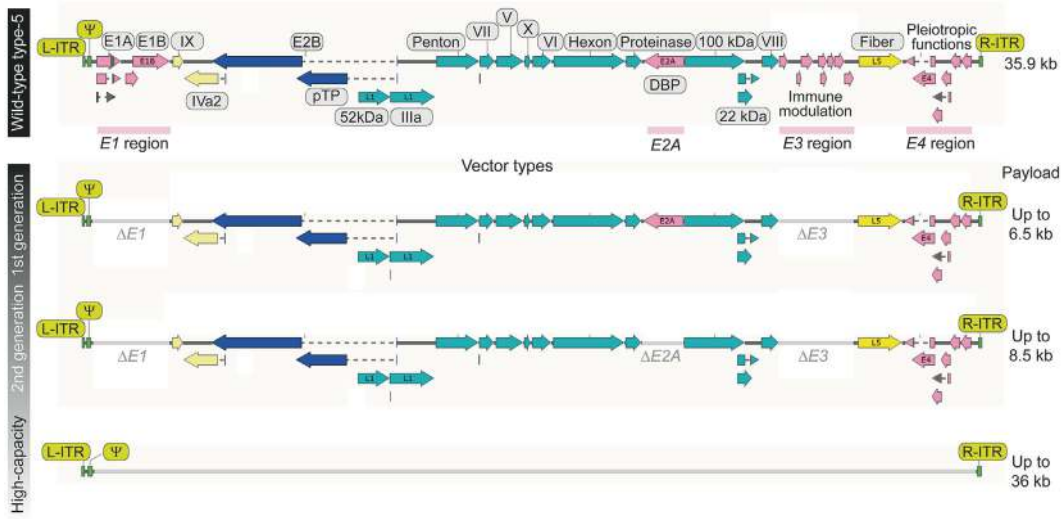


Fig. 1 Diagrams of wild-type adenovirus and recombinant adenoviral vector systems. The genome organization of the prototypic human adenovirus type-5 is drawn in relation to that of first-generation (*E1*-deleted), second-generation (*E1*- and *E2A*-deleted), and third-generation or high-capacity adenoviral vector particles. The noncoding *cis*-acting elements involved in vector DNA replication and encapsidation, common to all vector platforms, are the inverted terminal repeat (ITR) and packaging signal (Ψ) sequences, respectively. Regulatory functions involved in the activation of the viral gene expression cascade are encoded by the early (E) regions *E1A*, *E1B*, *E2A*, *E2B*, *E3*, and *E4* (pink and dark blue arrows). The proteins needed for the assembly and proteolytic processing of virion capsids are encoded by the late (L) regions *L1* through *L4* (cyan arrows) and *L5* (dark yellow arrow). The *L5* reading frame yields cell receptor-interacting fiber proteins. The full activation of the late viral gene expression program involves upregulation of the major late promoter (MLP, not shown) that occurs only after the onset of viral DNA replication. The reading frames coding for the intermediate proteins IX and IVa2 are also shown (light-yellow arrows). Other reading frames, e.g., *VAI* and *VAII* encoding small noncoding RNAs, are not depicted

terminal repeat (ITR) and packaging signal (Ψ) sequences, which are indispensable for vector DNA replication and encapsidation in producer cells, respectively [6,11–13].

CRISPR-derived genome-editing tools, comprising Cas nucleases and cognate guide RNAs (gRNAs), have established versatile, protein-engineering-free genome-editing systems that, as corollary, have become instrumental to the field [14]. Yet, nuclease-induced DSBs can lead to untoward bystander effects due to the activation and engagement of error-prone end joining DNA repair processes, e.g., nonhomologous end joining (NHEJ) and microhomology-mediated end joining (MMEJ) [15]. Bystander effects include loss of cell fitness [16], on-target and off-target mutations, chromosomal rearrangements, and, in DSB-sensitive cell types such as stem/progenitor cells, apoptosis [17–19]. Instead, genome editing based on nickases [20,21] or on nickases fused to heterologous effector domains can achieve seamless genome editing, as single-stranded DNA breaks, or nicks, are substrates for neither NHEJ nor MMEJ.

Base editors and prime editors are examples of RNA-programmable nickases endowed with heterologous effector domains, in this case, deaminases and reverse transcriptases, respectively. Base editors, consisting of cytidine or adenine deaminases, typically fused to a $Cas9^{D10A}$ nickase, install C•G-to-T•A or A•T-to-G•C transitions, respectively [22–24]. More recent base editors can install C•G-to-G•C and A•T-to-C•G transversions instead [25–27]. Prime editors are more versatile than base editors in that they can establish all 12 bp substitutions as well as defined small insertions and deletions [28,29]. Broadly, prime editing encompasses a prime editing gRNA (pegRNA) and a prime editor protein formed by a $Cas9^{H840A}$ nickase fused to an engineered reverse transcriptase (RT). The pegRNA consists of a gRNA covalently linked at its 3′ end to an RT template that encodes the edit(s) of interest and a primer-binding site (PBS). Hence, the pegRNA defines both the target site and edit(s) of interest. After target-site nicking by a prime editor:pegRNA complex, the generated 3′ genomic DNA flap anneals to the PBS of the pegRNA, providing a 3′-OH primer for RT-driven DNA synthesis along the linked RT template. The resulting synthesized DNA subsequently partially hybridizes with the complementary genomic DNA. Finally, after the resolution of nonhybridizing DNA flaps, DNA repair or replication leads to the incorporation of edits at the chromosomal target site [28]. This basic prime editing system, named PE2, is complemented by using an auxiliary guide RNA that, via the generation of a proximal nick at the nontarget strand, fosters DNA editing frequencies. However, due to coordinated nicking of the "top" and "bottom" DNA strands, this prime editing system, dubbed PE3, typically yields higher frequencies of bystander indels than the PE2 system [28].

To increase the efficacy and scope of prime editing, next-generation prime editing modalities are being investigated [29]. Dual prime editing is a particularly powerful and versatile modality as it offers a wider range of targetable genomic sequences, edit types, and edit sizes via the programming of pegRNA pairs. Dual prime editors work together to locally generate complementary DNA flaps that, upon hybridization, can directly install precise DNA changes that are larger than those achieved via, for instance, base editing (i.e., 1-bp substitutions) or standard prime editing (i.e., up to 40-bp edits) [29]. Moreover, in addition to their capacity to install larger edits, dual prime editors also tend to be more precise than standard PE3 because their bipartite target sequences are more separated, preventing residual DSBs arising from nicking of the "top" and "bottom" DNA strands [30]. More recently, CRISPR-Paste builds on prime editing by inserting a recognition site for a large serine recombinase (e.g., Bxb1 and variants thereof) that subsequently serves as a genomic "landing pad" for targeted gene-sized donor DNA integration [31,32]. Another emerging large-scale genome-editing strategy is the use of CRISPR-associated transposition, which employs

multimeric proteins and donor DNA transposons to enable DSB-free targeted exogenous DNA insertions in mammalian cells [33,34].

AdVPs constitute a valuable platform for evaluating and applying advanced genome-editing systems owing to their attractive attributes. Specifically, (i) vast payload capacity (up to 36 kb), (ii) lack of cytotoxic and immunogenic viral genes, (iii) strict episomal nature; (iv) high particle stability and homogeneity; and (v) efficient entry into both dividing and post-mitotic cells in vitro and in vivo. Examples of the co-option of AdVPs for nuclease-free genome editing in biomedical contexts include the delivery of base editing and prime editing systems targeting alleles associated with Duchenne muscular dystrophy (DMD; OMIM #310200) [35] and hemoglobinopathies [36–38]. In fact, regarding the latter prevalent blood disorders, studies using capsid-modified AdVPs have already provided notable proof-of-principle for in vivo base editing and prime editing in hematopoietic stem/progenitor cells [36–38].

Notwithstanding these advances, both ex vivo and in vivo AdVP-based gene therapies employing next-generation genome editing technologies will benefit from further research aimed at overcoming well-defined biological and technical limitations. In particular, a deeper understanding of vector particle-cell interactions that trigger pro-inflammatory cytokine release (e.g., interleukin-6 and tumor necrosis factor) or activate intracellular innate immune sensors (e.g., Toll-like receptors and the cGAS-STING pathway) is warranted [39]. Insights gained from such studies are expected to inform strategies for transiently modulating these signaling pathways, thereby improving vector performance and downstream genome-editing outcomes. Moreover, in the context of in vivo gene therapy, continued progress in capsid engineering to achieve liver de-targeting and strict cell- or tissue-specific transduction is expected to become increasingly critical [40]. Equally important from a translational standpoint is the optimization of upstream and downstream AdVP manufacturing pipelines. In this regard, the production of AdVPs is intrinsically more complex than that of earlier-generation adenoviral vectors due to the requirement for a complementing *E1*-deleted helper vector that should be removed as thoroughly as possible from the final AdVP preparations. Indeed, effective helper depletion relies on efficient recombinase-mediated excision of the helper packaging signal in producer cells, followed by physical separation of AdVPs from residual helper particles through isopycnic (buoyant density) ultracentrifugation (Fig. 2). The typical range of helper vector contamination in AdVP preparations, often quantified by PCR-based assays, is 0.01%–1% of the total vector particles. Helper levels above 2% are undesirable in that cytotoxic effects in vitro or higher immunogenicity in vivo can become significant when using high AdVP amounts.

In this chapter, we present a detailed protocol for research-scale AdVP rescue, propagation, and purification, and validate a storage

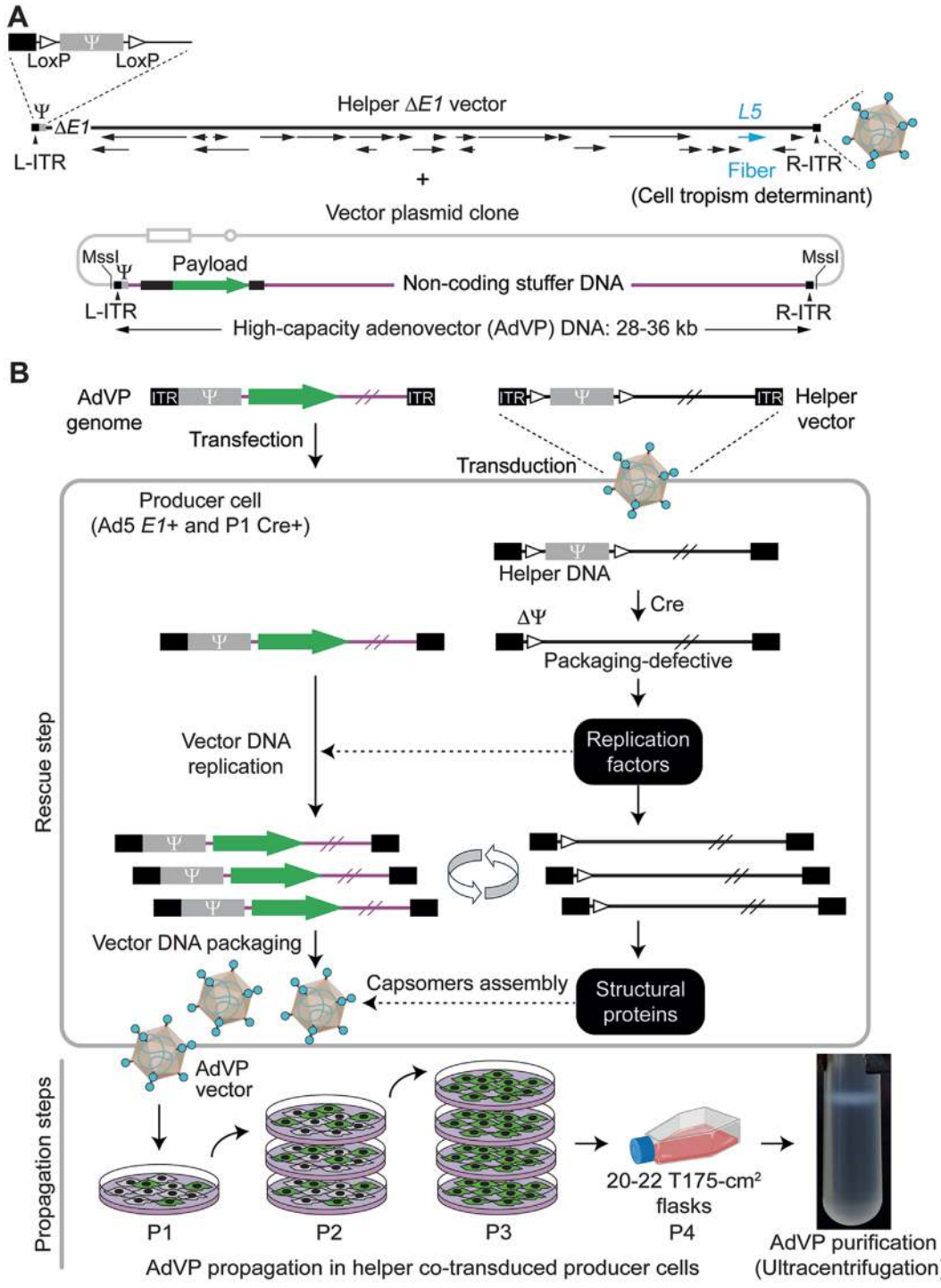


Fig. 2 Overview of research-scale production and purification of high-capacity adenoviral vector particles. (**A**) AdVP production components. First-generation (*E1*-deleted) helper adenoviral vector and AdVP plasmid molecular clone. The helper has its packaging signal elements (Ψ) framed by a direct repeat of LoxP sites for selective Cre/LoxP-mediated excision in packaging cells; the AdVP is devoid of all adenovirus DNA sequences except for the *cis*-acting packaging signal and "left" and "right" inverted terminal repeats (L-ITR and R-ITR, respectively). In addition to the ITR and Ψ sequences, AdVP genomes contain the genetic payload(s) of interest

buffer formulation that preserves AdVP titers following repeated freeze–thaw cycles. We further demonstrate the structural integrity and functionality of complex genome-editing cargos packaged in AdVP capsids, focusing on multiplexing dual nuclease and dual prime-editing systems developed for the correction of pathogenic alleles underlying DMD [35,41]. Finally, we describe general guidelines regarding the design and structure of AdVP and helper vector genomes.

2 Materials

2.1 Rescue and Propagation of AdVP Vectors

2.1.1 Reagents

1. 70% disinfectant ethanol.
2. 1% disinfectant sodium dodecyl sulfate (SDS) solution.
3. Cell culture-grade pH 7.4 phosphate-buffered saline (PBS).
4. Cell culture-grade 0.05% trypsin-ethylenediaminetetraacetic acid (EDTA) solution.
5. AdVP packaging cells (Table 1) and respective culture medium without marker-gene selection drugs.
6. AdVP plasmid clone with recognition sequences for a restriction enzyme (e.g., MssI) flanking the ITR elements.
7. Restriction enzyme (e.g., MssI) and corresponding buffer.
8. Agarose gel electrophoresis materials.
9. 1 mg/mL Polyethylenimine (PEI) transfection polycation: dissolve 45 mg of linear 25 kDa PEI in 40 mL of Milli-Q water pre-heated to 80°C. Allow the solution to cool down to room temperature. Adjust the pH to 7.4 with 1 M HCl. Add Milli-Q

Fig. 2 (continued): and "stuffer" DNA. The "stuffer" DNA, ideally of human origin and without extensive repetitive sequences, serves to increase vector genome length to a minimum size of approximately 28 kb. (**B**) AdVP production steps. AdVP assembly (rescue of vector genomes into adenovirus capsids) starts by transfecting into adenovirus type-5 *E1*-complementing and bacteriophage P1 Cre-expressing packaging cells, linear AdVP genomes spanning from the "left" to the "right" ITR. Before DNA transfection, the AdVP genomes are released from the respective plasmid clone backbone by restriction enzyme digestion (e.g., MssI). Transfected packaging cells are subsequently transduced with the helper that provides *in trans* all the adenovirus replication factors and structural proteins necessary for, respectively, replication and encapsidation of AdVP DNA into adenovirus capsids. As corollary, the cell or tissue tropism of AdVP vectors is defined by that of the helper used. The main determinants of tropism underlying cell binding and entry are the fibers and penton bases. Critically, the selective removal of the packaging signal from the helper vector DNA by Cre/LoxP-mediated recombination renders the helper vector packaging-defective. Rescued AdVPs are subsequently collected and amplified through a series of propagation steps in increasing amounts of helper-transduced packaging cells. After the final propagation step (typically, the fourth), AdVPs are collected and purified from producer cell lysates

Table 1
Representative packaging cell lines for high-capacity adenoviral vector production

Cell line	Parental cells	Complementation	Recombinase	References
293Cre4	HEK293	*E1A E1B (E1)*	Cre	[12]
293Cre415	293Cre4	*E1*	Cre	[42]
CreE	E2T	*E1 E2A*	Cre	[43]
293FLP	HEK293	*E1*	FLPe	[44]
293CreFLP	293Cre4	*E1*	Cre FLPe	[44]
293-FLPe6	HEK293	*E1*	FLPe	[45]
C7-Cre	C-7	*E1 E2B*	Cre	[46]
116	293N3S	*E1*	Cre	[47]
PER.C6-Cre	PER.C6	*E1*	Cre	[48]
Per.tTA.Cre43	PER.C6	*E1*	Cre	[49]
PEC3.30	PER.E2A	*E1 E2A*	Cre	[50]

water to a final volume of 45 mL. Sterilize the solution by filtration through 0.22-μm cellulose filters. Freeze and thaw at least three times before first use. Aliquot and store at −80°C.

10. 150 mM NaCl solution in pH 7.4 PBS. Sterilize the solution by filtration through 0.22-μm cellulose filters or by autoclaving at 121°C for 20 min.
11. Helper *E1*-deleted adenoviral vector with packaging signal flanked by recognition sequences for a site-specific recombinase (e.g., bacteriophage P1 Cre or *S. cerevisiae* FLP recombinase, or variants thereof).
12. Liquid nitrogen N_2.

2.1.2 Equipment

1. Vertical laminar air flow cabinet.
2. Humidified CO_2 Incubator.
3. Pipetboy and disposable sterile pipettes: 1, 2, 5, 10, and 25 mL.
4. Sterile pipette filter tips: 10, 20, 200, and 1000 μL.
5. Sterile 15-mL and 50-mL screw cap polypropylene centrifuge tubes.
6. Sterile 1.5-mL and 2.0-mL Eppendorf tubes.
7. Cell counting chamber and cell counter or automatic cell counter apparatus.
8. Six-well cell culture plates (Greiner Bio-One).
9. T75-cm^2 and T175-cm^2 cell culture flasks (Greiner Bio-One).
10. Dry oven (37°C).
11. Agarose gel electrophoresis materials and apparatus.

12. Vortex apparatus.
13. Tabletop centrifuge with cooling option.
14. Water bath (37°C).

2.2 Concentration and Purification of AdVP Vectors

2.2.1 Reagents

1. 70% disinfectant ethanol.
2. 1% disinfectant SDS.
3. Cell culture-grade pH 7.4 PBS.
4. Research-scale cell lysate.
5. Deoxycholate (DOC) detergent: 5% (w/v) diluted in Milli-Q water. Sterilize the solution by filtration through a cellulose filter with a 0.22-μm pore size.
6. 1 M $MgCl_2$ in 100 mL Milli-Q water. Sterilize the solution by autoclaving or by filtration through a cellulose filter with a 0.22-μm pore size.
7. 10 mg/mL DNaseI: dissolve 100 mg DNaseI in 10 mL pH 7.4 PBS. Sterilize by filtration through a cellulose filter with a 0.22-μm pore size, aliquot and store at −20°C.
8. 1 M pH 8.0 Tris-Cl in 1 L Milli-Q water and 1 M pH 7.5 Tris-Cl in 1 L Milli-Q water. Sterilize the solutions by autoclaving.
9. Cesium chloride (CsCl) buffered solution with a density of 1.4 g/mL supplemented with 5% glycerol: 264.4 g CsCl (dissolve at 65°C), 15 mL 1 M pH 7.5 Tris-Cl, 25 mL 100% glycerol, adjust to 500 mL with Milli-Q. Sterilize the solution by autoclaving. Check by weighing 1 mL of the final solution (range: 1.39–1.42 g).
10. CsCl buffered solution with a density of 1.33 g/mL supplemented with 5% glycerol: 227.2 g CsCl (dissolve at 65°C), 15 mL 1 M pH 7.5 Tris-Cl, 25 mL 100% glycerol, adjust to 500 mL with Milli-Q water. Sterilize the solution by autoclaving. Check by weighing 1 mL of the final solution (range: 1.31–1.34 g).
11. CsCl buffered solution with a density of 1.2 g/mL supplemented with 5% glycerol: 138.65 g (dissolve at 65°C), 15 mL 1 M pH 7.5 Tris-Cl, 25 mL 100% glycerol, adjust to 500 mL with Milli-Q water. Sterilize the solution by autoclaving. Check by weighing 1 mL of the final solution (range: 1.20–1.22 g).
12. AdVP storage buffer (A195): 10 mM Tris, 75 mM NaCl, 5% (w/v) sucrose, 0.02% (w/v) polysorbate 80 (Tween 80), 1 mM $MgCl_2$, 100 μM EDTA, 0.5% (v/v) ethanol, 10 mM histidine, pH 7.4. Sterilize the solution by filtration through cellulose filters with 0.22-μm pore size.

2.2.2 Equipment

1. Vertical laminar air flow cabinet.
2. Pipetboy and disposable sterile pipettes: 1, 2, 5, 10, and 25 mL.
3. Sterile pipette filter tips: 10, 20, 200, and 1000 μL.
4. Sterile 15-mL and 50-mL screw cap polypropylene centrifuge tubes.
5. Sterile 0.5-mL Eppendorf tubes.
6. Tabletop centrifuge with cooling option.
7. Water bath (37°C).
8. Ultracentrifuge, such as Optima XE-90 with SW28 or SW32Ti rotor and VTi65.1 rotor (Beckman Coulter).
9. Polypropylene ultracentrifuge tubes (25 × 89 mm) (Beckman Coulter).
10. Quick-Seal ultracentrifuge tubes (16 × 76 mm) (Beckman Coulter), metal caps, and tube heat-sealing apparatus (Beckman Coulter). Alternatively, OptiSeal polyallomer ultracentrifuge tubes and plugs (16 × 67 mm) (Beckman Coulter).
11. Sterile forceps.
12. 10-mL Syringes.
13. 20 G × 1 ½" Nr.1 (0.9 × 38 mm) and 23 G × 1 ¼" Nr.14 (0.6 × 32 mm) needles.
14. Amicon Ultra-15 centrifuge filter tubes with 100 kDa Molecular Weight Cutoff (MWCO) (Merck Millipore).
15. Analytical weighing scale.

2.3 Characterization of AdVP Genomes by Restriction Fragment Length Analysis (RFLA)

2.3.1 Reagents

1. 70% disinfectant ethanol.
2. 1% disinfectant SDS.
3. 50–80 μL of purified AdVP stock.
4. 10 mg/mL DNaseI.
5. 10× digestion buffer: 130 mM pH 7.5 Tris-Cl, 1.2 mM $CaCl_2$, and 50 mM $MgCl_2$.
6. 0.5 mM pH 8.0 EDTA.
7. 10% SDS solution.
8. 20 mg/mL Proteinase K.
9. AdVP and helper plasmid clones.
10. Restriction enzymes and corresponding buffers.
11. Agarose gel electrophoresis materials.
12. Elution buffer: 10 mM pH 8.0 Tris-Cl.

2.3.2 Equipment

1. Vertical laminar air flow cabinet.
2. Sterile pipette filter tips: 10, 20, 200, and 1000 μL.
3. Sterile 1.5-mL Eppendorf tubes.
4. Dry oven (37°C).
5. Metal heating block (55°C).
6. QIAEX II Gel Extraction Kit (Qiagen) or similar.
7. Agarose gel electrophoresis apparatus.
8. SnapGene software package or similar.

3 Methods

The work activities involving the production and handling of adenoviral vectors occur in a laboratory with biosafety level 2 (BSL-2) following the pertinent national practices. Regular subculturing of AdVP packaging cell lines (Table 1) can instead take place under a BSL-1 confinement level. Rinse and discard disposable pipettes and pipette tips in 1% SDS. After work termination, clean nondisposable materials and flow cabinet surfaces with a 1% SDS solution, then with 70% ethanol. Turn off and close the flow cabinet, then light up the UV irradiation for at least 15 min.

3.1 Rescue of AdVP Vector Genomes into Adenoviral Capsids (P0)

1. On day 0, seed AdVP packaging cells at a density that guarantees a confluency of approximately 70%–80% the next day. The number of cells seeded depends on the cell line used (*see* **Note 1**).
2. Set up a preparative digestion of the AdVP plasmid molecular clone using the appropriate enzyme (e.g., MssI). This is needed for releasing the AdVP vector genome, spanning from the "left" to the "right" ITR, from the plasmid backbone (Fig. 2A). To this end, add to a sterile Eppendorf tube: 7.5 μg of AdVP plasmid DNA, 2 μL of the appropriate restriction enzyme (10 units), and 4 μL of the respective 10× restriction enzyme buffer. Bring the final volume to 40 μL by using sterile Milli-Q water and incubate at 37°C (optimal temperature for most restriction enzymes) in a dry oven for 4–5 h. Next, load 4 μL of the digestion mixture in 1× loading buffer on a 0.75% (w/v) agarose gel containing a DNA dye in 1× Tris-acetate-EDTA (TAE) running buffer to confirm digestion reaction completion through DNA electrophoresis (*see* **Note 2**).
3. On day 1, apply a DNA transfection method to introduce the linearized AdVP DNA into the packaging cells (Fig. 2B). A low-cost and efficient nucleic acid transfection option makes use of 25 kDa linear PEI, a highly cationic water-soluble polymer that, after binding to DNA acts via the "proton sponge effect" for cell entry and endosomal escape. On

a per six-well basis, dilute 6.25 μg of digested AdVP plasmid DNA in 150 mM NaCl to a final volume of 200 μL. Next, add 20.6 μL of 1 mg/mL PEI to the plasmid DNA solution and vortex immediately for approximately 10 s. Let the PEI-DNA complexes form for 15–20 min at room temperature, then add the entire transfection mixture directly to the 2 mL packaging-cell culture medium, and homogenize the medium and inoculum thoroughly by gentle swirling (*see* **Note 3**). For this DNA transfection step, upscale if needed the number of wells using the relevant reagent amounts, e.g., production of different AdVP vector batches. When generating different AdVP vectors, assign distinct six-well plates to each AdVP assembly to mitigate the risk of vector cross-contamination.

4. After 6 h, remove the circa 2 mL of transfection medium and add 3 mL of fresh culture medium containing the helper *E1*-deleted adenoviral vector at a multiplicity of infection (MOI) in vector units per cell that yields full cytopathic effect (CPE) within 2 to 4 days post-transduction (Fig. 2B) (*see* **Note 4**).
5. At full CPE, collect into 15-mL or 50-mL screw cap polypropylene tubes the suspension of producer cells transfected with the linearized AdVP vector DNA and transduced with the helper vector and either store it at −80°C, or proceed by lysing the cells by three cycles of freezing and thawing using liquid nitrogen (N_2) and 37°C water baths, respectively (*see* **Note 5**).
6. Centrifuge the screw cap tubes at 2000 × *g* for 10 min at 16°C to pellet cell debris and transfer the supernatants to new screw cap polypropylene tubes inside the laminar flow cabinet. Store the clarified cell lysates at −80°C or proceed with AdVP vector propagation.

3.2 Propagation of AdVP Vectors in Producer Packaging Cells

3.2.1 First Propagation Round (P1)

1. Seed the AdVP packaging cells 20–24 h prior to the start of the first propagation round (P1) at a density that guarantees monolayers at ~70%–80% confluency with evenly distributed cells. Prepare three wells of six-well plates per AdVP vector. The number of cells seeded depends on the cell line used (*see* **Note 1**). When generating different AdVP vectors, allocate distinct six-well plates for each AdVP propagation to mitigate vector cross-contamination risks.
2. Start P1 by removing the 2 mL of culture medium and adding 300–400 μL of clarified cell lysate (P0) diluted in 1.7–1.6 mL of culture medium containing the helper *E1*-deleted adenoviral vector at an MOI leading to full CPE within 2 to 4 days post-transduction (*see* **Note 4**). Next, distribute 2 mL of the

gently homogenized inoculum per well of a six-well plate per AdVP vector.

3. At full CPE, pool and collect P1 producer cell suspensions corresponding to individual AdVP preparations in 15-mL or 50-mL screw cap polypropylene tubes and store them at −80°C. Alternatively, proceed with cell lysis by applying three cycles of freezing and thawing in liquid N_2 and 37°C water baths, respectively (*see* **Note 5**).
4. Clarification of producer cell lysates (see Sect. 3.1.6).

3.2.2 Second Propagation Round (P2)

1. Seed the AdVP packaging cells 20–24 h prior to the initiation of the second propagation round (P2) at a density that ensures monolayers at ~70%–80% confluency with evenly distributed cells. Prepare three T75-cm² cell culture flasks per AdVP vector. The number of cells seeded depends on the cell line used (*see* **Note 1**).
2. Initiate P2 by removing the 10 mL of culture medium and adding 2–3 mL of clarified cell lysate (P1) diluted in 8–7 mL of culture medium containing the helper *E1*-deleted adenoviral vector at an MOI leading to full CPE within 2 to 4 days post-transduction (*see* **Note 4**). Next, distribute 10 mL of the gently homogenized inoculum per T75-cm² flask per AdVP vector.
3. At full CPE, pool and collect P2 producer cell suspensions corresponding to individual AdVP preparations in 50-mL screw cap polypropylene tubes and store them at −80°C or advance with cell lysis by applying three cycles of freezing and thawing in liquid N_2 and 37°C water baths, respectively (*see* **Note 5**).
4. Clarification of P2 producer cell lysates (see Sect. 3.1.6).

3.2.3 Third Propagation Round (P3)

1. Seed the AdVP packaging cells 20–24 h prior to the start of the third propagation round (P3) at a density that assures monolayers at ~70%–80% confluency with evenly distributed cells. Prepare three T175-cm² cell culture flasks per AdVP vector. The number of cells seeded depends on the cell line used (*see* **Note 1**).
2. Start P3 by removing the 20 mL of culture medium and adding 1–3 mL of clarified cell lysate (P2) diluted in 19–17 mL of culture medium containing the helper *E1*-deleted adenoviral vector at an MOI leading to full CPE within 2 to 4 days post-transduction (*see* **Note 4**). Next, distribute 20 mL of the gently homogenized inoculum per T175-cm² flask per AdVP vector.
3. At full CPE, pool and harvest P3 producer cell suspensions corresponding to individual AdVP preparations in 50-mL screw cap polypropylene tubes and store them at −80°C or

proceed to cell lysis by applying three cycles of freezing and thawing in liquid N_2 and 37°C water baths, respectively (*see* **Note 5**).

4. Clarification of P3 producer cell lysates (see Sect. 3.1.6).

3.2.4 Fourth Propagation Round (P4)

1. Seed the AdVP packaging cells 20–24 h before the fourth propagation round (P4) is initiated at a density that yields monolayers at ~70%–80% confluency with uniformly distributed cells. Prepare 20–22 T175-cm^2 cell culture flasks per AdVP vector. The number of cells seeded depends on the cell line used (*see* **Note 1**).
2. Remove the 20 mL of culture medium and add 1–3 mL of clarified cell lysate (P3) diluted in 19–17 mL of culture medium containing the helper *E1*-deleted adenoviral vector at an MOI leading to full CPE within 2 to 4 days post-transduction (*see* **Note 4**). Next, distribute 20 mL of the gently homogenized inoculum per T175-cm^2 flask per AdVP vector.
3. At full CPE, pool and gather P4 producer cell suspensions corresponding to individual AdVP preparations in 50-mL screw cap polypropylene tubes. The cells remaining attached can be collected by mechanical detachment by tapping each well-closed T175-cm^2 culture flask (*see* **Note 6**).
4. Rinse the surface of all T175-cm^2 flasks with 20 mL of PBS pH 7.4 using a pipetboy connected to a 50-mL disposable pipette and transfer the resulting cell suspension to the collected bulk cell suspension in culture medium.
5. Centrifuge the cell suspensions in 50-mL screw cap polypropylene tubes at 2000 × *g* for 10 min at 16°C. Discard the supernatants and resuspend the cell pellets in a total of 30 mL of culture medium. Rinse all 50-mL tubes with a total of 7 mL of culture medium using a 10-mL disposable pipette and transfer the resulting material to the bulk cell suspensions. Divide the approximately 40-mL material into two 50-mL tubes and store at −80°C; or move to the AdVP vector concentration and purification procedures.

3.3 Concentration and Purification of AdVP Vectors

3.3.1 Release of AdVP Vectors from Producer Cells

1. Add 2.2 mL of 5% DOC detergent in Milli-Q to each 50-mL tube with the collected producer-cell suspension and incubate in a water bath at 37°C for 30 min. Homogenize the mixture every 5–10 min by gentle tube swirling or repeated inversions.

2. Add 0.8 mL of $MgCl_2$ (1.0 M) and 40–60 μL of DNaseI (10 mg/mL) to each 50-mL tube with the collected producer-cell suspension and incubate in a water bath at 37°C for 30 min. Homogenize the mixture every 5–10 min by gentle tube swirling or inversions.
3. Centrifuge at 2000 × *g* for 10 min at 16°C, transfer the supernatant to a new 50-mL screw cap polypropylene tube and centrifuge at 3000 × *g* for 10 min at 16°C. Transfer the resulting supernatant to a new screw-cap polypropylene tube.

3.3.2 Preparation of the CsCl Block Gradient

1. For either SW32Ti or SW28 swinging-bucket rotors (Beckman Coulter), place the respective ultracentrifuge tube holders and lids inside the flow cabinet. Each SW32Ti and SW28 rotor holds positions for ultracentrifugation of six tubes.
2. Add 2 mL of 1% SDS and cap the ultracentrifuge tube holders with the respective lids. Invert the tube holders several times, discard the washing 1% SDS solution, and place the tube holders and lids upside down on a clean tissue to allow the remaining solution to drain out. Repeat these procedures using 70% ethanol instead, and ensure there are no residual 1% SDS or 70% ethanol to avoid subsequent AdVP inactivation. Finally, irradiate the tube holders for at least 20 min by using the sterilizing UV lamp built into the flow cabinet.
3. Prepare in a 50-mL screw cap polypropylene tube a buffered CsCl solution with a density (ρ) of 1.24 g/mL by mixing 16 mL and 4 mL of buffered CsCl solutions with densities of 1.2 g/mL and 1.4 g/mL, respectively. One 20-mL 1.24 g/mL mixture is sufficient for processing 40 mL of clarified AdVP producer cells divided in two ultracentrifugation tubes, i.e., 38.5 mL Open-top thin-wall polypropylene round bottom tubes (25 × 89 mm).
4. Add 10 mL of the CsCl solution ($\rho = 1.24$ g/mL) to the bottom of an Open-top thin-wall polypropylene ultracentrifugation tube (25 × 89 mm), keeping the walls dry.
5. Place the tip of a disposable pipette containing 7 mL of CsCl ($\rho = 1.4$ g/mL) at the bottom of the 25 × 89 mm ultracentrifuge tube and gently dispense 5 mL of this heavy solution underneath the lighter 10 mL of CsCl ($\rho = 1.24$ g/mL)(*see* **Note 7**). Mark with a waterproof ink pencil the sharp boundary between the 1.4 g/mL and 1.24 g/mL CsCl density layers, visible due to light diffraction.
6. Carefully, add the clarified AdVP producer cell lysate onto the CsCl block gradients, taking care to avoid mixing the different layers (Fig. 3A). If needed, add PBS pH 7.4 until the surface of the cumulative fluid is ~0.5 cm underneath the opening of the

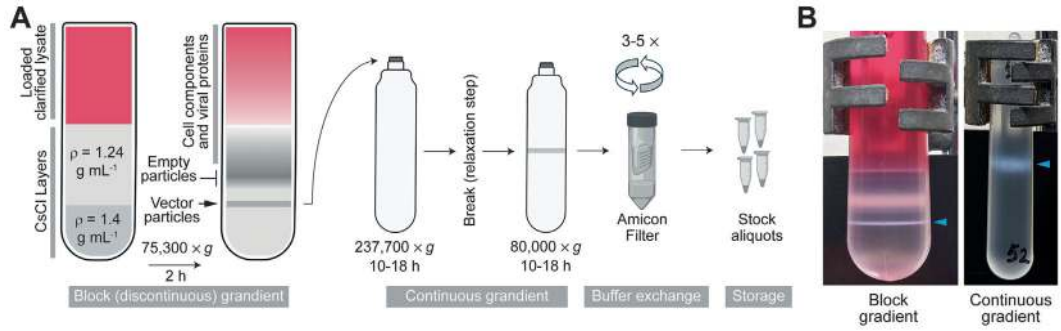


Fig. 3 Downstream processing of AdVP vectors. (**A**) Sequential ultracentrifugation and ultrafiltration steps. (**B**) Representative images of AdVP material (arrowheads) after discontinuous and continuous CsCl density banding (left and right images, respectively). See text for details

ultracentrifuge tube. Carefully, transfer the filled ultracentrifuge tubes to the tube holders with the aid of sterilized forceps.

7. Balance each pair of holders containing filled ultracentrifugation tubes and their respective caps using a calibrated analytical weighing scale (*see* **Note 8**). Before placing the analytical weighing scale inside the flow cabinet, clean it thoroughly with a tissue soaked in 70% ethanol, then remove excess moisture with a dry tissue.
8. Screw the lids of the properly balanced tube holders and carefully append the capped tube holders containing the loaded ultracentrifugation tubes into the respective hooks in a SW32Ti or SW28 swinging-bucket rotor.

3.3.3 CsCl Block Gradient Ultracentrifugation

1. In a Beckman Coulter XE-90 ultracentrifuge, or similar apparatus, centrifuge the tubes at 75,300 × *g* for 2 h at 10°C with the acceleration and deceleration speed set to slow (i.e., 7 and 8, respectively). The vector band should be located at the interface between the 1.4 g/mL and 1.24 g/mL CsCl densities (Fig. 3A).
2. Prepare a stand with a fastened clamp and arrange a black background inside the flow cabinet (Fig. 3B). Before placing these materials inside the flow cabinet, clean them by using a tissue infused with 1% SDS and subsequently with 70% ethanol. Eliminate excess humidity with a dry tissue.
3. Place a tray containing 1% SDS under the clamp and, after opening the tube holder inside the flow cabinet, remove the corresponding ultracentrifuge tube with the aid of sterilized forceps. Each ultracentrifuge tube is processed individually. Clean the side wall of the ultracentrifuge tube using tissues soaked in 1% SDS, then 70% ethanol. Eliminate thoroughly any excess humidity with a dry tissue. Next, fasten the ultracentrifugation

tube to the stand by carefully tightening the clamp to avoid disturbing the banded layers.

4. Plug a 20 G × 1½" Nr.1 (0.9 × 38 mm) needle to a 10-mL syringe. After removing the cap from the needle, move the plunger of the syringe a couple of times up and down to ensure a continuous air column. Pierce through the cleaned ultracentrifuge tube's side wall just beneath the AdVP band and gently recover the vector particles using syringe suction, taking care to avoid mixing the banded layers.

3.3.4 CsCl Continuous Gradient Ultracentrifugation

1. Transfer the recovered AdVP vector material into an 11.2 mL OptiSeal polyallomer tube 16 × 67 mm with plug; or into a 13.5 mL Quick-Seal polyallomer tube 16 × 76 mm. The former tubes have a lower volume capacity but do not require a dedicated metal cap-heating apparatus for sealing. Make sure that, after removing the needle, the dripping from the hole is collected inside the tray containing 1% SDS. Moreover, release the centrifuge tube from the clamp and discard it into the 1% SDS solution.
2. Fill the continuous-gradient ultracentrifugation tubes to the neck of each tube with a buffered CsCl solution mixture tailored to the estimated buoyant density of the AdVP undergoing purification, e.g., 1.31–1.32 g/mL (*see* **Note 9**).
3. Balance each pair of loaded ultracentrifuge tubes in an analytical weighing scale by using an aliquot of CsCl solution for weight equilibration, making sure that the weight differences between tube pair members do not exceed ±0.02 g. Seal the ultracentrifuge tubes.
4. Introduce the sealed tubes in the tube holders embedded in a VTi 65.1 rotor (Beckman Coulter), place the gold metal caps on top of each sealed tube and screw the lids. Close all rotor-embedded tube holders with the respective lids, even if some of the tube holders remain empty.
5. In a Beckman Coulter XE-90 ultracentrifuge, or analogous apparatus, centrifuge the tubes at 237,700 × *g* for 10–18 h at 10°C.
6. After 10–18 h of ultracentrifugation, reduce the speed from 237,700 × *g* to 80,000 × *g* for an additional 10–18 h at 10°C (relaxation step) with the apparatus set to slow acceleration and break off (*see* **Note 10**). The vector band should be located at or around the central portion of the ultracentrifugation tube (Fig. 3A, B).
7. Perform the procedures described in items 2 and 3 under Sect. 3.3.3.

8. Plug a 20 G × 1½" Nr.1 (0.9 × 38 mm) needle to a 10-mL syringe. After removing the cap from the needle, move the plunger of the syringe a couple of times up and down to ensure a continuous air column. Pierce the top of the OptiSeal or Quick-Seal ultracentrifugation tube with a 23 G × 1¼" Nr.14 (0.6 × 32 mm) needle next to the neck to allow AdVP vector band retrieval by using the 10-mL syringe connected to the needle.
9. Pierce through the cleaned ultracentrifuge tube side wall just underneath the AdVP band and gently recover the vector particles through syringe suction. Make sure that after removing the needle, any dripping from the needle's hole is collected in the tray containing 1% SDS. Moreover, release the centrifuge tube from the clamp and discard it into the 1% SDS solution.

3.3.5 Buffer Exchange Through Ultrafiltration

1. Add 10 mL of storage buffer A195 [51] into an Amicon Ultra-15 centrifugal tube containing filters with 100 kDa MWCO (Fig. 3A) and equilibrate the filter membranes by rinsing at 2000 × *g* at 15°C until ±500 µL of A195 storage buffer is left as retentate in the filter unit (*circa* 7 min) (*see* **Note 11**). Discard the flow through and place the filter unit back into the respective acceptor tube.
2. Transfer the collected AdVP material into the pre-rinsed filter unit connected to the empty acceptor tube.
3. Fill the filter unit with A195 storage buffer until full, and centrifuge the filled Amicon Ultra-15 tubes at 2000 × *g* at 15°C until approximately 500 µL of AdVP retentate is left in the filter unit (*see* **Note 12**). Discard the flow through and place the filter unit back into the respective acceptor tube.
4. Repeat buffer exchange Step 3 at least three times, making sure that the AdVP retentate left after the last buffer exchange cycle is around 0.5 mL. Collect the AdVP retentate material into a sterile Eppendorf tube.
5. Rinse the surface of the filter membranes with 150 µL of A195 storage buffer several times using a pipette connected to a 200-µL filter tip to recover absorbed AdVP material. Take care that the filter tip does not touch the filter membrane throughout the rinsing cycles to prevent membrane damage. Transfer the membrane washing A195 buffer solution into the AdVP stock. Repeat this AdVP recovery step two additional times.
6. Homogenize the final volume of AdVP stock by gentle pipetting, then aliquot it into sterile 0.5 mL Eppendorf tubes (20–40 µL per tube) (Fig. 3A). Store the AdVP aliquots at −70°C or −80°C until use.

3.4 Characterization of AdVP Genomic DNA Structure by RFLA

1. Collect 50–80 µL of purified AdVP stock in a 1.5-mL Eppendorf tube and add 8 µL of DNAseI (10 mg/mL), 12 µL of 10× digestion buffer and Milli-Q water to a total volume of 120 µL. Homogenize the digestion mixture by pipetting and incubate it at 37°C for 30 min.
2. Add 2.4 µL EDTA (0.5 mM, pH 8.0), 6 µL of 10% SDS and 1.5 µL of Proteinase K (20 mg/mL). Homogenize the mixture by pipetting and incubate it at 55°C for 60 min in a heat block.
3. Concentrate and purify the isolated DNA by using a DNA extraction kit based on nucleic acid adsorption to and elution from microbeads, such as the QIAEX II Gel Extraction Kit.
4. Add 500 µL Buffer QX1 and 10 µL of beads, mix well by gentle inversion and incubate at 55°C for 20 min, mix every 3–5 min by inversion.
5. Centrifuge at 17,900 × *g* for 30 s and discard the supernatant. Wash the bead pellet once with 500 µL of Buffer QX1 and twice with 500 µL of Buffer PE.
6. Air-dry the bead pellet until it becomes white, while paying attention not to over-dry it.
7. Add 40 µL of Elution buffer or Milli-Q water and incubate at 55°C for 15 min while shaking every couple of minutes.
8. Centrifuge at 17,900 × *g* for 30 s and collect the supernatant with the eluted DNA into a new Eppendorf tube. Measure the DNA concentration at 260 nm by using a Nanodrop or similar device.
9. Perform RFLA of the eluted DNA by agarose gel electrophoresis in 1× TAE running buffer. To this end, digest 150–200 ng of DNA with restriction enzymes expected to yield multiple fragments spanning the payload(s) in the vector genome, taking along equal amounts of the parental AdVP and helper plasmid clones used for vector-stock generation. To evaluate the structural integrity of vector genomes in purified AdVP preparations, compare the observed in-gel versus the expected *in silico* RFLA patterns using, as a marker, an appropriate DNA molecular weight ladder. Concordant in-gel and in silico RFLA patterns indicate that AdVP vector genomes did not undergo major structural rearrangements during rescue and propagation in helper-transduced packaging cells (Fig. 4).

3.5 Testing AdVP Preparations

Following the further characterization of AdVP preparations (*see* **Note 13**), the testing and application of genome-editing approaches enabled through AdVP delivery can commence. To illustrate AdVP-assisted multiplexing gene editing (Fig. 5), fiber-modified vectors AdVP.SaC9::SpC9.dgR$^{\Delta 51}$F50 and AdVP.Dual.PE$^{\Delta 51}$F50 were assessed for *DMD* reading frame correction in dystrophin-defective

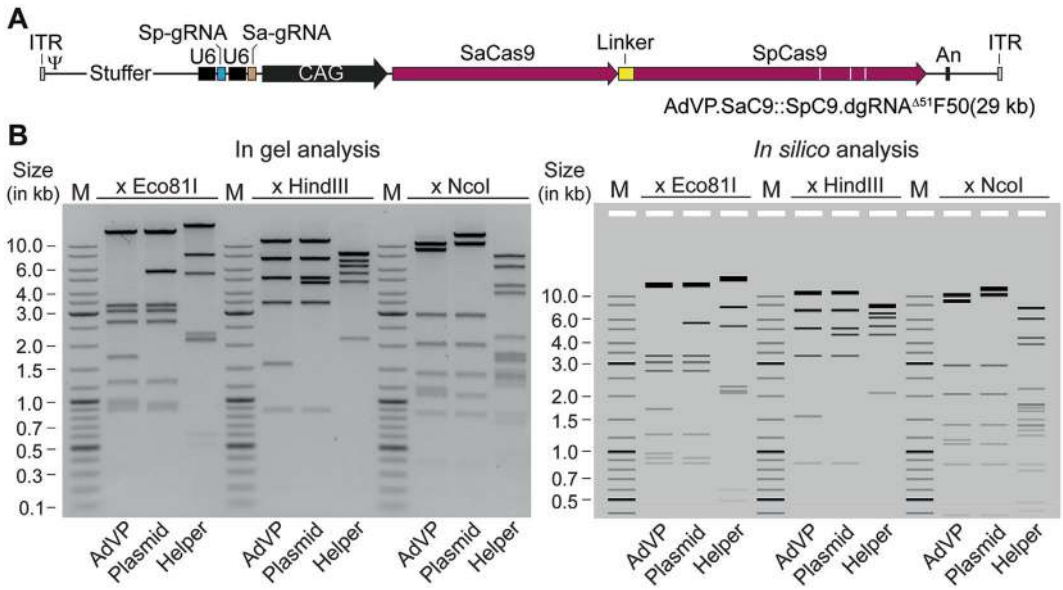


Fig. 4 Structural analysis of AdVP for all-in-one delivery of forced CRISPR-Cas9 heterodimers. (**A**) AdVP genomic structure. AdVP.SaC9::SpC9.dgR$^{\Delta 51}$F50 encodes a fusion between orthogonal *S. aureus* Cas9 and *S. pyogenes* Cas9 nucleases (SaC9::SpC9). The forced SaC9::SpC9 heterodimer and cognate dual gRNA (i.e., Sa-gRNA and Sp-gRNA) synthesis is controlled by the hybrid CAG and human U6 promoters, respectively. ITR and Ψ, adenoviral inverted terminal repeats and packaging signal, respectively. An, polyadenylation signal. (**B**) Evaluation of AdVP genomic integrity. Restriction fragment length analysis (RFLA) of AdVP.SaC9::SpC9.dgR$^{\Delta 51}$F50 vector DNA isolated from purified vector particles using the indicated enzymes. Plasmid clones containing AdVP and helper genomes, treated with the same restriction enzymes, served as molecular weight references, together with the GeneRuler DNA Ladder Mix (M). In-gel and *in silico* RFLA analyses are presented

human muscle cells by targeted excision of the splice acceptor of exon 51 or of the whole exon 51 sequence, respectively (Figs. 5 and 6). Both DNA editing approaches result in *DMD* exon 51 skipping amenable to the restoration of the dystrophin-encoding reading frame of *circa* 13%–14% of DMD patient genotypes. This subgroup represents the largest single patient population that can, in principle, be treated with exon-skipping therapies based on DNA or RNA targeting.

4 Notes

1. As guidance for vector DNA transfections in 293Cre4 cells, seed 1.6×10^6 cells in 2 mL per well of a six-well plate. In parallel, as a contingency, seed also cells at ±1.3-fold densities relative to this value to maximize the chances of obtaining evenly distributed monolayers at the proper confluency of 70%–80%. As guidance for vector propagation in 293Cre4

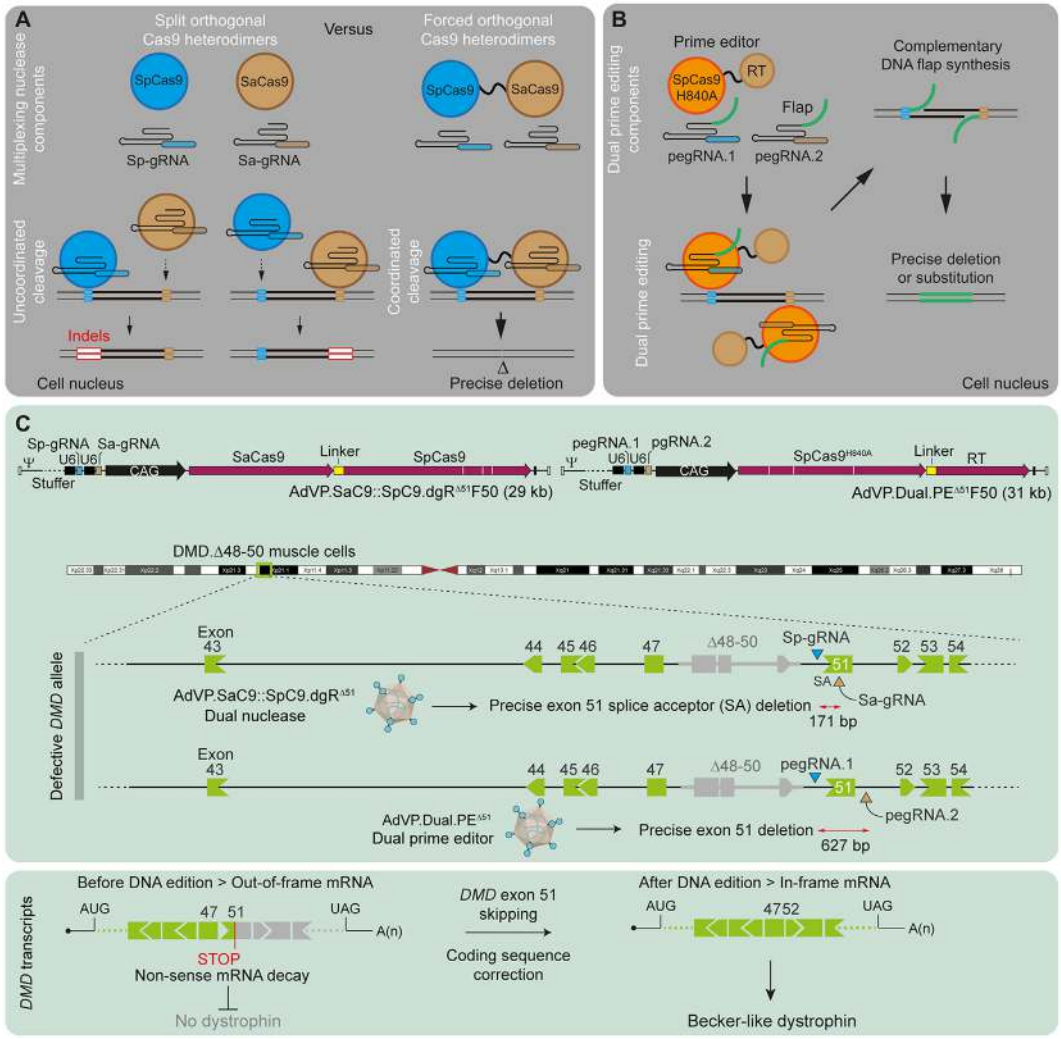


Fig. 5 Advanced gene editing strategies enabled through AdVP delivery. (**A**) Targeted DNA deletions using split versus forced CRISPR-Cas9 heterodimers. CRISPR complexes formed by the forced SaC9::SpC9 heterodimer coupled to its cognate gRNAs favor, upon coordinated DNA cleavage at bipartite target sequences, precise genomic deletions over imprecise end-joining-derived small insertions and deletions (indels). (**B**) Targeted DNA deletions or substitutions using dual prime editing. CRISPR complexes consisting of a prime editor protein and a pegRNA pair generate offset-positioned complementary DNA flaps that, upon hybridization, yield precise pegRNA-programmed genomic substitutions or deletions without concomitant buildup of bystander indels. (**C**) Schematics of *DMD* reading frame repair strategies. The fiber 50-modified AdVPs encoding forced CRISPR-Cas9 heterodimer and dual prime-editing complexes AdVP.SaC9::SpC9.dgR$^{\Delta 51}$F50 and AdVP.Dual.PE$^{\Delta 51}$F50, respectively, are designed for *DMD* reading frame repair through targeted DNA deletions. The synthesis of the heterologous proteins and RNA transcripts is driven by the hybrid CAG and human U6 promoters, respectively. AdVP.SaC9::SpC9.dgR$^{\Delta 51}$F50 transduction leads to NHEJ-mediated exon 51 splice acceptor (SA) removal, whilst AdVP.Dual.PE$^{\Delta 51}$F50 transduction results in dual prime editing-mediated whole exon 51 excision. Both AdVP-assisted approaches yield in-frame *DMD* transcripts coding for a partially functional Becker-like dystrophin in muscle cells containing *DMD* alleles with specific intragenic deletions (e.g., Δ48–50). Both DNA editing maneuvers result in *DMD* exon 51 skipping, amenable to circa 13%–14% of DMD patient genotypes

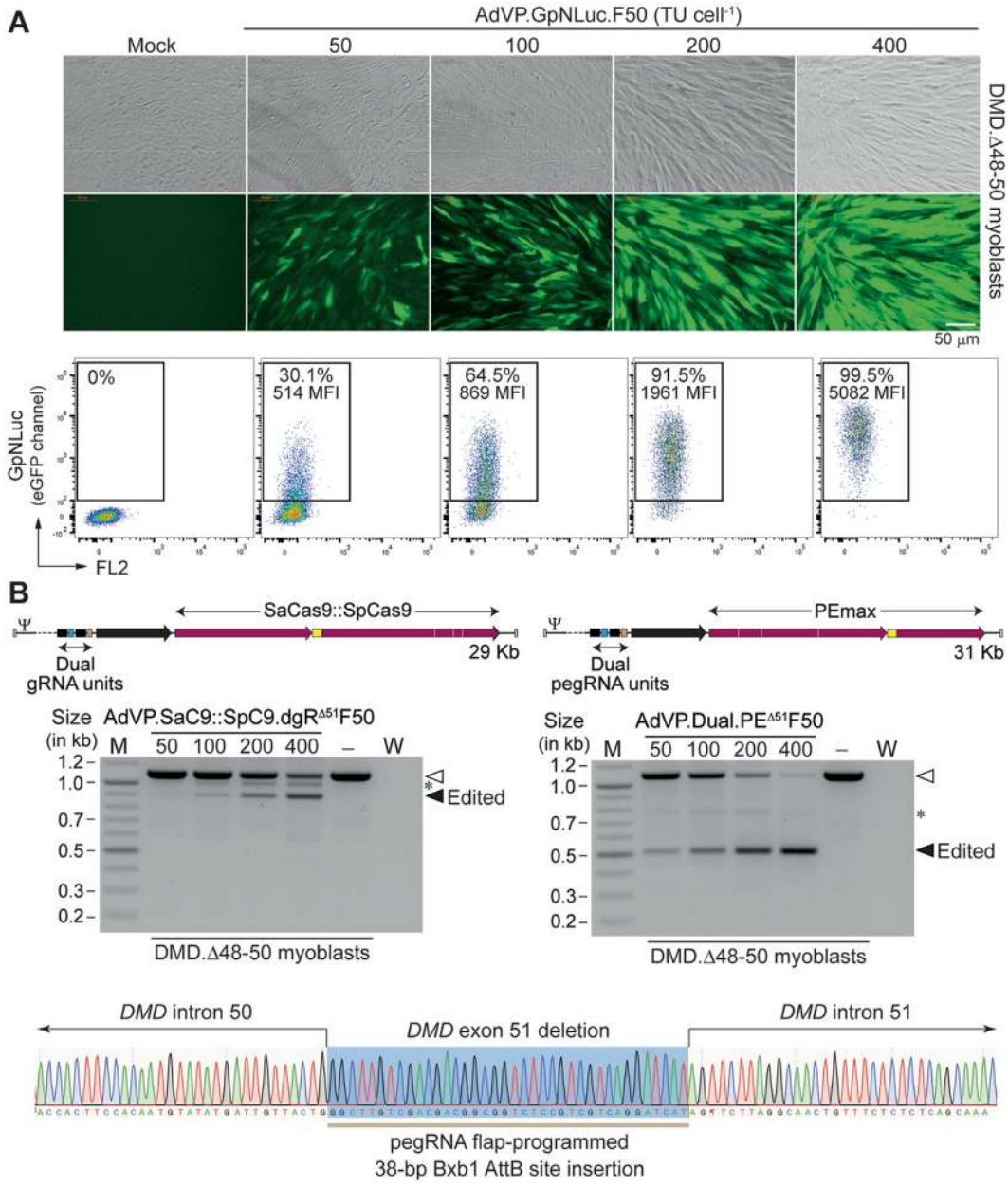


Fig. 6 Testing advanced gene editing strategies enabled through AdVP delivery. (**A**) Transduction of dystrophin-defective muscle cells with tropism-modified AdVPs. Human myoblasts with an intragenic *DMD* deletion spanning exons 48 through 50 (DMD.Δ48–50) were exposed overnight to AdVP.GpNLuc.F50. The vector AdVP.GpNLuc.F50 encodes a fusion product between the eGFP and NanoLuc reporters (GpNLuc) [70], and displays fiber motifs from adenovirus type-50 that bind CD46, a cell receptor abundantly present on the surface of human muscle cells. Mock- and AdVP-transduced muscle cells were analyzed through light microscopy and flow cytometry at 3 days post-transduction (top and bottom panels, respectively). Bright and direct fluorescence microscopy fields are shown. TU, transducing units as determined by qPCR analysis of vector DNA isolated from HeLa cells subjected to AdVP end-point titrations; MFI, mean fluorescence intensity. (**B**) Evaluation of AdVP delivery of multiplexing prime editor and nuclease complexes. Human DMD.Δ48–50 myoblasts were transduced overnight with the fiber 50-modified vectors AdVP.SaC9::SpC9.dgR$^{\Delta 51}$F50 and AdVP.

cells, seed 10–12 × 10^6 cells in 10 mL per T75-cm^2 flask, and 23–27 × 10^6 cells in 20 mL per T175-cm^2 flask.

2. To serve as efficient substrates for the initiation of adenovirus-dependent DNA replication, the ITR sequences containing the viral origins of replication need to be freed from covalently attached DNA, hence the need for this vector DNA linearization step. Indeed, in the context of circular supercoiled plasmid DNA, AdVP genomes yield minimal vector particles during the initial rescue step.
3. If the AdVP packaging cells are regularly subcultured in the presence of a marker-gene selection drug (e.g., puromycin or hygromycin), seed the cells in drug-free medium or exchange drug-containing medium for drug-free medium prior to the DNA transfection or the AdVP vector propagation.
4. Full CPE is identified when roughly 90% of the packaging producer cells have rounded up and detached from the culture vessel surface. The cells remaining attached can be mobilized by gentle pipetting, shaking, or tapping the cell culture vessel(s). To ensure synchronous CPE across wells or flasks during each propagation round, a master mix of clarified cell lysate and medium should be prepared prior to transduction. The total volume should slightly exceed the required amount to account for losses during aliquoting and pipetting. The timing of CPE development per helper vector MOI is, in part, dependent on the characteristics of the packaging cell line and helper vector used. Hence, the helper MOI leading to full CPE within 2 to 4 days post-transduction needs to be identified empirically *a priori* via helper dose-response transduction experiments in the selected AdVP packaging cells. Examples of Cre recombinase-susceptible helpers are: H10 [52], H14 [52], Av1nBgflx [53], AdNG163R-2 [47], AdV.SRa.lacZ.1.5 [54], and AdV.SRa.lacZ.1.50 [54]. The MOI dosage units can be expressed in infectious units (IU) or vector particles (VP) per cell. Helper IUs can be determined through, for instance, tissue culture infectious dose 50% ($TCID_{50}$) or plaque-forming units (PFU) titration assays in *E1*-complementing cells; helper VPs can instead

Dual.PE$^{\Delta 51}$F50, encoding forced CRISPR-Cas9 heterodimer and dual prime-editing complexes, respectively. Both vectors are designed to repair *DMD* reading-frame mutations through targeted DNA deletions (Fig. 5).
Fig. 6 (continued): Mock- and AdVP-transduced cells were analyzed at 4 days post-transduction by PCR and agarose gel electrophoresis (top panel). Asterisks mark the positions of heteroduplex species formed during PCR by the hybridization of upper and lower DNA chains. Sanger sequencing confirmed the accurate substitution of the target DNA encompassing *DMD* exon 51 with the serine recombinase Bxb1 recognition site upon dual-prime editing (bottom panel). The indicated vector dosages correspond to TU per cell. TU determined by qPCR analysis of vector DNA isolated from HeLa cells subjected to AdVP end-point titrations. M, GeneRuler DNA Ladder Mix

be established via, for instance, optical absorbance of vector components at OD_{260} [55], qPCR of vector DNA isolated from purified particles using vector DNA calibration curves [56,57]; or fluorometric assays based on double-stranded DNA dyes [54,58]. With the exception of $TCID_{50}$ and PFU assays, all the above-indicated titration methods can also be used to titrate AdVP preparations. Finally, for AdVPs harboring a reporter unit, end-point titrations based on applying limiting dilutions of AdVP stocks on indicator cells followed by reporter-directed flow cytometry can be used to determine AdVP titers in terms of transducing units per mL.

5. In between each cycle, vortex the cell suspension vigorously for 5 s to aid cell disruption and vector release. After the final thawing step, dry the tubes with a tissue and clean them with 70% ethanol.
6. At the last propagation round, it is important to avoid harvesting the producer cells too long after the emergence of full CPE to mitigate vector particle loss into the medium due to prolonged helper-induced cell lysis.
7. Dispensing only 5 of 7 mL of CsCl ($\rho = 1.4$ g/mL) leaves inside the pipette 2 mL. This procedure minimizes the generation of air bubbles that would otherwise disturb the formation of a sharp CsCl block gradient.
8. In the loaded rotor, holder 1 will be paired opposite holder 4, 2 opposite 5, and 3 opposite 6. For the balancing of the holder pairs, use a pipetboy connected to a 1-mL disposable pipette for adding in a dropwise fashion, weight-equilibrating PBS pH 7.4 solution. Importantly, the weight difference between loaded holder pair members should not exceed ± 0.02 g. Place the properly balanced tube-holders capped with their lids in the rotor. Place all six tube holders in the rotor, even if some holders remain empty.
9. The density (mass/volume) of a recombinant adenovirus vector (third-generation or otherwise) is directly proportional to the ratio of its DNA content to its protein capsid volume. Since the protein capsid has a fixed volume size, a vector carrying a smaller genome (e.g., 28 kb) is less dense than a wild-type virion or a helper containing 36-kb of packaged double-stranded DNA whose buoyant density is ~1.34 g/mL. Specifically, an AdVP carrying a 28-kb genome has an estimated buoyant density of 1.31 to 1.32 g/mL in a CsCl continuous gradient. Hence, for maximizing the separation between the AdVP vector and helper remnants resulting from Cre/LoxP recombination escape, it is advisable to use AdVP and helper vectors with substantially distinct DNA contents. For instance, AdVP and helper vectors with, respectively, 28–31 kb and 36–37.5 kb genomes, or vice versa. These

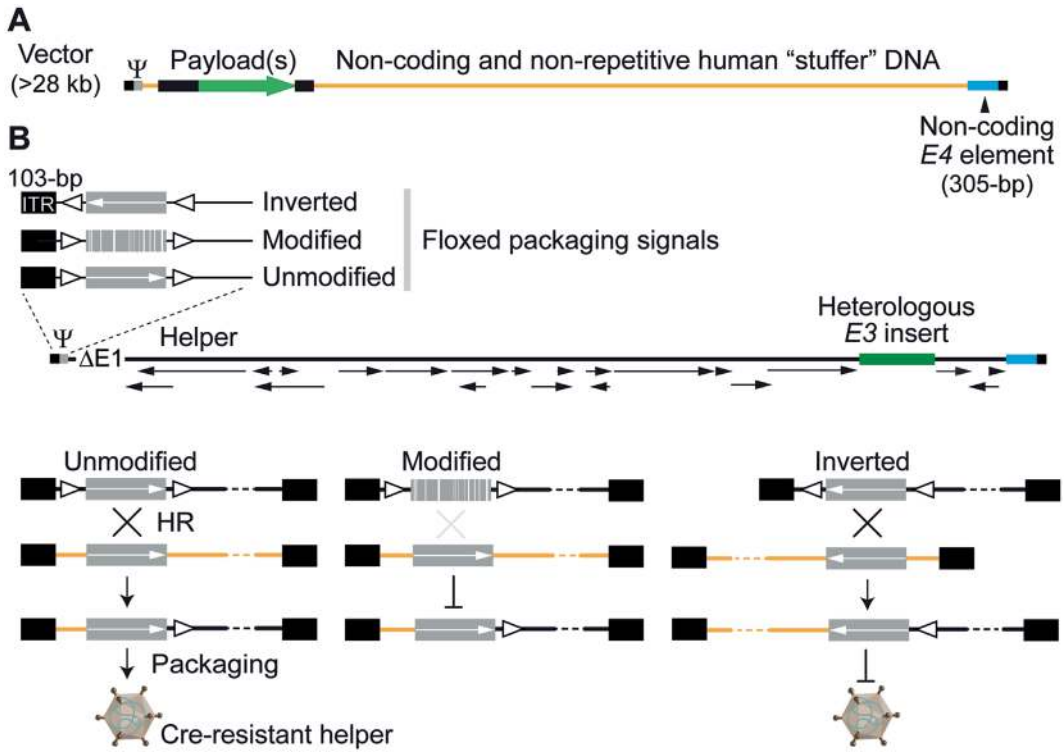


Fig. 7 Considerations on the design of AdVP production components. (**A**) Composition of AdVP DNA. To maximize genetic stability during AdVP production, vector genomes should be larger than 28 kb from the "left" to the "right" ITR and contain sequences that are neither extensively repetitive nor homologous to the helper DNA. Retaining the noncoding *cis*-acting *E4* sequence linked to the "right" ITR (cyan region) is advantageous to enhance selective AdVP DNA packaging. (**B**) Composition of helper DNA. Helpers with modified and inverted packaging signals dampen the risk for the emergence of Cre-resistance byproducts by, respectively, mitigating vector-helper homologous recombination and assembling byproducts too large for packaging. Incorporation of "stuffer" DNA in the *E3* region mitigates the amplification of replication-competent adenovirus (RCA) byproducts created through homologous recombination events involving *E1* sequences located in helper and HEK293-derived cell line DNA. See text for details

DNA lengths are guided by earlier studies defining that adenoviral vectors remain genetically stable upon propagation (i.e., without DNA rearrangements) when vector genomes range from ~75%–80% (27–29 kb) to ~105% (37.7–38 kb) of the wild-type size [59–61] (Fig. 7). To meet these size requirements, "stuffer" DNA sequences are frequently incorporated. These nonfunctional filler DNA fragments are introduced into the vector genome to achieve an optimal length that supports efficient packaging, genome stability, and vector production, without contributing coding or regulatory functions. Choosing AdVP DNA shorter than helper DNA reduces "stuffer" tract requirements and favors vector over helper genome replication buildup. On the other hand, selecting AdVP DNA longer than helper DNA improves the

thermostability of AdVP vectors [61,62]. Regardless, it is worth noting that the "stuffer" DNA is not necessarily an inert component, as it can impact AdVP production and/or performance. In this regard, noncoding "stuffers" of human origin are preferable, as earlier research has demonstrated that bacteriophage λ sequences, for example, can trigger immune responses and transgene silencing, in contrast to human DNA [63,64]. Moreover, although adenoviral vectors have a substantially higher genetic stability than lentiviral vectors [65], "stuffers" with extensive repetitive tracts and recombinogenic vector-helper homologous sequences should be reduced or avoided to maximize vector DNA stability during propagation in producer cells (Fig. 7). Indeed, homologous recombination between DNA shared by AdVP and helper can yield Cre-resistant helper species leading to high levels of helper contamination [52]. For this reason, helpers with packaging signals modified by site-directed mutagenesis or inverted have also been developed (Fig. 7). The former strategy reduces the likelihood of homologous recombination via limiting contiguous packaging signal homologies [52]; the latter creates helper species too large for packaging following homologous recombination [47,66]. To further improve selective AdVP DNA packaging, a *cis*-acting *E4* sequence located next to the "right" ITR is, ideally, kept in AdVP genomes (Fig. 7) [52]. Finally, the AdVP producer cell line can also affect the likelihood with which untoward byproducts emerge. Specifically, replication-competent adenovirus (RCA) byproducts can arise through homologous recombination if *E1*-deleted helper and adenoviral sequences in *E1*-complementing packaging cells overlap [67]. In HEK293 cells [68], and their recombinase-expressing derivatives (Table 1), genomic adenoviral sequences extend beyond the minimal *E1* region, creating overlapping homology for RCA generation. Importantly, to curtail RCA emergence in HEK293-derived AdVP producer cells, heterologous "stuffer" DNA should be added to the dispensable *E3* region so that acquisition of *E1* sequences by helper genomes renders them too large for packaging [12,44–47,52]. In PER.C6 cells [69], and their recombinase-expressing derivatives (Table 1), trimmed *E1* sequences lack homology with helper DNA, which impedes RCA generation.

10. This two-tier centrifugation speed scheme within a single run involves the generation of a continuous CsCl density gradient at the highest speed, followed by a "relaxation" equilibrium step at the lower speed. This procedure allows vectors with differently sized genomes to move further away from each other, enhancing, as a result, separation resolution and, ultimately, AdVP purification levels (Fig. 8).

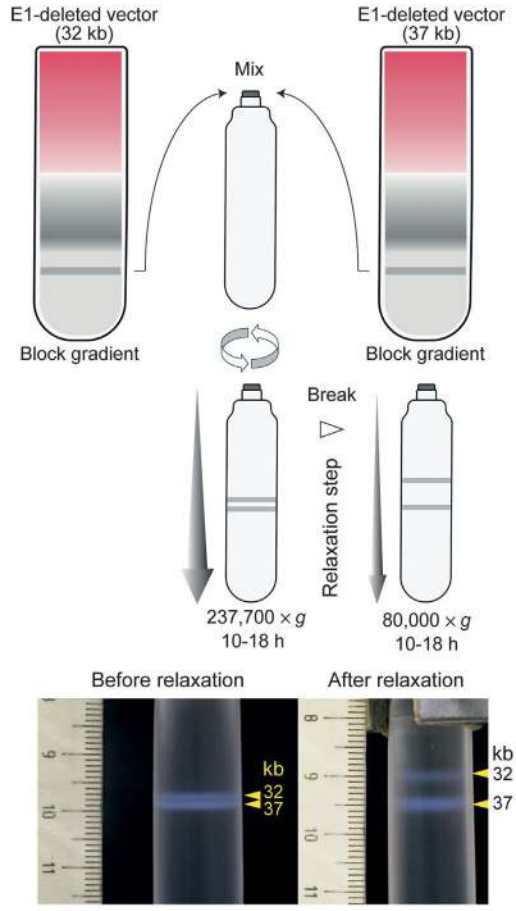


Fig. 8 Illustration of the relaxation step based on a two-speed ultracentrifugation regimen. After CsCl block gradient ultracentrifugation, two *E1*-deleted adenoviral vectors differing in their DNA content by 5 kb were subjected to CsCl buoyant density ultracentrifugation. Pictures of banded vector particles taken before and after the relaxation step midway through the CsCl continuous gradient ultracentrifugation are depicted. See text for details

11. The A195 solution was developed as a formulation that stabilizes long-term storage of *E1*-deleted viral vector vaccines based on the adenovirus type-5 [51]. This formulation contains a nonionic surfactant, a cryoprotectant, and excipients that inhibit free-radical oxidation. The surfactant prevents capsid adsorption to storage vessel surfaces, whilst the cryoprotectant mitigates vector inactivation caused by temperature changes. Adenoviral vectors with genomes over ~33.3 kb are as stable as the 36-kb parental adenovirus type-5 virion [61]. Yet, AdVPs often contain genomes smaller than 33.3 kb with decreasing DNA content directly correlating with lower vector particle thermostabilities [61,62]. Importantly, keeping

regular and tropism-modified AdVPs containing a 29.6-kb genome in the A195 buffer formulation resulted in the maintenance of functional vector particle titers upon multiple cycles of freezing and thawing (Fig. 9). In contrast, storing the same AdVPs in a conventional storage buffer formulation (20 mM pH 8.0 Tris-Cl, 25 mM NaCl, 0.25% glycerol in Milli-Q water), led to a clear decrease in functional vector particle titers as a function of freeze-thaw cycle number (Fig. 9).

12. The centrifugation time required for leaving *circa* 500 µL of retentate in the filter units depends on the AdVP vector concentration. Hence, start by spinning for 7 min, check the volume of retentate left and estimate the additional centrifugation time needed to reach *circa* 500 µL of retentate. Repeat if needed, while taking care that this additional spinning cycle does not lead to the drying of the filter membranes.

13. Further characterization of AdVP preparations includes determining their functional and physical vector particle titers by using established methods [e.g., *see* 54–58]. The residual *E1*-deleted helper levels present in each AdVP preparation can be equally determined by using established procedures, e.g., helper DNA-specific quantitative PCR assays.

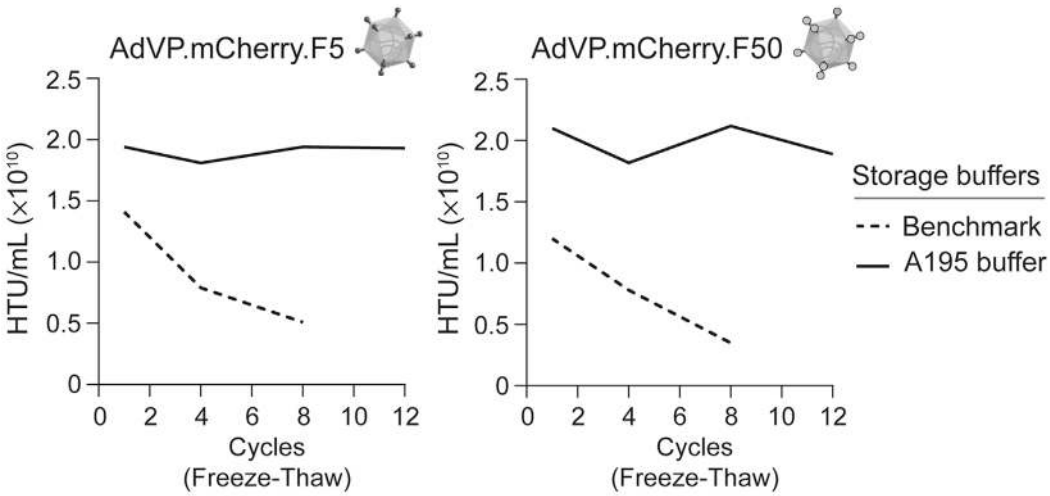


Fig. 9 Evaluation of AdVP stability in storage buffer A195. Conventional vector AdVP.mCherry.F5 with type-5 fibers and tropism-modified AdVP.mCherry.F50 vector with type-50 fibers binding to the cell surface receptors CAR and CD46, respectively, were subjected to the indicated numbers of freeze-thaw cycles. After each cycle, functional vector particles were quantified by end-point titrations on permissive HeLa cells followed by mCherry-directed flow cytometry at 3 days post-transduction. Prior to the freeze-thaw treatments, aliquots of each primary AdVP stock were diluted 50-fold in benchmark and test A195 storage buffers

Acknowledgments

This publication is based upon work by COST Action CA21113: Genome Editing for the Treatment of Human Diseases (https://www.genehumdi.eu), supported by European Cooperation in Science and Technology (COST). The authors thank Vincent Mouly (Sorbonne University, Paris, France) for providing the DMD.Δ 48–50 myoblasts (AB1098) used in this chapter, and Antoine A. F. de Vries (Department of Cardiology, Leiden University Medical Center, the Netherlands) for the source construct encoding the GpNLuc reporter. This work was supported by the Prinses Beatrix Spierfonds, the Dutch Neuromuscular Foundation (grant W.OR21-01). Xiaoling Wang is the recipient of a PhD fellowship from the China Scholarship Council–Leiden University Joint Scholarship Program. Research in the authors' laboratory is further supported by the Dutch Duchenne Parent Project, the Horizon Europe Program, and the Dutch Research Council (NWO). Authors in this study are members of the European Reference Network for Neuromuscular Diseases (ERN EURO-NMD).

Conflict of Interest The authors have no conflicts of interest to declare that are relevant to the content of this chapter.

References

1. Curiel DT, Parker AL (eds) (2025) Adenoviral vectors for gene therapy. Academic Press, London
2. Russell WC (2009) Adenoviruses update on structure and function. J Gen Virol 90:1–20
3. de Pablo PJ, San Martín C (2022) Seeing and touching adenovirus: complementary approaches for understanding assembly and disassembly of a complex virion. Curr Opin Virol 52:112–122
4. Greber UF, Suomalainen M (2022) Adenovirus entry: stability, uncoating, and nuclear import. Mol Microbiol 118:309–320
5. Greber UF, Gomez-Gonzalez A (2021) Adenovirus—a blueprint for gene delivery. Curr Opin Virol 48:49–56
6. Tasca F, Wang Q, Gonçalves MAFV (2020) Adenoviral vectors meet gene editing: a rising partnership for the genomic engineering of human stem cells and their progeny. Cells 9:953
7. Chen X, Gonçalves MAFV (2016) Engineered viruses as genome editing devices. Mol Ther 24:447–457
8. Gao J, Mese K, Bunz O, Ehrhardt A (2019) State-of-the-art human adenovirus vectorology for therapeutic approaches. FEBS Lett 593:3609–3622
9. Kovesdi I, Hedley SJ (2010) Adenoviral producer cells. Viruses 2:1681–1703
10. Havenga MJ, Holterman L, Melis I et al. (2008) Serum-free transient protein production system based on adenoviral vector and PER C6 technology high yield and preserved bioactivity. Biotechnol Bioeng 100:273–283
11. Ricobaraza A, Gonzalez-Aparicio M, Mora-Jimenez et al. (2020) High-capacity adenoviral vectors expanding the scope of gene therapy. Int J Mol Sci 21:3643
12. Parks RJ, Chen L, Anton M et al. (1996) A helper-dependent adenovirus vector system removal of helper virus by Cre mediated excision of the viral packaging signal. Proc Natl Acad Sci 93:13565–13570
13. Schiedner G, Morral N, Parks RJ et al. (1998) Genomic DNA transfer with a high-capacity adenovirus vector results in improved in vivo gene expression and decreased toxicity. Nat Genet 18:180–183
14. Doudna JA, Charpentier E (2014) Genome editing the new frontier of genome engineering with CRISPR-Cas9. Science 346:1258096

15. Xue C, Greene EC (2021) DNA repair pathway choices in CRISPR-Cas9-mediated genome editing. Trends Genet 37:639–656
16. Chen X, Tasca F, Wang Q et al. (2020) Expanding the editable genome and CRISPR-Cas9 versatility using DNA cutting-free gene targeting based on in trans paired nicking. Nucleic Acids Res 48:974–995
17. Kosicki M, Tomberg K, Bradley A (2018) Repair of double-strand breaks induced by CRISPR-Cas9 leads to large deletions and complex rearrangements. Nat Biotechnol 36:765–771
18. Haapaniemi E, Botla S, Persson J et al. (2018) CRISPR-Cas9 genome editing induces a p53 mediated DNA damage response. Nat Med 24:927–930
19. Ihry RJ, Worringer KA, Salick MR et al. (2018) p53 inhibits CRISPR-Cas9 engineering in human pluripotent stem cells. Nat Med 24:939–946
20. Chen X, Janssen JM, Liu J et al. (2017) In trans paired nicking triggers seamless genome editing without double-stranded DNA cutting. Nat Commun 8: 657
21. Nakajima K, Zhou Y, Tomita A et al. (2018) Precise and efficient nucleotide substitution near genomic nick via noncanonical homology-directed repair. Genome Res 28:223–230
22. Komor AC, Kim YB, Packer MS et al. (2016) Programmable editing of a target base in genomic DNA without double-stranded DNA cleavage. Nature 533:420–424
23. Nishida K, Arazoe T, Yachie N et al. (2016) Targeted nucleotide editing using hybrid prokaryotic and vertebrate adaptive immune systems. Science 353:aaf8729
24. Gaudelli NM, Komor AC, Rees HA et al. (2017) Programmable base editing of AT to GC in genomic DNA without DNA cleavage. Nature 551:464–471
25. Kurt IC, Zhou R, Iyer S et al. (2021) CRISPR C-to-G base editors for inducing targeted DNA transversions in human cells. Nat Biotechnol 39:41–46
26. Chen L, Park JE, Paa P et al. (2021) Programmable C:G to G:C genome editing with CRISPR-Cas9 directed base excision repair proteins. Nat Commun 12: 1384
27. Chen L, Hong M, Luan C et al. (2024) Adenine transversion editors enable precise efficient A•T-to-C•G base editing in mammalian cells and embryos. Nat Biotechnol 42:638–650
28. Anzalone AV, Randolph PB, Davis JR et al. (2019) Search-and-replace genome editing without double-strand breaks or donor DNA. Nature 576:149–157
29. Chen PJ, Liu DR (2023) Prime editing for precise and highly versatile genome manipulation. Nat Rev Genet 24:161–177
30. Tao R, Wang Y, Jiao Y et al. (2022) Bi-PE bi-directional priming improves CRISPR/Cas9 prime editing in mammalian cells. Nucleic Acids Res 50:6423–6434
31. Yarnall MTN, Ioannidi EI, Schmitt-Ulms C et al. (2023) Drag-and-drop genome insertion of large sequences without double-strand DNA cleavage using CRISPR-directed integrases. Nat Biotechnol 41:500–512
32. Pandey S, Gao XD, Krasnow NA et al. (2025) Efficient site-specific integration of large genes in mammalian cells via continuously evolved recombinases and prime editing. Nat Biomed Eng 9:22–39
33. Lampe GD, King RT, Halpin-Healy TS et al. (2024) Targeted DNA integration in human cells without double-strand breaks using CRISPR-associated transposases. Nat Biotechnol 42:87–98
34. Witte IP, Lampe GD, Eitzinger S et al. (2025) Programmable gene insertion in human cells with a laboratory-evolved CRISPR-associated transposase. Science 388:eadt5199
35. Wang Q, Capelletti S, Liu J et al. (2024) Selection-free precise gene repair using high-capacity adenovector delivery of advanced prime editing systems rescues dystrophin synthesis in DMD muscle cells. Nucleic Acids Res 52:2740–2757
36. Li C, Georgakopoulou A, Mishra A et al. (2021) In vivo HSPC gene therapy with base editors allows for efficient reactivation of fetal γ-globin in β-YAC mice. Blood Adv 5:1122–1135
37. Li C, Georgakopoulou A, Newby GA et al. (2022) In vivo base editing by a single i.v. vector injection for treatment of hemoglobinopathies. JCI Insight 7:e162939
38. Li C, Georgakopoulou A, Newby GA et al. (2023) In vivo HSC prime editing rescues sickle cell disease in a mouse model. Blood 141:2085–2099
39. Wang Y, Shao W (2023) Innate immune response to viral vectors in gene therapy. Viruses 15:1801
40. Barry MA, Rubin JD, Lu SC (2020) Retargeting adenoviruses for therapeutic applications and vaccines. FEBS Lett 594:1918–1946
41. Tasca F, Brescia M, Liu J et al. (2023) High-capacity adenovector delivery of forced CRISPR-Cas9 heterodimers fosters precise chromosomal deletions in human cells. Mol Ther Nucleic Acids 31:746–762
42. Chen L, Anton M, Graham FL (1996) Production and characterization of human 293 cell lines expressing the site-specific recombinase Cre. Somat Cell Mol Genet 22:477–488
43. Zhou H, Zhao T, Pastore L et al. (2001) A Cre-expressing cell line and an E1/E2a

double-deleted virus for preparation of helper-dependent adenovirus vector. Mol Ther 3:613–622
44. Ng P, Beauchamp C, Evelegh C et al. (2001) Development of a FLP/frt system for generating helper-dependent adenoviral vectors. Mol Ther 3:809–815
45. Umaña P, Gerdes CA, Stone D et al. (2001) Efficient FLPe recombinase enables scalable production of helper-dependent adenoviral vectors with negligible helper-virus contamination. Nat Biotechnol 19:582–585
46. Barjot C, Hartigan-O'Connor D, Salvatori G et al. (2002) Gutted adenoviral vector growth using E1/E2b/E3-deleted helper viruses. J Gene Med 4:480–489
47. Palmer D, Ng P (2003) Improved system for helper-dependent adenoviral vector production. Mol Ther 8:846–852
48. Sakhuja K, Reddy PS, Ganesh S et al. (2003) Optimization of the generation and propagation of gutless adenoviral vectors. Hum Gene Ther 14:243–254
49. Gonçalves MAFV, Van der Velde I, Janssen JM et al. (2002) Efficient generation and amplification of high-capacity adeno-associated virus/adenovirus hybrid vectors. J Virol 76:10734–10744
50. Brescia M, Janssen JM, Liu J et al. (2020) High-capacity adenoviral vectors permit robust and versatile testing of DMD gene repair tools and strategies in human cells. Cells 9:869
51. Evans RK, Nawrocki DK, Isopi LA et al. (2004) Development of stable liquid formulations for adenovirus-based vaccines. J Pharm Sci 93:2458–2475
52. Sandig V, Youil R, Bett AJ et al. (2000) Optimization of the helper-dependent adenovirus system for production and potency in vivo. Proc Natl Acad Sci USA 97:1002–1007
53. Reddy PS, Sakhuja K, Ganesh S et al. (2002) Sustained human factor VIII expression in hemophilia A mice following systemic delivery of a gutless adenoviral vector. Mol Ther 5:63–73
54. Janssen JM, Liu J, Skokan J et al. (2013) Development of an AdEasy-based system to produce first- and second-generation adenoviral vectors with tropism for CAR- or CD46-positive cells. J Gene Med 15:1–11
55. Mittereder N, March KL, Trapnell BC (1996) Evaluation of the concentration and bioactivity of adenovirus vectors for gene therapy. J Virol 70:7498–7509
56. Gallaher SD, Berk AJ (2013) A rapid Q-PCR titration protocol for adenovirus and helper-dependent adenovirus vectors that produces biologically relevant results. J Virol Methods 192:28–38
57. Tasca F, Brescia M, Wang Q et al. (2022) Large-scale genome editing based on high-capacity adenovectors and CRISPR-Cas9 nucleases rescues full-length dystrophin synthesis in DMD muscle cells. Nucleic Acids Res 50:7761–7782
58. Holkers M, Cathomen T, Gonçalves MAFV (2014) Construction and characterization of adenoviral vectors for the delivery of TALENs into human cells. Methods 69:179–187
59. Bett AJ, Prevec L, Graham FL (1993) Packaging capacity and stability of human adenovirus type 5 vectors. J Virol 67:5911–5921
60. Parks RJ, Graham FL (1997) A helper-dependent system for adenovirus vector production helps define a lower limit for efficient DNA packaging. J Virol 71:3293–3298
61. Saha B, Wong CM, Parks RJ (2014) The adenovirus genome contributes to the structural stability of the virion. Viruses 6:3563–3583
62. Smith AC, Poulin KL, Parks RJ (2009) DNA genome size affects the stability of the adenovirus virion. J Virol 83:2025–2028
63. Parks RJ, Bramson JL, Wan Y et al. (1999) Effects of stuffer DNA on transgene expression from helper-dependent adenovirus vectors. J Virol 73:8027–8034
64. Ross PJ, Kennedy MA, Parks RJ (2009) Host cell detection of noncoding stuffer DNA contained in helper-dependent adenovirus vectors leads to epigenetic repression of transgene expression. J Virol 83:8409–8417
65. Holkers M, Maggio I, Liu J et al. (2013) Differential integrity of TALE nuclease genes following adenoviral and lentiviral vector gene transfer into human cells. Nucleic Acids Res 41:e63
66. Ng P, Evelegh C, Cummings D et al. (2002) Cre levels limit packaging signal excision efficiency in the Cre/loxP helper-dependent adenoviral vector system. J Virol 76:4181–4189
67. Hehir KM, Armentano D, Cardoza LM et al. (1996) Molecular characterization of replication-competent variants of adenovirus vectors and genome modifications to prevent their occurrence. J Virol 70:8459–8467
68. Graham FL, Smiley J, Russell WC et al. (1977) Characteristics of a human cell line transformed by DNA from human adenovirus type 5. J Gen Virol 36:59–74
69. Fallaux FJ, Bout A, van der Velde I et al. (1998) New helper cells and matched early region 1-deleted adenovirus vectors prevent generation of replication-competent adenoviruses. Hum Gene Ther 9:1909–1917
70. Schaub FX, Reza MS, Flaveny CA et al. (2015) Fluorophore-NanoLuc BRET reporters enable sensitive in vivo optical imaging and flow cytometry for monitoring tumorigenesis. Cancer Res 75:5023–5033

Open Access This chapter is licensed under the terms of the Creative Commons Attribution-NonCommercial-NoDerivatives 4.0 International License (http://creativecommons.org/licenses/by-nc-nd/4.0/), which permits any noncommercial use, sharing, distribution and reproduction in any medium or format, as long as you give appropriate credit to the original author(s) and the source, provide a link to the Creative Commons license and indicate if you modified the licensed material. You do not have permission under this license to share adapted material derived from this chapter or parts of it.

The images or other third party material in this chapter are included in the chapter's Creative Commons license, unless indicated otherwise in a credit line to the material. If material is not included in the chapter's Creative Commons license and your intended use is not permitted by statutory regulation or exceeds the permitted use, you will need to obtain permission directly from the copyright holder.





Chapter 9

Adeno-Associated Viral Vector (AAV)-Mediated In Vivo CRISPR-Cas9 Delivery

Andrea Llanos-Ardaiz, Nerea Zabaleta, Laura Torella and Gloria Gonzalez-Aseguinolaza

Abstract

CRISPR-based gene editing is a growing therapeutic strategy for modifying or silencing disease-causing genes. This chapter focuses on the in vivo delivery of CRISPR systems using recombinant adeno-associated viral (rAAV) vectors. Specifically, we detail a methodology using a rAAV vector carrying *Staphylococcus aureus* Cas9 (SaCas9) to target the murine *Hao1* gene in liver parenchymal cells as a curative treatment for primary hyperoxaluria type 1 (PH1). We provide comprehensive protocols for plasmid design and cloning, rAAV production, animal administration, and evaluation of editing efficacy.

Keywords CRISPR-SaCas9, rAAV, Gene editing, In vivo, Liver, Mouse

1 Introduction

Implementation of in vivo gene editing using the CRISPR-Cas9 system has brought tremendous advances to biomedical research, offering opportunities to knock down detrimental gene expression, correct mutations, or introduce functional versions of a gene into a target. While numerous in vitro studies have established the efficacy of CRISPR systems, translating this machinery into in vivo models requires safe, tissue-specific, and efficient delivery vehicles. Recombinant adeno-associated viral (rAAV) vectors have emerged as a preferred delivery vehicle for gene-editing tools due to their lack of pathogenicity and their ability to transduce both dividing and nondividing cells. However, a major limitation of rAAVs is their restricted packaging capacity [1–3]. To overcome this hurdle, the smaller *Staphylococcus aureus* Cas9 (SaCas9) nuclease is frequently utilized instead of the traditional *Streptococcus pyogenes* Cas9 (SpCas9) [4,5]. Using SaCas9 allows efficient packaging of the nuclease and its required guide RNAs (gRNAs) into a single rAAV vector.

Duško Lainšček et al. (eds.), *CRISPR Delivery*, Methods in Molecular Biology, vol. 3075,
https://doi.org/10.1007/978-1-0716-5547-4_9,
© The Author(s) 2027

Gene editing holds promise for treating monogenic liver diseases, such as primary hyperoxaluria type 1 (PH1). By directing rAAV-delivered SaCas9 specifically to liver parenchymal cells, specific genes can be efficiently targeted for knockdown. For instance, knocking down expression of the murine *Hao1* gene, which encodes the glycolate oxidase (GO) protein, serves as a successful therapeutic strategy for PH1 [6–9].

Here, we describe a comprehensive protocol for the in vivo delivery of CRISPR systems, concretely those carrying SaCas9 nuclease targeting the liver. We outline all critical steps, from the design and cloning of plasmids containing the gRNA, SaCas9, and rAAV ITRs, to the production and purification of rAAV vectors using HEK 293T cells. Furthermore, we detail how these vectors should be administered intravenously to mice and describe the analyses that can be performed to evaluate the efficacy of the designed editing approach, including liver processing and protein knockdown assessment.

2 Materials

2.1 CRISPR-Cas9 and gRNA-Containing Plasmid Cloning

2.1.1 Reagents

1. Bottle Assembly, Polypropylene, 250 mL, 62 × 120 mm.
2. AAV vector plasmid, expressing CRIPSR (e.g., Addgene plasmid # 61593).
3. T4 Polynucleotide Kinase.
4. T4 DNA ligase.
5. T4 DNA ligation Buffer.
6. BsaI-High Fidelity (HF) enzyme.
7. LB broth.
8. LB agar plates.
9. Petri dishes.
10. Ampicillin (or antibiotic of choice).
11. One Shot top10 chemically competent *E. coli* (or similar).
12. SOC medium.
13. NucleoSpin Plasmid Transfection-grade, Mini kit for ultrapure plasmid DNA (or similar).
14. NucleoBond Xtra Maxi plus (or similar).
15. NucleoSpin Gel and PCR Clean-up, Mini kit for gel extraction or PCR clean-up.
16. 15 mL polypropylene conical tubes.

2.1.2 Equipment

1. Eppendorf Thermomixer compact.
2. Vortex.
3. Eppendorf Centrifuge 5804R, or similar.
4. Eppendorf Centrifuge 5810R, or similar.
5. Avanti Centrifuge J-26XP, or similar.
6. J-Lite JLA-16.250 Rotor, or similar.
7. Pipetus.
8. Bunsen burner.
9. 37°C incubator.
10. Shaker incubator.
11. 0.5–10 µL micropipette.
12. 2–20 µL micropipette.
13. 20–200 µL micropipette.
14. 100–1000 µL micropipette.
15. NanoDrop™ 1000 spectrophotometer (Thermo Scientific, #ND-1000).

2.2 rAAV Production, Purification, and Titration

2.2.1 Reagents

1. 50 mL polypropylene conical tubes.
2. 5 mL serological pipette.
3. 10 mL serological pipette
4. 25 mL serological pipette.
5. 18 G × $1^{1/2}$ needle.
6. 19 G × $1^{1/2}$ needle.
7. 21 G × $1^{1/2}$ needle.
8. 1000 µL barrier pipette tip.
9. 200 µL barrier pipette tip.
10. 20 µL barrier pipette tip.
11. 0.1–10 µL barrier pipette tip.
12. Ultraclear centrifuge tubes (25*89 mm).
13. Amicon ultra centrifugal filters-ultracel 100 KDa.
14. 10 mL syringe.
15. 15 mL tubes.
16. Aspiration pipettes.
17. P150 cell culture plates.
18. Screw cap 2 mL micro tube.
19. 1.5 mL micro tube.

20. Spin X-Centrifuge Tube Filter 0.22 μm.
21. HEK293T cells.
22. DMEM, high glucose, pyruvate.
23. Fetal bovine serum (FBS).
24. Dulbecco's phosphate-buffered saline (DPBS).
25. Penicillin/Streptomycin.
26. Polyethyleneimine.
27. Lysis buffer: 50 mM Tris, 150 mM NaCl, 2 mM $MgCl_2$, 0.1% Triton X-100
28. KCl.
29. PEG-8000.
30. DNAse I.
31. RNase A.
32. Pluronic F-68.
33. Sodium chloride solution 0.9%.
34. Phenol red.
35. Iodixanol
36. Sucrose.
37. pDP8.ape plasmid (Plasmid Factory, #PF478).
38. High-purity Viral DNA kit (Roche, #11858874001).
39. IQTM SYBR® Green Supermix.
40. ITR-specific primers.

2.2.2 Equipment

1. Biological Safety cabinet class II.
2. Water bath.
3. 100–1000 μL Micropipettes
4. 20–200 μL Micropipettes.
5. 2–20 μL Micropipettes.
6. 0.5–10 μL Micropipettes.
7. Table centrifuge.
8. Type 70 Ti rotor.
9. Optima L-90 K Ultracentrifuge, or similar.
10. Tube sealer.
11. Seal former.
12. Retort stand with a utility clamp.
13. Cell incubator.
14. Ultra-low temperature freezer.
15. Eppendorf Centrifuge 5804R, or similar.

16. Eppendorf Centrifuge 5810R, or similar.
17. Pipetus.
18. CFX96TM Real-Time System thermocycler.

2.3 rAAV Intravenous Administration into Mice

2.3.1 Reagents

1. Insulin syringes (0.3 mL).
2. Isofluorane.

2.3.2 Equipment

1. Biosafety hood.
2. Inhalation anesthesia system.
3. Scale.

2.4 Liver Extraction and Processing

2.4.1 Reagents

1. DPBS.
2. Dry ice.
3. Wet ice.
4. Maxwell® RSC simplyRNA Tissue Kit (Promega, #AS1340).
5. Maxwell® RSC simplyDNA Tissue Kit (Promega, #AS1610).
6. RIPA buffer.
7. PMSF.
8. Orthovanadate.
9. Protease inhibitor cocktail.

2.4.2 Equipment

1. Surgical scissors.
2. Anatomical surgical forceps.
3. Surgical blades.
4. Petri dishes.
5. 1.5 mL tubes.
6. Promega DNA and RNA Extraction System | Maxwell RSC 48.
7. GloMax® microplate luminometer, or similar.
8. NanoDrop™ 1000 spectrophotometer.
9. Maxwell® RSC 48 Instrument.
10. BCA protein assay kit (ThermoFisher Scientific, #PI23225).

2.5 Analysis of Liver Transduction

2.5.1 Reagents

1. PCR plates.
2. PCR plate seals.

3. 1.5 mL tubes.
4. 0.2 mL tubes.
5. M-MLV reverse transcriptase.
6. DNase.
7. DNase buffer.
8. 5× first-strand buffer.
9. dNTPs.
10. Random primers.
11. RNase OUT.
12. 0.1 M DTT.
13. GOTaq PCR master mix 2×, or similar.
14. SaCas9-specific primers.
15. Housekeeping gene-specific primers.

2.5.2 Equipment

1. Chemical hood.
2. PCR hood.
3. PCR thermal cycler.
4. Real-Time PCR Machine.
5. QuantStudio™ Design and Analysis software.
6. Image Lab Software.

2.6 Editing Efficiency Analysis

2.6.1 Reagents

1. Nitrocellulose membranes.
2. Acrylamide.
3. 10% SDS.
4. TMED.
5. 10% APS.
6. Methanol.
7. 10× Tris/Glycine Buffer for Western Blots and Native Gels.
8. 10× Tris/Glycine/SDS Buffer.
9. Tris-HCl 1.5 M pH 8.8.
10. Tris-HCl 0.5 M pH 6.8.
11. Q5® High-Fidelity 2× Master Mix, or similar.
12. Kapa HiFi HotStart ReadyMix PCR Kit (Roche, #KK2601)
13. Nonfat Dry Milk.
14. TBS (20 mM Tris base 150 mM NaCl)-Tween20 0.05%.
15. Ponceau red.
16. α-GAPDH, mouse monoclonal antibody.
17. α-target protein antibody.

18. α-rabbit IgG.
19. α-mouse IgG.
20. SuperSignal West Femto Maximum Sensitivity Substrate.
21. Agencourt AMPure XP system (Beckman Coulter, #A63881).
22. Qubit quantitation (Invitrogen™ Qubit™ dsDNA HS and BR Assays).
23. TapeStation assay (Agilent Technology D1000 ScreenTape Assay for TapeStation Systems).

2.6.2 Equipment

1. Sequencer (for Sanger sequencing).
2. Electrophoresis Cell.
3. Transference Cell.
4. High-current power supply.
5. Chemidoc MP, or similar.
6. ImageLab software, or similar.

3 Methods

3.1 Synthesis of the rAAV Plasmid Carrying SaCas9 and the Guide RNAs (gRNAs)

Here we are describing the preparation of the rAAV, delivering SaCas9 and gRNAs targeting the *Hao1* mouse gene. The gRNAs targeting the exon 2 of the *Hao1* mouse gene were designed and selected using Benchling software, based on the best predicted on-target [10] and off-target score (*see* **Note 1**) [11]. The target sequence consisted of 21 nucleotides (nt) followed by 5′-NNGRRT-3′ PAM sequence, required for SaCas9 to bind and cut (*see* **Note 2**). The sequences of the two gRNAs (Hao1-g1 and Hao1-g2) were 5′-TCCGTGGATAGAGCTTCCATC-3′ and 5v-GTCAACTTCTGTTTTAGGACA-3′ . The plasmid with the SaCas9 system, pX602-AAV-TBG::NLS-SaCas9-NLS-HA-OLLAS-bGHpA;U6::BsaI-sgRNA, was obtained from Addgene plasmid # 61593 (Fig. 1). The plasmid contains the SaCas9 gene tagged by HA-OLLAS tag and flanked by nuclear localization sequences (NLS), and its expression is controlled by the

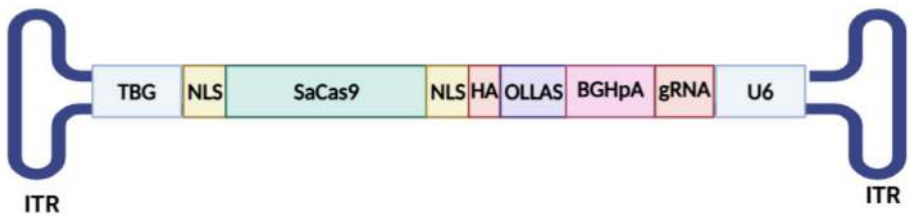


Fig. 1 Schematic representation of the cloned rAAV genome. The vector genome contains the TBG promoter, the SaCas9, the BGHpA, and the gRNA flanked by the ITRs. Created in https://BioRender.com

tyroxine-binding globulin (TBG) promoter and a bovine growth hormone polyadenylation sequence (BGHpA). The gRNA is expressed under the control of the human U6 promoter (*see* **Note 3**). The plasmid also incorporates the inverted terminal repeats (ITR) sequences necessary for AAV vector production (*see* **Note 4**).

3.1.1 gRNA Cloning for Hao1

The two gRNAs *Hao1*-g1 and *Hao1*-g2 were cloned by standard molecular biology techniques.

a) Design oligos for each gRNA.
Hao-g1: 5′-CACCGTCCGTGGATAGAGCTTCCATC-3′ and 5′-CACCGTCAACTTCTGTTTTAGGACA-3′.
Hao-g2: 5′-AAACGATGGAAGCTCTATCCACGGAC-3′ and 5′-AAACTGTCCTAAAACAGAAGTTGAC-3′.
The oligos are complementary except for the 5′ ends, which are designed to create overhangs upon hybridization.

b) Digest the cloning plasmid (2 μg) (pX602-AAV-TBG::NLS-SaCas9-NLS-HA-OLLAS-bGHpA;U6:BsaI-sgRNA) with the BsaI-HF enzyme (1 μL) in 1×rCutSart buffer.

c) Perform phosphorylation and hybridization of the oligos by mixing 1 μL of 100 μM of each oligo, 0.5 μL of PNK enzyme (NEB), 1 μL of the Buffer of T4 ligase (NEB), and 6.5 μL of water. Incubate the mix for 30 min at 37°C followed by 5 min at 97°C. Left the mix to cool down to room temperature slowly.

d) Ligate 1:100 and 1:250 dilutions of the hybridized oligos with 100 ng of the digested and purified vector using T4 ligase in 1×Ligation buffer.

e) Transform the competent *E. coli* with the ligation mixture. Incubate the *E. coli* first on ice (30 min) by adding the ligation mixture to the tube, containing the *E. coli*.

f) Perform heat shock of the *E. coli*: transfer the tube, containing *E. coli,* to the heating plate (42°C) for 3 min. After that, add 500 μL of LB medium and shake the tube for 30 min at 300 rcf on a shaker.

g) Spin down the tube, discard the supernatant and put the *E. coli* pellet on an LB plate containing the appropriate antibiotic resistance. Incubate overnight in the incubator at 37°C.

h) The next day, pick some clones, transfer them into LB medium (10 mL), and incubate overnight again at 37°C.

i) The next day, isolate plasmid DNA using a plasmid DNA isolation kit.

j) Sequence a few positive clones by Sanger sequencing using a primer in the U6 promoter (5′ -ACTATCATATGCTTACCGTAAC-3′) to confirm the correct cloning of the gRNAs.

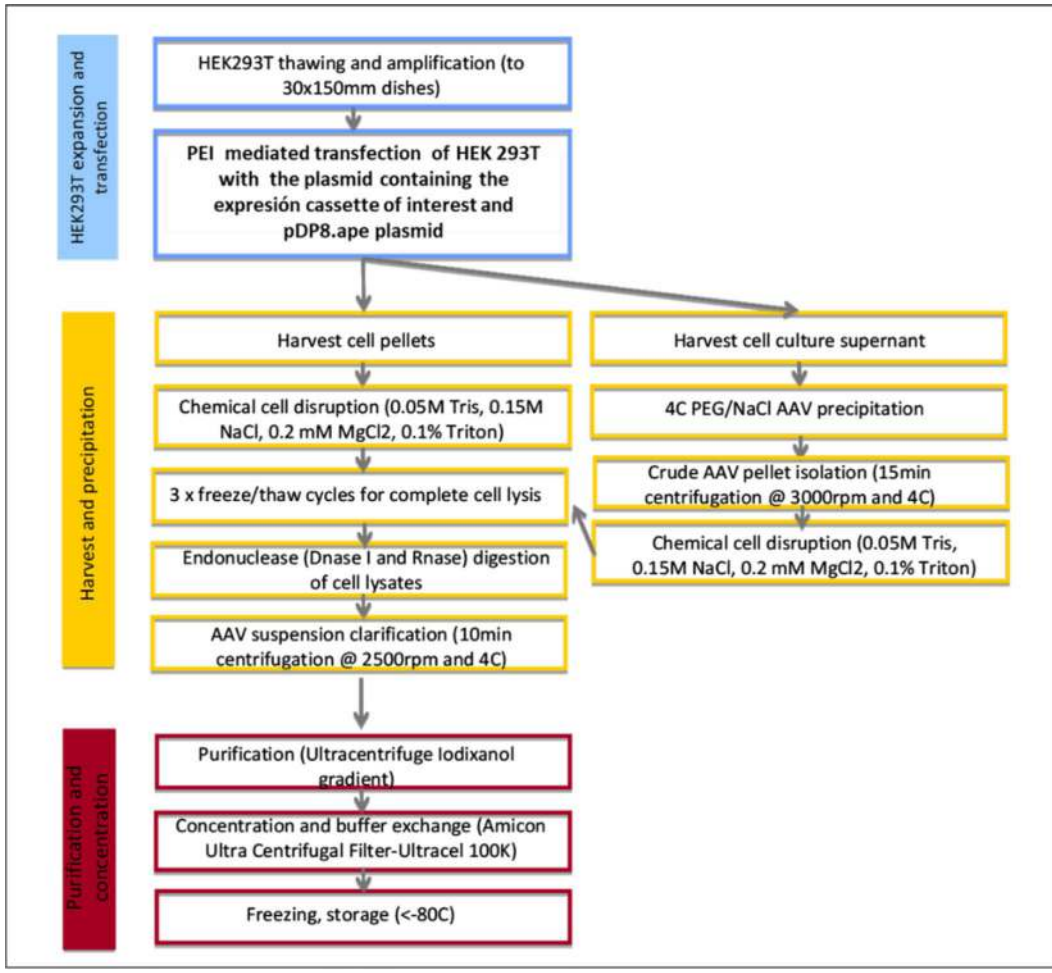


Fig. 2 Schematic summary of the rAAV production process. All the previously described steps are summarized here in chronological order

3.2 rAAV Production (see Note 5)

3.2.1 Cell Transfection

For the production of rAAV8 vectors (Fig. 2), HEK-293T cells are cultured in 150 mm plates in Dulbecco's modified Eagle's medium (DMEM) with pyruvate supplemented with 10% heat-inactivated fetal bovine serum (FBS), 1% penicillin–streptomycin.

a) Day 1: Seed $8–10 \times 10^6$ cells in 150 mm plates, and culture in an incubator at 37°C and with a 5% carbon dioxide (CO_2) concentration for 24 h (*see* **Note 6**).

b) Day 2: One hour before cell transfection, change the cell media to DMEM with pyruvate supplemented with 2% FBS.

c) After that, transfect the cells with a plasmid mix (*see* **Note 7**). Transfection is performed using PEI:DNA in a ratio Nitrogen:Phosphate (N:P) of 3:1. The amount of PEI needed is calculated based on the following equation PEI (μL) = $3 \times D \times R/S$, where D is the total among of plasmid DNA used (in μg), R is the N:P ratio (ratio of nitrogen content in PEI to phosphorous content in DNA) and S is the concentration of the PEI stock (mM) [12].

d) Seventy-two hours after cell transfection, harvest the cells and culture medium separately.

e) For cell collection: centrifuge the cells in a 5810R centrifuge at room temperature (RT) and 1200 × *g* for 10 min.

f) Resuspend the cell pellets in lysis buffer and perform three freeze-thaw cycles to release the viral vector particles (*see* **Note 8**).

g) Incubate the cell medium, which also contains viral vector particles with 40% poly-ethylene glycol (PEG)-8000 in 2.5 NaCl for 48–72 h to allow viral particle precipitation.

h) After that, centrifuge the PEG-treated supernatant at 2400 × *g* for 15 min and resuspend the pellet in lysis buffer and combine with the vector solution obtained from the cell pellet lysis (*see* **Note 9**).

3.2.2 Vector Purification

a) For vector purification, centrifuge the cell lysates and culture supernatants at 1200 × g for 10 min at 4°C.

b) Treat the resulting supernatant, which contains the vector particles, with 0.1 mg/10 μL of DNAse I and RNase A for 1 h at 37°C to remove free DNA and RNA (*see* **Note 10**).

c) Next, centrifuge the solution at 2500 × *g* for 10 min at 4°C to remove any remaining cellular debris.

d) Meanwhile, the supernatant containing the viral particles is subjected to ultracentrifugation in an iodixanol gradient. To this end, prepare different iodixanol concentrations (15, 25, 40, and 57% with miliQ water) and add them to an ultracentrifuge tube together with vector preparations. 25% and 57% solutions contain phenol red to facilitate the distinction of the different bands, including the band containing the viral vector.

e) Heat-seal the tubes and centrifuge them at 69,000 rpm for 2.5 h at 16°C.

f) After centrifugation, recover the rAAV particles from the interface between the 40% and 57% iodixanol layers using an 18–19 G gauge needle.

g) To remove iodixanol and concentrate the vector particles, add the ~1 mL fraction containing the purified virus to 13–14 mL

of DPBS 5% sucrose, place it on an Amicon Ultra-4 centrifugal filter, and centrifuge the solution for 5 min at 4000 rpm and 4°C. Repeat three times to complete the buffer exchange, which ends when 45–50 mL of flowthrough is collected.

h) In the end, sterilize 1 mL of the vector-containing solution by using a column with 0.22 μm pore membrane and centrifuge for 1-min at 15,000 × *g* at 4°C.

i) Finally, aliquot the purified viral vector in screw cap micro tubes and store at −80°C for its conservation until use.

3.2.3 Viral Vector DNA Extraction and Titering by qPCR

a) For viral vector titration, extract the viral DNA using the High Pure Viral DNA kit following the manufacturer's instructions.

b) First, mix 20 μL of viral vector with 180 μL of saline solution and 200 μL of binding buffer supplemented with polyA and 50 μL of proteinase K.

c) Incubate the mixture for 10 min at 72°C, and add 100 μL of binding buffer.

d) Load the sample into a high-purity filter tube and centrifuge for 1 min at 8000 rpm. Then, add 500 μL of inhibitor removal and centrifuge for 1 min at 8000 rpm.

e) Perform two washes with 450 μL of wash buffer by centrifuging the mixture twice for 1 min at 8000 rpm.

f) Perform a final centrifugation for 10 s at maximum speed to dry the filter.

g) Finally, elute the viral DNA by adding 30–50 μL of sterile water into the column, that is placed in a clean Eppendorf tube, and perform a 1 min centrifugation at 8000 rpm.

h) Titration is performed by quantification of viral copies, amplifying the ITR sequence via qPCR. First, make a standard curve ranging from 10^9 to 10^2 copies of a plasmid carrying the ITR sequences.

i) Next, dilute the purified viral DNAs 1/10, 1/100, and 1/1000 times in water.

j) For qPCR, the reactions are performed in a final volume of 10 μL. Mix 2 μL of the different dilutions of the viral genomes, 0.2 μL of the forward and reverse primers for the ITR sequence (15 μM, Fw: 5′-GGAACCCCTAGTGATGGAGTT-3′ and Rv: 5′-CGGCCTCAGTGAGCGA-3′), 2.6 μL of sterile water and 5 μL of the IQTM SYBR® Green Supermix.

k) Prepare the different samples inside the PCR cabin, and then perform the qPCR in a CFX96TM Real-Time System thermocycler, or similar (PCR conditions are: 95°C-10' (95°C-15", 60°C-1', 72°C 25", 80°C-10") * 40 cycles and 4°C − ∞).

3.3 rAAV Administration into Mice

All animal procedures were reviewed and approved in advance by the Institutional Animal Care and Use Committee (IACUC). Up to six mice should be placed in an isoflurane inhalation anesthesia chamber. Prior to rAAV administration, each mouse must be weighed to determine the appropriate injection volume, considering a range of 5–10 μL per gram of body weight and a target dose of 5×10^{12} vector genomes per kilogram (vg/kg).

a) Weigh the mice. After weighing, return the mouse to the anesthesia chamber until the time of injection.

b) The rAAV solution must be maintained on ice throughout the entire procedure.

c) Once the required volume has been calculated, load a 0.3 mL insulin syringe with the corresponding amount of rAAV solution.

d) Perform intravenous administration via the retro-orbital route.

e) Remove the anesthetized mouse from the chamber and place it laterally. Injection may be carried out in either eye, according to the operator's preference.

f) With the nondominant hand, gently stretch the skin surrounding the eye to improve exposure.

g) Position the syringe with the needle directed toward the medial canthus, with the bevel facing upward.

h) Insert approximately half the length of the needle into the orbital sinus, keeping it parallel to the snout at an angle of

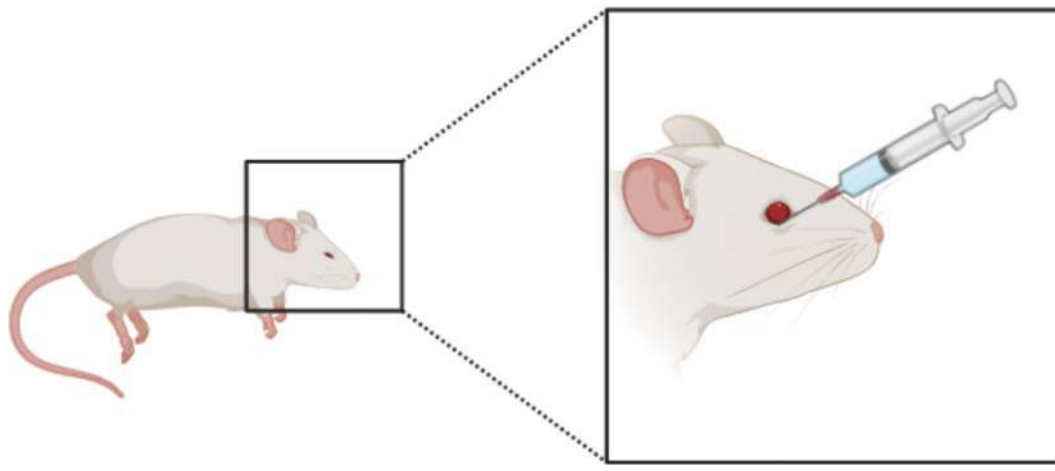


Fig. 3 Schematic representation of intravenous administration of rAAV. In this representation, we see the proper way to place the mouse (on its side to facilitate access to the eye) and a zoomed square into the positioning of the needle inside the eye for proper rAAV injection. Created in https://BioRender.com

approximately 45° (*see* Fig. 3). Once properly positioned, inject the solution slowly and steadily (*see* **Note 11**).

i) After completing the injection, return the mouse to its cage and monitor until full recovery.

j) Repeat these steps for each animal until all mice have been treated.

3.4 Liver Extraction and Processing

3.4.1 Liver Extraction

a) Euthanize the animals using an IACUC-approved method.

b) Open the abdominal cavity of the mouse using surgical scissors to access the liver.

c) Isolate and extract the whole liver.

d) Clean the organ by submerging it in DPBS.

e) Once cleaned, separate the different lobes of the liver using forceps and surgical blades. If immunohistochemistry is going to be performed, select the lobes for analysis and include them in a tube containing 4% paraformaldehyde solution.

f) Dissect the rest of the liver into pieces of around 45–50 mg, and store some in different 1.5 mL tubes for DNA, RNA, and protein extractions. The remaining or excess organ can be stored in a cryotube.

g) Snap-freeze these samples using either liquid nitrogen or dry ice and keep at −80°C until their use.

3.4.2 Genomic DNA (gDNA) Extraction from Liver Tissue

For gDNA extraction from liver samples, use the Maxwell® RSC Tissue DNA Kit, following the provider's instructions.

a) First, add 100 µL of TE buffer to each piece of tissue sample.

b) Homogenize the tissue sample using a pestle.

c) Load the homogenized tissue into the cartridge.

d) Run the "Tissue DNA" protocol in the Maxwell® RSC 48 instrument.

e) Elute the samples in 100 µL of a mixture of elution buffer and RNaseA (4 mg/mL), in a proportion 4:1.

f) Determine the DNA concentration (app. 1 µL of solution) using the NanoDrop™ 1000 spectrophotometer (Thermo Scientific, #ND-1000) or similar.

3.4.3 RNA Extraction from Liver Tissue

Perform RNA extraction from tissue samples using the Maxwell® RSC simply RNA Tissue Kit, following the manufacturer's instructions.

a) First, add 196 µL of homogenization buffer and 4 µL of thioglycerol per sample.
b) Homogenize the samples with the buffer using a pestle.
c) Incubate the samples at 70°C for 2 min.
d) Then, add 200 µL of lysis buffer per sample.
e) Thoroughly vortex before loading into the cartridges.
f) Add 10 µL of DNAse into the specific well of the cartridge.
g) Add the plungers to their specific well.
h) Run the protocol "RNA Tissue" in the Maxwell® RSC 48 instrument.
i) Elute RNA in 50 µL nuclease-free water and quantify using the NanoDrop™ 1000 spectrophotometer, or similar.

3.4.4 Protein Extraction and Quantification

Total protein is extracted using RIPA buffer supplemented with 1 M sodium orthovanadate, 100 mM PMSF, 0.5 M sodium pyrophosphate, and a protease inhibitor cocktail.

a) Approximately add 300 µL of this solution to a liver piece of 40–50 mg.
b) Using a pestle, disrupt the tissue.
c) After homogenizing the tissue, incubate it for 30 min in ice. Vortex the samples every 10 min to ensure proper homogenization.
d) After that, centrifuge the tubes at 15,000 rpm for 20 min at 4°C and collect the supernatant, containing the extracted protein, in a new tube.
e) For protein quantification, use a BCA protein assay kit.

3.5 Analysis of rAAV Liver Transduction

3.5.1 PCR for rAAV Genomes Quantification

a) For the quantification of viral genomes, genomic DNA (gDNA) extraction, qPCR is performed using 50 ng of total gDNA mixed with the GOTaq PCR master mix 2× and primers specific for the detection of SaCas9 (5′-AAGCCATCCCTCTGGAAGAT-3′ and 5′-TGCCCTTCTTGCTGTTTTCT-3′) and mGAPDH (5′ -TGCACCACCAACTGCTTA-3′ and 5′-GGATGCAGGGAT GATGTTC-3′) as a housekeeping.
b) The qPCR is run on the Applied Biosystems QuantStudio™ 5 Real-Time PCR Machine or a similar instrument.
   - All reactions should be performed in triplicate.
c) Levels of vector genomes are then assessed by calculating the 2ΔCT: $2^{(\text{Ct of the housekeeping gene} - \text{Ct of the desired gene})}$.

3.5.2 RT-PCR to Evaluate SaCas9 and Hao1 *Expression*

SaCas9 expression is quantified by RT-qPCR using 50 ng of cDNA, retrotranscribed from 500 ng of the total extracted RNA using the M-MLV reverse transcriptase.

a) To prepare the RNA for cDNA synthesis, dilute 500 or 1000 ng of RNA in nuclease-free water to reach a final volume of 7 μL in a 0.2 mL tube.

b) Then, add 1 μL of 10× TURBO DNase buffer, 0.15 μL of DNase Turbo, and 0.85 μL of nuclease-free water to the RNA samples.

c) Incubate the mixture for 30 min at 37°C.

d) Next, to inactivate the DNase activity, add 1 μL of 25 mM EDTA to each tube and incubate the mixture for 10 min at 75°C.

e) To perform the retro transcription, prepare a mixture of 4 μL of 5× First Strand Buffer, 2 μL of dNTPs (10 mM), 2 μL of random primers (250 ng/μL), 1 μL of DTT (0.1 M), 0.4 μL of RNase OUT and 0.6 μL of M-MLV RT per sample. Add 10 μL of this mixture to each tube.

f) Finally, incubate the mixture for 1 h at 37°C and 1 min at 95°C. Then, dilute the resulting cDNA to obtain a concentration of 10.8 ng/μL; e.g.: add 46 μL of nuclease-free water to the obtained 20 μL of cDNA if you start from 500 ng of RNA.

g) For qPCR, 4.6 μL of cDNA (10.8 ng/μL) is mixed with 0.2 μL/each of *SaCas9* (5′-AAGCCATCCCTCTGGAAGAT-3′ and 5′-TGCCCTTCTTGCTGTTTTCT-3′), *Hao1* (5′-GTCAGTGTATGACTATTACAGGTCT-3′ and 5′-GTGGATAGAGCTTCCATCTAGAAA-3′) and *m-β-actin* (5′-ACGGCCAGGTCATCACTATTG-3′ and 5′-CAAGAAGGAAGGCTGGAAAAGA-3′) specific primers (15 mM), and 5 μL GOTaq PCR master mix 2× (Promega, #A600A).

h) The qPCR is run in the Applied Biosystems QuantStudio™ 5 Real-Time PCR Machine.

- All reactions are performed in triplicate.

i) Relative expression of SaCas9 is then assessed by calculating the 2ΔCT: $2^{(\text{Ct of the housekeeping gene} - \text{Ct of the desired gene})}$.

3.6 Analysis of Editing Efficiency

3.6.1 PCR for the Amplification of the CRISPR-Cas9 Target Region

To evaluate the efficiency of editing of the SaCas9 + gRNA, several analyses can be performed. Most require, as a first step, the performance of a PCR to amplify the region within our target gene where the cut is made by our selected approach.

a) For that purpose, primers flanking the target sequence are designed (*see* **Note 12**).

b) PCR is then run mixing 50 ng of gDNA, 1.25 μL/each of the previously designed primers (10 mM each) and 12.5 μL of the Q5® High-Fidelity 2× Master Mix.

c) Next, the PCR is run on the thermal cycler.

d) Finally, PCR products should be purified using the NucleoSpin Gel and PCR Clean-up, Mini kit for gel extraction or PCR clean up, or similar. The resulting purified product is then quantified using the Qubit™ Flex Luminometer, or similar.

3.6.2 Sanger Sequencing to Evaluate Editing Efficiency with TIDE or Similar Tools

To analyze the editing efficiency, Sanger sequencing from the purified PCR products is performed using one of the primers used to generate the amplification product. An unedited control sample must be added to this analysis. Once the sequencing results are obtained, different methods can be used to evaluate the editing efficiency. Here, we describe the use of the TIDE web tool [13]. TIDE is a tool designed to analyze SpCas9-mediated indels, and therefore, the input information needs to be modified when analyzing SaCas9 editing (*see* **Notes 13 and 14**).

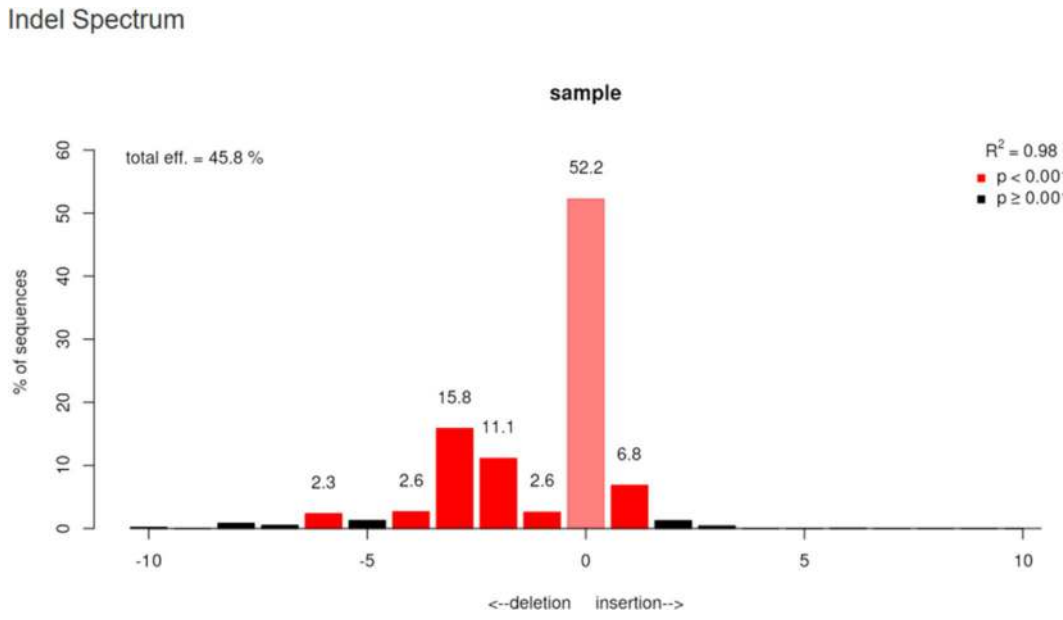


Fig. 4 Example of the data obtained using the TIDE webpage. This sample has a sequence homology with the unedited control of 52.2%, meaning that this percentage of reads contains unedited DNA. As the analysis shows, in the upper left corner, the editing efficiency (total eff.) of the rAAV in this sample was of 45.8%, meaning that this percentage of reads contains either insertions or deletions that make them different from the original DNA sequence

a) The tool requests a 20nt gRNA sequence, and therefore, we input the 20nt adjacent to the PAM recognizing sequence. There are no further adjustments required, as both SpCas9 and SaCas9 introduce a double-strand break (DSB) 3 bp upstream of the PAM.

b) After indicating the gRNA sequence in the "guide sequence" field, upload the sequencing results from the unedited control, in the "Control sample chromatogram" field, and finally, the sequencing results from the edited samples, one by one, into the "Test sample chromatogram" field.

c) Click on "update view".

d) Next, the program will calculate the percentage of homology between the edited sample and the unedited control, and it will show the percentage of edited reads, and of the insertions and deletions generated (see Fig. 4).

3.6.3 Deep Sequencing analysis to Determine INDEL Characteristics

a) Perform a first PCR round by mixing 250 ng of template and primers flanking the target region.

b) Purify the PCR product using the Agencourt AMPure XP system and elute in 10 µL nuclease-free H_20.

c) Quantify the purified PCR product using the Qubit™ Flex Luminometer or similar and perform a TapeStation assay to quantify and determine the purity of the first amplicon before proceeding with the second PCR step (*see* **Note 15**).

d) Then, mix 40 ng of the PCR product with primers carrying partial universal adapters for Illumina amplicons.

e) Purify 450 bp amplicons as described above and send them to GENEWIZ (GENEWIZ Germany GmbH) for Amplicon-EZ analysis.

f) Raw FASTQ files are the results of Amplicon-EZ analysis trimmed with Trimmomatic v0.36 [14].
For the analysis of all editing events, a bash script can be developed to characterize AAV insertion-bearing reads and ensure they originate from the mouse genome (*see* **Note 16**).

   a) First, align all the reads to the mm10 reference genome with BWA MEM v0.7.17 [15] and remove unmapped read-pairs from the alignment files with samtools v1.6 [16] (*see* **Note 17**).

   b) Then, covert filtered BAM files back to FASTQ files with bedtools v2.30 bamToFastq [17] and map with BWA MEM to the vector genome used in each experiment.

   c) Finally, employ samtools and bedtools once more to only recover the reads that map to the vectors and the reads that do not map. A virus-free BAM file is obtained with

minimap2 v2.17 [18] with alignment options -A5 -B4 -O25 -E1.

d) Analyze the editing events in the vector-sequence-free BAM files with the CrispRVariants R package [19], then the reads with known vector insertions are added to these results.

3.6.4 WB Analysis for the Evaluation of Protein Knockdown

To evaluate GO protein knockdown, 20 µg of total protein is separated by SDS polyacrylamide gel electrophoresis (SDS-PAGE) and then transferred onto nitrocellulose membranes following the wet procedure using the BIO-RAD trans-blot machine.

1. Polyacrylamide gel preparation.
   a) First, set up the glass plates where the gel is going to be formed. To do so, align the back (larger) and front (shorter) plates (1.5 mm thick) and put them into the casting frame or stand.
   b) Make sure the assembly does not leak by adding water up to the top and waiting for a few minutes to see whether there is any leakage. Readjust if needed.
   c) After confirming there are no leaks, start preparing the 10% resolving (percentage of resolving gel might change depending on the size of the protein to be studied) and 4% stacking gels. Add the comb of your required size to the 4% before it polymerizes.

2. Samples preparation and electrophoresis.
   a) For protein expression analyses, 20 µg of total protein is mixed with LB 4× and incubated for 10 min at 95°C to denaturalize the proteins.
   b) Prepare the electrophoresis chamber by including the gel in the gel stands (also add a ghost gel in the stand in case you need it). Next, put the stand containing the gel/gels inside the electrophoresis chamber, and fill the space between the two gels with running buffer. Keep filling the rest of the chamber until the 2-gel mark of the electrophoresis chamber.
   c) Once the electrophoresis chamber is ready, remove the comb from the gel/gels.
   d) Next, load the samples and your ladder of choice into the gel.
   e) Close the chamber with the lid and attach the cables to the electrophoresis power supply.
   f) Run the electrophoresis for around 2 h at 90 V or until the sample front has reached the lower part of the gel.

3. Protein transfer from the gel to the nitrocellulose membrane.
   a) Once electrophoresis has been completed, remove the gel from the stand and from the glass plates.
   b) Prepare the "sandwich" for the transfer of proteins from the gel to the nitrocellulose membrane. To do so, wet two transference sponges in transfer buffer. Open the transfer cassette and put the first wet sponge onto the transparent side (corresponding to the anode). Next, add a pre-wetted Whatman paper (of a size similar to the gel) and place the also pre-wetted nitrocellulose membrate on top of it. Next, put the gel on top of the membrane. After that, add another wetted Whatman paper. Use a pipette or a small roller to remove any bubbles that may have formed during the sandwich preparation. Finally, the other wetted transfer sponge is added, and the transfer cassette is closed.
   c) Once the sandwich is prepared, put it inside the transfer chamber.
   d) Put an ice pack, that should fit into the chamber, in order to help with the maintenance of the cold temperature needed for the transfer.
   e) Fill the chamber until the specific mark for transference with transfer buffer.
   f) Close the chamber with the lid and attach it to the power supply system. This should be done at 4°C. The transfer should be performed at 80 V for 1-1 and a half hours.
   g) Once the transfer has ended, protein transfer is assessed by staining the membranes with Ponceau Red. To do so, remove the nitrocellulose membrane from the sandwich and put it inside a container where it fits. Add 5 mL of Ponceau Red and agitate in darkness for 1 min. If transference has happened, all protein bands should be stained. If more than one protein needs to be studied, membranes can be cut at this point to then treat them independently with each specific antibody.
   h) After cutting the membrane, remove the ponceau red stain and clean the membrane by performing several washes with TBS-Tween20 0.05% until no red remains on it.
4. Blocking of unspecific antibody interactions.
   a) Unspecific antibody interactions are avoided by blocking the membranes with 5% nonfat milk in TBS-Tween20 0.05% for 30 min at RT on a shaker.
5. Incubation with primary and secondary antibodies and protein imaging.

a) After blocking, membranes are incubated O/N at 4°C in a shaker with primary antibodies against α-GO and α-GAPDH as a housekeeping control. First, remove the blocking solution and later on, add enough antibody-containing solution to cover the membrane and incubate.

b) To remove unbound primary antibody molecules, three 5 min washes with TBS-T are performed.

c) Next, membranes are incubated with horseradish peroxidase (HRP)-conjugated α-rabbit IgG or HRP-conjugated α-mouse IgG diluted 1/5000 for 1 h in a shaker at RT.

d) To remove unbound secondary antibody molecules, three 5 min washes with TBS-T are performed.

e) Finally, to visualize the target proteins, the peroxidase signal is developed using SuperSignal West Femto Maximum Sensitivity Substrate and a ChemiDoc MP imaging system is used for image generation.

f) Band quantification can be performed using the Image Lab software (BioRad) or similar (Fig. 5). Protein of interest levels should be normalized to those of the housekeeping protein.

4 Notes

1. SaCas9 Specific Constraints: When designing gRNAs for the SaCas9 system, the target sequence must consist of exactly 21 nucleotides. This 21-nucleotide sequence must be immediately followed by a 5′-NNGRRT-3′ PAM sequence, which is strictly required for the SaCas9 nuclease to efficiently bind and cut the DNA.

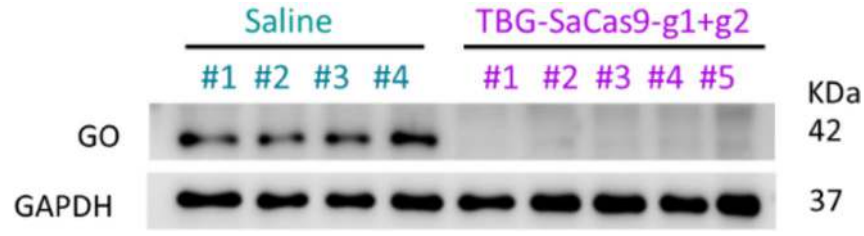


Fig. 5 Example of GO protein knockdown evaluation with WB. The first four lanes correspond to protein samples coming from four different control mice treated with saline to assess basal GO levels in the liver. The next five lanes correspond to protein samples coming from five mice treated with the rAAV expressing SaCas9 and gRNAs 1 and 2. Here, we can observe the efficient GO protein knockdown achieved with the rAAV treatment

2. Predictive Software: It is highly recommended to use design software, such as Benchling, to select the best gRNAs based on their predicted on-target and off-target scores.
3. Additionally, an extra G nucleotide was added to the 5′ end of the spacer to ensure proper RNA transcription under the control of the U6 promoter.
4. Changes in the plasmid design can be made in order to change the promoter or any other regulatory sequences that are wanted to be included in the resulting rAAV vectors.
5. Handling of AAV Material: Recombinant AAV production and handling are generally considered Biosafety Level 2 (BSL-2) activities. Ensure all work—especially the initial harvesting and lysis steps—is performed in a Class II Biological Safety Cabinet.
6. HEK293T Cell Confluency: for optimal rAAV vector production, HEK293T cells should ideally be at 70%–80% confluency at the time of transfection. Culturing them for 24 h prior to transfection typically achieves this state. Overconfluent cells can lead to reduced transfection efficiency and significantly lower viral titers.
7. PEI Transfection Ratio: When preparing the PEI transfection mixture, ensure that the nitrogen-to-phosphate (N:P) is 3:1. Allow the PEI-plasmid mix to incubate at room temperature for 15–20 min to allow the complexes to form properly before adding them to the culture media. The composition of the plasmid mix is different depending on the rAAV expression cassette. For this particular study, this mix contained the pDP8.ape plasmid for AAV8 serotype vectors production (this plasmid contains the Adenoviral sequences required for AAV genome replication, the AAV serotype 2 Rep gene, and the AAV serotype 8 Cap gene) plus the plasmid carrying the AAV recombinant genome containing the SaCas9 and gRNA cassettes and the AAV2 serotype ITRs.
8. Freeze-Thaw Cycles: To efficiently release the viral vector particles from the cell pellet, ensure the three freeze-thaw cycles are rigorous. Use a dry ice/ethanol bath for freezing and a 37°C water bath for thawing to quickly fracture the cell membranes without degrading the viral capsids.
9. PEG-8000 Precipitation: During the viral vector precipitation step using 40% PEG-8000 in 2.5 M NaCl, it is critical to respect the full 48–72 h incubation period. Premature centrifugation can lead to incomplete recovery of viral particles from the cell medium and reduce your final yield.
10. DNAse I Treatment: Treatment with DNAse I (0.1 mg/mL) is a crucial purification step. It digests any residual

unencapsidated plasmid DNA from the transfection step that could later interfere with quantitative PCR titrations

11. In Vivo Administration: When performing intravenous injections using insulin syringes, warming the mouse slightly (e.g., using a heat lamp) can help dilate the tail vein, making the injection smoother and less stressful for the animal.
12. Primer Design for Evaluation: To evaluate editing efficiency (using either Sanger or deep sequencing), you must first design specific primers that accurately flank the target region where the CRISPR-Cas9 cut is made.
13. TIDE Analysis Adjustments: If you are using the TIDE web tool to analyze Sanger sequencing results, be aware that the web interface asks for a 20-nucleotide guide sequence.
14. Trimming for TIDE: Because of TIDE's 20-nucleotide input restriction, you may need to manually remove some nucleotides from your original gRNA sequence prior to input, particularly ensuring that the PAM sequence is excluded.
15. Amplicon Quality Control: Before adding partial universal adapters in the second PCR step for deep sequencing, the purity and quantity of your first PCR amplicon must be accurately determined. This quality control can be performed using Qubit quantitation and TapeStation assays.
16. AAV Vector Integration: When analyzing INDEL characteristics from deep sequencing, your bioinformatics pipeline must be designed to characterize potential AAV insertion-bearing reads.
17. Dual-Mapping Strategy: To properly identify these insertions, reads must first be aligned to the reference mouse genome (e.g., mm10), and the resulting files must then be converted and remapped to the specific vector genome used in your experiment.

Acknowledgments

The publication is based upon work by COST Action CA21113: Genome Editing for the Treatment of Human Diseases (https://www.genehumdi.eu), supported by European Cooperation in Science and Technology (COST). Figures were created using Biorender.com.

Conflict of Interest The authors have no conflicts of interest to declare that are relevant to the content of this chapter.

References

1. Ngo W, Wu JLY, Wasko KM et al. (2026) Targeted delivery of genome editors in vivo. Nat Biotechnol 44:49–59
2. Colella P, Ronzitti G, Mingozzi F (2018) Emerging issues in AAV-mediated in vivo gene therapy. Mol Ther Methods Clin Dev 8:87–104
3. Wang D, Tai PWL, Gao G (2019) Adeno-associated virus vector as a platform for gene therapy delivery. Nat Rev Drug Discov. 18:358–378
4. Ran FA, Cong L, Yan WX et al. (2015) In vivo genome editing using *Staphylococcus aureus* Cas9. Nature 520:186–191
5. Stevanovic M, Piotter E, McClements ME et al. (2021) CRISPR systems suitable for single AAV vector delivery. Curr Gene Ther 22:1–14
6. Martin-Higueras C, Luis-Lima S, Salido E (2016) Glycolate oxidase is a safe and efficient target for substrate reduction therapy in a mouse model of primary hyperoxaluria Type I. Molecular Therapy 24:719–725
7. Frishberg Y, Saland JM, Lieske JC et al. (2026) Final results of the ILLUMINATE-A phase 3 clinical trial of lumasiran for primary hyperoxaluria 1. Clin J Am Soc Nephrol 21:377–388
8. Zabaleta N, Barberia M, Martin-Higueras C et al. (2019) Re: CRISPR/Cas9-mediated glycolate oxidase disruption is an efficacious and safe treatment for primary hyperoxaluria type I. J Urol 201:853–854
9. Torella L, Klermund J, Bilbao-Arribas M et al. (2024) Efficient and safe therapeutic use of paired Cas9-nickases for primary hyperoxaluria type 1. EMBO Mol Med 16:112–131
10. Doench JG, Hartenian E, Graham DB et al. (2014) Rational design of highly active sgRNAs for CRISPR-Cas9-mediated gene inactivation. Nat Biotechnol 32:1262–1269
11. Hsu PD, Scott DA, Weinstein JA et al. (2013) DNA targeting specificity of RNA-guided Cas9 nucleases. Nat Biotechnol 31:827–834
12. Reed SE, Staley EM, Mayginnes JP et al. (2006) Transfection of mammalian cells using linear polyethylenimine is a simple and effective means of producing recombinant adeno-associated virus vectors. J Virol Methods 138:85–98
13. Brinkman EK, van Steensel B (2019) Rapid quantitative evaluation of CRISPR genome editing by TIDE and TIDER. Method Mol Biol 1961:29–44
14. Bolger AM, Lohse M, Usadel B (2014) Trimmomatic: a flexible trimmer for Illumina sequence data. Bioinformatics 30:2114–2120
15. Li H (2013) Aligning sequence reads, clone sequences and assembly contigs with BWA-MEM. ArXiv
16. Danecek P, Bonfield JK, Liddle J, Marshall J, Ohan V, Pollard MO, Whitwham A, Keane T, McCarthy SA, Davies RM, & Li H (2021) Twelve years of SAMtools and BCFtools. GigaScience 10(2):giab008
17. Quinlan AR, Hall IM (2010) BEDTools: a flexible suite of utilities for comparing genomic features. Bioinformatics 26:841–842
18. Li H (2018) Minimap2: pairwise alignment for nucleotide sequences. Bioinformatics 34:3094–3100
19. Lindsay H, Burger A, Biyong B et al. (2016) CrispRVariants charts the mutation spectrum of genome engineering experiments. Nat Biotechnol 34:701–702

Open Access This chapter is licensed under the terms of the Creative Commons Attribution-NonCommercial-NoDerivatives 4.0 International License (http://creativecommons.org/licenses/by-nc-nd/4.0/), which permits any noncommercial use, sharing, distribution and reproduction in any medium or format, as long as you give appropriate credit to the original author(s) and the source, provide a link to the Creative Commons license and indicate if you modified the licensed material. You do not have permission under this license to share adapted material derived from this chapter or parts of it.

The images or other third party material in this chapter are included in the chapter's Creative Commons license, unless indicated otherwise in a credit line to the material. If material is not included in the chapter's Creative Commons license and your intended use is not permitted by statutory regulation or exceeds the permitted use, you will need to obtain permission directly from the copyright holder.



Part III

Non-Viral Delivery Methods



Chapter 10

Lipid Nanoparticle-Mediated Delivery of CRISPR–Cas9 Components for Genome Editing

Amalie Lykke Olsen, Camilla Blunk Brandt, Rasmus Karred Larsen and Yonglun Luo

Abstract

Lipid nanoparticles (LNPs) are a clinically validated nonviral platform for the delivery of CRISPR-associated components. Composed of ionizable lipids, phospholipids, cholesterol, and PEG–lipids, LNPs enable the efficient encapsulation, protection, and cytosolic delivery of therapeutic cargo such as DNA, RNA, or proteins. The clinical relevance of LNPs has already been shown by multiple FDA-approved therapies, including siRNA-based treatments and mRNA vaccines. Compared with viral vectors, LNPs offer several advantages, including reduced immunogenicity, absence of genomic integration, scalable manufacturing, and flexibility in cargo size, while supporting transient expression, which is desirable for genome editing applications. However, challenges remain, including limited tissue specificity and inefficient endosomal escape. Recent advances in lipid chemistry optimization and surface modification have improved delivery performance. Among available formulation techniques, microfluidic mixing has emerged as a preferred method due to its reproducibility, scalability, and precise control over particle properties. This protocol describes a standardized microfluidic workflow for reproducible LNP formulation, providing practical guidance on lipid preparation, nanoparticle assembly, and quality control.

Keywords Lipid nanoparticles, Nonviral delivery, CRISPR SpCas9, Microfluidic mixing

1 Introduction

Lipid nanoparticles (LNPs) are a clinically validated nonviral delivery system, now widely used for intracellular delivery of nucleic acids, such as messenger RNA (mRNA), small interfering RNA (siRNA), and CRISPR-associated components [1]. Structurally, LNPs are self-assembled nanoparticles, typically ranging from 50 to 200 nm, and are composed of four main lipid types [2]. These include an ionizable lipid, a phospholipid, a sterol lipid (typically cholesterol), and a polyethylene glycol (PEG)-conjugated lipid. Together, these components enable efficient cargo encapsulation and protection

These authors Amalie Lykke Olsen and Camilla Blunk Brandt are contributed equally to this work.

Duško Lainšček et al. (eds.), *CRISPR Delivery*, Methods in Molecular Biology, vol. 3075,
https://doi.org/10.1007/978-1-0716-5547-4_10,
© The Author(s) 2027

against degradation while facilitating systemic delivery and cytosolic release [1]. Multiple LNP-mediated nucleic acid therapies are currently FDA-approved, highlighting the clinical relevance of the delivery platform. Notable examples include the siRNA drug patisiran (Onpattro®) targeting hereditary transthyretin amyloidosis, as well as the mRNA-based SARS-CoV-2 vaccines from Moderna and Pfizer. These successes have positioned LNPs as one of the leading delivery platforms for nucleic acid therapeutics, particularly where transient expression or genome editing is required [3]. Compared with viral vectors like lentivirus and adeno-associated virus (AAV), LNPs offer several advantages. These include reduced immunogenicity, absence of genomic integration, high biocompatibility, scalable manufacturing, and greater flexibility in terms of cargo size [4]. In contrast to physical delivery methods such as electroporation or microinjection, LNPs enable systemic administration and are compatible with *in vivo* applications [5]. Indeed, several LNP-based *in vivo* CRISPR therapeutic trials have yielded promising results in patients, such as NTLA-2001, an LNP-mediated delivery of a single guide RNA (sgRNA) targeting human TTR and a SpCas9 mRNA for treating transthyretin amyloidosis [6], and k-abe, an LNP-mediated delivery of the SpCas9 nickase-derived adenine base editor 8e (ABE8e) and an sgRNA targeting the human *CPS1* gene with Q335X variant for treating a neonate with severe carbamoyl-phosphate synthetase 1 deficiency [7]. However, LNP-mediated delivery is also associated with limitations, including restricted tissue distribution and inefficient endosomal escape, all of which necessitate careful formulation and optimization [8–10].

Each lipid component of LNPs contributes a distinct set of properties to the final particle (Fig. 1). Ionizable lipids, such as DLin-MC3-DMA, ALC-0315, and SM-102, are essential for efficient nucleic acid encapsulation during formulation and promote intracellular release after uptake through their pH-dependent protonation. Phospholipids, commonly DSPC (1,2-Distearoyl-sn-glycero-3-phosphocholine) or DOPE (dioleoylphosphatidylethanolamine), stabilize the lipid membrane layer and influence membrane fusion. Sterol lipids, such as cholesterol, modulate particle stability and membrane rigidity, while PEG–lipids, such as DMG-PEG2000, improve colloidal stability and control particle size but may also affect cellular uptake and circulation time [1]. In addition, PEG–lipids are essential for the functionalization of LNPs to improve the cell- and tissue-specific delivery efficiency by conjugating to, for example, cell-specific antibodies and ligands.

As shown in Fig. 1, the cellular uptake of LNPs occurs via endocytosis, after which delivery relies on efficient endosomal escape to release the cargo into the cytosol. Despite extensive studies, endosomal escape remains a major bottleneck, and only a small fraction of the packaged nucleic acid cargos reaches the cytosol [8].

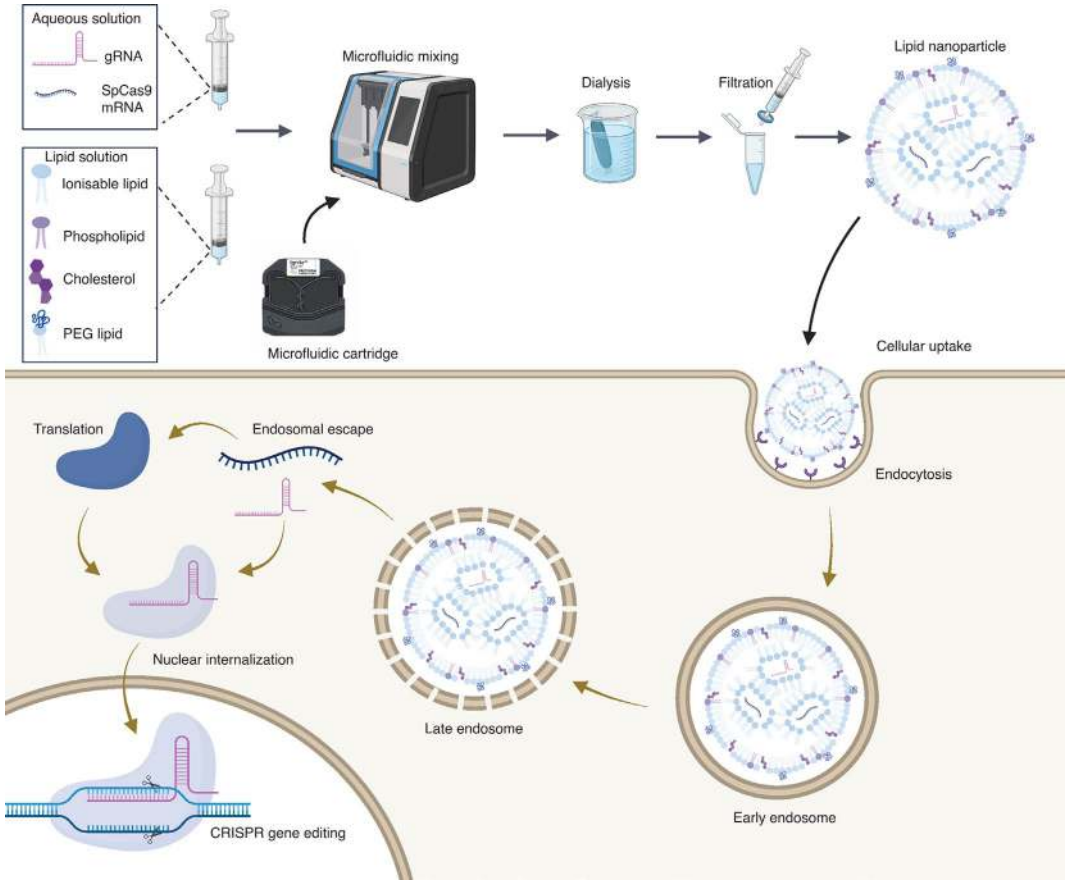


Fig. 1 Schematic illustration of LNP-based CRISPR delivery. Top. Illustration of the aqueous solution and lipid solution used for generating LNP using microfluidic mixing. Four technical steps, including microfluidic mixing, dialysis, filtration, and quality control of the LNP generated, are provided in this protocol. Bottom. Schematic illustration of LNP uptake in cells via endocytosis and intercellular endosomal escape for the generation of CRISPR ribonucleoprotein (RNP) complex and final gene editing at the genomic DNA

Furthermore, most conventional LNP formulations exhibit strong liver tropism following systemic administration. This is primarily due to the adsorption of apolipoprotein E (ApoE), which mediates uptake by hepatocytes via lipoprotein receptors. While this is advantageous for liver-targeted therapies, it represents a limitation for applications requiring efficient delivery to extrahepatic tissues (e.g., lungs, spleen, or immune cells) [11], highlighting the need for continued optimization of the LNP formulations.

Recent advances in LNP-mediated delivery have generally focused on the systematic optimization of lipid chemistry and molar ratios, while particle surface modifications have also shown significant effects. These advancements are particularly relevant for emerging therapeutic applications, e.g., CRISPR-based genome editing (Fig. 1), where efficient, transient, and *in vivo* delivery is essential

[12–15]. Multiple formulation methods exist for LNP manufacturing, including ethanol injection, lipid film hydration, manual bulk mixing, and microfluidic mixing. Among these, microfluidic mixing has become the preferred approach, offering high reproducibility, scalability, and precise control over particle size and encapsulation efficiency. Rapid mixing of an ethanol-dissolved lipid phase with an aqueous nucleic acid phase under controlled flow conditions enables consistent production of well-defined LNPs [16].

This protocol describes a standardized microfluidic formulation workflow for LNP-mediated nucleic acid delivery, providing practical guidance on lipid preparation, particle assembly, quality control, and critical parameters influencing LNP performance.

2 Materials

2.1 Reagents

1. 14 kDa MWCO dialysis tubing (e.g., Spectrum Laboratories Inc. #132700).
2. 50 mL Falcon tubes.
3. 15 mL Falcon tubes.
4. 1.5 mL Eppendorf tubes.
5. Nuclease-free water.
6. 2 L wide-mouth bottles.
7. 0.9% (w/v) NaCl (9 g NaCl dissolved in 1 L Milli-Q water).
8. Milli-Q water.
9. 70% ethanol.
10. Absolute ethanol.
11. 100 mg/mL SM-102 lipid.
12. 20 mg/mL DSPC lipid.
13. 20 mg/mL Cholesterol.
14. 25 mg/mL DMG-PEG2000 lipid.
15. SpCas9 mRNA (or your cargo of interest).
16. 1 M Sodium acetate pH 4.5.
17. Ice.
18. IgniteTM NxGenTMcartridge (e.g., Cytiva #NIN0062).
19. 1 mL syringe (e.g., BraunTM #9161406V).
20. 3 mL syringe (e.g., BD, #309658).
21. 20 mL syringe.
22. Blunt fill needle (18 G).
23. Paired standard and weighted closures.

24. Parafilm.
25. Sterile 0.2 μm cellulose acetate syringe filter.
26. Sterile 0.2 μm non-pyrogenic filters.
27. Sucrose powder.
28. Phosphate-buffered saline (PBS, pH 7.4).
29. Quant-iT RiboGreen Assay kit (e.g., Invitrogen #R11490).
30. Triton X-100.
31. Black 96-well plate.
32. Tin foil.
33. DTS1070 cell and stoppers.
34. 20× TE buffer.

2.2 Equipment

1. Positive displacement pipettes.
2. Heating cabinet (37°C).
3. Laboratory scissors.
4. Thermomixer suitable for 1.5 mL Eppendorf tubes.
5. Mini benchtop centrifuge.
6. Benchtop vortex.
7. Microfluidic mixer (e.g., NanoAssemblr™ Ignite machine, Cytiva).
8. Sterile laminar flow hood.
9. Magnetic stirring bars and a magnet stirrer.
10. Plate reader (e.g., GloMax Discover, Promega).
11. Particle size quantification equipment (e.g., Zetasizer Ultra, Malvern).

3 Methods

In this protocol, we describe the generation of LNPs with SpCas9 mRNA as cargo. This protocol can also be applied to other nucleic acids, such as sgRNA. For generating LNPs with both SpCas9 mRNA and sgRNA, a 1:1 or 2:1 weight ratio between the Cas9 mRNA and the sgRNA was used.

3.1 Lipid Nanoparticle Formulation

3.1.1 Preparation Prior to Lipid Nanoparticle Formulation

1. Prepare a 14 kDa MWCO dialysis tubing by soaking a 5 cm piece of tube in a 50 mL Falcon tube with nuclease-free water for 20–30 min before use.

2. Prepare two 2-L solutions of 0.9% (w/v) NaCl and store at 4°C until use.
3. Prepare lipid stocks in absolute ethanol at the following concentrations (Table 1, *see* **Note 1**).
4. Calculate the required volumes for LNP formulation of each component for the lipid solution according to Table 2 (also *see* **Note 2**).
5. Calculate the required volumes of each component for the aqueous solution according to Table 3, using a nitrogen-to-phosphate (N/P) ratio of 5 (*see* **Note 2**).

Table 1
Preparation of lipid stocks, sealed with parafilm and saved at −20°C

Lipid	Molecular weight (μg/μmol)	Stock [mg/mL]
SM-102	710.2	100
DSPC	790.16	20
Cholesterol	386.65	20
DMG-PEG2000	2509.2	25

Table 2
Calculation of lipid volume according to a molar ratio of 50:10:39:1 for the four lipid types

Pipetting order	Lipid	Molar ratio	[μL]
1	Absolute ethanol, a final volume of 308 μL		60.9
2	SM-102	50	54.7
3	DSPC	10	60.8
4	Cholesterol	39	116.1
5	DMG-PEG2000	1	15.5
	Total volume		308

Table 3
Nucleic acid cargo required for the preparation of one batch of LNP using an NP ratio of 5

Calculations for aqueous solution	Volume (μL)
Cas9 mRNA [1 μg/μL]	495.9
1 M Sodium acetate [μL]	123.2
Nuclease-free water [μL], to a final of 1232 μL	612.9

3.1.2 Lipid Nanoparticle Formulation With NanoAssemblr Ignite Machine

1. Incubate lipid stock solutions at 37°C for at least 10 min before mixing.
2. Centrifuge lipid stocks briefly, vortex, and centrifuge briefly again. Ensure that no precipitation is present and that no lipids remain on the sides of the vials.
3. Prepare 308 μL of lipid solution in a 1.5 mL Eppendorf tube as described in Table 2. Add components in the listed order.
4. Place the lipid solution tube in a thermomixer at 37°C until use.
5. Thaw RNA (SpCas9 mRNA) on ice.
6. Mix RNA, sodium acetate, and nuclease-free water in a 1.5 mL Eppendorf tube according to Table 3.
7. Place the tube with the aqueous solution on ice.
8. Start the microfluidic mixing machine (e.g., NanoAssemble Ignite).
9. Clean the machine using 70% ethanol and leave the lid open to let it fully evaporate.
10. Place a 15 mL Falcon tube without a lid for waste collection and a second 15 mL Falcon tube for sample collection.
11. Check that the 15 mL Falcon tube holder can slide back and forth easily.
12. Place a new single-use cartridge in the cartridge holder.
13. Right before use, vortex the lipid solution, gently invert the aqueous solution, and briefly centrifuge both solutions.
14. Lipid solution: Using a 1 mL syringe with an 18 G needle, aspirate the entire volume and attach the syringe to the port on the right (*see* **Note 3**).
15. Aqueous solution: Using a 3 mL syringe with an 18 G needle, aspirate the entire volume and attach the syringe to the port on the left (*see* **Note 3**).
16. On the NanoAssemblr, create a protocol by:
    a. Selecting “recipes.”
    b. Selecting “edit recipe.”
    c. Adjusting syringes and volumes.
    d. Syringe C: bd3 (1.23 mL) and R: br1 (0.31 mL).
    e. Defining flow conditions: C (4.00) and R (1.00). Total volume 1.54 mL. Total flow rate: 5.00 mL/min.
    f. Setting “start waste” at 0.35 mL and “end waste” at 0.05 mL.
    g. Save and name the recipe.
17. Press “Run,” which takes less than 1 min.
18. Collect the LNP sample for dialysis.

3.1.3 Dialysis

1. Wash the inside of the dialysis tube with nuclease-free water using a 1000 µL pipette.
2. Attach a weighted closure to the bottom of the dialysis tube, then gently add the entire volume of LNP product using a 1000 µL pipette.
3. Close the dialysis tube with a non-weighted closure.
4. Attach a string of parafilm to the top closure of the dialysis tube, then place the tube in one of the 2-L containers containing NaCl solution.
5. Secure the parafilm to the edge of the container to prevent the dialysis tube from sinking.
6. Add a magnetic stirring bar and cover the opening with parafilm.
7. Place on a magnet stirrer at 4°C with gentle stirring.
8. After a few hours, replace the saline buffer with the second premade NaCl solution.
9. Cover the opening with parafilm and stir gently overnight at 4°C.

3.1.4 Filtering of Lipid Nanoparticles

1. Extract the LNP product from the dialysis tube using a 1000 µL pipette, then transfer it to a 1.5 mL Eppendorf tube.
2. Note the approximate volume of the LNP product in µL.
3. Carry out the following procedures in a sterile laminar flow hood.
4. Using a 3 mL syringe and needle, extract the LNP product from the Eppendorf tube.
5. Detach the needle from the syringe and ensure no excess air before attaching a sterile 0.2 µm cellulose acetate syringe filter.
6. Slowly filter the LNP product and collect it in a sterile 1.5 mL Eppendorf tube.

3.2 Quality Control of Lipid Nanoparticle Formulation

3.2.1 Preparation for Quant-iT RiboGreen Assay

1. Prepare a 1× TE buffer by adding 2.5 mL 20× TE buffer (provided in the Quant-iT RiboGreen Assay kit) to 47.5 mL nuclease-free water and mix well.
2. Prepare a 1× TE buffer with 2% Triton X-100 by adding 200 µL Triton X-100 to 9.8 mL 1× TE buffer and mixing well.
3. Prepare the RNA standard solution (provided in the Quant-iT RiboGreen Assay kit) to a working concentration of 4 µg/mL by adding 8.8 µL RNA standard to 211.2 µL 1× TE buffer.
4. Calculate the required dilution of the LNP sample needed for a 210 µL solution for use in the Quant-iT RiboGreen Assay (*see* **Note 4**).

Allow the RiboGreen dye (provided in the Quant-iT RiboGreen Assay kit) to thaw at room temperature, protected from light.

3.2.2 Concentration Measurement and Estimation of Encapsulation Efficiency With RNA Detection Kit

1. Using a black 96-well plate, prepare all samples in duplicate as follows
2. Prepare RNA standard to a final volume of 100 µL per well, as follows:
   a. Add 40 µL 1× TE buffer and 10 µL RNA standard.
   b. Add 45 µL 1× TE buffer and 5 µL RNA standard.
   c. Add 47.5 µL 1× TE buffer and 2.5 µL RNA standard.
   d. Add 49 µL 1× TE buffer and 1 µL RNA standard.
   e. Add 50 µL 1× TE buffer (blank control).
3. Bring all wells to 100 µL total volume with 1× TE buffer.
4. Prepare RNA standard with detergent conditions to a final volume of 100 µL per well, as follows:
   a. Add 50 µL RNA standard.
   b. Add 25 µL 1× TE buffer and 25 µL RNA standard.
   c. Add 45 µL 1× TE buffer and 5 µL RNA standard.
   d. Add 49 µL 1× TE buffer and 1 µL RNA standard.
   e. Add 50 µL 1× TE buffer (blank control).
5. Bring all wells to 100 µL total volume using 1× TE buffer containing 2% Triton X-100.
6. For measuring nonencapsulated RNA, add 50 µL of diluted LNP samples to 50 µL of 1× TE buffer.
7. For measuring total RNA, add 50 µL of diluted LNP samples to 50 µL of 1× TE buffer containing 2% Triton X-100.
8. Incubate the 96-well plate at room temperature for 10 min to allow complete LNP disruption in the Triton-containing wells.
9. Meanwhile, prepare a 1:200 dilution of the dye (provided in the Quant-iT RiboGreen Assay kit) in 1× TE buffer in a 5 mL Eppendorf tube wrapped in tin foil.
10. Add 100 µL of the diluted dye to each well in the 96-well plate.
11. Gently swirl the plate to mix the contents.
12. Incubate the 96-well plate for 2–5 min at room temperature in the dark by covering it with tin foil.
13. Turn on the plate reader.
    a. Open the program and choose “Fluorescence Quick Read” with the parameters: 475 nm Excitation, 500–550 nm Emission.

b. Click the door icon in the top-right corner and place the plate so that well A1 is in the corner marked "A1."
c. Remove the lid from the 96-well plate.
d. Measure the fluorescence intensity.
e. Export file, close the program, and shut down the plate reader.

14. Perform data analysis as follows:
15. Generate standard curves from the measurements of RNA standards prepared in 1× TE buffer and 1× TE buffer with 2% Triton X-100.
16. Calculate the RNA concentration from LNP samples measured in 1× TE (nonencapsulated RNA) and 1× TE buffer with 2% Triton X-100 (total RNA).
17. Determine encapsulated RNA by subtracting the measured concentration of 1× TE (nonencapsulated RNA) and 1× TE buffer with 2% Triton X-100 (total RNA).

3.2.3 Measurements of Size and ζ-Potential

1. *Prepare the DTS1070 cell, which allows for both size (hydrodynamic diameter, Z-Average (nm)) and* ζ-potential (surface charge, (mV)) measurements on the Zetasizer Ultra.
2. Attach two syringes (1 mL or 3 mL), one to the inlet and the other to the outlet of the cell, one filled with 70% ethanol and the other empty.
3. Rinse the cell thoroughly by repeatedly flushing 70% ethanol back and forth through the capillary.
4. Repeat the cleaning procedure in steps 2 and 3 using deionized water.
5. Carefully withdraw the remaining water to ensure that the capillary is free of residual liquid.
6. Set up the experiment and measure on the DLS machine (e.g., Zetasizer Ultra machine):
   a. Open the ZS Explore software on the computer and select "measure."
   b. Use the drop-down menu to select the cell DTS1070.
   c. Use the drop-down for materials to select "polystyrene latex."
   d. Use the drop-down menu for dispersant to select "water."
   e. Select "size" and set the number of runs to 3.
   f. Select "Zeta potential" and set the number of runs to 3.
   g. Set the measurement temperature to 25°C.

7. Dilute the LNP sample by gently mixing 20 μL of the LNP sample with 980 μL of nuclease-free water in a 1.5 mL Eppendorf tube.
8. Briefly spin the tube to collect all solutions to the bottom of the tube.
9. Aspirate the entire diluted LNP sample using a needle attached to a 3 mL syringe.
10. Detach the needle from the syringe and ensure that no air bubbles are present before attaching the syringe to the cell.
11. Invert the cell and slowly inject the sample from its syringe into the cell, filling the U-tube in the cuvette to just over halfway.
12. Turn the cell upright and continue injecting slowly until the liquid reaches the fill area.
13. Check for air bubbles in the cell; if so, tap gently to dislodge them.
14. Remove the syringe.
15. Attach stoppers to the inlet and outlet of the cell.
16. Insert the cell into the Zetasizer instrument and ensure that the Malvern logo faces toward the front of the instrument. Press down until the cell clicks into place.
17. Run the experiment by selecting "start method" in the ZS Explore software.

3.3 Storage of Lipid Nanoparticles

1. Make a 50% sucrose solution by weighing 20 g sucrose powder and transferring it to a 50 mL Falcon tube. Add 1× PBS pH 7.4 to 30–35 mL, put the lid on, and dissolve the sucrose by repeatedly inverting the tube or vortexing. Once dissolved, add PBS up to a final volume of 40 mL.
2. Carry out this and the following procedures in a sterile laminar flow hood.
3. Sterilize the sucrose solution by filtering the solution through a sterile 0.2 μm non-pyrogenic filter.
4. Mix nine parts LNPs with one part sterile 50% sucrose solution.
5. Aliquot the LNP samples to sterile Eppendorf tubes to avoid repeated freeze–thaw cycles.
6. Store the LNPs at −80°C (*see* **Note 5**).

4 Notes

1. Use positive displacement pipettes, if available, when working with lipid solutions.
2. Calculations for LNP formulation:
   To formulate a 1000 µL LNP batch with waste settings defined, $V_{\text{waste start}} = 350\ \mu\text{L}$ and $V_{\text{waste end}} = 50\ \mu\text{L}$ perform the following calculation to determine the required total volume. An additional 10% is included to account for potential losses during the process.

$$V_{\text{LNP}}\ (\mu\text{L}) = (V_{\text{LNP wanted}}\ (\mu\text{L}) + V_{\text{waste start}}\ (\mu\text{L}) + V_{\text{waste end}}\ (\mu\text{L}))$$

$$V_{\text{LNP}} = (1000\,\mu\text{L} + 350\,\mu\text{L} + 50\,\mu\text{L}) \cdot 1.1 = 1540\,\mu\text{L}$$

   The NanoAssemblr formulates the LNPs in a flow rate ratio of 1:4 (lipid solution: aqueous solution). Hence, the following volumes of the lipid and aqueous solution are required for the experiment:

$$V_{\text{Lipid}}\ (\mu\text{L}) = \frac{1}{5} \cdot V_{\text{LNP}}\ (\mu\text{L})$$

$$V_{\text{Lipid}}\ (\mu\text{L}) = \frac{1}{5} \cdot 1540\ \mu\text{L} = 308\ \mu\text{L}$$

$$V_{\text{Aqueous}}\ (\mu\text{L}) = \frac{4}{5} \cdot V_{\text{LNP}}\ (\mu\text{L})$$

$$V_{\text{Aqueous}}\ (\mu\text{L}) = \frac{4}{5} \cdot 1540\ \mu\text{L} = 1232\ \mu\text{L}$$

   The following calculations show the volume needed of each of the four lipid types for a given molar ratio. This is based on a wanted total lipid concentration of $c_{\text{lipid}} = 10\ \text{mM} = 0.010\ \frac{\mu\text{mol}}{\mu\text{L}}$. The amount of substance for all lipids is:

$$n_{\text{lipid}}\ (\mu\text{mol}) = c_{\text{lipid}} \left(\frac{\mu\text{mol}}{\mu\text{L}} \right) \cdot V_{\text{LNP}}\ (\mu\text{L})$$

The SM102 lipid constitutes 50% of the amount of substance:

$$\begin{aligned} & n_{\mathrm{SM102}}\ (\mu\mathrm{mol}) \\ & = 0.50 \cdot n_{\mathrm{lipid}}\ (\mu\mathrm{mol}) \\ & = 0.50 \cdot c_{\mathrm{lipid}} \left(\frac{\mu\mathrm{mol}}{\mu\mathrm{L}} \right) \cdot V_{\mathrm{LNP}}\ (\mu\mathrm{L}) \end{aligned}$$

With a stock solution of c_{SM102} for the SM102 lipid, another way of calculating the amount of substance is:

$$n_{\mathrm{SM102}}\ (\mu\mathrm{mol}) = \frac{c_{\mathrm{SM102}} \left(\frac{\mu\mathrm{g}}{\mu\mathrm{L}} \right) \cdot V_{\mathrm{SM102}}\ (\mu\mathrm{L})}{M_{\mathrm{SM102}} \left(\frac{\mu\mathrm{g}}{\mu\mathrm{mol}} \right)}$$

These equations for n_{SM102} can be combined as:

$$0.50 \cdot c_{\mathrm{lipid}} \left(\frac{\mu\mathrm{mol}}{\mu\mathrm{L}} \right) \cdot V_{\mathrm{LNP}}\ (\mu\mathrm{L}) = \frac{c_{\mathrm{SM102}} \left(\frac{\mu\mathrm{g}}{\mu\mathrm{L}} \right) \cdot V_{\mathrm{SM102}}\ (\mu\mathrm{L})}{M_{\mathrm{SM102}} \left(\frac{\mu\mathrm{g}}{\mu\mathrm{mol}} \right)}$$

And solved for V_{SM102}:

$$V_{\mathrm{SM102}}\ (\mu\mathrm{L}) = \frac{0.50 \cdot c_{\mathrm{lipid}} \left(\frac{\mu\mathrm{mol}}{\mu\mathrm{L}} \right) \cdot V_{\mathrm{LNP}}\ (\mu\mathrm{L}) \cdot M_{\mathrm{SM102}} \left(\frac{\mu\mathrm{g}}{\mu\mathrm{mol}} \right)}{c_{\mathrm{SM102}} \left(\frac{\mu\mathrm{g}}{\mu\mathrm{L}} \right)}$$

The molecular weight of SM102 is $M_{\mathrm{SM102}} = 710.2\ \frac{\mu\mathrm{g}}{\mu\mathrm{mol}}$, and the stock solution is $c_{\mathrm{SM102}} = 100\ \frac{\mu\mathrm{g}}{\mu\mathrm{L}}$ (see Table 1):

$$V_{\mathrm{SM102}} = \frac{0.50 \cdot 0.010\ \frac{\mu\mathrm{mol}}{\mu\mathrm{L}} \cdot 1540\,\mu\mathrm{L} \cdot 710.2\ \frac{\mu\mathrm{g}}{\mu\mathrm{mol}}}{100\ \frac{\mu\mathrm{g}}{\mu\mathrm{L}}} = 54.7\,\mu\mathrm{L}$$

Similar calculations can be performed for DSPC, cholesterol, and DMG-PEG2000, with the molecular weights and stock solutions stated in Table 1.

As shown in Table 2, the volumes of the different lipid solutions are summarized, and the remaining volume $V_{\mathrm{Lipid}} = 308\ \mu\mathrm{L}$ consists of absolute ethanol.

$$V_{\text{absolute ethanol}}\ (\mu\text{L}) = V_{\text{Lipid}}\ (\mu\text{L}) - V_{\text{SM102}}\ (\mu\text{L}) - V_{\text{DSPC}}\ (\mu\text{L}) - V_{\text{cholesterol}}\ (\mu\text{L}) - V_{\text{DMG-PEG2000}}\ (\mu\text{L})$$

$$\begin{aligned} V_{\text{absolute ethanol}} &= 308\ \mu\text{L} - 54.7\ \mu\text{L} - 60.8\ \mu\text{L} - 116.1\ \mu\text{L} \\ &\quad - 15.5\ \mu\text{L} \\ &= 60.9\ \mu\text{L} \end{aligned}$$

The amount of RNA, SpCas9 mRNA, is determined by the N/P ratio, here set to 5. N units are the number of protonatable amine groups per ionizable lipid (1 per lipid). P units are the effective number of phosphate groups per nucleic acid in the RNA (1 per nucleic acid). For an N/P ratio of 5, the amount of substance of SM102 must be five times that of nucleic acid:

$$n_{\text{SM102}}\ (\mu\text{mol}) = 5 \cdot n_{\text{nucleic acid}}\ (\mu\text{mol})$$

Or

$$n_{\text{nucleic acid}}\ (\mu\text{mol}) = \frac{n_{\text{SM102}}\ (\mu\text{mol})}{5}$$

The amount of substance of nucleic acid is:

$$n_{\text{nucleic acid}}\ (\mu\text{mol}) = \frac{m_{\text{nucleic acid}}\ (\mu\text{g})}{M_{\text{nucleic acid}}\left(\frac{\mu\text{g}}{\mu\text{mol}}\right)}$$

Combining these equations gives:

$$\frac{m_{\text{nucleic acid}}\ (\mu\text{g})}{M_{\text{nucleic acid}}\left(\frac{\mu\text{g}}{\mu\text{mol}}\right)} = \frac{n_{\text{SM102}}\ (\mu\text{mol})}{5}$$

Solving for the amount of nucleic acid needed:

$$m_{\text{nucleic acid}}\left(\mu\text{g}\right) = \frac{n_{\text{SM102}}\ (\mu\text{mol})}{5} \cdot M_{\text{nucleic acid}}\left(\frac{\mu\text{g}}{\mu\text{mol}}\right)$$

The equation for n_{SM102} from earlier can be used:

$$m_{\text{nucleic acid}}\left(\mu\text{g}\right) = \frac{0.50 \cdot c_{\text{lipid}}\left(\frac{\mu\text{mol}}{\mu\text{L}}\right) \cdot V_{\text{LNP}}\ (\mu\text{L})}{5} \cdot M_{\text{nucleic acid}}\left(\frac{\mu\text{g}}{\mu\text{mol}}\right)$$

An average molecular weight of $M_{\text{nucleic acid}} = 322\ \frac{\mu\text{g}}{\mu\text{mol}}$ is used:

$$m_{\text{nucleicacid}} = \frac{0.50 \cdot 0.010\ \frac{\mu\text{mol}}{\mu\text{L}} \cdot 1540\,\mu\text{L}}{5} \cdot 322\ \frac{\mu\text{g}}{\mu\text{mol}} = 495.9\,\mu\text{g}$$

Using a SpCas9 stock concentration of 1.0 µg/µL (theoretical number), the needed volume is:

$$V_{\text{nucleic acid}}\ (\mu\text{L}) = \frac{m_{\text{nucleic acid}}\ (\mu\text{g})}{c_{\text{nucleic acid}}\left(\frac{\mu\text{g}}{\mu\text{L}}\right)}$$

$$V_{\text{nucleic acid}}\ (\mu\text{L}) = \frac{495.9\ \mu\text{g}}{1.0\ \frac{\mu\text{g}}{\mu\text{L}}} = 495.9\ \mu\text{L}$$

The sodium acetate 1 M is added with a dilution factor of 10:

$$V_{\text{sodium acetate}}\ (\mu\text{L}) = \frac{1}{10} \cdot V_{\text{Aqueous}}\left(\mu\text{L}\right)$$

$$V_{\text{sodiumacetate}} = \frac{1}{10} \cdot 1232\,\mu\text{L} = 123.2\,\mu\text{L}$$

And the remaining volume consists of nuclease-free water:

$$V_{\text{nuclease-free water}}\ (\mu\text{L}) = V_{\text{Aqueous}}\ (\mu\text{L}) - V_{\text{nucleic acid}}\ (\mu\text{L}) - V_{\text{sodium acetate}}\left(\mu\text{L}\right)$$

$$V_{\text{nuclease-free water}} = 1232\ \mu\text{L} - 495.9\ \mu\text{L} - 123.2\ \mu\text{L} = 612.9\ \mu\text{L}$$

3. Ensure no excess air in the syringe before attaching it to the machine.
4. In our experience, a concentration of 0.005 µg/µL is fitting with the RNA standard. Using this equation to calculate the

volume of LNP sample required for a final concentration of 0.005 µg/µL in 210 µL solution.

$$V_{\text{LNPsample}}\,(\mu\text{L}) = \frac{c_{\text{wanted}}\left(\frac{\mu\text{g}}{\mu\text{L}}\right) \cdot V_{\text{1xTE-buffer}}\,(\mu\text{L})}{c_{\text{theoretical}}\left(\frac{\mu\text{g}}{\mu\text{L}}\right)}$$

The theoretical concentration is calculated based on the amount of packaging RNA (in this case, 495.9 µg SpCas9 mRNA) and the noted volume of the LNP product after dialysis (1300 µL theoretical number) from Sect. 3.1.4.2.

$$V_{\text{LNPsample}} = \frac{0.005\,\frac{\mu\text{g}}{\mu\text{L}} \cdot 210\,\mu\text{L}}{\frac{495.9\,\mu\text{g}}{1300\,\mu\text{L}}} = 2.75\,\mu\text{L}$$

Add this to a 1× TE buffer volume of:

$$V_{\text{1x TE-buffer}}\left(\mu\text{L}\right) = V_{\text{total}}\left(\mu\text{L}\right) - V_{\text{LNP sample}}\left(\mu\text{L}\right)$$

$$V_{\text{1x TE-buffer}} = 210\ \mu\text{L} - 2\,.75\ \mu\text{L} = 207\,.25\ \mu\text{L}$$

The LNP sample is diluted in 1× TE buffer in a sterile laminar flow hood.

5. For short time storage, the LNP solution could be saved 4°C up to one week. Keeping the LNP solution at 4°C for over 1 week will lead to LNP particle aggregation and a decrease in efficiency. We observed that the size of LNP will increase upon increasing storage time at 4°C, and a decrease in CRISPR editing efficiency.

Acknowledgments

The publication is based upon work by COST Action CA21113: Genome Editing for the Treatment of Human Diseases (https://www.genehumdi.eu), supported by European Cooperation in Science and Technology (COST). This project is supported by the Lundbeck Foundation (R396-2022-350). The figure is created in BioRender. Luo, Y. (2026). https://BioRender.com/7vx1960.

Competing Interests The authors declare no competing interests.

References

1. Hou X, Zaks T, Langer R, Dong Y (2021) Lipid nanoparticles for mRNA delivery. Nat Rev Mater 6(12):1078–1094. https://doi.org/10.1038/s41578-021-00358-0
2. Pavlin N et al (2025) Analysis of lipid nanoparticles using two-dimensional chromatography: simultaneous determination of encapsulation efficiency, nucleic acid integrity, and size of LNP formulations. J Chromatogr B 1265:124751. https://doi.org/10.1016/j.jchromb.2025.124751
3. Makkar SK (2025) Advances in RNA-based therapeutics: current breakthroughs, clinical translation, and future perspectives. Front Genet 16. https://doi.org/10.3389/fgene.2025.1675209
4. Wang C et al (2023) Emerging non-viral vectors for gene delivery. J Nanobiotechnol 21(1):272. https://doi.org/10.1186/s12951-023-02044-5
5. Li M et al (2024) Lipid nanoparticles outperform electroporation in delivering therapeutic HPV DNA vaccines. Vaccines 12(6):666
6. Gillmore JD et al (2021) CRISPR-Cas9 *in vivo* gene editing for transthyretin amyloidosis. N Engl J Med 385(6):493–502. https://doi.org/10.1056/NEJMoa2107454
7. Musunuru K et al (2025) Patient-specific *in vivo* gene editing to treat a rare genetic disease. N Engl J Med 392(22):2235–2243. https://doi.org/10.1056/NEJMoa2504747
8. Chatterjee S, Kon E, Sharma P, Peer D (2024) Endosomal escape: a bottleneck for LNP-mediated therapeutics. Proc Natl Acad Sci USA 121(11):e2307800120. https://doi.org/10.1073/pnas.2307800120
9. Wang J et al (2024) Recent advances in lipid nanoparticles and their safety concerns for mRNA delivery. Vaccines (Basel) 12(10) https://doi.org/10.3390/vaccines12101148
10. Johansson JM et al (2025) Cellular and biophysical barriers to lipid nanoparticle mediated delivery of RNA to the cytosol. Nat Commun 16(1):5354. https://doi.org/10.1038/s41467-025-60959-z
11. Hosseini-Kharat M, Bremmell KE, Prestidge CA (2025) Why do lipid nanoparticles target the liver? Understanding of biodistribution and liver-specific tropism. Mol Ther Methods Clin Dev 33(1):101436. https://doi.org/10.1016/j.omtm.2025.101436
12. Tafech B, Mohabatpour F, Hedtrich S (2024) Surface modification of lipid nanoparticles for gene therapy. J Gene Med 26(1):e3642. https://doi.org/10.1002/jgm.3642
13. Hashiba K et al. (2023) Branching ionizable lipids can enhance the stability, fusogenicity, and functional delivery of mRNA. Small Sci 3(1):2200071. https://doi.org/10.1002/smsc.202200071
14. Zhang L et al. (2025) Role of PEGylated lipid in lipid nanoparticle formulation for *in vitro* and *in vivo* delivery of mRNA vaccines. J Control Release 380:108–124. https://doi.org/10.1016/j.jconrel.2025.01.071
15. Cheng Q et al. (2020) Selective organ targeting (SORT) nanoparticles for tissue-specific mRNA delivery and CRISPR–Cas gene editing. Nat Nanotechnol 15(4):313–320. https://doi.org/10.1038/s41565-020-0669-6
16. Seo H, Jeon L, Kwon J, Lee H (2023) High-precision synthesis of RNA-loaded lipid nanoparticles for biomedical applications. Adv Healthc Mater 12(13):2203033. https://doi.org/10.1002/adhm.202203033

Open Access This chapter is licensed under the terms of the Creative Commons Attribution-NonCommercial-NoDerivatives 4.0 International License (http://creativecommons.org/licenses/by-nc-nd/4.0/), which permits any noncommercial use, sharing, distribution and reproduction in any medium or format, as long as you give appropriate credit to the original author(s) and the source, provide a link to the Creative Commons license and indicate if you modified the licensed material. You do not have permission under this license to share adapted material derived from this chapter or parts of it.

The images or other third party material in this chapter are included in the chapter's Creative Commons license, unless indicated otherwise in a credit line to the material. If material is not included in the chapter's Creative Commons license and your intended use is not permitted by statutory regulation or exceeds the permitted use, you will need to obtain permission directly from the copyright holder.





Chapter 11

CRISPR/Cas9 Delivery Using Extracellular Vesicles

Peter Pečan and Mateja Manček-Keber

Abstract

Extracellular vesicles (EVs), particles released from cells, have the potential to become an important in vivo delivery vehicle for CRISPR machinery. Unlike viral vectors such as Adeno-associated virus (AAV), EVs reduce risks associated with immunogenicity, long-term expression, and potential off-target effects. EVs can efficiently deliver CRISPR/Cas9 ribonucleoprotein (RNP) complexes, which provide transient, ready-to-function editing machinery with reduced off-target risk compared with plasmid DNA or mRNA delivery. RNP loading into EVs can occur without specific targeting signals, although strategies such as membrane anchoring, inducible dimerization systems, or fusion with EV-associated proteins can enhance cargo enrichment. EVs are typically produced by transfecting producer cells with plasmids encoding Cas9 and sgRNA, followed by vesicle release into culture media. Purification requires removal of cellular debris and enrichment of vesicles using methods such as ultracentrifugation, ultrafiltration, chromatography, or precipitation. As no single gold-standard purification approach exists, method selection should balance yield and purity, and characterization using vesicle markers and size distribution profiling is recommended.

Keywords Extracellular vesicles, Exosomes, Microvesicles, In vivo delivery, CRISPR/Cas9, Ultracentrifugation

1 Introduction

The successful development of genome editing treatment using CRISPR machinery undoubtedly involves the development of a targeted delivery vehicle. A major drawback of viral delivery (e.g., AAV) is its immunogenic nature, the ability to induce inflammatory and adverse immunogenic responses. Also importantly, viral delivery relies on genomic integration, long-lasting expression, and increased probability of off-target effects. To avoid or reduce some of these effects, new delivery vehicles are being developed: extracellular vesicles (EVs), virus-like particles (VLPs), and lipid nanoparticles (LNPs) (reviewed in [1]. All three delivery systems are compatible with ribonucleoprotein (RNP) delivery, EVs, and LNPs; however, they can also be used to deliver nucleic acids (e.g., mRNA or plasmid DNA) as well. RNPs, over plasmid DNA and mRNA, provide

Duško Lainšček et al. (eds.), *CRISPR Delivery*, Methods in Molecular Biology, vol. 3075,
https://doi.org/10.1007/978-1-0716-5547-4_11,
© The Author(s) 2027

ready-to-go functional complexes, with short half-life and low chance of off-target effects. All three systems also differ in the principles of their loading. RNPs loading into EVs do not need specific signals [2, 3], though some of them improve the packaging [4–7]. In the VLP system, Cas9 needs to be fused to a structural protein, such as Gag [7], to be actively recruited to VLPs. Also, loading of RNPs to LNPs requires additional modifications of lipid composition and loading conditions to ensure RNP encapsulation and stability [8].

There have already been more than 15 publications on using EVs as a delivery system of CRISPR/Cas9. EVs are cell-released particles delimited by a lipid bilayer, with a size of virus or bacteria (30 nm–1 μm). Due to their diversity, EVs' nomenclature according to MISEV2018 is preferentially based on their clear measurable common feature, most commonly the size (small EVs, medium/large EVs, and large EVs), unless the authors can establish reliable specific markers of subcellular origin [9]. On the basis of EV origin, small EVs are almost exclusively exosomes (30–150 nm), and medium/large and large EVs are ectosomes (further divided to microvesicles and apoptotic bodies): [1] exosomes originate as intraluminal vesicles formed through complex endosomal pathways. Exosomes mature into multivesicular bodies (MVBs) by inward budding and are released when MVBs fuse with the plasma membrane [2]; microvesicles are formed from plasma membrane budding and released from the cell surface; [3] apoptotic bodies are formed in the process of apoptosis due to cell fragmentation and are excluded as a suitable delivery vehicle. Neither the size nor the EV origin is sufficient to isolate a certain type of EVs. Due to diverse cell formation and release, EVs contain different combinations of cytosolic and membrane proteins, proteins of the cytoskeleton, stress, and transport, which are not EV-type specific.

One of the most important features of EVs that is being exploited in CRISPR delivery is the ability of EVs to deliver diverse molecules to distinct tissues and organs. As highly flexible vehicles in these terms, they also enable in vivo studies of their biodistribution and determination of specific target cells. The lipid bilayer protects the cargo from digestion. How the cargo is being sorted to EVs is still not fully resolved, but transfecting the EV-producing cells with plasmids encoding Cas9 and cognate sgRNA is sufficient for loading RNP into EVs [2, 3]. However, diverse possibilities to enrich RNPs in EVs have been described. To improve loading efficiency, Cas9 was added a myristoylation signal [7], or it was anchored to vesicle-enriched transmembrane proteins usually through dimerization. Split-GFP system was used to co-encapsulate vesicular stomatitis virus G protein (VSV-G) with Cas9 in EVs 5), and CD63–GFP and Cas9–GFP nanobody to enrich RNPs in exosomes [6]. More efficient cargo loading was also demonstrated by using an inducible dimerization system, where a membrane-associated protein containing the DmrA

domain was physically associated with the DmrC domain present on the Cas9 RNP after addition of rapamycin analog [4].

EVs for Cas9 RNP delivery are produced in cell cultures following transfection of relevant plasmid DNA. EVs are released into the medium, which is then collected. There is no gold standard for EV isolation and purification. The first step in EV isolation is the removal of cell debris, which is achieved by low-speed centrifugation. There are several possibilities for the method of EV purification: ultracentrifugation, ultrafiltration, chromatography, and precipitation. Each technique has its strengths and drawbacks in terms of EV purity and yields, so the choice of method depends on the desired product and application. It is also important to note that each technique enriches a certain type of vesicle population; detection of specific molecular markers and size distribution profiles is recommended.

2 Materials

2.1 EV-Associated Work

2.1.1 Reagents

1. Human embryonic kidney (HEK) 293T cells (ATTC).
2. Dulbecco's Modified Eagle's Medium (DMEM) supplemented with 10% heat-inactivated fetal bovine serum (FBS).
3. Dulbecco's Modified Eagle's Medium (DMEM) supplemented with 10% heat-inactivated exosome-depleted fetal bovine serum (FBS).
4. Phosphate-buffered saline (PBS).
5. Trypsin–EDTA solution.
6. 0.4% Trypan blue solution.
7. Dimethyl sulfoxide (DMSO).
8. Plasmids for CRISPR/Cas9 system expression (e.g., pgRNA-humanized and pDNA Cas9 expressing)
9. Polyethyleneimine (PEI), linear, MW 25,000.
10. 150 mM NaCl.
11. Antibodies: rabbit anti-CD63 (diluted 1:1000; Santa Cruz), mouse anti-CRISPR-Cas9 (diluted 1:500; Abcam), mouse anti-Tsg101 (diluted 1:1000; Santa Cruz), rabbit anti-calnexin (diluted 1:500; Abcam), rabbit anti-alpha/beta tubulin (diluted 1:1000; Cell Signaling Technology). Secondary Ab goat polyclonal anti-rabbit IgG-HRP (diluted 1:4000; Abcam), goat anti-mouse IgG-HRP (diluted 1:4000; Santa Cruz).
12. Total protein quantification kit (e.g., QuantiPRO BCA assay kit or equivalent).

13. 60 w/V % iodixanol in distilled water (OptiPrep™).
14. 0.25 M sucrose buffer: 6 mM EDTA and 60 mM Tris-HCl, pH7.4.
15. 4× SDS sample buffer.
16. Any kD™ Mini-PROTEAN® TGX™ precast polyacrylamide gels (or equivalent).
17. SDS electrophoresis buffer.
18. WB transfer buffer: 25 mM Tris, 192 mM glycine, 20 % methanol, pH 8.3.
19. Nitrocellulose membrane (pore size 0.45 μm) (or equivalent).
20. Filter papers.
21. 0.2% (m/v) I-BLOCK (or equivalent).
22. PBS + 0.01% Tween 20 buffer (or equivalent).
23. Super Signal West Pico Chemiluminescent Substrate (or equivalent).

2.1.2 Equipment

1. Biosafety cabinet (class II, Type A or B)
2. Automated cell counter (or equivalent—hemocytometer or microscope).
3. T-75 tissue culture flask (treated for adherent cells).
4. 10 cm tissue culture-treated dish.
5. Individually wrapped sterile serological pipettes.
6. Benchtop centrifuge.
7. 1.5 ml microtubes.
8. Conical sample tubes (15 ml and 50 ml; sterile)
9. Humidified CO_2 incubator.
10. Ultracentrifuge (UC).
11. Beckman Colter ultracentrifuge rotors 50Ti or 42.1 (or equivalent).
12. Polypropylene ultracentrifuge tubes (13.2 ml and 35.5 ml; sterile)
13. Inverted light microscope.
14. Nanoparticle tracking analysis (NTA) device (or equivalent).
15. Microplate reader SynergyMx (or equivalent).
16. Spectrophotometer.
17. Mini-PROTEAN Vertical Electrophoresis Cell (or equivalent).
18. Mini Trans-Blot® Electrophoretic Transfer Cell (or equivalent).
19. G:BOX documentation and analysis system with GeneTools program (or equivalent).

2.2 In Vivo Tracking and Quantification of Genome Editing

2.2.1 Reagents

1. BALB/c mice or any other strain.
2. DiD (1,1′-Dioctadecyl-3,3,3′,3′-Tetramethylindodicarbocyanine Perchlorate) oil.
3. UC isolated extracellular vesicles.
4. Sterile phosphate buffer solution.
5. 0.2 μm filters.
6. 27 G needles, placed on 1 ml syringe.
7. 70% ethanol or any other disinfectant.
8. Isoflurane.
9. Eye ointment.
10. Petri dish.
11. T7E1 endonuclease.
12. Genomic DNA isolation kit (DNeasy Blood and Tissue Kit (Qiagen) or any equivalent).
13. PCR primers for the amplification of the genomic region of interest.
14. 10%–15% native PAGE gel.
15. SYBR Gold DNA stain.
16. KAPA HiFi HotStart Ready Mix for PCR amplification (or any equivalent).
17. PCR Cleanup kit (NEB or any equivalent).
18. NEB 2.1 buffer.

2.2.2 Equipment

1. Inhalation anesthesia system.
2. Heated surgical table.
3. IVIS® Lumina LT Series III Imaging system with integrated 150 W Tungsten/Halogen Lamp for fluorescence detection (PerkinElmer) or equivalent.
4. Living Image® 4.7.2 Software (PerkinElmer) or equivalent.
5. Tissue homogenizer (IKA or equivalent).
6. PCR Thermal Cycler machine.
7. G:BOX documentation and analysis system with GeneTools program (or equivalent).
8. Scissors and forceps.
9. 10 ml Falcon tubes.
10. ImageJ software.

3 Methods

3.1 General Maintenance of Cell Line

Here, we describe general guidance for the maintenance of adherent HEK293 cells. All protocols involving cells should be performed under sterile conditions in a laminar flow hood.

1. Thaw the vial containing the cells in a 37°C water bath or put the vial for 2 min to 37°C preheated thermoblock.
2. Rapidly transfer thawed cells to a conical tube (15 ml) containing 10 ml of prewarmed DMEM supplemented with 10% FBS.
3. Centrifuge cells at 300 × *g* for 5 min.
4. Discard the cell supernatant, resuspend the cell pellet in prewarmed 10 mL DMEM supplemented with 10% FBS, and transfer the cell suspension to a T-75 flask.
5. Incubate the cells at 37°C and 5% CO_2 in a humidified incubator, and when they reach approximately 90% confluence, pass the cells.
6. Remove the spent culture media and wash cells with the 10 ml PBS (*see* **Note 1**).
7. Discard the PBS from the flask, add 2 ml of trypsin–EDTA solution, and wait for the cells to detach from the flask surface.
8. Once detached, add 8–10 ml of DMEM supplemented with 10% FBS to inactivate the trypsin and transfer the cells into a conical tube (15 ml).
9. Centrifuge the cells at 300 × *g* for 5 min.
10. Discard the supernatant and resuspend the cell pellet in 10 ml of DMEM supplemented with 10% FBS.
11. Dilute the sample of cell suspension in a 1:1 ratio (v/v) with trypan blue vital stain and count live (unstained) and dead (stained) cells using an automated cell counter.
12. For subculturing the cells, seed them in a T-75 tissue culture flask at a concentration of $2–3 \times 10^5$ cells/ml in as many flasks as necessary (*see* **Note 2**) or follow Sect. 3.2, for plating cells for transfection.
13. To maintain the cell line (*see* **Note 3**).

3.2 Extracellular Vesicles Production

Here, we describe a protocol for EV production by transient transfection of HEK293 cells with plasmids for Cas9 and sgRNA.

1. Seed ten 10 cm culture dishes (*see* **Note 4**) with 4×10^6 HEK293 cells per dish in 10 ml DMEM supplemented with 10% exosome-depleted FBS.

2. Incubate the cells overnight at 37°C and 5% CO_2 in a humidified incubator to achieve approximately 80%–90% confluency.
3. Prepare transfection mixture in two 15 ml conical tubes (amount for one 10 cm culture dish):
   a) **Tube 1** (plasmid mixture): dilute the plasmids (e.g., 10 μg pCMV-dCas9-VPR, 10 μg pgRNA—total amount of 20 μg) in 150 mM NaCl to a total volume of 500 μl (*see* **Note 5**).
   b) **Tube 2** (transfection reagent): Dilute PEI in 500 μL 150 mM NaCl. Generally, for 1 μg of plasmid DNA mixture, 6–12 μL of PEI solution will be required.
4. Pipette the solution from tube 2 to the solution in tube 1, vortex the conical tube, and incubate for 20–30 min at room temperature, then pipette the solution dropwise into the dish containing HEK293 cells. To evenly distribute the transfection mixture, gently swirl the dish back and forth (*see* **Note 5**).
5. Incubate the cells at 37°C and 5% CO_2 in a humidified incubator for 24 h.

3.3 Extracellular Vesicle Purification

3.3.1 Total EV Purification

Here, we describe total EV purification. If you want to separate small EVs (e.g., exosomes) from medium/large EVs (e.g., microvesicles) using ultracentrifugation, follow Sect. 3.3.2. after point 2. If you want to separate EVs depending on density follow follow Sect. 3.3.3, point 10.

1. Harvest the supernatant, containing EVs, in conical tubes (50 ml).
2. Centrifuge the supernatant at 800 × *g* for 15 min to pellet the cells and remove cell debris.
3. Collect the supernatant by using sterile serological pipettes (*see* **Note 6**) and transfer the supernatant to ultracentrifuge tubes.
4. Balance the ultracentrifuge tubes to within 0.1 g and centrifuge at 100,000 × *g* (42.1 or SW32Ti rotor) for 1 h at 4°C.
5. Pour the supernatant from the ultracentrifuge tube into a waste bottle. The EV pellet should be visible at the bottom of the tube.
6. Add 10 ml of cold PBS and wash the pellet.
7. Ultracentrifuge again at 100,000 × *g* for 1 h at 4°C.
8. Remove the supernatant and resuspend the pellet in 100 μl of PBS by gently pipetting up and down multiple times.

9. Collect the EVs and determine the EV concentration using the BCA QuantiPRO BCA assay kit.
10. Store the sample at 4°C (*see* **Note 7**).

3.3.2 Separation of Small EVs and Medium/large EVs (see Note 8)

1. After the removal of cell pellet and debris (point 2 in Sect. 3.3.1), collect the supernatant by using sterile serological pipettes (*see* **Note 6**) and transfer the supernatant to conical tubes (50 ml).
2. Centrifuge at 10,000 × *g* (SW32Ti rotor) for 1 h at 4°C (*see* **Note 8**).
3. The pellet contains an enriched fraction of medium/large EVs.
4. Collect the supernatant by using sterile serological pipettes (*see* **Note 9**) and transfer the supernatant to ultracentrifuge tubes.
5. Balance the ultracentrifuge tubes to within 0.1 g and centrifuge at 100,000 × *g* (SW32Ti rotor) for 1 h at 4°C.
6. Pour the supernatant from the ultracentrifuge tube into a waste bottle. The enriched small EV pellet should be visible at the bottom of the tube.
7. Add 10 ml of cold PBS and wash the pellet.
8. Ultracentrifuge again at 100,000 × g for 1 h at 4°C.
9. Remove the supernatant and resuspend the small EV pellet in 100 µl of PBS by gently pipetting up and down multiple times.
10. Collect the EVs and determine the small EV and medium/large EV concentration using the BCA QuantiPRO BCA assay kit.
11. Store the samples at 4°C.

3.3.3 Density Gradient Ultracentrifugation (DGUC) of EVs

Density gradient ultracentrifugation is a purification technique used to separate EVs on their physical properties (density, size, and shape) with high reproducibility. Here we describe DGUC, which can be used to either further purify the EVs (*see* **Note 10**) or to more closely analyze the EVs in terms of their origin (e.g., coexistence of specific markers and RNPs determined by subsequent immunoblotting; see Sect. 3.4).

1. Dilute 60 w/V % iodixanol to 40, 20, 10, and 5% in 0.25 M sucrose buffer.
2. Layer 3.0 ml of 40% solution on the bottom of a 13.5 ml ultracentrifuge tube.
3. Take a UC tube and a 1 ml pipette and hold the tube angled (approximately 20°–40°).

4. Pipette 3.0 ml of 20% solution on top of 40% iodixanol solution slowly and carefully. Do not touch the previous layer.
5. Pipette 3.0 ml of 10% solution on top of 20% iodixanol solution slowly and carefully. Do not touch the previous layer.
6. Pipette 2.5 ml of 5% solution on top of 10% iodixanol solution slowly and carefully. Do not touch the previous layer.
7. Slowly return the tube to the vertical position (*see* **Note 11**).
8. On the top, put 0.5 ml of isolated EVs (*see* **Note 12**).
9. Put the UC tubes into the precooled rotor and balance the tubes.
10. Ultracentrifuge at 100,000 × *g* for 16 h at 4°C.
11. Collect 1 ml fractions of density gradient layers from the top (fr. 1–fr. 9).
12. Analyze fractions for protein content by BCA assay using QuantiPRO BCA Assay kit.
13. To measure the density of fractions, 100 µl of the fractions are diluted with 100 µl of water and put on a 96-well plate in triplicate. Add also 5% (1.054 g/ml), 10% (1.079 g/ml), 20% (1.127 g/ml), and 40% (1.211 g/ml) iodixanol standards for the calibration curve (*see* **Note 13**).
14. Measure the absorbance at 340 nm with a microplate reader.
15. Calculate the density of samples based on their iodixanol concentration.
16. Keep fractions at 4°C or store at −80°C before use.

3.4 Determination of EV Markers Using Immunodetection

For the detection of Cas9 and EV markers (small EVs and medium/large EVs) within different EV samples and EV density fractions, SDS PAGE and Western blot can be performed, and Cas9, Tsg101, CD63, and/or calnexin can be detected.

1. Mix 30 µg of proteins in the isolated EV sample and an appropriate amount of 4× SDS reducing sample buffer. Heat the samples for 5 min at 95°C.
2. Or mix 100 µl of each density fraction with 30 µl 4× SDS reducing sample buffer (*see* **Note 14**). Heat the samples for 5 min at 95°C.
3. Load the samples onto a precast polyacrylamide gel.
4. Prepare the Mini-PROTEAN Vertical Electrophoresis Cell.
5. Run the electrophoresis in SDS electrophoresis buffer at 200 V for 60 min.
6. Rinse the polyacrylamide gel with water and soak it in WB transfer buffer.

7. Soak the nitrocellulose membrane, the filter papers, and the fiber pads in WB transfer buffer.
8. Prepare the cassette for Mini Trans-Blot® Electrophoretic Transfer Cell in cooled WB transfer buffer.
9. Perform the WB transfer for 1.5 h at 350 mA.
10. Wash the membrane with water and incubate for 1 h while shaking at room temperature using 0.2% (m/v) of I-BLOCK to block the free binding sites on the membrane.
11. Incubate the nitrocellulose membrane for 3 h while shaking at room temperature with appropriate dilutions of primary antibody (anti-Cas9, anti-Tsg101, anti-CD93, anti-calnexin, or anti-tubulin) in 0.2% (m/v) of I-BLOCK.
12. Wash the membrane three times for 5 min in PBS + 0.01% Tween 20 buffer while shaking.
13. Incubate the membrane with appropriate secondary antibody (anti-mouse or anti-rabbit) conjugated with HRP in 0.2% (m/v) of I-BLOCK at room temperature for 1 h while shaking.
14. Wash the membrane three times for 5 min in PBS + 0.01% Tween 20 buffer while shaking.
15. Coat the membrane for 5 min at room temperature with Super Signal West Pico Chemiluminescent Substrate.
16. Remove the reagent by touching the paper.
17. Place the membrane in a G: BOX system and analyze the image in the GeneTools program (Fig. 1).

3.5 Tissue and Organ Tracking of Extracellular Vesicles

Here, we describe DiD-labeled EV injection as an in vivo fluorescence imaging model, the process of obtaining the whole body in vivo fluorescent signals, and ex vivo organ imaging. All animal experiments must be performed according to the national legislation upon obtaining an appropriate permit, with emphasis on FELASA recommendations and the 3 R rule. All procedures on animals should be performed using a minimal invasive approach, whereas injections should be administered aseptically and under general anesthesia, offering supportive care when appropriate.

3.5.1 Labeling of EVs with DiD

1. Add 1 μM DiD oil in PBS to UC isolated EVs.
2. Stain for 10 min at room temperature, protected from light.
3. Add 10 ml of PBS.
4. Ultracentrifuge for 1 h at 100,000 × *g* at 4°C.
5. Resuspend the pellet in PBS.
6. Analyze for protein content by BCA assay using QuantiPRO BCA Assay kit.

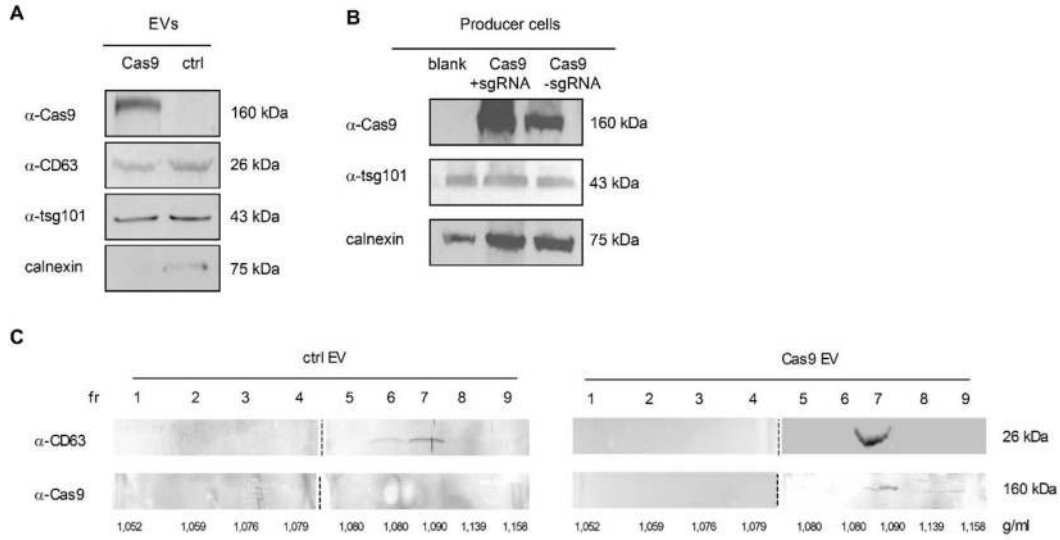


Fig. 1 Generation of the EVs for CRISPR delivery and its efficiency in functional CRISPR/Cas9 delivery. (**A**) HEK293 cells were transiently transfected with the Cas9/sgRNA plasmid vector for 24 h. EVs were subjected to immunoblot analysis using antibodies against Cas9, CD63, tsg101 (an extracellular vesicle marker), and against calnexin, an apoptotic bodies marker. A representative image from three independent experiments is shown. (**B**) HEK293, blank, and GEDEX producing cells (cells that were transiently transfected with Cas9 with or without the sgRNA plasmid vector for 24 h) were lysed and immunoblotted against Cas9, tsg101, and calnexin. (**C**) Extracellular vesicles were purified using an OptiPrepTM density gradient ultracentrifugation. Fractions of Ctrl and Cas9 EVs were immunoblotted against Cas9 protein and CD63 protein, an EV marker. Also, the specific density of fractions was determined. The dashed line presents merged blots (2)

3.5.2 In Vivo Imaging

In vivo imaging is performed under general anesthesia, using the IVIS Lumina LT Series III system with integrated Living Image software, but any other instrument capable of detecting fluorescence can be used.

1. Place the BALB/c mouse in an isoflurane inhalation anesthesia chamber. For induction, use 1.5–1.7 MAK; for maintenance of anesthesia, use 1.2–1.5 MAK.
2. Set the mouse on the heated surgical table with continuous inhalation anesthesia and apply the eye ointment to avoid corneal ulceration.
3. Obtain good lateral tail vein visualization (*see* **Note 15**).
4. Disinfect the tail with 70% ethanol and wait to dry.
5. Inject 150 μg DiD labeled EVs in a total volume of 100 μl PBS using a 27 G needle intravenously in the tail vein of the BALB/c mice (*see* Note **15**).
6. After 3 h, transfer the mouse into the IVIS in vivo imaging chamber connected to the inhalation anesthesia. The IVIS machine should be initialized before the imaging, resulting in

cooling the CCD camera at −90°C and heating the platform at 37°C (green light stating readiness for imaging). Turn on the Quartz Halogen Lamp (*see* Note **15**).

7. Adjust the settings: FOV (field of view) to D and check the mode fluorescent and photograph. Set binning to 8 and adjust the exposure time first to Auto. The excitation and emission filters should be open for the values depending on the fluorophore that we are monitoring (DiD; Excitation 640 nm, Emission 670 nm). F/Stop is set to 2. The focus should be adjusted to the subject's height (1.5 cm) (*see* **Notes 16–19**). Check the Lamp Level to High. Click Acquire to obtain the image.
8. Process the images. In the Units section, set parameters to Radiant Efficiency or Efficiency. In the Correction section, check Adaptive FL Background Subtraction. To determine the whole fluorophore spectra, acquire the whole spectra by setting up the Imaging wizard (*see* **Notes 20** and **21**).
9. To compare different fluorescent signals (e.g., DiD signal, tissue fluorescence, food fluorescence) to exclude a certain signal, perform the Spectral Unmixing. In the Sect. "Spectral Unmixing," check the Automatic Method, and then click Start Unmixing. Determine the Threshold on the Photograph. Select the two components (DiD, Tissue Autofluorescence) that you want to unmix. PCA (principal component analysis) should be checked; the value should be approximately 100%. An alternative to spectral unmixing is Image Math (*see* **Note 22**).
10. Check the images and Radiant Efficiency, where the sole DiD signal of EVs or Tissue Autofluorescence (AF) is presented. Unmixing results additionally in a composite image of DiD and Tissue AF, depicted in different colors. By spectral unmixing, different fluorescent and bioluminescent reporters can be monitored at the same time (*see* **Note 23**) (Fig. 2).

3.5.3 Ex Vivo Imaging of Organs

1. Mice are euthanized using an approved method 3 h after i.v. injection of DiD-labeled EVs (see Sect. 3.5.2) (*see* Note **15**).
2. Heart, lungs, spleen, liver, kidney, and brain are collected and put into a petri dish using scissors and forceps after disinfecting the skin of the animals with 70% ethanol.
3. Transfer the petri dish into the IVIS in vivo imaging chamber and proceed with the imaging as written in Sect. 3.5.2.

3.5.4 Genome Editing Quantification from Isolated Organs Using The T7E1 Assay

1. Place the organs in 10 ml falcon tubes.
2. Place sufficient volume of lysis buffer from the Genomic DNA isolation kit.
3. Isolate the genomic DNA according to the manufacturer's instructions.

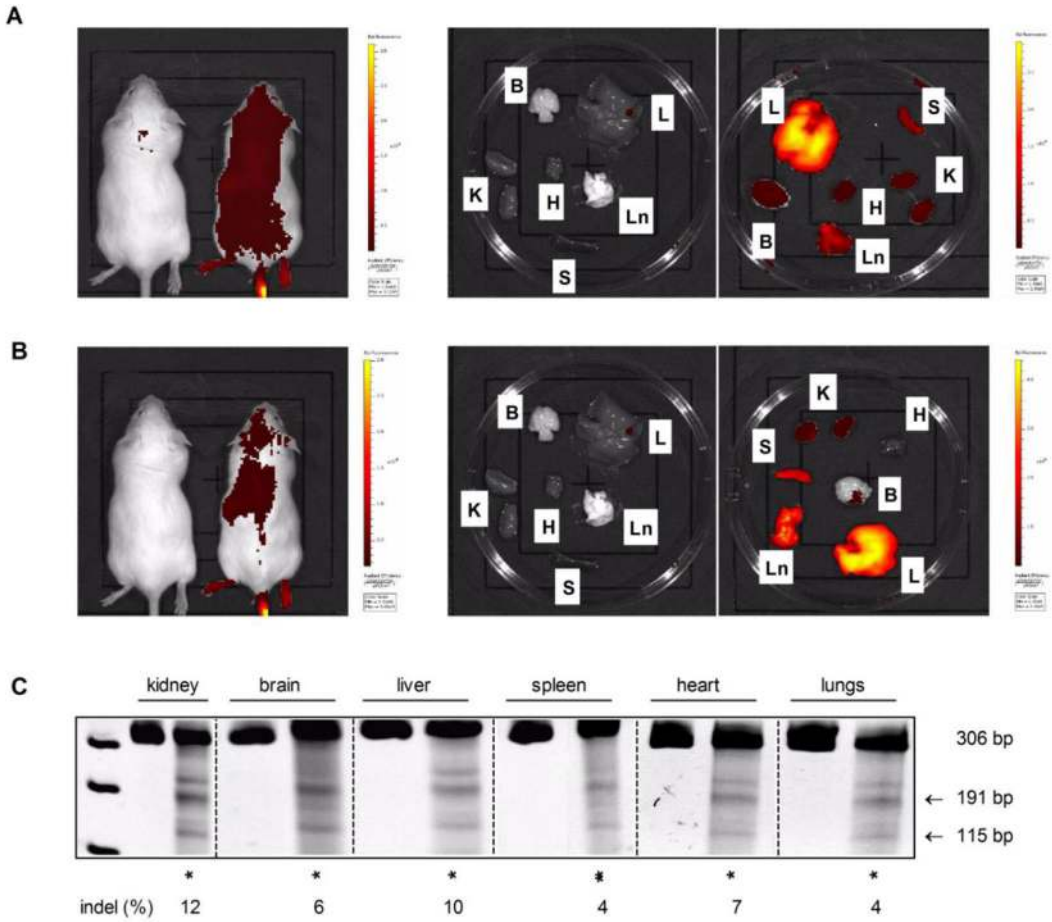


Fig. 2 Extracellular vesicles in vivo tracking and genome editing quantification. DiD-stained EVs were intravenously injected into BALB/c mice. Mice and then ex vivo organs were subjected to fluorescence imaging. (**A**) Three hours after DiD-stained administration in the mice (left mouse/Petri dish, untreated; right mouse/Petri dish, 150 μg of stained EVs). (**B**) Twenty-four hours after DiD-stained administration in the mice (left mouse/Petri dish, untreated; right mouse/Petri dish, 150 μg of stained EVs). (**C**) Indel mutations caused by *Ptgs1*-EVs in different tissues of the BALB/c mice that were i/v injected with 150 μg *Ptgs1*-EVs (*). After 48 h, organs were harvested and subjected to a T7E1 assay. A representative image from two independent experiments is shown ($n = 3$). Arrows depict the cleaved PCR product. The lane without * has cells treated with the control EVs. The dashed line represents merged pictures. Abbreviations: K kidney, B brain, S spleen, H heart, Ln lung, L liver (2)

4. Amplify the genomic region of interest using selected forward and reverse primers using KAPA HiFi HotStar Ready Mix on a PCR cycler (*see* **Note 24**).
5. Purify the PCR product using the PCR Cleanup Kit following the manufacturer's instructions.
6. For the T7E1 assay, 200 ng of isolated amplified genomic DNA is used. Make a 20 μl reaction by using 1× NEB 2.1 buffer (*see* **Note 25**).

7. To form heteroduplexes, recognize by the T7E1 endonuclease, denature and reanneal the PCR amplicon using the next program on the PCR Cycler (95°C for 10 min; 95 to 85°C ramping at −2°C/s; 85 to 25°C at −0.25°C/s; and 25°C hold for 1 min).
8. After the reannealing process, add 1 μL of T7 Endonuclease I. Incubate 15–30 min at 37°C.
9. Place the products on PAGE native gel-run at 150 V for 60 min.
10. Stain the gels with SYBR gold DNA stain for 30 min.
11. Visualize the cleavage with a DNA bioimaging system.
12. Calculate the genome editing efficiency (indel formation in %) using ImageJ following the next formula: $100(1-(1-(b+c)/(a+b+c))1/2)$, where a is the integrated intensity (determined by using ImageJ software) of the undigested PCR product, wherein b and c are integrated intensities of cleaved PCR product (Fig. 2).

4 Notes

1. Carefully, without disturbing the cells, add PBS to the corner of the T-75 tissue culture flask to prevent the loss of the cells. Then gently swirl the flask a few times to wash the cells.
2. Subculture the cells every 2–3 days or when they reach approximately 90% confluence. Check the flask under an inverted light microscope every 24 h.
3. Human adherent and suspension cell lines should be expanded rapidly, and stocks should be frozen in liquid nitrogen in a cryopreservation medium (FBS with 10% DMSO) at a low passage number. We usually freeze at approximately 2×10^6 cells per cryovial.
4. We are describing production in a volume of 100 ml, which usually results in EV stocks of 1 mg/ml. We prefer using 10 cm culture dishes, but any format can be used.
5. The plasmid ratio should be examined prior to obtaining the best transfection efficiency. The culture medium should be replaced with a fresh one after several hours post-transfection to remove the transfection mixture.
6. Pipette the supernatant slowly and leave the last cm of supernatant to avoid the transfer of cells.
7. EVs are stable at 4°C for up to 3–4 weeks and at −80°C for up to 4–6 months. We recommend avoiding freeze–thaw cycles as each cycle reduces efficiency.

8. By centrifugation of supernatant at 10,000 × *g* with subsequent ultracentrifugation at 100,000 × *g*, medium/large EV and small EV fractions are only enriched but not fully separated. Analysis of specific markers using immunoblot is necessary.
9. Pipette the supernatant slowly and leave the last centimeter of supernatant to avoid the transfer of medium/large EVs.
10. Mind that further purification increases the EV purity but decreases the yield. The choice depends on the desired product and application.
11. If layering is careful, you must see the borders between the layers. If not, discard the tube and repeat the layering.
12. Be careful and avoid sudden moves.
13. Density numbers for 5%, 10%, 20%, and 40% iodixanol are given at 20°C.
14. For the detection of CD63, use 4× SDS nonreducing buffer.
15. For a good lateral tail visualization, provoke vasodilatation by placing the tail in a 40°C water bath for 1 min. The concentration of injected EVs can vary. The time point of animal visualization can vary (30 min–24 h).
16. FOV is determined by the distance between the lens and the sample. FOV A presents a 5 cm distance, FOV B 7.5 cm, FOV C 10 cm, and FOV D 12.5 cm. Some instruments have also FOV E (24 cm) and FOV Z (2.6 cm) options.
17. Exposure time is proportional to how long the light is collected through the open shutter. A shorter exposure time improves throughput, and a longer exposure time increases intensity. Recommended maximum exposure time should be below 5 min.
18. F/Stop (Lens Aperture) determines the amount of light that is collected by the CCD camera. The maximum light collection is at F/Stop 1 (default settings for luminescence), whereas 16 (default settings for photo) is the smallest aperture, where we obtain the best resolution.
19. Binning gives the possibility to change sensitivity and resolution. It refers to grouping the pixels of the photo into a larger super-pixel. Large binning (set value 8) enables higher sensitivity with lower resolution, whereas small binning (value 2) offers lower sensitivity with higher resolution.
20. Radiant Efficiency is a calibrated measurement and states a radiance per incident excitation power ($\mu W/cm^2$). To perform Adaptive FL Background Subtraction, you first set the Threshold on the image where you want to do the subtraction.

21. The imaging wizard is used for sequence acquisition, meaning that the animal is imaged at different wavelength excitations with resulting different emissions. Mark the excitations and emissions that you want to compare. Obtain the sequence. You can also alter the excitation length for each fluorophore. Additionally, you can set up a time series study, determining the time interval. Then, perform spectral unmixing by choosing different fluorescence sources. As an alternative, you can use Overlaying Multiple Images. Click on the Tools-Image Overlay and then choose two images.
22. Image math is an alternative to spectral unmixing for removing the autofluorescence background signal from the image. Image math combines two images and mathematically creates a new image. In the Tools, select Image Math and then choose two images that you want to combine. Image A is the primary image, whereas image B is the image with the background signal. Then click Compute 'k' from ROI. To see the new image, click Image display.
23. Spectral unmixing can be performed by using Auto Mode or by Manual Mode, where you individually choose the fluorophores that you want to compare.
24. The program for PCR amplification has to be optimized for the specific genomic region of interest and the primers used. For the T7E1 assay, you can use a direct amplified PCR reaction if there is a single-band PCR. If not, place the PCR reaction on the 0.8% agarose gel, excise the appropriate PCR amplicon, clean it, and then proceed with the T7E1 assay.
25. If you want to avoid the T7E1 assay, you can send the PCR amplicon for Sanger sequencing and check the genome editing efficiency using online free software (e.g., TIDER (https://apps.datacurators.nl/tider/) or ICE (https://ice.editco.bio/#/).

Acknowledgments

The publication is based upon work by COST Action CA21113: Genome Editing to Treat Humans Diseases (https://www.gene-humdi.eu), supported by European Cooperation in Science and Technology (COST).

Competing Interests The authors declare no competing interests.

References

1. Dipalo LL, Mikkelsen JG, Gijsbers R et al. (2025) Trojan horse-like vehicles for CRISPR-Cas delivery: engineering extracellular vesicles and virus-like particles for precision gene editing in cystic fibrosis. Human Gene Ther 36(15-16):1021–1052
2. Lainšček D, Kadunc L, Keber MM et al. (2018) Delivery of an artificial transcription regulator dCas9-VPR by extracellular vesicles for therapeutic gene activation. ACS Synth Biol 7(12):2715–2725
3. Chen R, Huang H, Liu H et al. (2019) Friend or Foe? Evidence indicates endogenous exosomes can deliver functional gRNA and Cas9 protein. Small (Weinheim an der Bergstrasse, Germany) 15(38):e1902686
4. Campbell LA, Coke LM, Richie CT et al. (2019) Gesicle-mediated delivery of CRISPR/Cas9 ribonucleoprotein complex for inactivating the HIV provirus. Mol Ther 27(1):151–163
5. Zhang X, Xu Q, Zi Z et al. (2020) Programmable extracellular vesicles for macromolecule delivery and genome modifications. Dev Cell 55(6):784–801.e789
6. Ye Y, Zhang X, Xie F et al. (2020) An engineered exosome for delivering sgRNA:Cas9 ribonucleoprotein complex and genome editing in recipient cells. Biomater Sci 8(10):2966–2976
7. Whitley JA, Kim S, Lou L et al. (2022) Encapsulating Cas9 into extracellular vesicles by protein myristoylation. J Extracell Vesicles 11(4):e12196
8. Kazemian P, Yu SY, Thomson SB et al. (2022) Lipid-nanoparticle-based delivery of CRISPR/Cas9 genome-editing components. Mol Pharm 19(6):1669–1686
9. Théry C, Witwer KW, Aikawa E et al. (2018) Minimal information for studies of extracellular vesicles 2018 (MISEV2018): a position statement of the International Society for Extracellular Vesicles and update of the MISEV2014 guidelines. J Extracell Vesicles 7(1):1535750

Open Access This chapter is licensed under the terms of the Creative Commons Attribution-NonCommercial-NoDerivatives 4.0 International License (http://creativecommons.org/licenses/by-nc-nd/4.0/), which permits any noncommercial use, sharing, distribution and reproduction in any medium or format, as long as you give appropriate credit to the original author(s) and the source, provide a link to the Creative Commons license and indicate if you modified the licensed material. You do not have permission under this license to share adapted material derived from this chapter or parts of it.

The images or other third party material in this chapter are included in the chapter's Creative Commons license, unless indicated otherwise in a credit line to the material. If material is not included in the chapter's Creative Commons license and your intended use is not permitted by statutory regulation or exceeds the permitted use, you will need to obtain permission directly from the copyright holder.





Chapter 12

Preparation of Polymeric Nanoparticles for Gene Delivery

Emre Şefik Çağlar and Emine Saldamlı

Abstract

Gene delivery strategies include two main approaches: viral and nonviral systems to deliver the genetic material to target cells. Although viral vectors have high transfection efficacy, their clinical usage has been limited due to the risks of immunogenicity and mutagenesis. Therefore, nonviral delivery strategies such as polymeric nanoparticles gained considerable interest, since they are safer and more flexible. In this chapter, we comprehensively explained the protocols for preparing chitosan, a natural polymer, as well as poly(beta-amino esters) and poly(lactic-co-glycolic acid) nanoparticles, which are synthetic biodegradable polymers, and discussed their characterization. Within the scope of the chapter, we reviewed the ionic gelation method for chitosan, the nanoprecipitation and self-assembly methods for poly(beta-amino esters) systems, and the emulsion-solvent evaporation method for poly(lactic-co-glycolic acid). Particularly, the pH sensitivity and high transfection efficacy of poly(beta-amino esters) and the FDA-approved bioavailability and controlled-release characteristics of poly(lactic-co-glycolic acid) are discussed. Moreover, we explained the efficiency of these systems in gene delivery, basic physicochemical characterization methods such as particle size and polydispersity analysis with dynamic light scattering, and surface charge assessment with zeta potential, in addition to the biological performance criteria such as nucleic acid binding capacity, enzymatic protection, and serum stability. This section aims to provide a holistic guide to design and evaluate polymeric gene delivery systems.

Keywords Polymeric nanoparticles, Gene delivery, Poly-ß-aminoesters (PßAE), Chitosan, Polylactic-co-gylcolic acid (PLGA)

1 Introduction

Gene delivery approaches are broadly divided into two categories: viral and nonviral systems. Although viral vectors are frequently used due to their high gene transfer efficiency, several drawbacks, such as limited loading capacity, the potential to trigger immune responses, and the risk of insertional mutagenesis [1, 2], limit their clinical applicability. As a result, nonviral systems have gained increasing attention as safe and more versatile strategies of nucleic acid delivery.

Physical and chemical approaches are the two most common methods of viral gene delivery. Electroporation, microinjection, and gene gun-mediated transfer are physical approaches that allow

Duško Lainšček et al. (eds.), *CRISPR Delivery*, Methods in Molecular Biology, vol. 3075,
https://doi.org/10.1007/978-1-0716-5547-4_12,
© The Author(s) 2027

transient cell membrane penetration for intracellular delivery [3]. In contrast, chemical approaches rely on synthetic carriers specifically engineered to concentrate, protect, and transport genetic material to target cells. Due to their adaptability, relatively low immunogenicity, and targeted delivery capabilities, polymeric nanoparticles, liposomes, and cationic lipids have gained increasing attention [4–6].

Along with natural polymers, synthetic biodegradable polymers such as poly(beta-amino esters) (PßAE) have become a major focus of research. PßAEs are cationic polymers prepared via the Michael addition reaction, which facilitates a rapid library screening to detect the best structures for certain types of cells [7]. When compared to gold standards such as polyethylenimine (PEI), their rapid breakdown in physiological settings reduces the risk of long-term cytotoxicity without compromising transfection efficiency [8]. Gene transporters have also developed specialized polymeric structures to overcome intracellular and extracellular barriers, such as "Olga" polymers, which are oligomers with complex branching or particular sequences [9]. The charge density and hydrophobicity can be fine-tuned with these sequence-or architecture-controlled polymers, which provide improved stabilities and the ability to silence genes or regulate gene expression profiles in challenging biological contexts.

Biodegradable nanoparticles have significant advantages compared to non-biodegradable systems, such as low risk of toxicity and facilitated elimination without tissue accumulation. Poly(D,L-lactide-co-glycolide) (PLGA) is an FDA-approved biodegradable and biocompatible polymer used for certain human therapeutic applications. PLGA nanospheres are effective carriers for gene transfer due to their safety profiles and sustained release characteristics. The degradation time of PLGA nanoparticles might change from weeks to months by adjusting the molecular weight of the copolymer or the lactic acid/glycolic acid ratio of the copolymer [10].

PLGA undergoes degradation through hydrolysis of ester bonds in aqueous media, resulting in the formation of natural metabolites such as poly(lactic acid) (PLA) and poly(glycolic acid) (PGA) [11]. Lactic acid and glycolic acid, two metabolites produced by the breakdown of the PLGA polymer, are natural substances metabolized during the Krebs cycle, which significantly reduces the toxicity of these metabolites. PLGA nanoparticles are small hydrophobic and hydrophilic drugs that can encapsulate various active compounds, including nucleic acids and proteins. Moreover, due to their positive charges and hydrophobic characteristics, PLGA nanoparticles efficiently associate with molecules that modulate circulation duration, enabling targeted adhesion to specific cell types [12].

Within the scope of this chapter, the protocols to prepare the polymeric nanoparticles using chitosan, PßAE, and PLGA are discussed systematically. The protocols cover ionic gelation for chitosan nanoparticles, nanoprecipitation and electrostatic self-assembly for PßAE systems, and emulsion–solvent evaporation for PLGA formulations.

Following the synthesis protocols, the basic characterization methods used to evaluate the efficacy of the prepared nanoparticle systems in gene delivery are discussed. In this context, we reviewed the physicochemical characterization techniques such as dynamic light scattering (DLS) to measure the particle size and polydispersity index, and zeta potential analysis to determine the surface charge. Additionally, analytical methods for the evaluation of nucleic acid binding capacity, protective efficacy against enzymatic degradation, and serum stability are explained.

2 Materials

2.1 Reagents

2.1.1 Polymers and Lipids

1. 10–150 mg Poly(D,L-lactide-co-glycolide) (PLGA).
2. 0.5–5 mg/mL Chitosan (low, medium, or high molecular weight; degree of deacetylation ≥ 75%).
3. 5–10 mg/mL Poly(β-amino ester) (PßAE).
4. 0–25% (w/w) 1,2-Dioleoyl-3-trimethylammonium propane (DOTAP).

2.1.2 Organic Solvents

1. Dichloromethane (DCM).
2. Chloroform.
3. Dimethyl sulfoxide (DMSO).
4. Acetone.
5. Acetonitrile.

2.1.3 Aqueous Phase, Buffers and pH Adjustment

1. 18 MΩ cm at 25°C Ultrapure water.
2. 10 mM Tris-HCl, 1 mM EDTA, pH 7.5 TE buffer.
3. 10–25 mM, pH 5.0–5.2 Sodium acetate buffer.
4. Phosphate-buffered saline (PBS).
5. HEPES buffer.
6. DEPC-treated water.
7. 0.1%–1% (v/v) Acetic acid solution.
8. Sodium hydroxide (NaOH).
9. 96% (v/v) Ethanol (EtOH).

2.1.4 Crosslinking Agents and Inorganic Components

1. 0.5–2 mg/mL, pH 8.0–9.5 Sodium tripolyphosphate (TPP).
2. 31.25 mM Calcium nitrate.
3. 18.7 mM Diammonium hydrogen phosphate.

2.1.5 Stabilizers and Surfactants

1. 2% (w/v) Poly(vinyl alcohol) (PVA).

2. Poloxamer.
3. Tween 80.

2.1.6 Characterization Reagents

1. 50–100 IU/mL Heparin.
2. 1% (v/v) Triton X-100.
3. PicoGreen stain (for DNA quantification).
4. RiboGreen stain (for RNA quantification).
5. 1%–2.5% (w/v) Sodium dodecyl sulfate (SDS).
6. 5%–50% (v/v) Fetal bovine serum (FBS).
7. Ethylenediaminetetraacetic acid (EDTA).
8. 0.4 IU per 1 μg pDNA, DNase enzyme.
9. 0.07% RNase enzyme.
10. 0.8%–2% (w/v) agarose.
11. (150 ng) DNA/RNA ladder.
12. Ethidium bromide or SYBR Safe (gel staining).
13. 5, 10, 25, 50, 100 ng/mL DNA/RNA standards (standard curve series).

2.1.7 Cryoprotectants

1. 5%–10% (w/v) Trehalose.
2. 5%–10% (w/v) Sucrose.
3. 5%–10% (w/v) Mannitol.

All solutions should be prepared using ultra-pure water (prepared by purifying deionized water to obtain a sensitivity of 18 MΩ cm at 25°C). Analytical grade reagents should be used while preparing the solutions. Unless otherwise specified, the experiments need to be performed at room temperature. If a genetic element is involved, DNase/RNase-free water should be used. All equipment and water should be autoclaved in advance. If possible, DNase/RNase-free equipment, vials, beakers, pipettes, etc., should be used. Nanoparticle preparation is highly suggested to be performed in biosafety cabinets. Otherwise, the experimental area should be cleaned using 96% EtOH.

2.2 Equipment

1. Magnetic stirrer with hot plate.
2. Fine needle syringe (e.g., 27 G) or syringe pump.
3. Probe sonicator and/or bath sonicator.
4. Ultrasonic processor.
5. Centrifuge (capable of 20,000–38,000×*g*).
6. Ultracentrifuge (capable of 38,000×*g* for PLGA protocols).
7. Rotary evaporator.
8. pH meter.

9. 0.22 μm syringe filters.
10. Dynamic Light Scattering (DLS) device.
11. Zeta potential analyzer.
12. Microplate reader (480 nm excitation/520 nm emission).
13. Vortex mixer.
14. Freeze dryer (lyophilizer).
15. Biosafety cabinet.
16. Autoclave.
17. Horizontal agarose gel electrophoresis system.
18. UV transilluminator or gel documentation system.
19. −80°C freezer.
20. −20°C freezer.
21. Disposable cuvettes (for DLS and zeta potential measurements).
22. 96-well plate.
23. DNase/RNase-free microcentrifuge tubes.
24. DNase/RNase-free pipette tips.

3 Methods

3.1 Preparation of Chitosan Nanoparticles

Chitosan nanoparticles are frequently synthesized via the ionic gelation technique, which occurs due to the electrostatic attraction between the positively charged amino groups of the chitosan and the negatively charged phosphate groups of tripolyphosphate (TPP) [13] (*see* **Note 1**). Restraining the necessity of chemical solvents or high temperatures, this cross-linking reaction takes place spontaneously under mild aqueous conditions, which makes it particularly beneficial to encapsulate the sensitive biological macromolecules such as plasmid DNA, siRNA, and mRNA. Thus, the resulting nanoparticles have pivotal characteristics that are highly preferable in gene delivery applications, such as increased biocompatibility, biodegradability, and mucoadhesiveness.

Nucleic acids are integrated into chitosan nanoparticles either through the pre-complexation method or the post-loading procedure. The pre-complexation method involves mixing the nucleic acid with the chitosan solution prior to introducing TPP. In this method, the nucleic acid is electrostatically adsorbed onto the positively charged chitosan chains before the cross-linking takes place, which results in the encapsulation within the nanoparticle matrix. On the other hand, the post-loading approach involves adding the nucleic acid to the

preformed nanoparticle suspension and allowing it to adsorb onto the nanoparticle surface through electrostatic interactions.

1. Dissolve the chitosan in 0.1%–1% (v/v) acetic acid solution, typically at a concentration of 0.5–5 mg/mL. This may vary depending on the nanoparticle size (*see* **Note 2**) and the application.
2. Stir the solution gently at room temperature or at 40–50°C until it is fully dissolved. This might take from 1 to 3 h, depending on the chitosan's molecular weight (*see* **Note 3**).
3. Once the chitosan is completely dissolved, use a dilute NaOH solution to adjust the pH of the chitosan solution to 4.5–5.5. The specified pH range is critical to make sure that the amino groups are sufficiently protonated, thereby preserving the solubility.
4. Filter the solution using a 0.22 μm syringe filter to eliminate any undissolved particles or aggregates.
5. Dissolve TPP (*see* **Note 1)** in ultrapure water until a concentration of 0.5–2 mg/mL.
6. Stir to dissolve fully and filter the solution using a 0.22 μm syringe filter. The TPP solution usually has a pH value between 8.0 and 9.5. Adjust it accordingly, if needed.
7. Transfer the chitosan solution to a clean glass vial or beaker. Stir the solution on a magnetic stirrer at 500–1000 rpm while the nanoparticles are forming.
8. Using a 100 μL pipette tip, syringe, or syringe pump, add the TPP solution dropwise to the chitosan solution at a controlled rate, generally between 0.2 and 1 mL/min, or one drop for every 10 s (*see* **Notes 4** and **5**). Nanoparticle formation happens spontaneously when TPP is added due to the electrostatic cross-linking between the oppositely charged components.
9. After adding TPP solution completely, stir the suspension for 30–60 min at ambient temperature to facilitate thorough cross-linking and nanoparticle stabilization.
10. In the pre-complexation method, prepare the nucleic acid solution using ultrapure water or a buffer with a minimal ionic strength. Mix the chitosan solution with the nucleic acid solution at the specified N/P ratio (molar ratio of nitrogen in chitosan to phosphate in the nucleic acid) (*see* **Note 6**). Incubate the mixture at room temperature for 15–30 min to speed up the initial formation of the complex. Then, add the TPP solution dropwise, as indicated in Step 8.
11. In the post-loading method, prepare the nucleic acid solution using ultrapure water or a buffer with a low ionic strength.

Then, mix this solution with the chitosan nanoparticle dispersion, adjusting the ratios of each component.

12. Centrifuge the solution at 10,000–20,000×*g* for 20–30 min at 4°C to purify the nanoparticle suspension. Discard the supernatant and resuspend the particles using ultrapure water or a suitable buffer such as phosphate-buffered saline (PBS) or HEPES. Wash the samples 2–3 times to discard unbound TPP, free nucleic acid, and other contaminants (*see* **Note 7**).

3.2 Preparation of PßAE Nanoparticles

The process of nanoprecipitation depends on the rapid diffusion of a water–miscible organic solvent, which contains the polymer, into an aqueous phase. This process causes the spontaneous formation of nanoscale particles [14–16]. The generation of relatively uniform nanoparticles under moderate conditions for PßAE-based systems is facilitated by this method, which might be modified for studies involving nucleic acid complexation or encapsulation.

Two strategies are primarily used to incorporate nucleic acids into PßAE-based nanoparticle systems. The post-loading/surface complexation approach involves introducing DNA, siRNA, or mRNA after the formation of the nanoparticles. This process facilitates electrostatic adsorption onto the positively charged surface of preformed PßAE nanoparticles. Conversely, the simultaneous precipitation/encapsulation method necessitates the precise optimization of formulation parameters due to the potential impact on loading reproducibility of the nucleic acid's presence in the aqueous phase during the nanoprecipitation process. Post-formation electrostatic complexation is generally regarded as the more reproducible strategy for the majority of PßAE-based gene delivery systems since it is more compatible with the polymer's cationic nature and enables more precise control over the efficacy of nucleic acid loading [7, 17].

1. Dissolve the PßAE polymer (5–10 mg/mL) in a water-miscible organic solvent, such as acetone, DMSO, ethanol, or acetonitrile. Dissolve the polymer by gently stirring the solution (*see* **Note 13**) and filter the solution using a 0.22 µm filter if particulate matter is present.
2. Use ultrapure water or a buffer with a low ionic strength to prepare the aqueous phase. Use a stabilizer, such as 0.1%–1% (w/v) PVA, to enhance colloidal stability by incorporating it into the water phase. Sodium acetate buffer at pH 5.0–5.2 is widely preferred for gene delivery applications since mildly acidic conditions facilitate the formation of nanoparticles and PßAE protonation [17,18].
3. Transfer the aqueous phase to a clear glass vial or a beaker. A uniform mixture is typically achieved by agitating at a moderate speed, typically between 750 rpm on a magnetic stirrer.

4. Add PßAE-containing organic phase to the aqueous phase dropwise using a 100 µL pipette tip, syringe, or syringe pump. Slow and controlled addition processes are essential to produce homogeneous and small nanoparticles. The initial addition rate is typically between 0.2 and 1 mL/min. In this phase, the polymer precipitates as nanosized particulates as a result of the rapid diffusion of the organic solvent into the aqueous medium.
5. Agitate the suspension continuously at ambient temperature for 60–120 min (*see* **Note 14**). The extended agitation period stabilizes the nanoparticles and facilitates the partial diffusion of the solvent.
6. Slightly sonicate the suspension in case of aggregation using a solution sonicator or a probe sonicator at a reduced intensity. Avoid excessive sonication to prevent polymer degradation or particle damage.
7. Magnetic stirring under ambient conditions or mild vacuum, rotary evaporation when compatible with the batch size, or dialysis against water or buffer should be used to eliminate residual organic solvent (*see* **Note 14**). The solvent removal process is maintained until the formulation is suitable for biological applications.
8. Centrifuge the nanoparticle suspension at 10,000–20,000× *g* for 10–30 min, depending on the particle size and density. Discard the supernatant and resuspend the particle in ultrapure water or a suitable buffer (*see* **Note 15**).
9. Prepare the nucleic acid solution separately using a low ionic strength buffer, such as sodium acetate buffer. Subsequently, introduce the PßAE nanoparticle suspension into the nucleic acid solution at the intended polymer: nucleic acid ratio, or N/P ratio, and then incubate for 15–30 min (*see* **Note 16**) at room temperature to facilitate stable complex formation.

3.3 Preparation of PLGA Nanoparticles

Emulsion-solvent evaporation or solvent replacement techniques are the most frequently used methods to produce PLGA nanoparticles. These techniques enable the encapsulation of high molecular weight therapeutic agents, such as DNA and antisense oligonucleotides, as well as low molecular weight lipophilic or hydrophilic drugs. The physical properties of the particles and their cellular incorporation might be affected by the persistent presence of specific excipients on the nanoparticle surface during formulation. The hydrophilicity of the nanoparticles may be enhanced by a higher concentration of excipient on the surface, which could potentially reduce cellular absorption. As a result, the number of excipients on the surface might be altered to act on the physical characteristics of the nanoparticles and their interactions with cells [19].

The complexation of nucleic acids with cationic excipients is a commonly used approach to enhance charge. Cationic compounds, including PEI, DOTAP, and other polyamines, enhance the affinity between molecules and particle matrices by establishing electrostatic interactions with negatively charged nucleic acids. This has the potential to enhance the encapsulation efficiency of nanoparticles and accelerate the charging rate. The discharge of charged substances may be delayed by cationic excipients, which frequently raise potential toxicity concerns. Consequently, it is crucial to create alternative methods to improve charging and to thoroughly evaluate the impact of formulation and production parameters on encapsulation efficiency. Research has demonstrated that the encapsulation efficiency of macromolecular therapeutics within PLGA particles is substantially influenced by specific formulation and process parameters [20]. The methodology to integrate genetic material into double emulsion PLGA nanoparticles is detailed in Sect. 3.3.1. and the approach to transfer genetic material onto cationic polymer PLGA nanoparticles is explained in Sect. 3.3.2.

3.3.1 Double Emulsion Solvent Evaporation

1. Prepare the necessary concentrations of nucleic acids or CRISPR/Cas9 components in RNase/DNase-free TE buffer [21]. Mix 10 µL (1000 ng/µL) of nucleic acid (specifically, the CRISPR/Cas9 plasmid) with 105 µL of each of the following solutions: 31.25 mM calcium nitrate and 18.7 mM diammonium hydrogen phosphate. Vortex the mixture, and then allow it to settle on ice for 5 min to facilitate the formation of the CaP/Cas9 complex. Dilute the final complex in ultrapure water before using (*see* **Note 25**) [22].
2. Mix the complex with dichloromethane (DCM) containing 10–150 mg of PLGA (*see* **Note 21**).
3. Sonicate the complex using an ultrasonic processor to form the primary water-in-oil (w_1/o) emulsion. Maintain consistent sonication parameters, including amplitude, duration, and pulse intervals during the entire procedure.
4. Add 2 mL of 2 mL of 2% (w/v) PVA in ultrapure water directly to the primary emulsion. Emulsify the mixture using sonication for an additional 60 s to form the $w_1/o/w_2$ double emulsion.
5. Finally, let the DCM evaporate by stirring the emulsion with a magnetic stirrer at room temperature for 3 h.
6. Collect the PLGA nanoparticles via ultracentrifugation, applying 38,000×*g* for 10 min at 4°C, and then wash them twice with ultrapure water.
7. Resuspend the harvested nanoparticles in 6 mL of DEPC-treated water.
8. Freeze-dry the PLGA nanoparticles using an appropriate cryoprotectant, then powder the lyophilized cake and store it at −20°C until needed [23].

3.3.2 Cationic Modified Preparation Method

1. Dissolve 125 µL of 8 µM nucleic acid solution in TE buffer
2. Dissolve PLGA in chloroform, then incorporate DOTAP at concentrations between 0 and 25% (w/w), ensuring the total DOTAP/PLGA concentration remains at 60 mg/mL (*see* **Note 24**).
3. Add 250 µL of the DOTAP/PLGA solution to the nucleic acid solution, and sonicate the mixture via an ultrasonic processor for 90 s to make the initial water-in-oil (w_1/o) emulsion.
4. Finally, add 1 mL of a 2% (w/v) PVA solution to the primary emulsion, and sonicate for 60 s to produce the $w_1/o/w_2$ double emulsion.
5. Dilute the double emulsion with 5 mL of a 2% (w/v) PVA solution, and evaporate chloroform using a rotary evaporator.
6. Centrifuge the dispersion at 18,000×*g* for 12 min at 4°C. Discard the supernatant, and redisperse the nanoparticle pellet in ultrapure water.
7. Repeat the centrifugation and washing procedure for three times to remove any remaining PVA [24].

3.4 Characterization of Nanoparticles

The ideal nanoparticle size for gene transport should be below 200 nm, which is important both for the recruitment of nanoparticles into the cell and for overcoming various barriers in the body [25]. Another important parameter is the zeta potential of the developed nanoparticles. In particular, the cationic surface charge is required for the binding of the nucleic acid to the nanoparticle and the uptake of the nanoparticle by the cell. This load is generally preferred to be between 20 and 40 mV. High zeta potential also increases toxicity [26]. After the ideal nanoparticle is prepared and the nucleic acid is loaded, the binding capacity of the nucleic acid to the nanoparticle, in other words, its loading efficiency, should be analyzed thoroughly. Likewise, nucleic acid protection assays (serum stability, DNase/RNase stability) and lyophilization optimizations should be performed to detect the physiological environment and long-term stability. Thus, we explained the characterization methods of nanoparticles in this section.

3.4.1 Particle Size and Polydispersity Index, and Zeta Potential Measurements

1. Slightly mix the sample upside down to have a homogeneous mixture while preparing the samples for measurement. Load the sample into disposable cuvettes, avoiding any air bubbles, and dilute the sample with DNase/RNase-free water or preparation buffer if needed. The aim here is to obtain the appropriate scattering signal and reduce multiple scattering.
2. While writing a standard operation procedure (SOP) on the device, select "size" or "zeta" as the measurement type in accordance with the type of measurement. Select room temperature unless otherwise indicated. Set the equilibration time

to 120 s. Prefer at least three to five technique repetitions for each sample reading. Use three different batches for the measurement to obtain a correct measurement.

3. In the optical and dispersant information section of the SOP, enter the dispersant refractive index, dispersant viscosity, material refractive index, and absorption information. If water is used for the dispersant refractive index and dispersant viscosity, set the water from the device. For the material refractive index, enter the known value or the value specified by previous studies. If it is not known, measure with the help of a refractometer and a viscometer, and enter the values obtained. For the absorption value, follow the software recommendation of the device.
4. Prefer the backscatter mode for the measurement angle if it is available. This mode corresponds to approximately 173° on many devices.
5. Set the measurement time to 10–15 runs and three repetitions.
6. Transfer the samples of the appropriate volume to the cuvette. Be careful to avoid any bubbles in the sample, have the outer surface of the cuvette clean, avoid scratches, stains, or drops on the cuvette, and place the cuvette in the chamber in the correct orientation. Close the lid. Write the sample name, analyst name if necessary, and measurement notes into the device. Start the measurement by selecting the correct SOP and evaluating the results obtained after the measurement.

3.4.2 Binding and Encapsulation Efficacy

1. Mix nanoparticles and nucleic acids in varying ratios. For example, Polymer:Nucleic acid ratio might be 1:1, 2:1, 3:1, 5:1, 10:1, 40:1, etc. (w/w). Keep the complex at room temperature or 37°C for 30 min by gently tapping the bottom of the tube.
2. The total amount of nucleic acid used (W_{total}) is noted.
3. Centrifuge at 20,000–30,000×*g* for 30 min at 4°C if the free nucleic acid (W_{free}) needs to be separated from the prepared nanoparticle suspension. In case no precipitation is observed after the centrifugation, use filtered centrifuge tubes of appropriate molecular weight to allow the passage of the free nucleic acid.
4. Transfer the supernatant into a separate tube without disturbing the pellet.
5. Add heparin (50–100 IU/mL), or 1% SDS or Triton X-100 degradation buffer to the pellet. Incubate for 60 min to allow separation of the nucleic acid from the polymer.
6. Prepare a standard series of at least five points using DNA or RNA standards of known concentration (i.e., 5, 10, 25, 50, 100 ng/mL).

7. Add 100 µL of standard or sample from the supernatant or the pellet to each well of the 96-well plate.
8. Add 100 µL of PicoGreen dye for DNA or RiboGreen dye for RNA to each well and leave at room temperature for 5–10 min while protecting from the light.
9. Using a microplate reader, measure the absorbance at 480 nm excitation and 520 nm emission.
10. Plot the regression equation of the standard curve and calculate the concentration of nucleic acid in the samples by using this equation.
11. Calculate the binding efficiency (BE), i.e., the free amount in the supernatant, according to Eq. 1, and the encapsulation efficiency (EE), i.e., the amount obtained from the degraded pellet, according to Eq. 2.

$$\text{BE} \quad (\%) \quad = \quad \left(\frac{W_{\text{total}} - W_{\text{free}}}{W_{\text{total}}} \right) \quad \times \quad 100 \qquad (1)$$

$$\text{EE} \quad (\%) \quad = \quad \left(\frac{W_{\text{encapsulated}}}{W_{\text{total}}} \right) \quad \times \quad 100 \qquad (2)$$

3.4.3 Gel Retardation Assay

This study is performed as a control experiment of binding or entrapment efficacy.

1. Prepare an agarose gel ranging from 0.8% to 2%, depending on the size of the nucleic acid.
2. Load the free nucleic acid, as the control group, and nucleic acid complexed with nanoparticles in different ratios into the wells.
3. Run the samples at 80–100 V for 60 min.
4. Bands that remain in the well or do not migrate confirm successful binding/encapsulation. In other words, a moving band is not observed in the wells where the coupling takes place.

3.4.4 DNase/RNase Stability

The aim of this study is to evaluate the protective efficacy of nucleic acid-loaded nanoparticles against nucleases. The results are evaluated by comparing them with free nucleic acid.

1. Prepare nucleic acid-loaded nanoparticles according to the Sects. 3.1, 3.2, or 3.3 with a different polymer-to-nucleic acid ratio.

2. Add 0.4 IU DNase enzyme per 1 μg pDNA or 0.07% RNAse enzyme to the polymer–nucleic acid complex. Incubate for 45 min.
3. EDTA can be used to inactivate the enzyme activity. Similarly, short-term heating (such as 65°C for 10 min) might be applied as well.
4. Separate the nucleic acid from the polymer complex using heparin, SDS, or Triton-X100 and run in agarose gel as described above. In the control group, the amount of nucleic acid loaded into the nanoparticle is used. Analyze protection against enzyme activity by comparing the band densities on the gel.

3.4.5 Serum Stability

The aim of this study is to evaluate the stability and nucleic acid conservation capacity of polymeric nanoparticles in serum medium (in the presence of protein, salt, and nuclease). Size change, aggregation, and nucleic acid degradation in nanoparticles are assessed in the presence of serum.

1. Keep the serum at room temperature. Add 5%–50% fetal bovine serum, depending on the route of application of the nanoparticle.
2. Add the serum to the nucleic acid-loaded nanoparticle suspension. Stir gently and incubate at 37°C.
3. Take samples from media at certain time points (e.g., a minimum of 150 ng for pDNA) that will yield bands in the agarose gel.
4. Evaluate size, polydispersity indexes, and zeta potentials with the DLS method.
5. Perform a gel retardation study to analyze the preservation of the integrity of the nucleic acid.

3.4.6 Lyophilization for Long-Term Stability

For long-term storage, lyophilization is highly recommended. Cryoprotectants such as trehalose (5%–10% w/v), sucrose, or mannitol should be added prior to freeze–drying to prevent irreversible aggregation during the freezing and drying process. Lyophilized nanoparticles are generally stored at −20°C for extended periods and reconstituted in ultrapure water before use.

1. Prepare nucleic acid-loaded nanoparticles according to the standard protocol.
2. Add cryoprotectant to the suspension.
3. Transfer the prepared solution to the vials by filling 1/3 of them.
4. Freeze the vials at −80°C, preferably overnight.

5. Place frozen samples in a freeze dryer at −50°C and lyophilize by first primary heating and then by secondary heating. Never allow the samples to melt in the freeze dryer.
6. At this point, the samples should have a cake-like appearance and be white and porous.
7. Redisperse the final product with the same amount of water as the nanoparticle suspension before the freeze–drying process. The final product should be able to redisperse in less than 30 s.
8. The size and PDI value of the restored samples should not differ from the pre-freeze–drying value by more than 15%–20%.
9. A gel retardation experiment can be performed to analyze the nucleic acid integrity.

4 Notes

1. TPP is not the only cross-linking agent for chitosan; it is the most frequently used one. Other agents such as glutaraldehyde, genipin, and fucoidan are available as well [27, 28].
2. The overall stability of the colloidal system, the polydispersity index (PDI), zeta potential, and particle size are significantly influenced by the mass ratio of chitosan to TPP while preparing the chitosan nanoparticles. Any imbalance in this ratio may result in incomplete crosslinking or particle aggregation, which may affect the uniformity and the structure of the nanoparticles.
3. Below, we demonstrated a sample calculation to be used while preparing 0.01% and 0.025% chitosan nanoparticles with varying CS:TPP ratios (Table 1).
4. Our experimental findings suggest that the uniformity of the nanoparticle formulations produced is significantly enhanced by allowing chitosan to dissolve at ambient temperature for a full day. During the subsequent ionic gelation process, this extended dissolution phase ensures that the polymer chains are thoroughly hydrated and distributed evenly within the acidic environment, a critical factor in achieving a monodisperse particle size distribution [29, 30].
5. A more controlled ionic gelation process is obtained using a smaller orifice or a higher gauge needle while adding TPP dropwise, which causes a more uniform and monodisperse nanoparticle distribution.
6. The ratio of chitosan to TPP solution is a crucial factor, typically optimized between 3:1 and 6:1 (v/v).

Table 1
Calculation to prepare 0.01% and 0.025% chitosan nanoparticles with varying CS:TPP ratios

Nanoparticle dispersion (5 mL)				
Chitosan (%)	**Volume of chitosan solution (mL)**	**Chitosan:TPP Ratio**	**TPP volume (mL)**	**Distilled water (mL)**
0.01% (0.4 mg Chitosan/5 mL Distilled Water)	0.133	3:1	0.133	4.734
		4:1	0.100	4.767
		5:1	0.080	4.787
		6:1	0.067	4.800
		7:1	0.057	4.810
0.025% (1.25 mg Chitosan/5 mL Distilled Water)	0.417	3:1	0.417	4.166
		4:1	0.313	4.271
		5:1	0.250	4.333
		6:1	0.208	4.375
		7:1	0.179	4.404

7. The N/P ratio is a critical parameter since it has a significant impact on the size, surface charge, encapsulation efficiency, and transfection efficacy of nanoparticles. N/P ratios, which typically range from 5:1 to 50:1, require optimization for each specific application in chitosan-based gene delivery systems.
8. Once synthesized, chitosan nanoparticles can be stored at 4°C for limited periods, typically up to 1–2 weeks, to maintain colloidal stability.
9. A higher molecular weight of chitosan typically results in the formation of larger particles, which demonstrates enhanced mechanical stability.
10. A greater degree of chitosan deacetylation leads to a higher positive charge density, which improves nucleic acid binding, although it might cause cytotoxicity.
11. Larger particles are typically produced at higher chitosan concentrations.
12. The pH of the chitosan solution significantly affects the protonation of amino groups, which in turn influences cross-linking efficiency.
13. Smaller particles are generally produced by rapidly adding the solution and stirring at higher speeds.

14. Based on our experiences, letting chitosan dissolve at room temperature for 24 h significantly improves the uniformity of the resulting nanoparticle formulations.
15. For small-scale formulations, the organic phase evaporates completely within 2–4 h, depending on the total sample volume.
16. The washing procedure can be repeated 1–3 times to eliminate any remaining solvent, unbound polymer, or surfactant.
17. Our experimental results suggest that the formation of more robust and stable polymer–DNA complexes was obtained by incubation at 37°C for 45 min, likely due to the intensified electrostatic interactions at physiological temperature.
18. It is generally recommended to use freshly prepared PßAE nanoparticles promptly. Formulations may be stored at 4°C for short periods if necessary; however, colloidal stability should be confirmed prior to use.
19. Transfection efficiency and cytotoxicity are affected by the polymer's molecular weight, the distribution of its molecular weights, and its concentration [31].
20. Among the other critical parameters that control nanoparticle preparation are the rate of addition, stirring speed, pH, and ionic strength of the aqueous phase, the presence and concentration of stabilizer, and the polymer-to-nucleic acid ratio. Additionally, the type of organic solvent and the organic-to-aqueous phase volume ratio are all noteworthy [32–35]. In general, lower polymer concentration, slower addition, and higher dilution tend to favor the formation of smaller particles.
21. The incorporation of methyl side groups in the PLA structure of PLGA renders it more hydrophobic than PGA, resulting in lactide-rich PLGA copolymers being less hydrophilic, absorbing less water, and thus exhibiting slower degradation rates. The alterations in PLGA characteristics during polymer biodegradation influence the release and breakdown rates of the encapsulated medicinal molecules [36].
22. The end-group chemistry of PLGA (acid-terminated or ester-terminated) substantially influences the polymer's hydrophobicity, water absorption, and hydrolytic degradation rate. Previous studies indicate that acid-terminated PLGA possesses more hydrophilicity due to its free carboxylic acid groups, resulting in accelerated breakdown relative to ester-terminated PLGA. In contrast, ester-terminated PLGA exhibits greater hydrophobicity, leading to reduced hydrolysis rates and prolonged drug release patterns [37]. Electrostatic

interactions between the positively charged amine end groups and the negatively charged phosphate backbone of DNA accelerate encapsulation and arrest. The end-group chemistry of PLGA determines its interaction with DNA through electrostatic and hydrophobic interactions. Consequently, PLGA with amine terminal groups enhances the retention of additional electrostatic interactions with negatively charged DNA. In contrast, PLGA with an ester end cap exhibits a hydrophobic nature at its terminal carbon chain, resulting in less interaction with hydrophilic DNA due to reduced electrostatic interaction and heightened hydrophobicity, hence causing a slower acceleration [38].

23. The size of PLGA nanoparticles is affected by the polymer's molecular weight [39].
24. Surfactants, including polyvinyl alcohol, poloxamers, and polyethylene glycol, are commonly used to improve the stability of PLGA nanoparticles. These substances prevent aggregation by reducing interfacial tension, thereby improving colloidal stability. Furthermore, in some cases, they may delay the circulation time. The surfactant's specific type, concentration, and molecular weight might affect particle size and encapsulation efficiency as well. Careful adjustment of these parameters is essential for the development of reliable and consistent PLGA nanocarrier systems [40]. For instance, one study demonstrates that increasing the concentration of PVA, used as a surfactant, from 0.5% to 2% results in an increase in the zeta potential, from -31.3 ± 1.6 mV to -6.5 ± 1.7 mV [39].
25. The size of nanoparticles and the loading efficiency of the drugs depend on the organic solvent that is being used. The interfacial tension values for dichloromethane (DCM) (20.4) and chloroform (CR) (31.4) were significantly higher than that of ethyl acetate (EA) (6.78). As a result, the size of the microsphere particles increased with the interfacial tension in the water phase. A solvent with low interfacial tension with water generates smaller droplets when making an emulsion [41]. Their boiling points are known to be 39.75°C for DCM, 77°C for EA, and 61–62°C for CR [42]. Since a solvent that evaporates quickly produces smaller emulsion droplets, DCM is often used for PLGA nanoparticles [41]. Nevertheless, the cationic lipids like DOTAP have better solubility in chloroform, and therefore, the polymer solution (PLGA/DOTAP) is prepared by dissolving it in chloroform [43].
26. Calcium phosphate formation around Cas9 creates a CaP transporter. This process stabilizes Cas9, which helps it enter cells more easily and then be released [44].

Acknowledgments

The publication is based upon work by COST Action CA21113: Genome Editing for the Treatment of Human Diseases (https://www.genehumdi.eu), supported by European Cooperation in Science and Technology (COST). The authors used a combination of generative AI programs to improve grammar, academic language, and readability. After using these tools, the authors reviewed and edited the content as needed and took full responsibility for the content of the publication.

Competing Interests The authors declare no competing interests.

References

1. Naldini L (2015) Gene therapy returns to centre stage. Nature 526:351–360
2. Ginn SL, Amaya AK, Alexander IE, et al. (2018) Gene therapy clinical trials worldwide to 2017: an update. J Gene Med 20, e3015.
3. Wells DJ (2004) Gene therapy progress and prospects: electroporation and other physical methods. Gene Ther 11:1363–1369
4. Mintzer MA, Simanek EE (2008) Nonviral vectors for gene delivery. Chem Rev 109:259–302
5. Pack DW, Hoffman AS, Pun S, Stayton PS (2005) Design and development of polymers for gene delivery. Nat Rev Drug Discov 4:581–593
6. Mao S, Sun W, Kissel T (2010) Chitosan-based formulations for delivery of DNA and siRNA. Adv Drug Deliv Rev 62:12–27
7. Karlsson J, Rhodes KR, Green JJ, Tzeng SY (2020) Poly(beta-amino ester)s as gene delivery vehicles: challenges and opportunities. Expert Opin Drug Deliv 17:1395
8. Lynn DM, Langer R (2000) Degradable poly(β-amino esters): synthesis, characterization, and self-assembly with plasmid DNA. J Am Chem Soc 122:10761–10768
9. Scholz C, Wagner E (2012) Therapeutic plasmid DNA versus siRNA delivery: common and different tasks for synthetic carriers. J Control Release 161:554–565
10. Zou W, Liu C, Chen Z, Zhang N (2009) Studies on bioadhesive PLGA nanoparticles: a promising gene delivery system for efficient gene therapy to lung cancer. Int J Pharm 370:187–195
11. Rai R, Alwani S, Badea I (2019) Polymeric nanoparticles in gene therapy: new avenues of design and optimization for delivery applications. Polymers (Basel) 11(4):745.
12. López-Royo T, Sebastián V, Moreno-Martínez L, et al. (2021) Encapsulation of large-size plasmids in PLGA nanoparticles for gene editing: comparison of three different synthesis methods. Nanomaterials 11(10), 2723.
13. Garg U, Chauhan S, Nagaich U, Jain N (2019) Current advances in chitosan nanoparticles based drug delivery and targeting. Adv Pharm Bull 9:195
14. Martínez-Muñoz OI, Ospina-Giraldo LF, Mora-Huertas CE et al (2020) Nanoprecipitation: applications for entrapping active molecules of interest in pharmaceutics. Nano- and Microencapsulation - Techniques and Applications
15. Salatin S, Barar J, Barzegar-Jalali M et al. (2017) Development of a nanoprecipitation method for the entrapment of a very water soluble drug into Eudragit RL nanoparticles. Res Pharm Sci 12:1
16. Kuddushi M, Kanike C, Xu BB, Zhang X (2025) Recent advances in nanoprecipitation: from mechanistic insights to applications in nanomaterial synthesis. Soft Matter 21:2759–2781
17. Green JJ, Zugates GT, Langer R, Anderson DG (2009) Poly (β-amino esters): procedures for synthesis and gene delivery. Methods Mol Biol 480:53
18. Luly KM, Yang H, Lee SJ et al. (2022) Poly(beta-amino ester)s as high-yield transfection reagents for recombinant protein production. Int J Nanomedicine 17:4469
19. Panyam J, Labhasetwar V (2003) Biodegradable nanoparticles for drug and gene delivery to cells and tissue. Adv Drug Deliv Rev 55:329–347
20. Cun D, Jensen DK, Maltesen MJ et al. (2011) High loading efficiency and sustained release of siRNA encapsulated in PLGA nanoparticles: quality by design optimization and characterization. Eur J Pharm Biopharm 77:26–35
21. Cun D, Foged C, Yang M et al. (2010) Preparation and characterization of

poly(dl-lactide-co-glycolide) nanoparticles for siRNA delivery. Int J Pharm 390:70–75
22. Bao W, Ji P, Xi WS, et al. (2026) Genome editing of Spp1 by inhalable CRISPR/Cas9 formulation for treating pulmonary fibrosis. J Controll Release 389, 114424.
23. Cun D, Jensen DK, Maltesen MJ et al. (2011) High loading efficiency and sustained release of siRNA encapsulated in PLGA nanoparticles: quality by design optimization and characterization. Eur J Pharm Biopharm 77:26–35
24. Jensen DK, Jensen LB, Koocheki S et al. (2012) Design of an inhalable dry powder formulation of DOTAP-modified PLGA nanoparticles loaded with siRNA. J Control Release 157:141–148. https://doi.org/10.1016/J.JCONREL.2011.08.011
25. Barar J (2015) Bioimpacts of nanoparticle size: why it matters?. Bioimpacts 5:113
26. Shao XR, Wei XQ, Song X et al. (2015) Independent effect of polymeric nanoparticle zeta potential/surface charge, on their cytotoxicity and affinity to cells. Cell Prolif 48:465–474
27. Fang Y, Zhang T, Song Y, Sun W (2020) Assessment of various crosslinking agents on collagen/chitosan scaffolds for myocardial tissue engineering. Biomed Mater 15:045003
28. Choi DG, Venkatesan J, Shim MS (2019) Selective anticancer therapy using pro-oxidant drug-loaded chitosan-fucoidan nanoparticles. Int J Mol Sci 20(13), 3220.
29. Çağlar EŞ EkerFidanEB, Gök MK et al. (2025) Development and in vitro characterization studies of novel chitosan nanoparticles for the treatment of Huntington's disease. ACTA Pharm Sci 63:249–270
30. Gan Q, Wang T, Cochrane C, McCarron P (2005) Modulation of surface charge, particle size and morphological properties of chitosan–TPP nanoparticles intended for gene delivery. Colloids Surf B Biointerfaces 44:65–73
31. Eltoukhy AA, Siegwart DJ, Alabi CA et al. (2012) Effect of molecular weight of amine end-modified poly(β-amino ester)s on gene delivery efficiency and toxicity. Biomaterials 33:3594
32. Pulingam T, Foroozandeh P, Chuah JA, Sudesh K (2022) Exploring various techniques for the chemical and biological synthesis of polymeric nanoparticles. Nanomaterials 12:12
33. Kuddushi M, Kanike C, Xu BB, Zhang X (2025) Recent advances in nanoprecipitation: from mechanistic insights to applications in nanomaterial synthesis. Soft Matter 21:2759–2781
34. Routkevitch D, Sudhakar D, Conge M et al. (2020) Efficiency of cytosolic delivery with poly(beta-amino ester) nanoparticles is dependent on the effective pKa of the polymer. ACS Biomater Sci Eng 6:3411
35. Ding J, Zhang H, Dai T et al. (2024) TPGS-b-PBAE copolymer-based polyplex nanoparticles for gene delivery and transfection in vivo and in vitro. Pharmaceutics 16:213
36. Makadia HK, Siegel SJ (2011) Poly lactic-co-glycolic acid (PLGA) as biodegradable controlled drug delivery carrier. Polymers (Basel) 3:1377
37. Lu Y, Cheng D, Niu B, et al. (2023) Properties of poly (lactic-co-glycolic acid) and progress of poly (lactic-co-glycolic acid)-based biodegradable materials in biomedical research. Pharmaceuticals 16(3):454.
38. Fabrication and characterization of PLGA nanoparticles encapsulating large CRISPR–Cas9 plasmid | Enhanced Reader
39. Astete CE, Sabliov CM (2006) Synthesis and characterization of PLGA nanoparticles. J Biomater Sci Polym Ed 17:247–289
40. Stevanović MM, Qian K, Huang L, Vukomanović M (2025) PLGA-based co-delivery nanoformulations: overview, strategies, and recent advances. Pharmaceutics 17(12), 1613.
41. Ito F, Fujimori H, Honnami H et al. (2009) Study of types and mixture ratio of organic solvent used to dissolve polymers for preparation of drug-containing PLGA microspheres. Eur Polym J 45:658–667
42. Sahana DK, Mittal G, Bhardwaj V, Kumar MNVR (2008) PLGA nanoparticles for oral delivery of hydrophobic drugs: Influence of organic solvent on nanoparticle formation and release behavior in vitro and in vivo using estradiol as a model drug. J Pharm Sci 97:1530–1542
43. Sousa F, Lee H, Almeida M et al. (2024) Immunostimulatory nanoparticles delivering cytokines as a novel cancer nanoadjuvant to empower glioblastoma immunotherapy. Drug Deliv Transl Res 14:2655–2667
44. Wei CG, Zhang R, Wei LY, et al. (2022) Calcium phosphate-based nanomedicine mediated CRISPR/Cas9 delivery for prostate cancer therapy. Front Bioeng Biotechnol 10, 1078342.

Open Access This chapter is licensed under the terms of the Creative Commons Attribution-NonCommercial-NoDerivatives 4.0 International License (http://creativecommons.org/licenses/by-nc-nd/4.0/), which permits any noncommercial use, sharing, distribution and reproduction in any medium or format, as long as you give appropriate credit to the original author(s) and the source, provide a link to the Creative Commons license and indicate if you modified the licensed material. You do not have permission under this license to share adapted material derived from this chapter or parts of it.

The images or other third party material in this chapter are included in the chapter's Creative Commons license, unless indicated otherwise in a credit line to the material. If material is not included in the chapter's Creative Commons license and your intended use is not permitted by statutory regulation or exceeds the permitted use, you will need to obtain permission directly from the copyright holder.





Chapter 13

Quantitative Analysis of CRISPR Encoding Plasmid DNA–Nanocarrier Interactions by Gel Electrophoresis and Densitometry

Cecilia Vasti, Laura E. Valenti and Carla E. Giacomelli

Abstract

Nanoparticle-based carriers are key systems for the transport and delivery of nucleic acids in gene therapy, RNA therapeutics, and genome editing applications. The development of efficient delivery systems for CRISPR–Cas technologies requires reliable methods to evaluate nanocarrier–nucleic acid interactions, binding efficiency, and loading capacity. Agarose gel electrophoresis is commonly used to study these interactions through gel retardation assays, but results are often interpreted qualitatively based on visual inspection of DNA band migration. In this chapter, we present a quantitative approach that combines agarose gel electrophoresis with densitometric analysis of plasmid DNA (pDNA) bands to evaluate the interaction between pDNA and inorganic nanocarriers. The method relies on quantifying the fraction of free pDNA that migrates through the gel, while nanocarrier–pDNA systems remain near the loading wells. Band intensities are analyzed using ImageJ software to determine the amount of free pDNA and to estimate binding efficiency through depletion analysis. This protocol provides a simple and accessible strategy to quantify the loading of pDNA encoding CRISPR components, guide RNA constructs, or other nucleic acid cargos, facilitating the development and optimization of nanoparticle-based delivery systems for genome editing applications.

Keywords Nanocarrier–pDNA interaction, Agarose gel electrophoresis, Densitometric analysis, Depletion assay

1 Introduction

Nanocarriers have emerged as powerful systems to transport and deliver nucleic acids in biomedical and biotechnological applications [1]. The rapid development of gene therapy, RNA therapeutics, and genome-editing technologies has intensified the need for efficient strategies capable of introducing genetic material into cells [2, 3]. Compared to direct administration of naked nucleic acids, nanocarriers enhance stability, protect cargo from enzymatic degradation, and promote cellular uptake. Most nanocarrier–nucleic acid systems rely on electrostatic interactions between negatively charged

Duško Lainšček et al. (eds.), *CRISPR Delivery*, Methods in Molecular Biology, vol. 3075,
https://doi.org/10.1007/978-1-0716-5547-4_13,
© The Author(s) 2027

nucleic acids and positively charged nanoparticle surfaces [4]. The phosphate backbone of plasmid DNA, messenger RNA, and other nucleic acids enables their association with cationic nanomaterials, leading to the formation of nanoscale systems that condense and protect the genetic cargo while facilitating transport across biological barriers [5]. Among available systems, inorganic nanocarriers have attracted particular interest because of their structural robustness, tunable surface chemistry, and potential for multifunctional design. Nanomaterials such as layered double hydroxides and metal oxides, and other inorganic nanostructures can be engineered to efficiently bind nucleic acids while providing additional capabilities, including imaging, controlled release, and environmental responsiveness [6]. Their relevance has further increased with the emergence of genome-editing technologies such as CRISPR/Cas, for which efficient intracellular delivery of plasmid DNA, guide RNAs, or other components remains a key challenge [7]. Given the central role of nanocarrier–nucleic acid interactions in these systems, understanding the mechanisms that rule binding and loading efficiency is essential to optimize the performance of the nanocarrier in both in vitro and in vivo applications [8]. The efficiency of nucleic acid binding directly influences the stability of the formulation, its protection against enzymatic degradation, and its ability to transport genetic material into target cells. Consequently, several analytical techniques have been developed to evaluate the interaction between nanocarriers and nucleic acids.

Traditionally [9, 10], the interactions between nanocarriers and molecular cargo are studied through batch experiments, in which nanocarriers are incubated with a defined concentration of the molecule of interest under controlled conditions of pH, ionic strength, and temperature until steady-state conditions are reached. Afterward, the amount of loaded and free molecules is quantified by measuring the decrease in the concentration of the molecule remaining in solution (depletion analyses), using techniques such as UV–vis and fluorescence spectroscopies, or chromatographic methods. By varying the initial concentration of the molecule of interest as well as the solution conditions, key parameters such as loading capacity and binding affinity can be evaluated [9, 11]. These methodologies are conceptually simple, experimentally accessible, and compatible with a wide range of analytical techniques. However, these experiments generally require relatively large sample volumes and significant amounts of both nanocarriers and cargo molecules, which can become costly or impractical when working with biomolecules such as proteins or nucleic acids.

To overcome this limitation, agarose gel electrophoresis–based assays, commonly referred to as gel retardation assays or electrophoretic mobility shift assays, are commonly used due to their simplicity and accessibility. The principle of the method is based on

the electrophoretic mobility of nucleic acids [11, 12, 13]. Free DNA migrates through the agarose matrix according to its size and charge when an electric field is applied. However, the electrophoretic mobility of loaded nucleic acids is typically reduced due to changes in size, charge, and overall conformation. In many cases, the resulting nanocarrier–nucleic acid systems are sufficiently large or electrically neutralized to prevent migration through the gel, causing them to remain near the loading wells. As a result, gel retardation assays allow qualitative evaluation of nucleic acid loading by comparing the intensity of the migrating DNA band with that of the free DNA control. A decrease in the intensity of the migrating band indicates increasing nucleic acid loading capacity of the nanocarrier.

Despite their widespread use, conventional gel retardation assays are often interpreted qualitatively, relying primarily on visual inspection of DNA band disappearance. This approach may limit the ability to accurately compare different nanocarrier formulations or to quantitatively determine loading efficiency. However, when combined with fluorescence staining and digital image analysis, it can also provide quantitative information about the amount of DNA present in each band. The fluorescence emitted by nucleic acid–intercalating dyes, such as ethidium bromide or SYBR-based stains, is proportional to the amount of nucleic acid within the gel over a defined linear range of detection. As a result, the intensity of a DNA band can be used as an indirect measure of the quantity of nucleic acid present in the sample. Quantitative analysis of DNA bands relies on the relationship between fluorescence signal intensity and nucleic acid concentration. Within the linear dynamic range of the detection system, the measured intensity of a band increases proportionally with the amount of DNA loaded in the gel. This relationship enables the construction of calibration curves using lanes containing known amounts of plasmid DNA. By comparing the intensity of unknown samples to these standards, it is possible to estimate the amount of DNA present in each lane [14]. For this reason, the integration of densitometric analysis of gel images has emerged as a valuable strategy to transform these assays into semiquantitative or quantitative methods to evaluate nanocarrier–nucleic acid interactions.

The use of digital image analysis software has greatly facilitated densitometric quantification of nucleic acids in electrophoresis gels. Programs such as ImageJ or its distribution Fiji allow the measurement of band intensity through integrated density calculations or lane profile analysis. These tools enable the extraction of quantitative information from gel images while maintaining reproducibility and transparency in data processing. When applied to nanocarrier–nucleic acid interaction studies, densitometric analysis of agarose gels can be used to quantify the fraction of free nucleic acid that remains capable of migrating through the gel [15]. By comparing the intensity of the migrating DNA band with that of the free DNA control, the amount

of nucleic acid associated with nanoparticles can be estimated through depletion analysis. This approach provides a simple, reliable, and accessible strategy for quantifying the loading capacity and efficiency of the nanocarriers using small volumes and low concentrations without requiring specialized instrumentation.

In this chapter, we present a practical gel-based protocol that combines agarose electrophoresis and densitometric analysis to enable quantitative assessment of plasmid DNA binding to inorganic nanocarriers (Fig. 1).

2 Materials

2.1 Reagents

1. Agarose.
2. Plasmid DNA (pDNA).
3. Nanoparticle suspension (e.g., inorganic nanoparticles such as layered double hydroxide nanoparticles [16–19]).
4. DNA molecular weight marker (DNA ladder).
5. DNA loading buffer.
6. DNA intercalating dye (e.g., ethidium bromide, GelRed, or SYBR Safe).
7. Nuclease-free ultra-pure water.
8. TAE buffer (1×): 40 mM Tris-acetate, 1 mM EDTA.
9. TAE buffer (50× stock): 2 M Tris base, 1 M acetic acid, 50 mM EDTA.
10. Prepare 1× TAE running buffer by diluting the 50× stock solution 1:50 in ultra-pure water.

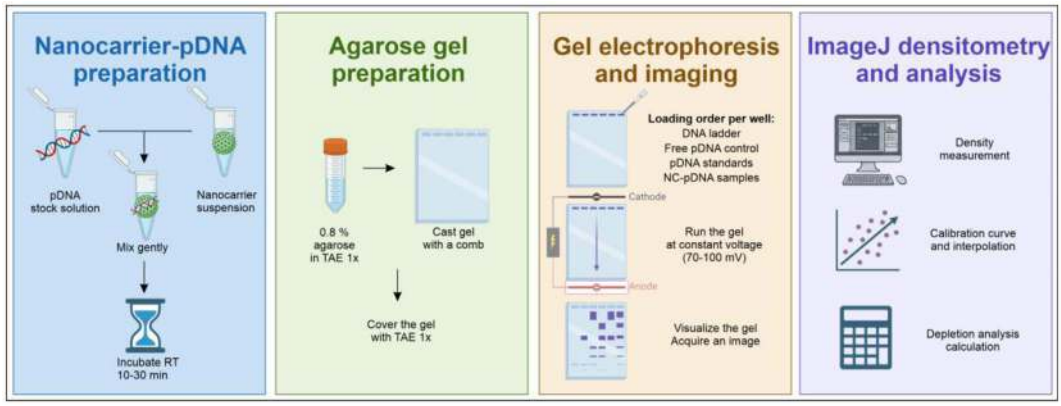


Fig. 1 Schematic workflow of the four sequential stages for the quantitative analysis of nanocarrier–pDNA interactions: (**a**) preparation of nanocarrier–pDNA system, (**b**) preparation of agarose gels in TAE buffer and casting, (**c**) electrophoretic separation and imaging, and (**d**) densitometric analysis

11. Add ultra-pure water up to 1 L.

DNA loading buffer: commercially available loading dye containing tracking dyes and density agents (e.g., glycerol or Ficoll).

2.2 Equipment

1. Horizontal agarose gel electrophoresis chamber.
2. Power supply for electrophoresis.
3. Gel casting tray and combs.
4. Microwave oven or heating plate for agarose dissolution.
5. Conical polypropylene centrifuge microtube.
6. Micropipettes and sterile pipette tips.
7. Gel documentation system.
8. UV or blue-light transilluminator.
9. Computer for image analysis.
10. Open-source image analysis software (e.g., Fiji/ImageJ, ROI Manager, and Gel Analyzer).

3 Methods

3.1 Preparation of Nanocarrier–Nucleic Acid Systems

Nanocarrier–plasmid DNA (pDNA) systems were prepared by mixing pDNA solutions with nanocarrier suspensions at different nanoparticle-to-DNA ratios. This preparation should be carried out under sterile conditions when the formulations are intended for biological applications.

1. Prepare pDNA stock solutions in an appropriate buffer (e.g., nuclease-free water or 5 mM buffer). Determine the pDNA concentration spectrophotometrically and adjust the solution to the desired working concentration (*see* **Note 1**).
2. Prepare the nanocarrier suspension in the same buffer used for the pDNA solution whenever possible to minimize ionic strength differences that may affect the loading capacity (*see* **Note 2**).
3. Calculate the required volumes of nanocarrier suspension and pDNA solution to reach the desired nanocarrier-to-pDNA (nanocarrier/pDNA) ratios. Depending on the system under study, several nanocarrier/pDNA ratios (ranging between 10:1 and 1000:1) should be tested to evaluate the interaction range and loading capacity.
4. In a conical polypropylene centrifuge microtube, add the pDNA solution first and then slowly add the nanocarrier suspension while gently mixing the solution to promote homogeneous formation.

5. Mix the samples gently by pipetting up and down or by mild vortexing for a few seconds. Avoid vigorous mixing that could shear pDNA.
6. Incubate the mixtures at room temperature for an appropriate period (typically 10–30 min) until reaching steady state conditions.
7. After incubation, do not centrifuge nor filtrate the samples. The nanocarrier–pDNA systems are typically too large to migrate through the agarose matrix and therefore remain in or near the loading well during electrophoresis, whereas free pDNA migrates through the gel. Consequently, the samples should be loaded directly onto the agarose gel (see Sect. 3.2) to evaluate the amount of free pDNA by electrophoretic separation and subsequent densitometric analysis (*see* **Note 3**).

3.2 Preparation of Agarose Gels

Agarose gels are prepared using standard electrophoresis conditions suitable for pDNA migration. The agarose percentage indicated below provides good resolution for pDNA molecules under typical electrophoresis conditions.

1. Prepare a 0.8% (w/v) agarose gel by weighing the appropriate amount of agarose and adding it to TAE buffer (1×). For example, dissolve 0.4 g agarose in 50 mL of TAE buffer (*see* **Note 4**).
2. Heat the suspension using a microwave or heating plate until the agarose is completely dissolved and the solution becomes clear.
3. Allow the agarose solution to cool to approximately 50–60°C before adding the DNA intercalating dye. The agarose solution should be cooled to 40°C before adding DNA stains, particularly when using temperature-sensitive dyes. Excessively hot agarose may reduce staining efficiency or degrade the dye.
4. Add an appropriate DNA intercalating dye (e.g., ethidium bromide or a safer alternative such as SYBR Safe or GelRed) according to the manufacturer's recommendations (*see* **Note 5**).
5. Pour the molten agarose into a gel casting tray fitted with a comb to create wells.
6. Allow the gel to solidify completely at room temperature (typically 20–30 min).
7. Once polymerized, carefully remove the comb and place the gel into the electrophoresis chamber.
8. Cover the gel with 1× TAE running buffer, ensuring that the gel is completely submerged.

3.3 Agarose Gel Electrophoresis

Electrophoresis is used to separate free pDNA from nanocarrier–pDNA systems. Under typical conditions, these systems remain near the loading wells, while free pDNA migrates through the agarose matrix, as schematically shown in Fig. 2.

1. Prepare the samples by mixing each pDNA or nanocarrier–pDNA system with an appropriate loading buffer (pDNA/loading buffer 5:1 and 20 µL final volume).
2. Load the gel wells with a molecular weight marker or DNA ladder to allow visualization of migration and approximate size estimation.
3. Load at least four wells containing known amounts of free pDNA (ranging between 10 and 100 ng/µL) to generate the calibration curve required for densitometric quantification.
4. Load the nanocarrier–pDNA systems prepared as described in Sect. 3.1.
5. Place the lid on the electrophoresis chamber and connect the electrodes.
6. Run the gel at constant voltage (typically 70–100 V) until the loading dye has migrated up to 80% through the total gel length.
7. After electrophoresis, visualize the gel using a UV or blue-light transilluminator and acquire an image suitable for densitometric analysis as described in Sect. 3.4.

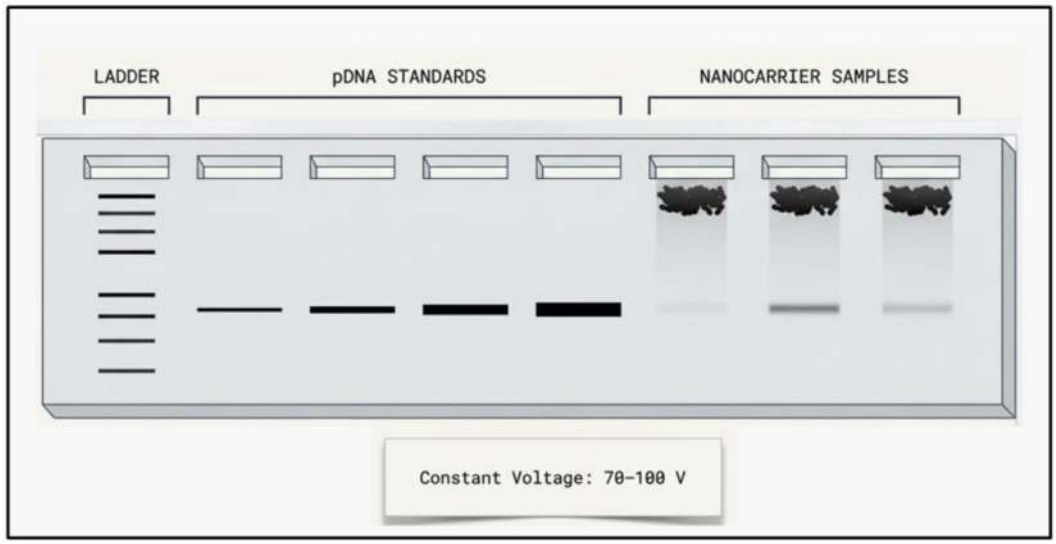


Fig. 2 Representative agarose gel layout and band pattern used for the quantitative assessment of nanocarrier–pDNA interactions. The gel includes three distinct regions: a molecular weight ladder, a series of pDNA standards for calibration, and nanocarrier–pDNA samples prepared at defined experimental conditions. Free pDNA migrates from nanocarrier-adsorbed pDNA, which remains partially or fully retained in the loading wells

3.4 Densitometric Analysis Using ImageJ

General considerations: Densitometric analysis is performed to quantify the amount of free pDNA remaining in each sample after incubation with nanocarriers. The method assumes that the fluorescence intensity of the DNA band is proportional to the amount of nucleic acid present within the linear range of detection. Thus, a calibration curve is generated using lanes loaded with known amounts of free pDNA, and the intensity measured for each unknown sample is interpolated against this curve to estimate the amount of unbound pDNA. Binding efficiency is then calculated by depletion analysis (Fig. 1).

3.4.1 Image Acquisition Requirements

1. After electrophoresis, place the gel on a UV or blue-light transilluminator and acquire the image using a gel documentation system.
2. Use the same exposure settings for all samples intended to be compared quantitatively within the same experiment (*see* **Note 6**).
3. Avoid saturated bands (Fig. 3), since signal saturation prevents reliable densitometric analysis (*see* **Note 7**).
4. Save the image in a non-compressed format, preferably TIFF, to preserve pixel intensity values (*see* **Note 8**).
5. Include in the same gel:
   a. a molecular weight marker,
   b. a free pDNA control,
   c. a series of free pDNA standards of known concentration, and
   d. the nanocarrier–pDNA samples to be analyzed.

3.4.2 Opening and Preparing the Image in ImageJ/Fiji

1. Open Fiji/ImageJ.

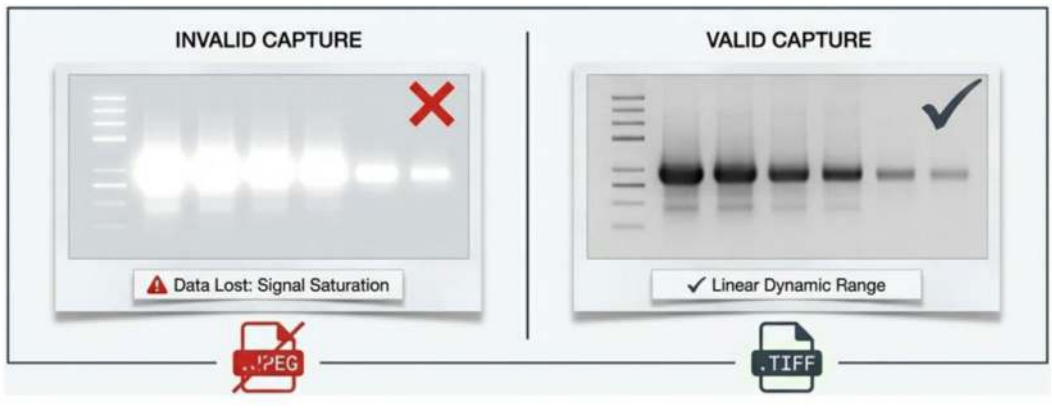


Fig. 3 Comparative agarose gel images illustrating the impact of image acquisition conditions on the reliability of densitometric quantification of nanocarrier–pDNA interactions. Gels compare suboptimal and optimized imaging settings, highlighting common artifacts such as signal saturation, low contrast, uneven illumination, and background noise

2. Import the gel image by selecting File > Open and choosing the corresponding TIFF file.
3. If the image is in color, convert it to grayscale by selecting Image > Type > 8-bit.
4. If necessary, invert the image using Edit > Invert, so that bands appear as dark peaks on a light background or according to the preferred analysis mode. The same approach must be maintained for all analyzed images.
5. Inspect the image visually to verify that (see Fig. 3):
   a. all lanes are clearly resolved,
   b. bands are not overexposed,
   c. background is reasonably uniform, and
   d. no major artifacts interfere with band detection.

3.4.3 Background Correction

1. Apply background subtraction to reduce uneven fluorescence across the gel.
2. Select Process > Subtract Background.
3. Use the same rolling-ball radius or background subtraction settings for the entire image and for all comparable gels within the same analysis series.
4. Do not modify individual lanes separately, since this may introduce bias in the quantitative comparison.
5. After subtraction, verify that the bands remain clearly identifiable and that the background is flattened without loss of real signal.

3.4.4 Definition of Regions of Interest (ROIs)

1. Select the rectangle tool in ImageJ.
2. Draw a rectangular region of interest enclosing the first lane to be analyzed as indicated in Fig. 4.
3. The rectangle should:
   a. include the entire width of the lane,
   b. cover the migration region containing the band of interest, and
   c. extend over the same vertical range for all lanes.
4. Add the selected region to the ROI Manager by pressing Add.
5. Move the same rectangle horizontally to the next lane without changing its dimensions (*see* **Note 9**).
6. Repeat this procedure for all lanes, including standards, free pDNA controls, and nanocarrier-containing samples (*see* **Note 10**).

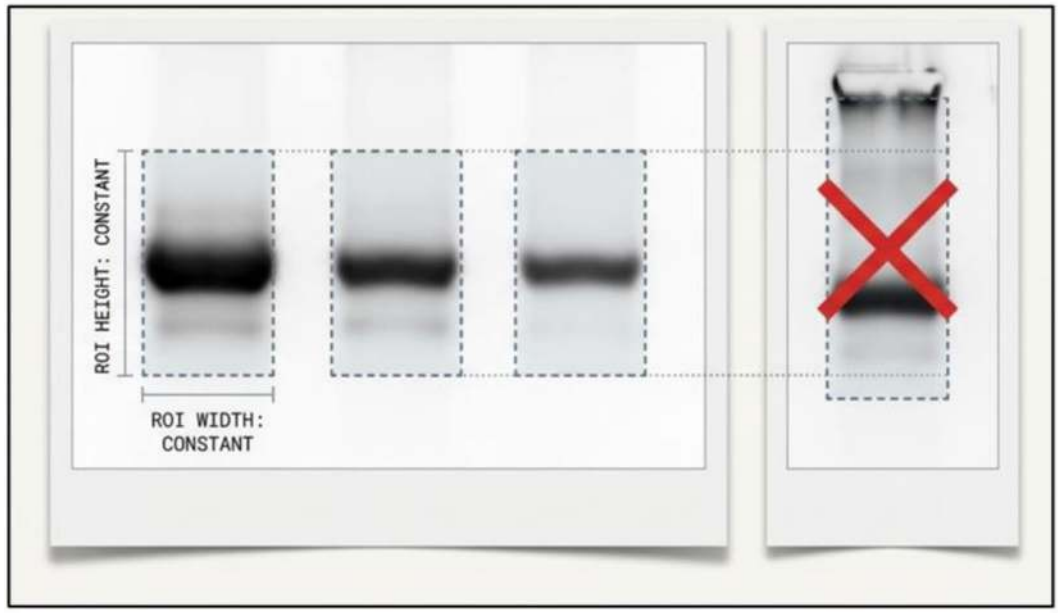


Fig. 4 Zoomed-in view of agarose gel bands illustrating the selection of regions of interest (ROI) for densitometry analysis of pDNA. Well-resolved bands enable accurate delineation of ROI and reliable integration of signal intensity, whereas unresolved or poorly resolved bands complicate ROI definition and introduce significant uncertainty in intensity measurements

7. Keep the ROI size strictly constant across all lanes analyzed in the same gel.

3.4.5 Lane Profile Extraction

1. Once the ROIs are defined, select the first lane ROI.
2. Generate the intensity profile using Analyze > Gels > Plot Lanes or, alternatively, record the corresponding integrated density directly if the band is well isolated.
3. For gel profile analysis, identify the peak corresponding to the migrating free pDNA band.
4. Use the straight-line tool to define the baseline beneath the peak if needed (*see* **Note 11**).
5. Measure the peak area corresponding to the free pDNA.
6. Repeat the same analysis for all lanes using the same criteria for baseline selection and peak integration.
7. Record all values in a spreadsheet for subsequent calculations.

3.4.6 Integrated Density Measurement Approach

As an alternative to peak integration from lane plots, the free pDNA signal may be quantified using the integrated density of the selected band region, as shown in Fig. 5.

1. Select a rectangular ROI around the band of interest.

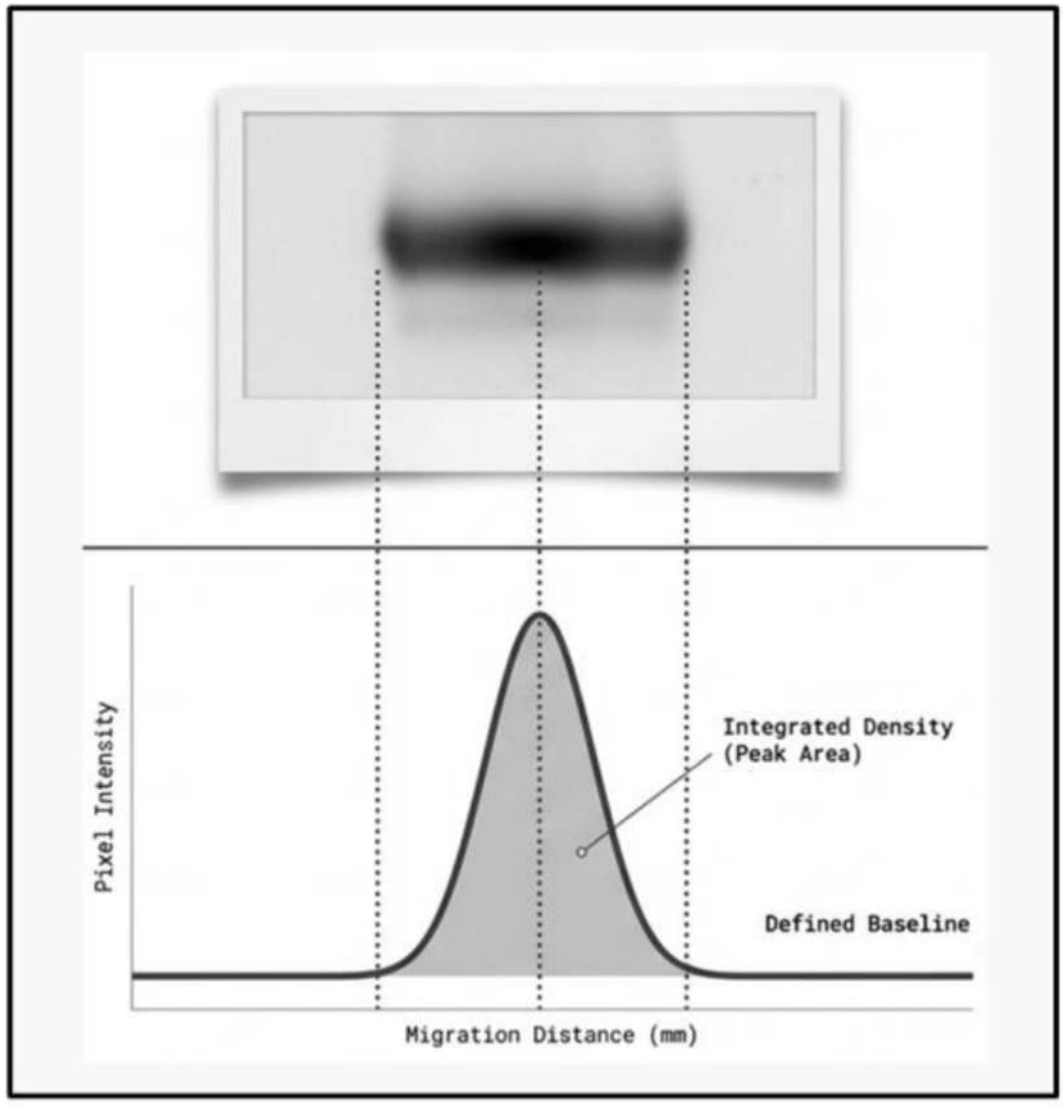


Fig. 5 Enlarged view of agarose gel band and the corresponding intensity profile used to calculate the integrated density of pDNA. The shaded area under the curve defines the integrated density after appropriate baseline subtraction

2. Go to Analyze > Set Measurements and select at least:
   a. area,
   b. mean gray value, and
   c. integrated density.
3. Measure each band using Analyze > Measure.
4. Record the integrated density values for all standards and unknown samples.

5. When this approach is used, the same band area and background treatment must be applied consistently to all lanes.

3.4.7 Construction of the Calibration Curve

1. Load into the gel a set of free pDNA standards spanning the concentration range expected for the unknown samples (Fig. 2).
2. Measure the band intensity of each standard using the same workflow applied to the experimental lanes.
3. Build a calibration curve by plotting as shown in Fig. 6:
   - *x*-axis: amount or concentration of free pDNA loaded in the gel lanes,
   - *y*-axis: measured band intensity (peak area or integrated density).
4. Fit the data using linear regression, but only within the range where the relationship between signal and pDNA amount is linear.
5. Verify that the coefficient of determination (R^2) of the calibration curve is sufficiently high (typically $R^2 \geq 0.98$) to ensure reliable quantitative analysis.
6. If any standard falls outside the linear region because of a very weak or saturated signal, exclude it from the final fit and repeat the calibration if necessary.

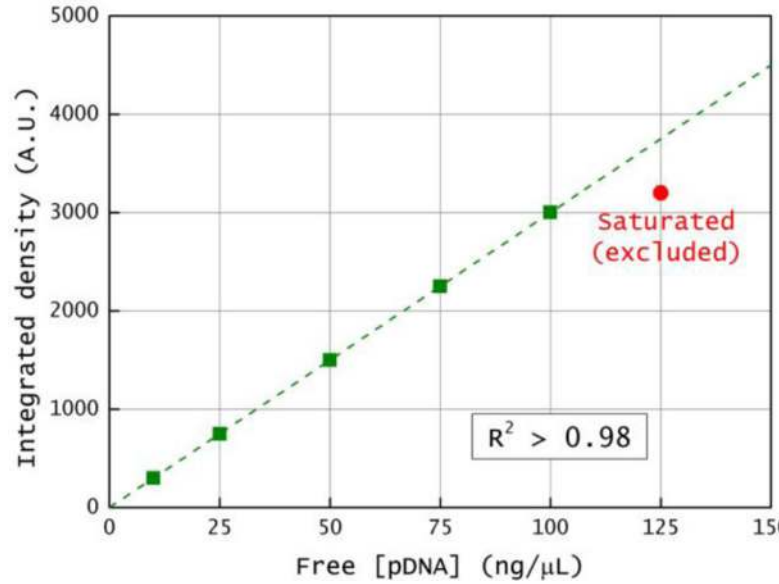


Fig. 6 Calibration curve obtained from the intensity profiles of pDNA standards

3.4.8 Determination of Free pDNA in Nanocarrier-Containing Samples

1. Measure the band intensity of each nanocarrier–pDNA sample using the same analysis parameters defined for the standards.
2. Interpolate the measured intensity in the calibration curve to estimate the amount of free pDNA present in the lane.
3. Correct for dilution factors if the original sample was diluted before loading.
4. Express the result as shown in Fig. 7:
   a. ng of free pDNA loaded in the gel lane,
   b. concentration n of free pDNA in the analyzed sample,
   c. or fraction of free pDNA relative to the input control.

3.4.9 Calculation of Depletion and Binding Efficiency

The amount of pDNA associated with nanocarriers is determined indirectly from the depletion of free pDNA:

$$p\mathrm{DNA}_{\mathrm{bound}} = p\mathrm{DNA}_{\mathrm{total}} - p\mathrm{DNA}_{\mathrm{free}}$$

Where $p\mathrm{DNA}_{\mathrm{total}}$ is the amount of pDNA initially added to the formulation and $p\mathrm{DNA}_{\mathrm{free}}$ is the amount quantified by densitometric analysis in the free migrating band.

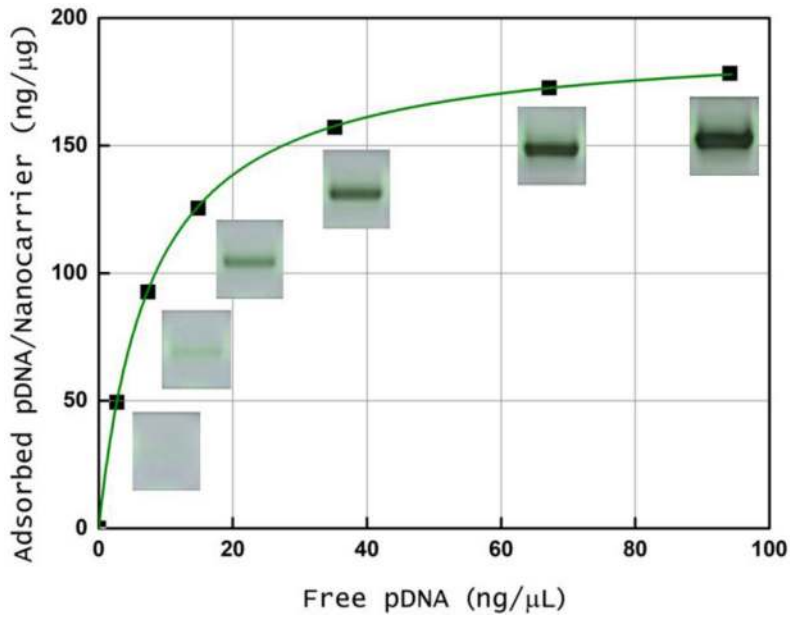


Fig. 7 Nanocarrier–pDNA interactions plot showing the loading capacity. An enlarged view of agarose gel bands is included to show the intensity band corresponding to free pDNA in each experimental condition

Binding efficiency was calculated as:

$$\text{Binding efficiency (\%)} = \left(\frac{p\text{DNA}_{\text{bound}}}{p\text{DNA}_{\text{total}}} \right) \times 100$$

3.4.10 Replicates and Data Treatment

1. Perform at least three independent experiments whenever possible.
2. Within each gel, include technical replicates if lane availability allows.
3. Analyze all replicate images using the same ImageJ settings.
4. Report results as mean ± standard deviation or mean ± standard error, depending on the statistical treatment adopted.
5. When comparing formulations, use the same gel composition, electrophoresis conditions, staining protocol, and image acquisition settings to minimize inter-experimental variability.

4 Notes

1. pDNA purity and integrity are critical for reproducible nanocarrier–pDNA formation. Highly pure plasmid preparations with A260/A280 ratios between approximately 1.8 and 2.0 are recommended. Degraded DNA or contaminants such as salts or proteins may affect nanocarrier binding efficiency and electrophoretic behavior.
2. The ionic strength and composition of the buffer can significantly influence nanocarrier–pDNA interactions, particularly when electrostatic interactions are involved. For this reason, nanocarrier suspensions should preferably be prepared in the same buffer used for the pDNA solution.
3. Incubation time may require optimization depending on the nanocarrier. While 10–30 min is sufficient for many electrostatic driven interactions, some systems may require longer incubation times to reach steady state conditions.
4. The agarose concentration may need to be adjusted depending on plasmid size and the resolution required. Lower agarose percentages (e.g., 0.7%–0.8%) facilitate migration of large plasmid DNA molecules, whereas higher concentrations (1.0%–1.5%) may improve resolution of smaller fragments or closely migrating bands.
5. Safer nucleic acid stains such as SYBR Safe or GelRed can be used instead of ethidium bromide when reduced toxicity is

desired. However, fluorescence intensity and detection sensitivity may vary depending on the stain used.

6. For quantitative analysis, all images must be acquired using identical exposure settings. Variations in exposure time or detector sensitivity can significantly affect fluorescence intensity measurements and compromise the comparison between samples.
7. Signal saturation occurs when fluorescence intensity exceeds the dynamic range of the detector. Saturated pixels cannot be quantified reliably because intensity information is lost. If saturation occurs, reduce the exposure time and reacquire the image.
8. Images intended for densitometric analysis should be saved in non-compressed formats such as TIFF. Compressed image formats (e.g., JPEG) may alter pixel intensity values and reduce the accuracy of quantitative measurements.
9. The ROI should include only the region containing the migrating pDNA band. Regions containing strong background fluorescence, gel artifacts, or signal from retained nanocarrier–pDNA systems near the loading wells should be excluded whenever possible.
10. The same ROI dimensions must be used for all lanes within the gel. Changing the width or height of the ROI between lanes introduces systematic errors in integrated density measurements and compromises quantitative comparison.
11. Accurate baseline definition is essential for reliable peak integration. When using the lane profile method, ensure that the baseline is placed consistently beneath each peak to avoid overestimation or underestimation of band intensity.

Acknowledgments

The publication is based upon work by COST Action CA21113: Genome Editing for the Treatment of Human Diseases (https://www.genehumdi.eu), supported by European Cooperation in Science and Technology (COST). The authors acknowledge CONICET (PIP 11220210100267CO) and Secretaría de Ciencia y Tecnología-Universidad Nacional de Córdoba (Formar 2023) and Fondo para la Investigación Científica y Tecnológica (PICT-2020 SERIE A-02476) for financial support.

Competing Interests The authors declare no competing interests.

References

1. Kim M, Hwang Y, Lim S et al. (2024) Advances in nanoparticles as non-viral vectors for efficient delivery of CRISPR/Cas9. Pharmaceutics 16:1197. https://doi.org/10.3390/pharmaceutics16091197
2. Khirallah J, Eimbinder M, Li Y, Xu Q (2023) Clinical progress in genome-editing technology and in vivo delivery techniques. Trends Genet. 39:208–216
3. Guzmán-Sastoque P, Rodríguez CF, Monsalve MC et al. (2025) Nanotheranostics revolutionizing gene therapy: emerging applications in gene delivery enhancement. J Nanotheranostics 6:10. https://doi.org/10.3390/jnt6020010
4. Bian X, Zhou L, Luo Z et al. (2025) Emerging delivery systems for enabling precision nucleic acid therapeutics. ACS Nano 19:4039–4083. https://doi.org/10.1021/acsnano.4c11858
5. Ita K (2020) Polyplexes for gene and nucleic acid delivery: progress and bottlenecks. Eur J Pharm Sci 150:105358. https://doi.org/10.1016/j.ejps.2020.105358
6. Vasti C, D'Alessandro L, Aristizabal Bedoya D et al. (2026) From surface chemistry to nuclear targeting: the multifaceted challenge of genetic delivery via inorganic nanoparticles. Hybrid Adv 12:100586. https://doi.org/10.1016/j.hybadv.2025.100586
7. Seijas A, Cora D, Novo M et al. (2025) CRISPR/Cas9 delivery systems to enhance gene editing efficiency. Int J Mol Sci 26:4420. https://doi.org/10.3390/ijms26094420
8. Mendes BB, Conniot J, Avital A et al (2022) Nanodelivery of nucleic acids. Nat Rev Methods Primers 2:24
9. Bedoya DA, Vasti C, Rojas R, Giacomelli CE (2017) Risedronate functionalized layered double hydroxides nanoparticles with bone targeting capabilities. Appl Clay Sci 141:257–264. https://doi.org/10.1016/j.clay.2017.03.001
10. Vasti C, Pfaffen V, Ambroggio E et al. (2017) A systematic approach to the synthesis of LDH nanoparticles by response surface methodology. Appl Clay Sci 137:151–159. https://doi.org/10.1016/j.clay.2016.12.023
11. Vasti C, Aristizabal Bedoya D, Bonnet LV et al. (2020) Synthetic and biological identities of layered double hydroxides nanocarriers functionalized with risedronate. Appl Clay Sci 199:105880. https://doi.org/10.1016/j.clay.2020.105880
12. Stowell JAW, Tang TTL, Seidel M, Passmore LA (2021) Gel-based analysis of protein–nucleic acid interactions. In: Hennig J (ed) Protein–ligand interactions. Methods in molecular biology, vol 2263. Humana, New York, NY, pp 321–339
13. Ream JA, Lewis LK, Lewis KA (2016) Rapid agarose gel electrophoretic mobility shift assay for quantitating protein: RNA interactions. Anal Biochem 511:36–41. https://doi.org/10.1016/j.ab.2016.07.027
14. Tomlinson C, Rajasekaran A, Brochu-Gaudreau K et al. (2024) A convenient analytic method for gel quantification using ImageJ paired with Python or R. PLoS ONE 19:e0308297. https://doi.org/10.1371/journal.pone.0308297
15. Qin WJ, Yung LYL (2007) Nanoparticle-based detection and quantification of DNA with single nucleotide polymorphism (SNP) discrimination selectivity. Nucleic Acids Res 35:e111. https://doi.org/10.1093/nar/gkm602
16. Giacomelli CE, Rojas R (2015) Size-tunable LDH-protein hybrids toward the optimization of drug nanocarriers. J Mater Chem B 3:2778–2785. https://doi.org/10.1039/C4TB01992J
17. Rojas R, Vasti C, Giacomelli CE (2015) LDH nanoparticles: synthesis, size control and applications in nanomedicine. In: Layered Double Hydroxides (LDHs): Synthesis, Characterization and Applications. pp 101–120
18. Vasti C, Borgiallo A, Giacomelli CE, Rojas R (2017) Layered double hydroxide nanoparticles customization by polyelectrolyte adsorption: mechanism and effect on particle aggregation. Colloids Surf A Physicochem Eng Asp 533:316–322. https://doi.org/10.1016/j.colsurfa.2017.09.002
19. Rojas R, Aristizabal Bedoya D, Vasti C, Giacomelli CE (2014) LDH nanoparticles: synthesis, size control and applications in nanomedicine. In: Sherman IT (ed) Layered double hydroxides (LDHs). Synthesis, characterization and applications. pp 101–119

Open Access This chapter is licensed under the terms of the Creative Commons Attribution-NonCommercial-NoDerivatives 4.0 International License (http://creativecommons.org/licenses/by-nc-nd/4.0/), which permits any noncommercial use, sharing, distribution and reproduction in any medium or format, as long as you give appropriate credit to the original author(s) and the source, provide a link to the Creative Commons license and indicate if you modified the licensed material. You do not have permission under this license to share adapted material derived from this chapter or parts of it.

The images or other third party material in this chapter are included in the chapter's Creative Commons license, unless indicated otherwise in a credit line to the material. If material is not included in the chapter's Creative Commons license and your intended use is not permitted by statutory regulation or exceeds the permitted use, you will need to obtain permission directly from the copyright holder.





Chapter 14

Cell-Penetrating Peptide Delivery for CRISPR Applications

Abhik Paul, Hye Young Lee and Jan Tuma

Abstract

Cell-penetrating peptides (CPPs) provide a modular nonviral strategy for intracellular delivery of CRISPR/Cas9 components, particularly preassembled Cas9 ribonucleoprotein (RNP) complexes. This chapter summarizes key principles of CPP-mediated Cas9 RNP delivery, including noncovalent complexation and covalent CPP–Cas9 conjugation strategies. A representative protocol is provided for the preparation and evaluation of Cas9-K5 RNP, including in vitro uptake and reporter-editing assays, nucleofection-based functional controls, local intracranial delivery, immunofluorescence staining, and quantitative analysis of reporter activation in brain tissue.

Keywords Cell-penetrating peptides, CRISPR/Cas9, Cas9-K5 RNP, Nonviral delivery, Genome editing, Covalent conjugation, Noncovalent complexation, Intracellular delivery

1 Introduction

Cell-penetrating peptides (CPPs) represent a versatile class of short peptides capable of mediating the intracellular delivery of diverse molecular cargos, including proteins, nucleic acids, small molecules, and imaging probes [1,2]. Since the original observations that short cationic peptide motifs derived from proteins such as HIV-1 trans-activator of transcription (TAT) and *Antennapedia* homeodomain (pAntp) could cross biological membranes and accumulate intracellularly, CPPs have been extensively investigated as nonviral delivery systems in both basic research and translational applications [3–6]. CPPs are particularly useful as delivery tools because they can promote cellular uptake while preserving membrane integrity, and because their modular design allows compatibility with a wide range of biologically relevant cargos [7,8].

CPPs have recently gained attention as delivery platforms for CRISPR/Cas9 systems, particularly for preassembled Cas9 ribonucleoprotein complexes (Cas9 RNPs). Cas9 RNPs consist of Cas9 protein bound to sgRNA and provide a transient genome-editing format with limited nuclease exposure [9–11]. In CPP-mediated

Duško Lainšček et al. (eds.), *CRISPR Delivery*, Methods in Molecular Biology, vol. 3075,
https://doi.org/10.1007/978-1-0716-5547-4_14,
© The Author(s) 2027

workflows, the RNP can be assembled before cellular application and delivered directly into target cells. Efficient delivery requires CPP-dependent membrane interaction, cellular uptake, endosomal escape, cytosolic release, preservation of Cas9 activity, and nuclear import. Thus, CPP sequence, charge, amphipathicity, cargo format, and conjugation strategy are key determinants of CRISPR/Cas9 delivery efficiency [12,13].

CPPs are often classified according to physicochemical properties into cationic, amphipathic, and hydrophobic peptides, and may also be grouped by origin into protein-derived, chimeric, or fully synthetic sequences [8,14,15]. These classifications are useful because they reflect properties that influence delivery behavior. Charge distribution, amphipathicity, secondary-structure propensity, and sequence architecture all influence membrane binding, uptake pathways, endosomal escape, intracellular trafficking, and cargo complexation behavior [16–18]. In practice, this means that CPP-based CRISPR delivery does not represent a single universal platform, but rather a heterogeneous methodological field in which peptide design, cargo format, formulation conditions, and target cell type together determine delivery outcome.

Mechanistically, CPP-mediated uptake can proceed through multiple, nonmutually exclusive pathways. Depending on the peptide and cargo, cellular entry may involve direct translocation across the plasma membrane, energy-dependent endocytic pathways, or a combination of both [16,18,19]. Initial membrane association is typically driven by electrostatic interactions between positively charged CPPs and anionic membrane components, including glycosaminoglycans and negatively charged phospholipids [20,21]. Arginine-rich sequences often show particularly efficient uptake, likely due to favorable interactions of guanidinium groups with membrane-associated anionic moieties [22–24]. However, cellular internalization alone is not sufficient for successful genome editing. In many systems, endosomal escape remains a major rate-limiting step, because internalized complexes can otherwise be trapped in endosomes and ultimately degraded in lysosomes [25–27]. For Cas9 RNP delivery, intracellular release must then be followed by nuclear import, typically mediated by nuclear localization signals (NLSs) encoded within the Cas9 protein [28].

From a formulation perspective, CPP-based CRISPR delivery systems can be broadly divided into noncovalent and covalent strategies. In noncovalent systems, CPPs associate with Cas9 RNPs through supramolecular interactions, driven primarily by electrostatic attraction between cationic peptide residues and the negatively charged phosphate backbone of sgRNA, and in some systems further stabilized by hydrophobic contributions [2,9,18]. This approach is especially well-suited for negatively charged biomacromolecules and offers clear practical advantages, including formulation flexibility and

the possibility of simple aqueous mixing without chemical modification of the cargo. Representative systems include simple polycationic CPPs such as TAT or polyarginines, amphipathic peptides such as penetratin and transportan-related sequences, and more structurally optimized lipid-modified systems such as members of the PepFect family [3,6,29,30]. At the same time, noncovalent CPP systems may be highly sensitive to ionic strength, serum exposure, peptide:cargo ratio, and target cell context, which can complicate reproducibility and cross-system comparison [30,31].

In contrast, covalent CPP delivery systems rely on direct attachment of CPPs to Cas9, typically by recombinant fusion or chemical conjugation, followed by assembly of the CPP–Cas9 construct with sgRNA to generate the functional RNP complex [18,32,33]. Compared with noncovalent approaches, covalent systems provide better-defined composition, improved stoichiometric control, and often greater formulation reproducibility. These advantages are particularly relevant when precise control over carrier:cargo architecture is desired. However, covalent approaches also introduce additional complexity, including the need for protein engineering or site-selective chemical modification, and may interfere with Cas9 folding, activity, intracellular trafficking, or release if the design is suboptimal [13,33,34]. Covalent systems may be further divided into noncleavable and cleavable formats. In noncleavable constructs, the CPP remains permanently linked to Cas9 throughout the delivery process, whereas cleavable systems are designed to release the cargo in response to intracellular stimuli such as reducing conditions, acidic pH, or enzyme activity [33,35,36]. Although conceptually attractive, the practical development of such systems remains comparatively limited in the specific context of CPP-mediated Cas9 delivery.

Recent experimental studies illustrate both the promise and diversity of CPP-based CRISPR delivery. Amphipathic peptides such as LAH5 have supported in vitro delivery of Cas9 RNPs together with donor templates for genome editing and correction approaches [11]. Lipid-modified CPPs such as PF14 have been formulated with Cas9 RNPs under defined aqueous conditions and have demonstrated efficient peptide-mediated intracellular delivery in cultured cells [30]. Covalent or fusion-based systems further extend this concept. For example, the coiled-coil-forming peptide $(KVSALKE)_5$ (K5) has been fused to Cas9 and shown to enhance intracellular delivery of protein cargo while retaining measurable genome-editing activity in vitro and in vivo [37]. Similarly, engineered self-deliverable CPP-fused Cas9 systems have enabled editing in neural progenitor cells and detectable modification of endogenous loci in brain tissue [38]. Taken together, these studies indicate that CPP-based CRISPR delivery is not a single protocol-defined technology, but rather a set of related strategies that differ substantially in peptide architecture, cargo assembly, intracellular behavior, and evaluation workflow.

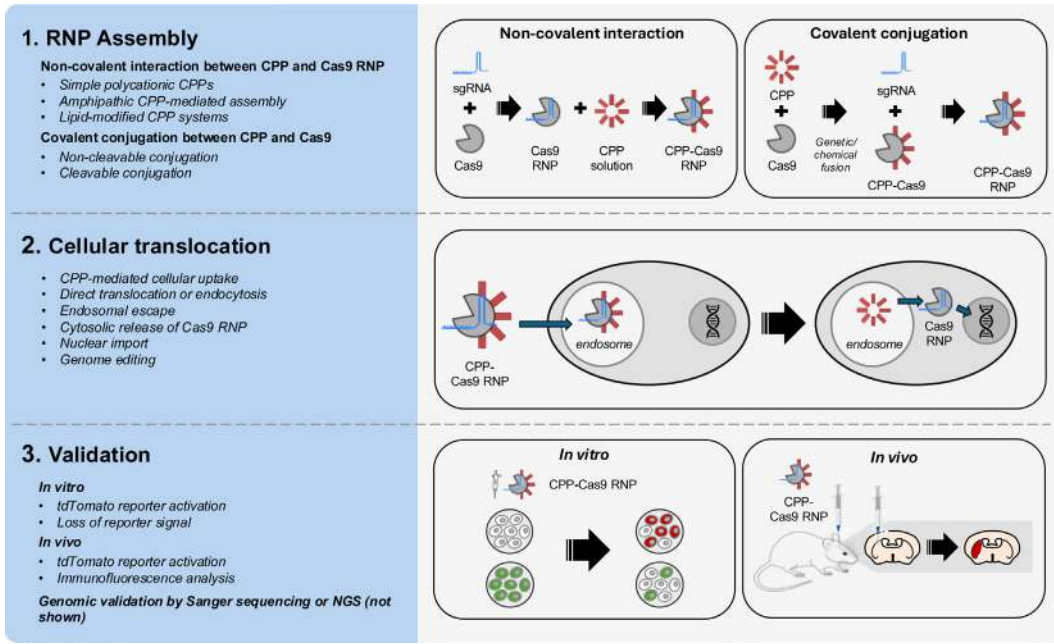


Fig.1 Schematic overview of CPP-mediated delivery of CRISPR/Cas9 RNP complexes. In the noncovalent strategy, CPPs interact with preassembled Cas9 RNPs to form supramolecular complexes. In the covalent strategy, CPPs are first conjugated to Cas9, followed by association with sgRNA to form CPP-Cas9 RNP complexes. These complexes can be applied in vitro or in vivo. Following CPP-mediated cellular uptake, direct translocation or endocytosis may occur, followed by endosomal escape, cytosolic release of Cas9 RNP, nuclear import, and genome editing. Functional delivery and editing can be validated in vitro by reporter activation (e.g., tdTomato) or loss of reporter signal (e.g., GFP), and in vivo by reporter activation (e.g., tdTomato) and immunofluorescence analysis. Indel efficiency and precise genomic modifications can be further assessed by Sanger sequencing or next-generation sequencing (NGS), although these readouts are not shown in the figure

Because of the heterogeneity of CPPs, a single universal protocol cannot be defined for all CPP-mediated CRISPR systems. Therefore, this chapter presents a representative protocol for the preparation and evaluation of Cas9-K5 RNP as an example of a noncleavable covalent CPP–Cas9 delivery strategy. The overall workflow of CPP-mediated CRISPR/Cas9 RNP delivery and validation is summarized in Fig. 1.

2 Materials

2.1 Cells and Animals

1. NIH 3T3—mouse embryonic fibroblasts.
2. HeLa—human cervical cancer cells.
3. Ai9 NIH 3T3—NIH 3T3 fibroblasts engineered to contain a loxP-flanked STOP cassette upstream of a tdTomato reporter gene; genome editing-mediated removal of the STOP cassette results in tdTomato expression (Fig. 2).

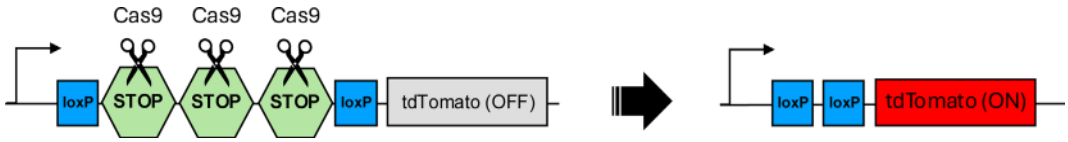


Fig.2 Schematic representation of the Ai9/tdTomato reporter system used to assess CPP-mediated delivery and CRISPR/Cas9 genome editing. In the unedited state, a loxP-flanked STOP cassette prevents tdTomato expression (tdTomato OFF). Following Cas9-mediated deletion of the STOP sequence, tdTomato expression is activated (tdTomato ON), enabling fluorescent detection of edited cells

4. GFP HEK and BFP HEK—human embryonic kidney (HEK) reporter cell lines expressing green fluorescent protein (GFP) or blue fluorescent protein (BFP) reporter genes, respectively, and used for reporter knockout assays.
5. Ai9 (B6.Cg-*Gt(ROSA)26Sor* $^{tm9(CAG\text{-}tdTomato)}$*Hze*/J) reporter mice (2–3 months old) for in vivo studies.

2.2 Reagents

1. Recombinant Cas9-K5, containing an N-terminal 6His-MBP-TEV tag and two C-terminal SV40 NLS peptides. The stock concentration of purified Cas9-K5 may vary between preparations and should be determined before each RNP assembly by measuring absorbance at 280 nm using a NanoDrop 2000 or equivalent spectrophotometer. The critical assembly parameter is the Cas9-K5:sgRNA molar ratio rather than a fixed stock concentration.
2. sgRNA targeting the locus of interest (e.g., Ai9-targeting sgRNA: AAGTAAAACCTCTACAAATG; BFP/GFP-targeting sgRNA: GCTGAAGCACTGCACGCCAT). The sgRNA stock concentration may vary depending on the source or preparation method. Before RNP assembly, determine or obtain the sgRNA concentration, and calculate the amount required to achieve a Cas9-K5:sgRNA molar ratio of 1:1.2.
3. Control solutions: Sterile saline or sterile phosphate-buffered saline (PBS), pH 7.4, for vehicle control injections; native Cas9 RNP may be used as an additional control where appropriate.
4. ATTO 550-labeled sgRNA, supplied at a known stock concentration, for intracellular uptake studies. Use instead of unlabeled sgRNA for Cas9-K5 RNP assembly at a Cas9-K5:sgRNA molar ratio of 1:1.2.
5. Protein storage buffer: 50 mM HEPES, pH 7.5, 300 mM NaCl, 10% glycerol, 100 μM TCEP
6. Complete culture medium: High-glucose Dulbecco's modified Eagle medium (DMEM; 4.5 g/L glucose, with L-glutamine, with or without sodium pyruvate, according to

cell-line requirements) supplemented with 10% fetal bovine serum (FBS) and 1% penicillin–streptomycin.

7. Opti-MEM or equivalent reduced-serum medium for direct transfection/editing assays.
8. SE Cell Line 4D-Nucleofector Solution or another cell-type-compatible nucleofection buffer recommended by the manufacturer.
9. Accutase, ready-to-use solution, or trypsin-EDTA, e.g., 0.05% trypsin-EDTA, depending on the cell line.
10. PBS, pH 7.4, sterile for cell culture applications.
11. Flow cytometry buffer, if used for resuspension before flow cytometry.
12. Anesthesia (e.g., 4% isoflurane for induction and 2% isoflurane for maintenance).
13. Analgesia, according to institutional guidelines (e.g., carprofen 5 mg/kg SC).
14. 4% paraformaldehyde (PFA) in PBS (filtered, pH 7.4).
15. 30% Sucrose in PBS.
16. Cryoembedding molds for O.C.T. embedding.
17. Citrate buffer for antigen retrieval: 0.294% sodium citrate, 0.05% Tween 20 in distilled water, pH 6.0.
18. Blocking solution: 5% goat serum, 0.2% Triton X-100 in PBS (filtered).
19. Primary antibodies against RFP/tdTomato, NeuN (neuronal nuclei marker), and GFAP (glial fibrillary acidic protein).
20. Fluorophore-conjugated secondary antibodies.
21. DAPI (4′,6-diamidino-2-phenylindole).
22. Antifade mounting medium.
23. O.C.T. compound (Tissue-Tek®).
24. Low-binding microcentrifuge tubes.
25. Tissue culture-treated 96-well plates.
26. Hydrophobic barrier pen for slide-mounted immunostaining.
27. Adhesive microscope slides, such as Superfrost Plus or equivalent positively charged slides, for mounting cryosections.
28. Coverslips suitable for fluorescence microscopy.
29. Cryostat supplies: Cryostat-compatible specimen holders/chucks, disposable microtome blades, anti-roll plate or brush, forceps, and slide storage boxes.
30. Surgical consumables: Sterile drapes, sterile gloves, sterile gauze pads, cotton swabs, sterile saline, antiseptic solution for skin preparation, e.g., povidone-iodine or chlorhexidine, 70%

ethanol, ophthalmic ointment, absorbable or nonabsorbable sutures or wound clips, and sterile injection needles/syringe tips compatible with the stereotaxic injection setup.

2.3 Equipment

1. NanoDrop or equivalent instrument for determining protein concentration by absorbance at 280 nm.
2. Humidified CO_2 incubator, set to 37°C and 5% CO_2.
3. Nucleofection system, e.g., Lonza 4D-Nucleofector.
4. Flow cytometer: Attune NxT flow cytometer or equivalent instrument equipped with appropriate lasers and emission filters for GFP, BFP, tdTomato/RFP, and ATTO 550 detection. Representative settings include a 488 nm laser with a 530/30 nm emission filter for GFP, a 405 nm laser with a 450/40 nm emission filter for BFP, and a 561 nm laser with an orange/red emission filter, such as 585/16, 586/15, or 610/20 nm, for tdTomato/RFP and ATTO 550.
5. Fluorescence microscope: Inverted epifluorescence microscope for in vitro reporter and uptake imaging (e.g., EVOS M5000), or confocal/confocal-like fluorescence microscope for immunostained tissue sections and cell-type-specific colocalization analysis (e.g., Zeiss Axio Observer 7 with Apotome), equipped with channels suitable for DAPI/BFP, GFP, tdTomato/RFP, ATTO 550, and the selected secondary antibody fluorophores. Representative settings include 350–405 nm excitation/~450 nm emission for DAPI/BFP, 488 nm excitation/~510–540 nm emission for GFP, and 540–561 nm excitation/~570–620 nm emission for tdTomato/RFP and ATTO 550.
6. Stereotaxic apparatus with microinjector.
7. An anesthesia system, including an induction chamber, an isoflurane vaporizer, an oxygen supply, and a nose cone.
8. Thermostatically controlled heating pad for maintaining body temperature during surgery and recovery.
9. Stereotaxic microscope.
10. Mouse stereotaxic atlas, e.g., Paxinos and Franklin [39].
11. Hamilton Neuros syringe for intracranial injections.
12. Perfusion setup, such as a peristaltic pump or a syringe-based transcardiac perfusion system, with appropriate tubing and perfusion needles.
13. Cryostat.
14. Surgical instruments: Small animal surgical instrument set suitable for stereotaxic intracranial injection, including fine scissors, forceps, needle holder, microdrill with sterile drill bits, and suturing instruments.

3 Methods

3.1 Preparation of Cas9-K5 RNP

Note: This protocol starts from purified recombinant Cas9-K5 protein and does not include protein expression or purification (*see* **Note 1**).

1. Thaw the Cas9-K5 protein aliquot on ice immediately before RNP preparation.
2. Keep the Cas9-K5 protein on ice throughout the procedure.
3. Mix the thawed Cas9-K5 protein gently by pipetting. Do not vortex.
4. Briefly centrifuge the tube to collect the liquid at the bottom.
5. Blank a NanoDrop 2000 or equivalent spectrophotometer with the corresponding protein storage buffer.
6. Load the Cas9-K5 protein sample onto the measurement pedestal.
7. Measure absorbance at 280 nm.
8. Determine the Cas9-K5 protein concentration from the A280 measurement using the instrument software (*see* **Note 2**).
9. Obtain or prepare the sgRNA corresponding to the target sequence of interest. For the Ai9 reporter assay, use sgRNA targeting sequence AAGTAAAACCTCTACAAATG. For BFP or GFP reporter assays, use sgRNA targeting sequence GCTGAAGCACTGCACGCCAT.
10. If cellular uptake will be analyzed by fluorescence microscopy or flow cytometry, use ATTO 550-labeled sgRNA.
11. Calculate the amount of sgRNA required to achieve a Cas9-K5:sgRNA molar ratio of 1:1.2 (*see* **Notes 2 and 3**).
12. Transfer the required amount of Cas9-K5 protein into a nuclease-free low-binding microcentrifuge tube kept on ice.
13. Add the calculated amount of sgRNA to the Cas9-K5 protein.
14. Mix gently by pipetting.
15. Incubate the mixture on ice for 15 min to allow Cas9-K5 RNP formation (*see* **Note 3**).
16. Use the assembled Cas9-K5 RNP immediately for downstream applications.
17. For direct in vitro cellular delivery/editing experiments, use the assembled Cas9-K5 RNP or native Cas9 RNP in Opti-MEM. Use 100 μL Opti-MEM per well containing RNP corresponding to 16.6 μg Cas9-K5 or native Cas9 protein (*see* **Note 4**).

18. For nucleofection-based functional controls, use the assembled Cas9-K5 RNP or native Cas9 RNP in SE Cell Line 4D-Nucleofector Solution. For each nucleofection reaction, use 200,000 cells in 20 µL SE Cell Line 4D-Nucleofector Solution containing 31.25 pmol Cas9-K5 or native Cas9 protein and 37.5 pmol sgRNA (*see* **Note 4**).
19. For in vitro cleavage assays, use the assembled Cas9-K5 RNP or native Cas9 RNP with the corresponding DNA template. Use 500 ng Cas9-K5 RNP or native Cas9 RNP with 500 ng Ai9 template DNA (*see* **Note 4**).
20. For intracellular uptake studies, prepare fluorescent Cas9-K5 RNP using ATTO 550-labeled sgRNA following the same assembly procedure (*see* **Note 5**).

3.2 In Vitro Evaluation of Cas9-K5 RNP Delivery and Editing

3.2.1 Intracellular Uptake Assay

Note: Maintain NIH 3T3, HeLa, Ai9 NIH 3T3, GFP HEK, or BFP HEK cells in DMEM supplemented with 10% FBS and 1% penicillin–streptomycin at 37°C in a humidified incubator containing 5% CO_2. Passage cells using Accutase (or Trypsin) when they reach approximately 80% confluency.

1. Seed NIH 3T3 and HeLa cells in tissue culture-treated 96-well plates at a density of 10,000 cells per well 1 day before treatment. Prepare the cell suspension at 1×10^5 cells/mL and seed 100 µL per well.
2. Prepare Cas9-K5 RNP or native Cas9 RNP as described in Sect. 3.1.
3. Add ATTO 550-labeled Cas9-K5 RNP or native Cas9 RNP to the cells in 100 µL medium per well. Use an RNP amount corresponding to the selected experimental condition; for consistency with the direct in vitro editing assay, 16.6 µg Cas9-K5 or native Cas9 protein per 100 µL may be used as a representative amount (*see* **Notes 4–6**).
4. Incubate the cells at 37°C for 4 h.
5. Wash the cells three times with PBS (100–200 µL per well) to remove noninternalized material.
6. Analyze uptake by fluorescence microscopy or flow cytometry. Detect ATTO 550 fluorescence using excitation at ~554 nm and emission at ~576 nm. Quantify uptake as the percentage of ATTO 550-positive cells (*see* **Notes 5 and 6**).

3.2.2 In Vitro Genome Editing after Direct Exposure

1. Seed Ai9 NIH 3T3 or GFP HEK cells in 96-well plates at a density of 10,000 cells per well in 100 µL complete culture medium, corresponding to 1×10^5 cells/mL, 1 day before treatment.
2. Prepare Cas9-K5 RNP or native Cas9 RNP as described in Sect. 3.1.
3. Dilute the assembled Cas9-K5 RNP or native Cas9 RNP in Opti-MEM to obtain a final volume of 100 µL per well. Each well should receive RNP corresponding to 16.6 µg of Cas9-K5 or native Cas9 protein (*see* **Note 4**).
4. Remove the culture medium from each well immediately before treatment.
5. Add the prepared RNP-containing Opti-MEM from Step 3 to each well.
6. Incubate the cells with RNP-containing Opti-MEM for 4 h at 37°C in a humidified incubator with 5% CO_2.
7. After incubation, replace the RNP-containing Opti-MEM with complete culture medium (DMEM supplemented with 10% FBS and 1% penicillin–streptomycin).
8. After medium replacement, culture the cells for an additional 24 h or 72 h at 37°C in a humidified incubator with 5% CO_2 (*see* **Note 6**).
9. Remove the culture medium and wash the cells once with 100–200 µL PBS per well.
10. Add 30–50 µL Accutase (or 0.05% trypsin-EDTA) to each well, ensuring that the well bottom is covered, and incubate at 37°C until the cells detach.
11. Transfer the detached cells to flow cytometry tubes or a 96-well V-bottom plate.
12. Centrifuge the cells at 600 × g for 3 min.
13. Remove the supernatant and resuspend the cell pellet in 100–200 µL PBS or flow cytometry buffer.
14. Analyze the cells using a flow cytometer with appropriate fluorescence channels for tdTomato or GFP detection. For tdTomato, use 561 nm excitation with an orange/red emission filter, such as 585/16, 586/15, or 610/20 nm. For GFP, use 488 nm excitation with a 530/30 nm emission filter (*see* **Note 7**).
15. Use untreated cells to define the fluorescence gates separating negative and positive populations. Apply the same gates to all treated samples within the experiment.
16. For Ai9 NIH 3T3 cells, quantify editing as the percentage of tdTomato-positive cells among all analyzed viable single

cells: Editing efficiency (%) = (tdTomato-positive cells/total analyzed viable single cells) × 100 (*see* **Notes 7 and 9**).

17. If untreated cells show background tdTomato positivity, report background-corrected editing efficiency as: Corrected editing efficiency (%) = % tdTomato-positive treated cells − % tdTomato-positive untreated cells.
18. For GFP HEK cells, quantify reporter knockout as the percentage of GFP-negative cells. Calculate background-corrected editing efficiency as: Editing efficiency (%) = % GFP-negative treated cells − % GFP-negative untreated cells (*see* **Note 7**).

3.2.3 Optional Nucleofection-Based Functional Control

1. Use Ai9 NIH 3T3 or BFP HEK cells harvested at approximately 70%–80% confluency. Aspirate the medium, rinse once with PBS, and add enough Accutase (or 0.05% trypsin-EDTA) to cover the cell monolayer, typically 0.5–1 mL per well of a 6-well plate. Incubate at 37°C until cells detach. Collect the cells in complete culture medium, centrifuge at 600 × *g* for 3 min, discard the supernatant, and wash the cell pellet once with PBS.
2. Resuspend 200,000 cells in 20 μL SE Cell Line 4D-Nucleofector Solution containing 31.25 pmol Cas9-K5 or native Cas9 protein and 37.5 pmol sgRNA (*see* **Notes 4 and 8**).
3. Nucleofect the cells using a Lonza 4D-Nucleofector according to the manufacturer's protocol, using a program appropriate for the selected cell type (*see* **Note 8**).
4. After nucleofection, centrifuge the cells at 600 × *g* for 3 min, resuspend them in 500 μL fresh complete DMEM supplemented with 10% FBS and 1% penicillin–streptomycin, and culture for 5 days at 37°C in a humidified incubator with 5% CO_2 before flow cytometric analysis.
5. Analyze cells by flow cytometry using appropriate fluorescence channels for tdTomato/RFP or BFP detection. For tdTomato/RFP, use 561 nm excitation with an orange/red emission filter, such as 585/16, 586/15, or 610/20 nm. For BFP, use 405 nm excitation with an emission filter around 450/40 nm.
6. Determine editing efficiency as the percentage of tdTomato-positive cells in Ai9 NIH 3T3 cells or as the percentage of BFP-negative cells in BFP HEK cells. In BFP reporter assays, calculate background-corrected editing efficiency as: Editing efficiency (%) = % BFP-negative treated cells − % BFP-negative untreated cells (*see* **Note 7**).

3.3 In Vivo Evaluation of Cas9-K5 RNP

3.3.1 Stereotaxic Intracranial Injection

Note: All in vivo experiments must be approved by the relevant institutional animal care and use committee or equivalent regulatory authority and performed in accordance with applicable national and institutional guidelines for animal welfare. Appropriate anesthesia, analgesia, postoperative monitoring, and humane endpoints must be included in the approved protocol.

1. Use adult male and female Ai9 reporter mice for in vivo evaluation of Cas9-K5 RNP delivery and editing (*see* **Note 9**).
2. Induce anesthesia in an induction chamber using 4% isoflurane in oxygen until the animal loses the righting reflex and shows no response to a gentle toe pinch.
3. Maintain anesthesia with approximately 2% isoflurane delivered through a nose cone throughout the procedure. Apply ophthalmic ointment to prevent corneal drying. Place the animal on a thermostatically controlled heating pad and maintain body temperature throughout the surgery.
4. Place the mouse in a stereotaxic frame by securing the upper incisors in the bite bar and gently positioning the ear bars in the external auditory canals. Adjust the ear bars symmetrically to stabilize the head and confirm a stable surgical plane of anesthesia.
5. Shave the scalp and disinfect the surgical area using alternating applications of antiseptic solution and sterile saline or 70% ethanol, according to institutional surgical guidelines.
6. Make a midline scalp incision using sterile scissors or a scalpel to expose the skull surface.
7. Gently clear connective tissue from the skull using sterile cotton swabs.
8. Identify bregma and lambda under a stereotaxic microscope or magnifying lens.
9. Level the skull by adjusting the head position until bregma and lambda are aligned in the dorsoventral plane.
10. Using bregma as the reference point, mark the injection coordinates on the skull for the selected brain region (*see* **Note 11**).
11. Drill a small burr hole at each marked injection site using a microdrill, taking care not to damage the dura or underlying brain tissue.
12. Load the Cas9-K5 RNP formulation or control solution into a Hamilton Neuros syringe, avoiding air bubbles. Prepare

sufficient volume for all planned injection sites, allowing extra volume for syringe dead space.

13. Lower the injection needle slowly through the burr hole to the target dorsoventral coordinate.
14. Inject Cas9-K5 RNP into one hemisphere and the appropriate control solution, such as saline or native Cas9 RNP, into the contralateral hemisphere.
15. Inject 1.5 μL per site at a controlled infusion rate of 0.5 μL min^{-1}. Use Cas9-K5 RNP at the selected final concentration; representative concentrations are 0.6 or 2.5 μg μL^{-1} (*see* **Notes 4 and 10**).
16. Leave the injector in place for 5 min after infusion to facilitate diffusion and minimize backflow.
17. Slowly withdraw the needle from the brain.
18. Close the scalp incision using sutures or wound clips.
19. Disinfect the incision area according to institutional surgical guidelines.
20. Allow the animal to recover on a heating pad and monitor it according to the approved animal protocol.
21. Allow the desired post-injection interval (14–21 days) before tissue collection. Monitor the animal and incision site daily until the wound is fully healed and provide wound care or antiseptic treatment as required by the approved animal protocol to prevent infection (*see* **Note 10**).

3.3.2 Tissue Processing and Immunostaining

1. At the selected post-injection time point, deeply anesthetize the animal according to the approved animal protocol until no response to toe pinch is observed.
2. Place the animal in a supine position on a dissection surface and secure the limbs.
3. Open the thoracic cavity using scissors to expose the heart.
4. Insert a perfusion needle into the left ventricle and make a small incision in the right atrium to allow drainage.
5. Perfuse the animal with ice-cold PBS, pH 7.4, until the effluent runs clear, typically 20–30 mL for an adult mouse.
6. Switch to 4% PFA in PBS, pH 7.4, and continue perfusion with 20–30 mL fixative to fix the tissue.
7. Decapitate the perfused animal using appropriate surgical scissors according to the approved animal protocol.
8. Remove the skin and soft tissue from the skull using fine scissors and forceps.

9. Make a midline cut through the skull from the foramen magnum toward the frontal bone using fine scissors, taking care not to damage the underlying brain.
10. Gently peel the skull plates laterally using fine forceps.
11. Carefully detach the brain from the cranial cavity by gently lifting it from the caudal side while cutting or releasing the cranial nerves as needed.
12. Transfer the isolated brain immediately into 10–20 mL 4% PFA in PBS for post-fixation for 4 h at 4°C.
13. Wash the brain once with 10–20 mL PBS, pH 7.4.
14. Transfer the brain to 10–20 mL 30% sucrose in PBS, pH 7.4 and incubate at 4°C for 2–3 days, or until the tissue sinks to the bottom of the tube, indicating sufficient cryoprotection.
15. Remove the cryoprotected brain from 30% sucrose and gently blot excess sucrose solution from the tissue surface using filter paper.
16. Embed the cryoprotected brain in O.C.T. compound using a cryoembedding mold, orient the tissue for coronal sectioning, freeze the block on dry ice or in cooled isopentane, and store at −80°C until sectioning.
17. Cut 20 µm coronal sections containing the brain area of interest, such as the striatum or hippocampus, and collect the sections directly onto positively charged microscope slides. Because the sections are thin and fragile, avoid free-floating handling to minimize mechanical damage.
18. Rinse sections once in PBS, pH 7.4, by immersing the slides in a Coplin jar or staining dish. Replace with fresh PBS and wash sections three times for 5 min each at room temperature, using enough PBS to fully cover the tissue sections.
19. Perform heat-induced epitope retrieval by incubating the slides in pre-warmed citrate buffer, pH 6.0, in a steamer for 15 min, ensuring that the sections remain fully submerged and that the citrate buffer temperature does not exceed 70°C. After the antigen retrieval, cool the slides in the same buffer on ice for 10 min before washing.
20. Rinse sections once in PBS, pH 7.4, by immersing the slides in a Coplin jar or staining dish. Replace with fresh PBS and wash sections three times for 5 min each at room temperature, using enough PBS to fully cover the tissue sections.
21. Draw a hydrophobic barrier around the tissue sections using a hydrophobic barrier pen. Allow the barrier to dry for 1–2 min before applying blocking solution.
22. Apply approximately 70 µL of blocking solution (5% goat serum, 0.2% Triton X-100 in PBS) per brain section within

the hydrophobic barrier, ensuring that each section is fully covered. Incubate the slides in a humidified chamber for 1 h at room temperature.

23. Apply approximately 70 µL of primary antibody solution per brain section within the hydrophobic barrier, ensuring that each section is fully covered. Incubate sections overnight at 4°C in a humidified chamber. Primary antibodies against RFP/tdTomato, NeuN, and GFAP are diluted in blocking solution (5% goat serum, 0.2% Triton X-100 in PBS) (*see* **Note 12**).
24. Rinse sections once in PBS, pH 7.4, by immersing the slides in a Coplin jar or staining dish. Replace with fresh PBS and wash sections three times for 5 min each at room temperature, using enough PBS to fully cover the tissue sections.
25. Apply approximately 70 µL of fluorophore-conjugated secondary antibody solution per brain section within the hydrophobic barrier and incubate for 2 h at room temperature in a humidified chamber protected from light (*see* **Note 12**).
26. Rinse sections once in PBS, pH 7.4, by immersing the slides in a Coplin jar or staining dish protected from light. Replace with fresh PBS and wash sections three times for 5 min each at room temperature, using enough PBS to fully cover the tissue sections. Keep the slides protected from light during all washing steps.
27. Apply approximately 70 µL of DAPI solution diluted 1:1500 in PBS from a 5 mg/mL stock solution, corresponding to a final concentration of 3.33 µg/mL, per brain section within the hydrophobic barrier. Incubate for 10 min at room temperature in a humidified chamber protected from light.
28. Rinse sections once in PBS, pH 7.4, by immersing the slides in a Coplin jar or staining dish protected from light. Replace with fresh PBS and wash sections three times for 5 min each at room temperature, using enough PBS to fully cover the tissue sections. Keep the slides protected from light during all washing steps.
29. After the final PBS wash, gently remove excess liquid without drying the tissue. Mount the sections with 1–2 drops of antifade mounting medium, apply a coverslip, and keep the slides at 4°C protected from light until imaging.
30. Image the sections using a confocal/confocal-like fluorescence microscope with excitation and emission settings appropriate for the selected fluorophores. Representative settings include 350–405 nm excitation/~450 nm emission for DAPI, 488 nm excitation/~510–540 nm emission for green fluorophores, 540–561 nm excitation/~570–620 nm emission for tdTomato/RFP, and 633–647 nm excitation/~660–720 nm

emission for far-red fluorophores. Acquire z-stack images through the region of interest to capture the full labeled tissue volume and improve visualization of reporter-positive and marker-positive cells. Generate maximum-intensity projections for visualization and quantitative analysis, keeping acquisition parameters constant across experimental groups (*see* **Note 13**).

3.3.3 Quantification of Editing Efficiency

Note: For clarity, full terms (e.g., tdTomato-positive, DAPI-positive, NeuN-positive, or GFAP-positive) are used in descriptive text, whereas abbreviated notation (e.g., tdTomato$^+$, DAPI$^+$, NeuN$^+$, or GFAP$^+$) is used in co-localization analyses and quantitative expressions.

1. For studies, analyze a defined ROI that is kept constant across animals and conditions. Count tdTomato-positive, DAPI-positive, NeuN-positive, and GFAP-positive cells within defined ROI (*see* **Notes 13 and 14**).
2. Calculate local editing efficiency as the percentage of tdTomato-positive cells among all DAPI-positive cells (*see* **Notes 13 and 14**): Local editing efficiency (%) = (tdTomato-positive cells/total DAPI-positive cells) × 100.
3. To assess cell-type specificity among edited cells, calculate the proportion of tdTomato$^+$; NeuN$^+$ and tdTomato$^+$; GFAP$^+$ cells among all tdTomato$^+$ cells: Neuronal fraction among edited cells (%) = (tdTomato$^+$; NeuN$^+$ cells/total tdTomato$^+$ cells) × 100. Astrocytic fraction among edited cells (%) = (tdTomato$^+$;GFAP$^+$ cells/total tdTomato$^+$ cells) × 100 (*see* **Note 14**).
4. To assess editing within each lineage, calculate the percentage of edited neurons and edited astrocytes among all cells of the corresponding lineage (*see* **Note 14**): Neuronal editing efficiency (%) = (tdTomato$^+$; NeuN$^+$ cells/total NeuN$^+$ cells) × 100. Astrocytic editing efficiency (%) = (tdTomato$^+$;GFAP$^+$ cells/total GFAP$^+$ cells) × 100.

Reporter-based quantification may be complemented by genomic validation where appropriate (*see* **Note 15**). Uptake, reporter editing, and genomic validation should be interpreted as complementary readouts rather than interchangeable endpoints (*see* **Note 16**).

4 Notes

1. **Cas9-K5 protein source:** This protocol starts from purified recombinant Cas9-K5 protein and does not include protein expression or purification. In Li et al. [37], Cas9-K5

contained the K5 peptide fused to the N-terminus of Cas9 and two SV40 NLS sequences at the C-terminus. The protein was expressed in *Escherichia coli* BL21(DE3) from a custom pET-based vector and purified to homogeneity, yielding approximately 10 mg/L.

2. **Cas9-K5 and sgRNA concentration:** The stock concentration of purified Cas9-K5 should be determined before each RNP assembly by measuring absorbance at 280 nm using a NanoDrop 2000 or equivalent spectrophotometer, as it may vary between preparations. The sgRNA stock concentration should also be known or determined before use. Based on these measured concentrations, calculate the required amounts of Cas9-K5 and sgRNA for each experiment to achieve the Cas9-K5:sgRNA molar ratio of 1:1.2.
3. **RNP assembly conditions:** The critical assembly parameter is the Cas9-K5:sgRNA molar ratio rather than a fixed stock concentration. For Cas9-K5 RNP preparation, mix Cas9-K5 protein and sgRNA at a 1:1.2 molar ratio and incubate the mixture on ice for 15 min. These assembly conditions were used by Li et al. [37] and should be maintained unless specific optimization is required.
4. **Assay-dependent RNP amounts:** The amount and concentration of Cas9-K5 RNP should be selected according to the downstream application. The representative conditions used in this protocol are 16.6 μg Cas9-K5 or native Cas9 protein in 100 μL Opti-MEM for direct in vitro cellular delivery/editing, 31.25 pmol Cas9-K5 or native Cas9 protein with 37.5 pmol sgRNA in 20 μL SE Cell Line 4D-Nucleofector Solution for nucleofection-based controls, 500 ng Cas9-K5 RNP or native Cas9 RNP with 500 ng Ai9 template DNA for in vitro cleavage assays, and final Cas9-K5 RNP concentrations of 0.6 or 2.5 μg μL^{-1} for in vivo intracranial injection.
5. **Fluorescent uptake readout:** For intracellular uptake studies, use ATTO 550-labeled sgRNA to quantify cellular internalization of Cas9-K5 RNP or native Cas9 RNP independently of downstream genome editing. The ATTO 550 signal reflects RNP internalization rather than functional editing and is therefore useful for comparing delivery efficiency between native Cas9 RNP and Cas9-K5 RNP.
6. **Uptake versus editing assay format:** In Li et al. [37], intracellular uptake was assessed after a 4 h incubation, whereas direct in vitro editing assays used 48 h exposure in Opti-MEM followed by medium replacement and additional culture before reporter analysis. The uptake assay measures cellular internalization of fluorescent RNP, whereas the editing assay

measures functional genome editing and should not be interpreted as an uptake readout.

7. In vitro **quantification of editing efficiency:** Edited cells can be quantified by flow cytometry according to the reporter system used. In Ai9 NIH 3T3 cells, editing is measured as a gain of tdTomato signal and reported as the percentage of tdTomato-positive cells. In GFP HEK or BFP HEK reporter knockout assays, editing is measured as loss of reporter signal and reported as the percentage of GFP-negative or BFP-negative cells. Where appropriate, values should be normalized to untreated or nontargeting controls to correct for background reporter-positive or reporter-negative populations.
8. **Nucleofection-based functional control:** Nucleofection is used as a functional control to confirm that fusion of K5 to Cas9 does not abolish nuclease activity or reporter-editing capacity. Because nucleofection bypasses CPP-mediated uptake, it helps distinguish impaired delivery from impaired intrinsic Cas9 activity. Nucleofection programs should be selected according to the cell type and manufacturer's recommendations; in Li et al. [37], EN-158 or CM-130 programs were used depending on the cell type.
9. **Ai9 reporter system and alternative reporter lines:** In Ai9-based reporter systems (Fig. 2), activation of the tdTomato signal serves as a primary functional readout of editing. Successful genome editing removes the transcriptional STOP cassette located upstream of the reporter, thereby enabling tdTomato expression [40]. Because Ai9 is a highly sensitive Cre-dependent reporter, low background or apparent "leaky" reporter activation may occur depending on the experimental context, driver system, and tissue analyzed. Appropriate negative controls, such as untreated samples, nontargeting RNP controls, contralateral saline-treated tissue, or contralateral tissue treated with native Cas9 RNP, are therefore essential to distinguish true editing from background reporter activity [41]. Other Cre-dependent reporter lines, such as Ai14 mice, may be used if the sgRNA target site, reporter design, and downstream readout are adapted accordingly.
10. **Stereotaxic surgery, delivery route, and scope of the** in vivo **workflow:** The in vivo workflow described here is a representative local intracranial delivery model for evaluating brain CPP–CRISPR/Cas9 delivery in Ai9 reporter mice. Direct intracerebral administration bypasses the blood–brain barrier and enables local assessment of Cas9-K5 RNP delivery and editing in defined brain regions, such as the striatum and hippocampus. This workflow should be interpreted as a representative in vivo validation paradigm rather than a universal

assay for all CPP-based delivery systems. Exact anesthesia, analgesia, aseptic preparation, drilling, injection, wound closure, and postoperative monitoring procedures must follow the approved institutional animal protocol and be performed by trained personnel. For studies targeting tissues outside the brain, this stereotaxic workflow may be omitted and replaced by an appropriate delivery route, such as intravenous administration or local tissue injection.

11. **Stereotaxic coordinates:** Target coordinates should be selected according to the brain region of interest, animal age, strain, and the stereotaxic atlas used [39]. In Li et al. [37], Cas9-K5 RNP was injected into the striatum and hippocampus of adult Ai9 mice. The coordinates used, relative to bregma, were: striatum, AP +0.50 mm, ML ±1.87 mm, DV −3.47 mm; hippocampus, AP −2.56 mm, ML ±1.55 mm, DV −2.00 mm. AP, ML, and DV denote anteroposterior, mediolateral, and dorsoventral coordinates, respectively. Coordinates should be verified and adjusted if a different mouse strain, age, atlas, or surgical setup is used.
12. **Antibody selection, dilution, and cell-type-specific markers:** Primary and secondary antibody dilutions should be optimized for the specific antibody clone, supplier, tissue fixation conditions, section thickness, target tissue, and imaging setup. In Li et al. [37], brain sections were incubated with rabbit anti-RFP for tdTomato detection (1:500), mouse anti-NeuN (1:500), and chicken anti-GFAP (1:1000) to identify edited cells, neurons, and astrocytes, respectively. Fluorophore-conjugated secondary antibodies can be used at 1:500 as an initial working dilution. If CPP–CRISPR/Cas9 delivery is evaluated in other tissues, lineage or cell-type-specific markers should be selected according to the target organ and biological question. Antibody concentrations should be adjusted according to signal intensity, background staining, and manufacturer recommendations.
13. In vivo **image acquisition, ROI definition, and cell counting:** tdTomato-positive cells can be visualized in fixed brain sections and further characterized by co-immunostaining with lineage markers such as NeuN and GFAP to assess editing in specific cell populations. For quantitative analysis, define the region of interest (ROI) before analysis and keep the ROI, section thickness, imaging settings, magnification, exposure time, and z-stack parameters constant across animals, treatment groups, and control conditions. In Li et al. [37], each injected brain area was quantified from five z-stack images with a 10 μm z-depth acquired at 40× magnification.

Cells were counted using the Cell Counter plugin for ImageJ (NIH); equivalent image-analysis software may also be used.

14. **Cell-type-specific in vivo quantification:** For cell-type-specific in vivo analysis, the tdTomato signal should be interpreted together with lineage-marker staining, such as NeuN for neurons and GFAP for astrocytes, because overall reporter activation alone does not distinguish neuronal from astrocytic editing. Separate quantification of tdTomato$^+$; NeuN$^+$ and tdTomato$^+$; GFAP$^+$ cells provides information on both cell tropism among edited cells and lineage-specific editing efficiency.
15. **Genomic validation of editing:** Although reporter activation is a convenient functional readout, it should be complemented, where possible, by direct analysis of editing outcomes at the genomic level. Indel formation can be evaluated by extracting genomic DNA from treated cells or homogenized tissue, amplifying the target locus by high-fidelity PCR, and analyzing the purified amplicons by Sanger sequencing or next-generation sequencing (NGS). Sanger chromatograms can be analyzed using tools such as TIDE or ICE to estimate the frequency of NHEJ-mediated insertions and deletions, whereas NGS enables more detailed quantification of indel spectra and precise genomic modifications. This orthogonal approach is particularly useful when reporter activation is unavailable or when direct confirmation of editing at the endogenous locus is required.
16. **Interpretation of assay endpoints:** Because the Cas9-K5 system combines a delivery function with a genome-editing cargo, assay endpoints should be interpreted as complementary rather than interchangeable. It is useful to distinguish at least three readout categories: RNP uptake, functional reporter editing, and genomic validation. Combining these readouts strengthens data interpretation and helps distinguish inefficient cellular internalization from impaired Cas9 activity, insufficient nuclear delivery, or limited editing at the target locus.

Acknowledgments

The publication is based upon work by COST Action CA21113: Genome Editing for the Treatment of Human Diseases (https://www.genehumdi.eu), supported by European Cooperation in Science and Technology (COST). This chapter was supported by the Ministry of Health of the Czech Republic (grant No. NW26-08-00119) and the Cooperatio Program (NEUR and MED/DIAG

research areas) funded to J.T. This chapter was also supported by the National Institute of Mental Health (R01MH125979), the UT Rising STARs award, the FRAXA Research Foundation, the Simons Foundation (SFI-AN-SURFiN-00013585 and SFI-AN-SURFiN-00028092) funded to H.Y.L.

Conflict of Interest The authors declare no competing interests.

References

1. Dinca A, Chien WM, Chin MT (2016) Intracellular delivery of proteins with cell-penetrating peptides for therapeutic uses in human disease. Int J Mol Sci 17(2):263. https://doi.org/10.3390/ijms17020263
2. Said Hassane F, Saleh AF, Abes R, Gait MJ, Lebleu B (2010) Cell penetrating peptides: overview and applications to the delivery of oligonucleotides. Cell Mol Life Sci 67(5):715–726. https://doi.org/10.1007/s00018-009-0186-0
3. Frankel AD, Pabo CO (1988) Cellular uptake of the tat protein from human immunodeficiency virus. Cell 55(6):1189–1193. https://doi.org/10.1016/0092-8674(88)90263-2
4. Green M, Loewenstein PM (1988) Autonomous functional domains of chemically synthesized human immunodeficiency virus Tat trans-activator protein. Cell 55(6):1179–1188. https://doi.org/10.1016/0092-8674(88)90262-0
5. Joliot A, Pernelle C, Deagostini-Bazin H, Prochiantz A (1991) Antennapedia homeobox peptide regulates neural morphogenesis. Proc Natl Acad Sci USA 88(5):1864–1868. https://doi.org/10.1073/pnas.88.5.1864
6. Derossi D, Joliot AH, Chassaing G, Prochiantz A (1994) The third helix of the Antennapedia homeodomain translocates through biological membranes. J Biol Chem 269(14):10444–10450
7. Sawant R, Torchilin V (2010) Intracellular transduction using cell-penetrating peptides. Mol Biosyst 6(4):628–640. https://doi.org/10.1039/b916297f
8. Gori A, Lodigiani G, Colombarolli SG, Bergamaschi G, Vitali A (2023) Cell penetrating peptides: classification, mechanisms, methods of study, and applications. Chemmedchem 18(17):e202300236. https://doi.org/10.1002/cmdc.202300236
9. Xie J, Bi Y, Zhang H, Dong S, Teng L, Lee RJ, Yang Z (2020) Cell-penetrating peptides in diagnosis and treatment of human diseases: from preclinical research to clinical application. Front Pharmacol 11:697. https://doi.org/10.3389/fphar.2020.00697
10. Sioson VA, Kim M, Joo J (2021) Challenges in delivery systems for CRISPR-based genome editing and opportunities of nanomedicine. Biomed Eng Lett 11(3):217–233. https://doi.org/10.1007/s13534-021-00199-4
11. Oktem M, Mastrobattista E, de Jong OG (2023) Amphipathic cell-penetrating peptide-aided delivery of Cas9 RNP for in vitro gene editing and correction. Pharmaceutics 15(10). doi:https://doi.org/10.3390/pharmaceutics15102500
12. Tripathi PP, Arami H, Banga I, Gupta J, Gandhi S (2018) Cell penetrating peptides in preclinical and clinical cancer diagnosis and therapy. Oncotarget 9(98):37252–37267. https://doi.org/10.18632/oncotarget.26442
13. van Hees M, Slott S, Hansen AH, Kim HS, Ji HP, Astakhova K (2022) New approaches to moderate CRISPR-Cas9 activity: addressing issues of cellular uptake and endosomal escape. Mol Ther 30(1):32–46. https://doi.org/10.1016/j.ymthe.2021.06.003
14. Du JJ, Zhang RY, Jiang S, Xiao S, Liu Y, Niu Y, Zhao WX, Wang D, Ma X (2025) Applications of cell penetrating peptide-based drug delivery system in immunotherapy. Front Immunol 16:1540192. https://doi.org/10.3389/fimmu.2025.1540192
15. Kalafatovic D, Giralt E (2017) Cell-penetrating peptides: design strategies beyond primary structure and amphipathicity. Molecules 22(11). doi:https://doi.org/10.3390/molecules22111929
16. Madani F, Lindberg S, Langel U, Futaki S, Graslund A (2011) Mechanisms of cellular uptake of cell-penetrating peptides. J Biophys 2011:414729. https://doi.org/10.1155/2011/414729
17. Jobin ML, Alves ID (2014) On the importance of electrostatic interactions between cell penetrating peptides and membranes: a pathway toward tumor cell selectivity? Biochimie 107 Pt A:154–159. https://doi.org/10.1016/j.biochi.2014.07.022
18. Ruseska I, Zimmer A (2020) Internalization mechanisms of cell-penetrating peptides. Beilstein J Nanotechnol 11:101–123. https://doi.org/10.3762/bjnano.11.10

19. Henriques ST, Quintas A, Bagatolli LA, Homble F, Castanho MA (2007) Energy-independent translocation of cell-penetrating peptides occurs without formation of pores. A biophysical study with pep-1. Mol Membr Biol 24(4):282–293. https://doi.org/10.1080/09687860601142936
20. Walrant A, Correia I, Jiao CY, Lequin O, Bent EH, Goasdoue N, Lacombe C, Chassaing G, Sagan S, Alves ID (2011) Different membrane behaviour and cellular uptake of three basic arginine-rich peptides. Biochim Biophys Acta 1808(1):382–393. https://doi.org/10.1016/j.bbamem.2010.09.009
21. Ziegler A, Seelig J (2011) Contributions of glycosaminoglycan binding and clustering to the biological uptake of the nonamphipathic cell-penetrating peptide WR9. Biochemistry (Mosc) 50(21):4650–4664. https://doi.org/10.1021/bi1019429
22. Mitchell DJ, Kim DT, Steinman L, Fathman CG, Rothbard JB (2000) Polyarginine enters cells more efficiently than other polycationic homopolymers. J Pept Res 56(5):318–325. https://doi.org/10.1034/j.1399-3011.2000.00723.x
23. Wender PA, Mitchell DJ, Pattabiraman K, Pelkey ET, Steinman L, Rothbard JB (2000) The design, synthesis, and evaluation of molecules that enable or enhance cellular uptake: peptoid molecular transporters. Proc Natl Acad Sci USA 97(24):13003–13008. https://doi.org/10.1073/pnas.97.24.13003
24. Mishra A, Gordon VD, Yang L, Coridan R, Wong GC (2008) HIV TAT forms pores in membranes by inducing saddle-splay curvature: potential role of bidentate hydrogen bonding. Angew Chem Int Ed Engl 47(16):2986–2989. https://doi.org/10.1002/anie.200704444
25. Richard JP, Melikov K, Vives E, Ramos C, Verbeure B, Gait MJ, Chernomordik LV, Lebleu B (2003) Cell-penetrating peptides. A reevaluation of the mechanism of cellular uptake. J Biol Chem 278(1):585–590. https://doi.org/10.1074/jbc.M209548200
26. Kaplan IM, Wadia JS, Dowdy SF (2005) Cationic TAT peptide transduction domain enters cells by macropinocytosis. J Control Release 102(1):247–253. https://doi.org/10.1016/j.jconrel.2004.10.018
27. Erazo-Oliveras A, Muthukrishnan N, Baker R, Wang TY, Pellois JP (2012) Improving the endosomal escape of cell-penetrating peptides and their cargos: strategies and challenges. Pharmaceuticals 5(11):1177–1209. https://doi.org/10.3390/ph5111177
28. Lange A, Mills RE, Lange CJ, Stewart M, Devine SE, Corbett AH (2007) Classical nuclear localization signals: definition, function, and interaction with importin alpha. J Biol Chem 282(8):5101–5105. https://doi.org/10.1074/jbc.R600026200
29. Veiman KL, Mager I, Ezzat K, Margus H, Lehto T, Langel K, Kurrikoff K, Arukuusk P, Suhorutsenko J, Padari K, Pooga M, Lehto T, Langel U (2013) PepFect14 peptide vector for efficient gene delivery in cell cultures. Mol Pharm 10(1):199–210. https://doi.org/10.1021/mp3003557
30. Gustafsson O, Radler J, Roudi S, Lehto T, Hallbrink M, Lehto T, Gupta D, Andaloussi SE, Nordin JZ (2021) Efficient peptide-mediated in vitro delivery of Cas9 RNP. Pharmaceutics 13(6). https://doi.org/10.3390/pharmaceutics13060878
31. Keller AA, Mussbach F, Breitling R, Hemmerich P, Schaefer B, Lorkowski S, Reissmann S (2013) Relationships between cargo, cell penetrating peptides and cell type for uptake of non-covalent complexes into live cells. Pharmaceuticals 6(2):184–203. https://doi.org/10.3390/ph6020184
32. Ramakrishna S, Kwaku Dad AB, Beloor J, Gopalappa R, Lee SK, Kim H (2014) Gene disruption by cell-penetrating peptide-mediated delivery of Cas9 protein and guide RNA. Genome Res 24(6):1020–1027. https://doi.org/10.1101/gr.171264.113
33. Behzadipour Y, Hemmati S (2024) Covalent conjugation and non-covalent complexation strategies for intracellular delivery of proteins using cell-penetrating peptides. Biomed Pharmacother 176:116910. https://doi.org/10.1016/j.biopha.2024.116910
34. Suresh B, Ramakrishna S, Kim H (2017) Cell-penetrating peptide-mediated delivery of Cas9 protein and guide RNA for genome editing. Methods Mol Biol 1507:81–94. https://doi.org/10.1007/978-1-4939-6518-2_7
35. Kristensen M, Birch D, Morck Nielsen H (2016) Applications and challenges for use of cell-penetrating peptides as delivery vectors for peptide and protein cargos. Int J Mol Sci 17(2). doi:https://doi.org/10.3390/ijms17020185
36. He M, Li J, Han H, Borges CA, Neiman G, Roise JJ, Hadaczek P, Mendonsa R, Holm VR, Wilson RC, Bankiewicz K, Zhang Y, Sadlowski CM, Healy K, Riley LW, Murthy N (2020) A traceless linker for aliphatic amines that rapidly and quantitatively fragments after reduction. Chem Sci 11(33):8973–8980. https://doi.org/10.1039/d0sc00929f
37. Li J, Tuma J, Han H, Kim H, Wilson RC, Lee HY, Murthy N (2022) The coiled-coil forming peptide (KVSALKE)(5) is a cell penetrating peptide that enhances the intracellular delivery of proteins. Adv Healthc Mater

11(9):e2102118. https://doi.org/10.1002/adhm.202102118
38. Chen K, Stahl EC, Kang MH, Xu B, Allen R, Trinidad M, Doudna JA (2024) Engineering self-deliverable ribonucleoproteins for genome editing in the brain. Nat Commun 15(1):1727. https://doi.org/10.1038/s41467-024-45998-2
39. Paxinos G, Franklin K (2007) The mouse brain in stereotaxic coordinates. Elsevier,
40. Madisen L, Zwingman TA, Sunkin SM, Oh SW, Zariwala HA, Gu H, Ng LL, Palmiter RD, Hawrylycz MJ, Jones AR, Lein ES, Zeng H (2010) A robust and high-throughput Cre reporting and characterization system for the whole mouse brain. Nat Neurosci 13(1):133–140. https://doi.org/10.1038/nn.2467
41. Nakashiba T, Sugiyama T, Iwano S, Iwama M, Yoshiki A, Miyawaki A, Abe K (2026) Assessing leaky expression of Cre-dependent DNA constructs in the mouse genome using sensitive bioluminescent reporters. Cell Rep Methods 101369. https://doi.org/10.1016/j.crmeth.2026.101369

Open Access This chapter is licensed under the terms of the Creative Commons Attribution-NonCommercial-NoDerivatives 4.0 International License (http://creativecommons.org/licenses/by-nc-nd/4.0/), which permits any noncommercial use, sharing, distribution and reproduction in any medium or format, as long as you give appropriate credit to the original author(s) and the source, provide a link to the Creative Commons license and indicate if you modified the licensed material. You do not have permission under this license to share adapted material derived from this chapter or parts of it.

The images or other third party material in this chapter are included in the chapter's Creative Commons license, unless indicated otherwise in a credit line to the material. If material is not included in the chapter's Creative Commons license and your intended use is not permitted by statutory regulation or exceeds the permitted use, you will need to obtain permission directly from the copyright holder.





Chapter 15

Oligo-Modified Poly(β-Amino Ester)-Mediated mRNA Delivery: A Protocol for Gene Editing Applications

Laia Martí-Melero, Sara Pérez Martín, Salvador Borrós Gómez and Marta Guerra-Rebollo

Abstract

Oligopeptide-modified poly(β-amino ester)s (OM-pBAEs) are polymer-based delivery systems that enable the encapsulation and intracellular transport of nucleic acids, including messenger RNA (mRNA) and mixtures of mRNA with DNA. OM-pBAEs form cationic nanoparticles (NPs) through electrostatic interactions with nucleic acids, protecting them from degradation and enhancing cellular uptake. Terminal oligopeptides composed of lysine, arginine, or histidine enhance polyplex stability, nucleic acid binding, and endosomal escape. This chapter describes a protocol for preparing OM-pBAE nanoparticles, including polymer synthesis, peptide modification, controlled mixing with nucleic acids to form polyplexes, precipitation in RNase-free water, stabilization with excipients, and optional freeze-drying for long-term storage. Nanoparticle formation occurs at a constant temperature of 25°C, with incubation to ensure reproducible self-assembly. Nanoparticles are characterized by using dynamic light scattering (DLS) to determine particle size, polydispersity, and surface charge, while nucleic acid encapsulation efficiency is assessed to evaluate loading capacity. This protocol provides a versatile, nonviral platform for efficient nucleic acid delivery, supporting applications such as gene-editing experiments.

Keywords Oligopeptide-modified poly(β-amino ester), Nonviral delivery, Nucleic acid nanoparticles, Gene editing, CRISPR/Cas9 delivery, Endosomal escape, Polymeric vectors

1 Introduction

Efficient intracellular delivery of nucleic acids is a key challenge for experimental and therapeutic applications. Poly(β-amino ester)s (pBAEs) are biodegradable cationic polymers that form nanoscale polyplexes upon complexation with nucleic acids through electrostatic interactions [1]. These polymers are typically synthesized via Michael addition, allowing precise control over polymer length and composition, and they combine high transfection efficiency with low cytotoxicity and favorable biodegradation profiles [2–4].

Laia Martí-Melero and Sara Pérez Martín have contributed equally to this work.

Duško Lainšček et al. (eds.), *CRISPR Delivery*, Methods in Molecular Biology, vol. 3075,
https://doi.org/10.1007/978-1-0716-5547-4_15,
© The Author(s) 2027

To further enhance their performance, oligopeptide end-modified pBAEs (OM-pBAEs) have been developed. Terminal oligopeptides composed of cationic amino acids, such as lysine, arginine, or histidine, improve nucleic acid binding, stabilize polyplexes, and facilitate endosomal escape [5–8]. By tuning the type and ratio of these oligopeptides, OM-pBAEs can be optimized for different cargos, particle sizes, and cellular targets, providing a versatile and efficient platform for non-viral gene delivery [9].

The protocol described here outlines the preparation of OM-pBAE polyplexes for encapsulating nucleic acids. It covers the formulation of nanoparticles using either mRNA alone or mRNA–DNA mixtures, highlighting the steps necessary for controlled polyplex assembly, stabilization, and handling. These procedures ensure efficient electrostatic complexation between OM-pBAEs and nucleic acids, forming stable nanoparticles suitable for in vitro delivery and testing. By following this workflow, researchers can adapt the system to a variety of nucleic acid cargoes, demonstrating the flexibility of OM-pBAEs as a non-viral delivery platform for a wide range of gene-editing applications. In particular, these nanoparticles are compatible with the intracellular delivery of CRISPR/Cas components, enabling genome editing applications [10,11].

2 Materials

2.1 Polymer Synthesis

1. 91.2 mmol of 1,4-butanediol diacrylate. Store protected from light at 4°C (*see* **Note 1**).
2. 38 mmol of 1-hexylamine.
3. 38 mmol of 5-amino-1-pentanol. Store in a desiccator.
4. 50 mL round-bottom flask.
5. Amber glass vial.
6. Cys–His–His–His peptide in trifluoroacetic acid (TFA), supplied as a lyophilized powder. Stored at −20°C
7. Cys-Lys-Lys-Lys peptide in trifluoroacetic acid (TFA), supplied as a lyophilized powder. Stored at −20°C.
8. Cys-Arg-Arg-Arg peptide in trifluoroacetic acid (TFA), supplied as a lyophilized powder. Stored at −20°C
9. 0.1 M hydrochloric acid (HCl) solution.
10. 50 mL plastic tube.
11. DEPC reagent for RNase-free water. This reagent is important to treat MilliQ water to remove any RNases from the buffers.
12. Anhydrous dimethyl sulfoxide.

13. 50 mL round-bottom flask
14. Magnetic stirrer with heating plate
15. Diethyl ether/acetone (7:3, v/v) solution. Stored at −20°C.
16. Chloroform-d.
17. Dimethyl sulfoxide-d6.

2.2 Nanoparticle Formulation and Analysis

1. 12.5 mM sodium acetate buffer (AcONa) (pH 5.2). Filtered and stored at 4°C for a maximum of 3 months.
2. 20 mM HEPES buffer (pH 7.4). Filtered and stored at 4°C for a maximum of 1 month.
3. Sucrose 4% in 20 mM HEPES buffer. Filtered and stored at 4°C for a maximum of 1 month.
4. RNase-free water (prepared or commercially obtained DEPC-treated water).
5. 100 mg/mL of pBAEs stock (in anhydrous DMSO. Store at −20°C.
6. Nucleic acid stock solution. Store at −20°C in aliquots.
7. Agarose.
8. 1× TAE buffer (1 L: 4.84 g Tris base, 0.37 g EDTA, 1.14 mL glacial acetic acid). Autoclave and store at room temperature.

2.3 Equipment

1. Silicone oil bath (90°C).
2. Magnetic stirrer with heating plate and temperature probe (e.g., MR Hei-Connect Temperature, Heidolph Instruments GmbH & Co.).
3. 400 MHz JEOL NMR spectrometer (e.g., JEOL Ltd., Tokyo, Japan).
4. Standard 5 mm outer diameter (O.D.) borosilicate glass NMR tubes.
5. Water bath (25°C or controlled temperature as required).
6. Freezing at –80°C freezer.
7. Centrifugation at 4000 rpm.
8. Vacuum drying system (vacuum desiccator or rotary vacuum drying, as applicable).
9. Freezing at –20°C freezer.
10. Vortex mixer.
11. ZetaSizer is based on dynamic light scattering (DLS). Malvern Panalytical Nano Z.
12. Agarose gel electrophoresis system (gel tank and power supply) and gel imaging system with UV or blue-light transilluminator.
13. ZetaSizer software, Malvern Panalytical DTS Application.

14. Micropipettes.
15. Disposable micropipette tips.
16. Pasteur pipettes and pipette bulbs.
17. 0.2 mL microcentrifuge tubes.

3 Methods

3.1 Polymer Synthesis

Here, we describe the synthesis of OM-C6 pBAE by Michael addition, including reaction conditions and subsequent validation of polymer structure by ^{1}H NMR.

3.1.1 Polymerization of C6 pBAE

1. Combine 3.9 g (38 mmol) of 5-amino-1-pentanol and 3.8 g (38 mmol) of 1-hexylamine in a 50 mL round-bottom flask and mix thoroughly.
2. Add 18 g (91.2 mmol) of 1,4-butanediol diacrylate to the mixture.
3. Preheat a silicone oil bath to 90°C, immerse the flask, and stir the reaction with a magnetic stir bar for 20 h. After completion, turn off the heat and stirrer, and allow the mixture to cool to room temperature (*see* **Note 2**).
4. Transfer the polymer product from the flask to an amber glass vial, weigh it, and store at –20°C.
5. It is essential to validate the structure of the obtained C6 pBAE by ^{1}H NMR analysis (Fig. 1A, B). Figure 1B shows the expected spectrum after polymerization, with characteristic signals corresponding to the polymer backbone and terminal acrylate groups. In particular, the presence of acrylate vinyl proton signals (~5.5–6.5 ppm) confirms that the polymer retains reactive end groups required for subsequent peptide conjugation. The appearance of broad peaks corresponding to the β-amino ester backbone further indicates successful polymer formation (*see* **Note 3**). The sample is prepared by dissolving 5–10 mg of product in deuterated chloroform.

3.1.2 Peptide Conjugation

Polymer end-capping can be carried out using different peptides according to the protocol described below. Commonly used peptides include Cys-His-His-His, Cys-Lys-Lys-Lys, and Cys-Arg-Arg-Arg. The steps described in the following sections are applicable to any of these peptide end-capping approaches.

1. Dissolve the peptide with 200 mg of TFA in 20 mL of 0.1 M HCl in a pre-weighed 50 mL Falcon tube suitable for freeze-drying (*see* **Note 4**). Stir manually until a clear solution is obtained.

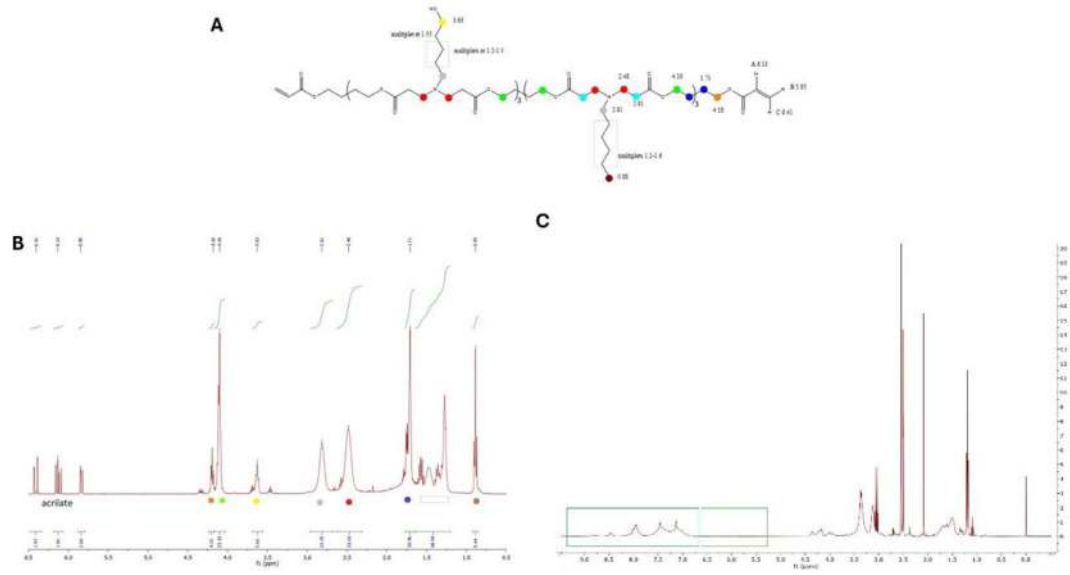


Fig. 1 Chemical structure and ^{1}H NMR characterization of the synthesized C6 pBAE and oligopeptide modification of C6-pBAE. (**A**) Chemical structure of the polymer with colored circles indicating the different proton environments. (**B**) Corresponding ^{1}H NMR spectrum with signal assignments matching the labeled proton environments. (**C**) 1H-NMR of the OM-pBAE after the modification with the cysteine-terminated arginine oligopeptide (Cys-Arg-Arg-Arg). The disappearance of acrylate signals is marked in green, indicating the correct addition of the arginine oligopeptide to the C6-pBAE polymer (peptide signal marked in blue)

2. Freeze the solution at −80°C for 1 h and lyophilize to obtain the peptide hydrochloride, confirming the final weight matches the theoretical value.
3. Prepare a solution of 113 mg (0.054 mmol) of C6 pBAE in 1.1 mL anhydrous DMSO and a solution of 99 mg (0.13 mmol) of peptide hydrochloride in 1 mL anhydrous DMSO. Combine the two solutions in a screw-cap tube and close securely.
4. Stir the mixture in a water bath maintained at 25 ± 2°C with a magnetic stir bar for 20 h.
5. Add the reaction mixture dropwise to 10 mL of 7:3 (v/v) diethyl ether/acetone to precipitate the product (*see* **Note 5**). Centrifuge at 4000 rpm for 10 min and remove the supernatant.
6. Wash the solid twice with 5 mL of 7:3 (v/v) diethyl ether/acetone and dry under vacuum.
7. Prepare a stock solution of 100 mg/mL of the final product in DMSO and store at −20°C until further use.
8. Following peptide conjugation (end-capping), ^{1}H NMR analysis should be repeated to confirm successful modification. In this case, the disappearance or significant reduction of the acrylate vinyl proton signals (~5.5–6.5 ppm), Fig. 1C (*see*

Note 6), indicates consumption of the reactive end groups. Additionally, new signals corresponding to the incorporated oligopeptides (e.g., side-chain protons from lysine, arginine, or histidine) should be observed, confirming successful attachment of the peptide moieties. The sample is prepared by dissolving 5–10 mg of product in deuterated DMSO-d6.

3.2 Nanoparticle Formulation

Here, we describe the formulation of OM-pBAE polyplex nanoparticles through electrostatic complexation with nucleic acids, including mRNA alone or mixtures of mRNA and DNA. This method enables the reproducible formation of stable nanoparticles suitable for in vitro applications and subsequent physicochemical characterization. All procedures should be carried out at a constant temperature of 25°C. Nanoparticles can be prepared at different w/w ratios (polymer:nucleic acid) using the protocol described below. Typically, ratios of 75:1 and 25:1 are selected as optimal formulations for in vitro and in vivo studies using OM-pBAEs.

1. Thaw the 100 mg/mL peptide-modified polymer stock and homogenize by briefly vortexing. Dilute to the desired working concentration (as required) in 12.5 mM sodium acetate buffer by pipetting up and down, and allow the solution to equilibrate for 10 min (*see* **Note 7**).
2. Prepare the nucleic acid solution (e.g., Cas9 mRNA, DNA, or a 1:1 mixture) at the desired working concentration (0.5 mg/mL). Handle RNA gently and avoid vortexing; DNA may be vortexed.
3. Combine the previous polymer and nucleic acid solutions in a 1:1 volume ratio by pipetting up and down vigorously, then incubate at 25°C for 30 min to allow nanoparticles to self-assemble. For optimal results, add the previously prepared genetic material solution to the polymer solution, rather than vice versa. Do the mixture in 0.2 mL microcentrifuge tubes since small volumes are used.
4. Precipitate the nanoparticles by slowly adding the previous mixture to RNase-free water at the appropriate ratio (typically 1:1, previously prepared sample:water) while gently pipetting to avoid aggregation.
5. Immediately after, add excipients to the nanoparticle solution in water (either 20 mM HEPES buffer, pH 7.4 or, if a subsequent lyophilization is planned, 20 mM HEPES buffer supplemented with 4% sucrose) in an equal volume to the nanoparticle mixture (corresponding to the volume before the addition of water).
6. Mix gently by pipetting up and down to ensure homogeneity. At this stage, the sample is diluted approximately threefold,

and the nanoparticles are stabilized for short-term handling. The nanoparticles remain stable for several hours at room temperature and can be used for immediate in vitro applications.

7. For long-term storage, freeze the nanoparticles at –80°C, lyophilize them, and store at −20°C. Resuspend in RNase-free water at the desired concentration prior to use.

3.3 Nanoparticle Physicochemical Characterization

Here, we describe the physicochemical characterization of OM-pBAE polyplex nanoparticles, including particle size, surface charge, and nucleic acid encapsulation efficiency. These analyses are performed using dynamic light scattering (DLS) and agarose gel electrophoresis to confirm successful nanoparticle formation, evaluate colloidal stability, and assess nucleic acid complexation prior to in vitro applications.

3.3.1 Size and Zeta Potential Measurements of Nanoparticles Using Dynamic Light Scattering (DLS)

1. Switch on the DLS instrument and the connected computer. Open the software and ensure the LED indicator shows green. Allow the instrument to stabilize for approximately 30 min before measurements.
2. *Particle size measurement:* Pre-rinse a microcuvette with filtered dilution media. Fill the cuvette with at least 50 µL of nanoparticle suspension prepared according to the nanoparticle formulation protocol (*see* **Sect.** 3.2), and ensure no bubbles are present in the optical window. Insert the cuvette fully into the instrument, create an appropriate size analysis (considering the main buffer solution of the nanoparticle suspension, the cuvette used and reading temperature), enter the sample name, and start the measurement by clicking "Play." After completion, select the results to obtain the average particle size, polydispersity index (PDI), standard deviation, and graphical outputs (Fig. 2A) (*see* **Note 8**).
3. *Zeta potential measurement:* Dilute the nanoparticle sample 1:10 with 20 mM HEPES buffer to adjust pH to ~7. Filter the dispersant before use. Ensure the final nanoparticle concentration is between 200 and 2200 µg/mL (based on polymer content). Pre-rinse a disposable folded capillary cuvette with filtered buffer and fill completely with the diluted nanoparticles using a 1 mL syringe, avoiding bubbles. Insert the cuvette into the DLS. Create an appropriate SOP file for zeta potential analysis, enter the sample name, and run the measurement. After completion, obtain the average zeta potential, standard deviation, and graphical outputs (Fig. 2B) (*see* **Note 9**).
4. Remove the cuvettes and retain samples if necessary. Clean with Milli-Q water, followed by ethanol and water, and dry under a compressed air stream. The equipment is ready for the next measurement (*see* **Notes 10 and 11**).

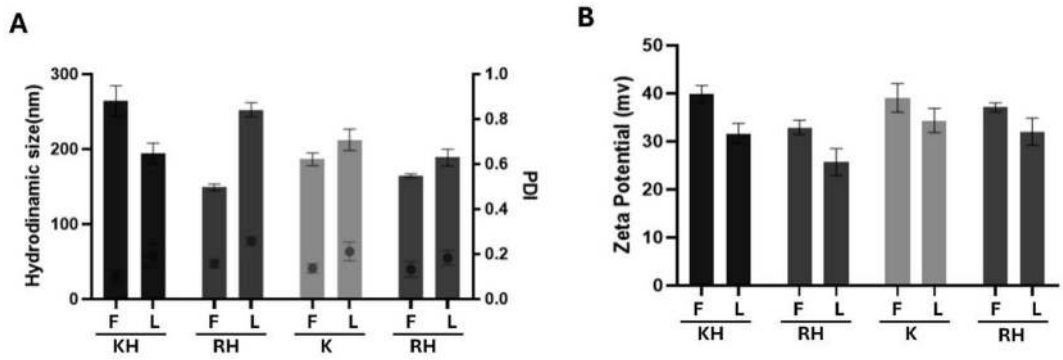


Fig. 2 Physical characterization of OM-pBAE polyplexes composed of single polymers (K, R) and polymer blends KH (60% K/40% H) and RH (60% R/40% H) under fresh (F) and lyophilized (L) conditions.(**A**) Hydrodynamic diameter (nm), typically between 100 and 200 nm, was measured by DLS. Slight deviations above 200 nm were observed in some samples, but are not considered significant. (**B**) Zeta potential (mV), typically between +20 and +40 mV depending on polymer composition, was measured by DLS

3.3.2 Encapsulation Efficiency Measurement Using Agarose Gel Electrophoresis

1. Prepare a 2% agarose gel in 1× TAE buffer and add a suitable nucleic acid stain (such as GelRed or ethidium bromide). Cast the gel in a gel tray and allow it to solidify.
2. Prepare the desired nanoparticle samples (*see* **Note 12**) containing mRNA, DNA, or mixtures of both (*see* **Note 13**) to be analyzed. The prepared nanoparticles should be resuspended in RNase-free water or buffer to the desired concentration.
3. Prepare control samples containing equivalent amounts of free mRNA and/or DNA (non-encapsulated) to serve as references.
4. Load equal volumes of nanoparticle samples and control samples into the wells of the agarose gel. Include a molecular weight or nucleic acid size marker if needed. Be careful that the agarose gel is not covered with 1× TAE buffer after sample loading (*see* **Note 14**).
5. Run the electrophoresis gel approximately 5 min at 60 V (until the dye front has migrated sufficiently to resolve free nucleic acids). Then, cover the agarose gel with 1× TAE buffer and run the gel at 120 V for 40–60 min.
6. Visualize the gel using an appropriate imaging system. Compare the migration of free nucleic acids to that of nanoparticle samples. Complete encapsulation is indicated by the absence or reduction of free nucleic acid bands in the nanoparticle lanes (Fig. 3). This assay is qualitative and does not provide a quantitative measurement of encapsulation efficiency (*see* **Note 15**).

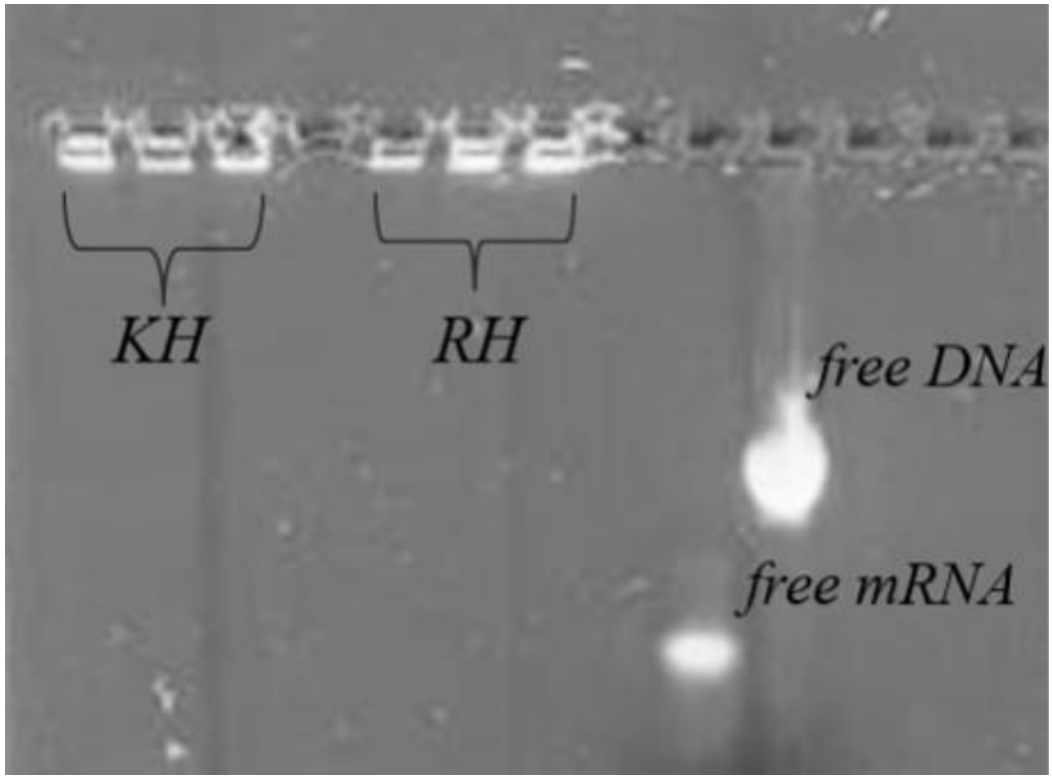


Fig. 3 Agarose gel electrophoresis analysis of lyophilized KH and RH nanoparticles formulated with a 1:1 ratio of DNA and mRNA, compared to free mRNA and free DNA controls. The absence of free nucleic acid bands in the nanoparticle lanes indicates complete encapsulation of both components

4 Notes

1. Handle 1,4-butanediol diacrylate inside a fume hood while wearing appropriate personal protective equipment. Avoid skin contact and inhalation, as acrylate monomers may cause irritation and skin sensitization. Acrylate monomers are prone to spontaneous polymerization; therefore, store the reagent tightly closed and protected from light and heat to prevent unwanted polymerization.
2. The obtained product is a viscous, pale yellow, honey-like liquid.
3. NMR spectra are recorded on a 400 MHz JEOL NMR instrument (JEOL Ltd., Japan) using chloroform-d as the solvent.
4. Peptide powder is highly electrostatically charged and can easily disperse and adhere to the outside of plastic Falcon tubes, so care must be taken. Measure outside of the analytical balance box.

5. In case no precipitation occurs, repeat this step using a solution with a higher diethyl ether concentration, since the end-capped C6 pBAE is insoluble in this solvent.
6. It is important to note the disappearance (or substantial reduction) of olefin signals, while peptide signals will appear.
7. The final polymer concentration depends on the selected NP ratio. For a 25:1 NP ratio with nucleic acid at 0.5 mg/mL, the polymer concentration after mixing will be 12.5 mg/mL.
8. The expected size of OM-pBAE nanoparticles is typically between 100 and 200 nm.
9. The expected zeta potential of OM-pBAE nanoparticles is positive, typically between +20 and +40 mV, depending on the polymer composition.
10. Cuvettes with scratches must be discarded; if additional cleaning is required, use specially formulated solutions and avoid ultrasonic baths.
11. Remove samples promptly to prevent residue adherence. Proper handling ensures reproducible measurements and extends cuvette life.
12. Ensure the nanoparticle samples are handled gently to avoid premature disruption.
13. Using a 1:1 ratio of mRNA to DNA has been shown to result in complete encapsulation of both nucleic acid components within the nanoparticles.
14. For better results, load the samples directly into the wells of the dry gel while the gel is placed in the cuvette outside the electrophoresis chamber. After loading, carefully transfer the gel (with the cuvette) into the electrophoresis chamber, allowing the 1× TAE buffer to contact the gel surface without completely covering the wells.
15. Additional quantification can be performed by densitometry if needed.

Acknowledgments

The publication is based upon work by COST Action CA21113: Genome Editing for the Treatment of Human Diseases (https://www.genehumdi.eu), supported by European Cooperation in Science and Technology (COST).

Conflict of Interest The authors have no conflicts of interest to declare that are relevant to the content of this chapter.

References

1. Zhang J, Cai X, Dou R et al (2023) Poly(β-amino ester)s-based nanovehicles: structural regulation and gene delivery. Mol Ther Nucleic Acids 32:568–581
2. Liu Y, Li Y, Keskin D et al (2019) Poly(β-amino esters): synthesis, formulations, and their biomedical applications. Adv Healthc Mater 8:e1801359
3. Kamat CD, Shmueli RB, Connis N et al (2013) Poly(β-amino ester) nanoparticle delivery of TP53 has activity against small cell lung cancer in vitro and in vivo. Mol Cancer Ther 12:405–415
4. Karlsson J, Rhodes KR, Green JJ et al (2020) Poly(beta-amino ester)s as gene delivery vehicles: challenges and opportunities. Expert Opin Drug Deliv 17:1395–1410
5. Segovia N, Dosta P, Cascante et al (2014) Oligopeptide-terminated poly(β-amino ester)s for highly efficient gene delivery and intracellular localization.. Acta Biomater 10:2147–2158
6. Fornaguera C, Guerra-Rebollo M, Lázaro MÁ et al (2018) mRNA delivery system for targeting antigen-presenting cells in vivo. Adv Healthc Mater 7:e1800335
7. Fornaguera C, Guerra-Rebollo M, Lázaro MÁ et al (2019) In vivo retargeting of poly(beta amino ester) (OM-pBAE) nanoparticles is influenced by protein corona. Adv Healthc Mater 8:e1900849
8. Fornaguera C, Castells-Sala C, Borrós S (2020) Unraveling polymeric nanoparticles cell uptake pathways: two decades working to understand nanoparticles journey to improve gene therapy. Adv Exp Med Biol 1288:117–138
9. Navalón-López M, Dols-Perez A, Grijalvo S et al (2023) Unravelling the role of individual components in pBAE/polynucleotide polyplexes in the synthesis of tailored carriers for specific applications: on the road to rational formulations. Nanoscale Adv 5:1611–1623
10. Gao X, Jin Z, Tan X et al (2020) Hyperbranched poly(β-amino ester) based polyplex nanoparticles for delivery of CRISPR/Cas9 system and treatment of HPV infection-associated cervical cancer. J Control Release 321:654–668
11. Parés M, Fornaguera C, Vila-Julià F et al (2021) Preclinical assessment of a gene-editing approach in a mouse model of mitochondrial neurogastrointestinal encephalomyopathy. Hum Gene Ther 32:1210–1223

Open Access This chapter is licensed under the terms of the Creative Commons Attribution-NonCommercial-NoDerivatives 4.0 International License (http://creativecommons.org/licenses/by-nc-nd/4.0/), which permits any noncommercial use, sharing, distribution and reproduction in any medium or format, as long as you give appropriate credit to the original author(s) and the source, provide a link to the Creative Commons license and indicate if you modified the licensed material. You do not have permission under this license to share adapted material derived from this chapter or parts of it.

The images or other third party material in this chapter are included in the chapter's Creative Commons license, unless indicated otherwise in a credit line to the material. If material is not included in the chapter's Creative Commons license and your intended use is not permitted by statutory regulation or exceeds the permitted use, you will need to obtain permission directly from the copyright holder.





Chapter 16

Virus-Like Particles as a Nonviral CRISPR/Cas Editing Delivery Tool

Antonio Carusillo, Asma Naseem and Alessia Cavazza

Abstract

Virus-like particles (VLPs) are self-assembling viral protein complexes that mimic native virions while lacking replicative and infectious capacity. By retaining efficient cellular entry and cargo protection, they overcome key limitations of viral vectors, including insertional mutagenesis and strong immunogenicity. Their ease of production, flexible cargo capacity, and tunable tropism make them highly versatile tools. Here, we describe a protocol for generating VSV-G-pseudotyped VLPs that deliver CRISPR/Cas9 RNPs and their functional validation in surrogate cell lines.

Keywords Virus-like particles (VLPs), CRISPR/Cas9, RNP delivery, VSV-G pseudotyping, Genome editing, Nonviral delivery, Nucleic acid delivery, Gene editing

1 Introduction

Virus-like particles (VLPs) are self-assembling structures composed of viral structural proteins that organize into virion-like particles; however, unlike fully competent viruses, they lack the ability to replicate and infect cells [1].

As a result, VLPs retain key advantageous properties of viruses, such as efficient cellular entry, endosomal escape, and protection of their cargo, while avoiding several limitations associated with viral vectors, including the risk of random genomic integration (as observed with retroviruses) and strong immunogenicity.

Although VLPs were initially developed and widely used in vaccinology, they are increasingly being explored as delivery systems for a variety of cargos, including both nucleic acids and proteins, such as CRISPR-based platforms [2]. What makes VLPs particularly attractive is that: (a) they can be produced in the laboratory using protocols similar to those employed for lentiviral vector production; (b) unlike viral vectors, they are not constrained by the same packaging limitations; and (c) their tropism can be readily engineered,

Duško Lainšček et al. (eds.), *CRISPR Delivery*, Methods in Molecular Biology, vol. 3075,
https://doi.org/10.1007/978-1-0716-5547-4_16,
© The Author(s) 2027

for example by modifying the envelope glycoprotein (e.g., VSV-G vs. SFV) or by incorporating adaptor proteins (e.g., scFvs) during VLP production [3,4]. These features make VLPs highly suitable for applications that require robust and adaptable delivery systems.

In this chapter, we describe a protocol covering the key steps required to produce VSV-G–enveloped VLPs packaging a CRISPR/Cas9–sgRNA ribonucleoprotein (RNP) complex, as well as methods to functionally validate them in surrogate cell lines (Fig. 1).

2 Materials

2.1 VLP Preparation

2.1.1 Reagents

1. Plasmid for VSV-G pseudo-typing: pCMV-VSV-G [5].
2. Plasmid for VLPs assembly: pMMLV-gag-pol [6].
3. Plasmid for VLPs payload:
   a. BIC-gag-Cas9 [7].
   b. gag-YFP [8].
   c. sgRNA [9].
4. DMEM-GlutaMax.
5. Fetal Bovine Serum (heat inactivated).
6. Penicillin/Streptomycin.
7. PBS Store at 4°C.
8. Trypsin-EDTA (store at 4°C).
9. Transfection reagents [e.g., JetPRIME® (PolyPlus). Store at 4°C].

2.1.2 Equipment

1. Fluorescence microscope.
2. Automated cell-counter or Hemacytometer.
3. Ultracentrifuge.
4. Flow-cytometer.
5. qPCR Thermocycler.

2.2 VLP Purification and Titration Reagents

1. PEG-it Virus Precipitation Solution. Store at 4°C.
2. Filter Units 0.45л PVDF. Keep at RT, use under the flow hood.
3. Sucrose. 20% (w/v) in PBS
4. Lysis (Laemmli) Sample Buffer. Store short-term at RT or long-term at 4°C.
5. 1× Cell Extraction Buffer. Store at 4°C.

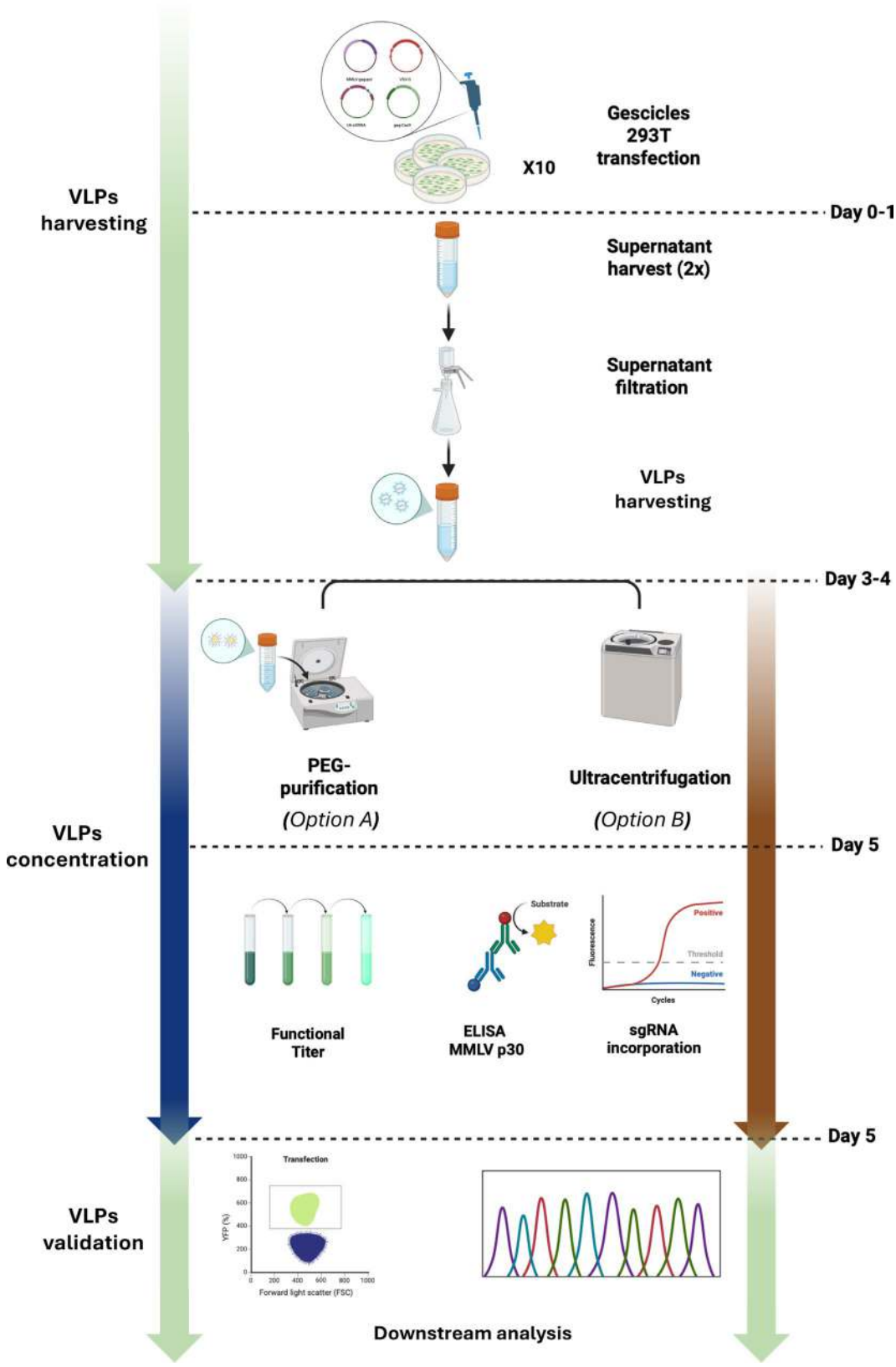

VLPs harvesting
Gescicles 293T transfection
X10
Day 0-1
Supernatant harvest (2x)
Supernatant filtration
VLPs harvesting
Day 3-4
PEG-purification
(Option A)
Ultracentrifugation
(Option B)
VLPs concentration
Day 5
Functional Titer
Substrate
ELISA MMLV p30
Positive
Threshold
Negative
Fluorescence
Cycles
sgRNA incorporation
Day 5
VLPs validation
Transfection
YFP (%)
Forward light scatter (FSC)
Downstream analysis

Fig. 1 Workflow for VLP production, purification, and functional validation. Gesicle Producer 293T cells are transfected with VLP-forming and payload plasmids (Day 0–1), followed by the collection of the supernatant containing VLPs. VLPs are subsequently purified and concentrated either by PEG-based precipitation or ultracentrifugation (Day 3–4). Purified VLPs are then quantified using p30 ELISA or qPCR and functionally validated through downstream assays, including flow cytometry and Sanger sequencing (Day 5)

6. QuickTiter™ MuLV Core Antigen ELISA Kit (MuLV p30). Store at 4°C.
7. TBST buffer. Store at RT.
8. Blocking buffer solution.
9. Anti-Cas9 antibody.
10. Anti-MLV p30.
11. Anti-VSV-G.

3 Methods

3.1 VLP Production in Gesicle Producer 239T Cells—Duration 5 days

In this protocol, we describe how VLPs can be purified and concentrated either via PEG-it (5a) or via ultracentrifugation (5b). The first approach is suitable when an ultracentrifuge is not available and/or when it is not necessary to obtain highly concentrated VLPs, as PEG-it can concentrate VLPs up to ~100-fold. The second approach is recommended when highly pure and highly concentrated VLPs are required, for example, when they are intended to be used on sensitive cells (e.g., hematopoietic stem cells) or for in vivo applications (*see* **Note 1**).

In parallel to CRISPR-VLPs, it is also possible to prepare VLPs containing only a reporter gene (e.g., YFP), which can be used as a proxy to evaluate and optimize the infection conditions of target cells via flow cytometry. Before starting, check the **Note** (**1–5**).

3.1.1 Gesiscles Producer 293T Cells Seeding (Day 0)

1. Take the Gesiscles 293T on the 10-cm dish out of the incubator.
2. Remove the medium using a vacuum pump.
3. Wash the cells with 5 mL of pre-warmed (37°C) PBS.
4. Remove the PBS and detach cells by adding 1 mL Trypsin-EDTA.
5. Place the cells in the incubator at 37°C for 5 min.
6. Add 9 mL of prewarmed (37°C) medium to inactivate trypsin.
7. Count the cells using either a manual hemocytometer or an automatic cell counter.
8. Seed 5 million cells per plate. We recommend using T-75 flask with ventilated cap.

9. Centrifuge the required number of cells at 100 × *g* for 5 min (see **Note 3**).
10. Resuspend the cells in the appropriate volume of medium, then seed them into a T-75 flask.
11. Seed 5 million cells per flask.
12. After seeding, gently swirl the flask to ensure even distribution of the cells.
13. Place the cells back in the incubator.

3.1.2 Transfecting VLP-Forming Plasmids and the Payload Plasmid in Gesicles (Day 1)

1. Take JetPRIME® and JetPRIME®buffer out of the fridge, place them under the cell hood, and allow them to reach room temperature.
2. Meanwhile, prepare the DNA mix in the laminar flow hood in a 1.5 mL Eppendorf tube as listed in Tables 1 and 2.
3. Add 500 µL of JetPRIME® buffer to the DNA mix.
4. Vortex briefly (5 s) and spin down.
5. Add JetPRIME® at a 2:1 ratio (JetPRIME®: µg DNA). For example, for 9929 ng of DNA, add 18.59 µL of JetPRIME®.

Table 1
VLPs plasmid mix for CRISPR-loaded VLPs

Construct	ng	tot DNA 9929 ng
VSV-G	400	
MMLV-gag-pol	3375	
Gag-ABE	1124	
sgRNA	4400	

Table 2
VLPs plasmid mix to test cell infectivity

	ng	tot DNA
VSV-G	400	
MMLV	3375	
YFP-gag	1500	5275

6. Mix gently by pipetting, avoiding bubble formation, and spin down.
7. Incubate at room temperature for 10 min.
8. Distribute evenly DNA:JetPRIME® mix onto the cells. For this we suggest tilting the flask to one side to collect the medium in a corner and adding there the mix. When the flask is back in its original position the medium will distribute evenly the mix to the cells.
9. Swirl the flask to evenly distribute the transfection mix.
10. Place the cells back in the incubator.
11. After 4 h, remove the medium and carefully add fresh medium.
12. Place the cells back in the incubator.

3.1.3 Collection of Supernatant 1 Out 2 (Day 3)

1. At 48 h post-transfection, collect the supernatant in a 50 mL Falcon tube and replace it with fresh medium, taking care not to detach the cells.
2. Remove potential debris from the supernatant by centrifuging at 500 × *g* for 5 min.
3. Transfer the supernatant to a new Falcon tube and store it at 4°C.

3.1.4 Collection of Supernatant 2 out of 2 and Purification (Day 4)

1. Collect the supernatant and discard the cell plate
2. Remove potential debris from the supernatant by centrifuging at 500 × *g* for 5 min.
3. Take out of the fridge the supernatant from Day 3.
4. Pool the two supernatants and filter using 0.45л PVDF filter.
5. Place the filtered supernatant at 4°C.
6. Proceed to purify and concentrate the VLPs either via PEG-it (Sect. 3.2.1) or Ultra-Centrifuge (Sect. 3.2.2).

3.2 VLP Purification

3.2.1 PEG Purification (Day 4 to Day 5)

1. Place the PEG-it Virus Precipitation Solution in the cell culture hood.
2. For PEG-it precipitation, one volume of PEG-it is mixed with four volumes of filtered supernatant. For example 5 mL of PEG-it with 20 mL of filtered supernatant.
3. Take the filtered supernatant out of the fridge and distribute it into an appropriate number of 50 mL Falcon tubes. For example, 100 mL of filtered supernatant should be transferred to 4 × 50 mL Falcon tubes (25 mL each). This will ensure to have enough volume to accommodate the PEG-it.
4. Add PEG-it (6.25 mL in 25 mL) and carefully mix by pipetting up and down ten times or until the PEG-it is fully mixed.

5. Parafilm the Falcon tubes and transfer them back to the fridge.
6. Incubate the supernatant with PEG-it for at least 12 h and up to 4 days.
7. 12 h later, transfer and prechill the centrifuge at 4°C.
8. Set an ice bucket next to the laminar flow hood and pre-chill cryogenic vials.
9. Transfer the Falcons into the centrifuge and spin down $1500 \times g$ for 30 min at 4°C.
10. After centrifugation, a greyish pellet should be visible. (Optional) Carefully transfer the supernatant to a new Falcon and repeat the centrifugation to collect potential residues of PEG-it aggregated VLPs.
11. Discard the supernatant, then leave the Falcon tube inverted and gently tap it on tissue paper to remove as much liquid as possible.
12. Leave the Falcon tube inverted for 5 min or until the majority of the liquid on the walls has been removed.
13. Resuspend the pellet in cold PBS (pH 7.4) by slowly pipetting up and down to avoid forming bubbles until it is fully dissolved. Resuspend using between 1/10 and 1/100 of the original volume. For example, 100 µL for 10 mL of filtered supernatant.
14. The resuspended solution should appear cloudy. Make single-use aliquots by distributing the resuspended solution in prechilled cryovials.
15. Transfer and keep at −80°C until use.

(Optional) If the VLPs are packaged with a fluorescent protein (e.g., YFP), it is possible to estimate functionality by performing a serial dilution, transfecting the cells, and measuring the numbers of positive and negative cells using a flow cytometer.

3.2.2 Ultracentrifuge Purification (Day 4 to Day 5)

1. Set an ice bucket next to the laminar flow hood and prechill cryogenic vials.
2. Turn on the Ultracentrifuge.
3. Clean and inspect the ultracentrifuge tubes for cracks or abnormalities.
4. Add 33 mL of filtered supernatant to the Ultracentrifuge tubes.
5. Take 3 mL of filtered sucrose with a serological pipette, place it in the Ultracentrifuge tube, and let it settle to the bottom without touching it.
6. Slowly start dispensing the filtered sucrose. A clear cushion should form at the bottom.

7. Weigh the tubes and top up with additional supernatant.
8. Concentrate the filtered supernatant 1000–3000-fold by Ultracentrifuge at 121,896×*g* for 2 h 15 min at 4°C.
9. When the Ultracentrifugation is done, carefully open the tube canister to remove the Ultracentrifuge tube. Use tweezers to not touch the supernatant.
10. Carefully discard the supernatant, invert the tube, and tap it on tissue paper to remove any remaining liquid.
11. Leave the tube inverted for 5 min. If an excess of liquid is still visible, you can use tissue paper to absorb it from the interior walls.
12. Resuspend the pellet in cold PBS (pH 7.4) by slowly pipetting up and down to avoid forming bubbles until it is fully dissolved. Resuspend using between 1/10 and 1/100 of the original volume. For example, 100 µL for 10 mL of filtered supernatant.
13. Make single-use aliquots by distributing the resuspended solution in prechilled cryovials.
14. Transfer and keep at −80°C until use.

3.3 VLPs Titration by MLV p30 ELISA—Only if VLPs Purified via Ultracentrifuge [10]

This protocol assumes ultracentrifuge-purified VLPs that have been concentrated 1000–5000×.

3.3.1 Lyse VLPs

(Option A)

1. Prepare lysis (Laemmli) buffer by mixing 50 mM Tris-HCl, pH 8, 2% sodium dodecyl sulfate (SDS) with 10% (v/v) glycerol and 2 mM dithiothreitol (DTT). Store short-term at RT or long-term at 4°C.

Table 3
Standard preparation

Standard tubes	MuLV p30 standard (µL)	Assay diluent (µL)	MuLV p30 concentration
1	2 of Stock standard (10 µg/mL)	998	20 ng/mL
2	300 of tube#1	300	10 ng/mL
3	300 of tube#1	300	5 ng/mL
4	300 of tube#1	300	2.5 ng/mL
5	300 of tube#1	300	1.25 ng/mL
6	300 of tube#1	300	0.625 ng/mL
7	300 of tube#1	300	0.313 ng/mL
8	300 of tube#1	300	0

2. Lysate eVLPs in lysis buffer by adding one volume of lysis buffer to one volume of purified eVLPs.
3. Heat at 95°C for 15 min.

(Option B)

1. Prepare cell extraction buffer (1×) by mixing together FastScan™ ELISA Cell Extraction Buffer (5×) and FastScan™ ELISA Cell Extraction Enhancer Solution (50×) with deionized water.
2. Lysate VLPS in CEB, one volume of VLPs per one volume of CEB.
3. Incubate on ice for 5 min.
4. Centrifuge at 13,000 for 5 min at 4°C.
5. Recover the supernatant.

3.3.2 Preparation of Standards

Prepare the standards following the manufacturer's instructions (Table 3).

3.3.3 Preparation of Quantification Curve

1. Add 100 µL of samples/standards, and shake 2 h at 300 rpm at RT.
2. Wash five times with 250 µL wash buffer.
3. Add 100 µL anti-MuLV p30 antibody.
4. Shake the plate 1 h at 16 G, RT.
5. Wash five times with 250 µL of wash buffer.
6. Add 100 µL secondary antibody.
7. Shake the plate for 1 h at 16 G, RT.
8. Wash five times 250 µL wash buffer.
9. Add 100 µL TMB substrate and incubate the plate for 5–10 min at RT (*see* **Note 6**).
10. Add 100 µL of STOP solution.
11. Read OD at 450 nm.

3.3.4 Data Analysis

1. Generate a linear standard curve using the p30 standards.
2. Use sample absorbance values within the linear range to calculate p30 concentration (ng/mL) in the original undiluted sample
3. Convert p30 concentration to molarity using: MW(p30) = 32.941 kDa.

3.3.5 Estimation of VLP Concentration

Estimate VLP concentrations from p30 ELISA measurements by using the following parameters based on previous work [10]:

1. p30 molecular weight: 32.941 kDa.
2. No. of p30 molecules per particle: 1800.

3. Percentage of VLP-associated p30 per particle: 20% VLP-associated p30 [10, 11].
4. Conversion from ng/mL p30 to VLPs/μL uses a constant factor of 2030.566434 derived from Avogadro's number and unit conversions (*see* **Note 7**).

Example Calculation
Measured p30 concentration: 539,000 ng/mL
Calculated values:

- $p30 = 1.64 \times 10^7$ pM.
- $p30 = 9.85 \times 10^{12}$ molecules/μL.

Assuming 20% VLP association and 1800 p30 molecules per particle:
VLP concentration $= 1.09 \times 10^9$ particles/μL.
(*see* **Notes 8 and 9**)

3.3.6 Validation of VLP Protein Content by Dot Blot Analysis

1. Lyse eVLPS as described in Sect. 3.3.1.
2. Spot lysed VLP samples onto a dry nitrocellulose membrane.
3. Allow the membrane to air-dry for 30 min at RT.
4. Prepare TBST buffer by mixing 100 mL of 10× TBS with 1 mL Tween detergent and 900 mL of deionized water. Store at RT.
5. Prepare a blocking buffer with TBST buffer and 1% BSA. Store at RT
6. Block the membrane by incubating with the blocking buffer for 1 h at RT with rocking.
7. Next, incubate the membrane overnight at 4°C with rocking in blocking buffer containing one of the following primary antibodies: anti-Cas9, anti-MLV p30, or anti-VSV-G.
8. Wash the membrane three times for 10 min each at room temperature in TBST.
9. Incubate the membrane with the corresponding secondary antibody for 1 h at room temperature with rocking.
10. Wash the membrane again three times for 10 min each in TBST.
11. Develop the blot.
12. Visualize chemiluminescence on a dedicated apparatus (e.g., Bio-Rad ChemiDoc).

3.3.7 Quantifying sgRNA Packaging in VLPs via qPCR (see Note 11)

1. Extract RNA from VLPs (*see* **Note 10**).
2. Retrotranscribe extracted RNA using sgRNA-specific primers (*see* **Notes 11 and 12**).
3. Generate a standard curve using tenfold serial dilutions (e.g., 10^8–10^2 copies) of a plasmid containing your sgRNA sequence.

4. Perform quantitative real-time PCR with SYBR Green dye.
5. The plasmid constructs used for VLPs production can be used as positive control and standards during this step.
6. Determine amplification efficiency from the standard curve (acceptable range: 90%–110%) and ensure linearity ($R^2 \geq 0.99$).
7. Quantify sgRNA copy number in samples by interpolation from the plasmid standard curve.
8. Normalize sgRNA abundance to MLV p30 content.
9. Calculate sgRNA abundance per eVLP as $\log_2(\Delta Cq)$ relative to VLPs.

3.4 Functional Testing Cell Infectivity via VLPs (Duration 2 Days)

After VLPs production and quantification (only if VLPs were purified via Ultracentrifugation), it is important to verify if the VLPs can deliver their cargo. As we are describing the production of VLPs packaging a reporter protein (YFP), this can be tested via flow cytometry.

3.4.1 H293T Cells Seeding (Day 1) (see Notes 13 and 14)

1. Remove media using a vacuum pump.
2. Wash cells with prewarmed (37°C) PBS.
3. Remove PBS and detach cells by adding Trypsin-EDTA.
4. Put the cells into the incubator at 37°C for 5 min.
5. Add prewarmed (37°C) medium to inactivate the trypsin.
6. Count the cells using either a manual hemacytometer or an automatic Cell-Counter device.
7. Spin down the required number of cells at $300 \times g$ for 5 min.
8. Resuspend the cells in the appropriate volume of medium and seed 150,000 cells in a 24-well plate.
9. After seeding, gently swirl the plate carefully to ensure even distribution of the cells on the plate surface.
10. Place the cells back in the incubator.

3.4.2 H293T Cells Transduction with VLPs and Flow Cytometry (Day 2)

1. Take the cryogenic vials containing VLPs from the −80°C and place them on an ice bucket, allowing them to slowly thaw.
2. When VLPs are thawed, take the cells out of the incubator.
3. For VLPs, we recommend using no more than 1/10 of the volume present in the well where cells have been seeded. For example, if 500 μL of media has been used to seed the cells in, do not use more than 50 μL.
   (Optional) Make a series of dilutions of your VLPs in PBS to test different amounts. For example, 1:2, 1:4, and 1:8.
4. Add the VLPs to the cells dropwise, and after gently rocking the plate to allow even spreading of the VLPs. If highly concentrated PEG-purified VLPs are used, an initial grayish stain may be observed on the media surface. Rock the plate until evenly distributed.

5. Place the cells back in the incubator.
6. As the VLPs are packaging a reporter protein, this is readily expressed, and a strong signal can be observed already at 4–6 h post-transfection.
7. After 4–6 h collect the cells and run them through the flow-cytometer to check for cells positive to the reporter protein used to package the VLPs with. For YFP or EGFP packaging VLPs, the signal can be observed using a 488 nm Laser with a 525/550 nm filter. For an efficient VSVG-VLPs production, it is expected to see between 60% and 90% YFP/EGFP positive HEK293T cells.

4 Notes

1. To ensure the best results, we recommend preparing each plasmid used for VLP production as Maxi preparation and ensuring it is free of endotoxins; we recommend using the EndoFree MaxiPrep kit from Qiagen (#12362). We suggest storing the plasmid DNA at −20°C for improved preservation.
2. Gesicles Producer 293T cells (Takara, #632617) should not be older than passage 16–17 to ensure the highest quality of produced VLPs. We recommend, upon arrival, expanding the Gesicles 293T cells and freezing and storing as many aliquots as possible at early passage to always have early passages as a starting point for VLP production.
3. The protocol assumes seeding five T-75 flasks with 5million cells each, per construct. The number of plates can be scaled up or down depending on the required amount of VLPs, but conditions should be checked on a case-by-case basis.
4. Gesicles Producer 293T cells are quite sensitive; exceeding 100 g may negatively affect their viability and the overall procedure.
5. As a transfection reagent, we recommend using jetPRIME®®-JetPRIME® (Polyplus, 101000006). Take JetPRIME®®e and jetPRIME®®JetPRIME®buffer out of the fridge, place them under the cell hood, and allow them to reach room temperature.
6. Monitor color to make sure it doesn't get too saturated (depends on your plate reader sensitivity).
7. To convert measured p30 concentration (ng/mL) to VLP concentration (particles/μL), apply the following dimensional analysis.

8. Assumptions: (i) Molecular weight of p30 = 32,941 ng/nmol, (ii) 1 nmol = 6.02×10^{14} molecules, (iii) 1800 p30 molecules per VLP, and (iv) 20% of p30 is associated with VLPs.
9. Dimensional analysis

$$[p30]\left(\frac{ng}{mL}\right) \times \frac{1 \quad ml}{10^2 \quad \not{L}} \times \frac{1 \quad nmol}{32941 \quad ng} \times \frac{6.02 \times 10^{14} \quad molecules}{1 \quad nmol} \times \frac{1 \quad VLP}{1800 \quad molecules} \times 0.2$$

10. We recommend using the QiaAMP Viral RNA mini kit (Qiagen) following the manufacturer's protocol.
11. We recommend using SuperScript™ III First-Strand Synthesis SuperMix (Invitrogen).
12. Since sgRNAs are small and structured, they may not be efficiently reverse-transcribed with Random hexamers or Oligo(dT) (as they are not polyadenylated). For this reason, it is important to design a primer that binds specifically to your sgRNA scaffold sequence.
    For example, for SpCas9, the reverse primers can be complementary to the end of the sgrNA (5′-GTTTTAGAGCTAGAAATAGCAAGTTAAAATAAGGCTAGTCCGTTATCAACTTGAAAAAGTGGCACCGAGTCGGTGC-3′), while the Forward can be specific for the spacer of the sgRNA of interest.
13. If using VSVG as an envelope, the VLPs will have a broad tropism, allowing them to infect various types of cell lines and primary cells. Therefore, while this experiment uses HEK293T cells, other cell types can be used. However, the efficiency of infection may vary across cell lines.
14. If VLPs are packaging a reporter protein (e.g., EGFP, YFP), you may observe a diffused signal under the microscope. These are not cells, but mainly the packaged YFP present in VLPs, still outside of the cells, emitting the signal. Therefore, a sole visual evaluation may be deceiving; however, the accurate percentage of transduction efficiency can be obtained by FACS by gating in the GFP channel.

Acknowledgments

The publication is based upon work by COST Action CA21113: Genome Editing for the Treatment of Human Diseases (https://www.genehumdi.eu), supported by European Cooperation in Science and Technology (COST). This work was supported by the

Italian Ministry of Education, University and Research (MUR) under the FIS—Fondo Italiano per la Scienza program (Grant No. FIS2023-00171). This work was also supported by Fondazione Telethon, Italy (Grant No. GMR24T2036).

Conflict of Interest The authors declare no conflicts of interest.

References

1. Bachmann MF, van Damme P, Lienert F et al. (2025) Virus-like particles: a versatile and effective vaccine platform. Expert Rev Vaccines 24(1):444–456
2. Cavazza A, Molina-Estevez FJ, Plaza Reyes A et al. (2025) Advanced delivery systems for gene editing: a comprehensive review from the GenE-HumDi COST Action Working Group. Mol Ther Nucleic Acids 36(1):102457
3. Enoch YPark, Robert Minkner (2025) A systematic approach for scalable purification of virus-like particles. Protein Expr Purif ume 228(2025):106664. ISSN 1046-5928
4. Han J, Bai H, Li F et al. (2025) Engineering a streamlined virus-like particle for programmable tissue-specific gene delivery. Nat Commun 16: 9157
5. Stewart SA, Dykxhoorn DM, Palliser D et al (2003) Lentivirus-delivered stable gene silencing by RNAi in primary cells. RNA (4):493–501. https://doi.org/10.1261/rna.2192803
6. pBS-CMV-gagpol was a gift from Patrick Salmon (Addgene plasmid # 35614), https://www.addgene.org/35614/
7. Mangeot PE, Risson V, Fusil F et al. (2019) Genome editing in primary cells and in vivo using viral-derived Nanoblades loaded with Cas9-sgRNA ribonucleoproteins. Nat Commun 10(1):45
8. Sherer NM, Lehmann MJ, Jimenez-Soto LF et al (2003) Visualization of retroviral replication in living cells reveals budding into multivesicular bodies. Traffic 4(11):785–801
9. Ran FA, Hsu PD, Wright J et al. (2013) Genome engineering using the CRISPR-Cas9 system. Nat Protoc 8(11):2281–2308
10. Banskota S, Raguram A, Suh S et al. (2022) Engineered virus-like particles for efficient in vivo delivery of therapeutic proteins. Cell 185(2):250–265
11. Renner TM, Bélanger K, Lam C, Gerpe MCR, McBane JE, Langlois MA (2018) Full-Length Glycosylated Gag of Murine Leukemia Virus Can Associate with the Viral Envelope as a Type I Integral Membrane Protein. J Virol 92(6), e01530-17. https://doi.org/10.1128/JVI.01530-17

Open Access This chapter is licensed under the terms of the Creative Commons Attribution-NonCommercial-NoDerivatives 4.0 International License (http://creativecommons.org/licenses/by-nc-nd/4.0/), which permits any noncommercial use, sharing, distribution and reproduction in any medium or format, as long as you give appropriate credit to the original author(s) and the source, provide a link to the Creative Commons license and indicate if you modified the licensed material. You do not have permission under this license to share adapted material derived from this chapter or parts of it.

The images or other third party material in this chapter are included in the chapter's Creative Commons license, unless indicated otherwise in a credit line to the material. If material is not included in the chapter's Creative Commons license and your intended use is not permitted by statutory regulation or exceeds the permitted use, you will need to obtain permission directly from the copyright holder.



Part IV

Physical Delivery Methods



Chapter 17

Production and Purification of Cas9 Protein for Ribonucleoprotein Complex Formation

Mojca Skrbinek and Jure Bohinc

Abstract

Cas9–guide RNA ribonucleoprotein (RNP) complexes are widely used for genome editing because they provide rapid, transient nuclease activity without introducing exogenous DNA into target cells. Efficient RNP delivery requires a highly purified, correctly folded Cas9 protein that is free of contaminating nucleases and small-molecule impurities. This chapter describes the expression of N-terminally His-tagged Cas9 from a pET28b vector in *Escherichia coli* Rosetta strains, followed by purification using Ni-NTA immobilized metal affinity chromatography (IMAC) and size exclusion chromatography (SEC) on a Superdex 200 Increase column. The protocol covers bacterial fermentation, cell lysis, IMAC with high-salt and graded-imidazole washes, SEC polishing, dialysis into a storage buffer, and concentration to RNP-ready stocks, with quality control by SDS-PAGE and optional western blotting and BCA assay. Finally, a short procedure for assembling Cas9 RNPs with in vitro–transcribed guide RNAs is provided, making the protocol directly applicable to CRISPR RNP delivery in mammalian cells.

Keywords CRISPR-Cas9, Ribonucleoprotein complex, His-tag purification, Immobilized metal affinity chromatography, Size exclusion chromatography, Fast protein liquid chromatography, *Escherichia coli* expression, Genome editing

1 Introduction

CRISPR–Cas9 RNP delivery offers several advantages over plasmid or viral delivery, including transient nuclease exposure, reduced off-target activity, and the elimination of integration-associated genotoxicity [1–4]. These properties are particularly attractive in therapies such as CAR-T cell manufacturing [5] and in advanced genome editing systems like CCExo [6] or prime editors [7], where precise and controllable editing is required. In all these applications, the performance of RNPs depends strongly on the quality of the Cas9 protein preparation: contaminants from bacterial lysates, partially folded Cas9, or residual imidazole can reduce editing efficiency and compromise cell viability (*see* **Note 1**) [8].

Duško Lainšček et al. (eds.), *CRISPR Delivery*, Methods in Molecular Biology, vol. 3075,
https://doi.org/10.1007/978-1-0716-5547-4_17,
© The Author(s) 2027

His-tagged Cas9 and Cas9-based fusions can be efficiently produced in T7-based *E. coli* expression systems such as pET28b [9] in engineered strains like Rosetta-Gami or NiCo21. Rosetta-type strains provide tRNAs for rare eukaryotic codons and improve expression of large eukaryotic proteins [9, 10], while NiCo21-like strains reduce the co-purification of endogenous histidine-rich proteins during Ni-NTA chromatography (*see* **Note 2**) [11]. IMAC on Ni-NTA resin provides a rapid first purification step [12], exploiting the coordination between the polyhistidine tag and immobilized Ni^{2+} ions. High-salt and low-imidazole washes remove weakly bound contaminants, and Cas9 is subsequently eluted with high imidazole concentrations. A second purification step by SEC on a Superdex 200 Increase removes aggregates and degradation products and allows assessment of monodispersity from the elution profile [12, 13].

This protocol integrates experience from the purification of spCas9 and related proteins (nCas9, PE2, Cas9-N5) [6, 7] to provide a detailed, stepwise method that yields milligram quantities of monomeric His-tagged Cas9 suitable for RNP formation and delivery into mammalian cells [14, 15].

2 Materials

Prepare all solutions with Milli-Q (MQ) water and analytical-grade reagents. Store buffers at 4°C unless otherwise indicated. Follow institutional guidelines for handling recombinant DNA and *E. coli* cultures and dispose of chemical and biological waste according to local regulations (*see* **Notes 3 and 4**).

2.1 Reagents

1. *Escherichia coli* Rosetta-Gami BL21 (DE3) pLysS competent cells or similar Rosetta-type strain (providing tRNAs for rare codons) (*see* **Note 2**).
2. pET28b expression vector encoding N-terminally His-tagged Cas9 (Cas9-N5 in the original work; treated here as Cas9) under the control of the T7 promoter and lac operator, with kanamycin resistance (*see* **Notes 3–5**). Preferably, the His-tag should be on the C terminus, which would ensure that only full-length proteins are purified.
3. LB broth: LB powder 25 g/L in demineralized water, autoclaved for 20 min at 121°C, 1.2 bar.
4. LB agar plates with kanamycin (LBK): LB 25 g/L, agar 15 g/L, kanamycin monosulfate 100 μg/mL (Gold Biotechnology), poured into Petri dishes after autoclaving and cooling to ~55°C.
5. 50 mg/mL kanamycin monosulfate in MQ water, filter-sterilized through a 0.22 μm filter, stored at −20°C.

6. Lysis buffer: 50 mM Tris HCl, pH 8.0, 500 mM NaCl, 10 mM imidazole, add just before use: 1 mM $MgCl_2$, benzonase 2 μL/20 mL lysate, CPI His-tag 40 μL/20 mL lysate, lysozyme 1 mg/mL (*see* **Notes 6–8**).
7. IMAC wash buffer A (high salt): 50 mM Tris HCl pH 8.0, 2 M NaCl, 20 mM imidazole, 10% (v/v) glycerol.
8. IMAC wash buffer B (low salt): 50 mM Tris HCl pH 8.0, 500 mM NaCl, 20–50 mM imidazole, 10% (v/v) glycerol.
9. IMAC elution buffer: 50 mM Tris HCl pH 8.0, 500 mM NaCl, 250–300 mM imidazole, 10% (v/v) glycerol.
10. SEC buffer: 20 mM Tris HCl pH 7.5, 150 mM NaCl, 10% (v/v) glycerol.
11. PBS 10×: 1.7 M NaCl, 34 mM KCl, 100 mM NaH_2PO_4, dilute 1:10 with MQ water to obtain PBS 1× (pH 7.4).
12. SDS-PAGE running buffer: 25 mM Tris, 192 mM glycine, 0.1% (w/v) SDS.
13. 4× SDS loading buffer: 250 mM Tris/HCl pH 6.8, 8% (w/v) SDS, 40% (v/v) glycerol, 20% (v/v) β-mercaptoethanol, 0.04% (w/v) bromophenol blue.
14. Resolving gel solution (12%): see Table 1.
15. Stacking gel solution (4%): see Table 1.
16. Optional long-term storage buffer: 10 mM Tris HCl pH 8.0, 300 mM NaCl, 0.1 mM EDTA, 20% (v/v) glycerol (*see* **Note 9**).
17. RNP assembly buffer: 20 mM Tris HCl pH 7.5, 150 mM NaCl, 5 mM $MgCl_2$, 5% (v/v) glycerol.
18. 30% Acrylamide/bis-acrylamide solution (29:1).
19. 10% Ammonium persulfate (APS).
20. TEMED.

Table 1
Composition of 12% resolving and 4% stacking SDS-PAGE gels (two 1.5 mm gels)

Reagent	12% Resolving gel	4% Stacking gel
MQ water	7.6 mL	5.95 mL
1.5 M Tris HCl, pH 8.8	5.2 mL	–
0.5 M Tris HCl, pH 6.8	–	2.5 mL
30% acrylamide	6.8 mL	1.34 mL
10% APS	200 μL	100 μL
10% SDS	200 μL	100 μL
TEMED	20 μL	10 μL

21. 10% SDS.
22. InstantBlue Coomassie Protein Stain.
23. PageRuler Plus Pre-stained Protein Ladder.
24. Ni-NTA agarose resin for IMAC (e.g., Qiagen or equivalent).
25. SEC column (e.g., Superdex 200 Increase 10/300 GL(Cytiva)).
26. 0.22 μm Millex syringe filters.
27. Dialysis tubing (e.g., Spectrum™ Labs Spectra/Por™ 3 dialysis tubing, 3.5 kDa MWCO).
28. Amicon Ultra centrifugal concentrators, 30 kDa MWCO.

2.2 Equipment

1. Orbital shaker incubator with temperature control (e.g., 16–37°C).
2. Autoclave.
3. Refrigerated floor and bench centrifuges.
4. FPLC system (e.g., ÄKTA pure 25 FPLC system).
5. SDS-PAGE system (e.g., Mini-PROTEAN Tetra).
6. Imaging System (e.g., GelDoc Go).
7. Spectrophotometer (e.g., Nanodrop ND-1000).
8. Magnetic stirrer and stirring bars.
9. Pipettes and appropriate sterile tips.

3 Methods

Carry out all protein purification steps at 4°C or on ice unless otherwise stated. Perform bacterial work in a Class 1 biosafety cabinet or equivalent if available and observe standard microbiological practice (*see* **Notes 3 and 4**).

3.1 Transformation and Pre-Culture

1. Thaw 50 μL aliquots of Rosetta-Gami BL21 (DE3) pLysS competent cells on ice.
2. Add 1–5 μL (10–100 ng) pET-28b-Cas9 plasmid to the cells, gently flick to mix, and incubate on ice for 30 min (*see* **Note 5**).
3. Heat-shock cells at 42°C for 45–60 s and immediately return to ice for 2–5 min.
4. Add 450–500 μL of pre-warmed LB broth and incubate at 37°C with shaking at 400–500 rpm for 1 h.
5. Plate 50–200 μL of the transformation mixture onto LBK agar plates (100 μg/mL kanamycin) and incubate overnight at 37°C.

6. Pick a single colony into 100 mL LB broth with 50 μg/mL kanamycin in a 500 mL flask, and incubate overnight at 37°C, 180 rpm.

3.2 Fermentation and Protein Induction

1. Measure the OD_{600} of the overnight culture (dilute 10× in LB if necessary) using LB broth as a blank.
2. In a 5 L baffled flask, combine 1.5 L LB broth and kanamycin to 50 μg/mL.
3. Calculate the required inoculum volume to obtain an initial OD_{600} of 0.1 using $V_1 \cdot OD_1 = V_2 \cdot OD_2$ and add this volume of overnight culture to the 1.5 L medium (*see* **Note 7**).
4. Incubate at 37°C, 180 rpm, monitoring OD_{600} every 30–60 min until it reaches 0.5–0.6.
5. Induce Cas9 expression by adding IPTG to a final concentration of 0.2 mM and mix by gentle swirling.
6. Immediately reduce the incubation temperature to 18°C and continue shaking at 180 rpm overnight (*see* **Note 8**).
7. Harvest cells by centrifugation at 5500 rpm (~5000 × *g*) for 5–10 min at 4°C.
8. Discard the supernatant, resuspend pellets loosely with a spatula, and freeze at −80°C until protein purification (*see* **Note 10**).

3.3 Cell Lysis

1. Thaw frozen cell pellets from 1.5 L culture on ice.
2. Add 30 mL ice-cold lysis buffer per pellet and resuspend thoroughly by gentle mixing with a glass rod, followed by vortexing and pipetting (*see* **Note 6**).
3. Incubate on ice for 30 min to allow lysozyme digestion, mixing gently every 10 min.
4. Lyse cells by sonication on ice using 1 s on/2 s off cycles at 40% amplitude until a total of 2 min sonication time is reached (*see* **Note 11**).
5. Centrifuge lysates at 12,000 rpm for 30 min at 4°C to pellet cell debris.
6. Carefully transfer the supernatant (soluble fraction) to fresh pre-chilled tubes; keep on ice (*see* **Note 12**).

3.4 Purification of Cas9 by IMAC

1. Pack a gravity-flow column with 10–15 mL Ni-NTA resin, allowing storage ethanol to drain completely.
2. Wash the resin with ten column volumes (CV) of MQ water, then equilibrate with 5 CV lysis buffer.
3. Load the clarified lysate onto the column, collect the flow-through, and reload it again if maximal binding is desired (*see* **Note 13**).

4. Wash the column with ≥5 CV IMAC wash buffer A until the absorbance at 280 nm (A_{280}) and at 260 nm (A_{260}) of the flow-through are both <0.02 (*see* **Note 14**).
5. Wash with ≥5 CV of IMAC wash buffer B, again until A_{280} is <0.02, to remove more tightly bound contaminants.
6. Elute bound Cas9 with IMAC elution buffer, collecting 1 mL fractions.
7. Measure A_{280} of each fraction and pool those with the highest absorbance (typically fractions 2–6).
8. Analyze samples from lysate, flow-through, wash A, wash B, and selected elution fractions by SDS-PAGE (Sect. 3.5) to assess purity and recovery (Fig. 1) (*see* **Notes 9**, **13–15**).

3.5 SDS-PAGE

3.5.1 Gel Preparation

1. Assemble 1.5 mm gel cassettes in a casting stand.

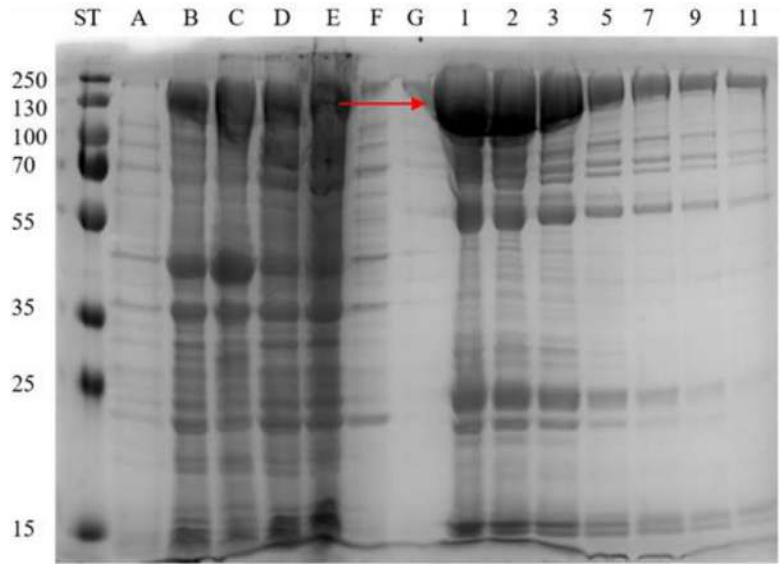


Fig. 1 SDS-PAGE analysis of Cas9-N5 purification by immobilized metal affinity chromatography (IMAC). Protein samples collected at each purification step were resolved on an 8% polyacrylamide gel under denaturing conditions and stained with Coomassie Brilliant Blue. *Lane ST*: PageRuler Plus prestained protein size standard with molecular weight markers indicated in kDa. Pre-purification samples: *lane A*: bacterial cell supernatant collected prior to IPTG induction; *lane B*: total cell lysate after induction and lysis; *lane C*: insoluble fraction after centrifugation; *lane D*: soluble fraction loaded onto the Ni-NTA column; *lane E*: column wash with buffer A; *lane F*: column wash with buffer B. Elution fractions: *lanes 1–11*, fractions collected from the Ni-NTA affinity column; Cas9-N5 (~163 kDa, arrow) is progressively enriched across fractions 2–6. IMAC immobilized metal affinity chromatography, IPTG isopropyl beta-D-1-thiogalactopyranoside, Ni-NTA nickel-nitrilotriacetic acid, SDS-PAGE sodium dodecyl sulfate polyacrylamide gel electrophoresis

2. Prepare a 12% resolving gel solution as in Table 1, mix gently, and immediately pour between plates to ~¾ of the cassette height.
3. Overlay with isopropanol to exclude oxygen and level the gel; allow it to polymerize for ~30 min at room temperature.
4. Remove isopropanol by pouring it out and blotting with filter paper.
5. Prepare a 4% stacking gel solution as in Table 1 and pour it on top of the resolving gel.
6. Insert combs carefully to avoid air bubbles and allow gels to polymerize for ~30 min.
7. Use gels immediately or store at 4°C wrapped in wet paper for up to several days.

3.5.2 Electrophoresis and Staining

1. Assemble the gel cassette into the electrophoresis tank and fill the inner and outer chambers with SDS-PAGE running buffer.
2. Mix 30 µL of each sample with 10 µL of 4× SDS loading buffer; heat at 95°C for 5 min, then cool on ice and briefly spin down.
3. Load 10 µL protein ladder and 20–40 µL of each sample into separate wells.
4. Run at 200 V until the bromophenol blue dye front reaches the bottom of the gel (~45 min).
5. Remove the gel and immerse in InstantBlue stain, gently agitating for 15 min at room temperature.
6. Decant the stain and wash the gel in MQ water for 5 min with gentle agitation.
7. Image the gel on a GelDoc system, confirming a major band at ~160 kDa corresponding to Cas9, with minimal additional bands after SEC (see Sect. 3.6).

3.6 Size Exclusion Chromatography (SEC)

1. Equilibrate the Superdex 200 Increase 10/300 GL column with ≥2 CV of SEC buffer on an ÄKTA pure 25 system, monitoring the baseline at 280 nm.
2. Filter pooled IMAC fractions through a 0.22 µm Millex filter.
3. Inject filtered Cas9 sample onto the column, and run at 0.5 mL/min in SEC buffer.
4. Collect 200 µL fractions across the elution profile, recording A_{280}.
5. Identify the main Cas9 peak (typically a well-defined symmetric peak corresponding to monomeric Cas9) and any earlier aggregate or later fragment peaks (Fig. 2) (*see* **Notes 16 and 17**).

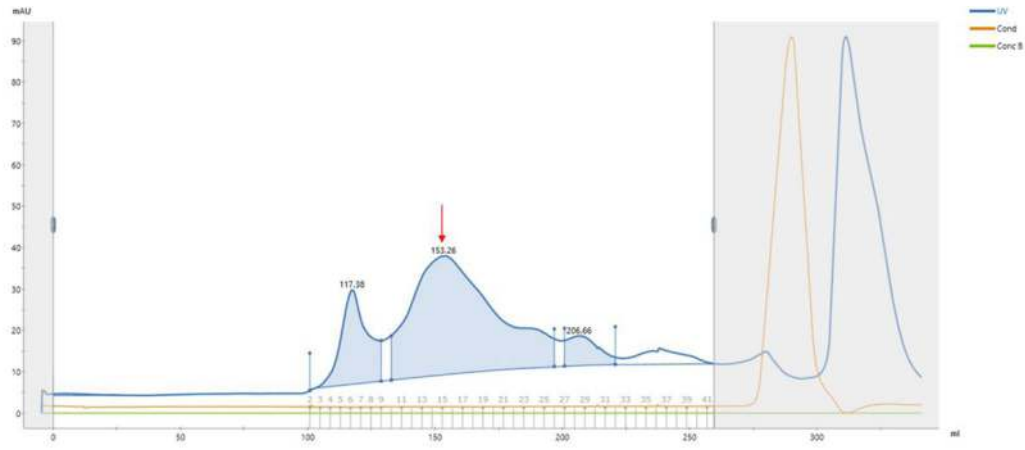


Fig. 2 SEC-MALS chromatogram of Cas9-N5 following IMAC purification, recorded on a Superdex 200 Increase 10/300 GL column using an ÄKTA pure 25 FPLC system. The *x*-axis shows elution volume (mL) with individual collected fractions indicated below; the *y*-axis shows UV absorbance at 280 nm (mAU). The main peak corresponding to monomeric Cas9-N5 is indicated by a red arrow. A minor shoulder at lower elution volume represents high-molecular-weight aggregates; minor peaks at higher elution volume correspond to degradation products or contaminants. FPLC fast protein liquid chromatography, mAU milli-absorbance units, SEC-MALS size-exclusion chromatography with multiangle light scattering

6. Analyze selected fractions across the main peak by SDS-PAGE as in Sect. 3.5 to determine which fractions contain the purest Cas9 (single strong band at ~160 kDa) (Fig. 3).
7. Pool the purest fractions for dialysis and concentration (Sect. 3.7).

3.7 Dialysis and Concentration

1. Pre-wet a piece of 3.5 kDa MWCO dialysis tubing in MQ water and then in 1× PBS.
2. Transfer the pooled SEC fractions to the tubing, remove air bubbles, and secure both ends with dialysis clips.
3. Place the tubing into 2 L of 1× PBS at 4°C with gentle stirring at ~150 rpm and dialyze overnight to remove imidazole and adjust buffer composition.
4. Optionally, replace the dialysis buffer with fresh PBS after 3–4 h to enhance imidazole removal (*see* **Note 9**).
5. Recover the dialyzed Cas9 and transfer it to a 30 kDa MWCO Amicon Ultra concentrator.
6. Centrifuge at 4°C according to the manufacturer's recommendations, periodically mixing and checking the volume.
7. Stop concentration when the volume has been reduced to ~1 mL or when A_{280} is approximately 1.0.

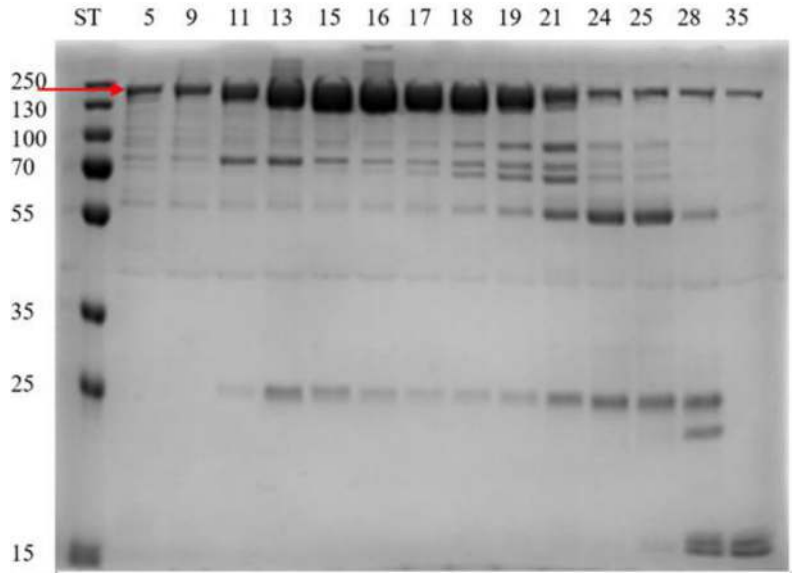


Fig. 3 SDS-PAGE analysis of fractions collected from SEC-MALS purification of Cas9-N5. Individual elution fractions from the FPLC column were resolved on an 8% SDS–polyacrylamide gel under denaturing conditions and stained with Coomassie Brilliant Blue. *Lane ST*: PageRuler Plus pre-stained protein size standard with molecular weight markers indicated in kDa; numbered lanes correspond to individual elution fractions. Band thickness is proportional to the amount of protein in each fraction. The highest concentration of Cas9-N5 (~163 kDa) was detected in fractions **13–19**, consistent with the main peak observed in the SEC-MALS chromatogram (Fig. 2). The location of Cas9-N5 on the gel is indicated by an arrow. Fractions 13–19 were pooled, dialyzed, and used for ribonucleoprotein (RNP) assembly. FPLC fast protein liquid chromatography, RNP ribonucleoprotein, SDS-PAGE sodium dodecyl sulfate polyacrylamide gel electrophoresis, SEC-MALS size-exclusion chromatography with multi-angle light scattering

8. Determine the final Cas9 concentration from A_{280} and the extinction coefficient, and verify by BCA assay if required (*see* **Note 15**).
9. Aliquot Cas9 into 50–100 µL portions, snap-freeze in liquid nitrogen, and store at −80°C. Avoid repeated freeze–thaw cycles.

3.8 Assembly of Cas9 RNPs

This protocol yields Cas9 suitable for forming RNP complexes with in vitro–transcribed gRNAs or synthetic sgRNAs [8, 14].

1. Thaw an aliquot of Cas9 on ice and dilute it in RNP assembly buffer to a working concentration (e.g., 10–20 µM).
2. Prepare gRNA at 20–40 µM in RNase-free water or RNP assembly buffer.

3. Mix Cas9 and gRNA at a molar ratio of 1:1 to 1:2 (Cas9:gRNA) [15], typically 2–5 µL Cas9 with appropriate gRNA volume and bring to the desired final volume with assembly buffer.
4. Incubate at room temperature for 10–15 min to allow RNP formation (*see* **Note 16**).
5. Keep RNPs on ice and use immediately for electroporation or lipid-based delivery into target cells. For electroporation of primary T cells, typical final Cas9 concentrations in the cuvette are in the low micromolar range but should be optimized per device and cell type. [14, 15]

4 Notes

1. Importance of protein quality for RNP editing. Contaminating bacterial proteins, nucleases, or residual imidazole can reduce editing efficiency and cell viability when Cas9 is delivered as RNPs, particularly to primary T cells and other sensitive cell types [8, 16]. SEC polishing and thorough buffer exchange are therefore strongly recommended.
2. Strain choice. Rosetta type strains provide rare codon tRNAs and improve the expression of large eukaryotic proteins such as Cas9 [9, 10]. NiCo21 strains further minimize the co-purification of endogenous His-rich proteins during Ni-NTA purification [11] and may yield cleaner IMAC eluates.
3. Acrylamide safety. Unpolymerized acrylamide is a neurotoxin. Handle powder and concentrated solutions in a fume hood, wear gloves and a mask, and dispose of acrylamide-containing waste as hazardous chemical waste.
4. Biological safety. The *E. coli* strains used are nonpathogenic laboratory strains and can be handled at Biosafety Level 1; nevertheless, follow institutional biosafety guidelines, wear appropriate PPE, and autoclave all cultures and solid waste before disposal.
5. Transformation efficiency. If few colonies appear after transformation, verify the quality and concentration of competent cells and plasmid DNA, and ensure that the antibiotic concentration on plates matches the plasmid resistance marker.
6. Lysis buffer composition. High salt (500 mM NaCl) improves solubility and reduces nonspecific interactions, while 10 mM imidazole reduces the binding of weakly interacting proteins to Ni-NTA. Adding benzonase, $MgCl_2$, and protease inhibitors immediately before use is crucial to limit DNA viscosity and proteolysis.

7. Inoculum calculation example. For an overnight culture at $OD_{600} = 3.0$ and a final volume of 1500 mL at $OD_{600} = 0.1$, the required inoculum is $(0.1 \times 1500\,\text{mL})/3.0 = 50\,\text{mL}$.
8. Induction temperature and time. Lower induction temperatures (25–30°C) lead to slower expression but yield more soluble protein and fewer inclusion bodies compared to 37°C. For more aggregation-prone constructs, overnight induction at 18–20°C may further improve solubility.
9. Buffer exchange and storage. Imidazole interferes with spectrophotometric assays and downstream biochemical experiments; thorough dialysis or diafiltration is essential. For long-term storage, a buffer containing 10%–20% glycerol and moderate salt (150–300 mM NaCl) helps preserve activity; inclusion of EDTA (0.1 mM) can improve stability by chelating trace metal ions, but should be avoided if metal-dependent downstream assays are planned.
10. Storage of cell pellets. Freezing cell pellets at −80°C for several days is compatible with high-quality protein purification and may even enhance lysis due to ice crystal formation. Avoid repeated freeze–thaw cycles.
11. Sonication and heat. Overheating during sonication can irreversibly denature Cas9 and activate proteases. Always keep tubes in an ice–water bath and use short pulses with pauses; if lysate warms, allow it to cool before continuing.
12. Solubility assessment. If most Cas9 is found in the pellet, consider lowering induction temperature, reducing IPTG concentration to 0.05–0.1 mM, shortening induction time, or switching to an alternative strain (e.g., NiCo21).
13. IMAC performance. If Cas9 appears in the flow-through, reduce the flow rate or reload the flow-through once more. If Cas9 elutes significantly during wash B, reduce the imidazole concentration in wash buffers and increase it in the elution buffer. High-salt wash A (up to 2 M NaCl) is useful when SDS-PAGE shows persistent contaminants that interact nonspecifically with the resin.
14. Absorbance at A_{260}. Because Cas9 is a positively charged protein, it binds nonspecifically to DNA present in the bacterial lysate. To remove this contaminating DNA during Ni-NTA purification, use a high-salt wash buffer. The effectiveness of DNA removal can be monitored by measuring the absorbance at 260 nm (A_{260}) of the Ni-NTA column flow-through. An elevated A_{260} in the flow-through of the first wash indicates that DNA is being successfully washed away from the bound protein.

15. Concentration determination and typical yields. A_{280}-based concentration estimates assume pure protein; residual contaminants or nucleic acids can bias results. Cross-checking with a BCA assay against BSA standards improves accuracy. For Cas9 variants expressed and purified by this protocol, typical yields after IMAC and SEC are 2–5 mg/L culture, with final concentrations of 1–5 mg/mL after concentration.
16. Interpreting SEC profiles and RNP assembly. A single symmetric main peak at the expected elution volume indicates monomeric Cas9; early peaks represent aggregates, while later peaks and smaller bands on SDS-PAGE represent degradation products or contaminants. RNP assembly usually proceeds efficiently at Cas9:gRNA molar ratios between 1:1 and 1:2 [15]; higher RNA excess can become cytotoxic in some cell types, as observed for epegRNA in HEK293 cells [7].
17. Adaptation to Cas9 fusions. The same expression and purification strategy has been successfully applied to Cas9 fusions with MMLVRT [7] and Cas9 linked to exonuclease III via coiled coils [6], with minor adjustments to buffer composition (e.g., addition of Triton X-100) and induction conditions. Users can adapt this protocol to related constructs by titrating salt, imidazole, and detergent concentrations based on SDS-PAGE and SEC results.

Acknowledgments

The publication is based upon work by COST Action CA21113: Genome Editing for the Treatment of Human Diseases (https://www.genehumdi.eu), supported by European Cooperation in Science and Technology (COST).

Conflict of Interest The authors have no conflicts of interest to declare that are relevant to the content of this chapter.

References

1. Kim S, Kim D, Cho SW et al (2014) Highly efficient RNA-guided genome editing in human cells via delivery of purified Cas9 ribonucleoproteins. Genome Res 24:1012–1019
2. DeWitt MA, Corn JE, Carroll D (2017) Genome editing via delivery of Cas9 ribonucleoprotein. Methods 121–122:9–15
3. Shen J, Zhang S, Li Y et al (2021) Strategies in the delivery of Cas9 ribonucleoprotein for CRISPR/Cas9 genome editing. Theranostics 11:614–648
4. Jinek M, Chylinski K, Fonfara I et al (2012) A programmable dual-RNA-guided DNA endonuclease in adaptive bacterial immunity. Science 337:816–821
5. Foy SP, Jacoby K, Bota DA et al (2023) Non-viral precision T cell receptor replacement for personalized cell therapy. Nature 615:687–696

6. Lainšček D, Forstnerič V, Mikolič V et al (2022) Coiled-coil heterodimer-based recruitment of an exonuclease to CRISPR/Cas for enhanced gene editing. Nat Commun 13: 3604
7. Anzalone AV, Randolph PB, Davis JR et al (2019) Search-and-replace genome editing without double-strand breaks or donor DNA. Nature 576:149–157
8. Lin S, Nguyen VQ, Lin S (2022) Preparation of Cas9 ribonucleoproteins for genome editing. Bio-protocol 12:e4420
9. Carmignotto GP, Azzoni AR (2019) On the expression of recombinant Cas9 protein in *E. coli* BL21(DE3) and BL21(DE3) Rosetta strains. J Biotechnol 306:62–70
10. Maxenberger DA, Padmaswari MH, Stokes AL et al (2024) Optimizing recombinant Cas9 expression: insights from *E. coli* BL21(DE3) strains for enhanced protein purification and genome editing. Biomedicines 12:1226
11. Robichon C, Luo J, Causey TB et al (2011) Engineering *Escherichia coli* BL21(DE3) derivative strains to minimize *E. coli* protein contamination after purification by immobilized metal affinity chromatography. Appl Environ Microbiol 77:4634–4646
12. Rajagopalan N, Song H, Kagale S et al (2018) A two-step method for obtaining highly pure Cas9 nuclease for genome editing, biophysical, and structural studies. Methods Protoc 1:17
13. Flottmann F, Pohl G, Brodehl A et al (2022) A detailed protocol for expression, purification, and activity determination of recombinant SaCas9. STAR Protoc 3:101276
14. Schumann K, Lin S, Boyer E et al (2015) Generation of knock-in primary human T cells using Cas9 ribonucleoproteins. Proc Natl Acad Sci USA 112:10437–10442
15. Seki A, Rutz S (2018) Optimized RNP transfection for highly efficient CRISPR/Cas9-mediated gene knockout in primary T cells. J Exp Med 215:985–997
16. Bloomer H, Khirallah J, Li Y et al (2022) CRISPR/Cas9 ribonucleoprotein-mediated genome and epigenome editing in mammalian cells. Adv Drug Deliv Rev 181:114087

Open Access This chapter is licensed under the terms of the Creative Commons Attribution-NonCommercial-NoDerivatives 4.0 International License (http://creativecommons.org/licenses/by-nc-nd/4.0/), which permits any noncommercial use, sharing, distribution and reproduction in any medium or format, as long as you give appropriate credit to the original author(s) and the source, provide a link to the Creative Commons license and indicate if you modified the licensed material. You do not have permission under this license to share adapted material derived from this chapter or parts of it.

The images or other third party material in this chapter are included in the chapter's Creative Commons license, unless indicated otherwise in a credit line to the material. If material is not included in the chapter's Creative Commons license and your intended use is not permitted by statutory regulation or exceeds the permitted use, you will need to obtain permission directly from the copyright holder.





Chapter 18

Electroporation for High-Efficiency Delivery of CRISPR to Hematopoietic Cells

Nikoletta Y. Papaioannou, Panayiota L. Papasavva, Petros Patsali and Carsten W. Lederer

Abstract

Recent advances in genome editing technologies have enabled transformative therapeutic strategies for hematological disorders. Efficient implementation of these approaches requires reliable delivery of genome editing components into primary hematopoietic stem and progenitor cells (HSPCs), which are particularly sensitive and resistant to conventional transfection methods. Electroporation has emerged as the most widely used strategy for ex vivo delivery of genome editing reagents into $CD34^+$ hematopoietic cells. Genome editing tools can be delivered in multiple formats, including plasmid DNA, messenger RNA (mRNA), and ribonucleoprotein (RNP) complexes. In HSPCs, mRNA- and RNP-based approaches are generally better tolerated than plasmid DNA and allow transient expression with reduced cytotoxicity. In this chapter, we describe optimized protocols for electroporation-based delivery of CRISPR/Cas9 RNP complexes and mRNA-encoded base editors into HSPCs using the Amaxa™ 4D-Nucleofector™ system. Detailed procedures are provided for cell preparation, guide RNA design, assembly of Cas9 RNPs, in vitro transcription and purification of base editor mRNA, electroporation parameters, and assessment of editing efficiency. Emphasis is placed on maximizing editing performance while preserving stem cell viability and functionality.

Keywords Electroporation, Nucleofection, HSPCs, HUDEP-2, CRISPR/Cas9, Base editor, In vitro transcription, Delivery, Genome editing, Editing efficiency

1 Introduction

Recent advances in genome editing (GE) technologies have enabled the development of transformative therapeutic strategies for genetic diseases, including hemoglobinopathies. These advances culminated in 2023 with the first marketing authorizations by the U.S. Food and Drug Administration and the European Medicines Agency for a GE-based therapy, CASGEVY™, for the treatment of sickle cell disease and β-thalassemia [1]. Beyond therapeutic applications, GE tools have also facilitated mechanistic studies and the identification of novel biological pathways, significantly advancing our understanding

Duško Lainšček et al. (eds.), *CRISPR Delivery*, Methods in Molecular Biology, vol. 3075,
https://doi.org/10.1007/978-1-0716-5547-4_18,
© The Author(s) 2027

of disease pathophysiology and supporting improved prognosis, as well as the development of new therapeutic interventions [2, 3].

GE technologies can broadly be classified into double-strand break (DSB)-dependent and DSB-independent platforms. DSB-dependent systems, including zinc finger nucleases (ZFNs) [4], transcription activator-like effector nucleases (TALENs) [5], and CRISPR/Cas9 [6], introduce targeted DNA breaks that are predominantly repaired through nonhomologous end joining (NHEJ) or in the presence of a donor template, by homology-directed repair (HDR) [7]. In contrast, DSB-independent precision-editing platforms include base editors (BEs) and prime editors (PEs). BEs enable precise base conversions (A-to-G or C-to-T) [8,9], while PEs use a reverse transcriptase to install defined edits directly at the target locus [10].

Successful implementation of these GE approaches depends on the efficient intracellular delivery of editing components into relevant cellular systems. In the context of hematological disorders, $CD34^+$ hematopoietic stem and progenitor cells (HSPCs) and human umbilical cord-derived erythroid progenitor cells (HUDEP-2) represent widely used experimental and therapeutic targets [11]. Efficient and reproducible delivery of GE tools into these cells is thus critical for evaluating candidate therapeutic editors, preclinical laboratory workflows, and ex vivo gene therapy applications [12–14].

Despite the availability of multiple delivery formats, primary human HSPCs remain particularly challenging to manipulate. These cells are predominantly quiescent and enriched in the G0/G1 phase of the cell cycle, which poses challenges for HDR-based precision editing, but are also sensitive to chemical and mechanical stress [15,16]. This sensitivity reduces the efficiency of common chemical transfection methods, harsh mechanical methods, and the use of plasmid-encoded editors [17,18]. Though efficiency concerns for HSPCs can be addressed by viral vectors, these carry physical delivery strategies for efficient ex vivo application of GE-based therapies.

Electroporation has been shown to significantly enhance the uptake of nucleic acids into cells [18,19]. Electroporation is based on the transient permeabilization of the plasma membrane upon exposure to pulsed electric fields, leading to a temporary loss of selective membrane barrier function. This process enables the intracellular entry of exogenous molecules, including DNA, RNA, proteins, and other small compounds [20]. Although early observations of electric field effects on biological tissues date back to the 18th century [21], the application of electroporation for cellular transfection was only established in the early 1980s [22,23].

Today, electroporation is one of the most widely used ex vivo delivery methods for GE reagents for hematopoietic stem cells, suitable for plasmid DNA, messenger RNA (mRNA), recombinant proteins, and pre-assembled ribonucleoprotein (RNP) complexes [24].

The choice of delivery format is particularly critical in sensitive primary HSPCs. Plasmid DNA is accessible and affordable, but in HSPCs, it frequently results in suboptimal editing efficiencies as it requires nuclear entry and transcription prior to editing, and as its prolonged intracellular persistence can contribute to cellular toxicity and reduced viability. Furthermore, plasmid-based delivery carries a risk of unintended genomic integration, which is particularly undesirable in therapeutic applications [25,26].

In contrast, delivery of recombinant nucleases as purified proteins or as Cas9-gRNA RNP complexes enables immediate editing activity upon entry into the cell and, by avoiding DNA components, avoids the risk of genomic integration altogether. Moreover, because the nuclease is degraded relatively rapidly, genome exposure to editing components is highly transient, which favors on-target editing activity at off-target sites, which are generally less efficiently edited [27]. On the downside, protein- or RNP-based strategies rely on preparative-scale purification of recombinant proteins. For most GE laboratories this entails the costly purchase of commercial protein products and limits their use to well-established enzyme components that are commercially available [28].

For many GE laboratories, in-house synthesis of custom mRNAs and RNA-based delivery of editing components can draw on standard know-how and equipment and thus represents a practicable, affordable, and versatile alternative. Following cytoplasmic entry, mRNA is rapidly translated without requiring nuclear transcription, allowing timely production of the editing enzyme while maintaining transient expression kinetics [29]. Compared with plasmid DNA, mRNA typically induces lower toxicity and avoids risks associated with genomic integration. In addition, this approach eliminates reliance on recombinant protein production, whether performed in-house or commercially, thereby reducing costs, increasing flexibility in experimental design, and enabling versatility in the use of niche or novel genome editors [30].

Various electroporation-based platforms are commercially available. In this chapter, we focus on the Lonza 4D-Nucleofector™ system (based on legacy Amaxa™ technology), an electroporation-based nucleofection platform that enables efficient cytoplasmic and nuclear delivery of GE components into human $CD34^+$ hematopoietic cells and supports 384-well to GMP-compliant large-volume formats [31]. Particular emphasis is placed on two delivery strategies widely used in hematopoietic GE: (i) RNP-based delivery of CRISPR/Cas9 nucleases and (ii) mRNA-based delivery of BE systems. For BE applications, we provide a detailed protocol for in vitro transcription (IVT) of editor-encoding mRNA, including preparation, purification, and quality assessment prior to electroporation.

This chapter therefore outlines optimized procedures for hematopoietic cell culture (thawing, expansion, and freezing), guide

RNA (gRNA) design, in vitro transcription of BE mRNA, preparation of Cas9 RNP complexes, electroporation parameters using the 4D-Nucleofector™ X Unit, and downstream assessment of editing efficiency (DNA extraction, PCR amplification, Sanger sequencing and editing assessment using dedicated software) (Fig. 1). The concluding panel Fig. 1F additionally provides an overview of the wide variety of common downstream procedures for which the cell material produced by the current protocol is suitable. These procedures are numerous and diverse and are therefore not detailed here. However, in addition to illustrating the utility of the current protocol, Fig. 1F provides context to prompt consideration of any downstream steps in the execution of the current protocol, so that, e.g., for bulk analyses, the required cell numbers and corresponding expansion times are considered, and for clonal analyses, timely initiation of isolation procedures shortly after GE can be accommodated. Collectively, the current protocol, with its detailed procedures, provides a robust and reproducible framework for efficient GE in hematopoietic cells, such as HSPCs and hematopoietic cell lines, with versatile downstream applications and an emphasis on balancing editing performance with the preservation of stem cell viability and functional integrity.

2 Materials

2.1 Cell Culturing and Counting

2.1.1 Reagents

Prepare all media using sterile technique under a biological safety cabinet. Prewarm all culture media to 37°C before use, unless otherwise stated. Stock validated 6-well culture plates, 15-mL conical tubes, and cryovials.

1. $CD34^+$ thawing medium: 94.4% Iscove's Modified Dulbecco's Medium (IMDM), 5.6% fetal bovine serum (FBS) Performance.
2. HUDEP-2 thawing medium: 94.4% IMDM, 5.6% FBS Secure.
3. $CD34^+$ expansion medium: StemSpan™ SFEM II, 1% StemSpan CC100, 2 IU/mL erythropoietin (EPO), 10^{-6} M dexamethasone, 1× penicillin/streptomycin (P/S).
4. HUDEP-2 expansion medium: StemSpan™ SFEM II, 100 ng/mL stem cell factor, 3 IU/mL EPO, 10^{-6} M dexamethasone, 2× P/S, 5 μg/mL doxycycline.
5. $CD34^+$ freezing medium: 40% IMDM, 50% FBS Performance, 10% dimethyl sulfoxide (DMSO).
6. HUDEP-2 freezing medium: 60% StemSpan™ SFEM II, 30% FBS Secure, 10% DMSO.
7. 0.4% trypan blue in phosphate-buffered saline.

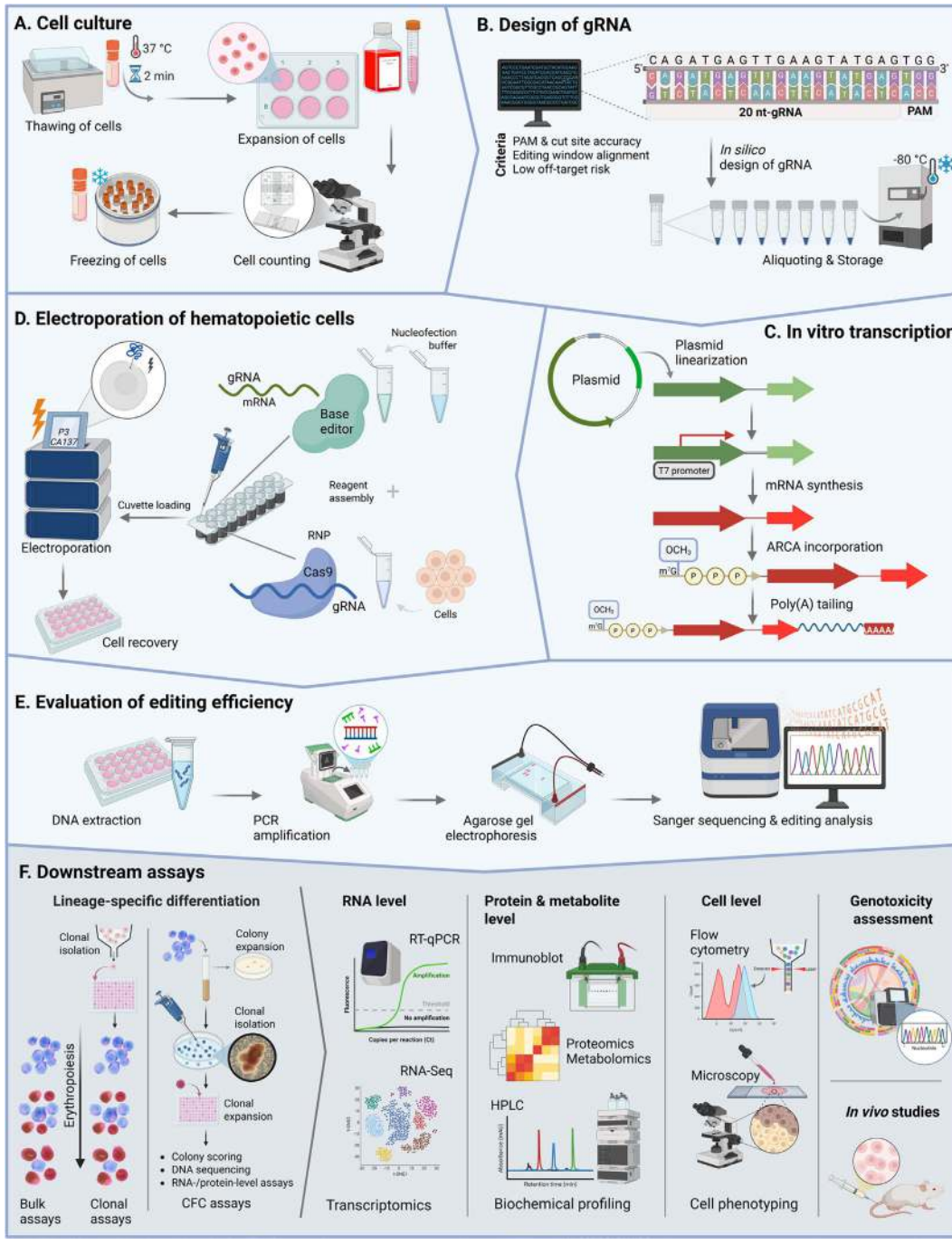


Fig. 1 Workflow for genome editing in hematopoietic cells using electroporation. Schematic overview of the optimized experimental pipeline described in this chapter, including potential downstream assays. **A** Hematopoietic cell handling, including thawing, expansion, cell counting, and cryopreservation. **B** In silico design of guide RNAs (gRNAs), illustrating identification of the 20-nt protospacer sequence adjacent to a PAM site, definition of the Cas9 cleavage position and/or base editing window, and application of key selection criteria (PAM positioning, editing window alignment, and off-target assessment), followed by aliquoting and storage.

2.1.2 Equipment

1. Class-II biological safety cabinet.
2. Humidified CO_2 incubator (37°C, 100% relative humidity, 5% CO_2).
3. Centrifuges and rotors compatible with 1.5-mL nuclease-free microcentrifuge tubes.
4. 15-mL conical tubes.
5. Controlled-rate freezing container.
6. Hemocytometer.
7. Light microscope.

2.2 Design of gRNA

2.2.1 Reagents

1. Synthetic gRNA: Chemically synthesized single gRNA.
2. Genomic DNA sequence: FASTA-format genomic DNA sequence of the gene of interest downloaded from a curated genomic database.

2.2.2 Equipment

1. Sequence visualization software: DNA visualization software capable of annotating exons, strand orientation, and nucleotide positions.
2. CRISPR design software: Web-based CRISPR gRNA design tool supporting off-target prediction and on-target scoring.

2.3 In Vitro Transcription

2.3.1 Reagents

Prepare all solutions using nuclease-free water. Perform all RNA-related procedures using RNase-free consumables and a dedicated clean workspace. Keep enzymes on ice at all times.

a) **DNA Template Preparation**

Fig. 1 (Continued) **C** In vitro transcription workflow for base editor (BE) mRNA production, including plasmid linearization, T7-driven transcription, ARCA cap incorporation, and poly(A) tailing to generate capped and polyadenylated mRNA. **D** Electroporation of $CD34^+$ hematopoietic stem and progenitor cells (HSPCs) or HUDEP-2 cells using the Lonza 4D-Nucleofector™ system (P3 buffer, program CA-137), including reagent assembly (mRNA:gRNA or Cas9 RNP complexes), cuvette loading, delivery (electroporation), and immediate cell recovery. **E** Evaluation of editing efficiency through genomic DNA extraction, PCR amplification of the target locus, agarose gel electrophoresis, Sanger sequencing, and downstream editing analysis using specialized software tools. **F** Downstream assays. Cell material generated using the current protocol is suitable for a wide variety of downstream assays, including bulk expansion, clonal isolation, and/or colony-forming cell (CFC) assays, before lineage-specific differentiation and functional and safety characterization. Corresponding analyses include RNA-, protein-, metabolite-, and cell-level assessments, as well as genotoxicity evaluation and in vivo engraftment studies of edited cells. RT-qPCR reverse-transcription quantitative PCR, HPLC high-performance liquid chromatography

1. Plasmid DNA: BE expression plasmid containing T7 promoter upstream of coding sequence.
2. Restriction digest reaction: Plasmid DNA (3 μg per reaction), 10× restriction enzyme buffer, 10 U/μL restriction enzyme cutting downstream of the open reading frame, nuclease-free water.
3. 0.8% m/v Agarose gel: 0.8 g agarose dissolved in 100 mL 1×TBE buffer, and adding an intercalating nucleic acid dye suitable for UV visualization, 6×loading dye, and DNA ladder (1 kb molecular weight marker).
   10×TBE buffer: 540 g Tris, 275 g boric acid, and 200 mL 0.5 M EDTA, pH 8.3.
4. DNA purification kit.

b) **In Vitro Transcription (IVT) and RNA Processing**

5. IVT reaction mix (30 μL total volume): ARCA/NTP mix (containing 1 mM GTP, 4 mM anti-reverse cap analog (ARCA), 1.25 mM CTP, 1.25 mM UTP, >1.25 mM ATP final concentrations, as specified by the manufacturer), 1.5 μg linearized DNA template, T7 RNA polymerase, nuclease-free water.
6. Deoxyribonuclease (DNase) I treatment: RNase-free DNase I enzyme.
7. Poly(A) tailing reaction (50 μL total volume): DNase-treated RNA, 10×poly(A) polymerase reaction buffer, poly(A) polymerase, nuclease-free water.
8. Lithium chloride precipitation: Lithium chloride (LiCl) solution.
9. 70% ethanol: 70% ethanol, 30% nuclease-free water by volume.

2.3.2 Equipment

1. Thermal block, incubator or thermal cycler (37°C).
2. Refrigerated microcentrifuge.
3. Gel electrophoresis apparatus.
4. UV or blue-light gel documentation system.
5. RNase-free microcentrifuge tubes.
6. Nanodrop spectrophotometer.
7. −80°C freezer.

2.4 Electroporation of Hematopoietic Cells

2.4.1 Reagents

Prepare all solutions under sterile conditions. Warm culture media to 37°C prior to use. Keep RNA- and protein-based reagents on ice throughout preparation.

a) **Cells**

1. Cell culture: CD34⁺ HSPCs and HUDEP-2 cells maintained in expansion medium (*see* Sect. 2.1).

b) **Genome Editing Components**

2. For mRNA-based base editing: In vitro transcribed base editor mRNA, synthetic gRNA.
3. For RNP-based CRISPR/Cas9 editing: Recombinant Cas9 protein, synthetic gRNA.
   All RNA components must be nuclease-free and stored at −80°C. For best results, it is recommended to store single-use gRNA aliquots in line with volume requirements for planned experimentation.
4. Nucleofector consumables: 16-well Nucleocuvette™ Strips, P3 Primary Cell Nucleofector™ Solution, P3 Supplement.
5. General plasticware: 1.5-mL nuclease-free microcentrifuge tubes, 15-mL conical tubes, 24-well tissue culture plates, sterile filtered pipette tips.

2.4.2 Equipment

1. Nucleofection system: 4D-Nucleofector™ instrument, including Core Unit and X Unit for nonadherent or detached adherent cells.

2.5 Evaluation of Genome Editing Efficiency

2.5.1 Reagents

Prepare all DNA solutions using nuclease-free water. Use aerosol-resistant tips to avoid cross-contamination.

a) **DNA Template Preparation**

1. DNA purification kit.

b) **PCR Amplification**

1. PCR reaction buffer (1× final): Tris-HCl, KCl, $MgCl_2$-containing high-fidelity polymerase buffer.
2. dNTP mix: 10 mM each deoxynucleotide triphosphate.
3. Forward and reverse primers: 0.5 μM final concentration each.
4. High-fidelity DNA polymerase: Proofreading enzyme suitable for amplicons used for Sanger sequencing.
5. 1% Agarose gel: 1 g agarose dissolved in 100 mL 1× TBE buffer, and adding an intercalating nucleic acid dye suitable for UV visualization, 6× loading dye, and DNA ladder (100 bp molecular weight marker). For TBE composition, *see* Sect. 2.3.

c) **Sanger Sequencing**

1. Cycle sequencing reaction mix: Dye-terminator sequencing mix, 5 × sequencing buffer, sequencing primer.
2. Purification system: Gel filtration spin columns or equivalent dye-terminator removal system.

2.5.2 Equipment

1. Thermal cycler.
2. Sanger sequencing equipment.

3 Methods

3.1 Culture of Hematopoietic Cells

Both HUDEP-2 and $CD34^+$ are suspension cells with different medium requirements but similar handling. In the following subsections, the thawing, culturing, freezing, and counting of cells will be explained. Materials "Sect. 2.1" indicate the medium composition for each cell type.

3.1.1 Thawing of Hematopoietic Cells

1. Pre-warm reagents (thawing medium, expansion medium) to 37°C in a water bath.
2. Transfer 9 mL thawing medium (*see* Sect. 2.1) into a 15-mL conical tube.
3. Remove the cryovial from liquid nitrogen and immediately place it in a 37°C water bath by gently swirling it until it is thawed (approximately 1–2 min).
4. Immediately disinfect the outside of the vial with 70% ethanol or an equivalent laboratory disinfectant.
5. Transfer the thawed cell suspension (~1 mL, cells in freezing medium) dropwise into the thawing medium.
6. Centrifuge at 300 × *g* for 5 min at room temperature (RT).
7. Carefully aspirate the supernatant without disturbing the pellet.
8. Resuspend the cell pellet in expansion medium at approximately 1 mL per 0.5×10^6 cells.
9. Transfer cells to a six-well plate and adjust the final volume based on the total cell number.
10. Incubate at 37°C, 5% CO_2.

3.1.2 Expansion of Hematopoietic Cells

1. Maintain cells in their respective expansion medium (*see* **Note 1**).
2. Keep cell density between $0.5–1 \times 10^6$ cells/mL (*see* **Note 2**).
3. For HUDEP-2 cells, add doxycycline to a final concentration of 5 μg/mL every 48 h (*see* **Note 3**).

4. For HUDEP-2 cells, perform a complete medium change at least once per week (*see* **Note 4**):
   a) Collect cells.
   b) Centrifuge at 300 × *g* for 5 min.
   c) Aspirate supernatant.
   d) Resuspend in fresh expansion medium.
5. $CD34^+$ cells should not be maintained in expansion medium for prolonged periods (*see* **Note 5**).

3.1.3 Freezing of Hematopoietic Cells

1. Prepare freezing medium fresh (*see* Sect. 2.1) (*see* **Note 6**).
2. Collect cells into a 15-mL tube.
3. Count cells using the trypan blue exclusion assay.
4. Adjust cell concentration to $0.5–1 \times 10^6$ cells per mL freezing medium.
5. Centrifuge at 300 × *g* for 5 min.
6. Aspirate supernatant completely.
7. Gently resuspend pellet in required mL freezing medium for the total number of vials (1 mL medium/vial).
8. Aliquot 1 mL per cryovial.
9. Place vials in a controlled-rate freezing container at RT.
10. Transfer container to −80°C overnight (o/n).
11. Move vials to liquid nitrogen for long-term storage.

3.1.4 Cell counting by the Trypan Blue Exclusion Assay

The number of live cells/mL of expansion medium is determined using the trypan blue exclusion assay.

1. Collect 10 µL of cells and add 10 µL of 0.4% trypan blue stain for a 1:1 dilution.
2. Mix well and transfer 10 µL to the Bright-Line Hemocytometer.
3. Visualize the hemocytometer with cells under a microscope with 10 × magnification.
4. For viable cells, count the number of unstained cells in the four large corner squares.
5. For dead cells, count the number of blue-stained cells in the four large corner squares.
6. Use the following equation to determine the corresponding number of cells per mL of medium.

$$\begin{aligned} cells/mL = {} & cell\#(from\,4\,squares) \\ & \times 2.5(to\ upscale\ cell\#from\,4\,to\,10 \\ & squares) \times 2(dilution\ factor) \\ & \times 1000(chamber\ volume) \end{aligned}$$

3.2 Design of gRNAs

1. Go to a curated genomic database, search for the gene you intend to target, and download its GenBank gene sequence.
2. Open the downloaded GenBank sequence in a sequence visualization software.
3. Locate the exact nucleotide position you intend to modify and confirm the strand orientation.

3.2.1 Manual gRNA Design

1. Scan the target region for a suitable PAM sequence (e.g., NGG for SpCas9).
2. Once a PAM sequence is identified (for a type-II enzyme, such as SpCas9), select the 20 nucleotides immediately upstream (5′ direction) of the PAM. This 20-nt sequence constitutes the gRNA protospacer.

3.2.2 Software-Assisted gRNA Design

1. Copy approximately 150–200 bp of genomic sequence surrounding the target site.
2. Open a CRISPR guide design platform of your interest (e.g., CRISPOR [https://crispor.gi.ucsc.edu/] CHOPCHOP [https://chopchop.cbu.uib.no/]).
3. Paste the copied sequence into the input field and select the appropriate reference genome (e.g., hg38 for human).
4. Submit the sequence to generate all possible gRNAs within the selected region.

3.2.3 General gRNA Selection Criteria

1. For CRISPR/Cas9 nuclease applications, ensure that the designed gRNA positions the predicted DNA cleavage correctly (*see* **Note 7**).
2. For base editing applications, design the gRNA to locate the intended nucleotide conversion within the editing window of the selected BE (*see* **Note 8**).
3. Evaluate the presence of additional editable nucleotides within the editing window and assess the likelihood of bystander editing events (*see* **Note 9**).
4. Define the experimental objective prior to selecting the final guide (*see* **Note 10**).
5. Select gRNAs with minimal predicted off-target sites (*see* **Note 11**).

6. Design at least two to three independent gRNAs per target locus whenever possible (*see* **Note 12**).
7. Order the selected synthetic gRNA from a commercial supplier. Upon resuspension, aliquot into single-use volumes and store at −80°C until use (*see* **Note 13**).

3.3 In Vitro Transcription of Base Editor mRNA

The IVT protocol described below was performed using a T7-based commercial mRNA synthesis kit with slight modifications [NEB; HiScribe® T7 ARCA mRNA Kit (with tailing)]; however, the procedure is compatible with any equivalent system that supports linearized template transcription, 5′ capping, DNase treatment, poly(A) tailing, and purification of the resulting mRNA.

3.3.1 Base Editor DNA Template Preparation

1. Digest 3 μg of plasmid DNA containing the BE coding sequence with a restriction enzyme that cuts downstream of the open reading frame (*see* **Note 14**) in a 50-μL reaction containing:
   a) 10× restriction enzyme buffer.
   b) 10 U/μL restriction enzyme.
   c) Nuclease-free water to the final volume.
2. Perform three parallel reactions to obtain approximately 9–10 μg total linearized template.
3. Incubate at 37°C for 3–4 h up to overnight (o/n).
4. Verify complete linearization (*see* **Note 15**) by loading 2 μL of each digestion reaction on a 0.8% agarose gel in 1× TBE buffer. A single linear band should be observed.
5. Purify the linearized DNA using a silica membrane–based spin column purification system according to the manufacturer's instructions (*see* **Note 16**).
   a) Mix the digestion reaction with chaotropic binding buffer (typically five volumes of binding buffer per one volume of reaction).
   b) Apply to a silica column and centrifuge at 17,900 × *g* for 1 min.
   c) Wash the column with ethanol-containing wash buffer and centrifuge at 17,900 × *g* for 1 min.
   d) Elute in nuclease-free water.
6. Measure DNA concentration and purity using a Nanodrop spectrophotometer (*see* **Note 17**).
7. The purified, linearized DNA is then used as a template for IVT (*see* **Note 18**).

3.3.2 Standard mRNA synthesis, DNase Treatment, Poly(A) Tailing, Purification, and Evaluation of mRNA

1. Assemble the reaction mix at RT and add each component in the following order to have a 30 μL total volume:
   a) Nuclease-free water.
   b) 3 μL of 2 × ARCA/NTP mix.
   c) 1.5 μg template DNA.
   d) 3 μL T7 RNA polymerase mix.
2. Incubate the reaction at 37°C for 45 min (*see* **Note 19**).
3. Add to the reaction 3 μL DNase I (1/10 of the initial reaction volume) and incubate at 37°C for 35 min (*see* **Note 20**).
4. Set up the poly(A) tailing reaction mix at RT in 50 μL reaction mix by adding the reagents in the following order:
   a) 7 μL nuclease-free water.
   b) 33 μL of the DNase-treated capped RNA.
   c) 5 μL of 10 × Poly(A) Polymerase reaction buffer.
   d) 5 μL Poly(A) polymerase.
5. Incubate the reaction at 37°C for 30 min (*see* **Note 21**).
6. Continue to mRNA purification by adding 25 μL LiCl to the 50 μL reaction and incubate at −20°C for 1 h.
7. After incubation, centrifuge the reaction mix at 4°C for 15 min at maximum speed.
8. Discard the supernatant and add ice-cold 70% ethanol to the pellet.
9. Centrifuge at 4°C for 10 min at maximum speed.
10. Discard the ethanol and air-dry the pellet (*see* **Note 22**).
11. Add 30 μL nuclease-free water to the pellet.
12. Heat the final mRNA at 65°C for 5 min.
13. Evaluate the mRNA concentration using the Nanodrop spectrophotometer. It is also recommended to assess RNA integrity (*see* **Note 23**).
14. Store the final product at −80°C (*see* **Note 24**).

3.4 Electroporation of Hematopoietic Cells

1. Thaw $CD34^+$ and HUDEP-2 cells 48 h pre-nucleofection (*see* **Note 25**).
2. On the day of nucleofection, collect the cells in a 15-mL tube and proceed to cell counting (see Sect. 3.1.4).
3. Use nuclease-free 1.5 mL Eppendorf tubes and transfer the appropriate cell volume corresponding to 200,000 cells (*see* **Note 26**).

4. Prepare a master mix of nucleofection buffer and keep it at RT. For one reaction of 20 μL in total, add:
   a) 16.4 μL P3 solution.
   b) 3.6 μL supplement.
5. Prepare the expansion medium based on your total reactions. For each reaction, 800 μL medium is required, which will be aliquoted into a 24-well plate. From the 800 μL medium, transfer 300 μL to another well in order to wash the cuvettes after the nucleofection. Place the 24-well plate into the incubator until needed (*see* **Note 27**).
6. **For mRNA nucleofection** (*see* **Note 28**): Immediately prior to nucleofection, prepare mRNA:gRNA mixture at a 1:1 mass ratio. Recommended amount: 2 μg base editor mRNA + 2 μg guide RNA.
7. **For RNP nucleofection** (*see* **Note 29**): Prepare Cas9:gRNA mixture at a 1:3 molar ratio. Recommended amount: 20 pmol Cas9 + 60 pmol guide RNA. Incubate mixture at RT for 10 min to allow RNP complex formation.
8. Centrifuge cells at 250 × *g* for 5 min.
9. Aspirate supernatant from cell pellet (*see* **Note 30**).
10. Add 20 μL nucleofection buffer and gently resuspend the cells (*see* **Note 31**).
11. Transfer the cells in the BE:gRNA or Cas9:gRNA mix and resuspend only twice (*see* **Note 32**).
12. Transfer the final mixture into the 16-well Nucleocuvette Strip (*see* **Note 33**).
13. At the Nucleofector instrument, select the P3 solution and the appropriate position in the cuvette and apply the CA-137 program (*see* **Notes 34 and 35**).
14. Initiate nucleofection.
15. Immediately after pulse, add 100 μL pre-warmed expansion medium to the cuvette (*see* **Note 36**).
16. Gently resuspend twice and transfer to the 500 μL pre-warmed medium well.
17. Wash the cuvette twice, using 100 μL each time, with the reserved 300 μL medium, and transfer the washes to the same well.
18. Place the plate in the incubator at 37°C, 5% CO_2 (*see* **Note 37**).

3.5 Evaluation of Editing Efficiency at DNA Level

3.5.1 DNA Extraction

Genomic DNA (gDNA) can be extracted from cells using a silica membrane spin column-based genomic DNA purification kit according to the manufacturer's protocol.

1. Five days post-nucleofection, approximately 3×10^5 cells are collected for DNA analysis (*see* **Note 38**). To pellet the cells, centrifuge for 5 min at 300 × *g*.
2. Discard the supernatant, and resuspend cells in 200 µL DPBS.
3. Add 400 µg proteinase K, 400 µg RNase A and 200 µL lysis buffer.
4. Pulse-vortex the sample for 15 s and incubate it at 56°C for 10 min.
5. Add 200 µL ethanol and pulse-vortex for 15 s.
6. Load the sample onto the provided spin column and centrifuge for 1 min at 6000 × *g*.
7. Transfer the column to a clean 2 mL tube.
8. Wash sequentially with the provided wash buffers (first centrifuge: 1 min 6000 × *g*, second centrifuge: 3 min at maximum speed).
9. Discard the flow-through and centrifuge for 1 min at maximum speed to remove any residual buffers.
10. Transfer the column to a 1.5-mL Eppendorf tube and add 30 µL nuclease-free water.
11. Incubate for 5 min at RT and centrifuge for 1 min at 6000 × *g*.
12. Evaluate the eluted product with Nanodrop spectrophotometry.

3.5.2 Polymerase Chain Reaction (PCR)

1. For the reaction, the following components are added at a final concentration of 50 µL volume:
   a) 1 × High-fidelity Reaction Buffer.
   b) 200 µM deoxynucleotide triphosphates (dNTPs).
   c) 0.5 µM Forward primer.
   d) 0.5 µM Reverse primer.
   e) 100 ng in total of template gDNA (i.e., 2 ng/µL).
   f) 0.02 U/µL proofreading DNA polymerase.
   g) Nuclease-free water.
2. Apply thermocycling conditions (*see* **Note 39**):
   a) 98°C for 30 s.

b) 35 cycles: 98°C 10–15 s, primer-specific annealing temperature 30 s, 72°C 30 s.

c) Final extension 72°C for 2 min, followed by a hold step at 4°C.

3. Verify amplification by loading 5 μL of PCR product on 1% agarose gel in 1× TBE.
4. Run gel at 100–120 V for ~30 min and confirm PCR amplification.
5. Purify remaining PCR product using silica column–based PCR purification system.
6. DNA Sequencing: Prepare two sequencing reactions of 10 to 20 μL each, one reaction using the forward primer and the other the reverse (*see* **Note 40**). Add the following according to the manufacturer's instructions: dye-terminator mix, sequencing buffer, a forward/reverse primer, purified PCR product (50 ng), and water.
7. Perform cycle sequencing:
   a) 96 °C 1 min.
   b) 25 cycles: 96°C 10 s, 50°C 5 s, 60°C 4 min.
8. Purify sequencing reactions using gel filtration columns.
9. Load purified samples on a capillary electrophoresis instrument.

3.5.3 Evaluation of Editing with EditR and ICE Software

1. For base editing, the EditR software (https://moriaritylab.shinyapps.io/editr_v10/) [32,33] can be used:
   - Upload Sanger sequencing trace files and the gRNA sequence to allow analysis (*see* **Note 41**).
   - The software output is area percentages for A/C/G/T base signals for each position of the provided gRNA.
2. For the evaluation of DSB-based editing, the Inference of CRISPR Edits (ICE) software can be used (https://ice.synthego.com/) [34,35].
   a) Upload Sanger sequencing trace files of a control and of edited samples (*see* **Note 41**).
   b) The Software output consists of the percentage of overall indel formation and an indication of significant individual insertion and deletion events.
3. Apply the same approach to assess predicted off-target sites (*see* **Note 42**).

4 Notes

1. Preparation of expansion medium: Expansion medium should be freshly prepared prior to use. Although individual components are stable when stored appropriately, repeated warming and storage of the complete medium can reduce cytokine activity and impact cell performance. It is also recommended to prepare aliquots of each reagent to avoid long-term freezing–thawing and to reduce the risk of contamination.
2. Cell density is a determinant of functional outcome: Maintaining hematopoietic cells at a density between $0.5–1 \times 10^6$ cells/mL is critical for preserving viability and functional integrity. Suboptimal density ($<0.5 \times 10^6$ cells/mL) reduces survival due to insufficient autocrine and paracrine support signals, whereas excessive density ($>1 \times 10^6$ cells/mL) promotes metabolic stress and accelerates spontaneous differentiation. Strict monitoring of cell density is therefore essential during expansion and prior to electroporation.
3. Doxycycline supplementation in HUDEP-2 cells: To maintain the expression of the HPV16-E6/E7 immortalization system in HUDEP-2 cells, doxycycline must be supplemented at 5 μg/mL every 48 h. Inconsistent doxycycline exposure may result in reduced proliferation and altered cellular phenotype. Whether performing on a partial or full medium change, add the appropriate concentration of doxycycline based on the total volume of culture medium, without accounting for residual doxycycline from previous additions.
4. Complete medium replacement in HUDEP-2 Cells: HUDEP-2 cells accumulate metabolic by-products and acidify the medium rapidly. At least once per week, a complete medium replacement is required. This should be performed by collecting the entire cell suspension, centrifugating, removing the conditioned medium, and resuspending in freshly prepared expansion medium.
5. Preservation of $CD34^+$ stemness: $CD34^+$ cells should be maintained in expansion medium for no longer than 7 days to avoid spontaneous differentiation. Primary $CD34^+$ HSPCs progressively lose stemness (proliferation and differentiation potential) during extended in vitro culture. The expansion medium in this protocol predisposes expanded cells to subsequent erythroid differentiation, whereas other expansion media favor NK, megakaryocyte, myeloid precursor, T and B cell differentiation instead [36–39]. Culture beyond 7 days under expansion conditions markedly reduces primitive stem cell characteristics and may negatively affect editing outcomes

and functional assays. GE experiments should therefore be performed within 1 week post-thaw whenever possible.

6. Addition of DMSO: DMSO should always be added last during preparation of freezing medium and mixed gently but thoroughly. Prolonged exposure of cells to DMSO at RT before controlled-rate freezing reduces viability and clonogenic potential.
7. Cas9 cleavage position: For CRISPR/Cas9 applications, DNA cleavage occurs approximately three nucleotides upstream of the PAM sequence.
8. Base editing window positioning: For base editing applications, confirm that the target nucleotide lies within the activity window of the selected base editor (commonly positions 4–8 from the 5′ end of the protospacer, though this varies by editor variant used). Different BE variants exhibit slightly different editing windows and sequence preferences. It is essential to verify the reported activity window for the specific editor used.
9. Bystander editing: BEs act within a defined activity window rather than at a single nucleotide position. If multiple editable bases (e.g., additional cytosines or adenines, respectively) are present within this window, unintended conversions may occur in addition to the intended modification; these are referred to as bystander edits. Such edits can introduce undesired sequence changes; therefore, all editable nucleotides within the predicted editing window should be carefully evaluated before final gRNA selection.
10. Functional targeting strategy: gRNA positioning must be aligned with the intended GE outcome. For CRISPR/Cas9-mediated gene knock-out, design the gRNA such that the predicted cleavage site (three nucleotides upstream of the PAM) lies within a critical coding exon, functional domain, or splice site to maximize the probability of generating a loss-of-function allele through indel formation. If base editing is used to induce gene disruption, position the target nucleotide within the editing window so that the resulting base conversion introduces a premature stop codon or alters a conserved splice consensus site. For gene or motif disruption, CRISPR/Cas9-mediated editing may be performed without a donor template, relying on NHEJ-mediated indel formation. For single-base substitution or other precision editing, CRISPR/Cas9-mediated editing generally requires an HDR donor template. Alternatively, base editing can be applied by positioning the desired nucleotide substitution within the editor's activity window. In base editing approaches, careful gRNA selection is required to minimize unintended bystander

edits (*see* **Note 9**), particularly where precision editing (rather than mere deactivation of target sequences) is required and where clonal selection of intended edits is not an option, as is typical of therapeutic applications based on $CD34^+$ HSPCs.

11. Off-target assessment: Select gRNAs with minimal predicted off-target sites, particularly avoiding candidates with potential matches in coding regions or regulatory elements. Computational prediction tools should be used as an initial screening step. Different CRISPR guide platforms provide in silico predictions of off-target events.
12. Empirical validation is essential: gRNA activity can vary substantially even among candidates with similar predicted scores. Design and test at least two to three independent gRNAs per target locus, if possible, to ensure reproducible and efficient editing.
13. gRNA storage and aliquoting: Synthetic gRNAs should be aliquoted into single-use volumes in nuclease-free tubes immediately upon resuspension and stored at −80°C. Repeated freeze–thaw cycles reduce RNA stability and may compromise editing efficiency. Preparing single-dose aliquots also simplifies nucleofection setup, as the editing component (mRNA or Cas9 protein) can be added directly to the pre-aliquoted gRNA, minimizing pipetting steps and potential RNA degradation.
14. Restriction site placement: The restriction enzyme must cut downstream of the open reading frame without truncating the coding sequence or polyadenylation region. Incorrect restriction site placement may result in incomplete transcripts or loss of functional mRNA elements.
15. Complete linearization is essential: Efficient in vitro transcription strictly depends on complete plasmid linearization. Residual circular plasmid markedly reduces transcription efficiency and increases template DNA contamination in the final product. Always verify linearization by agarose gel electrophoresis and confirm the presence of a single, sharp linear band before proceeding.
16. DNA purification: Silica membrane-based column purification is recommended over phenol–chloroform extraction to minimize organic contaminants that may impair enzymatic activity. When performing multiple digestion reactions, bind each reaction to a separate silica column. During elution, sequentially pass the same eluate (e.g. 30 μL) through each column and collect the final elution in a single tube to concentrate the linearized template.
17. Template quality: High-quality DNA template is critical for T7 polymerase activity. Poor A260/A280 ratios indicate

protein contamination, and A260/A230 ratios typically indicate residual salt or buffer contamination, both of which strongly reduce full-length RNA yield. Proceed only if the following criteria are met: A260/A280 ≥1.8 and A260/A230 is between 2.0 and 2.2.

18. RNase control is critical: RNA degradation is the most common cause of IVT failure. Strict RNase-free practices must be maintained throughout the procedure:
    a) Use RNase-free tubes and filtered tips.
    b) Decontaminate work surfaces and equipment with RNase inactivation solution.
    c) Change gloves frequently.
    d) Use nuclease-free water for all reactions.

    Failure to maintain RNase-free conditions can result in substantial transcript degradation.
19. Transcription reaction handling: The use of anti-reverse cap analog (ARCA) ensures correct 5′ cap orientation and significantly improves translation efficiency in hematopoietic cells. Optimal incubation time depends on template length and quality:
    a) For transcripts longer than 0.5 kb, 30 min at 37°C is generally sufficient to achieve maximal yield.
    b) For shorter transcripts (<0.5 kb), incubation for 1 h or longer is recommended.
    c) Reactions may be safely extended up to 16 h (overnight) if necessary.

    Do not heat the transcription reaction prior to DNase treatment. After transcription, proceed directly to DNase treatment and poly(A) tailing without intermediate purification. If necessary, the capped RNA reaction may be stored at −20°C for short-term storage prior to downstream processing.
20. DNase treatment is mandatory: DNase treatment is essential to remove residual template DNA. If not eliminated, contaminating plasmid DNA containing eukaryotic promoters may generate background expression during transfection experiments and confound downstream analyses.
21. Poly(A) tailing efficiency: A 30-min poly(A) tailing reaction typically yields ≥150 nucleotide tails for most mRNAs. For short RNA species (<300 nt), extending tailing to 1 h improves polyadenylation efficiency.
22. Avoid over-drying the RNA pellet: Excessive air-drying of the RNA pellet after ethanol wash makes resuspension difficult and may reduce apparent yield. Allow the pellet to dry only until residual ethanol has evaporated.

23. RNA integrity assessment (recommended): Assess RNA integrity prior to electroporation. Load 200–300 ng of RNA on a denaturing agarose gel or analyze using capillary electrophoresis. Intact mRNA should appear as a single high-molecular-weight band with minimal smearing.
    For gel-based evaluation:
    a) Decontaminate equipment with an RNase-inactivating solution and rinse thoroughly.
    b) Heat RNA samples at 65°C for 5 min prior to loading (do not place on ice afterward).
    c) Use an ssRNA ladder for size reference.
    d) Run the gel at 90 V for ~30 min while keeping the electrophoresis tank cooled.
24. mRNA aliquots and storage: It is recommended to resuspend the RNA pellet in nuclease-free water using a volume appropriate to the pellet size. Avoid excessive dilution in order to maintain a high RNA concentration suitable for low-volume nucleofection reactions. In most cases, 30 μL of nuclease-free water is sufficient for downstream applications. It is further recommended to aliquot the mRNA into single-use or limited-use volumes (e.g., corresponding to up to three reactions) to avoid repeated freeze-thaw cycles, which may reduce RNA stability. Store the final mRNA preparation at −80°C until use.
25. Cell health determines editing outcome: Only proceed with electroporation when cell viability exceeds 80% prior to nucleofection. Reduced pre-electroporation viability significantly compromises editing efficiency, post-pulse recovery, and downstream expansion. Suboptimal cell health is one of the most common causes of experimental failure.
26. Controlled cell concentration per reaction: Apply 200,000 cells per 20 μL nucleofection reaction unless prior optimization has been performed. Overloading the reaction reduces viability and alters pulse conductivity, leading to inconsistent editing efficiency.
27. Temperature of expansion medium: Medium must be prewarmed to 37°C. The addition of cold medium immediately after electroporation significantly reduces post-pulse recovery and survival.
28. RNA handling during mRNA-based editing: Keep mRNA and gRNA on ice at all times during preparation. Avoid repeated freeze–thaw cycles by using single-use aliquots of gRNA and maximum three-use aliquots of mRNA base editor. RNA degradation directly reduces editing efficiency and may increase variability between replicates.

29. RNP complex formation: For RNP-based editing, gently mix the Cas9 protein and gRNA using the edge of the pipette tip to avoid air bubbles or mechanical stress. Note incubation at RT and do not substantially exceed 10 min incubation time for stable complex formation prior to addition of cells.
30. Supernatant removal before resuspension: After centrifugation, aspirate the supernatant as completely as possible without disturbing the pellet. Residual medium may dilute the nucleofection buffer and alter the effective concentration of editing reagents, leading to reduced and inconsistent editing efficiency.
31. Limit exposure to nucleofection buffer: Do not leave cells suspended in nucleofection buffer for prolonged periods prior to pulsing. Exposure exceeding 5 min can negatively impact viability. Prepare editing complexes in advance and proceed promptly to nucleofection.
32. Minimize mechanical stress: Primary HSPCs are highly sensitive to mechanical stress. Limit pipetting steps to the absolute minimum. When mixing cells with nucleofection buffer and editing components (mRNA:gRNA or Cas9:gRNA), resuspend gently using no more than two pipetting actions before transferring to the cuvette.
33. Nucleofector components. As of this writing, the manufacturer offers different types of Nucleofection units in addition to the Core (control) Unit, suitable, respectively, for 384-well, 96-well, 16-well-strip & single-tube, and large-volume (LV) nucleofection, as well as nucleofection of strictly adherent cells (such as neurons). Standard experimentation for hematopoietic cells and for adherent but detachable/reattaching cells (such as HEK293T cells) is most commonly performed on the X Unit for 16-well-strip and single-tube nucleofection. Consider the throughput needs, running cost, cell types under study, and corresponding community resources before equipment purchases from this or other manufacturers.
    Buffers and cuvettes for Nucleofection equipment are costly and proprietary, but widespread use of the equipment has led to publication of protocols for the use of self-made buffers [40–42] and of suggestions for cleanup and multiple re-use of Nucleofector cuvettes [43], which may allow considerable cost savings. We have not evaluated these workarounds, and the current protocol is based on stock Nucleofector cuvettes and reagents.
34. Sequential processing of multiple samples: When performing multiple nucleofection reactions, avoid preparing and pulsing all samples simultaneously. Even for experienced operators,

processing no more than two reactions at a time is recommended, particularly for mRNA-based editing. Prolonged handling time before pulsing may reduce reproducibility and cell viability.

35. Avoid bubble formation: When transferring the cell suspension into the Nucleocuvette™, carefully avoid introducing air bubbles, as these can interfere with electrical conductivity and reduce transfection efficiency. After loading, gently tap the cuvette to ensure even distribution of the suspension at the bottom of the well.
36. Immediate post-pulse recovery: Do not leave cells in the cuvette for more than 1–2 min after electroporation. Delayed recovery increases cytotoxicity. Immediately add prewarmed expansion medium and transfer cells to culture plates.
37. Post-nucleofection handling: Do not split or excessively manipulate cells during the first 48 h post-electroporation. Early disturbance can negatively affect editing efficiency and survival. Allow cells to recover and stabilize before further processing.
38. Optimal time point for editing assessment: Editing efficiency is recommended to be assessed 5 days post-nucleofection. At this time point, transient nuclease or mRNA expression has subsided, edited alleles have stabilized, and sufficient time has elapsed for indel formation or base conversion to reach detectable levels. Earlier time points may underestimate editing efficiency. However, consider the biological context and potential negative selection of intended editing events when choosing the post-nucleofection time before editing analysis.
39. PCR optimization and annealing temperature: Accurate editing quantification depends on robust and specific PCR amplification of the target locus. Prior to experimental analysis, it is strongly recommended to optimize primer performance using a gradient-annealing-temperature PCR. Online tools such as the NEB Tm Calculator can be used to determine theoretical melting temperatures; however, empirical optimization remains essential. Suboptimal annealing conditions may result in nonspecific amplification, poor sequencing quality, and inaccurate editing analysis.
40. Bidirectional sequencing for initial validation: During initial optimization experiments, sequencing based on both forward and reverse primers is recommended. Bidirectional sequencing increases confidence in editing calls, improves resolution of mixed chromatograms, and helps identify potential sequencing artifacts.
41. Inclusion of an untreated control sample: An untreated (non-edited) control sample must always be sequenced in parallel.

Computational deconvolution tools such as ICE require a high-quality control chromatogram for accurate indel quantification. For base editing analysis, comparison to a control trace is essential to distinguish true editing from background signal variability.

42. Deconvolution analyses for off-target sites. Deconvolution of Sanger sequence traces is a cost-effective and informative means of assessing on-target editing outcomes and major off-target sites. It is similar in cost and, by providing estimates of specific indel events, superior in its analytical value to T7E1 and Surveyor assays originally employed in the field [44]. However, its accuracy and detection sensitivity for low-level edits are limited, inherent to the deconvolution approach but also dependent on the analysis algorithm used. For greater sensitivity, evaluation of short-listed editing tools for therapeutic application needs to employ targeted deep sequencing of potential off-target sites instead [45].

Acknowledgments

The publication is based upon work by COST Action CA21113: Genome Editing to Treat Human Diseases (https://www.gene-humdi.eu), supported by European Cooperation in Science and Technology (COST). Experimental work was supported by projects BETA-BET (EXCELLENCE/0524/0521) and EDIT-4-IRON (BILATERAL/ISRAEL (MOST)/0224/0024), co-financed by the European Regional Development Fund and the Republic of Cyprus through the Research and Innovation Foundation. The figure was created in BioRender. Papaioannou et al (2026) https://BioRender.com/4y546nu.

Conflict of Interest The authors have no conflicts of interest to declare that are relevant to the content of this chapter.

References

1. Parums DV (2024) Editorial: First regulatory approvals for CRISPR-Cas9 therapeutic gene editing for sickle cell disease and transfusion-dependent β-thalassemia. Med Sci Monit Int Med J Exp Clin Res 30:e944204
2. Traxler EA, Hotan Q, Shao Y, et al. (2026) An optimized CRISPR-Cas12a genome-wide screen reveals PTPA phosphatase pathway in fetal hemoglobin silencing. Blood 147:1999–2010.
3. Nguyen A-DH, Quang MT (2025) CRISPR/Cas9 Genome Editing in Oncology: Mechanisms, Therapeutic Platforms and Translational Challenges. Mol Biotechnol 68:2201–2229.
4. Urnov FD, Miller JC, Lee Y-L et al. (2005) Highly efficient endogenous human gene correction using designed zinc-finger nucleases. Nature 435:646–651
5. Joung JK, Sander JD (2013) TALENs: a widely applicable technology for targeted genome editing. Nat Rev Mol Cell Biol 14:49–55
6. Jinek M, Chylinski K, Fonfara I et al. (2012) A programmable dual-RNA–guided DNA

endonuclease in adaptive bacterial immunity. Science 337:816–821
7. Koniali L, Lederer CW, Kleanthous M (2021) Therapy development by genome editing of hematopoietic stem cells. Cells 10:1492
8. Komor AC, Kim YB, Packer MS et al. (2016) Programmable editing of a target base in genomic DNA without double-stranded DNA cleavage. Nature 533:420–424
9. Gaudelli NM, Komor AC, Rees HA et al. (2017) Programmable base editing of A•T to G•C in genomic DNA without DNA cleavage. Nature 551:464–471
10. Doman JL, Sousa AA, Randolph PB et al. (2022) Designing and executing prime editing experiments in mammalian cells. Nat Protoc 17:2431–2468
11. Papaioannou NY, Patsali P, Klermund J, et al. (2026) Functional correction and genome integrity with duplex base editing of β-thalassemic hematopoietic stem cells. Genome Biol 27:67.
12. Hardouin G, Antoniou P, Martinucci P et al. (2023) Adenine base editor-mediated correction of the common and severe IVS1-110 (G>A) β-thalassemia mutation. Blood 141:1169–1179
13. Antoniou P, Hardouin G, Martinucci P et al. (2022) Base-editing-mediated dissection of a γ-globin cis-regulatory element for the therapeutic reactivation of fetal hemoglobin expression. Nat Commun 13: 6618
14. Psatha N, Georgakopoulou A, Li C et al. (2021) Enhanced HbF reactivation by multiplex mutagenesis of thalassemic CD34+ cells in vitro and in vivo. Blood 138:1540–1553
15. Morgan RA, Gray D, Lomova A et al. (2017) Hematopoietic stem cell gene therapy: progress and lessons learned. Cell Stem Cell 21:574–590
16. Molaei Z, Jabbarpour Z, Omidkhoda A et al. (2024) Exploring non-viral methods for the delivery of CRISPR-Cas ribonucleoprotein to hematopoietic stem cells. Stem Cell Res Ther 15:233
17. Hendel A, Bak RO, Clark JT et al. (2015) Chemically modified guide RNAs enhance CRISPR-Cas genome editing in human primary cells. Nat Biotechnol 33:985–989
18. Maurisse R, De Semir D, Emamekhoo H et al. (2010) Comparative transfection of DNA into primary and transformed mammalian cells from different lineages. BMC Biotechnol 10: 9
19. Van Tendeloo VF, Ponsaerts P, Lardon F et al. (2001) Highly efficient gene delivery by mRNA electroporation in human hematopoietic cells: superiority to lipofection and passive pulsing of mRNA and to electroporation of plasmid cDNA for tumor antigen loading of dendritic cells. Blood 98:49–56
20. Shi J, Ma Y, Zhu J et al. (2018) A review on electroporation-based intracellular delivery. Molecules 23:3044
21. Rolong A, Davalos RV, Rubinsky B (2018) History of electroporation. In: Meijerink MR, Scheffer HJ, Narayanan G (eds) Irreversible electroporation in clinical practice. Springer International Publishing, Cham. pp 13–37
22. Neumann E, Schaefer-Ridder M, Wang Y et al. (1982) Gene transfer into mouse lyoma cells by electroporation in high electric fields. EMBO J 1:841–845
23. Potter H, Weir L, Leder P (1984) Enhancer-dependent expression of human kappa immunoglobulin genes introduced into mouse pre-B lymphocytes by electroporation. Proc Natl Acad Sci USA 81:7161–7165
24. Cavazza A, Molina-Estévez FJ, Reyes ÁP et al. (2025) Advanced delivery systems for gene editing: a comprehensive review from the GenE-HumDi COST Action Working Group. Mol Ther Nucleic Acids 36:102457
25. Yu K-R, Natanson H, Dunbar CE (2016) Gene editing of human hematopoietic stem and progenitor cells: promise and potential hurdles. Hum Gene Ther 27:729–740
26. Lattanzi A, Meneghini V, Pavani G et al. (2019) Optimization of CRISPR/Cas9 delivery to human hematopoietic stem and progenitor cells for therapeutic genomic rearrangements. Mol Ther 27:137–150
27. Kim S, Kim D, Cho SW et al. (2014) Highly efficient RNA-guided genome editing in human cells via delivery of purified Cas9 ribonucleoproteins. Genome Res 24:1012–1019
28. Glass Z, Lee M, Li Y et al. (2018) Engineering the delivery system for CRISPR-based genome editing. Trends Biotechnol 36:173–185
29. Kwon H, Kim M, Seo Y et al. (2018) Emergence of synthetic mRNA: In vitro synthesis of mRNA and its applications in regenerative medicine. Biomaterials 156:172–193
30. Papaioannou NY, Patsali P, Naiisseh B, et al. (2023) High-efficiency editing in hematopoietic stem cells and the HUDEP-2 cell line based on in vitro mRNA synthesis. Front Genome Ed 5, 1141618.
31. Lonza. (n.d.). Electroporation and Nucleofector® Technology. https://bioscience.lonza.com/nucleofector-technology
32. Kluesner, M.G. (2018). EditR—estimating base editing by Sanger sequencing, http://baseeditr.com/
33. Kluesner MG, Nedveck DA, Lahr WS, et al. (2018) EditR: a method to quantify base editing from Sanger Sequencing. CRISPR J 1:239–250.
34. Synthego (2018). How to use ice: a detailed guide for analyzing CRISPR editing results.

https://www.synthego.com/guide/how-to-use-crispr/ice-analysis-guide/
35. Conant D, Hsiau T, Rossi N et al. (2022) Inference of CRISPR edits from Sanger trace data. CRISPR J 5:123–130
36. Miller JS, Verfaillie C, McGlave P (1992) The generation of human natural killer cells from CD34+/DR- primitive progenitors in long-term bone marrow culture. Blood 80:2182–2187
37. Clinton J, Shapiro B (2015) Differentiation and expansion of hematopoietic precursor cells from bone-marrow derived CD34+ progenitors. ATCC Resour Appl Notes. ATCC
38. Reimann C, Dal-Cortivo L, Ternaux B et al. (2009) In vitro generation of human T-cell precursors from bone marrow CD34+ cells by short exposure to immobilized Notch-ligand delta-like 4. Blood 114:3532
39. Ichii M, Oritani K, Yokota T et al. (2010) Stromal cell-free conditions favorable for human B lymphopoiesis in culture. J Immunol Methods 359:47–55
40. Sommermann TG, O'Neill K, Plas DR et al. (2011) IKKβ and NF-κB transcription govern lymphoma cell survival through AKT-induced plasma membrane trafficking of GLUT1. Cancer Res 71:7291–7300
41. Chicaybam L, Barcelos C, Peixoto B et al. (2016) An efficient electroporation protocol for the genetic modification of mammalian cells. Front Bioeng Biotechnol 4:99
42. Bak RO, Porteus MH (2017) CRISPR-mediated integration of large gene cassettes using AAV donor vectors. Cell Rep 20:750–756
43. Danner E (2019) Lonza 4D nucleofection with effective homemade buffer (here using K562 with Cas9 plasmid). Protocols.io https://doi.org/10.17504/protocols.io.64qhgvw
44. Vouillot L, Thélie A, Pollet N (2015) Comparison of T7E1 and surveyor mismatch cleavage assays to detect mutations triggered by engineered nucleases. G3 5:407–415
45. Patsali P, Turchiano G, Papasavva P, et al. (2019) Correction of IVS I-110(GA) β-thalassemia by CRISPR/Cas-and TALEN-mediated disruption of aberrant regulatory elements in human hematopoietic stem and progenitor cells. Haematologica 104:e497–e501

Open Access This chapter is licensed under the terms of the Creative Commons Attribution-NonCommercial-NoDerivatives 4.0 International License (http://creativecommons.org/licenses/by-nc-nd/4.0/), which permits any noncommercial use, sharing, distribution and reproduction in any medium or format, as long as you give appropriate credit to the original author(s) and the source, provide a link to the Creative Commons license and indicate if you modified the licensed material. You do not have permission under this license to share adapted material derived from this chapter or parts of it.

The images or other third party material in this chapter are included in the chapter's Creative Commons license, unless indicated otherwise in a credit line to the material. If material is not included in the chapter's Creative Commons license and your intended use is not permitted by statutory regulation or exceeds the permitted use, you will need to obtain permission directly from the copyright holder.





Chapter 19

An Electroporation-Based Protocol for Ex Vivo Base Editing: From Design to Quantitative Assessment

Irene Peña-Gutierrez, Davide Mazzeo, Alex Bassons-Bascuñana, Sibtain Haider, Laura Garcia-Garcia, Beatriz Olalla-Sastre, Paula Río, Sergio López-Manzaneda and Manuel Mataix

Abstract

Base editing is a CRISPR variant approach that enables single-nucleotide conversions without generating double-strand breaks. Cytosine and adenine base editors mediate C•G to T•A and A•T to G•C transitions, respectively, by coupling a deaminase to a catalytically impaired Cas9, a modified nuclease that lacks DNA cleavage activity but retains DNA binding capability. By avoiding double-strand breaks, base editing limits reliance on unpredictable end-joining pathways and facilitates more precise outcomes. This chapter provides a practical protocol for base editing by electroporation in adherent and suspension stem cells. The workflow spans guide design aligned with the editor activity window, in vitro synthesis of mRNA-based editor components, and electroporation for transient delivery. We detail essential steps for cell handling and recovery, followed by standard readouts. Analytical endpoints focus on targeted sequencing to quantify base conversion and assess editing specificity, with guidance for basic interpretation of results. Troubleshooting notes address frequent pitfalls and practical remedies to optimize performance across cell types.

Keywords Base editing, CRISPR/Cas9, Precise editing, Ex vivo Gene Therapy, Electroporation, RNA delivery

1 Introduction

After the CRISPR/Cas9 revolution transformed the gene-editing field, numerous technologies were developed to adapt this platform to alternative approaches aiming to overcome its main limitations, particularly the induction of double-strand breaks (DSBs) and the inability to precisely control repair outcomes [1]. DSBs activate multiple competing DNA-repair pathways and can elicit p53-dependent DNA damage responses. These breaks are predominantly resolved through inherently uncontrollable, although somewhat predictable,

These authors contributed equally: Irene Peña-Gutierrez, Davide Mazzeo.

Duško Lainšček et al. (eds.), *CRISPR Delivery*, Methods in Molecular Biology, vol. 3075,
https://doi.org/10.1007/978-1-0716-5547-4_19,
© The Author(s) 2027

nonhomologous end joining (NHEJ) or microhomology-mediated end-joining (MMEJ), often resulting in insertions, deletions, duplications, or other disruptive genomic rearrangements [2, 3].

Among the new technologies, base editing emerged as a CRISPR-derived strategy enabling the direct conversion of individual nucleotides, typically C•G to T•A by cytosine base editors (CBEs) or A•T to G•C by adenine base editors (ABEs), without generating DSBs [4–7]. Early base editors relied solely on deamination of target nucleobases within a defined editing window, although recent variants have expanded the spectrum of possible nucleotide substitutions (Fig. 1) [8, 9].

Canonical base editors employ a single-guide RNA (sgRNA) to direct a catalytically impaired Cas9, most commonly dead Cas9 (dCas9) or nickase Cas9 (nCas9), to the genomic locus of interest. Upon target recognition, the sgRNA–Cas9 complex unwinds the DNA duplex, generating an R-loop in which the sgRNA forms an RNA–DNA heteroduplex while the opposite DNA strand remains exposed as single-stranded DNA (ssDNA). This ssDNA serves as the substrate for the fused deaminase. Following deamination, the cellular repair machinery processes the mismatch between the edited base and the unmodified complementary strand. To prevent mismatch repair from restoring the wild-type sequence, the nCas9 (D10A) variant introduces a single-strand nick in the non-edited strand, thereby biasing repair toward using the edited strand as the template [6].

This chapter describes a protocol to apply base editing technologies as an ex vivo strategy to precisely modify stem cells of diverse origins, including both adherent and suspension populations. To achieve efficient and transient delivery, we employ electroporation of the base-editing components in their RNA form, typically sgRNA and mRNA encoding the corresponding Cas9 variant and deaminase, thereby enabling high editing efficiencies while minimizing genomic integration risks. This approach has allowed us to systematically explore the applicability of base editors across distinct stem-cell systems and to advance their potential application in regenerative and therapeutic settings.

2 Materials

2.1 Cell Work

2.1.1 Reagents

1. 0.4% Trypan Blue solution for cell viability
2. Phosphate-buffered saline (PBS): pH 7.2–7.4
3. 10,000 U/mL Penicillin—10,000 µg/mL Streptomycin solution

2.1.2 Equipment

1. Incubator set to 37°C and 5% CO_2
2. Centrifuge
3. Flow cytometer

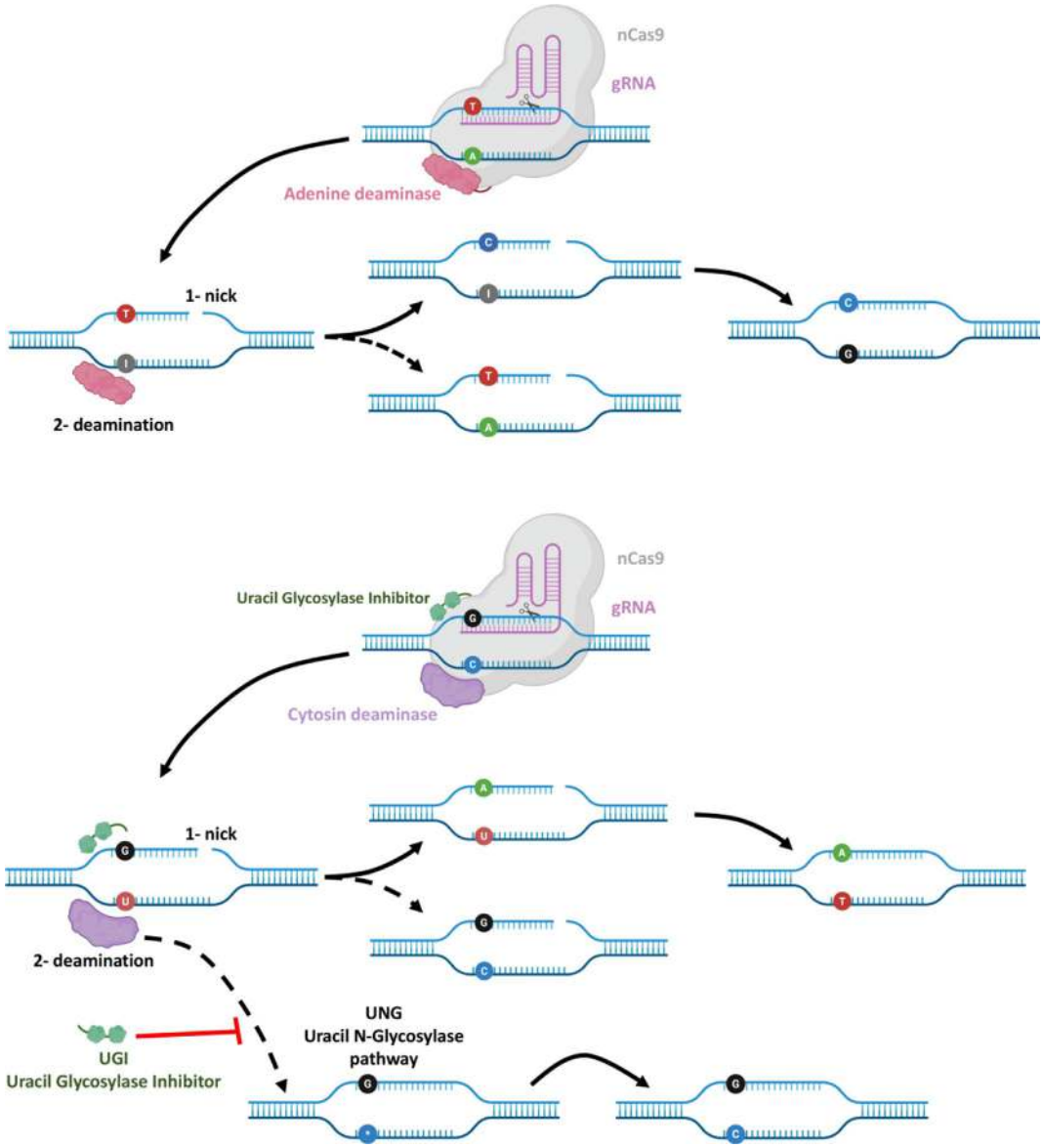


Fig. 1 Illustrative image of the base editing process. Description of deamination generated by adenosine (**A**) or cytosine (**B**) base editors and the nucleotide transitions induced. Figure created with Biorender.com

2.2 mRNA Production by In Vitro Transcription

2.2.1 Reagents

1. Plasmid DNA encoding the base editor downstream of a T7 or T3 promoter (Fig. 2)
2. Restriction enzyme to linearize the plasmid, cutting after the poly-A signal

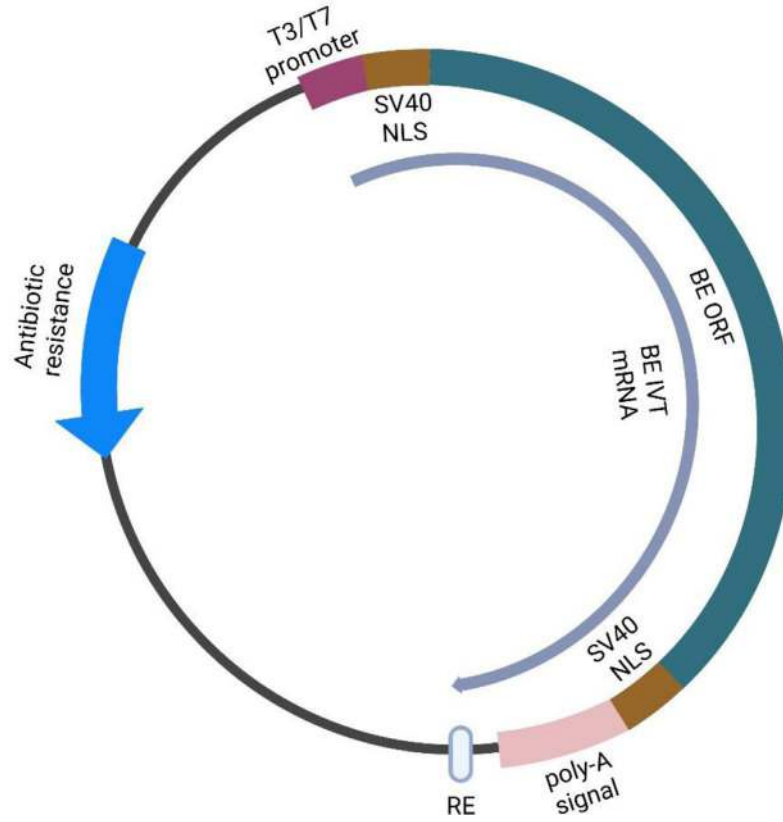


Fig. 2 Representative scheme of the BE encoding plasmid used for in vitro transcription. The BE transcript production is regulated under a T3/T7 promoter. The BE is flanked by SV40NLS (Simian Virus 40 Nuclear Localization Signal) sequences to enhance the translocation into the cell nucleus. RE: restriction enzyme motif to linearize the plasmid after the polyA signal using a unique cutter enzyme. Figure created with Biorender.com

3. 1% TBE agarose gel
4. Phenol:Chloroform:Isoamyl alcohol (25:24:1) pH 6.7
5. 3 M Sodium acetate, pH 5.5
6. Isopropanol
7. Ethanol
8. *In vitro* transcription kits:
   a. For T3 promoter (e.g., mMESSAGE mMACHINE T3 from Thermo Fisher)
   b. For the T7 promoter, multiple CAP analogs are available (e.g., mMESSAGE mMACHINE T7; mMESSAGE mMACHINE™ T7 ULTRA; and mMESSAGE mMACHINE™ T7 mRNA Kit with CleanCap™ Reagent AG, all from Thermo Fisher)

9. Poly(A) Tailing kit
10. RNeasy Mini columns kit
11. Qubit RNA Integrity and Quality assay kit (Thermo Fisher)

2.2.2 Equipment

1. Refrigerated centrifuge
2. Vortex
3. Fume hood
4. NanoDrop (Thermo Fisher)
5. Qubit 4 Fluorometer (Thermo Fisher)

2.3 Cell Electroporation

2.3.1 Reagents

1. Adenine base editor (ABE) mRNA or cytosine base editor (CBE) mRNA
2. sgRNA (single-guide RNA)
3. P3 Primary Cell 4D-Nucleofector™ X Kit S (Lonza):
   a. P3 Primary Nucleofector™ Solution (P3 buffer + Supplement)
   b. 16-well Nucleocuvette™ Strips
4. P3 Primary Cell 4D-Nucleofector™ X Kit L (Lonza):
   a. P3 Primary Nucleofector™ Solution (P3 buffer + = Supplement)
   b. Nucleocuvette™ Vessels (cuvettes)
5. Neon NxT Electroporation System 10-μL Kit (ThermoFisher):
   a. Electroporation buffer R

2.3.2 Equipment

1. Electroporator devices:
   a. 4D-nucleofector
   b. Neon™ NxT (ThermoFisher)

2.4 Specific Materials for CD34+ Cells

2.4.1 Reagents

1. Ficoll–Paque™ PLUS (density 1.077 g/mL)
2. PBE buffer: PBS supplemented with 0.5% bovine serum albumin (BSA) and 2 mM EDTA
3. 10 U/mL medium DNase I for cell culturing applications
4. Türk solution for cell counting
5. CD34 MicroBead Kit for human cells (Miltenyi)
6. LS and/or MS magnetic separation columns (Miltenyi)
7. 30 μm pre-separation filter (Miltenyi)

8. Prestimulation culture medium: StemSpan™ SFEM (Stemcell Technologies) expansion medium supplemented with 1% GlutaMAX™ (Gibco), 1% P/S solution, 100 ng/mL recombinant human stem cell factor (SCF) protein, 100 ng/mL recombinant human thrombopoietin (TPO) protein, 100 ng/mL recombinant human Flt3-Ligand (Flt3-L) protein, and 20 ng/mL human interleukin-3 (IL-3)
9. Antibody against hCD34 for flow cytometry applications

2.4.2 Equipment

1. QuadroMACS™ and/or OctoMACS™ magnetic separators compatible with LS/MS columns (Miltenyi)

2.5 Specific Materials for Adherent Cells

2.5.1 Reagents

1. Trypsin–EDTA—0.5 g porcine trypsin and 0.2 g EDTA
2. 0.25% Colagenase A in Dulbecco's Modified Eagle's Medium
3. Culture medium for fibroblasts and keratinocytes: DMEM supplemented with 10% fetal bovine serum (FBS)

2.5.2 Equipment

1. Mincing tools: Sterile scalpels or scissors for mechanical dissociation of the skin biopsy

2.6 Deep Sequencing Analysis Reagents

1. Illumina adapter sequences must be included in the sequencing primers:
   a. For the forward primer:
   5′-ACACTCTTTCCCTACACGACGCTCTTCCGATCT-3′
   b. For the reverse primer:
   5′-GACTGGAGTTCAGACGTGTGCTCTTCCGATCT-3′

3 Methods

3.1 Single-Guide RNA Design

1. sgRNAs must be designed depending on the editor's specific editing window to ensure that the target nucleotide falls within it.
2. The possible bystander introduction has to be considered, defined as an unintended editing event within the editing window of the employed base editing.
3. The design of the sgRNA strictly depends on the availability of the protospacer adjacent motif (PAM) at the target site (Fig. 3) (*see* **Note 1**).
4. The optimal editing window with the nucleotide to be targeted depends on the base editor selected. A summary of the most used adenine base editors is provided in Table 1, and the most common cytosine base editors are collected in Table 2.

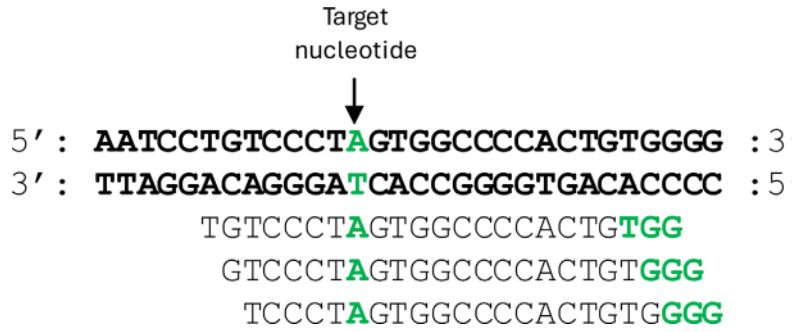


Fig. 3 sgRNA design across the target site. Schematic representation of sgRNAs tiled across the target region, showing their relative positions, orientations, and target sequences

5. Specialized software can be used for sgRNA design, such as Benchling (www.benchling.com), CRISPOR (https://crispor.gi.ucsc.edu/), or BE-designer (www.rgenome.net/be-designer).
6. BE-designer is a web-based tool optimized for base editing that facilitates sgRNA design based on the specific base editor employed in the experiment (selectable in the user interface) and the target genome of interest.

3.2 mRNA Production by In Vitro Transcription (IVT)

3.2.1 DNA Linearization Template for IVT

1. Linearize the plasmid DNA with an enzyme cutting after the poly-A sequence. If the selected enzyme does not exhibit STAR activity, the digestion can take place overnight (*see* **Notes 2** and **3**).
2. Confirm the plasmid linearization by running 2 µL of the digestion in a 1% agarose TBE gel.

3.2.2 DNA Template Purification

1. Purify the linearized plasmid by phenol–chloroform extraction and sodium acetate precipitation in a fume hood.
2. Add 1 volume of phenol–chloroform to the plasmid digestion, and vortex it for 15 s, the mix should get a whitish color.
3. Centrifuge the mixture for 10 min in a precooled centrifuge (4°C or lower) at 13,000 × *g*.
4. Collect the aqueous upper phase and add 0.1 volume of 3 M Sodium Acetate pH 5.2 solution, and 1 volume of cold isopropanol. Mix it by inversion and incubate it at −80°C for 30 min to precipitate the DNA.

Table 1
Most common adenosine base editors variants

	Base editor	Cas variant	Deaminase	Editing window	PAM	Addgene	Reference
Adenine base editors	ABE8e	SpCas9n D10A	TadA-8e	4–8	NGG	#138489	Richter et al. [10]
	ABEmax	SpCas9n D10A	TadA*	4–7	NGG	#112095	Koblan et al. [11]
	NG-ABE8e	SpCas9-NG	TadA-8e	4–11	NG	#138491	Richter et al. [10]
	ABE8e-SpRY	SpRY-nCas9 (D10A)	TadA*	4–8	NRN/NYN	#185671	Huang et al. [12]
	ABEmax-SpRY	SpRY-nCas9 (D10A)	TadA*	4–8	NRN/NYN	#140003	Walton et al. [13]
	ABEmax-NRTH	SpCas9n D10A	TadA*	4–8	NRTH	#136922	Miller et al. [14]
	ABEmax-NRCH	SpCas9n D10A	TadA*	4–8	NRCH	#136923	Miller et al. [14]

Table 2
Most common cytosine base editors variants

	Base editor	Cas variant	Deaminase	Editing window	PAM	Addgene	Reference
Cytosine base editors	BE4	SpCas9n D10A	rAPOBEC1	4–81	NGG	#100802	Komor et al. [15]
	BE4max	SpCas9n D10A	rAPOBEC1	4–8	NGG	#112093	Koblan et al. [11]
	evoAPOBEC1-BE4max	SpCas9n D10A	evoAPOBEC1	3–10	NGG	#122611	Thuronyi et al. [16]
	BE4max-SpRY	SpRY-nCas9 (D10A)	rAPOBEC1	3–10	NRN/NYN	#139999	Walton et al. [13]
	CBE-T1.52	SpCas9n D10A	TadA*8.20 + 15 directed evolution mutations	4–8	NGG	#193285	Lam et al. [17]
	TadCBEd	SpCas9n D10A	TadA-8e	4–7	NGG	#193835	Neugebauer et al. [18]

5. Centrifuge the mixture for 30 min in a precooled centrifuge at 13,000 × *g*.
6. Discard the supernatant with a pipette tip or by vacuum aspiration and wash the pellet with 400 µL of cold 100% ethanol.
7. Centrifuge it for 10 min in a precooled centrifuge (4°C) at 13,000 × *g*.
8. Discard the supernatant with a pipette tip or by vacuum aspiration and let the pellet dry in a fume hood for 10–15 min.
9. Once the pellet is absolutely dried, reconstitute it by adding 10 µL DNAse-RNase-free water and quantify the purified DNA by using a NanoDrop spectrophotometer (*see* **Notes 4–6**).

3.2.3 IVT for T3, T7, and T7 ARCA CAP

1. Prepare the in vitro transcription mixture using the reagents provided in an in vitro transcription kit. Briefly, the IVT reaction is described below:
   a. Up to 20 µL nuclease-free water
   b. 10 µL 2× NTP/CAP
   c. 2 µL 10× reaction Buffer
   d. 1 µg linearized plasmid DNA
   e. 2 µL enzyme mix
2. Pipette up and down carefully and incubate the reaction at 37°C for 2 h without agitation.
3. Spin down the reaction and add 1 µL of TURBO DNase per reaction. Incubate for 15 min at 37°C (mix carefully).

3.2.4 IVT for T7 mRNA CleanCap™ Reagent AG

1. Prepare the in vitro transcription mixture of the reagents provided in the kit according to the following guide:
   a. Up to 20 µL nuclease-free water
   b. 2 µL TheraPure™ ATP
   c. 2 µL TheraPure™ CTP
   d. 2 µL TheraPure™ GTP
   e. 2 µL TheraPure™ UTP (*see* **Note 7**)
   f. 1.5 µL CleanCap™ reagent AG
   g. 2 µL 10× T7 CleanCap buffer
   h. 1 µg linearized plasmid DNA
   i. 2 µL enzyme mix
2. Pipette up and down carefully and incubate the reaction at 37°C for 2 h without agitation.
3. Spin down the reaction and add 1 µL of TURBO DNase for four reactions and incubate it for 15′ at 37°C (mix carefully).

3.2.5 Poly(A) Tailing Procedure

1. Use the Poly(A) Tailing kit following the protocol provided by the supplier. A brief description of the IVT reaction is provided below:
   a. 21 µL IVT reaction
   b. 35 µL nuclease-free water
   c. 20 µL 5× E-PAP buffer
   d. 10 µL 25 mM $MnCl_2$
   e. 10 µL 10 mM ATP
   f. 4 µL E-PAP enzyme
2. Incubate the mixture at 37°C for 1 h (*see* **Note 8** and **9**).

3.2.6 mRNA Purification and Quantification

1. Use the RNeasy Mini columns kit to purify the mRNA following the manufacturer's protocol and using a precooled centrifuge. To concentrate the sample during the elution step, 30 µL of nuclease-free water is added directly to the membrane. This first elution is passed through the column twice to get the final mRNA (*see* **Notes 10** and **11**).
2. Place the collected mRNA on ice. Quantify the mRNA with the NanoDrop spectrophotometer.
3. Assess the quality of the mRNA by using the Qubit RNA Integrity and Quality assay following the manufacturer's protocol (*see* **Note 12**).
4. Aliquot the production and keep the mRNA at −80°C for long-term storage.

3.3 Base Editing in Hematopoietic Stem Cells

3.3.1 $CD34^+$ Cell Isolation

1. Transfer cord blood into sterile containers and carefully layer 10 mL over 5 mL Ficoll–Paque™ in a 15 mL conical tube without disturbing the interface (*see* **Note 13**).
2. Centrifuge at 500 × *g* for 25 min at room temperature with brake off.
3. Carefully collect the mononuclear cell (MNC) layer and transfer to a new 50 mL tube.
4. Wash the cells twice as follows:
   i. First wash: dilute with PBS at a 1:3 ratio and centrifuge at 500 × *g* for 7 min.
   ii. Second wash: resuspend in 20 mL PBE buffer and centrifuge at 500 × *g* for 7 min (*see* **Notes 14** and **15**).

5. Count cells using the Türk solution (1:20 dilution) to lyse erythrocytes.
6. Resuspend the cell pellet in 300 µL PBE buffer for each 1×10^8 cells.
7. Collect 10 µL of the cells for further flow cytometry analysis (unstained and CD34-stained samples).
8. Perform magnetic labeling at 4°C protected from light for 30 min. For every 300 µL (1×10^8 cells), add:
   a. 30 µL Fc Receptor Blocking Reagent
   b. 30 µL CD34 MicroBeads
9. To avoid any cell clump from obstructing the column, use a prefilter and equilibrate the column by adding 3 mL PBE buffer before loading the sample.
10. Wash the labeled cells with 20 mL PBE buffer and centrifuge at 500 × *g* for 7 min. Resuspend in 3 mL of PBE buffer.
11. Perform magnetic separation using LS or MS columns according to the manufacturer's instructions.
12. Collect the flow-through as the $CD34^-$ fraction.
13. Remove the column from the magnetic field and elute $CD34^+$ cells according to the manufacturer's instructions.
14. Count purified $CD34^+$ cells using Trypan Blue, distinguishing the live from the dead cells.
15. Collect an aliquot of $CD34^+$ cells for flow cytometry analysis to determine the percentage of $CD34^+$ cells, ensuring a recommended purity above 85%–90%.
16. Centrifuge purified $CD34^+$ cells at 500 × *g* for 7 min, resuspend in prestimulation medium at 1×10^6 cells/mL, and culture for 24 h under prestimulation conditions.
17. If required, perform a second round of magnetic selection using the $CD34^-$ fraction to recover additional $CD34^+$ cells.

3.3.2 Nucleofection of Base Editors (Adenine and Cytosine) in $CD34^+$ Cells

1. After the prestimulation, count $CD34^+$ cells and collect 2×10^5 cells per condition in a 1.5 mL microcentrifuge tube.
2. Wash once with PBS and centrifuge at 500 × *g* for 5 min. Carefully remove all residual PBS (*see* **Note 16**).
3. Resuspend the cell pellet in 20 µL P3 Primary Nucleofector™ Solution prepared as follows: 16.4 µL P3 buffer + 3.6 µL Supplement per 2×10^5 cells.
4. In a separate tube on ice, prepare the nucleofection mix containing:

a. 6 μg ABE or CBE mRNA (*see* **Note 17**)
b. 6.4 μg sgRNA

5. Mix gently without vortexing.
6. Combine the nucleofection mix with the cell suspension and gently mix.
7. Transfer the entire mixture to the appropriate nucleofection vessel, avoiding air bubbles (*see* **Note 18**).

a. For up to 2×10^5 cells, use 16-well Nucleocuvette™ Strips with the P3 Primary Cell Kit S
b. For up to 1×10^6 cells, use Nucleocuvette™ Vessels with the P3 Primary Cell Kit L

8. Perform nucleofection using the 4D-Nucleofector™ X Unit with program EO-100 (*see* **Note 19**).
9. Immediately incubate cells for 10 min at 37°C under standard culture conditions (normoxia, 5% CO_2).
10. Carefully transfer cells to prewarmed culture StemSpan expansion medium supplemented with the cytokines 1×10^6 cells/mL under standard conditions, in an appropriate plate 96-, 24-, or 6-well, depending on cell number.
11. Assess gene editing efficiency 5 days post-nucleofection.

3.4 Base Editing in Adherent Cells

3.4.1 Mechanical Dissociation

1. Mechanically mince the biopsy fragments into small pieces.

3.4.2 Primary Digestion (Fibroblasts Isolation)

1. Digest the skin fragments in a 0.25% Collagenase A solution supplemented with a penicillin–streptomycin antibiotic cocktail.
2. Incubate at 37°C with constant agitation for 2–4 h.
3. Following incubation, carefully collect the supernatant containing the dissociated cells, ensuring that no undigested skin fragments are transferred.
4. Centrifuge the supernatant at 500 × *g* for 10 min.
5. Resuspend the resulting pellet in the appropriate culture medium to obtain the fibroblast population.

3.4.3 Sequential Digestion (Keratinocyte Isolation)

1. Subject the remaining undigested tissue fragments to three cycles of Trypsin/EDTA digestion at 37°C under constant agitation (*see* **Note 20**).

2. Incubation times: The first cycle should last between 45 min and 1 h; subsequent cycles should last 30 min each.
3. After each cycle, collect the cell suspension (avoiding the carry-over of undigested fragments).
4. Inactivate the trypsin by adding complete medium (containing serum) and centrifuge at 500 × *g* for 10 min.
5. Resuspend the pellet to obtain the keratinocyte population.

3.4.4 Base Editing protocol for Adherent Cells (Keratinocytes and Fibroblasts)

1. Wash the adherent cells with 1× PBS and remove the PBS completely.
2. Add 1× Trypsin–EDTA and incubate the cells at 37°C and 5% CO_2.
3. Once cells are fully detached, inactivate the trypsin by adding a complete growth medium supplemented with FBS.
4. Count the cells with Trypan and transfer 2×10^5 cells per condition into a 1.5 mL microcentrifuge tube.
5. Centrifuge at 500 × *g* for 7 min. Discard the supernatant.
6. Wash the pellet with PBS and centrifuge again at 500 × *g* for 7 min.
7. Completely aspirate the PBS and resuspend the cell pellet in Buffer R (if using the Neon™ Transfection System) or Buffer P3 (if using the LONZA® system, as described above).
8. Prepare the nucleofection mix (adjusting the volume to a final volume of 10 µL):
    a. 6.4 µg ABE or CBE mRNA
    b. 6.4 µg sgRNA
9. Mix gently without vortexing and transfer the entire mixture into the nucleofection tips (Neon) or cuvettes (LONZA). Take care to avoid introducing air bubbles.
10. Execute the nucleofection using the following parameters:
    a. Keratinocytes: 1700 V/20 ms/1 pulse (Neon™) or program CM147 (LONZA®)
    b. Fibroblasts: 1400 V/20 ms/2 pulses (Neon™) or program DT130 (LONZA®)
11. Immediately after nucleofection, plate the cells in their respective culture medium.
12. Incubate under standard culture conditions to allow for recovery and subsequent growth:
    a. $1–2 \times 10^5$ cells in a 12-well plate
    b. $2–4 \times 10^5$ cells in a 6-well plate

3.5 Base Editing Result Analysis

3.5.1 General Considerations

1. Extract genomic DNA after Base Editing nucleofection to amplify the target region.
2. Sanger sequencing should be performed as a first screening analysis method, using a previously designed forward primer located inside the amplified amplicon (*see* **Note 21**).
3. A reverse primer may also be designed with the same objective as before, in case a low signal chromatogram is obtained.
4. Online free software, such as Primer-BLAST (https://www.ncbi.nlm.nih.gov/tools/primer-blast/) or Primer3plus (https://www.primer3plus.com/index.html), can be used for the PCR primers design.

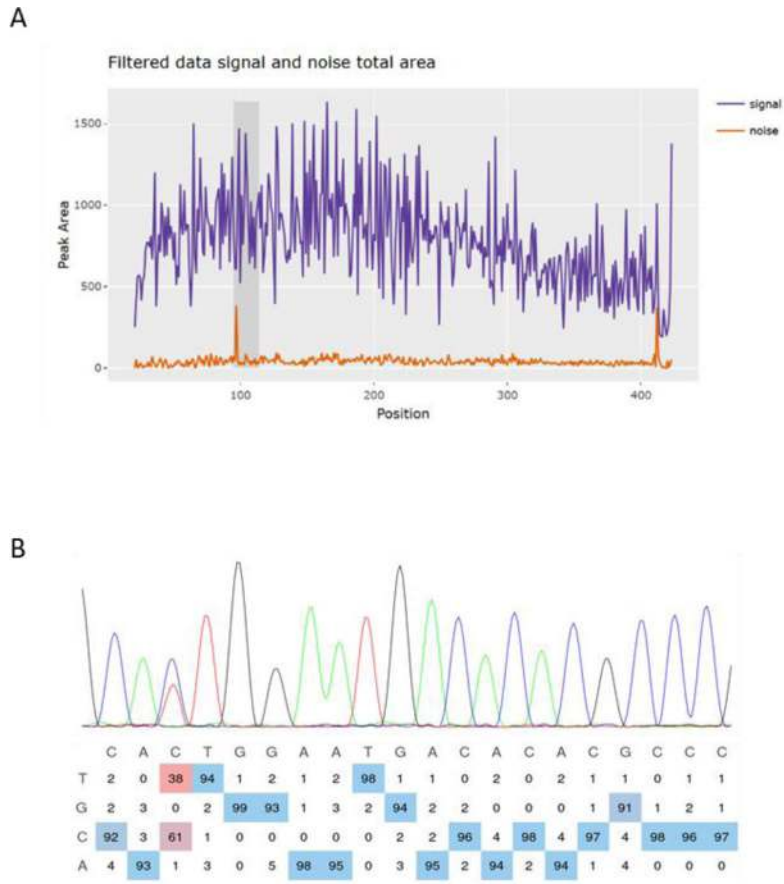


Fig. 4 Analysis of sequencing data using EditR. **A** Background noise levels in the analyzed samples were determined from Sanger sequencing chromatograms. **B** Quantification of base editing efficiency at the target site, showing the frequency of base conversions as calculated by EditR

5. In case quantitative information is needed from Sanger Sequencing, several open-source tools are available, such as EditR [19] and BEAT (base editing analysis tool) [20].
6. Due to the limited analytical depth of Sanger sequencing, targeted deep sequencing is highly recommended for analysis of base editing outcomes, based on its high read depth and capability of mutation identifications, even at very low frequencies, being able to detect bystanders in low frequency.

3.5.2 Editing Quantification by Sanger Sequencing

Option 1. EditR

1. This R-based software's quantification takes into account the area's change in the chromatogram peaks to quantify the percentages of base-edited nucleotides.
2. Provide the ~20 bp RNA guide sequence employed in the experiment, and the ab1 Sanger sequence file of the edited region (300–700 bp).
3. Refine the uploaded sequence file, providing information about the 5′ start and the 3′ end of the good-quality Sanger sequencing trace. In this way, low-quality regions can be trimmed manually.
4. The software automatically generates and provides to the user in the "Data QC" section insights in terms of the percent of noise detected across the sequence file analyzed. Evaluate the presence of some high-noise regions that may affect the sensitivity of the editing quantification (Fig. 4A).

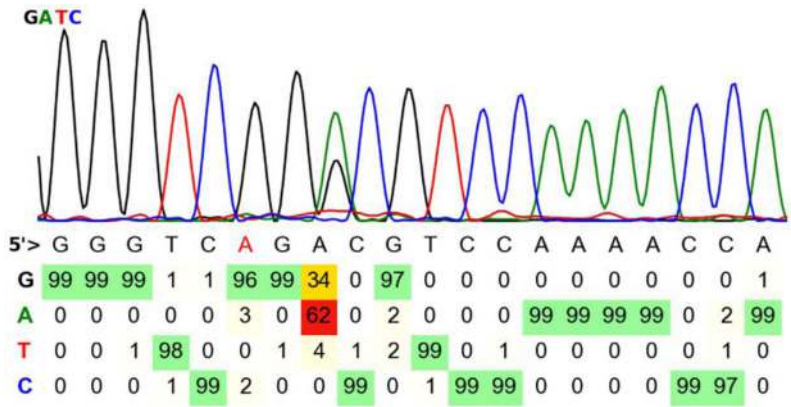


Fig. 5 Analysis of base editing efficiency by Sanger sequencing using BEAT. Editing efficiency at the target site was quantified from Sanger sequencing chromatograms using the BEAT analysis tool, showing the frequency of base conversions at the indicated positions

5. A chromatogram of the protospacer region is then generated to determine if the uploaded sequence correctly aligns with the sgRNA sequence provided (Fig. 4B) (*see* **Note 22**).

Option 2. BEAT

1. BEAT is a Python-based software developed to analyze and quantify base editing events from Sanger sequencing samples.
2. The ab1 sequence file has to be provided, coupled with the input name of the sample, the ~20 bp RNA protospacer sequence employed in the base editing experiment, and the target base position along the RNA guide sequence.
3. BEAT software automatically aligns the spacer sequence provided with the uploaded sequencing trace, detecting and determining the position of the target region (*see* **Note 23**).
4. The start and the end trimming positions of the sequence should be provided to ensure a correct estimation of the average background noise for each base in the trace (*see* **Note 24**).
5. The percentage of each base at each position is then calculated and represented in a heat map.

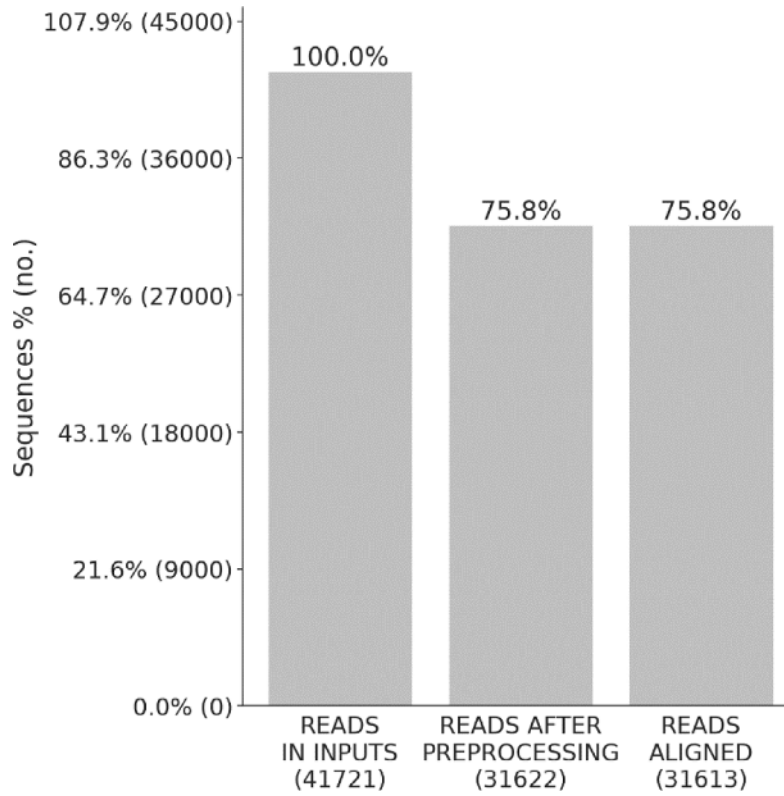


Fig. 6 Representation of the number and percentages of sequenced reads after preprocessing and alignment steps relative to the input reads

3.5.3 Deep Sequencing Analysis

Step 1. Sample Preparation Considerations for Targeted Deep Sequencing

1. Illumina® short-read sequencing can be easily used for base editing events analysis, with a designed amplicon spanning 150–500 bp and a final concentration of at least 500 ng of double-stranded DNA.
2. Illumina adapter sequences have to be included in the primer design in order to ensure a correct sequencing workflow during the library preparation by the company.
3. A minimum of 10,000–20,000 reads is generally recommended for bulk populations, but a higher coverage may be required for the detection of events with low detectability.
4. Editing levels at the target site should be compared with experimental unedited controls to establish if the detected editing levels are due to background noise or base editing activity (Fig. 5).

Step 2. Analysis of Deep Sequencing Data

1. CRISPResso2 [21] software, which is already configured for base editing events analysis, can be used for the analysis of Deep sequencing data.
2. This software analyses editing events in the sgRNA region and in its proximity, detecting on-target modifications as well as low-frequency events (Fig. 6).
3. The type of sequence analysis to be performed (paired-end reads, single-end reads, interleaved reads, or batch processing) has to be selected by the user.
4. Once selected, the input fastq raw files have to be uploaded, together with the target amplicon and the sgRNA used in the experiment.

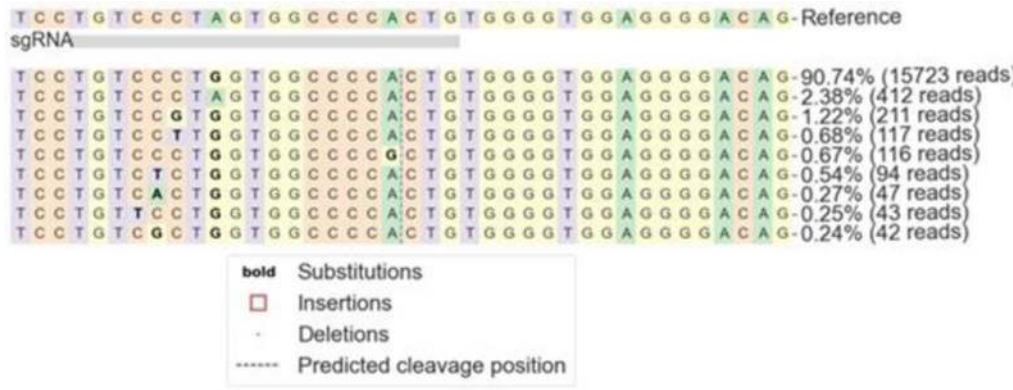


Fig. 7 Representation of the distribution of identified alleles around the sgRNA target site. The percentage of each allele is calculated and indicated, together with the number of reads detected, on the right

5. Some technical parameters can be further refined manually to optimize the sequence analysis by the software. The minimum homology for alignment to an amplicon can be chosen, for example, to define the threshold of homology between the input sequence and the target amplicon, below which reads are discarded.
6. The software finally generates a report comprised of several pieces of information related to the input fastq sequence analyzed. A graph with the distribution of identified alleles around the target site is generated (Fig. 7).

4 Notes

1. The NGG PAM is traditionally the one recognized by most of the base editors, but in recent years, new ones have been generated and defined near-PAMless editors. They are characterized by a less stringent PAM recognition, such as NYN or NRN (where R stands for A or G nucleotides, and Y stands for C or T nucleotides).
2. To increase the mRNA stability, the 3′ untranslated region (3′ UTR) from Xenopus β-globin or the bovine growth hormone, together with the polyadenylation (poly-A) signal, can be included at the end of the construct.
3. We recommend preparing the plasmid digestion in a 150–200 μL volume to facilitate the plasmid purification process. Depending on the number of reactions intended to prepare, up to 30 μg of plasmid is required for the digestion.
4. During linearized plasmid purification, to confirm that there are no traces of phenol–chloroform, you can vortex the collected aqueous phase, and if it turns whitish, repeat the phenol-chloroform purification until it remains transparent.
5. Alternatively, instead of plasmid linearization, PCR amplification can be performed using the Phusion U green multiplex master mix (NEB) following the manufacturer's protocol.
6. To increase the mRNA stability at the 5′ end, different CAP analogs can be used. ARCA nucleosides are more stable than standard cap analogs and are included in the mMESSAGE mMACHINE™ T7 ULTRA kit. The most stable nucleosides for the CAP are the CleanCap ones, available in the mMESSAGE mMACHINE™ T7 mRNA Kit with CleanCap™ Reagent AG. If using the mMESSAGE mMACHINE™ T7 mRNA Kit with CleanCap™ Reagent AG kit, be sure that the T7 promoter includes the AG motif, as described in the manufacturer's protocol.

7. For some applications, such as in vivo delivery, stabilization of BE mRNA may be enhanced by substituting nucleosides with modified analogs such as pseudouridine-5′triphosphate (Ψ-UTP).
8. This step is optional, but highly recommended.
9. All reagents are included in the mMACHINE™ T7 ULTRA kit, while for the rest of the kits described in this protocol, the poly(A) tailing kit needs to be bought separately.
10. To increase the mRNA concentration, two reactions from 1 μg DNA template can be purified together in a single column.
11. Alternatively, to the use of the RNeasy Mini columns kit, the mRNA can be precipitated with Lithium Chloride following the instructions described by the mMESSAGE mMACHINE protocol.
12. To confirm the size of the mRNA produced, this can be assessed using the Agilent Fragment Analyzer according to the manufacturer's guidance.
13. Bring the Ficoll to room temperature before use.
14. PBE can be prepared and stored at 4°C for up to 1 week.
15. If cell clumping occurs, add DNase I (10 μL per mL of wash volume), incubate for 5 min at room temperature, and gently pipette to dissociate aggregates.
16. It is crucial to wash the cells, as some proteins present in the growth medium can interfere with the electroporation.
17. For cytosine base editing in HSPCs, we recommend the use of CBE derived from ABEs (TAD versions) and the use of the T7 mRNA Kit with CleanCap™ Reagent AG for its production.
18. It is important to avoid air bubbles during electroporation as air bubbles cause arcing, compromising cell viability and transfection efficiency.
19. After the electroporation in Amaxa 4D Lonza, a green cross appears to indicate an accurate electroporation. If the cross is yellow or red, you can select the strip well or cuvette to get the error code and look for extra information in the manufacturer's protocol.
20. Incubation time with Trypsin–EDTA in adherent cells depends on cell type and confluency. Fibroblasts typically detach within 7–10 min, while keratinocytes may require 15–20 min depending on the degree of confluency.
21. In any case, the use of Sanger sequencing to assess editing efficiency is best suited for analyses that do not require a high level of analytical depth. It is generally required and advised as a cost-effective and rapid method for the assessment of

editing outcomes. Due to its low sensitivity, it reliably detects editing events corresponding to around 5%–10%. Below this threshold, data should be interpreted with caution due to potential bias from chromatogram noise.

22. Analysis of detected traces within these target regions is compared with the ones all along the sequencing files, in order to determine and quantify if there is a significant difference in the base editing activity detected. The percent of editing is calculated based on traces within the protospacer region, corresponding to each nucleotide (A, T, G, or C).
23. Sequencing files can also be uploaded and analyzed in batch if a common protospacer sequence has been employed.
24. By default, approximately the first 100 and the last 50 nucleotides of the sequence are trimmed to ensure a correct estimation of the average background noise for each base in the trace. The user can modify the standard parameters if the low-quality sequencing data have not been sufficiently removed.

Acknowledgments

The publication is based upon work by COST Action CA21113: Genome Editing for the Treatment of Human Diseases (https://www.genehumdi.eu), supported by European Cooperation in Science and Technology (COST).

Competing Interests The authors declare no competing interests.

References

1. Yeh CD, Richardson CD, Corn JE (2019) Advances in genome editing through control of DNA repair pathways. Nat Cell Biol 21:1468–1478
2. Paquet D, Kwart D, Chen A et al (2016) Efficient introduction of specific homozygous and heterozygous mutations using CRISPR/Cas9. Nature 533:125–129
3. Rees HA, Yeh WH, Liu DR (2019) Development of hRad51–Cas9 nickase fusions that mediate HDR without double-stranded breaks. Nat Commun 10:2212
4. Rees HA, Liu DR (2018) Base editing: precision chemistry on the genome and transcriptome of living cells. Nat Rev Genet 19:770–788
5. Kim JS (2018) Precision genome engineering through adenine and cytosine base editing. Nat Plants 4:148–151
6. Komor AC, Kim YB, Packer MS et al (2016) Programmable editing of a target base in genomic DNA without double-stranded DNA cleavage. Nature 533:420–424
7. Gaudelli NM, Komor AC, Rees HA et al (2017) Programmable base editing of T to G C in genomic DNA without DNA cleavage. Nature 551:464–471
8. Huang TP, Zhao KT, Miller SM et al (2019) Circularly permuted and PAM-modified Cas9 variants broaden the targeting scope of base editors. Nat Biotechnol 37:626–631
9. Wang Y, Zhou L, Liu N, Yao S (2019) BE-PIGS: a base-editing tool with deaminases inlaid into Cas9 PI domain significantly expanded the editing scope. Signal Transduct Target Ther 4:36
10. Richter MF, Zhao KT, Eton E et al (2020) Phage-assisted evolution of an adenine base

editor with improved Cas domain compatibility and activity. Nat Biotechnol 387(38):883–891
11. Koblan LW, Doman JL, Wilson C et al (2018) Improving cytidine and adenine base editors by expression optimization and ancestral reconstruction. Nat Biotechnol 36:843–848
12. Huang TP, Heins ZJ, Miller SM et al (2023) High-throughput continuous evolution of compact Cas9 variants targeting single-nucleotide-pyrimidine PAMs. Nat Biotechnol 41:96–107
13. Walton RT, Christie KA, Whittaker MN, Kleinstiver BP (2020) Unconstrained genome targeting with near-PAMless engineered CRISPR-Cas9 variants. Science 368:290–296
14. Miller SM, Wang T, Randolph PB et al (2020) Continuous evolution of SpCas9 variants compatible with non-G PAMs. Nat Biotechnol 38:471–481
15. Komor AC, Zhao KT, Packer MS et al (2017) Improved base excision repair inhibition and bacteriophage Mu Gam protein yields C:G-to-T:A base editors with higher efficiency and product purity. Sci Adv 3 (8):eaao4774
16. Thuronyi BW, Koblan LW, Levy JM et al (2019) Continuous evolution of base editors with expanded target compatibility and improved activity. Nat Biotechnol 37:1070–1079
17. Lam DK, Feliciano PR, Arif A et al (2023) Improved cytosine base editors generated from TadA variants. Nat Biotechnol 41:686–697
18. Neugebauer ME, Hsu A, Arbab M et al (2023) Evolution of an adenine base editor into a small, efficient cytosine base editor with low off-target activity. Nat Biotechnol 41:673–685
19. Kluesner MG, Nedveck DA, Lahr WS et al (2018) EditR: a method to quantify base editing from Sanger sequencing. Cris J 1:239–250
20. Xu L, Liu Y, Han R (2019) BEAT: a Python program to quantify base editing from Sanger sequencing. Cris J 2:223
21. Clement K, Rees H, Canver MC et al (2019) CRISPResso2 provides accurate and rapid genome editing sequence analysis. Nat Biotechnol 37:224–226

Open Access This chapter is licensed under the terms of the Creative Commons Attribution-NonCommercial-NoDerivatives 4.0 International License (http://creativecommons.org/licenses/by-nc-nd/4.0/), which permits any noncommercial use, sharing, distribution and reproduction in any medium or format, as long as you give appropriate credit to the original author(s) and the source, provide a link to the Creative Commons license and indicate if you modified the licensed material. You do not have permission under this license to share adapted material derived from this chapter or parts of it.

The images or other third party material in this chapter are included in the chapter's Creative Commons license, unless indicated otherwise in a credit line to the material. If material is not included in the chapter's Creative Commons license and your intended use is not permitted by statutory regulation or exceeds the permitted use, you will need to obtain permission directly from the copyright holder.





Chapter 20

Nucleofection-Based CRISPR/Cas Delivery in Human T Cells for Immunotherapy Applications

María Ortiz-Bueno, Alejandro Millán-López, Kornel Labun and Karim Benabdellah

Abstract

Electroporation-based delivery of CRISPR/Cas systems has emerged as a powerful and versatile approach for gene editing in primary human T cells, enabling efficient, transient, and nonviral modification while minimizing genomic integration risks. This chapter focuses on the principles and practical implementation of electroporation (nucleofection) for the delivery of Cas9 ribonucleoprotein (RNP) complexes into human T cells, highlighting critical parameters that influence editing efficiency, cell viability, and scalability for research and clinical applications. We provide a comprehensive protocol for multiplex gene editing in primary human T cells using Cas9 RNP electroporation, including optimization of cell activation status, buffer composition, electroporation settings, and post-electroporation recovery. Particular emphasis is placed on strategies to achieve high-efficiency disruption of target loci such as *TRAC* and *B2M*, enabling the generation of edited T cell products with defined functional properties. As a representative application, we describe how this delivery platform can be integrated with chimeric antigen receptor (CAR) engineering to produce edited CAR-T cells, including universal "off-the-shelf" designs with reduced risks of graft-versus-host disease and immune rejection. Downstream evaluation methods, including multiparameter flow cytometry for assessing editing efficiency and immunophenotype, are also outlined.

Keywords T cells, CRISPR/Cas9, RNP delivery, Electroporation, Nucleofection, Gene editing, Primary cells, Nonviral delivery

1 Introduction

Efficient delivery of gene editing reagents into primary human T cells is a critical determinant of successful genome engineering and remains a central technical challenge in the field [1]. Electroporation-based approaches, particularly nucleofection, have emerged as leading non-viral strategies for introducing CRISPR/Cas components directly

These authors contributed equally: María Ortiz-Bueno, Alejandro Millán-López

Duško Lainšček et al. (eds.), *CRISPR Delivery*, Methods in Molecular Biology, vol. 3075,
https://doi.org/10.1007/978-1-0716-5547-4_20,
© The Author(s) 2027

into T lymphocytes, enabling rapid, transient, and highly efficient genome editing while preserving cell viability and function [1–3].

These delivery platforms are especially well-suited for multiplex gene editing applications, such as the simultaneous disruption of *TRAC* and *B2M* to generate T cell receptor (TCR)- and HLA-deficient cells. Such double *knockout* (DKO) strategies are essential for the development of universal "off-the-shelf" T cell therapies, as they mitigate the risks of graft-versus-host disease and host immune rejection. The use of Cas9 ribonucleoprotein (RNP) complexes delivered via nucleofection further enhances editing precision and reduces prolonged nuclease exposure, thereby limiting *off-target* effects [4].

Within this framework, CRISPR/Cas-mediated engineering can be readily integrated with downstream applications such as CAR expression, enabling the generation of next-generation engineered T cell products with improved safety, scalability, and clinical potential [1–4]. In this context, nucleofection-based delivery represents a key enabling technology for advancing both fundamental studies and translational applications of gene-edited human T cells [1–4].

The combination of CRISPR/Cas9-based editing with CAR-T cell manufacturing has proven particularly powerful for the generation not only of allogeneic, off-the-shelf products through disruption of endogenous TCR and MHC class I expression, but also for the functional enhancement of autologous products via *knockout* of immune checkpoint genes [4–6]. Against this background, there has been growing interest in nonviral delivery methods that enable the transient introduction of gene editing components, thereby providing tighter temporal control over their activity while simplifying and reducing the cost of manufacturing processes. In particular, nucleofection-based delivery of CRISPR/Cas systems allows rapid but short-lived intracellular presence of editing machinery, which limits prolonged nuclease exposure and contributes to an improved safety profile compared to viral vectors [7–9]. Among these alternatives, electroporation has established itself as the most widely used nonviral technology for the intracellular delivery of plasmid DNA, mRNA, or ribonucleoprotein (RNP) complexes, including CRISPR/Cas9 components, into primary T lymphocytes [4–9]. Several recent reviews highlight that, relative to viral approaches, electroporation substantially reduces manufacturing costs and timelines, eliminates the risk of insertional mutagenesis, and achieves high transfection efficiencies with acceptable cell viabilities when pulse parameters and buffer formulation are appropriately optimized [6, 10, 11].

In this chapter, we describe a comprehensive protocol for CRISPR/Cas9-mediated multiplex genome editing in activated primary human T cells via electroporation-based RNP delivery, encompassing T cell isolation and activation, lentiviral CAR transduction, RNP complex assembly, electroporation using the MaxCyte® STX system, and downstream functional validation.

2 Materials

2.1 T Cell Isolation, Culture, and Electroporation

2.1.1 Reagents

1. Human peripheral blood mononuclear cells (PBMCs) were obtained from three independent healthy volunteer donors to account for interdonor biological variability in T cell composition and editing efficiency. Written informed consent was obtained from all donors in accordance with applicable ethical and institutional guidelines.
2. Pan T Cell Isolation Kit, Human (Miltenyi Biotec®, Bergisch Gladbach, Germany), for untouched negative immunomagnetic selection of the total T cell fraction from PBMCs.
3. TexMACS Medium (Miltenyi Biotec®), a serum-free, defined formulation optimized for primary human T lymphocyte expansion, was used as the base culture medium throughout isolation, activation, and pre-electroporation culture phases.
4. Penicillin/Streptomycin solution (e.g., 100×, BIOWEST) added to TexMACS medium (TX medium) at a final working concentration of 1× to prevent bacterial contamination during cell culture.
5. Recombinant human interleukin-2 (rhIL-2), interleukin-7 (rhIL-7), and interleukin-15 (rhIL-15), supplied as a 1000× concentrated stock solution (Miltenyi Biotec®), for supplementation of culture medium to support T cell survival, proliferation, and maintenance of a less differentiated phenotype during ex vivo expansion [12].
6. T Cell TransAct (Miltenyi Biotec®), a bead-free colloidal polymeric nanomatrix conjugated to humanized anti-CD3 and anti-CD28 agonistic antibody fragments, for polyclonal activation of primary human T cells prior to any editing.
7. Anti-CD3/CD28 activation beads for polyclonal T cell stimulation prior to electroporation, providing simultaneous TCR signal 1 (anti-CD3) and co-stimulatory signal 2 (anti-CD28).
8. Replication-incompetent lentiviral vector, produced by transient transfection of HEK293T cells (ATCC CRL-3216).
9. Phosphate-buffered saline (PBS, pH 7.4), prepared from standard laboratory reagents, for cell washing steps throughout the isolation and culture procedure.
10. Trypan blue solution (0.4% in PBS) for dye exclusion-based viability assessment in the improved Neubauer hemocytometer.

2.1.2 Equipment

1. Class II Type A2 biological safety cabinet (laminar airflow, 70% air recirculation with HEPA filtration).
2. AutoMACS Pro Separator (Miltenyi Biotec®) with automated depletion program for untouched negative isolation of CD3+ T cells from PBMC fraction, for automated immunomagnetic depletion of non-T cell populations and enrichment of CD3+ T cells.
3. CO_2 incubator set to 37°C with 5% CO_2 and ≥95% relative humidity.
4. Refrigerated benchtop centrifuge with swing-bucket rotor compatible with 15 and 50 mL conical tubes.
5. Improved Neubauer hemocytometer (depth 0.1 mm, 0.0025 mm^2 grid area) with coverslips, for trypan blue exclusion-based viability assessment.
6. BD FACS Canto II flow cytometer equipped with 488 and 633 nm laser lines and the standard three-detector configuration (FITC, PE, and APC channels), for immunophenotypic characterization of isolated T cell populations.
7. Inverted light microscope (10× and 40× objectives) for morphological inspection of cell cultures.
8. Calibrated micropipettes (range: 2–1000 µL) and serological pipettes.
9. Electronic pipette controller.
10. Water bath set to 37°C for reagent prewarming.
11. MaxCyte STX Scalable Transfection System (MaxCyte, Inc.®, Gaithersburg, USA), a flow electroporation platform that delivers precisely controlled electrical pulses to cell suspensions through closed, sterile processing assemblies. MaxCyte SOC (Static Optical Cuvette) Processing Assembly, model SOC25x3 (MaxCyte, Inc.®), with a nominal capacity of 25 µL per chamber and a three-chamber configuration, designed for small-scale process optimization and research-grade electroporation of primary human T cell samples.

2.2 RNP Complex Formation Reagents

1. Alt-R S.p. HiFi Cas9 Nuclease V3 (Integrated DNA Technologies®, Coralville, USA), a high-fidelity variant of *Streptococcus pyogenes* Cas9 engineered to reduce *off-target* double-strand break activity while maintaining *on-target* editing efficiency comparable to wild-type Cas9, supplied as a recombinant protein at a concentration of 61 µM in storage buffer [13].

2. Chemically synthesized single-guide RNAs (sgRNAs) targeting the *TRAC* locus (encoding the T cell receptor alpha constant region) and the *B2M* locus (encoding beta-2-microglobulin, a component of the MHC class I complex) with chemical modifications (2′ O-Methyl RNA/Phosphorothioated in both) at the 3′ and 5′ termini to confer nuclease resistance and enhance intracellular stability. The concentration used was 10 nmol.
3. MaxCyte Electroporation Buffer (MaxCyte, Inc.®, Gaithersburg, USA) for T cell nucleofection, ensuring physicochemical consistency between the RNP pre-complexing and delivery steps.
4. Nuclease-free water for preparation of sgRNA working dilutions and RNP assembly reactions.
5. Sterile low-binding microcentrifuge tubes (0.6 mL), RNase-free and DNA-free certified, for all RNP assembly and storage steps to minimize adsorptive loss of protein and RNA components to tube surfaces.

3 Methods

The following section describes a stepwise workflow for the generation of CRISPR/Cas9-edited, CAR-expressing primary human T cells, encompassing T cell isolation from cryopreserved PBMCs, lentiviral transduction with the CAR construct, and electroporation-based delivery of RNP complexes for simultaneous disruption of the *TRAC* and *B2M* loci (double *knockout*: "DKO"). All steps are performed under sterile conditions in a Class II Type A2 biological safety cabinet. Unless otherwise stated, centrifugation steps are carried out at 300 × *g* for 5 min at room temperature (RT), and all culture media are pre-warmed to 37°C prior to use.

3.1 Day 0: CD3+ T Cell Isolation, Seeding, and Activation

1. Thaw cryopreserved PBMCs from the desired donor in a 37°C water bath and transfer to a 15 mL conical tube containing prewarmed TX medium. Centrifuge at 300 × *g* for 5 min, discard the supernatant, and resuspend the pellet in an appropriate 10 mL of TX for cell counting and viability assessment by trypan blue exclusion using the improved Neubauer hemocytometer.
2. Proceed to $CD3^+$ T cell enrichment by automated negative immunomagnetic selection using the Pan T Cell Isolation Kit, Human (Miltenyi Biotec®), on the AutoMACS Pro Separator following the standard "T Cell (human) untouched" depletion program or equivalent.
3. Seed isolated $CD3^+$ T cells in G-REX 24-well plates at a density of 2×10^6 cells per well in 1 mL of TX medium supplemented

with penicillin/streptomycin (1×), IL-7 (150 U/mL), IL-15 (85 U/mL), and T Cell TransAct (10 µL per well; Miltenyi Biotec®) for polyclonal activation. This step is essential as T cell activation status critically affects editing efficiency.

4. Transfer the G-REX to the CO_2 incubator (37°C, 5% CO_2, 95% RH) and incubate undisturbed for 24 h (*see* **Note 1**).

3.2 Days 1 (+24 h) and 2 (+16 h): Lentiviral Transduction of T Cells and Medium Replenishment

1. Without removing the medium, add directly to each well the pre-calculated volume of titrated CAR lentiviral vector stock required to achieve the desired multiplicity of infection (MOI) (*see* **Note 2**). Do not replace the medium prior to transduction.
2. Return G-REX to the incubator and incubate for 16 h (until the next day).
3. Then, on day 2, perform a medium refill by adding TX medium supplemented only with IL-7 (150 U/mL) and IL-15 (85 U/mL) directly to each well to bring the total culture volume to 8 mL and return G-REX to the incubator (*see* **Note 3**). It is important not to remove the existing medium.

3.3 Day 3 (+24 h): Gene Editing by Electroporation (DKO TCR/HLA)

3.3.1 Pre-Electroporation Preparation

1. Switch on the MaxCyte® STX electroporation system and the heat block, and allow both to equilibrate to operating temperature prior to beginning cell preparation. Prewarm 1 mL of unsupplemented TX medium (without cytokines or penicillin/streptomycin) per electroporation condition in the incubator. This will be used for post-electroporation recovery culture.
2. Prepare the RNP complexes with all the reagents (kept on ice throughout to preserve enzymatic activity and prevent protein degradation) by combining the sgRNA and HiFi Cas9 protein components in MaxCyte® electroporation buffer at a molar ratio of 3:1 (sgRNA:Cas9) [7] according to the formulation below, and incubate at 37°C in the heat block for 20 min.

3.3.2 RNP Complex Formulation for SOC25x3 Cuvette (Per Condition, 2× 10^6 cells)

a) sgRNA 1 (TRAC): 0.3 µL
b) sgRNA 2 (B2M/HLA): 0.3 µL
c) Alt-R HiFi Cas9 protein: 0.32 µL
d) Total RNP volume: 0.92 µL
e) Cells resuspended in MaxCyte® Electroporation Buffer: 15 µL

Final Volume Per Chamber: ~20 µL

1. Remove 6 mL of conditioned medium from each G-REX well using a serological pipette and gently resuspend the cells in the remaining 2 mL. Transfer the suspension to a 15 mL conical

tube and centrifuge at 300 × *g* for 5 min. Aspirate the supernatant completely, resuspend the pellet in PBS, and perform a cell count and viability assessment. It is important to check this step as high cell density improves efficiency but may reduce viability, and, in this case, cell viability must be ≥80% before proceeding with electroporation.

2. Aliquot the volume of cell suspension corresponding to 2×10^6 cells per condition into individual 1.5 mL microcentrifuge tubes, topping up with PBS to 1 mL. Centrifuge using a minispin centrifuge at 300 × *g* for 5 min and carefully remove the supernatant with a P1000 pipette, ensuring the cell pellet is as dry as possible before adding the RNP–buffer mixture.
3. To prepare the electroporation master mix, strictly observe the following order of addition:
    a. aspirate 15 μL of MaxCyte® Electroporation Buffer, keeping the pipette tip only minimally submerged to avoid excess buffer on the outer tip surface;
    b. dispense the buffer directly onto the preassembled RNP and resuspend thoroughly; and
    c. transfer the complete RNP–buffer mixture onto the dry cell pellet and resuspend gently. This final volume (~20 μL) constitutes the sample to be loaded into the processing assembly (*see* **Note 4**).

3.3.3 Electroporation

1. Load the sample into the SOC25 × 3 cuvette processing assembly by inserting the pipette tip gently until it contacts the silicone base of the well. Dispense to the first stop of the pipette, then slightly retract the tip and expel the remaining volume from above the liquid surface to prevent bubble formation, which may compromise electroporation performance.
2. Prior to electroporating the experimental samples, perform a blank pulse using an empty or buffer-only assembly to initialize the instrument. Electroporate all samples using the "*Expanded T cell 3*" preprogrammed protocol on the MaxCyte® STX system.
3. Immediately after electroporation, transfer the processing assemblies to the CO_2 incubator and allow cells to recover undisturbed for 10 min at 37°C.
4. Recover cells from the assembly by washing the chamber with prewarmed unsupplemented TX medium. Resuspend and seed the recovered cells at a density of 2×10^6 cells/mL in 1 mL of unsupplemented TX medium per well in the G-REX. After 5 h of recovery at 37°C, add 7 mL of TX medium supplemented with IL-7 (150 U/mL), IL-15 (85 U/mL), and penicillin/

streptomycin (1×) per well. Return to the incubator and allow cells to expand undisturbed (*see* **Note 5**).

3.4 Day 8 (+7 Days Post-Transduction): Product Assessment

1. Carefully aspirate 6 mL of conditioned medium from each well using a serological pipette without disturbing the cell layer.
2. Harvest a representative aliquot of cells for flow cytometric assessment of gene editing efficiency (surface loss of CD3 and B2M) and CAR expression (%CAR+ cells). Therefore, based on the results of the editing and CAR expression analysis, proceed to the planning and scheduling of downstream functional assays (*see* **Note 6**).

3.5 Evaluation of Editing Efficiency

3.5.1 Flow Cytometry for the Efficiency of Gene Editing

Comprehensive downstream characterization of the edited T cell product is essential to confirm the efficiency and specificity of CRISPR/Cas9-mediated gene disruption and to assess the functional and phenotypic integrity of the cells following the electroporation procedure. In this protocol, downstream analysis encompasses two complementary approaches: multiparameter flow cytometry, which enables simultaneous quantification of editing efficiency through surface loss of the targeted proteins, and characterization of T cell subset composition, memory differentiation status, activation state, and co-inhibitor expression. Furthermore, genomic DNA extraction provides the cellular material required for molecular verification of indel formation at the *TRAC* and *B2M* loci, although the full ddPCR execution steps are not included in this protocol.

Fluorochrome-conjugated monoclonal antibodies for multiparameter flow cytometric immunophenotyping of edited T cell products, including assessment of gene editing efficiency (surface loss of CD3 and B2M), T cell subset distribution, memory and differentiation status, activation profile, and co-inhibitory receptor expression [14] (*see* **Notes 7 and 8**).

The efficiency of CRISPR/Cas9-mediated gene disruption was assessed by multiparameter flow cytometry on day 7 post-transduction, using surface loss of the targeted proteins as a direct functional readout of successful editing at each locus.

1. Abrogation of *TRAC* expression was evaluated by the absence of CD3 surface staining, as loss of the T cell receptor alpha constant region prevents assembly and membrane trafficking of the TCR/CD3 complex [15, 16]. Disruption of the *B2M* locus, encoding beta-2-microglobulin, the invariant light chain required for MHC class I complex folding and surface presentation, was confirmed by loss of B2M surface expression detected with an anti-B2M antibody conjugated to PE (BD Biosciences®).

2. Cells were co-stained with an anti-CD3 antibody conjugated to PerCP-Cy5.5 (BD Biosciences®) to allow simultaneous quantification of both *knockouts* within the same panel, and 7-AAD was included in all acquisitions for live/dead cell discrimination.
3. Additionally CAR surface expression was not assessed by antibody staining; instead, transduction efficiency was determined by direct detection of the blue fluorescent protein (BFP) reporter co-expressed with the CAR construct, allowing simultaneous and independent quantification of the transduced (%BFP+) and edited (CD3− B2M−) populations without additional staining steps or spectral compensation requirements (*see* **Note 9**).
4. All samples were acquired on a BD FACS Canto II flow cytometer and analyzed using appropriate gating strategies as illustrated in the figure below (Fig. 1).

3.5.2 Flow Cytometry Workflow for Phenotypic, Exhaustion, and Activation Profiling

On day 7 posttransduction, CAR DKO T cells were characterized by multiparameter flow cytometry using a BD FACS Canto II flow cytometer. Three independent panels were used to assess memory phenotype, exhaustion profile, and activation status within the

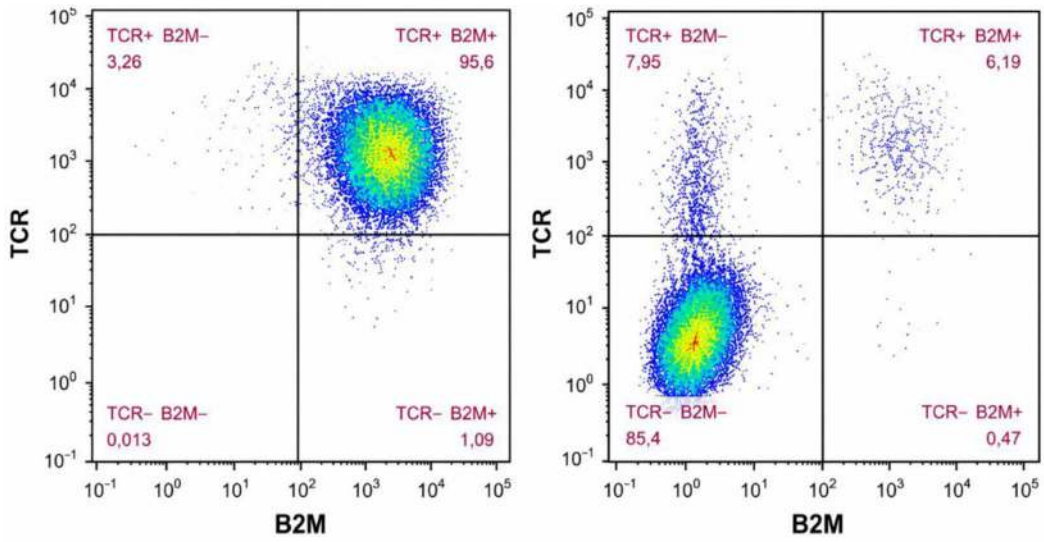


Fig. 1 Representative flow cytometry dot plots showing surface TCR (*TRAC*) and HLA class I (*B2M*) expression in bulk-edited T cells. Non-edited CAR WT cells are shown in the left panel, whereas CRISPR/Cas9-edited CAR DKO cells are shown in the right panel. Quadrants indicate the distribution of TCR and HLA expression patterns, and percentages are shown within each quadrant. The edited population displays the expected reduction in TCR and HLA co-expression together with enrichment of the TRAC^{-}B2M^{-} fraction, confirming efficient double *knockout* of the targeted loci

CAR-expressing population. CAR-expressing cells were identified by intrinsic BFP fluorescence encoded by the CAR construct rather than by antibody staining. Each panel was acquired independently using panel-specific compensation controls and fluorescence minus one (FMO) controls to support accurate gate placement and minimize spectral overlap.

1. For each staining condition, 2×10^5 cells were transferred into individual tubes, washed once with PBS, and resuspended in 100 µL of PBS. Cells were incubated for 20 min at 4°C in the dark with the corresponding antibody cocktail. Antibodies were used at a final dilution of 1:50, corresponding to 2 µL of each antibody per 100 µL staining volume. After incubation, cells were washed once with PBS and resuspended in acquisition buffer before analysis. For the exhaustion and activation panels, 7-AAD was added immediately before acquisition for live/dead discrimination.
2. Data analysis followed a hierarchical gating strategy. Lymphocytes were first identified according to forward scatter (FSC) and side scatter (SSC) properties, followed by singlet discrimination. For panels including 7-AAD, viable cells were selected by exclusion of 7-AAD-positive events. CAR+ cells were then identified on the basis of intrinsic BFP fluorescence and subsequently subdivided into CD4+ and CD8+ populations for downstream analysis. Finally, memory, exhaustion, and activation readouts were quantified as percentages of the parent CAR+ CD4+ or CAR+ CD8+ population.

Table 1

Phenotypic panel used for flow cytometric characterization of CAR DKO T cells on day 7 post-transduction. This panel was used to identify CAR+ CD4+ and CAR+ CD8+ T cells and to define memory differentiation subsets based on CD45RO, CCR7, CD62L, and CD95 expression

Channel	Fluorochrome	Marker	Clone
V1	BFP	CAR	–
V2	VioGreen	CD4	REA623
B1	FITC	CD3	REA613
B2	PE	CD95	REA738
B3	PerCP-Vio700	CCR7 (CD197)	REA546
B4	PE-Vio770	CD62L	REA615
R1	APC	CD45RO	REA611
R2	APC-Vio770	CD8	REA734

a) Phenotypic analysis
Phenotypic characterization was performed to define the differentiation profile of CAR DKO T cells by assessing the expression of CD45RO, CCR7 (CD197), CD62L, and CD95 within the CAR+ CD4+ and CAR+ CD8+ compartments. These markers were used to classify cells into naïve, stem cell memory, central memory, effector memory, and terminal effector subsets. They are all summarized in Table 1.
Furthermore, memory differentiation subsets within CAR^+ T cells were defined according to the criteria outlined below, in Table 2.

b) Exhaustion analysis
Exhaustion profiling was performed by assessing PD-1, TIM-3, and LAG-3 expressions within the CAR+ CD4+ and CAR+ CD8+ populations. Single-positive, double-positive,

Table 2

Definition of memory differentiation subsets within CAR+ T cells based on CD45RO, CCR7, CD62L, and CD95 expression. Subsets were assigned by hierarchical gating within the CAR+ CD4+ or CAR+ CD8+ compartment

Subpopulation	Gating strategy	CD45RO	CCR7	CD62L	CD95	Interpretation
Naïve	CAR+ → CD4+ /CD8+ → CD45RO− → CCR7+ → CD62L+ → CD95−	−	+	+	−	Undifferentiated T cells
Tscm	CAR+ → CD4+ /CD8+ → CD45RO− → CCR7+ → CD62L+ → CD95+	−	+	+	+	Stem cell memory, high persistence
Tcm	CAR+ → CD4+ /CD8+ → CD45RO+ → CCR7+ → CD62L+	+	+	+	+	Central memory, good expansion
Tem	CAR+ → CD4+ /CD8+ → CD45RO+ → CCR7−	+	−	−	+	Effector memory, rapid response
Temra	CAR+ → CD4+ /CD8+ → CD45RO− → CCR7−	−	−	−	+	Terminal effector

Table 3

Exhaustion panel used to evaluate inhibitory receptor expression in CAR DKO T cells on day 7 post-transduction. This panel was used to quantify PD-1, TIM-3, and LAG-3 expression within the CAR+ CD4+ and CAR+ CD8+ compartments. 7-AAD was included immediately before acquisition for live/dead discrimination

Channel	Fluorochrome	Marker	Clone
V1	BFP	CAR	_
V2	VioGreen	CD4	REA623
B1	FITC	CD3	REA613
B2	PE	PD-1	REA1165
B3	PerCP-Vio700	7-AAD	_
B4	PE-Vio770	LAG-3	REA351
R1	APC	TIM-3	REA635
R2	APC-Vio770	CD8	REA734

Table 4

Definition of exhaustion-associated subsets within CAR+ T cells based on PD-1, TIM-3, and LAG-3 expression. Exhaustion states were defined within the viable CAR+ CD4+ or CAR+ CD8+ compartment according to inhibitory receptor co-expression patterns

Population	Gating strategy	PD-1	TIM-3	LAG-3	Interpretation
PD-1+	CAR+ → CD4+/CD8+ → PD-1+	+	–	–	Initial chronic activation
TIM-3+	CAR+ → CD4+/CD8+ → TIM-3+	–	+	–	Progressive dysfunction
LAG-3+	CAR+ → CD4+/CD8+ → LAG-3+	–	–	+	Inhibitory regulation
PD-1+ TIM-3+	CAR+ → CD4+/CD8+ → PD-1+ → TIM-3+	+	+	–	Intermediate exhaustion
Triple+	CAR+ → CD4+/CD8+ → PD-1+ → TIM-3+ → LAG-3+	+	+	+	Deep exhaustion

and triple-positive populations were quantified to determine the extent of inhibitory receptor co-expression and to define progressive exhaustion-associated states. Within Table 3 are

detailed all the markers used to assess inhibitory receptor expression in CAR DKO T cells by flow cytometry, as described. Additionally, Table 4 shows that the exhaustion-associated subsets within CAR$^+$ T cells were classified according to the criteria described.

c) Activation analysis

Activation profiling was performed by assessing CD154 (CD40L), CD25, and CD137 (4-1BB) expression within the CAR+ CD4+ and CAR+ CD8+ populations. Single-positive, double-positive, and triple-positive populations were quantified to define early TCR activation, IL-2-associated proliferative signaling, CAR-specific activation, functional activation, and maximal activation states. The markers used to evaluate activation and functional responsiveness in CAR DKO T cells by flow cytometry are detailed in Table 5.

Following this, Table 6 outlines the definition of activation-associated subsets within CAR+ T cells based on CD154, CD25, and CD137 expression.

3.5.3 Genomic Analysis

1. Harvest an aliquot of at least $1–2 \times 10^6$ cells from the day 10 DKO CAR-T cell culture.
2. Centrifuge at $300 \times g$ for 5 min at room temperature and aspirate the supernatant completely.
3. Extract genomic DNA (gDNA) from the cell pellet using the DNeasy Blood & Tissue Kit (QIAGEN®), strictly following the manufacturer's protocol for cultured cells.

Table 5

Activation panel used to assess activation and functional responsiveness in CAR DKO T cells on day 7 post-transduction. This panel was used to quantify CD154, CD25, and CD137 expression within the CAR+ CD4+ and CAR+ CD8+ compartments. 7-AAD was included immediately before acquisition for live/dead discrimination

Channel	Fluorochrome	Marker	Clone
V1	BFP	CAR	_
V2	VioGreen	CD4	REA623
B1	FITC	CD3	REA613
B2	PE	CD154 (CD40L)	REA238
B3	PerCP-Vio700	7-AAD	_
B4	PE-Vio770	CD25	REAL128
R1	APC	CD137 (4-1BB)	REA765
R2	APC-Vio770	CD8	REA734

Table 6
Definition of activation-associated subsets within CAR+ T cells based on CD154, CD25, and CD137 expression. Activation states were defined within the viable CAR+ CD4+ or CAR+ CD8+ compartment according to the expression of early and late activation markers

Population	Gating strategy	CD154	CD25	CD137	Interpretation
CD154+	CAR+ → CD4+/CD8+ → CD154+	+	−	−	Early TCR activation
CD25+	CAR+ → CD4+/CD8+ → CD25+	−	+	−	IL-2 signaling/proliferation
CD137+	CAR+ → CD4+/CD8+ → CD137+	−	−	+	CAR-specific activation
CD154+ CD25+	CAR+ → CD4+/CD8+ → CD154+ → CD25+	+	+	−	Functional activation
Triple+	CAR+ → CD4+/CD8+ → CD154+ → CD25+ → CD137+	+	+	+	Maximal activation

4. Elute the gDNA in 50–100 µL of nuclease-free water or the provided elution buffer.
5. Store the extracted gDNA at −20°C until ready for downstream targeted amplicon sequencing or Droplet Digital PCR (ddPCR) analysis (*see* **Note 10**).

3.5.4 In Silico Off-Target Prediction and ddPCR Primer Design

1. Open a web browser and navigate to the CRISPR tools portal at https://crisprtools.org.
2. Select the *off-target* prediction tool CHOPOFF from the main interface to systematically assess the safety profile of the sgRNAs.
3. Fill in the job name field. Input the 20-nucleotide spacer sequences for the specific TRAC and B2M sgRNAs used in the electroporation step. Choose the target reference genome

(e.g., *Homo sapiens*) and select the specific nuclease utilized (e.g., Cas9).

4. Click the "Find *Off-Targets*" button and wait until this page refreshes and brings you to the results page.
5. Review the summary of *off-target* numbers for each sgRNA generated by the CHOPOFF (v1.0.3) [17] algorithm. Click on any of the guide rows to move to the detailed view for that specific sgRNA.
6. Examine the detailed view (Table 7), which displays all predicted *off-targets* with up to three mismatches, inserts, or bulges for your selected reference genome, alongside annotations of overlapping known genes. Note that results are sorted by editing distance and by the CRISPR-MFH predictive model, which ranks *off-targets* by their likelihood of actual cleavage [18] (*see* **Note 11** for guidelines on prioritizing *off-targets*).
7. Download the full list of these *off-target* loci by clicking the "Download *Off-targets*" button.
8. Design targeted primer pairs suitable for Droplet Digital PCR (ddPCR) validation [19] directly in the interface. Select the desired *off-target* rows in the "Design Primers" column, adjust the yield product sizes, and click the "Design Primers" button.
9. Once the calculation is initiated, click the "see Primers" expansion chevron for each *off-target* locus. Wait a minute and click the "Refresh" button until the designed primer sequences appear for your selected rows.

To conclude, a comprehensive workflow of this entire protocol is presented below in Fig. 2, illustrating the sequence of steps to be performed over a 1-week timeframe.

4 Notes

1. G-REX 24-well plates provide an enhanced gas-permeable surface area that supports high-density T cell expansion with minimal medium changes. Cells should not be disturbed during the first 24 h of activation to allow stable conjugation between TransAct and the T cell surface.
2. The MOI should be determined empirically for each viral batch based on the functional titer (TU/mL) established by flow cytometric titration. Selected MOI should yield stable CAR surface expression in ≥50% of transduced cells while minimizing the risk of multicopy lentiviral integration.
3. It is important to highlight that penicillin/streptomycin supplementation should be discontinued from the culture

Table 7

Representative in silico *off-target* prediction output for the B2M sgRNA generated using the CHOPOFF tool (crisprtools.org). Predicted *off-target* sites are ranked first by editing distance relative to the guide sequence and then by CRISPR-MFH score, with higher values indicating a greater predicted likelihood of *off-target* cleavage. Mismatched nucleotides relative to the guide sequence are highlighted in red in the alignment column (*Accessed April 21st, 2026*)

Rank	Distance	CRISPR-MFH	Location	Alignment	Genomic overlap
1	0	0.210	chr15:44711542:-	Guide: GGCCACGGAGCGAGACATCT Ref: GGCCACGGAGCGAGACATCT	B2M/N/A/ENSG00000166710
2	3	0.761	chr16:12288677:+	Guide: GG**C**CAC**G**GAGCGAGACATCT Ref: GG**T**G**A**CAGAGCGAGACATCT	None
3	3	0.707	chr1:241990371:-	Guide: GGC**C**AC**G**GAGCGAGACATCT- Ref: GGC**G**AC**A**GAGCGAGACATCT**C**	None
4	3	0.707	chr19:11815275:+	Guide: GGC**C**AC**G**GAGCGAGAC**T**CT Ref: GGC**A**AC**A**GAGCGAGAC**A**CT	None
5	3	0.697	chr11:14033327:-	Guide: GGCCA**C**GG-AG**C**GACACATCT Ref: GGCCA**T**GG**C**AG**T**GACACATCT	None
6	3	0.678	chr20:52174709:+	Guide: GG**C**CA**C**GGAG**C**GAGACATCT Ref: GG**A**CA**T**GGAG-GAGACATCT	None

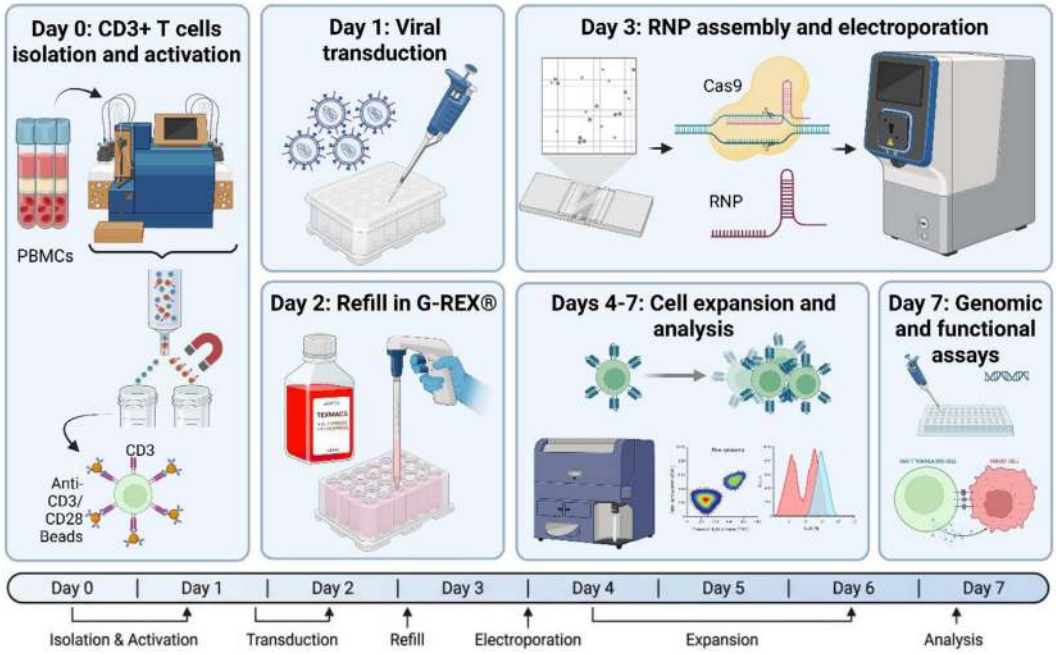


Fig. 2 Workflow for CRISPR/Cas9-mediated gene editing in human T cells by electroporation. Described workflow to obtain DKO TCR/HLA CAR-T cells from PBMCs in a week

medium at least 48 h prior to the scheduled electroporation step. Penicillin is a β-lactam antibiotic whose sodium and potassium salt counterions, as well as the ionic components of the streptomycin sulfate formulation, can alter the ionic composition and conductivity of the electroporation buffer upon carry-over, potentially interfering with the electrical pulse delivery and reducing both transfection efficiency and post-electroporation cell viability. Therefore, from day 1, medium refills and supplements should be prepared in antibiotic-free TX medium, and penicillin/streptomycin (1×) may be reintroduced following the post-electroporation recovery period.

4. The order of addition in Step 5 is critical. Adding buffer to the RNP before contacting the cell pellet ensures homogeneous RNP distribution and prevents localized osmotic stress on the cells. Any residual PBS in the pellet will dilute the electroporation buffer and may significantly impair transfection efficiency; complete removal of the supernatant in Step 4 is therefore essential.
5. The 5 h recovery period in unsupplemented medium following electroporation allows transient membrane resealing and reduces the cytotoxic impact of the electrical pulse before cytokine-supplemented expansion medium is added.

Addition of IL-7 and IL-15 prior to this recovery window is not recommended, as cytokine signaling during the immediate post-electroporation period may interfere with cellular stress responses and affect editing outcomes.

6. Although the initial protocol designates day 8 (7 days post-transduction) as the time point for product assessment, subsequent experimental optimization in our laboratory has established that delaying the evaluation to day 10 (9 days post-transduction) consistently yields superior outcomes. At this later point, a higher proportion of edited CAR+ cells are detected by flow cytometry, cell viability is better preserved, and the total cell number recovered is substantially greater, providing a more robust and reproducible starting population for the subsequent programming of cytotoxicity assays and serial rechallenge experiments.
7. Surface loss of CD3 and B2M is used as the primary flow cytometric readout of successful CRISPR/Cas9-mediated disruption of the *TRAC* and *B2M* loci, respectively. The CD3 antibody from BD Biosciences® (PerCP-Cy5.5) targets a distinct epitope from the Miltenyi Biotec® CD3–FITC clone.
8. The memory and differentiation markers (CD45RO, CD62L, CCR7, CD95) in combination enable classification of T cell subsets into naïve (T_N), stem cell memory (T_{SCM}), central memory (T_{CM}), effector memory (T_{EM}), and terminally differentiated effector (T_{EMRA}) subpopulations, providing a comprehensive assessment of the differentiation status of the edited product [14].
9. The use of BFP as an intrinsic reporter for CAR expression provides a reliable, antibody-independent surrogate for transduction efficiency that is spectrally compatible with the PerCP-Cy5.5 and PE channels used for CD3 and B2M detection on the BD FACS Canto II.
10. While flow cytometry confirms phenotypic editing, genomic-level validation is essential to assess the safety of the engineered product. Multiplexed disruption of *TRAC* and *B2M* may increase genotoxicity concerns, particularly with respect to *off-target* mutagenesis and interchromosomal translocations [20]. Current safety standards mandate a layered validation paradigm to address these liabilities [21]. The first layer focuses on unbiased discovery. Because biochemical assays (e.g., CHANGE-seq) lack chromatin context and generate high false-positive rates [22, 23], cellular assays like GUIDE-seq or DISCOVER-seq are prioritized to capture biologically relevant *off-target* cleavage [24, 25]. For detecting massive structural variants, unidirectional NGS (e.g., UDiTaS) or linker-mediated PCR (CAST-Seq) overcomes the amplification

dropouts inherent to standard sequencing [26, 27]. Because standard targeted amplicon sequencing is susceptible to PCR bias [28], to achieve absolute quantification of these nominated sites, droplet digital PCR (ddPCR) has emerged as the quantitative alternative offering unparalleled sensitivity (≤ 0.01%) and resilience to the chaotic breakpoint heterogeneity characteristic of NHEJ repair [29, 30].

11. Selecting which predicted *off-target* loci to prioritize for downstream experimental validation must be evaluated on a case-by-case basis. Given the impracticality of validating hundreds of predicted sites, we recommend the following hierarchical criteria for prioritization:

    - Editing distance (mismatches/bulges): prioritize loci with the lowest editing distance relative to the reference sequence. Sites with one or two mismatches are significantly more likely to be cleaved than those with three or more. (*Additional note: a distance of 0, visible in the first row of* Table 7, *represents the intended on-target site*).
    - Empirical validation (activity column): prioritize loci that have been previously identified as active *off-targets* in empirical databases or literature, as indicated in the platform's "Activity" column.
    - Genomic annotation: prioritize *off-targets* that overlap with known genes (especially exons, promoters, or regulatory elements of oncogenes or tumor suppressors). Unintended mutations in coding regions pose a vastly higher translational safety risk for clinical CAR-T products compared to deep intergenic or intronic mutations.
    - Predictive cleavage score: finally, utilize the CRISPR–MFH score to assess the relative danger of the remaining *off-targets*. Prioritize loci with higher CRISPR–MFH values, as these represent a higher computational probability of actual Cas9 cleavage.
    - General rule: try to scrutinize and experimentally validate as many high-priority *off-targets* as resources allow to ensure robust safety profiling of the engineered cells.

Acknowledgments

The publication is based upon work by COST Action CA21113: Genome Editing for the Treatment of Human Diseases (https://www.genehumdi.eu), supported by European Cooperation in Science and Technology (COST). Figures were created in BioRender. Benabdellah, K. (2026) https://BioRender.com/tsb89k8.

Competing Interests The authors declare no conflicts of interest and were guided by literature and conference evidence in content choices and conclusions. The funders had no role in the design of the study; in the collection, analyses, or interpretation of data; in the writing of the manuscript; or in the decision to publish the results.

References

1. June CH, O'Connor RS, Kawalekar OU et al (2018) CAR T cell immunotherapy for human cancer. Science 359:1361–1365
2. Tashiro H, Sauer T, Shum T et al (2017) Treatment of acute myeloid leukemia with T cells expressing chimeric antigen receptors directed to C-type lectin-like molecule 1. Mol Ther 25:2202–2213
3. Levine BL, Miskin J, Wonnacott K et al (2017) Global manufacturing of CAR T cell therapy. Mol Ther 4:92–101
4. Tao R, Han X, Bai X et al (2024) Revolutionizing cancer treatment: enhancing CAR-T cell therapy with CRISPR/Cas9 gene editing technology. Front Immunol 15:1354825
5. Lei T, Wang Y, Zhang Y et al (2024) Leveraging CRISPR gene editing technology to optimize the efficacy, safety and accessibility of CAR T-cell therapy. Leukemia 38:2517–2543
6. Harris E, Elmer JE (2021) Optimization of electroporation and other non-viral gene delivery strategies for T cells. Biotechnol Progress 37:3066
7. Seki A, Rutz S (2018) Optimized RNP transfection for highly efficient CRISPR/Cas9-mediated gene knockout in primary T cells. J Exp Med 215:985–997
8. Wu F, Ni L, Xiao Y et al (2026) Lipid nanoparticles for delivery of CRISPR gene editing components. Small Methods 10:2401632
9. VanderBurgh JA, Corso TN, Levy SL et al (2023) Scalable continuous-flow electroporation platform enabling T cell transfection for cellular therapy manufacturing. Sci Rep 13: 6857
10. Lukjanov V, Koutná I, Šimara P (2021) CAR T-cell production using nonviral approaches. J Immunol Res 2021:1–9
11. Khawar MB, Afzal A, Si Y et al (2024) Steering the course of CAR T cell therapy with lipid nanoparticles. J Nanobiotechnol 22: 380
12. Xu Y, Zhang M, Ramos AM et al (2014) Closely related T-memory stem cells correlate with in vivo expansion of CAR.CD19-T cells and are preserved by IL-7 and IL-15. Blood 123:3750–3759
13. Vakulskas CA, Dever DP, Rettig GR et al (2018) A high-fidelity Cas9 mutant delivered as a ribonucleoprotein complex enables efficient gene editing in human hematopoietic stem and progenitor cells. Nat Med 24:1216–1224
14. Gattinoni L, Lugli E, Ji Y et al (2011) A human memory T cell subset with stem cell–like properties. Nat Med 17:1290–1297
15. Poirot L, Philip B, Schiffer-Mannioui C et al (2015) Multiplex genome-edited T-cell manufacturing platform for "Off-the-Shelf" adoptive T-cell immunotherapies. Cancer Res 75:3853–3864
16. Ren J, Liu X, Fang C et al (2017) Multiplex genome editing to generate universal CAR T cells resistant to PD1 inhibition. Clin Cancer Res 23:2255–2266
17. Labun K, Rio O, Tjeldnes H et al (2025) CHOPOFF: symbolic alignments enable fast and sensitive CRISPR off-target detection. bioRxiv 2025.01.06.603201. https://doi.org/10.1101/2025.01.06.603201
18. Zheng Y, Zou Q, Li J et al (2025) CRISPR-MFH: a lightweight hybrid deep learning framework with multi-feature encoding for improved CRISPR-Cas9 off-target prediction. Genes 16:387
19. Untergasser A, Nijveen H, Rao X et al (2007) Primer3Plus, an enhanced web interface to Primer3'. Nucleic Acids Res 35:71–74
20. Stadtmauer EA, Fraietta J, Davis MM et al (2020) CRISPR-engineered T cells in patients with refractory cancer. Science 367:7365
21. FDA (2024) Human Gene Therapy Products Incorporating Human Genome Editing; Guidance for Industry. https://www.fda.gov/regulatory-information/search-fda-guidance-documents/human-gene-therapy-products-incorporating-human-genome-editing. Accessed 29 April 2026
22. Lazzarotto CR, Malinin NL, Li Y et al (2020) CHANGE-seq reveals genetic and epigenetic effects on CRISPR–Cas9 genome-wide activity. Nat. Biotechnol. 38(11):1317–1327
23. Atkins A, Chung C, Allen AG et al (2021) Off-target analysis in gene editing and applications for clinical translation of CRISPR/Cas9 in HIV-1 therapy. Front Genome Ed 3:673022
24. Tsai SQ, Zheng Z, Nguyen NT et al (2015) GUIDE-seq enables genome-wide profiling of off-target cleavage by CRISPR-Cas nucleases. Nat Biotechnol 33:187–197

25. Wienert B, Wyman SK, Richardson CK et al (2019) Unbiased detection of CRISPR off-targets in vivo using DISCOVER-Seq. Science 364:286–289
26. Turchiano G, Andrieux G, Klermund J et al (2021) Quantitative evaluation of chromosomal rearrangements in gene-edited human stem cells by CAST-Seq. Cell Stem Cell 28:1136–1147
27. Giannoukos G, Ciulla DM, Marco E et al (2018) UDiTaSTM, a genome editing detection method for indels and genome rearrangements. BMC Genomics 19: 212
28. Yin J, Liu M, Liu Y et al (2019) Optimizing genome editing strategy by primer-extension-mediated sequencing. Cell Discov 5:18
29. Miotke L, Lau BT, Rumma RT et al (2014) High sensitivity detection and quantitation of DNA copy number and single nucleotide variants with single color droplet digital PCR. Anal Chem 86:2618–2624
30. Findlay SD, Vincent KM, Berman JR et al (2016) A digital PCR-based method for efficient and highly specific screening of genome edited cells. PLoS ONE 11(4):153901

Open Access This chapter is licensed under the terms of the Creative Commons Attribution-NonCommercial-NoDerivatives 4.0 International License (http://creativecommons.org/licenses/by-nc-nd/4.0/), which permits any noncommercial use, sharing, distribution and reproduction in any medium or format, as long as you give appropriate credit to the original author(s) and the source, provide a link to the Creative Commons license and indicate if you modified the licensed material. You do not have permission under this license to share adapted material derived from this chapter or parts of it.

The images or other third party material in this chapter are included in the chapter's Creative Commons license, unless indicated otherwise in a credit line to the material. If material is not included in the chapter's Creative Commons license and your intended use is not permitted by statutory regulation or exceeds the permitted use, you will need to obtain permission directly from the copyright holder.





Chapter 21

Delivery of Targeting Constructs into Zygotes Using Electroporation

Michaela Vaskovicova, Vojtech Dolejs, Pavla Dostalova, Csilla Sustr Michalikova, Jan Prochazka and Radislav Sedlacek

Abstract

Zygote electroporation (EP) is a widely used technique for the delivery of targeting constructs into the embryos and has become very popular in the last few years in transgenic facilities all over the world. Zygote electroporation is technically simple, as it does not require equipment for microinjection. Moreover, zygote electroporation is less invasive, resulting in higher survival rates in comparison to pronuclear microinjection, leading to a reduction in the number of animals needed. Another advantage of zygote electroporation is a higher number of zygotes that can be targeted simultaneously, which minimizes the time required for zygote manipulation. Zygote electroporation is easily combined with the use of the CRISPR–Cas9 system.

Keywords Genome editing, Zygote electroporation, Blastocysts genotyping

1 Introduction

The introduction of CRISPR/Cas9 genome editing into mammalian systems in 2013 revolutionized the field of genetic engineering by enabling rapid, efficient, and programmable modification of the mouse genome [1,2]. This technological breakthrough rapidly replaced earlier gene-targeting strategies based on homologous recombination in embryonic stem cells, which were labor-intensive, time-consuming, and limited in scalability.

In parallel with the development of CRISPR-based genome editing, efficient methods for delivering editing reagents into mouse zygotes became a critical determinant of experimental success. Pronuclear microinjection has long been considered the gold standard for introducing nucleic acids and proteins into fertilized oocytes and has enabled the generation of a wide range of genetically modified mouse models [3]. However, microinjection requires substantial technical expertise, specialized equipment, and allows only limited

Duško Lainšček et al. (eds.), *CRISPR Delivery*, Methods in Molecular Biology, vol. 3075,
https://doi.org/10.1007/978-1-0716-5547-4_21,
© The Author(s) 2027

throughput, which poses constraints in high-demand settings such as transgenic core facilities and large-scale phenotyping initiatives.

To overcome these limitations, electroporation-based delivery methods have been developed as a practical alternative for introducing genome editing components into mouse zygotes. Zygote electroporation enables simultaneous processing of multiple embryos, reduces mechanical damage associated with micromanipulation, and significantly improves experimental scalability while maintaining high embryo viability [4,5]. Importantly, several studies have demonstrated that electroporation achieves genome editing efficiencies comparable to or exceeding those obtained by pronuclear microinjection, particularly for small insertions and deletions and for single-stranded donor-mediated knock-in strategies [6,7].

Electroporation is particularly well suited for the delivery of CRISPR/Cas9 ribonucleoprotein (RNP) complexes, which consist of recombinant Cas9 protein pre-complexed with guide RNA. In contrast to plasmid- or mRNA-based approaches, RNP delivery enables immediate genome editing activity upon entry into the zygote cytoplasm, thereby improving editing kinetics and reducing mosaicism. Furthermore, the transient presence of the Cas9 nuclease minimizes the risk of off-target effects [8,9].

In addition to knockout applications, the combination of electroporation with single-stranded oligodeoxynucleotide (ssODN) donors allows efficient generation of precise knock-in alleles, including disease-relevant point mutations. While this approach is highly effective for small sequence modifications, it remains less suitable for large DNA insertions, where alternative delivery strategies such as microinjection or viral vectors may still be required [7,10].

Despite its relative simplicity, successful implementation of zygote electroporation requires careful optimization of several experimental parameters, including electrical pulse conditions, reagent composition, embryo handling, and impedance control. Even minor deviations in these parameters can significantly affect both embryo survival and genome editing efficiency.

In this chapter, we provide a robust and reproducible protocol for the delivery of CRISPR–Cas9 RNP complexes into mouse zygotes using electroporation. The method is optimized for high-efficiency genome editing with minimal impact on embryo viability and is readily adaptable for both knockout and knock-in applications in standard transgenic workflows.

2 Materials

2.1 Reagents

- Alt-R™ CRISPR–Cas9 crRNA

- Alt-R™ CRISPR–Cas9 tracrRNA
- Alt-R S.p Cas9 nuclease V3, 100 μg
- Nuclease-free duplex buffer
- ssODN (4 nmole Ultramer™ DNA Oligo)
- KSOM (potassium simplex optimized medium)
- Opti-MEM (reduced-serum medium)
- M2 medium
- Mineral oil
- Lysis buffer (final concentration: 50 mM Tris pH 8, 1 mM EDTA, 0.5% (v/v) Triton X-100)
- 0.1–0.2 mg/ml Proteinase K
- DNA polymerase (DreamTaq PCR Master Mix (2×), or corresponding polymerases with buffers)-primers specific for the targeted region
- 1× TAE buffer (final concentration: 40 mM Tris, 20 mM acetic acid, 1 mM EDTA)
- DNA stain (Ethidium Bromide, or corresponding DNA stain)
- Gel loading dye
- Nuclease-free water

2.2 Equipment

- NEPA21 electroporator
- Electrode CUY501P1–1.5
- Petri dish
- Retransfer pipette (ID: 115–124 μm, TL: 40 mm)
- Aspirator tube assemblies for calibrated microcapillary pipettes
- Benchtop vortex
- Benchtop centrifuge
- PCR Thermal Cycler
- Agarose gel electrophoresis system, UV transilluminator

3 Methods

3.1 Preparation of crRNA:tracrRNA Duplex for Ex Vivo Zygote Electroporation

1. Dilute crRNAs in nuclease-free duplex buffer to a final concentration of 100 μM.
2. Dilute tracrRNA in nuclease-free duplex buffer to a final concentration of 100 μM.
3. Mix crRNA and tracrRNA 1:1, typically 5 μl of crRNA + 5 μl of tracrRNA.

4. Heat the crRNA:tracrRNA mix at 95°C for 3 min, then incubate for 5 min at room temperature, centrifuge briefly.
5. Add 4× volume of OptiMEM (i.e., add 40 µl of OptiMEM to 10 µl of crRNA:tracrRNA).
6. When using two gRNAs, combine both aliquots (final concentration of individual gRNAs is 5 µM, total gRNA concentration is 10 µM).
7. Prepare 10 µl aliquots and store at −20°C or use directly for EP (after adding Cas9 protein).

3.2 Preparation of RNPs (Ready to use for EP)

1. Thaw a 10 µl aliquot of gRNAs.
2. Add 0.5 µl (5000 ng) of Cas9 protein into a 10 µl crRNA:tracrRNA aliquot, mix well (final concentration of Cas9 protein is approximately 3 µM or 500 ng/µl).
3. Incubate 5 min at RT.
4. Keep on ice until electroporation (at least 15 min).

3.3 Preparation of RNPs + ssODN (Ready to use for EP)

1. Thaw a 10 µl aliquot of gRNAs.
2. Dilute ssODN in nuclease-free water to a final concentration of 100 µM.
3. Mix gRNA aliquot with ssODN aliquot 1:1 (5 µl of gRNA + 5 µl of ssODN).
4. Add 0.5 µl (5000 ng) of Cas9 protein into a 10 µl crRNA:tracrRNA aliquot, mix well (final concentration of Cas9 protein is approximately 3 µM or 500 ng/µl).
5. Incubate 5 min at RT.
6. Keep on ice until electroporation (at least 15 min).

3.4 Zygote Electroporation (EP)

1. After isolation (*see* **Note 1**), keep zygotes in KSOM overlaid with mineral oil in the incubator (37°C, 5% CO_2).
2. Prepare electrode CUY501P1–1.5 and set up the following parameters for electroporation using NEPA21 electroporator (*see* **Note 2**):
   a. Poring pulses: 40 V, 3.5 ms, 50 ms interval, four pulses, decay rate 10%, polarity+.
   b. Transfer pulses: 5 V, 50 ms, 50 ms interval, five pulses, decay rate 40%, polarity±.
3. Using a pipette, load 10 µl of RNPs or RNPs + ssODN in the gap of CUY501P1–1.5 electrode (Fig. 1).
4. Measure the impedance (Ω button), adjust impedance by removing the targeting construct or adding the OptiMEM

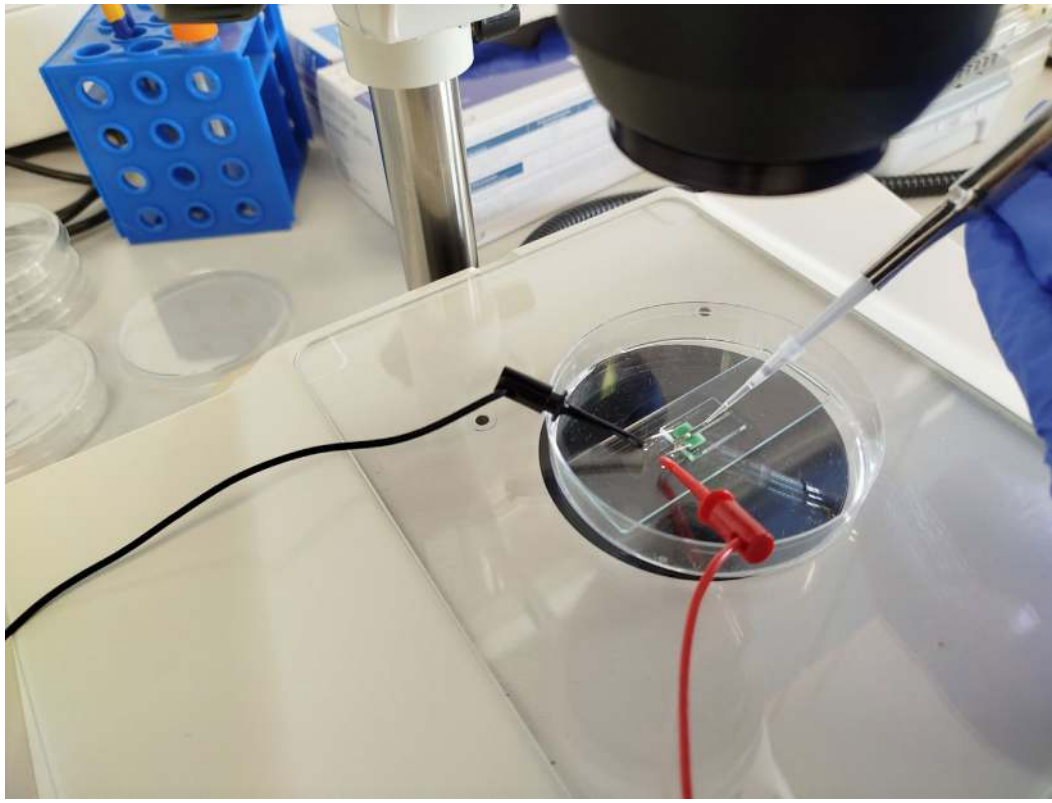


Fig. 1 Loading of targeting construct in the gap of CUY501P1–1.5 electrode. The targeting construct (CRISPR–Cas9 RNP complex with or without ssODN donor) is carefully pipetted into the gap between the electrodes mounted in a Petri dish. The solution forms a small droplet bridging the electrodes, into which zygotes are subsequently transferred. Precise positioning of the liquid column and avoidance of air bubbles are critical to ensure uniform electric field distribution and reproducible electroporation efficiency. The electrode is placed under a stereomicroscope to allow accurate manipulation and alignment of embryos prior to pulse application

(*see* **Note 3**). Optimal impedance should be in the range 0.18–0.22 kΩ.

5. Wash zygotes in three drops of OptiMEM (to remove oil) by aspiration and release using the retransfer pipette and aspiration tube.
6. Aspirate washed zygotes into the retransfer pipette and transfer them into the targeting construct in CUY501P1–1.5 electrode. Load a maximum of 50 zygotes, make sure zygotes are arranged in a row (clusters reduce efficiency of EP, *see* **Note 4**).
7. Measure the impedance (Ω button), adjust impedance by removing the targeting construct or adding the OptiMEM. Optimal impedance should be in the range 0.18–0.22 kΩ (see **Note 3**).
8. Apply the pulse (press start), and bubbles should appear as a marker of pulses.

9. Collect the zygotes and wash them in two drops of M2 and one drop of KSOM.
10. Culture zygotes till the blastocyst stage in KSOM overlayed with mineral oil in the incubator (37°C, 5% CO_2). Each day, check development (*see* **Note 5**). The timeline of preimplantation development is depicted in Fig. 2.

3.5 Embryo Collection and Genotyping

1. Collect embryos in the blastocyst stage (see Fig. 2)
2. Wash embryos in three drops of M2 media (to remove oil)
3. Aspirate a single embryo in the retransfer pipette and release the embryo into the PCR tube; make sure the embryos are at the bottom of the tube. Remove as much media as possible, store in −20°C, or continue directly with lysis
4. Add 0.5 µl of Proteinase K to 10 µl of lysis buffer
5. Shortly, centrifuge tubes with embryos (to have embryos at the bottom of the tubes)
6. Add 10 µl of lysis buffer with Proteinase K directly to each tube
7. Incubate for 30 min at 56°C
8. Incubate for 10 min at 95°C to inactivate Proteinase K
9. Vortex the samples for 10–15 s, cool briefly, and centrifuge shortly. Directly use samples as a template for DNA.
10. Gently vortex PCR buffer, dNTPs, and primers after thawing. Centrifuge briefly
11. Prepare Master mix by mixing water, PCR buffer, dNTPs, primers, and DreamTaq DNA polymerase according to Table 1. Keep Master Mix on ice.
12. Aliquot the Master Mix into individual PCR tubes and add template DNA

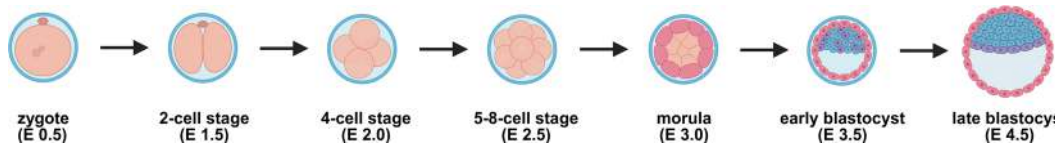


Fig. 2 Timeline of preimplantation development in mouse embryos. Schematic representation of mouse preimplantation development from the zygote (E0.5) to the late blastocyst stage (E4.5). Following fertilization, the zygote undergoes a series of cleavage divisions (2-cell, 4-cell, and 5–8-cell stages) leading to compaction and formation of the morula. Subsequent cavitation results in the formation of the blastocyst, characterized by the emergence of the inner cell mass and the surrounding trophectoderm. Zygote electroporation is typically performed at the pronuclear stage (E0.5), when genome-editing reagents can be introduced prior to the first cell division, thereby maximizing editing efficiency and minimizing mosaicism

13. Insert PCR tubes into the thermal cycler and perform the PCR reaction using specific thermal cycling conditions (see Table 2, *see* **Note 6**)
14. Prepare the agarose gel by melting agarose in 1× TAE buffer in a microwave. Cool under running water, add DNA stain for visualizing DNA, and mix well. Pour the gel into the tray, insert the comb, and allow it to solidify
15. Insert the gel in the electrophoresis chamber and cover with 1× TAE buffer; remove the comb
16. Mix the samples with loading dye for electrophoresis, if not already present in the PCR buffer
17. Pipette the samples into the wells, and load the DNA ladder into one lane to determine the size of amplified DNA

Table 1
Composition of Master Mix for PCR

reagent	Volume (μl)
10× DreamTaq Buffer	2.5
dNTP mix (2 mM each)	0.5
Primer forward (10 μM)	1.0
Primer reverse (10 μM)	1.0
DreamTaq DNA Polymerase	0.2
Template DNA	2.5
H_2O	17.3
Total volume	25.0

Table 2
PCR thermal cycling conditions

	Temperature (°C)	Time	Number of cycles
Initial denaturation	95	5 min	1
Denaturation	95	30 s	35–60
Annealing		30 s	
Extension	72	1000 bp/min	
Final extension	72	5 min	1
End	12	Infinity	

18. Close the lid and connect the electrodes, run the gel at constant voltage (80–100 V) until the loading dye front reaches the bottom of the gel
19. Visualize DNA fragments under a UV transilluminator
20. Determine the genotype of blastocysts and assess the effectiveness of targeting (*see* **Notes 7–10**)

4 Notes

1. After the dissection of the ovaries with the fallopian tubes from sacrificed animals, zygotes with cumulus cells are released from the ampulla. Treatment with Hyaluronidase is used for the removal of cumulus cells. Washed zygotes are cultured in KSOM media overlayed with mineral oil in the incubator at a stable temperature and atmosphere (37°C, 5% CO_2).
2. Although the parameters provided in this protocol serve as a robust starting point, optimal conditions may vary depending on the electroporation device, electrode geometry, embryo source, and reagent composition. Small adjustments in voltage, pulse duration, or number of pulses can have a significant impact on both embryo viability and editing efficiency. Therefore, initial pilot experiments are recommended when establishing the method in a new laboratory.
3. The electrical impedance of the electroporation chamber should be maintained within a narrow optimal range (typically 0.18–0.22 kΩ under the described conditions). If the impedance is lower than 0.18 kΩ adjust the impedance by removing the targeting construct. If the impedance is higher than 0.22 kΩ adjust by adding OptiMEM. Values below this range are often associated with insufficient delivery of RNP complexes, while higher impedance increases the risk of irreversible damage to embryos due to excessive local heating and membrane disruption. Impedance is influenced by medium composition, electrode condition, and the presence of air bubbles; therefore, it should be measured immediately prior to pulse delivery and adjusted if necessary by gently repositioning embryos or replacing the electroporation buffer.
4. Uniform alignment of embryos between the electrodes is essential for reproducible electroporation efficiency. Embryos should be arranged in a single line parallel to the electric field to ensure consistent exposure to the pulse. Clustering or overlapping embryos leads to uneven field distribution, resulting in variable uptake of reagents and reduced editing efficiency. Gentle pipetting with minimal medium volume facilitates proper positioning.

5. The developmental stage and overall quality of zygotes significantly affect both survival and editing outcomes. Optimal results are typically achieved when electroporation is performed at the pronuclear stage (PN stage), shortly after fertilization. Zygotes with visible abnormalities, delayed development, or compromised morphology should be excluded, as they are more sensitive to electroporation-induced stress. Differences between embryos derived from superovulation and natural mating may also impact outcomes and should be considered during experimental design.
6. PCR Master Mix and PCR thermal cycling conditions should be adjusted according to the specific DNA polymerase used. Always follow the manufacturer's instructions. Note that annealing temperature needs to be adjusted based on the melting temperature of specific primers. Extension time needs to be adjusted based on the length of the amplified sequence. Always include a non-template control reaction to check for contamination.
7. The use of preassembled Cas9 RNP complexes is strongly recommended over plasmid- or mRNA-based delivery systems. RNPs provide immediate genome editing activity and reduce the duration of Cas9 exposure within the cell, thereby minimizing mosaicism and potential off-target effects. To ensure maximal activity, RNP complexes should be freshly prepared, briefly incubated at room temperature to allow proper assembly, and kept on ice thereafter. Repeated freeze–thaw cycles should be avoided, as they can reduce nuclease activity.
8. Efficient knock-in using ssODN donors depends strongly on donor design. Homology arms of 50–100 nucleotides are typically sufficient, although asymmetric designs (longer homology arm on one side of the edit) have been reported to improve efficiency. The strand orientation relative to the target locus may also influence repair outcomes. It is advisable to introduce silent mutations to disrupt the PAM sequence or guide RNA binding site in order to prevent recutting of the edited allele.
9. Mosaicism remains a potential limitation of zygote-based genome editing and is influenced by the timing of DNA cleavage relative to the first cell division. The use of RNP complexes significantly reduces mosaicism by enabling rapid editing shortly after delivery. However, delayed activity or suboptimal reagent delivery may still result in mosaic embryos. Analysis at the blastocyst stage can help estimate the extent of mosaicism prior to establishing mouse lines.
10. While electroporation is highly effective for generating small insertions, deletions, and point mutations, it is less suitable for introducing large DNA fragments or complex genetic

constructs. In such cases, pronuclear microinjection or alternative delivery strategies may be required. The choice of method should therefore be aligned with the specific genetic modification being pursued.

Acknowledgments

The publication is based upon work by COST Action CA21113: Genome Editing for the Treatment of Human Diseases (https://www.genehumdi.eu), supported by European Cooperation in Science and Technology (COST). It was supported by the Czech Academy of Sciences RVO 68378050 and by the project LM2023036, Czech Center for Phenogenomics, provided by the Ministry of Education, Youth and Sports of the Czech Republic. We thank Petr Kasparek and Petr Nickl for their previous work on zygote electroporation protocols.

Competing Interests The authors have no conflicts of interest to declare that are relevant to the content of this chapter.

References

1. Cong L, Ran FA, Cox D et al. (2013) Multiplex genome engineering using CRISPR/Cas systems. Science 339:819–823
2. Mali P, Yang L, Esvelt KM et al. (2013) RNA-guided human genome engineering via Cas9. Science 339:823–826
3. Yang H, Wang H, Shivalila CS, Cheng AW et al. (2013) One-step generation of mice carrying reporter and conditional alleles by CRISPR/Cas-mediated genome engineering. Nat Biotechnol 31:684–686
4. Hashimoto M, Takemoto T (2015) Electroporation enables the efficient mRNA delivery into the mouse zygotes and facilitates CRISPR/Cas9-based genome editing. Sci Rep 5: 11315
5. Qin W, Dion SL, Kutny PM et al. (2015) Efficient CRISPR/Cas9-mediated genome editing in mice by zygote electroporation of nuclease. Genetics 200:423–430
6. Chen S, Lee B, Lee AYF et al. (2016) Highly efficient mouse genome editing by CRISPR ribonucleoprotein electroporation of zygotes. J Biol Chem 291:14457–14467
7. Modzelewski AJ, Chen S, Willis BJ et al. (2018) Efficient mouse genome engineering by CRISPR-EZ technology. Nat Protoc 13:1253–1274
8. Kim S, Kim D, Cho SW et al. (2014) Highly efficient RNA-guided genome editing in human cells via delivery of purified Cas9 ribonucleoproteins. Genome Res 24:1012–1019
9. Liang X, Potter J, Kumar S et al. (2015) Enhanced CRISPR/Cas9-mediated precise genome editing by improved design and delivery of gRNA, Cas9 nuclease, and donor DNA. J Biotechnol 208:44–53
10. Aida T, Chiyo K, Usami T et al. (2015) Cloning-free CRISPR/Cas system facilitates functional cassette knock-in in mice. Genome Biol 16: 87

Open Access This chapter is licensed under the terms of the Creative Commons Attribution-NonCommercial-NoDerivatives 4.0 International License (http://creativecommons.org/licenses/by-nc-nd/4.0/), which permits any noncommercial use, sharing, distribution and reproduction in any medium or format, as long as you give appropriate credit to the original author(s) and the source, provide a link to the Creative Commons license and indicate if you modified the licensed material. You do not have permission under this license to share adapted material derived from this chapter or parts of it.

The images or other third party material in this chapter are included in the chapter's Creative Commons license, unless indicated otherwise in a credit line to the material. If material is not included in the chapter's Creative Commons license and your intended use is not permitted by statutory regulation or exceeds the permitted use, you will need to obtain permission directly from the copyright holder.

